N73-28889
NASA CR-120918
D180-15296-1

DEVELOPMENT OF A FRACTURE CONTROL METHOD FOR COMPOSITE TANKS WITH LOAD SHARING LINERS

(Interim Report)

By
W. D. Bixler

BOEING
AEROSPACE COMPANY

Prepared For

NATIONAL AERONAUTICS AND SPACE ADMINISTRATION

NASA Lewis Research Center
Contract NAS 3-14380

1. Report No. NASA CR-120918	2. Government Accession No.	3. Recipient's Catalog No.
4. Title and Subtitle Development of a Fracture Control Method for Composite Tanks With Load Sharing Liners (Interim Report)		5. Report Date March 1973
		6. Performing Organization Code
7. Author(s) W. D. Bixler		8. Performing Organization Report No. D180-15296-1
		10. Work Unit No.
9. Performing Organization Name and Address Boeing Aerospace Company Research and Engineering Division Seattle, WA 98124		11. Contract or Grant No. NAS 3-14380
		13. Type of Report and Period Covered Contractor Report July 1971 through November 1972
12. Sponsoring Agency Name and Address National Aeronautics and Space Administration 21000 Brookpark Rd. Lewis Research Center Cleveland, OH 44135		14. Sponsoring Agency Code
15. Supplementary Notes Project Manager, James R. Faddoul Materials and Structures Division NASA Lewis Research Center Cleveland, OH 44135		

16. Abstract

This experimental program was undertaken to establish a fracture control method for composite tanks with load sharing liners. Uniaxial specimens containing surface flaws were loaded to failure (static fractured) and cycled to failure and the results were compared with burst tests and cyclic life tests of composite tanks having surface flaws present in the load sharing metal liners. The liner materials investigated were Inconel X750 STA, 2219-T62 aluminum and cryostretched 301 stainless steel at room temperature and at $78^{\circ}K$ ($-320^{\circ}F$) in liquid nitrogen. Differences were observed in comparing the uniaxial and tank test results. These differences should be resolved if an adequate fracture control method is to be developed.

17. Key Words (Suggested by Author(s)) Fracture Control, Composite Tanks, Load Sharing Liners, Uniaxial Specimens, Biaxial Specimens, Surface Flawed, Inconel X750 STA, 2219-T62 Aluminum, Cryoformed 301 Stainless Steel		18. Distribution Statement Unclassified, Unlimited	
19. Security Classif. (of this report) Unclassified	20. Security Classif. (of this page) Unclassified	21. No. of Pages 284	22. Price* $3.00

* For sale by the National Technical Information Service, Springfield, Virginia 22151

FOREWORD

This report describes the work performed by the Boeing Aerospace Company from July 1971 to November 1972 under Contract NAS 3-14380. The work was administered by Mr. James R. Faddoul of the NASA Lewis Research Center. Structural Composities Industries (SCI), acting in the capacity of an associate contractor, participated in the program. Boeing had overall responsibility for the program and conducted the experimental portion while SCI was primarily responsible for overwrapped tank design and analysis, and Inconel and aluminum specimen fabrication. Arde', Inc. also participated in the program in an advisory capacity and as a supplier of stainless steel specimens.

Boeing personnel who conducted the investigation include J. N. Masters, project supervisor and W. D. Bixler, technical leader. Specimen testing support was provided by A. A. Ottlyk and H. Olden, and the technical illustration and art work was done by D. Good. SCI personnel who contributed to the investigation include R. E. Landes, program supervisor and E. E. Morris, Vice-President. Arde' personnel who contributed to the investigation include A. Cozewith and D. Gleich.

The information contained in this report is also released as Boeing Document D180-15296-1.

TABLE OF CONTENTS

TABLE OF CONTENTS (Continued)

LIST OF FIGURES

LIST OF FIGURES (Continued)

LIST OF FIGURES (Continued)

LIST OF FIGURES (Continued)

LIST OF FIGURES (Continued)

LIST OF FIGURES (Continued)

LIST OF FIGURES (Continued)

LIST OF FIGURES (Continued)

LIST OF FIGURES (Continued)

LIST OF FIGURES (Continued)

LIST OF TABLES

LIST OF TABLES (Continued)

LIST OF TABLES (Continued)

LIST OF TABLES (Continued)

SUMMARY

The experimental work described herein was undertaken to establish a fracture control method which would guarantee the service life of composite tanks with load sharing liners. These tanks are made up of metallic liners which are overwrapped with glass filaments with epoxy resin. The tanks are designed so that the liners carry a significant portion of the membrane loads.

A tank design which incorporated a circumferentially (hoop) glass filament reinforced (GFR) cylinder with closed ends was established for three liner materials: (1) Inconel X750 STA, (2) 2219-T62 aluminum, and (3) cryoformed 301 stainless steel. Based on these designs, uniaxial and biaxial (tank) specimens containing artificially induced surface flaws were fabricated and fracture tested at 295°K (72°F) and 78°K (-320°F). Uniaxial specimens for each liner material investigated were pulled to failure and cycled to failure. Biaxial specimens with Inconel X750 STA and 2219-T62 aluminum liners were burst and cyclic tested. The static fracture and cyclic life results obtained from the uniaxial and biaxial specimens were compared to determine the extent that the uniaxial results could be used to predict the overwrapped tank fracture behavior. The comparison resulted in the following observations:

(1) Uniaxial surface flawed static fracture results can be used to predict burst test failures for hoop GFR Inconel X750 STA tanks with surface flawed liners having thicknesses of about 0.10 cm (0.040 in).

(2) Uniaxial surface flawed static fracture results underestimate the burst strength of hoop GFR 2219-T62 aluminum tanks with surface flawed liners having thicknesses of about 0.23 cm (0.090 in). This difference ranges from about 10 to 35% in the thickness tested.

(3) The cyclic life of both hoop GFR Inconel and aluminum tanks containing surface flawed liners are overestimated by uniaxial surface flawed specimens. The difference can range up to six times in the thickness tested.

(4) A leak mode-of-failure was observed for all hoop GFR Inconel and aluminum tanks that were burst tested at room temperature (RT) or cycled at RT or 78°K (-320°F).

The differences observed should be resolved if an adequate fracture control method for composite tanks with load sharing liners is to be developed.

1.0 INTRODUCTION

This document presents the first attempt to establish a fracture control method which would guarantee the service life of composite tanks with load sharing liners. The type of tanks being considered have filament overwrapped metal liners which are pressurized on the first cycle until the liner yields a predetermined amount and then the pressure is released. The filament overwrap material (S-glass) remains elastic throughout this pressure or sizing cycle. Upon releasing the pressure, the liner goes into compression while the filament overwrap remains in tension. The stress range for the metal liner on subsequent operating cycles is from compression at zero tank pressure to tension (always less than the liner stress at the sizing pressure) at tank operating pressure. The liner as well as the filament overwrap operates elastically during an operating pressure cycle. The sizing operation and subsequent operating cycles are schematically illustrated in Figure 1.

In general, the service life of all-metal tanks can be guaranteed by an effective proof test based on the application of linear elastic fracture mechanics. Such is not the case for composite tanks with load sharing liners, where the sizing cycle takes place well above the yield strength of the material; beyond the range of linear elastic fracture mechanic concepts.

It is anticipated that as with a proof test of an all-metal tank, the sizing cycle of a composite tank with a load sharing liner screens out flaws larger than a specific size. In doing so, a certain amount of flaw growth potential would be available for cyclic operation. This approach to assessing the allowable service life of composite tanks with load sharing liners is schematically illustrated in Figure 2.

Since no theory or fracture data was available for surface flawed materials stressed well above the material yield strength, a empirical approach was taken to develop static fracture data in this stress region. In addition, cyclic life data for liner materials which initially received a plastic sizing cycle were developed. Static fracture and cyclic life data were generated using semi-elliptical surface flawed uniaxial specimens of candidate liner materials; specifically Inconel X750 STA, 2219-T62 aluminum and cryostretched 301 stainless steel. Burst and service life tests were also conducted on non-overwrapped all-metal tanks and overwrapped tanks with surface flawed metal liners made of Inconel X750 STA and 2219-T62 aluminum. The static fracture and cyclic life results obtained from the uniaxial and biaxial (tank) specimens were compared to determine the extent that the uniaxial results could be used to predict the overwrapped tank fracture behavior.

2.0 TECHNICAL APPROACH

At the beginning of this contract a parametric design study was conducted to aid designers in selecting weight optimum composite tanks with load sharing liners for a specific design condition. From this study, a hoop glass filament reinforced (GFR) cylinder design for three liner materials was established which was representative of thicknesses and pressures covered in the design study. Uniaxial and biaxial (tank) fracture specimens were then fabricated and tested in accordance with the hoop GFR cylinder designs. The design study, hoop GFR cylinder designs and fracture testing program are discussed in the following paragraphs.

2.1 Parametric Design Study

The design study was conducted by Structural Composites Industries (SCI) and was published as a design guide handbook (Reference 1). GFR spheres, oblate spheroids and closed end cylinders constructed of Inconel X750 STA, 2219-T62 aluminum and cryoformed 301 stainless steel were considered in the parametric study. The design criteria for the GFR tanks is presented in Reference 1 and includes geometric parameters, material properties, and fabrication, sizing, operating and burst criteria. Operating temperatures ranged from $295^{\circ}K$ ($72^{\circ}F$) to $20^{\circ}K$ ($-423^{\circ}F$) and operating pressures ranged from 6.9 MN/m^2 (1000 psi) to 27.6 MN/m^2 (4000 psi) for these pressure vessels. The filament winding patterns considered were (1) axisymmetric, multiple angle for spheres, (2) longitudinal-in-plane for oblate spheroids, (3) and both circumferential only and longitudinal-in-plane complemented by circumferential along the cylindrical section for closed end cylinders. The closed end cylinders with only a circumferential filament winding pattern over the cylindrical section are commonly referred to as hoop GFR cylinders in this report.

The parametric design study was conducted using a computer program previously developed by SCI for the analysis of filament-wound, metal-lined pressure vessels (Reference 2). The program treats the filament shell by means of a netting analysis, which assumes that the stresses are constant along the filament path and that the resin makes a negligible structural contribution. The filament shell and the constant-thickness metal liner are combined by equating strains in the longitudinal and hoop directions and by adjusting the radii of curvature to match the combined material strengths at the design pressure. The filaments are assumed to have a linear stress/strain relationship until failure occurs whereas the metal liner stress/strain relationship is assumed to be bilinear. This bilinear representation is an engineering approximation to the elastic and plastic portions of the metallic stress/strain curve. The linearization was done in accordance with the schematic presented in Figure 3. Using the design guide one can define the GFR tank details, such as thicknesses, weight, sizing and burst pressures, given a pressure vessel shape, size, liner material and operating pressure requirements.

It should be noted that the GFR Inconel and aluminum tanks are sized at room temperature (RT), while the GFR cryoformed 301 tank is sized at 78°K (-320°F) in liquid nitrogen. Prior to sizing a 301 tank at 78°K (-320°F), the unreinforced tank is prestressed (σ_{ps}) at 78°K (-320°F) to about 932 MN/m^2 (135 ksi). This straining due to prestressing plus the straining due to sizing the GFR vessel, strengthens the cryoformed 301 to the desired level.

2.2 Hoop GFR Cylinder Design

For purposes of conducting the experimental fracture program presented in this document, a hoop GFR cylinder design was selected for each of the liner materials to be investigated. The design criteria for the hoop GFR cylinders is presented in Table 1. The cylinder dimensions used for design were 43 cm (17 in) long (cylindrical section) and 16.5 cm (6.5 in) in diameter with hemispherical end closures. The resulting liner design thicknesses were 0.10 cm (0.040 in) for the Inconel X750 STA, 0.23 cm (0.090 in) for the 2219-T62 aluminum and 0.071 cm (0.028 in) for the cryoformed 301 stainless steel.

The material properties used for the pressure vessel design are presented in Table 2. The mechanical properties were based on material properties obtained from the actual heats of materials used in fabricating the hoop GFR cylinders and uniaxial specimens. The cryoformed 301 stainless steel material properties are based on data obtained after a cryogenic prestress to about 932 MN/m^2 (135 ksi) in liquid nitrogen.

Computer derived membrane stresses in the cylindrical section of the pressure vessel are tabulated in Table 3 for the GFR Inconel tank, Table 4 for the GFR aluminum tank and Table 5 for the GFR 301 tank. The burst pressure for all hoop GFR tank designs are critical in the longitudinal direction in the liner, regardless of temperature. It was assumed that if a GFR pressure vessel was to be operated at a temperature other than that at which it was sized, the pressure vessel would receive a proof test at the operating temperature. The liner stress at the proof pressure was assumed to be equal to the offset yield point (see Figure 1) at the operating temperature. Figures 4, 5 and 6 present the hoop stress/strain relationships of the cylinders for both the ambient and cryogenic operating conditions. Computer output was also used to construct the pressure/hoop strain curves presented in Figures 7, 8 and 9 for the three different GFR pressure vessels. Pressure/hoop strain curves are used to compare the measured pressure/strain characteristics of the vessels with the predicted values.

The liner hoop stresses at the sizing and proof pressure (if applicable) are summarized below for the three different GFR pressure vessels analyzed:

GFR Pressure Vessel	SIZING			PROOFING		
	Temp. ^{o}K (^{o}F)	Pressure, p MN/m^2 (psi)	σ_s, Sizing Hoop Stress MN/m^2 (ksi)	Temp. ^{o}K (^{o}F)	Pressure, p MN/m^2 (psi)	σ_p, Proof Hoop Stress MN/m^2 (ksi)
Inconel X750 STA	295 (72)	19.6 (2840)	850 (123.3)	78 (-320)	20.9 (3030)	960 (139.1)
2219-T62 Aluminum	295 (72)	16.8 (2430)	332 (48.2)	78 (-320)	17.4 (2520)	381 (55.2)
Cryoformed 301 Stainless Steel	78 (-320)	23.9 (3460)	1442 (209.2)	295 (72)	21.8 (3160)	1235 (179.0)

The stress levels presented above are valid for other hoop GFR pressure vessels having the same diameter-to-thickness ratio.

2.3 Uniaxial Tests

Uniaxial specimens containing semi-elliptical surface flaws as depicted in Figure 10 were static fracture and fatigue tested at operating conditions equivalent to the hoop GFR cylinders presented in Paragraph 2.2. It was the object of these uniaxial tests to:

(1) Establish the stress-flaw size failure loci (Figure 2) and mode-of-failure [1] for various flaw sizes; especially above the yield strength of the material. The data would be used to determine the initial flaw size that would be screened by the sizing pressure and proof pressure (if applicable).

(2) Establish the cyclic life at various operating stresses for flaw sizes that are screened by the sizing cycle and proof test.

Uniaxial surface flawed specimens were made of base metal and weld metal of Inconel X750 STA, 2219-T62 aluminum and cryostretched 301 stainless steel and tested at $295^{\circ}K$ ($72^{\circ}F$) and $78^{\circ}K$ ($-320^{\circ}F$). All specimens tested were subjected to thermal and stress environments which closely simulated the processes the actual tank liners would experience. The primary exception to this rule was the cyclic stress condition where the uniaxial specimens were cycled from zero-to-maximum tension while the GFR liner experiences a compression-to-maximum tension cyclic profile during a zero-to-full tank pressure cycle.

Two thicknesses of uniaxial specimens were tested for each material; one equivalent to the hoop GFR cylinder design thickness presented in Paragraph 2.2 and one significantly thicker. The most emphasis during testing was placed on the thickness that was equivalent to the hoop GFR cylinder design. A summary of the thicknesses tested is presented below:

[1] Mode-of-failure can either be parting of the specimen (prior to leakage, and termed a fail mode) or the surface flaw can propagate through-the-thickness causing tank leakage (termed a leak mode).

Base Metal and Weld Metal Material	Thickness, cm (inch)	
	t_1	t_2
Inconel X750 STA	0.10 (0.040)	0.33 (0.13)
2219-T62 Aluminum	0.23 (0.090)	0.46 (0.18)
Cryostretched 301 Stainless Steel	0.071 (0.028)	0.26 (0.10)

The static fracture test matrices are schematically illustrated in Figures 11 and 12. For the Inconel and aluminum materials, the 295°K (72°F) static fracture specimens were pulled directly to failure whereas the 78°K (-320°F) static fracture specimens were pulled to failure after being stressed to the sizing value [1] at 295°K (72°F). The procedure was just reversed for the cryostretched 301; the 78°K (-320°F) static fracture specimens were pulled directly to failure (after experiencing an initial cryogenic prestress), whereas the 295°K (72°F) static fracture specimens were pulled to failure after being stressed to the sizing value at 78°K (-320°F). Static fracture data was generated for flaw depth-to-length (a/2c) ratios of about 0.10, 0.20 and 0.40, with most of the data obtained at an a/2c = 0.20. The selection of initial flaw sizes for the static fracture specimens tested at the sizing temperature were such that the failure loci was determined for flaw depths ranging up to the thickness of material being investigated, although the most emphasis was placed on obtaining fracture data in the plastic stress region. For static fracture specimens tested at a temperature other than the sizing temperature, the selection of initial flaw sizes was such that failure did not occur during the sizing operation.

The cyclic life test matrix is schematically illustrated in Figure 13. All cyclic specimens had flaws with an a/2c of about 0.20. For the Inconel and aluminum materials, a 295°K (72°F) sizing cycle [1] was put on the specimens prior to cycling to leakage at 295°K (72°F). In addition, the specimens to be cyclic tested at

[1] See Table in Paragraph 2.2, Page 7.

78°K (-320°F) were subjected to a proof test [1] after sizing. The cryostretched 301 specimens received a sizing cycle [1] at 78°K (-320°F) prior to cyclic testing and additionally, the specimens to be cycled at 295°K (72°F) received a 295°K (72°F) proof test [1]. Cyclic flaw growth tests were conducted generally at three different operating stress levels. These stress levels ranged from 60 to 100% of the sizing stress or proof stress (if applicable). The number of cycles at which the flaw grew through-the-thickness was recorded. The cyclic data results were presented as shown in Figure 14, so that for a given pressure vessel design and required cyclic life, the maximum permissible operating stress could be determined.

Table 6 summarizes the uniaxial tests conducted in this investigation along with the pertinent test parameters.

2.4 Biaxial Tests

Overwrapped and non-overwrapped tanks containing surface flaws in the cylindrical section of the metal shells were burst and fatigue tested at 295°K (72°F) and 78°K (-320°F). It was the object of these tests to establish failure loci and cyclic life data to be compared with the results of the uniaxial tests described in Paragraph 2.3. The biaxial specimen metal shells were made of Inconel X750 STA and 2219-T62 aluminum. The overwrapped tanks were fabricated per the respective design presented in Paragraph 2.2. GFR tank liners were used as the all-metal tanks. The purpose in testing all-metal tanks was to separate, in part, overwrapping effects from cylindrical biaxial stress effects.

The burst test matrix is schematically illustrated in Figure 15. The tanks tested at 295°K (72°F) were pressurized directly to failure or leakage, whereas the tanks tested at 78°K (-320°F) were sized at 295°K (72°F) prior to pressurizing to failure or leakage at 78°K (-320°F). The GFR tanks were sized per the table in Paragraph 2.2, Page 7. The all-metal tanks were burst tested only at 295°K (72°F). A single surface flaw with an a/2c of about 0.20 was present in each metal shell; one-half of the tank tests had flaws located in the weld metal. Flaws in the metal shells were

[1] See Table in Paragraph 2.2, Page 7

oriented in one of two directions; with the plane of the flaw parallel to the longitudinal axis of the shell or at $\pi/4$ rad. (45°) to the same reference axis. The pressure at tank leakage or burst was recorded.

The cyclic life test matrix is schematically illustrated in Figure 16. The GFR tanks cyclic tested at RT received a sizing cycle [1] at RT while the tanks cyclic tested in liquid nitrogen received a sizing cycle [1] at RT plus a cryogenic proof test [1]. The all-metal tanks were tested only at RT and received a simulated RT sizing cycle so that the hoop stress was equivalent to the GFR liner hoop stress. Each cyclic tank test had two surface flaws; one in the base metal and one in the weld metal. These flaws had an a/2c of about 0.20. The number of cycles at which the flaw grew through-the-thickness was recorded.

Table 7 summarizes the biaxial tests conducted in this investigation along with the pertinent test parameters.

[1] See Table in Paragraph 2.2, Page 7

3.0 MATERIALS AND PROCEDURES

3.1 Materials

The three liner materials investigated in this experimental program were Inconel X750 STA, 2219-T62 aluminum and cryostretched 301 stainless steel. S-glass with epoxy resin was used as the overwrap material for the composite tanks.

The Inconel X750 was purchased per AMS 5542, Revision G, in the annealed condition in sheet thicknesses of 0.10 cm (0.040 in) and 0.33 cm (0.130 in). The 0.10 cm (0.040 in) thick material (heat number HT 76C7X5) was used to fabricate uniaxial specimens as well as tank liners, whereas the 0.33 cm (0.130 in) thick material (heat number HT 0647X) was used only for uniaxial specimens.

The 2219 aluminum was obtained in the T87 temper in two thicknesses; 0.32 cm (0.125 in) for uniaxial specimens and tank liners and 1.27 cm (0.50 in) for other uniaxial specimens. Both thicknesses of material were fully annealed per BAC 5602 [1] prior to specimen fabrication. The 0.32 cm (0.125 in) thick material was obtained from a previously completed NASA contract, NAS 3-10290, and was purchased per BMS 7-105C. The 1.27 cm (0.50 in) thick material was purchased per MIL-A-8920A.

The 301 stainless steel (heat number 76235) was purchased from Arde', Inc. This heat of regular 301 material (unaged) was the same as used to fabricate some closed end cylinders which are presently in the NASA/Lewis inventory. Two thicknesses, 0.071 cm (0.028 in) and 0.26 cm (0.10 in), of annealed, unaged material were used to fabricate uniaxial specimens.

S-901 20 end glass roving pre-impregnated with NASA epoxy/polyurethane resin #2 was used as the overwrap material for the composite tanks. The S-glass was purchased per MIL-R-60346A.

[1] Heated in air at 687°K (775°F) for 2 hours minimum, furnace cooled at maximum rate of 28°K/hr (50°F/hr) to 534°K (500°F) or less, air cooled.

3.2 Uniaxial Specimen Fabrication

3.2.1 Inconel X750 STA Specimens

Inconel X750 STA base metal and weld metal uniaxial specimens were fabricated per the sketches presented in Figures 17, 18 and 19. The weld metal specimens were GTA welded per BAC 5980 Class "A" by laying a bead-on-plate with full penetration using Inconel 69 filler wire. No weld repairs were permitted. The weld bead was then leveled with the base metal. This was done because a slight sink-in of the weld bead had occurred during welding. The weld bead was subsequently ground flat with the base metal. The base metal and weld metal specimens were heat treated [1] and aged [2] per BAC 5616. The specimens were mechanically cleaned by air blasting with glass beads. The weld metal specimens were penetrant inspected per BAC 5423 and radiographically inspected per BAC 5915.

To introduce surface flaws, a starter notch with a terminating radius of less than 0.008 cm (0.003 in) was electric discharge machined (EDM) into the specimen. The EDM starter notch was then extended using low stress/high cycle fatigue; periodic examinations were conducted, using a microscope, to determine when a fatigue crack had been initiated around the entire periphery of the EDM notch. Between 1,600 to 70,000 cycles at stresses ranging from 207 MN/m^2 (30 ksi) to 483 MN/m^2 (70 ksi) were required to extend the precracks in the Inconel specimens, depending upon the EDM starter notch sharpness and depth relative to the specimen thickness. The precracking operation was done in air at RT at a frequency of 30 Hz (1800 cpm). The specimens were then subjected to a simulated resin cure cycle at 340°K (150°F) for 3 hours followed by 420°K (300°F) for 5 hours.

3.2.2 2219-T62 Aluminum Specimens

The 2219-T62 aluminum base metal and weld metal uniaxial specimens were fabricated per the sketches presented in Figures 20, 21 and 22. The welded specimens shown in

[1] Annealed in a vacuum at 1325°K (1925°F) for 30 minutes followed by a rapid quench by flooding the furnace with nitrogen gas.

[2] Heated in air at 978°K (1300°F) for 20 hours and air cooled.

Figure 22 were initially machined down in the test section to about 0.63 cm (0.25 in) prior to welding while the welded specimens shown in Figure 21 were welded in the stock sheet thickness of 0.32 cm (0.125 in). All weld metal specimens were GTA welded per BAC 5935, Class "A", by laying a bead-on-plate with full penetration using 2319 aluminum weld wire. No repair welds were permitted. The base metal and weld metal specimens were machined down in the test section to 0.23 cm (0.090 in) and 0.46 cm (0.18 in) for the two different thicknesses of specimens required. The base metal and weld metal specimens were then solution treated [1] and aged [2] per BAC 5602. The weld metal specimens were penetrant inspected per BAC 5423 and radiographically inspected per BAC 5915. Surface cracks were introduced into the aluminum specimens as previously outlined for the Inconel specimens, except that precracking stresses were less. Between 5,000 to 50,000 cycles at stresses ranging from 83 MN/m^2 (12 ksi) to 138 MN/m^2 (20 ksi) were required to extend the precracks. The specimens were then subjected to a simulated resin cure cycle as described in Paragraph 3.2.1.

3.2.3 Cryostretched 301 Stainless Steel Specimens

The cryostretched 301 stainless steel base metal and weld metal uniaxial specimens were fabricated per the sketches presented in Figures 23, 24 and 25. The weld metal specimens were GTA welded per Arde' welding specification AES 501C by laying a bead-on-plate with full penetration using 308L filler wire. No weld repairs were permitted. After welding, the weld beads were ground flush with the base metal. The base metal and weld metal specimens were then cleaned per Arde' specification AES 253D, annealed per AES 251A [3], pickled per AES 250D and passivated per AES 254C. The weld metal specimens were penetrant inspected per AES 451B and radiographically inspected per AES 450. Surface cracks were introduced into the 301 specimens as previously outlined for the Inconel specimens. The precracking was done after annealing and prior to cryogenically prestressing the specimen when testing

[1] Heated in air at 808°K (995°F) for 4 hours and then immediately quenched in water.

[2] Aged in air at RT for 96 hours and then aged in air at 463°K (375°F) for 36 hours.

[3] Heated in air at 1340°K (1950°F) for 15 minutes and then immediately quenched in water.

was first initiated. It was observed (Figure 82) that the fracture stress was reduced for these specimens as the precracking stress increased. The smaller the crack size, the higher the stress required to precrack it. Between 1,000 and 65,000 cycles at stresses ranging from 207 MN/m^2 (30 ksi) to 345 MN/m^2 (50 ksi) were required. This reduction in fracture stress with an increase in precrack stress was probably caused by cold working (at RT) the material at the crack tip during precracking. This in turn caused the material in the vicinity of the crack front to be very brittle and thereby inducing premature failure. The problem was eventually solved by re-annealing the specimens per AES 351A after precracking. This essentially would return the material at the crack front to a dead-soft condition. Further discussion of the results obtained are presented in Paragraph 4.3.2. After re-annealing, the 301 specimens were subjected to a prestress cycle of 932 MN/m^2 (135 ksi) at 78°K (-320°F). The specimens then received a simulated resin cure cycle as described in Paragraph 3.2.1 for the Inconel specimens.

3.3 Biaxial Specimen Fabrication

3.3.1 Inconel X750 STA Tanks

Cylindrical metal shells with hemispherical heads were fabricated per SCI assembly specification 9141-10. A sketch of the shell is shown in Figure 26. The cylindrical portion of the shell was roll formed, seam welded, and weld bead leveled in the same manner as the uniaxial Inconel X750 specimens (Paragraph 3.2.1). No repair of the weld was permitted in the longitudinal seam of the cylindrical shell. The material used for the cylindrical portion was 0.10 cm (0.040 in) thick and was made from the same heat of material (HT 76C7X5) as the uniaxial specimens. Boilerplate hemispherical heads of annealed Inconel X750 were welded to the cylindrical portion and the assembly was heat treated, aged and inspected per the specifications outlined for the uniaxial Inconel specimens (Paragraph 3.2.1).

Surface cracks were introduced into the outside of the cylindrical portion of the metal shells by machining a starter notch as was done with the uniaxial specimens, and then the shells were internally pressurized at 1 Hz (60 cpm) with hydraulic fluid to precrack the flaws. Shells to be burst tested contained only one flaw whereas those to be cyclic tested contained two flaws; one in the base metal and one in the weld metal. The two flaws were located circumferentially, π rad, (180°) apart, and axially about 10 cm (4 in) apart as illustrated in Figure 27. The tank with two flaws presented a potential precracking problem in that the fatigue cracks of both starter notches would not initiate at the same time, nor propagate at the same rate. This problem was due to inherent differences in the starter notch sharpnesses, flaw depths, local stress levels and base metal and weld metal properties. Thus, one flaw would reach its final dimensions while the other flaw would only be partially fatigue cracked. To obtain sharp crack fronts on both flaws and have the desired flaw size, the following technique was used. First, the tank was cyclic pressurized at a low stress level just as was done for a liner containing a single flaw. Both flaws were observed using a 10x microscope until one flaw reached its desired dimensions. Cycling was then terminated and a rigid restraining ring (see Figure 28) was positioned over the flaw that had been precracked and around the shell circumference to substantially reduce the local radial displacement, and consequently the shell stresses upon further low stress pressure cycling.

In order to provide a close fit between the restraint ring and the cylinder (required if cylinder displacements were to be significantly reduced), Teflon tape was used to fill the small gaps that existed. To verify that the hoop stresses were reduced under the restraining ring, strain gages were installed on the first shell containing two flaws. The measured hoop stress was reduced to about 30% of that in the non-restrained cylindrical portion.

The surface flaws in the cylindrical portion were oriented in one of two directions; with the plane of the flaw parallel to the longitudinal axis of the shell or at $\pi/4$ rad. (45°) to the same reference axis. These flaw orientations are referred to as 0 rad. (0°) and $\pi/4$ rad. (45°) flaws, respectively.

From 6,000 to 42,000 cycles were required for precracking the Inconel shells, using pressures that ranged from 3.5 MN/m^2 (500 psi) to 5.2 MN/m^2 (750 psi). These pressures corresponded to hoop stresses of about 276 MN/m^2 (40 ksi) and 414 MN/m^2 (60 ksi), respectively.

The majority of the surface flawed Inconel shell assemblies were hoop overwrapped with S-glass and epoxy resin per SCI fabrication procedure 1269298 and burst and cyclic tested. The remaining surface flawed shells were burst and cyclic tested as all-metal tanks with no overwrapping.

Overwrapped and non-overwrapped tanks were fitted with surface flaw breakthrough detection devices. The uniaxial static fracture and cyclic life data had demonstrated that flaw growth through-the-thickness of the specimen was a common occurrence with the materials investigated. Because of this, a device was necessary to detect the instant of flaw breakthrough in the overwrapped tanks, as well as in the non-overwrapped tanks. The breakthrough device had to work at liquid nitrogen temperatures and at ambient conditions. Observing the internal pressure for a pressure loss associated with flaw breakthrough was not feasible because of the very small amounts of liquid leaked at the instant of breakthrough. The system that was used successfully throughout the tank testing phase of the program is illustrated in Figure 29. A cylindrical hole was EDM into the surface flaw starter notch (prior to precracking) and a small tube (fabricated from a hypodermic needle) was inserted into this hole. For non-overwrapped tanks, the tubes were epoxied in place with Epon 901 and then the tank was subjected to a simulated resin cure cycle (to simulate thermally what an overwrapped tank would experience) at 340°K (150°F) for 3 hours followed by 420°K (300°F) for 5 hours. This simulated resin cure cycle was conducted in air. For overwrapped tanks, the tubes were epoxied in place with NASA resin #2 and cured at 345°K (160°F) for 8 hours followed by 420°K (300°F) for 15 minutes. During subsequent overwrapping the S-glass tape was split to straddle the tube. The composite tank was then cured at 348°K (165°F) for 4 hours, 360°K (190°F) for 2 hours, followed by 420°K (300°F) for 4 hours.

3.3.2 2219-T62 Aluminum Tanks

Cylindrical metal shells with hemispherical heads were fabricated per SCI assembly specification 9141-11. A sketch of the shell is shown in Figure 30. The cylindrical portion of the shell was roll formed and seam welded in the same manner as the uniaxial 2219 aluminum specimens (Paragraph 3.2.2). No repair of the weld was permitted in the longitudinal seam of the cylindrical shell. The material used for the cylindrical portion was 0.32 cm (0.125 in) thick and was made from the same heat of material as the uniaxial specimens.

Leveling of the longitudinal weld bead was performed in the as-welded condition. This leveling procedure which was not used on the uniaxial specimens did cause some premature failures of the tank specimens. The plastic straining resulting from this seam leveling resulted in abnormal grain growth in the vicinity of the weld fusion line during subsequent solution treatment and aging. If 2219 aluminum in the 0 temper is plastically strained a critical amount, from 2 to 7%, this situation will result. Coincidental with the abnormal grain growth is the formation of heavy grain boundary networks of the intermetallic compound, $CuAl_2$, resulting in a very brittle structure. Fortunately, surface flaws were introduced into the weld metal centerline (℄) where the microstructure was of normal proportions.

Boilerplate hemispherical heads of 2219-0 aluminum were welded to the cylindrical portion and the assembly was solution heat treated, aged and inspected per the specifications outlined for the uniaxial aluminum specimens (Paragraph 3.2.2). Another welding problem resulted in the premature failure of a few aluminum tanks. These failures resulted from an inadequate argon purge in the shell when attempting to weld the head-to-cylinder joint which, in turn, caused cracks.

Surface flaws were introduced in the aluminum shells in the same manner as the Inconel shells (Paragraph 3.3.1). From 1,300 to 30,000 cycles were required for precracking the aluminum shells, using pressures that ranged from 2.7 MN/m^2 (390 psi) to 3.9 MN/m^2 (560 psi). These pressures correspond to hoop stresses of about 97 MN/m^2 (14 ksi) and 138 MN/m^2 (20 ksi), respectively.

The majority of the surface flawed aluminum shell assemblies were hoop overwrapped with S-glass and epoxy resin per SCI specification procedure 1269301 and tested while other shells were tested as all-metal tanks. The same resin cure cycle and flaw breakthrough detection device as outlined in Paragraph 3.3.1 for the Inconel tanks were used for the aluminum tanks.

3.4 Uniaxial Specimen Test Procedures

Uniaxial specimens were tested to determine the mechanical properties, static fracture and cyclic life characteristics. The static fracture and cyclic life specimens were all surface flawed. All specimens containing flaws were instrumented with pressure cups as depicted in Figure 31. Low pressure, 3.45 kN/m^2 (5 psi), gaseous helium was supplied to the pressure cup opposite the surface flaw during specimen test. The non-pressurized pressure cup transducer output was observed as a function of uniaxial specimen load on an x-y plotter during the test to determine if and at what load the surface flaw broke through-the-thickness. This device was used at RT and in liquid nitrogen at 78°K (-320°F).

3.4.1 Inconel X750 STA Tests

Base metal and weld metal mechanical properties were determined by testing the specimen configurations shown in Figure 17. For welded specimens the weld nugget was instrumented with back-to-back strain gages in addition to a 5.1 cm (2.0 in) gage length extensometer, whereas the base metal specimens used only the extensometer. The mechanical property tests were conducted using a strain rate of 0.005 minutes^{-1} until the material yield strength was exceeded; the strain rate was then increased to 0.10 minutes^{-1} until failure.

Static fracture base metal and weld metal specimens (Figures 18 and 19) were tested at a loading rate such that failure resulted in about one minute after initial load application. Specimens tested in air at RT were loaded directly to failure, whereas specimens tested in liquid nitrogen at 78°K (-320°F) were first loaded (to simulate sizing a hoop overwrapped tank) to a stress of 850 MN/m^2 (123.3 ksi) at RT and unloaded. This necessitated that the specimens tested in liquid nitrogen have flaw depths less than that which would cause RT failure at 850 MN/m^2 (123.3 ksi).

Cyclic life base metal and weld metal specimens (Figures 18 and 19) tested at RT were sized to a stress of 850 MN/m^2 (123.3 ksi) at RT and then sinusoidally cycled at 0.8 Hz (50 cpm) until the flaw grew through-the-thickness. The maximum cyclic stress level was equal to or less than the sizing stress. Cyclic life specimens tested in liquid nitrogen were sized to a stress of 850 MN/m^2 (123.3 ksi) at RT, proofed to a stress of 960 MN/m^2 (139.1 ksi) at 78°K (-320°F) and then sinusoidally cycled at 78°K (-320°F) until the flaw grew through-the-thickness. The test was terminated at this point. The maximum cyclic stress level was equal to or less than the proof stress. All cyclic testing of uniaxial Inconel specimens was done at a $\sigma_{min}/\sigma_{max}$ ratio (R) of zero.

The majority of the cyclic life specimens tested were instrumented to measure the flaw opening displacement on the surface as the flaw grew due to cyclic loading. The change in flaw opening displacement can be related to the change in flaw size and instantaneous flaw growth rates can be calculated per the analysis outlined in Paragraph 3.6.3. The displacement measurement device is depicted in Figure 32.

3.4.2 2219-T62 Aluminum Tests

Mechanical properties were determined by testing the specimen configuration as shown in Figure 20 while the specimen configurations shown in Figure 21 and 22 were used to determine the static fracture and cyclic life characteristics. All of these specimens were tested using the same procedures as outlined for the uniaxial Inconel specimens in Paragraph 3.4.1, with the exception of sizing and proof stress levels. A RT sizing stress level of 332 MN/m^2 (48.2 ksi) and 78°K (-320°F) proof stress level of 381 MN/m^2 (55.2 ksi) were used.

3.4.3 Cryostretched 301 Stainless Steel Tests

Generally, uniaxial 301 specimens tested in this program received a cryogenic pre-stress to 932 MN/m^2 (135 ksi) prior to the testing discussed. As pointed out in Paragraph 3.2.3, the surface flaws were introduced into the uniaxial 301 specimens to be used for fracture testing prior to the cryogenic prestress cycle. Mechanical properties were determined by testing the specimen configuration shown in Figure 23 and by instrumenting fracture mechanics specimens (Figures 24 and 25) outside of the flaw area. Figure 23 mechanical property specimens were instrumented with a 5.1 cm (2.0 in) gage length extensometer. Figure 24 and 25 fracture specimens were instrumented with extensometers having 1.3 cm (0.5 in) and 2.5 cm (1.0 in) gage lengths, respectively. The mechanical property tests conducted using Figure 23 specimens, used a strain rate of 0.005 minutes^{-1} until the material yielded, then the strain rate was increased to 0.10 minutes^{-1} until failure.

Static fracture base metal and weld metal specimens (Figures 24 and 25) were tested so that failure resulted in about one minute after initial load application. Specimens tested in liquid nitrogen at 78°K (-320°F) were loaded directly to failure. Specimens failed in RT air were first loaded to 1442 MN/m^2 (209.2 ksi) in liquid nitrogen (to simulate sizing a hoop overwrapped tank) and then unloaded.

Cyclic life base metal and weld metal specimens (Figures 24 and 25) tested in liquid nitrogen were sized to a stress of 1442 MN/m^2 (209.2 ksi) in liquid nitrogen and then sinusoidally cycled at 0.8 Hz (50 cpm) until the flaw grew through-the-thickness. The maximum cyclic stress level was equal to or less than the sizing stress. Cyclic life specimens tested in RT air were sized to a stress of 1442 MN/m^2 (209.2 ksi) in liquid nitrogen, proofed to a stress of 1237 MN/m^2 (179 ksi) at RT and then sinusoidally cycled at RT until the flaw grew through-the-thickness. The test was terminated at this point. The maximum cyclic stress level was equal to or less than the proof stress. All cyclic testing of uniaxial 301 specimens was done at an R ratio of zero.

3.5 Biaxial Specimen Test Procedures

Burst and cyclic life tests were conducted with overwrapped and non-overwrapped tanks at RT and 78°K (-320°F). The test setup for the RT testing is shown in Figure 33, while the setup for the liquid nitrogen testing is shown in Figure 34. Test setup schematics are presented in Figures 35 and 36, respectively. The leak detection tubes that were installed in the surface flaws during tank fabrication (see Figure 37) were connected to a very sensitive pressure transducer to record the instant of flaw breakthrough if it occurred during the test. A closed circuit camera was also used as a backup to detect flaw breakthrough at RT. The pressurant (hydraulic fluid) would permeate the overwrap material when the liner flaw grew through-the-thickness. In addition to the breakthrough detection devices, a hoop deflection measurement device was installed for each test as shown in Figure 38. A nichrome wire was wrapped around the tank and each end was connected to one clip gage arm. The clip gage arm was strain gaged and calibrated to record displacements. As the tank was pressurized, the growth in tank circumference was recorded as the cantilevered arms of the clip gage were displaced. This device was calibrated directly in the test environment; either RT air or liquid nitrogen. Tank pressure versus hoop displacement was recorded for each test. On some selected overwrapped tank burst tests, the longitudinal displacement in the cylindrical portion of tank was recorded using a wire/clip gage device connected between two thumbtack type hard points which were positioned firmly in place by the overwrap material.

Tanks to be RT burst tested were pressurized directly to failure. The pressurization rate was such to cause failure in from one to two minutes after pressure initiation. Tanks to be burst tested at $78^{\circ}K$ ($-320^{\circ}F$) were first sized at RT. The overwrapped Inconel and aluminum liners were sized at 19.6 MN/m^2 (2840 psi) and 16.8 MN/m^2 (2430 psi), respectively. The non-overwrapped all-metal tanks burst tested at $78^{\circ}K$ ($-320^{\circ}F$) were first exposed to a simulated sizing pressure cycle of about 10.6 MN/m^2 (1530 psi) and 9.5 MN/m^2 (1375 psi) for Inconel and aluminum, respectively. These pressures cause hoop stresses that correspond to that experienced in the overwrapped tank liner during sizing.

Tanks to be RT cycled were first sized to the pressures outlined earlier in Paragraph 3.5. RT cyclic operating pressures of 17.8 MN/m^2 (2580 psi) and 14.1 MN/m^2 (2040 psi) were used for the overwrapped Inconel and aluminum liners, respectively. Based on the hoop overwrapped tank designs presented in Paragraph 2.2, these cyclic pressures stressed the liners to a maximum of 85 and 75% of the liner sizing hoop stress (σ_s) for the Inconel and aluminum, respectively. The corresponding operating pressures for the non-overwrapped all-metal tanks were 9.0 MN/m^2 (1300 psi) and 7.1 MN/m^2 (1030 psi) for the Inconel and aluminum, respectively. The cyclic tests conducted at RT utilized an approximate sinusoidal load profile at 0.5 Hz (30 cpm). Tanks to be cycled at $78^{\circ}K$ ($-320^{\circ}F$) received a cryogenic proof test after the sizing cycle and prior to cyclic testing. The overwrapped Inconel and aluminum liners were proof tested cryogenically at 20.9 MN/m^2 (3030 psi) and 17.4 MN/m^2 (2520 psi), respectively. Cryogenic cyclic operating pressures of 18.8 MN/m^2 (2730 psi) and

15.5 MN/m^2 (2240 psi) were used for the overwrapped Inconel and aluminum liners, respectively. These pressures represent 85% of proof hoop stress. The cyclic tests conducted at 78°K (-320°F) utilized a ramp loading profile with an exponential decay at about a 0.07 Hz (4 cpm) frequency. No non-overwrapped all-metal tanks were cyclic tested in liquid nitrogen.

A pressure ratio, p_{min}/p_{max}, of essentially zero was employed during most of the tank cyclic testing conducted. A minimum pressure of 68.9 kN/m^2 (100 psi) was maintained during liquid nitrogen testing, to prevent excessive boil-off of the nitrogen. The cyclic tests were terminated when the flaw grew through-the-thickness. The flaw area was then removed from the tank and pulled apart to reveal the flaw face.

3.6 Analysis Procedures

3.6.1 Stress Analysis of Uniaxial Specimens

As noted in the introduction, elastic/plastic deformation of the metal liners takes place during the sizing operation. This deformation in the hoop direction for the hoop GFR Inconel and aluminum tanks (presented in Paragraph 2.2) at the sizing pressure is about 1%. To duplicate the liner hoop stress levels at sizing in uniaxial specimens would also require about 1% strain. The hoop GFR vessels designed in Paragraph 2.2 do not permit liner yielding in the longitudinal direction at the sizing pressure and, therefore, the amount of hoop strain is considerably greater than if the stress field was 1 to 1 and plastic in both directions. If the design vessel had a true 1 to 1 stress field in the metal liner (such as a completely overwrapped GFR cylinder), the uniaxial strain would have to approach 2% if stresses at sizing were to be matched between the liner and the uniaxial specimen. Because of the relatively small amounts of strain involved at the sizing pressure with hoop GFR Inconel and aluminum tanks, engineering stresses (as opposed to true stresses) based on the original material thickness are adequate to describe their behavior up to at least the sizing stress level.

The same situation does not exist for the hoop GFR cryoformed 301 tanks. As pointed out in Paragraph 2.2, a 301 liner must receive a cryo-prestress to about 932 MN/m^2 (135 ksi) prior to being overwrapped and sized to bring the material up to the desired strength level. For the heat of 301 material investigated in this report, about 13% uniaxial strain would be required to achieve the prestress level of 932 MN/m^2 (135 ksi) as shown in Appendix A, Figure A-19. An unreinforced cylindrical liner would not require as much hoop straining to reach the same prestress level, but because of the significant deformation involved during prestressing, considerable thinning of the material results. Significant errors would be introduced into the tank analysis if engineering stresses were used which were based on the original liner thickness prior to prestressing. To handle this situation the liner properties, such as stress/strain characteristics and thickness, after prestressing were used in the Reference 2 computer program to design the hoop GFR 301 tanks. The same approach was utilized in analyzing the cryostretched 301 uniaxial specimens. The prestress cycle was based on the original specimen cross sectional area, but all load cycles applied thereafter were based on the cross sectional area at the end of the prestress cycle. The amount of strain at the cryogenic sizing stress level approaches 2% for both the hoop GFR tank and uniaxial specimens made of cryoformed 301 material, and engineering stresses can be used satisfactorily within this strain level. It should be mentioned that this relatively high amount of strain (2%) in a hoop GFR pressure vessel is a result of sizing at a temperature of 78°K (-320°F) where the filaments can be strained to a higher value than at RT.

3.6.2 Stress Analysis of Biaxial Specimens

The non-overwrapped metal shells were analyzed using the following equations:

$$\sigma_{L\theta} = \frac{p\bar{D}_L}{2t_L} \qquad (1)$$

$$\sigma_{L\phi} = \frac{p\bar{D}_L}{4t_L} \qquad (2)$$

where

$\sigma_{L\theta}$ = liner hoop stress

$\sigma_{L\phi}$ = liner longitudinal stress

p = internal pressure

$\bar{D}_L$ = mean liner diameter

t_L = liner thickness

The overwrapped tanks were analyzed for hoop stresses using the pressure/hoop displacement curves obtained during each loading cycle of the tank, while the longitudinal stresses were defined by Equation (2) above. The filaments were assumed to be elastic and full effective throughout the test of the tank. The initial "as fabricated" stress situation in the overwrapped tank was defined assuming no loss in filament tension during the cure cycle. The prestress in the filaments can be calcuated from the expression:

$$\sigma_{f\,ps} = \frac{TS_f}{A_f} \tag{3}$$

where

$\sigma_{f\,ps}$ = filament prestress

TS_f = tension per strand = 125 N (28 lbs)

A_f = cross-sectional area of strand = 2710 μcm^2 (420×10^{-6} in^2)

Thus, the filament prestress is

$$\sigma_{fps} = \frac{125}{2710} = 460 \text{ MN/m}^2 \text{ (66.7 ksi)}$$

The hoop prestress in the metal shell is defined by the relationship

$$\sigma_{L\,ps} = -\left(\frac{t_f}{t_L}\right) \sigma_{f\,ps} \tag{4}$$

where

$\sigma_{L\,ps}$ = liner prestress

t_f = filament thickness

Thus, the hoop prestress in the metal is only a function of the metal shell thickness for a specific wrap pattern. For the GFR Inconel tank

$$t_f = 4.73 \text{ TURNS/cm/layer} \times 4 \text{ layers} \times 2710\ \mu\,\text{cm}^2/\text{turn}$$

$$= 0.049 \text{ cm } (0.01932 \text{ inch})$$

The filament stress (σ_f) at any pressure can be calculated from the expression:

$$\sigma_f = \sigma_{f\,ps} + E_f \left(\frac{\Delta_L}{L}\right) \tag{5}$$

where

E_f = filament modulus of elasticity at ambient temperature = 85.5 GN/m^2 (12.4×10^6 psi)

Δ_L = measured circumferential deflection

L = circumference of GFR cylinder = $\pi(D_L + 2\,t_c)$

D_L = outside diameter of metal liner

t_c = composite thickness $\begin{cases} 0.076 \text{ cm } (0.030 \text{ in}) \text{ for GFR Inconel} \\ 0.074 \text{ cm } (0.029 \text{ in}) \text{ for GFR aluminum} \end{cases}$

A hoop load balance on the metal cylinder at any pressure defines the liner hoop stress ($\sigma_{L\theta}$) as

$$\sigma_{L\theta} = 2\sigma_{L\phi} - \sigma_f \left(\frac{t_f}{t_L}\right) \tag{6}$$

The longitudinal liner stress ($\sigma_{L\phi}$) is defined by Equation (2).

After the tank has been sized and filled with liquid nitrogen, a new zero pressure stress state exists in the filaments and metal shell. The assumption of strain compatibility between the two shells during the fill process results in the relationships:

$$\Delta\varepsilon = \left(\frac{\sigma_{fps}}{E_f}\right)^{78^\circ K} - \left(\frac{\sigma_{fps}}{E_f}\right)^{295^\circ K} + \alpha_f \, \Delta T \tag{7}$$

$$= \left(\frac{\sigma_{Lps}}{E_L}\right)^{78^\circ K} - \left(\frac{\sigma_{Lps}}{E_L}\right)^{295^\circ K} + \alpha_L \, \Delta T \tag{8}$$

where

$\Delta\varepsilon$ = change in hoop strain due to temperature change

α_f = coefficient of thermal expansion of filaments (see Table 2)

α_L = coefficient of thermal expansion of liner (see Table 2)

Δ_T = change of temperature from ambient to liquid nitrogen

A load balance of the filament and liner shells at zero pressure and liquid nitrogen temperature yields the relationship:

$$\sigma_{fps}^{78^\circ K} = -\left(\frac{t_L}{t_f}\right) \sigma_{Lps}^{78^\circ K} \tag{9}$$

Combining the strain compatibility relationships of Equations (7) and (8) with Equation (9) and solving for the hoop stress in the metal shell at zero pressure and liquid nitrogen temperature results in the expression:

$$\sigma_{Lps}^{78^\circ K} = \frac{\left(\frac{\sigma_{Lps}}{E_L}\right)^{295^\circ K} - \left(\frac{\sigma_{fps}}{E_f}\right)^{295^\circ K} - \left(\alpha_L - \alpha_f\right) \Delta T}{\frac{1}{E_L{}^{78^\circ K}} + \left[\left(\frac{t_L}{t_f}\right) \Big/ E_f{}^{78^\circ K}\right]} \tag{10}$$

Equations (2), (5) and (6) can now be used to calculate stresses in the filaments and metal shells at liquid nitrogen temperature for any set of pressure/hoop displacement data using the liquid nitrogen, zero pressure filament prestress resulting from Equations (9) and (10).

As mentioned at the beginning of Paragraph 3.6.2, the filaments were assumed to be elastic and fully effective throughout the test of the tank. This is consistant with results obtained in past test evaluations of glass filament-wound pressure vessels. However, if at very high filament stresses breakage of some filaments does occur, the overwrap stiffness would be effectively reduced; this condition would give rise to greater hoop displacements and if the elastic/fully effective overwrap analysis presented in the preceding paragraphs was applied, erroneous liner stresses would be calculated. The liner would be taking a greater load and consequently the overwrap a lesser load than calculated. Detailed analysis of some hoop GFR Inconel tank tests presented in Paragraph 5.1.2 suggests that this situation, or some other unexplained behavior, may have occurred.

Typical of some of these tests was Specimen BS-31, where the stress in the liner was calculated to increase until exceeding the sizing pressure and then decreased with increasing pressure to tank failure. Physically, this is not possible if the liner does not neck locally. The tank was inspected after the test and no signs of necking were observed in the liner. The filament stresses were calculated to be 2460 MN/m^2 (356 ksi) at tank failure. This phenomena is discussed in more detail in Paragraph 5.1.2.

The RT GFR aluminum tank tests did not strain the filaments to as high a level as did the GFR Inconel tanks and the problem discussed above was not encountered. The problem even in the GFR Inconel tanks, is somewhat academic since the analysis problems occur at pressures above the sizing pressure, which an actual tank to be put into service would never experience. The effect of the problem would be to slightly overestimate the vessel burst pressure capability.

3.6.3 Fatigue Crack Growth Rate Analysis

As mentioned in the introduction, fracture mechanics methods have not been developed to describe the failure or service life of flawed structures stressed to levels considerably above the yield strength of the material. Rather than attempt to develop new analysis tools or presentation methods, some techniques already employed in elastic fracture mechanic analysis of surface flaws were modified or applied directly to tests described in this report. This was particularly true in the area of fatigue crack growth rates. Investigators have shown that the fatigue crack growth rates due to tension loading can be adequately expressed as a function of stress intensity according to the expression

$$\frac{da}{dN} = C \Delta K^n \tag{11}$$

where

da/dN = fatigue crack depth growth rate

C = constant

ΔK = $K_{max} - K_{min}$

K = stress intensity

n = constant

In general, the fatigue crack depth growth rates in this program were determined for the specimens that were cycled using the following expression

$$\frac{da}{dN} = \frac{a_j - a_i}{N} \tag{12}$$

where

a_i = initial flaw depth

a_j = final flaw depth

N = number of cycles

The fatigue crack depth growth rates were then plotted on log-log paper as a function of stress intensity based on the maximum tension stress level. The results showed that equation (11) adequately expressed the relationship between da/dN and K. Stress intensity calculations for the surface flaws were based on Irwin's equation (Reference 3):

$$K_I = 1.1\sigma \left(\frac{\pi a}{Q}\right)^{1/2} \tag{13}$$

where

K_I = plane strain stress intensity

σ = applied stress field

a = semi-elliptical crack depth (see Figure 10)

Q = flaw shape parameter (see Figure 39)
$= [\Phi]^2 - 0.212\ (\sigma/\sigma_{ys})^2$

Φ = complete integral of the second kind

σ_{ys} = material yield strength

Equation (12) was not used to determine the fatigue crack growth rates for some Inconel and aluminum specimens. These specimens were instrumented with a crack opening displacement (COD) device as shown in Figure 32 so that the crack depth as a function of applied cycles could be determined and consequently instantaneous crack growth rates. The COD for a surface flaw can be approximated by the expression (details are presented in Reference 4).

$$\delta = J\,\frac{\sigma a}{\sqrt{Q}} \tag{14}$$

where

J = constant

[1] since the sizing cycle takes place above the material yield strength, the sizing stress or proof stress (if applicable) was used as the material yield strength.

The value of J can be determined at test initiation and termination from knowledge of the stress level, initial and final flaw sizes, and the corresponding COD as indicated below:

$$J_i = \frac{\delta_i}{\sigma} \left(\frac{\sqrt{Q}}{a}\right)_i$$

$$J_j = \frac{\delta_j}{\sigma} \left(\frac{\sqrt{Q}}{a}\right)_j \qquad (15)$$

where the subscripts i and i_j refer to initial and final conditions, respectively.

The value of J tends to increase with increasing crack size, rather than remain constant. Crack growth rate calculations in this report were based on an assumed linear variation in J between the known initial and final values.

In order to relate the flaw parameter $(a/\sqrt{Q})$ to δ for values of $(a/\sqrt{Q})$ between the initial and final values an assumption must be made as to the manner in which the flaw shape changes from test initiation to termination. It was assumed that

$$\frac{a - a_i}{a_j - a_i} = \frac{2c - (2c)_i}{(2c)_j - (2_c)_i} \qquad (16)$$

i.e., both flaw depth and width growth simultaneously reach the same percentage of their respective total growth from initial to final values. The flaw shape parameter (Q) can now be determined as a function of flaw depth and, in turn, can be related to crack depth using Equation (14). The number of cycles (N) corresponding to each selected flaw depth value can be determined from the test record and, consequently, the change in N for each increment of flaw depth is known. A series of da/dN data points are then derived from a single specimen where COD measurements are made and analyzed per the above discussion, as opposed to a single data point for a non-instrumented test specimen.

Consequently, fewer instrumented specimens are required to adequately define the fatigue crack growth rates as a function of stress intensity.

4.0 PRESENTATION AND ANALYSIS OF UNIAXIAL RESULTS

The data from all uniaxial tests conducted in this program are presented in this section. The results include mechanical property, static fracture and cyclic life tests of the three candidate liner materials; Inconel X750 STA, 2219-T62 aluminum and cryostretched 301 stainless steel.

4.1 Inconel X750 STA Uniaxial Results

4.1.1 Mechanical Properties

The results of the mechanical property tests are presented in Table 8 for the Inconel base metal and weld metal investigated. A summary of the yield strengths (0.2% offset) and ultimate strengths is presented below for the 0.10 cm (0.040 in) thick material:

Material	Temperature $^{\circ}K$ ($^{\circ}F$)	Strength, MN/m^2 (ksi)	
		Yield	Ultimate
Base Metal	295 (72)	762.6 (110.6)	1228.7 (178.2)
	78 (-320)	846.0 (122.7)	1520.3 (220.5)
Weld Metal	295 (72)	768.1 (111.4)	1172.2 (170.0)
	78 (-320)	850.8 (123.4)	1437.6 (208.5)

These values were obtained parallel to the rolling direction.

4.1.2 Static Fracture Tests

The results of the Inconel static fracture tests are presented in Figures 40 through 45 while the test parameters for each specimen are detailed in Tables 9 through 14. Figures 40 and 41 presents the static fracture failure loci as a function of initial flaw depth (a_i) for the 0.10 cm (0.040 in) thick base metal material at 295°K (72°F) and $78^{\circ}K$ ($-320^{\circ}F$), respectively. The data shows that as the flaw shape (a/2c) is decreased, the failure stress also decreases for a constant flaw depth. In other words, the most critical flaw shape for static fracture is a long shallow flaw with an aspect ratio approaching zero. This was true for tests conducted at $295^{\circ}K$ ($72^{\circ}F$) and $78^{\circ}K$ ($-320^{\circ}F$). A considerable amount of data was developed at an a/2c of about 0.2 and as the RT results indicate, the failure locus changes mode-of-failure at a stress slightly above the sizing stress (σ_s). The mode-of-failure changes from a leak to a fail mode at this point. Leakage of these specimens appeared to occur instantaneously with the resulting back side flaw equal in length to the surface flaw length. It also appears that at a constant stress level as the flaw shape ratio decreases the mode-of-failure changes from one of leakage to failure. The mode-of-failure at $78^{\circ}K$ ($-320^{\circ}F$) was failure regardless of stress level or flaw shape. It is interesting to point out that the cryogenic proof test to the offset yield strength did not screen a smaller flaw than was screened by the RT sizing cycle for the 0.10 cm (0.040 in) base metal material.

A test was conducted to verify that the specimen width was adequate for the static fracture testing. In general, the static fracture testing of the 0.10 cm (0.040 in) Inconel material was done with specimens having a specimen width (W)-to-flaw length (2c) ratio (W/2c) of ≥ 15. Three specimens were fabricated, two of standard width and one two times as wide. These specimens were heat treated as a special run and then flaws of essentially the same size were introduced into one of the standard width and the extra wide specimen. The results of these two RT tests are presented in Figure 40. Both specimens failed at a slightly higher stress (less than 10%) than the data generated with the standard width specimens heat treated as a regular run. The remaining standard width specimen (B-15) was then instrumented with an extensometer and pulled to failure to verify that all three specimens heat treated as a special run had the same mechanical properties as the other test specimens. The result of this test is presented in Table 8. Specimen B-15 showed a yield strength of about 10% higher and an ultimate strength of about 6% higher than the corresponding tensile specimens heat treated previously. This difference in mechanical properties could easily account for the slightly higher failing stresses for the two fracture specimens. It is believed that the specimen width was sufficiently wide during the static fracture tests.

A summary of the critical flaw depths at the sizing stress and proof stress for 0.10 cm (0.040 in) thick Inconel base metal is presented at the end of Paragraph 4.1.2.

Figures 42 and 43 present the static fracture failure loci for the 0.10 cm (0.040 in) thick weld metal material at 295°K (72°F) and 78°K (-320°F), respectively. The critical location for the surface flaw in the weld material was first established. Surface flaws were introduced into three areas; (1) the weld centerline (℄), (2) between the weld ℄ and the fusion line, and (3) heat affected zone (HAZ). As the RT results in Figure 42 indicate, the three tests yielded essentially the same failure stress with the one with the flaw located in the weld centerline slightly lower than the other two. Based on this result, all Inconel weld metal specimens were tested with flaws located in the weld centerline.

Essentially, the same results were observed for the Inconel weld metal as the base metal with regard to failure stresses, effects of flaw shape and mode-of-failure. The one disturbing thing was the inconsistency of the data generated. The curves presented in Figures 42 and 43 were completely defined when two RT and two 78°K (-320°F) failures were obtained (while attempting to size or proof specimens for cyclic life determination) which were lower than the expected failure locus at both test temperatures. Two of the specimens had been accidently subjected to a total of 60 hours at 420°K (300°F) during the simulated resin cure cycle while the other two specimens were originally visually rejected due to weld quality. The rejected weld specimens were intended to be cyclic tested at the end of the program to fill in data gaps. It is believed that the additional time at 420°K (300°F) did not alter the fracture characteristics of the weld metal, but that a more brittle weld existed in some specimens for presently unknown reasons. The welds were all made and inspected per BAC specifications as outlined in Paragraph 3.2.1. It was concluded that minor processing differences (e.g., welding) of Inconel X750 STA can have significant affects on the fracture characteristics. In light of this, the static fracture data presented herein should be used with caution.

The data presented in Figure 43 indicates that the cryogenic proof test does screen a smaller flaw than does the RT sizing cycle. A summary of the critical flaw depths at the sizing stress and proof stress for 0.10 cm (0.040 in) thick Inconel weld metal is presented at the end of Paragraph 4.1.2.

Figures 44 and 45 present the static fracture failure loci for the 0.33 cm (0.13 in) thick base metal and weld metal material at 295°K (72°F) and 78°K (-320°F). The results obtained are similar to the 0.10 cm (0.040 in) thick material results. A smaller flaw is screened by the cryogenic proof test than screened by the RT sizing cycle for both base metal and weld metal materials.

A summary of the critical flaw depths at the sizing stress and proof stress for the Inconel materials tested is presented below for $a/2c \approx 0.20$:

Inconel X750 STA Material		Critical Flaw Depth $(a_i)_{cr}$ cm (Inch) 295°K (72°F)	Critical Flaw Depth $(a_i)_{cr}$ cm (Inch) 78°K (-320°F)
0.10 cm (0.040 Inch)	Base Metal	0.079 (0.031)	0.081 (0.032)
	Weld Metal	0.081 (0.032)	0.069 (0.027)
0.33 cm (0.13 Inch)	Base Metal	0.198 (0.078)	0.165 (0.065)
	Weld Metal	0.198 (0.078)	0.188 (0.074)

NOTE: $\sigma_s = 850$ MN/m^2 (123.3 ksi)

$\sigma_p = 960$ MN/m^2 (139.1 ksi)

4.1.3 Growth-on-Loading

The fact that some specimens failed by leakage when loaded at RT suggests that stable flaw growth does take place during loading. The amount of flaw growth that occurred during the sizing cycle and proof test was easily determined on the cyclic life specimens because the growth that occurred was bracketed by fatigue bands representing the precrack and cyclic life portions of the test.

The growth-on-loading results are presented in Figures 46 through 49 for Inconel base metal and weld metal of both thicknesses tested. In general, the results for the 0.10 cm (0.040 in) thick material (Figures 46 and 47) showed essentially no differences in the amount of growth-on-loading which occurred between base metal and weld metal material and that the growth took place during the sizing cycle. The growth-on-loading results obtained for the 0.33 cm (0.13 in) thick material (Figures 48 and 49) did show significant differences between specimens that were sized only and those receiving a sizing cycle plus a cryogenic proof test. The specimens receiving a proof test exhibited more flaw growth than the ones that were sized only.

4.1.4 Cyclic Life Tests

Figures 50 through 57 present the cyclic life data generated for both thicknesses of Inconel tested as a function of both initial flaw depth (a_i) and operating stress (σ_o) while the test parameters for each specimen are detailed in Tables 15 through 22. The test results were plotted as a a_i versus cycles-to-leakage (N) for constant operating stress levels. This data was used to plot σ_o versus N for constant a_i.

In general, the cyclic life curves as a function of flaw depth are linear on a semi-log plot. A few specimens were cyclic tested with the flaw impregnated with resin to be used in overwrapping the liners. Figures 50 and 52 show that within the normal data scatter experienced these specimens did not experience cyclic lives any different than the non-resin impregnated flaw specimens.

All of the cyclic life data was analyzed to determine the flaw depth growth rate as a function of stress intensity based on the maximum tension stress level. The results of this analysis are presented in Figures 58 through 61. These rates were all based on the cyclic growth observed on the fracture face not including the amount of growth due to the sizing cycle or proof test. In general, at a given stress intensity the flaw depth growth rates are faster at RT than at 78°K (-320°F). As the figures show, the growth rate data can adequately be represented by the equation; $da/dN = C K^n$. Values of C and n for each material, thickness and temperature tested were evaluated and are presented in Table 23. The stress intensity range over which the values of C and n apply are also presented in Table 23.

4.2 2219-T62 Aluminum Uniaxial Results

4.2.1 Mechanical Properties

The results of the mechanical property tests are presented in Table 24 for the aluminum base metal and weld metal investigated. A summary of the yield strength (0.2% offset) and ultimate strengths is presented below for the 0.23 cm (0.090 in) thick material:

Material	Temperature °K (°F)	Strength, MN/m^2 (ksi)	
		Yield	Ultimate
Base Metal	295 (72)	293.7 (42.6)	431.6 (62.6)
	78 (-320)	360.6 (52.3)	524.7 (76.1)
Weld Metal	295 (72)	285.5 (41.4)	415.1 (60.2)
	78 (-320)	355.1 (51.5)	508.2 (73.7)

These values were obtained parallel to the rolling direction.

4.2.2 Static Fracture Tests

The results of the aluminum static fracture tests are presented in Figures 62 through 65 while the test parameters for each specimen are detailed in Tables 25 through 29. Figure 62 presents the static fracture failure loci as a function of initial flaw depth (a_i) for the 0.23 cm (0.090 in) thick base metal material at 295°K (72°F) and 78°K (-320°F). As with the Inconel data generated, the aluminum data also shows that the most critical flaw shape for static fracture is a long shallow flaw with an aspect ratio approaching zero. The mode-of-failure for all these static fracture tests was failure. Contrary to most of the Inconel results obtained, the cryogenic proof test for the aluminum specimens tested did not screen a smaller flaw than did the RT sizing cycle.

As with the Inconel material, a test was conducted to verify that the specimen width was adequate for the static fracture testing. In general, the static fracture testing of the 0.23 cm (0.090 in) aluminum material was done with specimens having a W/2c ratio of ≥ 7. One of the 0.46 cm (0.18 in) thick aluminum specimens (Figure 62) was machined down to a thickness of 0.23 cm (0.090 in) while retaining the 12.7 cm (5.0 in) width. This specimen was flawed so that the W/2c ratio was approximately 17 and then failed. The result is shown in Figure 62. The result of the extra wide specimen was within the scatter band of the other data generated and therefore the specimen width selected for the majority of the testing is believed adequate.

A summary of the critical flaw depths at the sizing stress and proof stress for 0.23 cm (0.090 in) thick aluminum base metal is presented at the end of Paragraph 4.2.2.

Figure 63 presents the static fracture failure loci for the 0.23 cm (0.090 in) thick weld metal material at 295°K (72°F) and 78°K (-320°F). The critical location for the surface flaw in the weld material was first established. Surface flaws were introduced into three areas; (1) the weld ℄, (2) weld fusion line, and (3) weld HAZ. As the RT results in Figure 63 indicate, no significant differences were noted; with the specimen with the flaw located in the weld centerline yielding a slightly lower failure stress than the other two. Based on this result, all aluminum weld metal specimens were tested with flaws located in the weld centerline. Essentially the same results were observed for the aluminum weld metal as the base metal with regard to the effects of flaw shape and mode-of-failure. The data presented in Figure 63 indicates that the cryogenic proof test does not screen a smaller flaw than does the RT sizing cycle. A summary of the critical flaw depths at the sizing stress and proof stress for 0.23 cm (0.090 in) thick aluminum weld metal is presented at the end of Paragraph 4.2.2.

Figures 64 and 65 presents the static fracture failure loci for the 0.46 cm (0.18 in) thick base metal and weld metal material at 295°K (72°F) and 78°K (-320°F). The results obtained are similar to the 0.23 cm (0.090 in) thick material results with RT sizing cycle screening a smaller flaw than is screened by the cryogenic proof test.

A summary of the critical flaw depths at the sizing stress and proof stress for the aluminum materials is presented below for $a/2c \approx 0.20$:

2219-T62 Aluminum		Critical Flaw Depth $(a_i)_{cr}$ cm (Inch)	
		295°K (72°F)	78°K (-320°F)
0.23 cm (0.090 Inch)	Base Metal	0.122 (0.048)	> 0.122 (0.048)
	Weld Metal	0.091 (0.036)	> 0.091 (0.036)
0.46 cm (0.18 Inch)	Base Metal	0.224 (0.088)	> 0.224 (0.088)
	Weld Metal	0.147 (0.058)	> 0.147 (0.058)

NOTE: $\sigma_s = 332 \text{ MN/m}^2$ (48.2 ksi)

$\sigma_p = 381 \text{ MN/m}^2$ (55.2 ksi)

4.2.3 Growth-on-Loading

As with the Inconel cyclic life specimens, growth-on-loading during the sizing cycle and proof test was observed for the aluminum cyclic life specimens. The amount of flaw growth-on-loading that occurred was easily determined on the cyclic life specimens because the growth that occurred was bracketed by fatigue bands representing the precrack and cyclic life portions of the test. The growth-on-loading results are presented in Figures 66 through 69 for aluminum base metal and weld metal of both thicknesses tested. As might be expected from the fact that the RT sizing cycle screens a smaller flaw than the cryogenic proof test, the growth-on-loading took place during the sizing cycle. The specimens receiving a cryogenic proof test after a RT sizing cycle did not show any more growth than those specimens receiving only a RT sizing cycle. This was true regardless of thickness of material tested and whether or not the material was base metal or weld metal.

4.2.4 Cyclic Life Tests

Figures 70 through 77 present the cyclic life data generated for both thicknesses of aluminum tested as a function of both initial flaw depth (a_i) and operating stress (σ_o) while the test parameters for each specimen are detailed in Tables 30 through 37. As with the Inconel cyclic life results the aluminum test results were plotted as a_i versus cycles-to-leakage (N) for constant operating stress levels and then this data was used to plot σ_o versus N for constant a_i.

In general, the cyclic life curves as a function of flaw depth are linear on a semi-log plot. A few specimens were cyclic tested with the flaw impregnated with the resin to be used in overwrapping the liners. Figure 70 and 72 shows that within the normal data scatter experienced these specimens did not experience cyclic lives any different than the non-resin impregnated flaw specimens.

All of the cyclic life data was analyzed to determine the flaw depth growth rate as a function of stress intensity based on the maximum tension stress level. The results of this analysis are presented in Figures 78 through 81. These rates were all based on the cyclic growth observed on the fracture face not including the amount of growth due to the sizing cycle or proof test. In general, at a given stress intensity, the flaw depth growth rates are faster at RT than at 78°K (-320°F). As the figures show the growth rate data can adequately be represented by the equation; $da/dN = CK^n$. Values of C and n for each material, thickness and temperature tested were evaluated and are presented in Table 38. The stress intensity range over which the values of C and n apply are also presented in Table 38.

4.3 Cryostretched 301 Stainless Steel

4.3.1 Mechanical Properties

The results of the mechanical property tests are presented in Table 39 for the cryostretched 301 stainless steel base metal and weld metal. A summary of the yield strengths (0.2% offset) and ultimate strengths is presented below for the 0.071 cm (0.028 in) thick material.

Material	Temperature °K (°F)	Strength, MN/m^2 (ksi)	
		Yield	Ultimate
Base Metal	78 (-320°)	1349.4 (195.7)	1954.7 (283.5)
	295 (72)	1197.7 (173.7)	1448.0 (210.0)
Weld Metal	78 (-320)		1772.0 (257.0)
	295 (72)		1244.5 (180.5)

These values were obtained parallel to the rolling direction. The mechanical properties at 78°K (-320°F) were obtained with specimens that were subjected to a cryogenic prestress (σ_{ps}) cycle of 932 MN/m^2 (135 ksi) and then loaded to failure at 78°K (-320°F). The mechanical properties at 295°K (72°F) were obtained with specimens that received a cryogenic sizing cycle to 1442 MN/m^2 (209.2 ksi) after the cryogenic prestress cycle of 932 MN/m^2 (135 ksi) and then were pulled to failure at RT. All mechanical property strength values were arrived at based on the specimen cross sectional area at the end of the cryogenic prestress cycle. The results presented in the above table do show that the weld metal strengths are about 10 to 15% less than the base metal strengths. The weld bead on these tests were ground flush with the base metal and re-annealed afterwards.

4.3.2 Static Fracture Tests

The results of the 301 static fracture tests are presented in Figures 82 through 85 while the test parameters for each specimen are detailed in Tables 40 through 43.

Figure 82 presents the static fracture failure locus as a function of initial flaw depth (a_i) for the 0.071 cm (0.028 in) thick base metal at 78°K (-320°F). An interesting observation was made while conducting the testing. The initial static fracture tests were run with specimens that were precracked in RT air at ≤ 276 MN/m^2 (40 ksi) and then tested. To generate cyclic life data, specimens with flaw depths less than about 0.036 cm (0.014 in) were required to successfully pass the cryogenic sizing cycle to 1442 MN/m^2 (209.2 ksi). To fabricate flaws less than this size required an increase in the precracking stress. As indicated in Figure 82, the result of the higher precrack stress was to reduce the failure stress of the specimen. In some cyclic life specimens that received high precracking stresses, but successfully passed the sizing cycle, a considerable amount of flaw growth-on-loading was observed. It appears that the material work hardens at the crack tip during the precracking operation, which is a function of the precracking stress level. In order to eliminate the effect of work hardening the crack tip during precracking, the specimens were re-annealed after precracking. This procedure appeared to solve the problem. As indicated in Figure 82, a single failure locus adequately describes the failure behavior of specimens that were re-annealed after precracking or precracked below 242 MN/m^2 (35 ksi).

Because of the precrack stress problem encountered, not as much static fracture and cyclic life data was generated as originally planned. In particular, the effect of flaw shape on the static fracture failure loci was not assessed; only a flaw shape of ≈ 0.2 was investigated. The mode-of-failure for the valid 0.071 cm (0.028 in) thick 301 base metal tested was failure at both 78°K (-320°F) and 295°K (72°F). Only two specimens were tested at RT, and both of them failed at about the ultimate strength of the material as shown in Figure 82. As with the RT results, the static fracture data generated at 78°K (-320°F) appears to be independent of flaw depth when the depth is ≤ 0.039 cm (0.012 in). Failure in specimens with flaws less than this amount fail at the ultimate strength of the material.

A summary of the critical flaw depths at the sizing and proof stress for the 0.071 cm (0.028 in) thick 301 base metal is presented at the end of Paragraph 4.3.2.

Figure 83 presents the static fracture failure loci for the 0.071 cm (0.028 in) thick 301 weld metal at 78°K (-320°F) and 295°K (72°F). The critical location for the surface flaw in the weld material was first established. Surface flaws were introduced into three areas; (1) the weld centerline, (2) weld fusion line, and (3) weld HAZ. These three specimens were not re-annealed after precracking but were precracked at a relatively low stress of 276 MN/m^2 (40 ksi). As the results in Figure 83 indicate, the specimen with the flaw located in the weld fusion line leaked during the cryogenic prestress cycle. Based on this result, all 301 weld metal specimens were tested with flaws located in the weld fusion line.

With one important difference, similar results were observed for the 301 weld metal and the base metal. As Figure 83 indicates, there is a definite discontinuity in the failure locus. For flaw depths > 0.030 cm (0.012 in), failure (leak mode) of the weld metal material can be expected at stresses significantly below that for the same size flaw in the base metal. For flaw depths < 0.030 cm (0.012 in), failure (fail mode) of the weld metal material can be expected to approach the base metal failure stress levels for the same size flaw. The physical change in properties of 301 stainless steel during cryogenic stretch (from an austenitic to martensitic structure) could account for the discontinuity although the phenomena was not observed in the 0.071 cm (0.028 in) thick base metal or in either the 0.26 cm (0.10 in) thick 301 base metal and weld metal results.

The data presented in Figure 83 indicates that the cryogenic sizing cycle screens a flaw that is less than or equal to that screened by a RT proof test. A summary of the critical flaw depths at the sizing stess and proof stress for 0.071 cm (0.028 in) thick 301 weld metal is presented at the end of Paragraph 4.3.2.

Figures 84 and 85 presents the static fracture failure loci for the 0.26 cm (0.10 in) thick 301 base metal and weld metal at 78°K (-320°F) and 295°K (72°F). The results obtained are similar to the 0.071 cm (0.028 in) thick 301 base metal results.

A summary of the critical flaw depths at the sizing stress and proof stress for the 301 materials tested is presented below for $a/2c \approx 0.20$:

Cryostretched 301 Stainless Steel		Critical Flaw Depth $(a_i)_{cr}$ cm (Inch)	
		78°K (-320°F)	295°K (72°F)
0.071 cm (0.028 Inch)	Base Metal	0.036 (0.014)	$\geq$ 0.036 (0.014)
	Weld Metal	0.028 (0.011)	$\geq$ 0.028 (0.011)
0.26 cm (0.10 Inch)	Base Metal	0.043 (0.017)	$\geq$ 0.043 (0.017)
	Weld Metal	0.043 (0.017)	$\geq$ 0.043 (0.017)

NOTE: σ_s = 1442 MN/m^2 (209.2 ksi)

σ_p = 1235 MN/m^2 (179.0 ksi)

4.3.3 Growth-on-Loading

Flaw growth-on-loading was observed in 301 cyclic life specimens which were not re-annealed after precracking. In general, the specimens that were re-annealed after precracking did not exhibit any growth-on-loading with one exception. Specimen 2C-15, Table 48, was sized with an initial flaw depth which was at 95% of critical.

Considerable flaw growth occurred in this specimen and would have probably failed if the load had not been immediately dropped to zero.

4.3.4 Cyclic Life Tests

Figures 86 through 93 present the cyclic life data generated for both thicknesses of 301 tested as a function a_i and σ_o while test parameters for each specimen are detailed in Tables 44 through 51. The test results were plotted as a_i versus cycles-to-leakage (N) for constant operating stress levels. This data was used to plot σ_o versus N for constant a_i. In general, the cyclic life curves as a function of flaw depth are linear on a semi-log plot. Some cyclic life plots were estimated from the flaw growth rate data generated during testing.

One important observation was made while cyclic testing the 0.26 cm (0.10 in) thick 301 material. Four specimens failed by fatigue outside of the artificially induced flaw. Generally, these flaws were semi-circular in shape and initiated on the specimen surface. Some failures resulted from the initiation of multiple flaws while other failures were the result of a single flaw. These failures occurred in the test section base metal at about 70% of the artificially induced flaw life, (see Figures 91, 92 and 93). The specimen data points with arrows indicates that leakage at the artificially induced surface flaw would have occurred after more cycles were put on the specimen. While this difference is not great relative to normal data scatter, it is significant that the life based on natural defects is less than that based on artificially induced flaws. It is apparent from these tests that a natural defect is probably somewhat more severe (higher crack growth rate) than the artificially induced flaw and therefore the 301 fracture characteristics presented herein should be used with caution.

All of the cyclic life data was analyzed to determine the flaw depth growth rates as a function of stress intensity, based on the maximum tension stress level. The results of this analysis are presented in Figures 94 through 97. The flaw growth rate data points shown are based on average values obtained by knowing the initial flaw size, the final flaw size and the number of cycles. The growth rate is plotted at the average stress intensity value. This approach is satisfactory in defining a flaw growth rate curve if the test specimens are not cycled over a very large stress intensity range (approximately a factor of two). As the stress intensity range gets larger , the average rate yields values that are considerably slower than actually experienced. For the Inconel, aluminum, and the thin 301 cyclic tested, the stress intensity range was relatively small and consequently average flaw growth rates adequately described the behavior. The thick 301 material tested was cycled to a final stress intensity that was about four times the initial value. Considerable error would result if an average growth rate analysis approach was used. It should be pointed out that this phenomena is not specifically a 301 material related problem but an analysis problem and could have occurred with Inconel or aluminum specimens.

Since all cyclic flaw growth rate data generated in this program was adequately described by the equation; $da/dN = CK^n$, it was decided to generate cyclic life curves using various values of C and n for the thick 301 and to select the constants which best described the cyclic life results. Key specimens were selected which were not cycled over large stress intensity ranges; the actual growth rate curve must pass through those data points. With this as a baseline, values of C and n were selected which best described the cyclic life behavior. As Figures 96 and 97 show, the estimated flaw growth rate curve represents a faster rate than the average rate values would indicate. Values of C and n for each material, thickness and temperature tested were evaluated and are presented in Table 52. The stress intensity range over which the values of C and n apply are also presented in Table 52.

5.0 PRESENTATION AND ANALYSIS OF BIAXIAL RESULTS

The data from all biaxial tests conducted in this program are presented in this section. The results include pressure/strain, static burst and cyclic life results of hoop GFR tanks made of Inconel X750 STA and 2219-T62 aluminum.

5.1 Inconel X750 STA Biaxial Results

5.1.1 Pressure/Strain Correlation

Figure 98 presents the extremes of pressure/hoop strain recorded for the hoop GFR Inconel tanks during the sizing cycle at RT. For comparison purposes the design curve based on data generated as described in Paragraph 2.2 is presented. As Figure 98 clearly shows, the hoop strains recorded at the sizing pressure are equal to or greater than the design value. This difference could be due to variations in the liner material yield strength, or residual wrapped-in filament prestress, or both. The differences observed could be accounted for entirely by about a 7% variation in material yield strength. As pointed out in Paragraph 4.1.2, Inconel X750 STA yield strengths and ultimate strengths can vary at least 10 and 6%, respectively. The majority of the hoop GFR Inconel tanks tested agreed very favorably with the design pressure/strain curve presented in Figure 98. The measured elastic loading portion of the pressure/strain curves were slightly steeper (indicating a slightly stiffer structure) than the elastic loading portion of the design curve, whereas the plastic loading slopes agreed very favorably between the measured and design values. The unloading portion of the test curves paralleled the elastic loading portion with only a slight apparent liner inelastic behavior.

As pointed out in Paragraph 2.2, if a tank was to be operated cryogenically it received a cryogenic proof test to the cryogenic offset yield point after being sized at RT. This essentially meant that during the cryogenic proof test the tank would not yield. Figure 99 illustrates what actually occurred in the hoop GFR Inconel tanks that were cryogenically proof tested. As the figure shows, the tank did yield slightly at the proof pressure causing a further increase in the liner compression stress.

5.1.2 Burst Tests

The results of the hoop GFR Inconel and all-metal Inconel tank burst tests are presented in Figures 100 through 103 while the test parameters for each test are detailed in Tables 53 and 54. The uniaxial static fracture data presented in Paragraph 4.1.2 are shown on these figures for reference purposes.

Figures 100 and 102 present the burst test results for surface flaws located in the base metal and weld metal centerline, respectively; both at RT. Within the range of stresses and flaw depths investigated, very good agreement between uniaxial and biaxial data exists, regardless of the orientation of the flaw plane, or whether the tank was overwrapped or not. The mode-of-failure also agreed between the uniaxial and biaxial results. The majority of hoop GFR Inconel tanks exhibited a leak mode-of-failure as shown in Figure 104. The hoop GFR Inconel tanks that exhibited a fail mode-of-failure all failed longitudinally (see Figure 105); the direction in which no overwrap was present. As noted in both Figures 100 and 102, the liners of some overwrapped tank burst tests are believed to have been at higher than calculated stresses at failure or leakage. Generally, these are tests where the filaments are stressed above 2000 MN/m^2 (290 ksi). As mentioned in Paragraph 3.6.2, the stress analysis used in defining the liner stresses is based on the assumption that the overwrap is fully effective and elastic. If the overwrap does not have the stiffness assumed, or some other effect is occurring to cause an apparent reduction in stiffness, the result would be to underestimate the liner hoop load. To resolve the problem of the actual failure stresses in the liners of highly pressurized overwrapped Inconel tanks will require additional tests and is not a part of the present program.

The burst test results conducted at 78°K (-320°F) in liquid nitrogen are presented in Figures 101 and 103 for flaws located in the base metal and weld metal centerline, respectively. Generally, all of these tanks failed or leaked at very high calculated filament stresses; > 2000 MN/m^2 (290 ksi), and consequently, the liner stresses are believed higher than calculated. No conclusions can be drawn from these results until the stress analysis problem is resolved.

5.1.3 Cyclic Life Tests

Figures 106 through 109 present the cyclic life data generated for the all-metal and hoop GFR Inconel tanks tested at RT and 78°K (-320°F). The tanks were cycled at a pressure so that the metal shell was stressed to a maximum operating stress (σ_o) of approximately 0.87 σ_s. The test parameters for each test are detailed in Tables 55 and 56. The uniaxial cyclic life data presented in Paragraph 4.1.4 are shown on these figures for reference purposes.

In general, the non-overwrapped tank cyclic life results agreed favorably with uniaxial results while the overwrapped tank cyclic lives were less than expected. A close examination of the data reveals that as the R ratio ($\sigma_{min}/\sigma_{max}$) decreases from zero to negative values the cyclic life also decreases. This phenomenon is more readily observed in the flaw growth rate data comparison made in Figures 110 and 111 between the uniaxial and biaxial results. The growth rates for the biaxial specimens were plotted as a function of the average stress intensity value calculated using the maximum tension stress level. As these figures indicate, the non-overwrapped tank flaw growth rates fall within the uniaxial data scatter bands at RT and as the R ratio decreases the cyclic rate increased. The hoop GFR Inconel flaw growth rates were a maximum of about 6 times the average uniaxial growth rate. This maximum difference was for the data generated with the lowest (highest negative) R ratio and the difference between hoop GFR and uniaxial flaw growth rates decreased as R ratio increased. The cyclic results obtained at 78°K (-320°F) were even more affected by R ratio, as shown in Figures 110 and 111.

It should be pointed out that no growth-on-loading due to the sizing cycle or proof test was observed in the biaxial cyclic life tests, while as pointed out in Paragraph 4.1.3, growth-on-loading was present in the uniaxial cyclic life specimens at comparable flaw depths.

5.2 2219-T62 Aluminum Biaxial Results

5.2.1 Pressure/Strain Correlation

Figure 112 presents the extremes of pressure/hoop strain recorded for the hoop GFR aluminum tanks during the sizing cycle at RT. For comparison purposes the design curve based on data generated as described in Paragraph 2.2 is presented. As Figure 112 clearly shows, the hoop strains recorded at the sizing pressure are less than the design value. This difference can be accounted for by (1) variations in the liner yield strength, (2) differences in the liner thickness between the design and actual, and (3) apparent increase in liner elastic stiffness in a biaxial stress field. A difference of only 10% in the liner yield strength or 10% in liner thickness could account for the variations observed in actual hoop GFR pressure/strain curves. The liner thickness assumed for the GFR design was 0.23 cm (0.090 in), whereas a nominal thickness for the actual liners was about 0.25 cm (0.098 in). This represents a 9% increase in stiffness of the structure and probably explains the variation in measured and predicted values based on the liner design thickness. The additional thickness would not have permitted the actual structure to displace as much as the design analysis indicated.

As Figure 112 indicates, the elastic loading portion of the actual pressure/strain curves is steeper than the design curve. This apparent increase in stiffness was also observed in the all-metal tank tests. The all-metal elastic modulus was calculated to be about 82.7 GN/m^2 (12×10^6 psi) using the general equations for elastic strain. Using this value combined with the elastic modulus of the filaments (see Table 2), yielded essentially the same measured elastic loading pressure/strain curve presented in Figure 112. The uniaxial elastic modulus for the aluminum is only about 73.1 GN/m^2 (10.6×10^6 psi) as reported in Table 2. The differences appear to be due to biaxiality, but in any event, does not permit the actual structure to deflect as much as indicated by the design analysis. It was first thought that the apparent difference was due to the displacement measurement setup. The calibration of the system was checked thoroughly and found to be satisfactory. Recorded displacements were also compared to actual measurements made at test initiation and termination and found to agree exactly. In addition, the recorded displacements were compared to strain gage data on one tank and found to agree satisfactorily. The displacement recording system was not in error. All of the above discussed items could account for differences observed between actual pressure/strain curves and design values.

Contrary to the hoop GFR Inconel tank results, the hoop GFR aluminum tanks yielded significantly in compression during the unloading portion of the pressure/strain curve as depicted in Figure 112. The tank design was based on no compression yielding after sizing. The phenomena observed is commonly known as a Bauschinger effect; where a metal if yielded significantly in tension has a subsequently reduced compressive yield strength (or vice-versa). Figure 112 also illustrates that the tank stiffness is apparently less during the release of pressure than during pressurization. This decrease in stiffness is due to the metal liner and was observed in the aluminum uniaxial specimens as reported in Appendix A.

As pointed out in Paragraph 2.2, if a tank was to be operated cryogenically it received a cryogenic proof test to the cryogenic offset yield point after being sized at RT. This essentially meant that during the cryogenic proof test the tank would not yield. Figure 113 illustrates what actually occurred in the GFR aluminum tanks that were cryogenically proof tested. As the figure shows, the tank did yield slightly at the proof pressure causing a further increase in the liner compression stress.

5.2.2 Burst Tests

The results of the hoop GFR aluminum and all-metal tank burst tests are presented in Figures 114 through 117 while the test parameters for each test are detailed in Tables 57 and 58. The uniaxial static fracture data presented in Paragraph 4.2.2 are shown on these figures for reference purposes.

Figures 114 and 116 present the burst test results for surface flaws located in the base metal and weld metal centerline, respectively, both at RT. As the figures illustrate, in general, close agreement between the biaxial data exists, regardless of the orientation of the flaw plane or whether the tank was overwrapped or not. The biaxial results do not agree with the uniaxial static fracture results. The biaxial results are between 10 to 35% higher. The range of flaw depths investigated was from about half of the thickness to flaw depths approaching the liner thickness. A possible explanation is that the material at the tip of the surface flaw is stressed differently in a uniaxial and biaxial tank specimen. With the uniaxial specimen, the presence of the flaw offsets the neutral axis in the immediate vicinity of the flaw causing a bending moment and giving rise to an additional tension stress at the flaw tip. The flaw located in a cylindrical tank is also stressed in a similar manner except that the stiffness due to curvature, tank material and thickness effectively react the local bending moment across the flaw front and the result is essentially a pure tension field over the remaining ligament below the flaw. In the uniaxial specimen the material is essentially free to deflect laterally and, therefore, reacts the bending with the material beneath the flaw. These differences could account for the high apparent static fracture strength of biaxial specimens over uniaxial specimens. As pointed out in Paragraph 5.1.2, good agreement was obtained between uniaxial and biaxial Inconel fracture results. The effective shell stiffness (curvature, tank material and thickness) is significantly less for the Inconel than the aluminum metal liners.

As the data presented in Figures 114 and 116 show, the overwrapped aluminum tanks all experienced a leak mode-of-failure (see Figure 118) while the non-overwrapped tanks had a fail mode-of-failure as did the RT uniaxial results.

The burst test results conducted at 78°K (-320°F) in liquid nitrogen are presented in Figures 115 and 117 for flaws located in the base metal and weld metal centerline, respectively. As with the RT results, the cryogenic biaxial tests resulted in failures above the uniaxial curve. The mode-of-failure at this temperature was mixed; with some leak modes and some fail modes (see Figure 119). The uniaxial static results were all fail mode-of-failures.

5.2.3 Cyclic Life Tests

Figures 120 through 123 present the cyclic life data generated for the all-metal and hoop GFR aluminum tanks tested at RT and 78°K (-320°F). The all-metal tanks were cycled at an operating stress (σ_o) equal to 0.75 σ_s whereas the hoop GFR tanks were cycled at a σ_o equal to about 0.84 σ_s; both at RT. The hoop GFR tanks tested at 78°K (-320°F) were cycled at a σ_o equal to about 1.02 σ_s. The test parameter for each test are detailed in Tables 59 and 60. The uniaxial cyclic life data presented in Paragraph 4.2.4 is shown on these figures for reference purposes.

In general, the non-overwrapped tank cyclic life results agreed favorably with uniaxial results while the overwrapped tank cyclic lives were slightly less than expected. As with the Inconel, a close examination of the data reveals that as the R ratio decreased from positive to negative values the cyclic life also decreases. This phenomenon is more readily observed in the flaw growth rate data comparison made in Figures 124 and 125 between the uniaxial and biaxial results. The growth rates for the biaxial specimens were plotted as a function of the average stress intensity value calculated using the maximum tension stress level. As these figures indicate, the non-overwrapped tank flaw growth rates fall within the uniaxial data scatter bands at RT and as the R ratio decreases the cyclic rate increases. The hoop GFR aluminum flaw growth rates were a maximum of about 4 times the average uniaxial growth rate. This maximum difference was for the data generated with the lowest (highest negative) R ratio and the difference between hoop GFR and uniaxial flaw growth rates decreased as R ratio increased. One hoop GFR tank (AS-22) was cycled at an R ratio of 0.20. This test demonstrated the lowest flaw growth rate obseved at a comparable stress intensity. The cyclic results obtained at 78°K (-320°F) were also slightly affected by R ratio, as shown in Figures 124 and 125.

As with the Inconel tests, no growth-on-loading due to the sizing cycle or proof test was observed in the biaxial cyclic life tests, while as pointed out in Paragraph 4.2.3, growth-on-loading was present in the uniaxial aluminum cyclic life specimens at comparable flaw depths.

6.0 OBSERVATIONS AND CONCLUSIONS

The major observations made from this investigation are presented below:

(1) Uniaxial surface flawed static fracture results can be used to predict burst test failures for hoop GFR Inconel X750 STA tanks with surface flawed liners having thicknesses of about 0.10 cm (0.040 in).

(2) Uniaxial surface flawed static fracture results underestimate the burst strength of hoop GFR 2219-T62 aluminum tanks with surface flawed liners having thicknesses of about 0.23 cm (0.090 in). This difference ranges from about 10 to 35% in the thickness tested.

(3) The cyclic life of both hoop GFR Inconel and aluminum tanks containing surface flawed liners are overestimated by uniaxial surface flawed specimens. The difference can range up to six times in the thickness tested.

(4) A leak mode-of-failure [1] was observed for all hoop GFR Inconel and aluminum tanks that were burst tested at RT or cycled at RT or $78^{\circ}K$ ($-320^{\circ}F$).

In conclusion, differences were observed between the uniaxial and biaxial test results obtained in this fracture test program. The exact reasons for these differences are not known but possible causes are detailed in Paragraphs 5.1.3, 5.2.2 and 5.2.3. With respect to the static fracture differences that occurred, one possible resolution of the problem could be obtained by the testing of some flawed uniaxial specimens with lateral restrain plates in the vicinity of the flaw. This would effectively transmit the local bending moment through the restraint plates and eliminate the addition tension component at the flaw tip. With respect to the cyclic life differences, additional overwrapped tanks cycled at an R ratio of zero should be conducted along with compression/tension uniaxial specimens.

In addition to the above areas for further investigation, the stress analysis problem

[1] Disregarding a few tanks which failed because of inadequate welds.

encountered with highly pressurized hoop GFR Inconel tanks (described in Paragraph 5.1.2) should be resolved. Testing of glass filament rings (fabricated in the same way the hoop GFR tanks were) to determine the stress/hoop displacement characteristics could possibly resolve this problem.

APPENDIX A

UNIAXIAL STRESS/STRAIN CURVES

The uniaxial stress/strain curves obtained for the mechanical property specimens are presented in this appendix. The materials include base metal and weld metal Inconel X750 STA, 2219-T62 aluminum and cryostretched 301 stainless steel tested at 295°K (72°F) and 78°K (-320°F). Both engineering stress and strain, and true stress and strain are presented. The true stress and strain are defined by the expressions:

$$\sigma' = \sigma (1 + \varepsilon) \qquad \text{(A-1)}$$

$$\varepsilon' = \ln (1 + \varepsilon) \qquad \text{(A-2)}$$

where

σ' = true stress

σ = engineering stress

ε' = true strain

ε = engineering strain

Figures A-1 through A-10 present the stress/strain relationships for the Inconel material. These tests were conducted by pulling the specimen directly to failure at the test temperature. All specimens received a simulated resin cure cycle [1] prior to testing. Figure A-11 presents the result of plastically deforming a uniaxial specimen at RT to a stress level simulating a sizing cycle followed by a cryogenic pull to failure. As Figure A-11 indicates, there is essentially no difference in the cryogenic portion of the stress/strain curve between this specimen and one pulled directly to failure without the RT sizing cycle. The unloading portion of the RT sizing cycle generated the same stress/strain slope as the initial loading portion.

Figures A-12 through A-17 present the stress/strain relationships for the aluminum material. These tests were conducted by pulling the specimen directly to failure at

[1] 340°K (150°F) for 3 hours followed by 420°K (300°F) for 5 hours.

the test temperature. All specimens received a simulated resin cure cycle [1] prior to testing. Figure A-18 presents the result of plastically deforming a uniaxial specimen at RT to a stress level simulating a sizing cycle followed by a cryogenic pull to failure. As with the Inconel, Figure A-18 indicates there is essentially no difference in the cryogenic portion of the stress/strain curve between this specimen and one pulled directly to failure without the RT sizing cycle. The unloading portion of the RT sizing cycle generated a stress/strain slope that was about 20% less than the slopegenerated during loading.

Figures A-19 through A-36 present the stress/strain relationships for the cryostretched 301 material. The majority of the tests conducted at $78^{\circ}K$ ($-320^{\circ}F$) utilized specimens that were first prestressed at $78^{\circ}K$ ($-320^{\circ}F$) to about 932 MN/m^2 (135 ksi), subjected to a simulated resin cure cycle [1], and then pulled to failure at $78^{\circ}K$ ($-320^{\circ}F$). The tests run at RT were conducted with specimens that were first prestressed at $78^{\circ}K$ ($-320^{\circ}F$) to about 932 MN/m^2 (135 ksi), subjected to a simulated resin cure cycle [1], loaded at $78^{\circ}K$ ($-320^{\circ}F$) to a simulated sizing stress of 1442 MN/m^2 (209.2 ksi) and then pulled to failure at RT. The calculations of stress for the first cryogenic stretch (prestress cycle) were based on the original specimen cross-sectional area, while subsequent stress cycles utilized the cross-sectional area at the end of the prestress cycle. This was done so that engineering stresses would be representative of true stresses during the simulated sizing operation. Figure A-37 illustrates what effect the simulated resin cure cycle (after cryo-prestressing) has on the subsequent stress/strain relationship of 301 stainless steel. Comparing the result with a 301 specimen pulled directly to failure at $78^{\circ}K$ ($-320^{\circ}F$) shows that an apparent strengthening results with the prestressed and resin cured specimen.

[1] $340^{\circ}K$ ($150^{\circ}F$) for 3 hours followed by $420^{\circ}K$ ($300^{\circ}F$) for 5 hours.

APPENDIX B

SYMBOLS

A	=	cross sectional area
a	=	semi-elliptical crack depth
a/2c	=	flaw shape
BM	=	base metal
C	=	constant
COD	=	crack opening displacement
D	=	outside diameter
D	=	mean diameter
$\frac{da}{dN}$	=	fatigue crack depth growth rate
E	=	modulus of elasticity
EDM	=	electric discharge machined
GFR	=	glass filament reinforced
HAZ	=	heat affected zone
J	=	constant
K	=	stress intensity
L	=	circumference of GFR cylinder
N	=	number of cycles or cycles-to-leakage
n	=	constant
OW	=	overwrapped
P	=	internal tank pressure
Q	=	flaw shape parameter
R	=	$\sigma_{min}/\sigma_{max}$
RT	=	room temperature
T	=	temperature
TS	=	tension per strand
t	=	thickness
W	=	thickness
WM	=	weld metal
2c	=	semi-elliptical crack length
℄	=	centerline

α	=	thermal coefficient of expansion
Δ	=	change or difference
δ	=	COD
ε	=	strain
ε'	=	true strain
θ	=	hoop direction
σ	=	stress
σ'	=	true stress
Φ	=	elliptical integral of the second kind
ϕ	=	longitudinal direction
Ψ	=	angle flaw plane makes with the longitudinal tank axis

SUBSCRIPTS

c	=	composite
cr	=	critical
f	=	filament
I	=	mode one crack opening
i	=	initial
j	=	final
L	=	liner
max	=	maximum
min	=	minimum
o	=	operating
p	=	proof
ps	=	prestress
s	=	sizing
ult	=	ultimate
ys	=	yield strength

REFERENCES

1. Landes, R.E.; "Glass Fiber Reinforced Metal Pressure Vessel Design Guide", NASA CR-120917, Structural Composites Industries, July 1972.

2. Darms, F.J. and Landes, R.E.; "Computer Program for the Analysis of Filament-Reinforced Metal-Shell Pressure Vessels", NASA CR-72124, Aerojet-General Corporation, Rev. May 1972.

3. Irwin, G.R.; "Crack Extension Force for a Part-Through Crack in a Plate", Journal of Applied Mechanics, Vol. 29, Trans. ASME, Vol. 84, Series E, December 1962.

4. Hall, L.R. and Bixler, W.D.; "Subcritical Crack Growth of Selected Aerospace Pressure Vessel Materials", NASA CR-120834, The Boeing Company, September 1972.

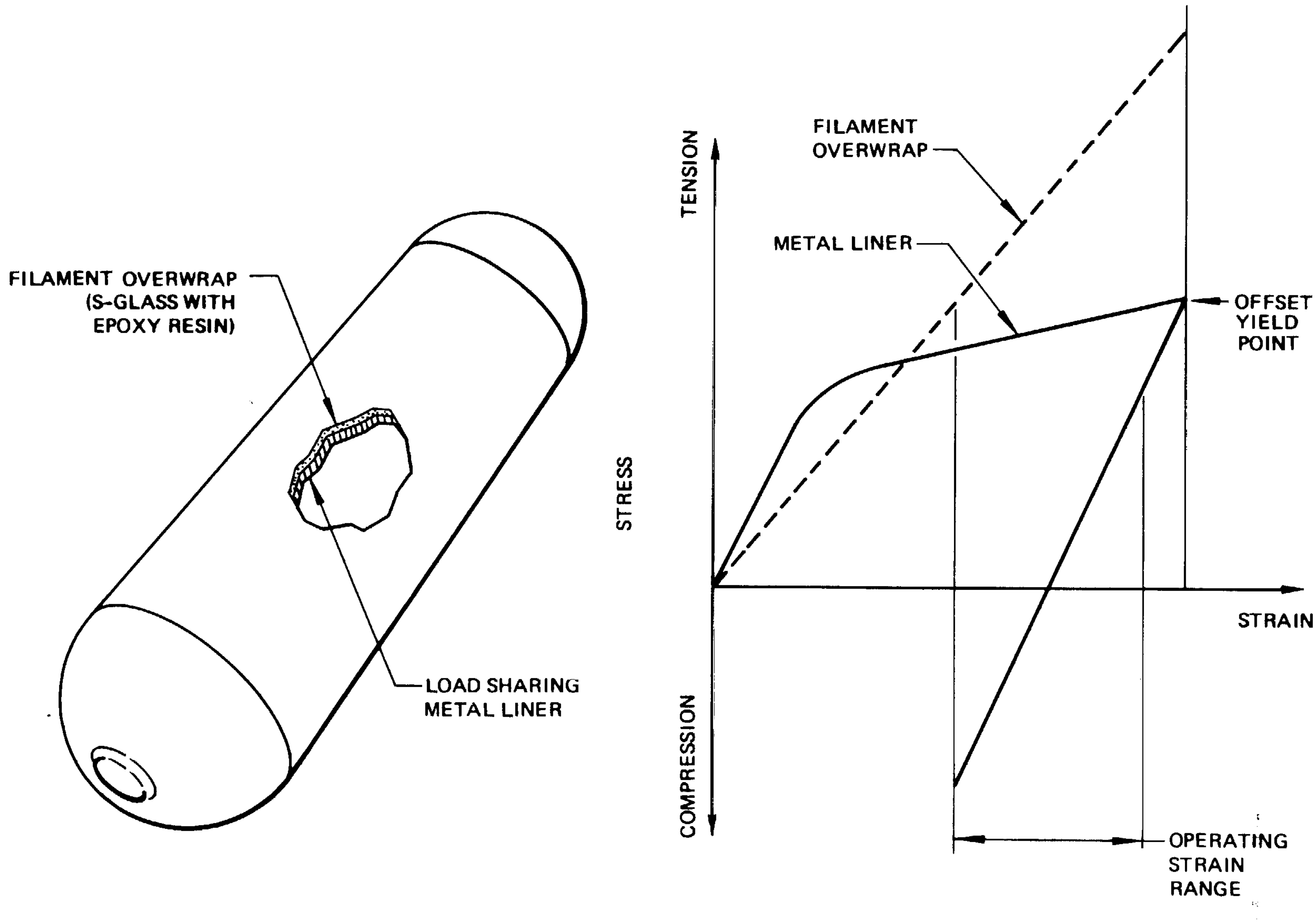

Figure 1 : Type of Tanks Being Evaluated

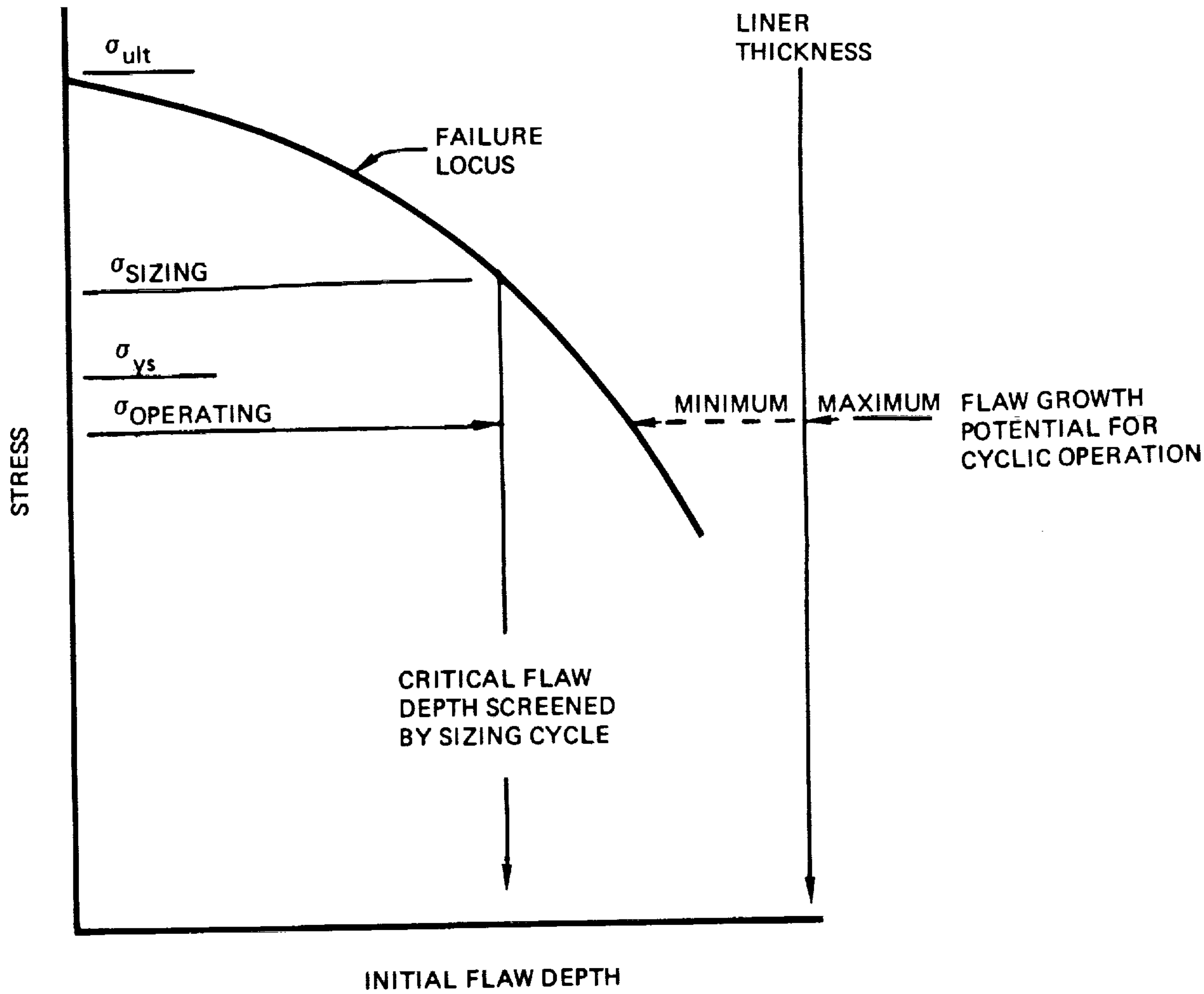

Figure 2: Fracture Mechanics Approach to Guaranteeing Service Life of Overwrapped Tanks

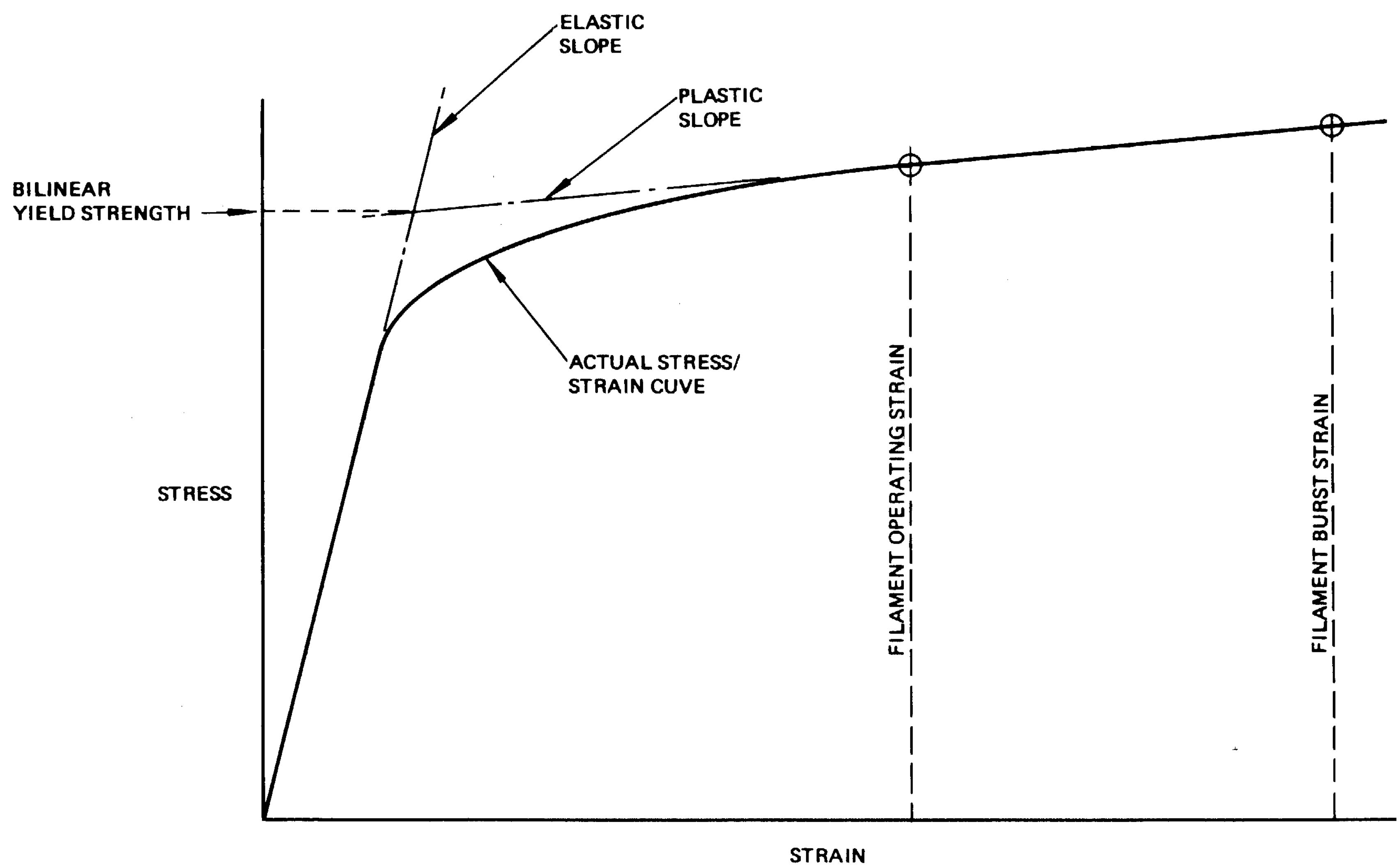

Figure 3 : Linearization of Metal Shell Stress/Strain Curve

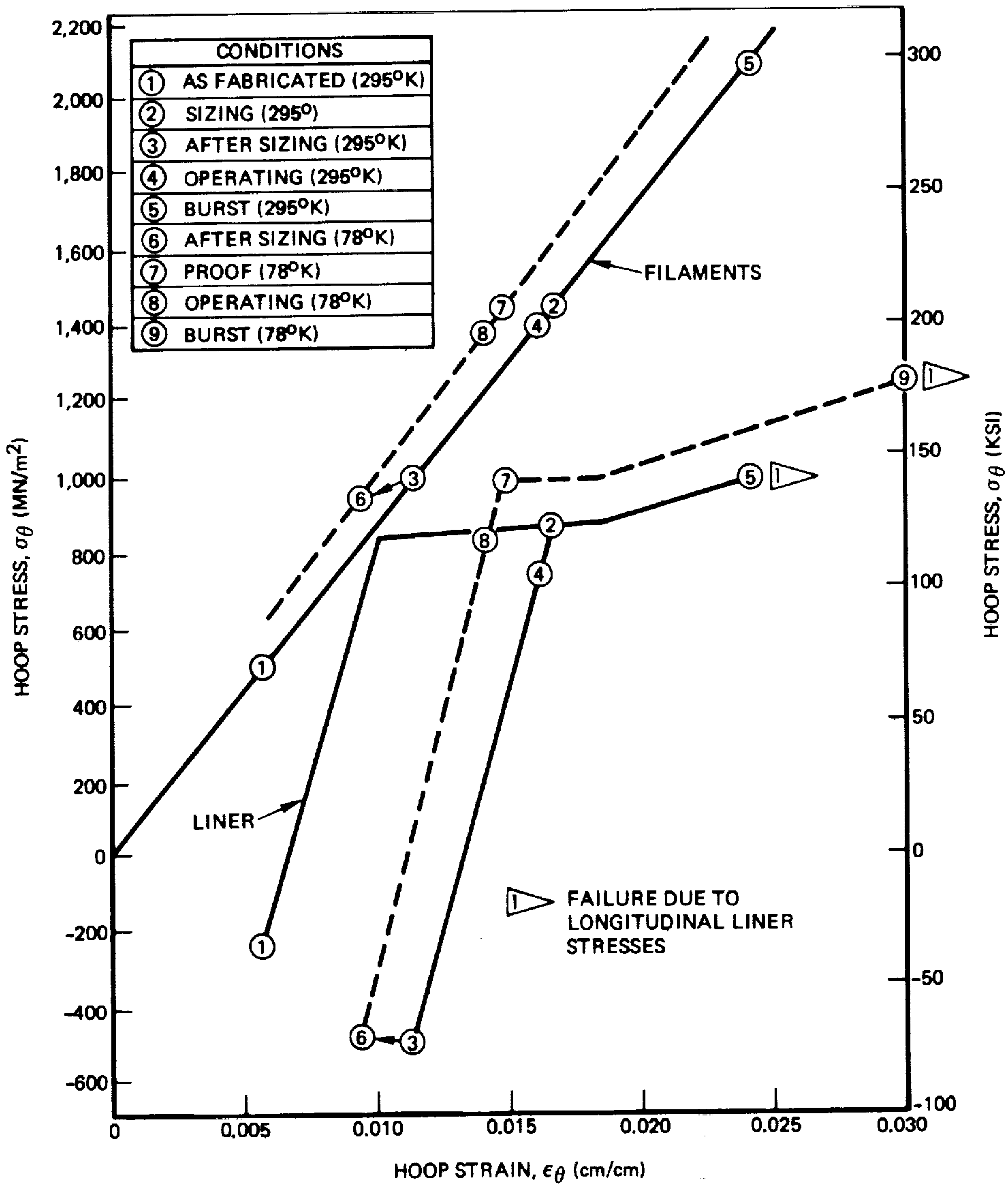

Figure 4: Stress/Strain Relationship for Hoop GFR Inconel X750 STA Tank

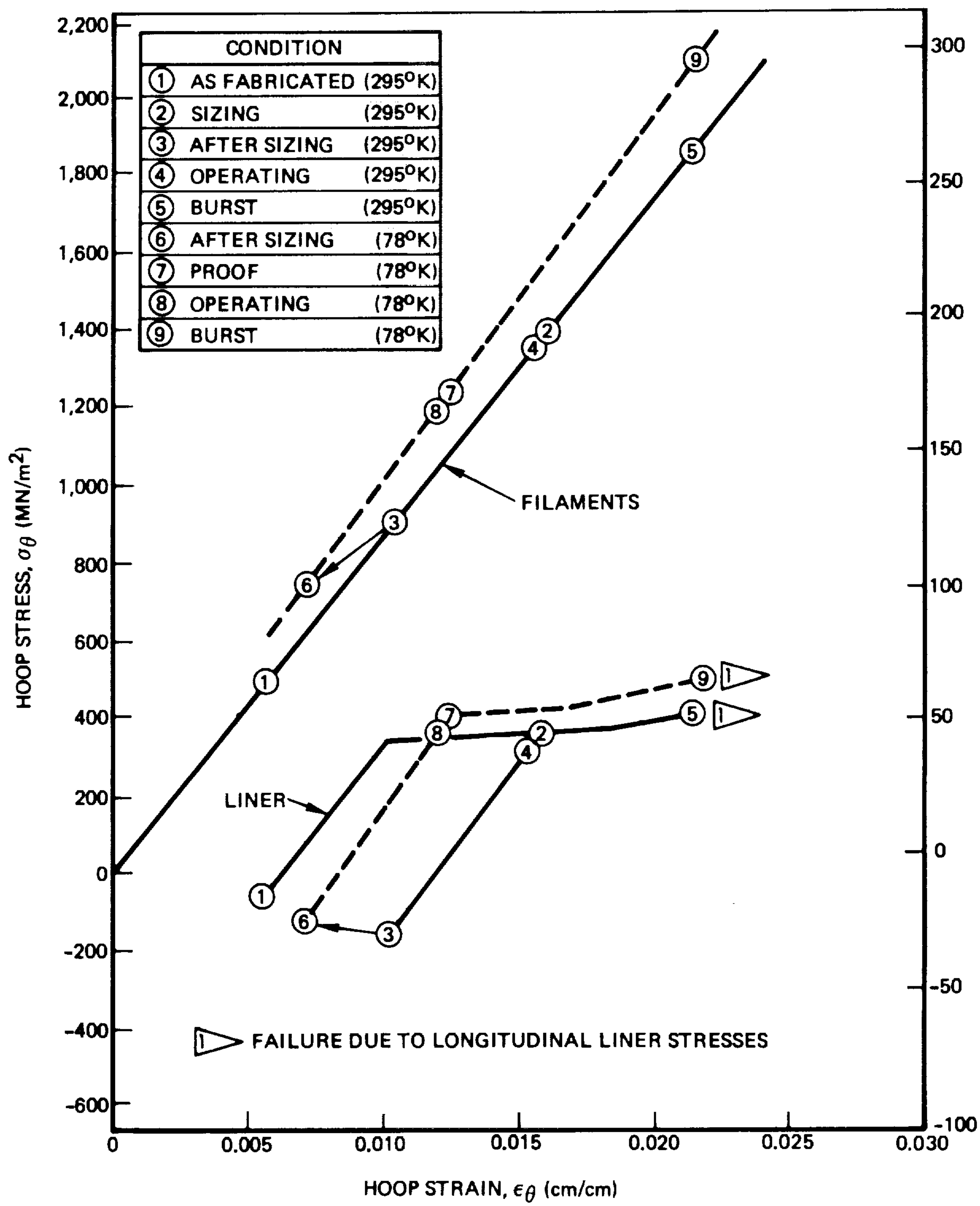

Figure 5: Stress/Strain Relationship for Hoop GFR 2219-T62 Aluminum Tank

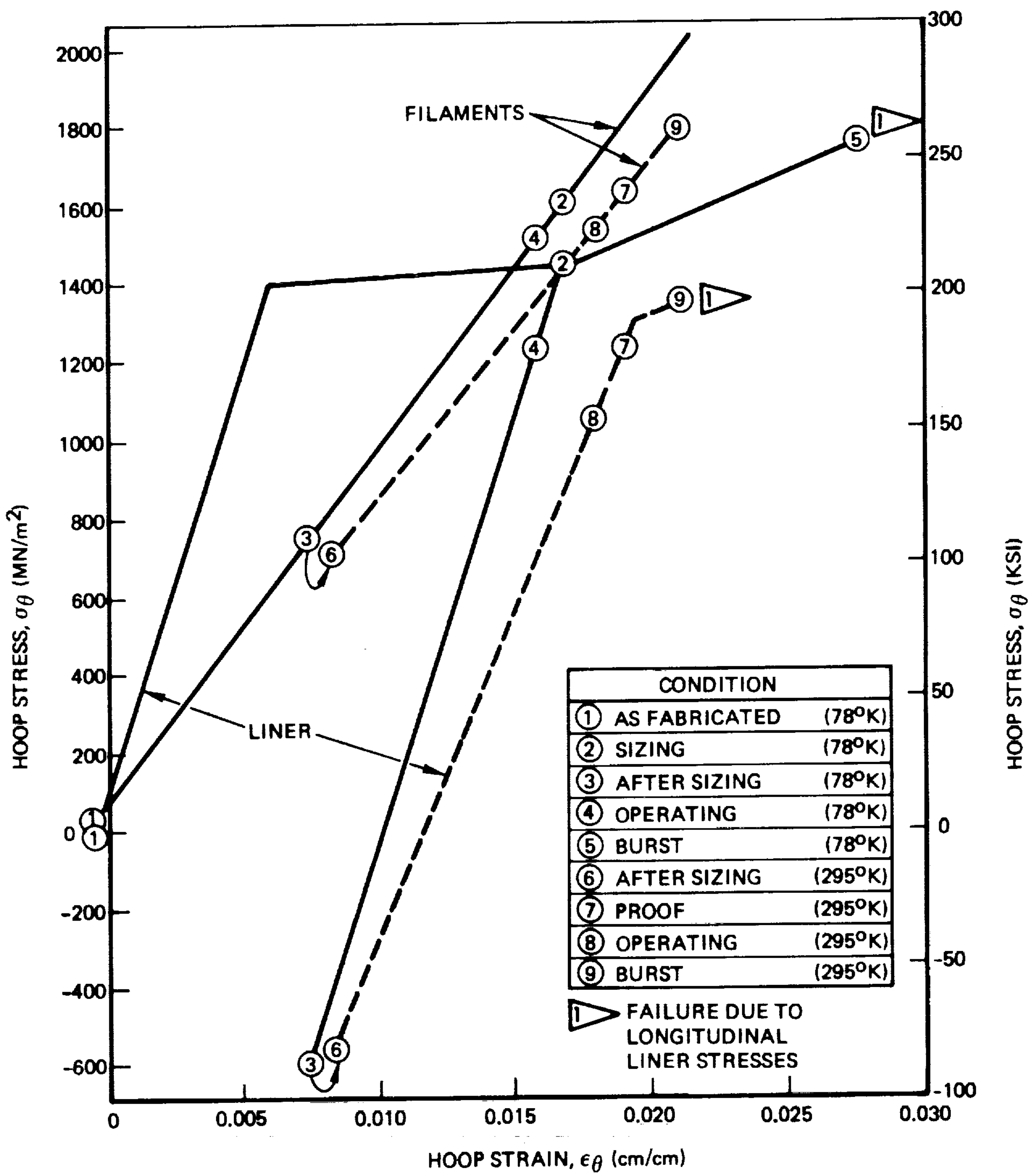

Figure 6: Stress/Strain Relationship for Hoop GFR Cryoformed 301 Stainless Steel Tank

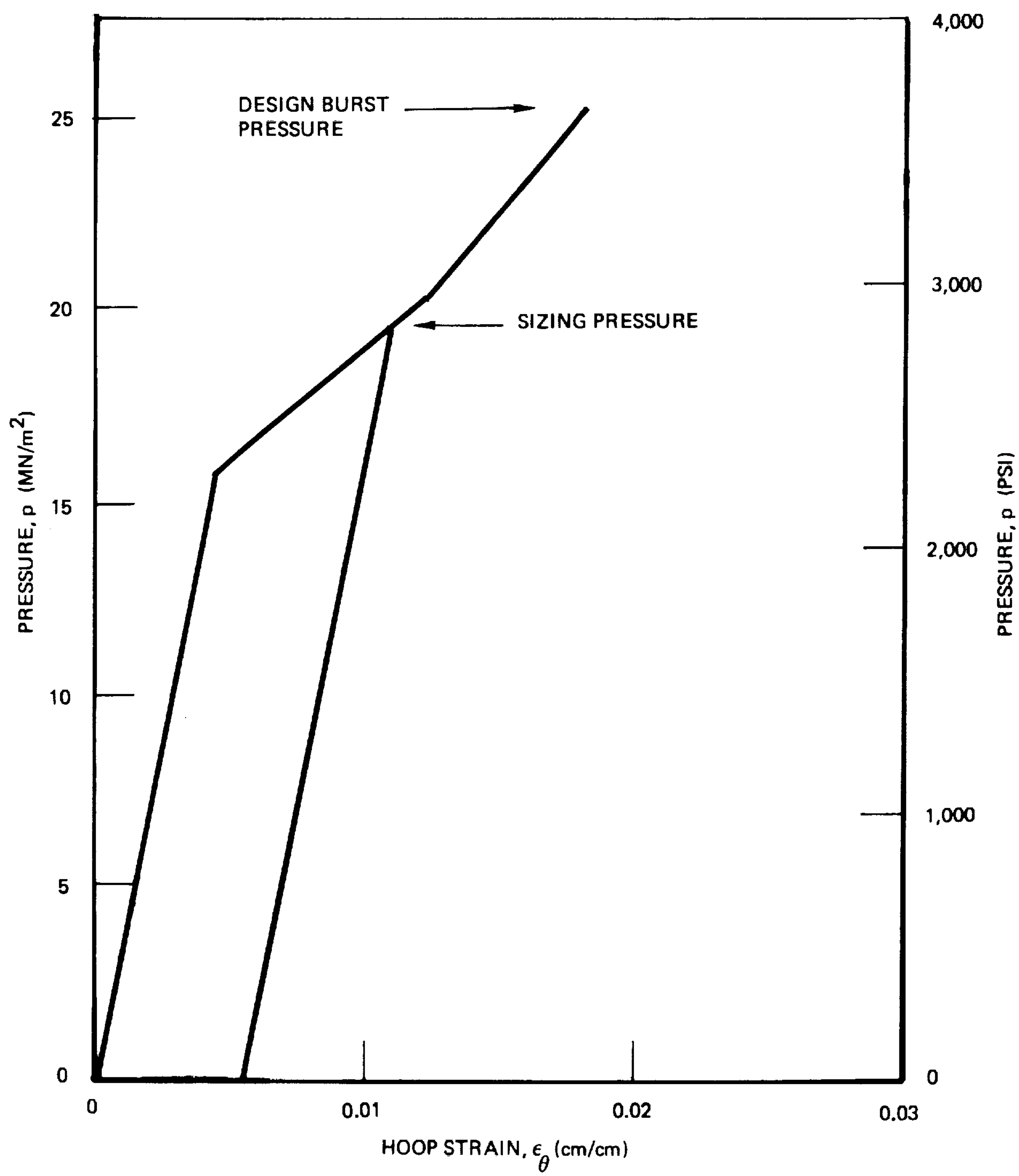

Figure 7: Ambient Pressure/Strain Relationships for Hoop GFR Inconel Tank

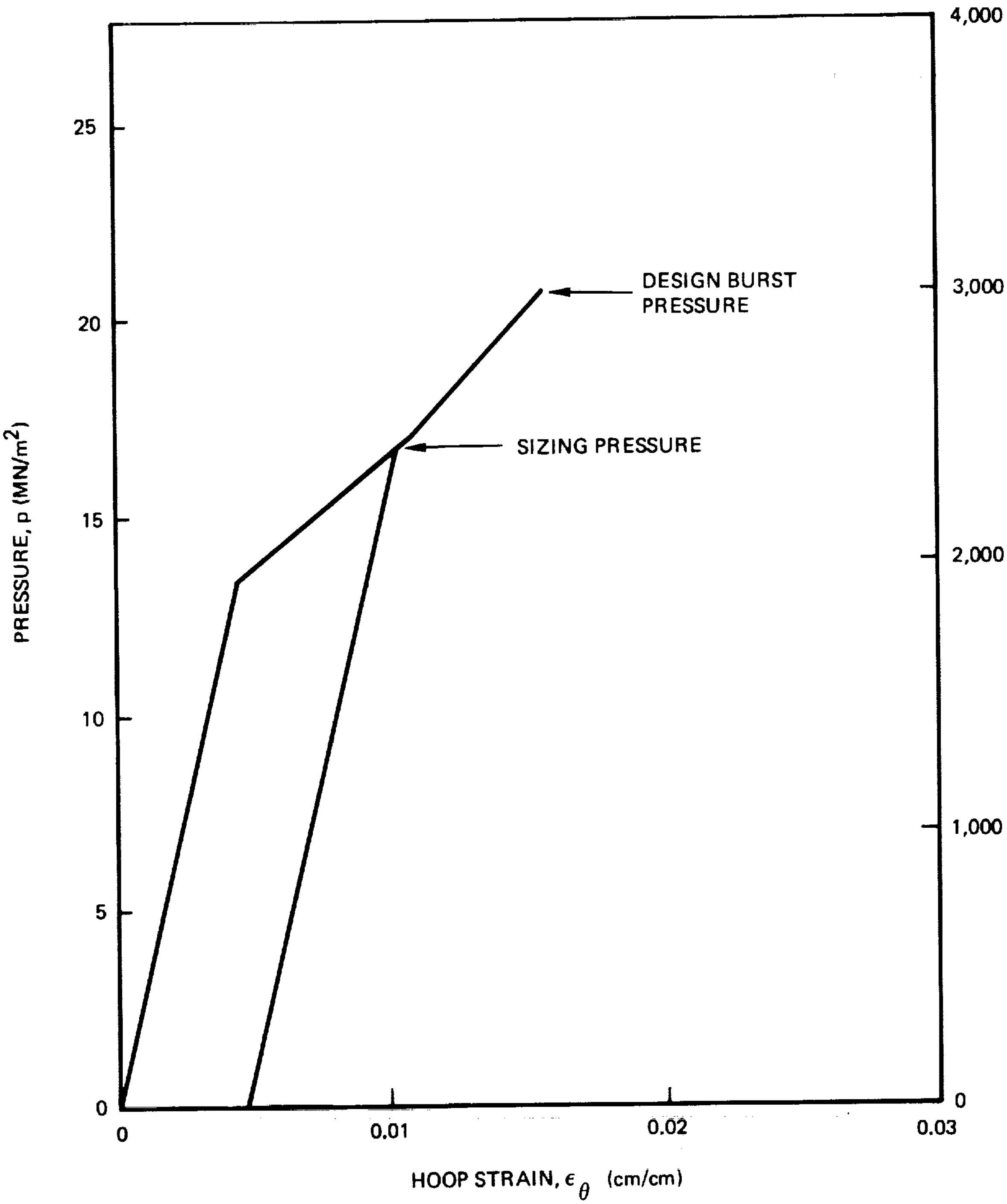

Figure 8: Ambient Pressure/Strain Relationships for Hoop GFR Aluminum Tank

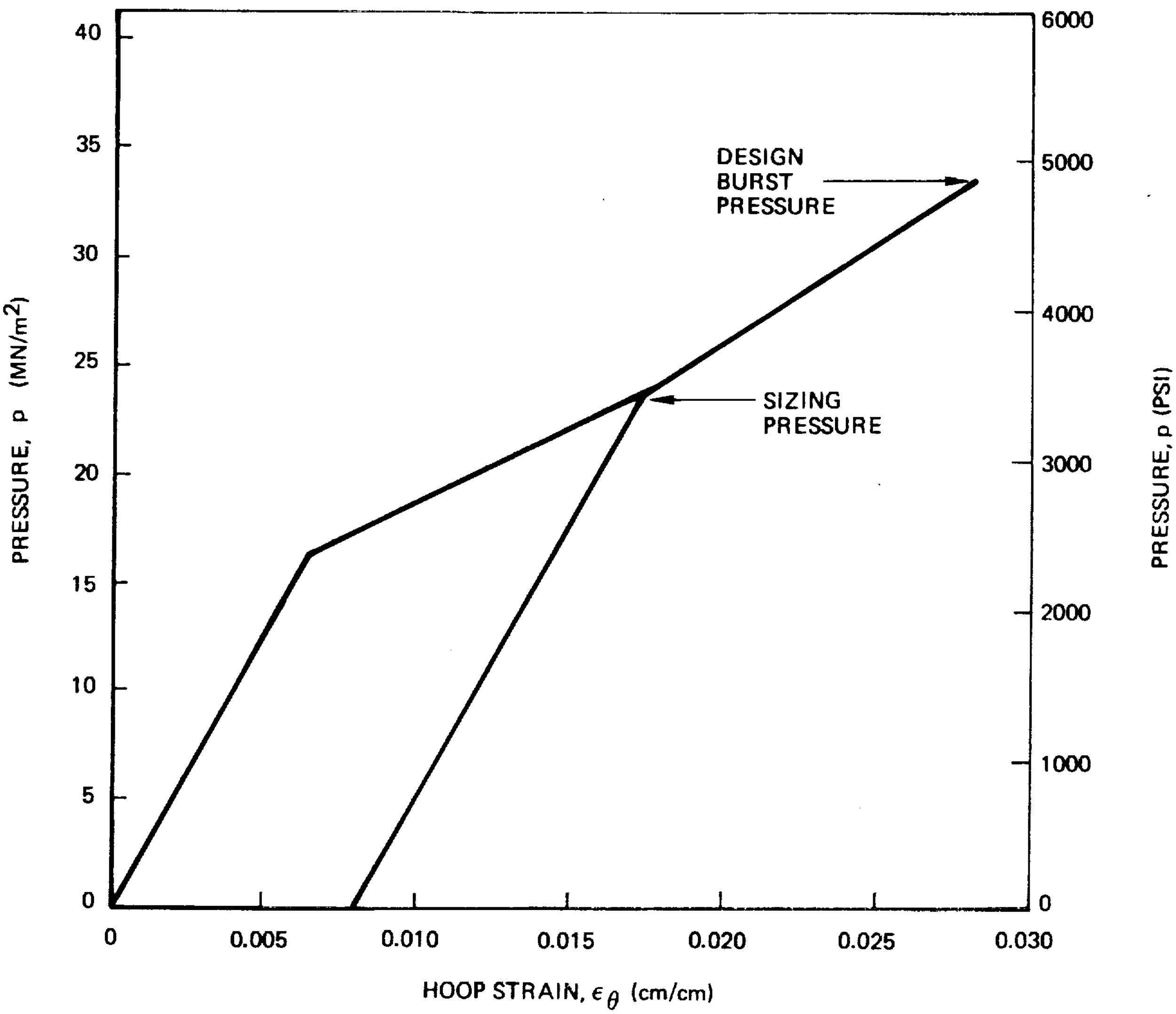

Figure 9: Cryogenic Pressure/Strain Relationships for Hoop GFR Cryoformed 301 Stainless Steel Tank

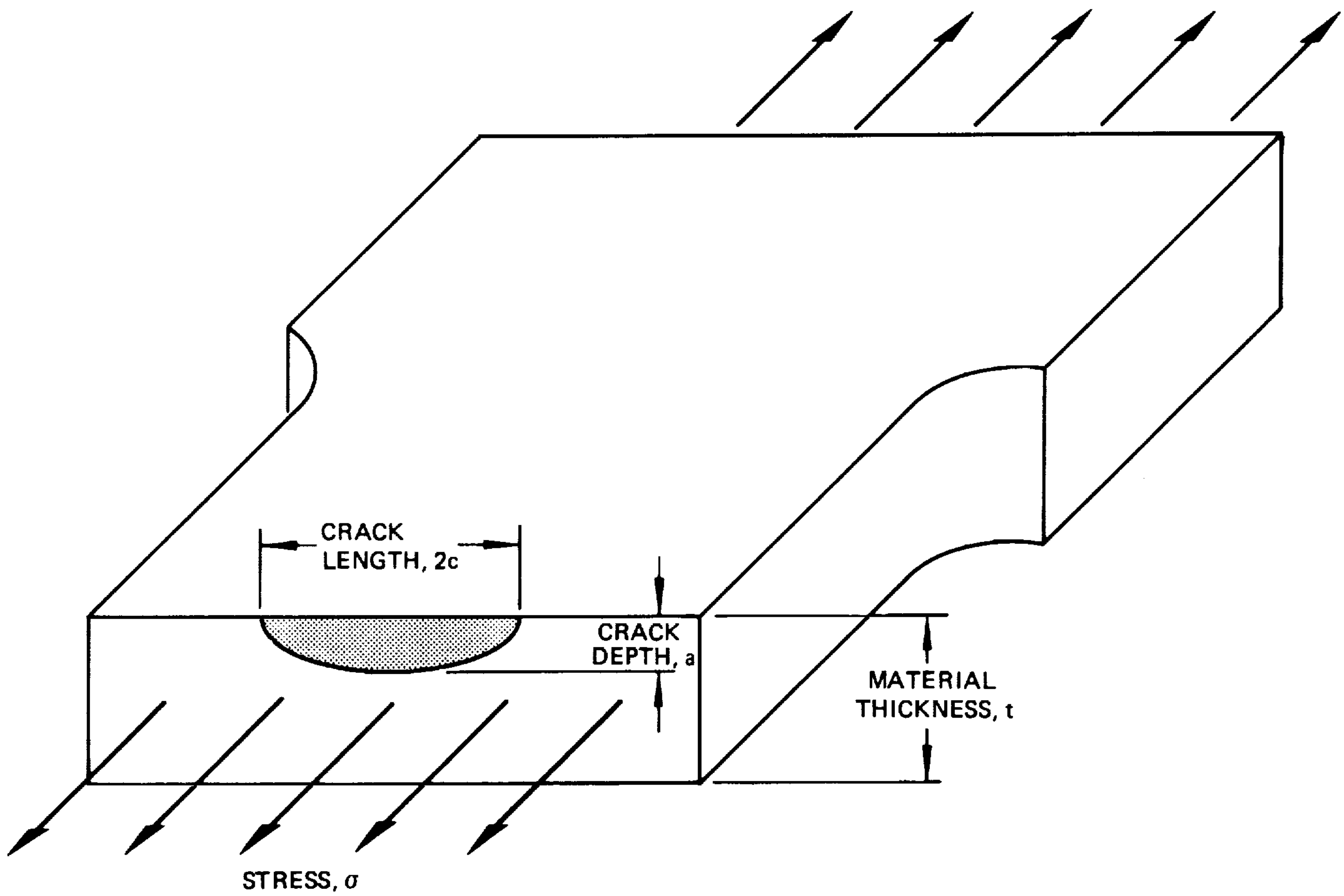

Figure 10: Semi-Elliptical Surface Flaw Configuration

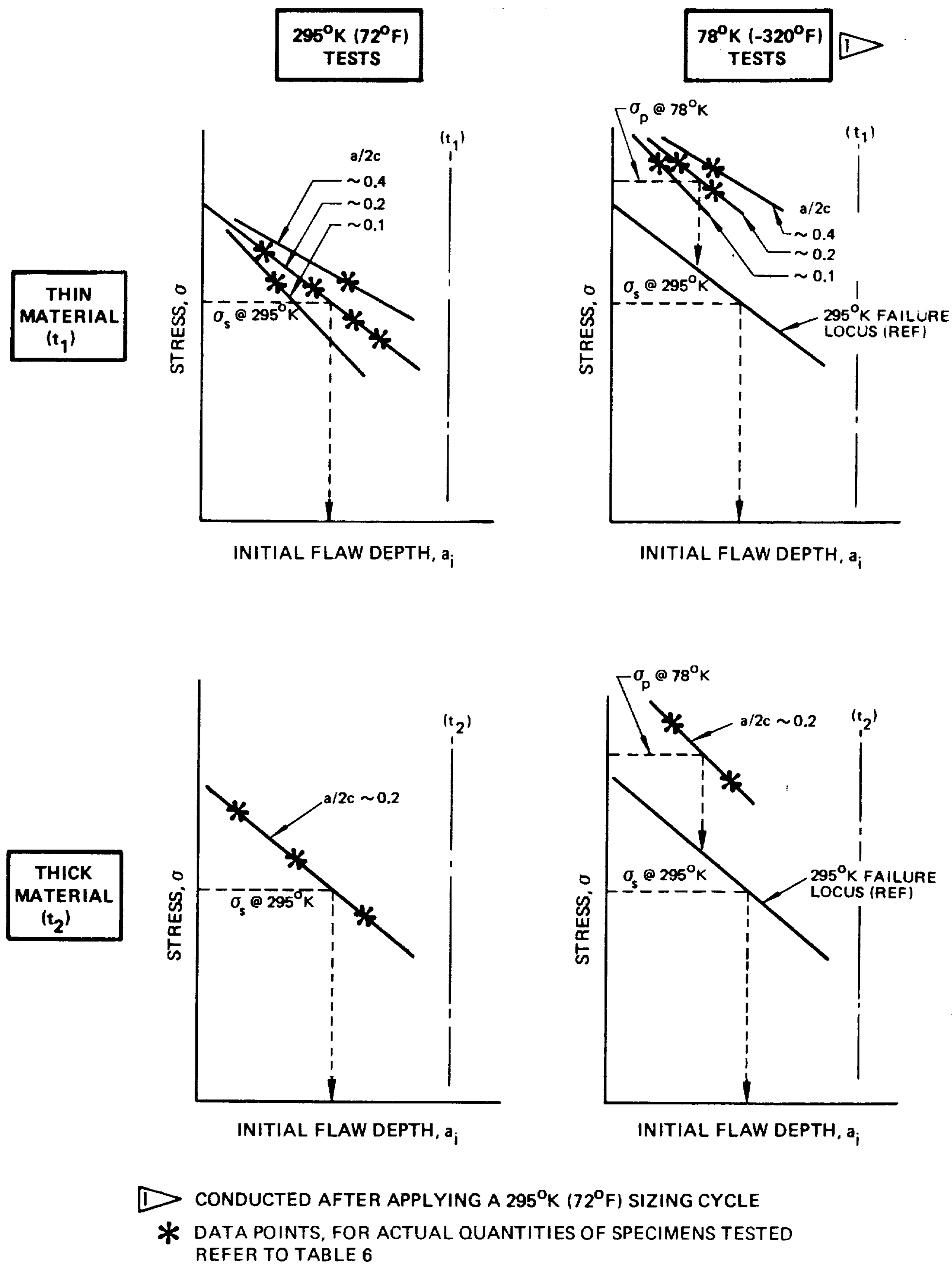

Figure 11: Schematic of Uniaxial Static Fracture Tests Conducted for Inconel X750 STA and 2219-T62 Aluminum (Base Metal and Weld Metal)

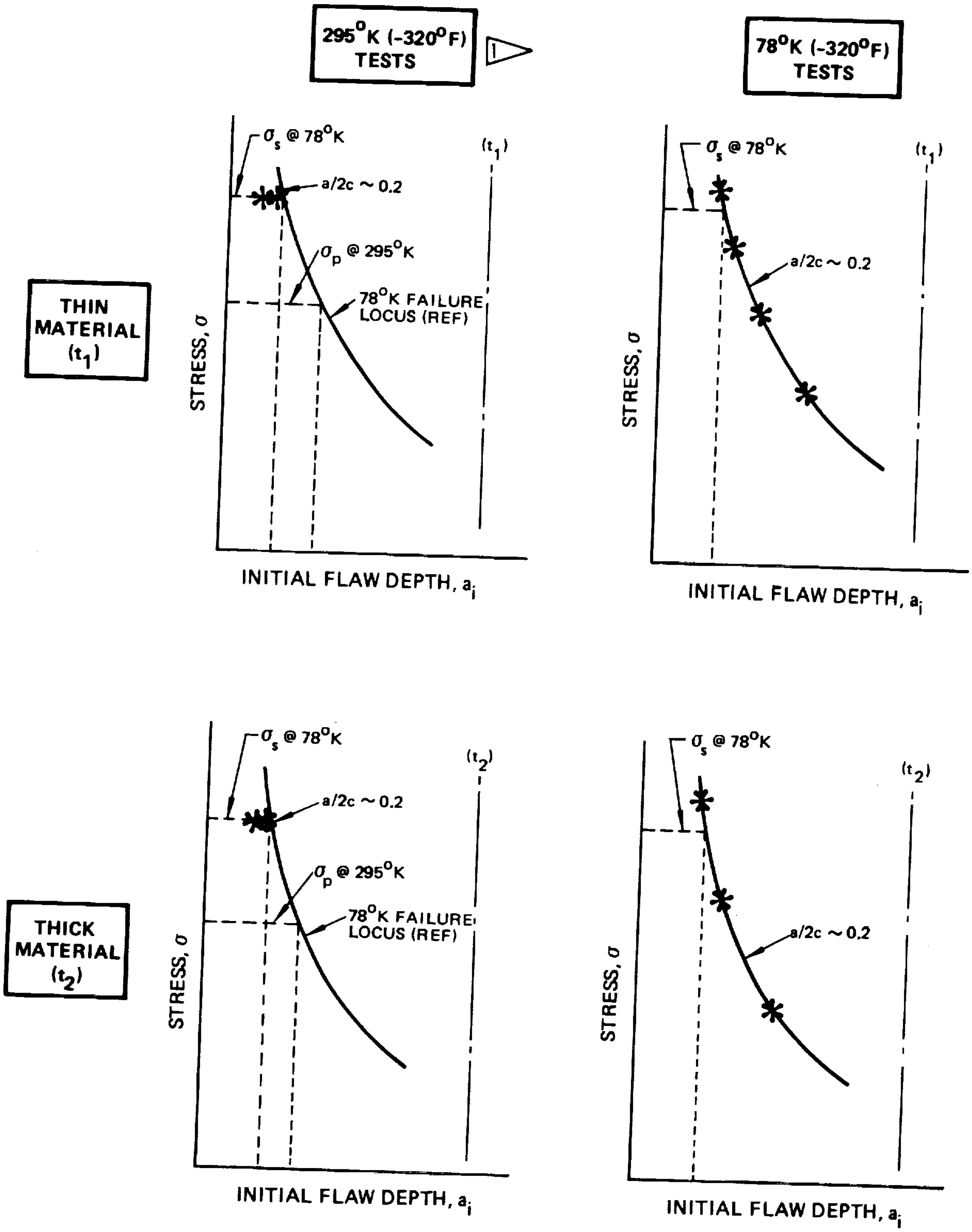

CONDUCTED AFTER APPLYING A 78°K (-320°F) SIZING CYCLE

* DATA POINTS, FOR ACTUAL QUANTITIES OF SPECIMENS TESTED REFER TO TABLE 6

Figure 12: Schematic of Uniaxial Static Fracture Tests Conducted for Cryo-Stretched 301 Stainless Steel (Base Metal and Weld Metal)

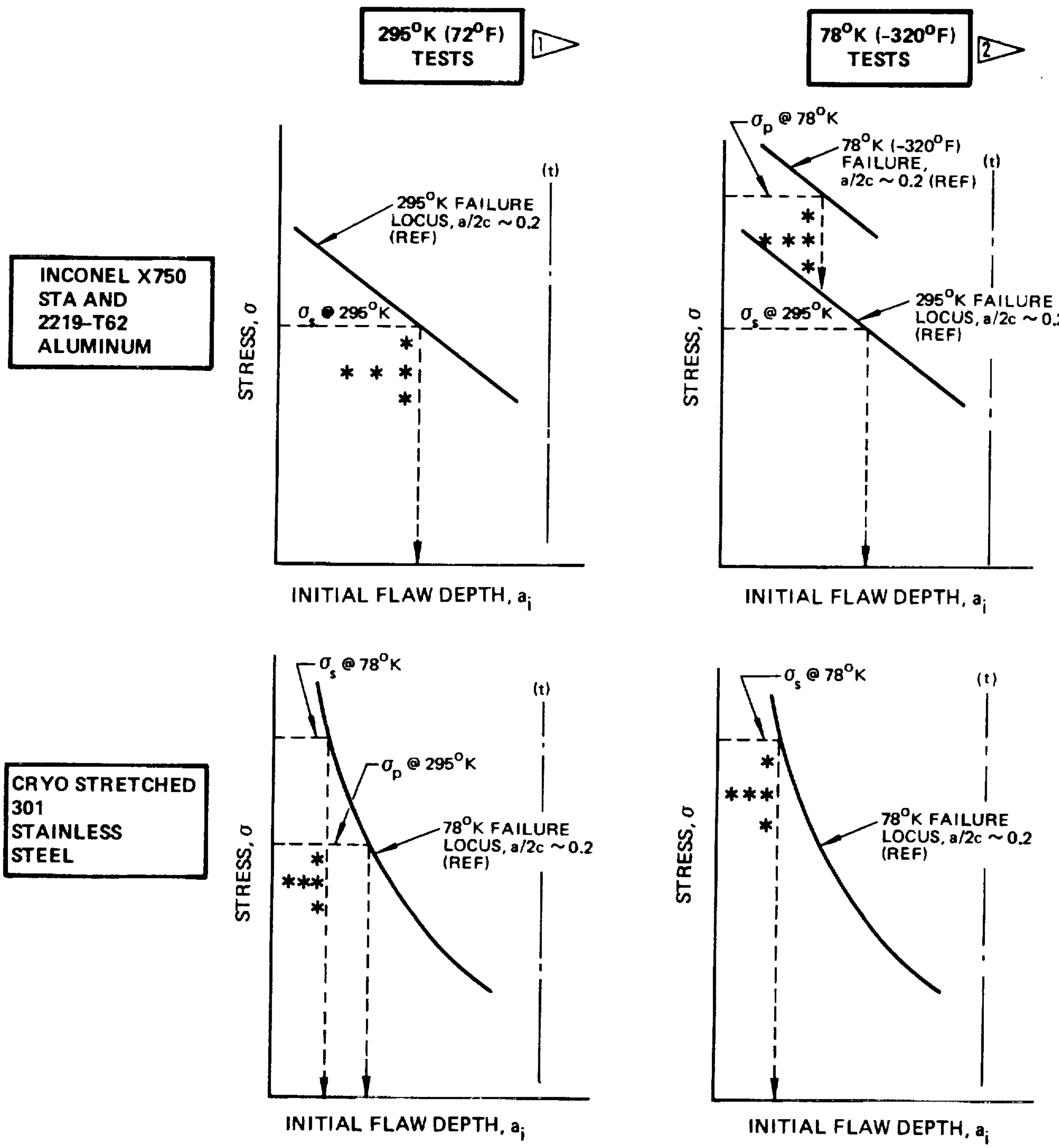

1 FOR INCONEL AND ALUMINUM CYCLIC TESTS CONDUCTED AFTER APPLYING A 295°K (72°F) SIZING CYCLE; FOR 301 CYCLIC TESTS CONDUCTED AFTER APPLYING A 78°K (-320°F) SIZING CYCLE PLUS A 295°K (72°F) PROOF TEST

2 FOR INCONEL AND ALUMINUM CYCLIC TESTS CONDUCTED AFTER APPLYING A 295°K (72°F) SIZING CYCLE PLUS A 78°K (-320°F) PROOF TEST; FOR 301 CYCLIC TESTS CONDUCTED AFTER APPLYING A 78°K (-320°F) SIZING CYCLE

* DATA POINTS, FOR ACTUAL QUANTITIES OF SPECIMENS TESTED REFER TO TABLE 6

Figure 13 : Schematic of Cyclic Life Tests for Program Materials (Both Thicknesses)

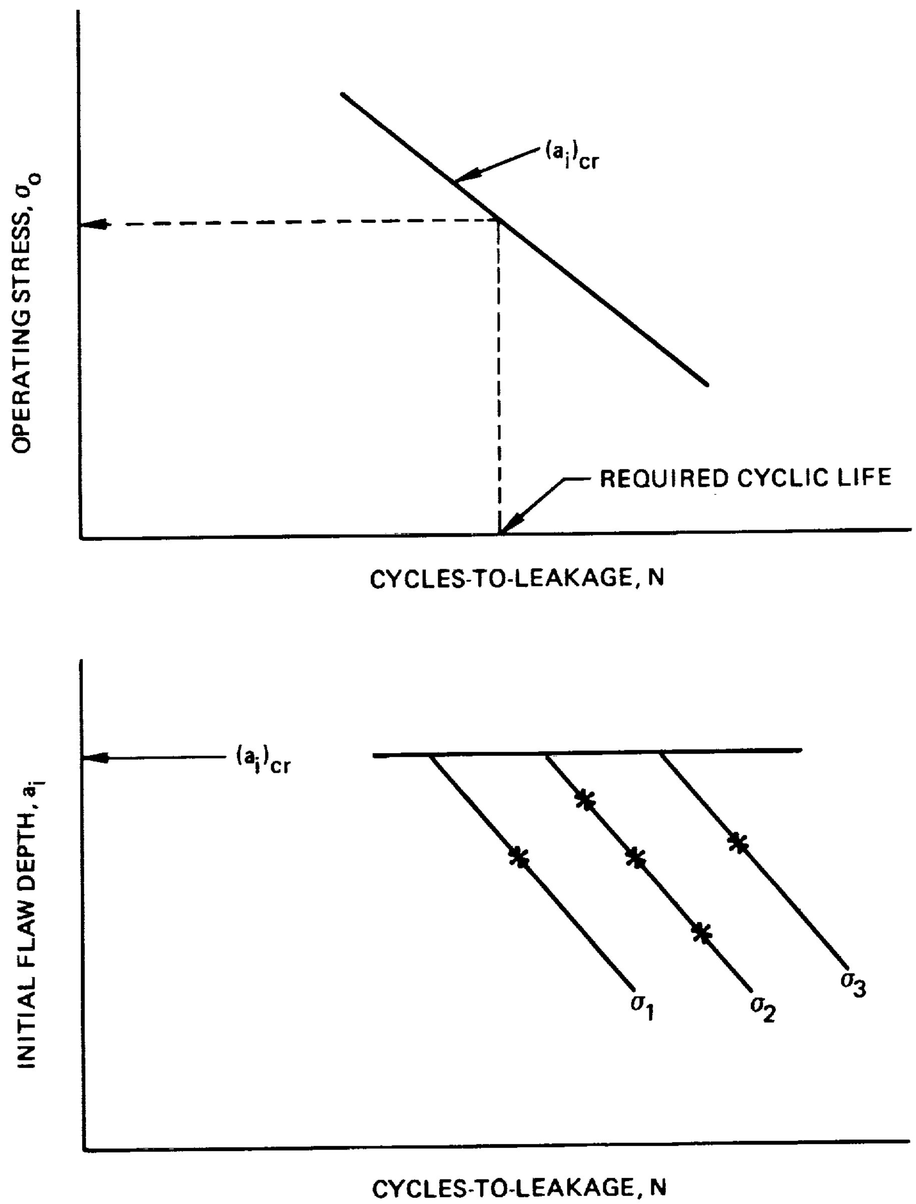

Figure 14 : Schematic of Cyclic Life Results Presentation

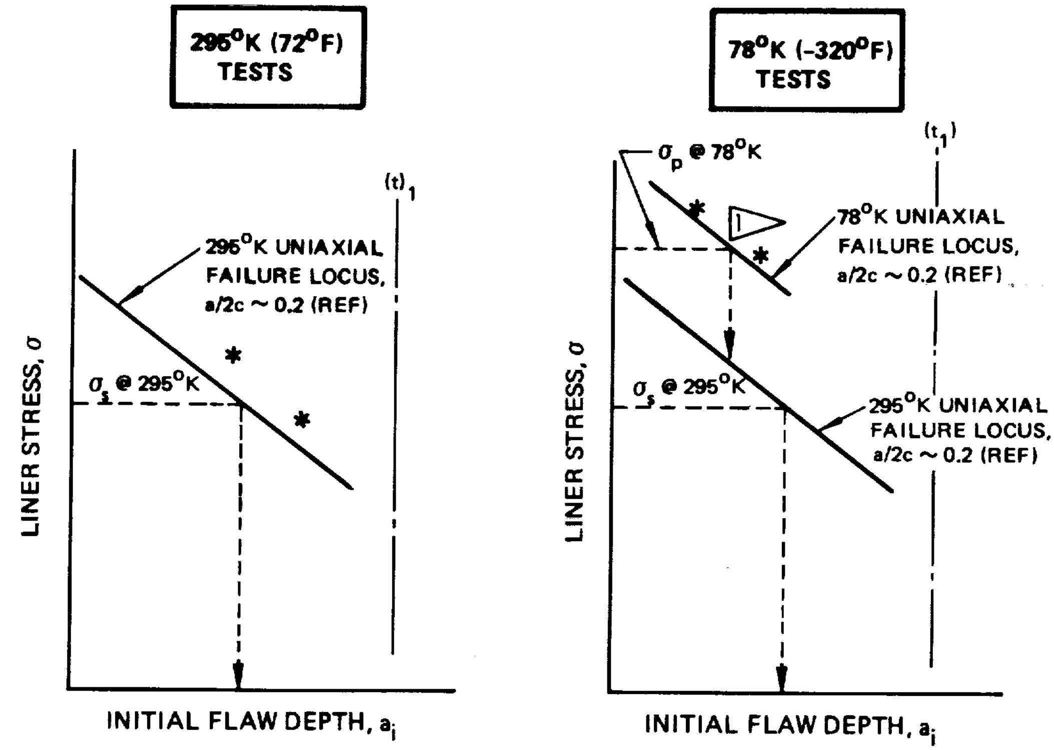

Figure 15: Schematic of Inconel and Aluminum Tank Static Burst Tests (Base Metal and Weld Metal)

1 CONDUCTED AFTER APPLYING A 295°K (72°F) SIZING CYCLE

2 CONDUCTED AFTER APPLYING A 295°K (72°F) SIZING CYCLE PLUS A 78°K (-320°F) PROOF TEST

* DATA POINTS, FOR ACTUAL QUANTITIES OF SPECIMENS TESTED REFER TO TABLE 7

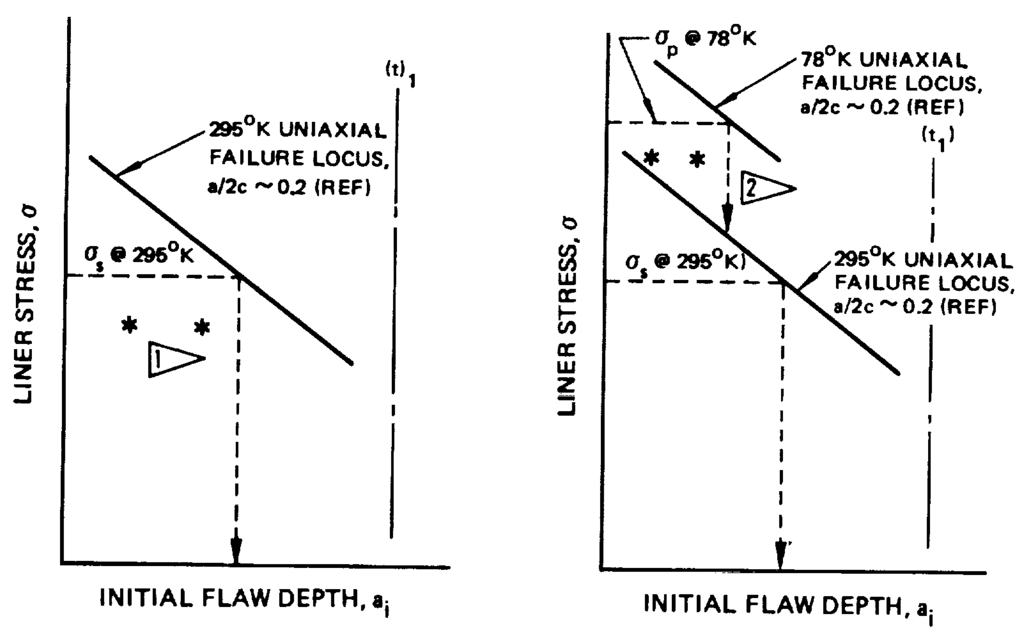

Figure 16: Schematic of Inconel and Aluminum Tank Cyclic Life Tests (Base Metal and Weld Metal)

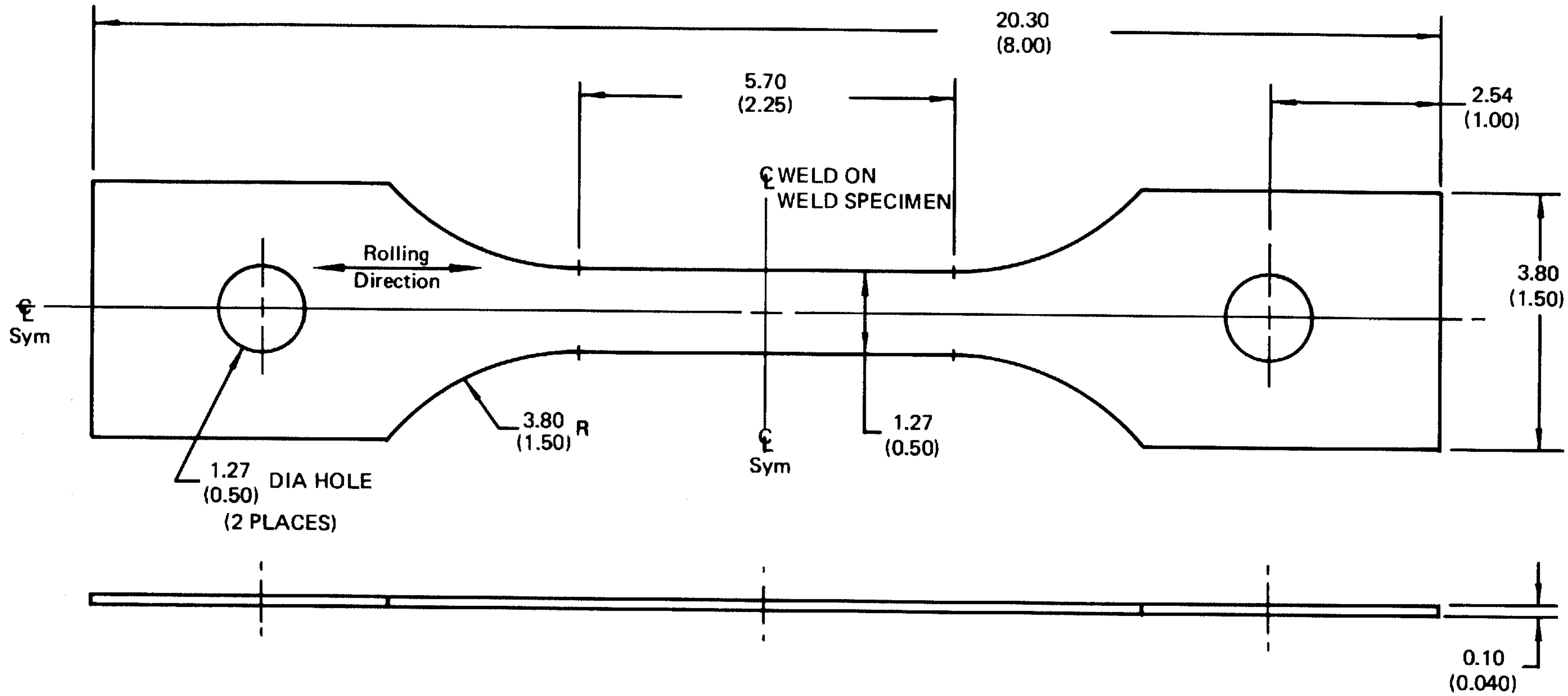

DIMENSIONS GIVEN IN CENTIMETERS (INCHES)

WELD BEAD MACHINED FLUSH ON WELDED SPECIMEN

Figure 17 : Inconel X750 STA Tensile Specimen (Base Metal and Weld Metal)

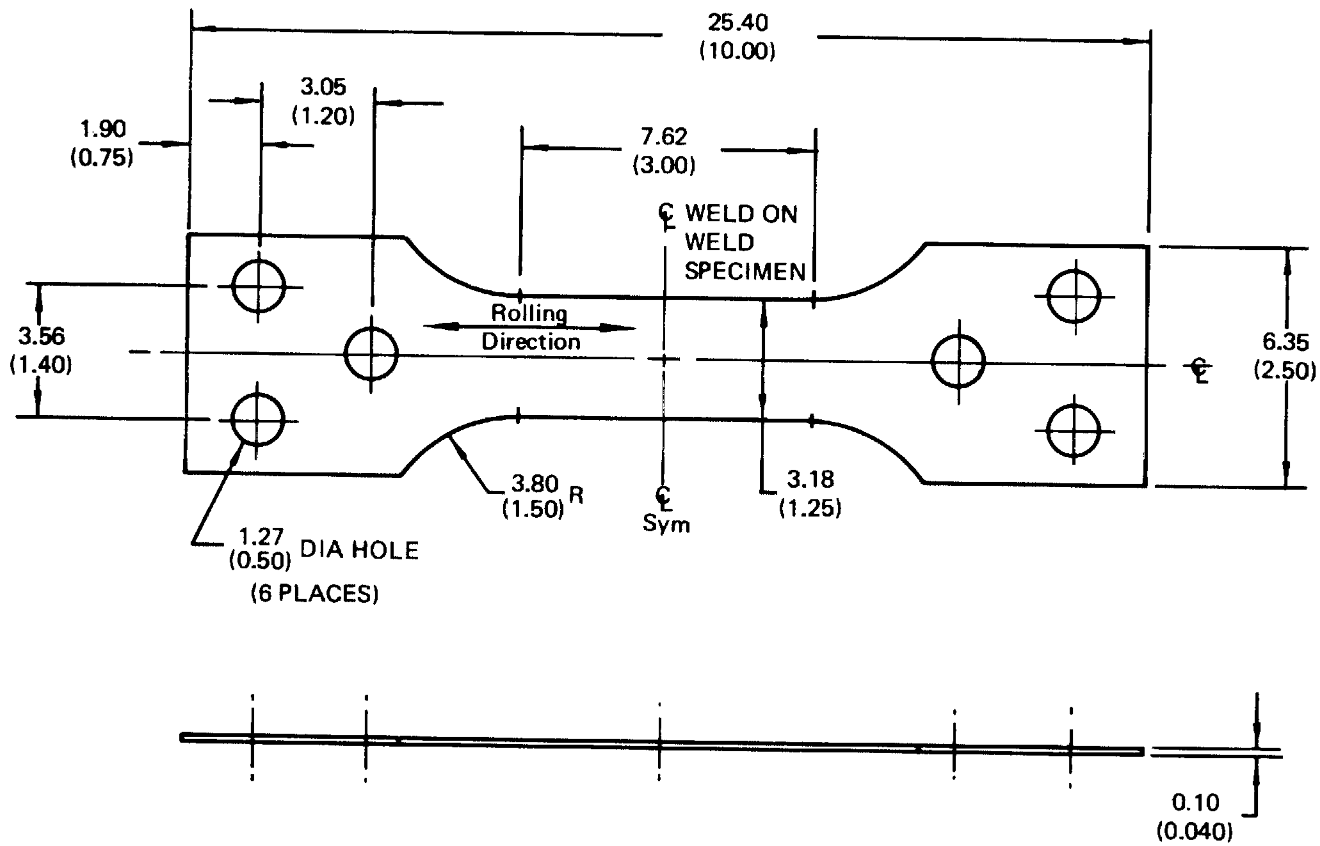

DIMENSIONS GIVEN IN CENTIMETERS (INCHES)

WELD BEAD MACHINED FLUSH ON WELDED SPECIMEN

Figure 18 : Inconel X750 STA "Thin" Fracture Specimen (Base Metal and Weld Metal)

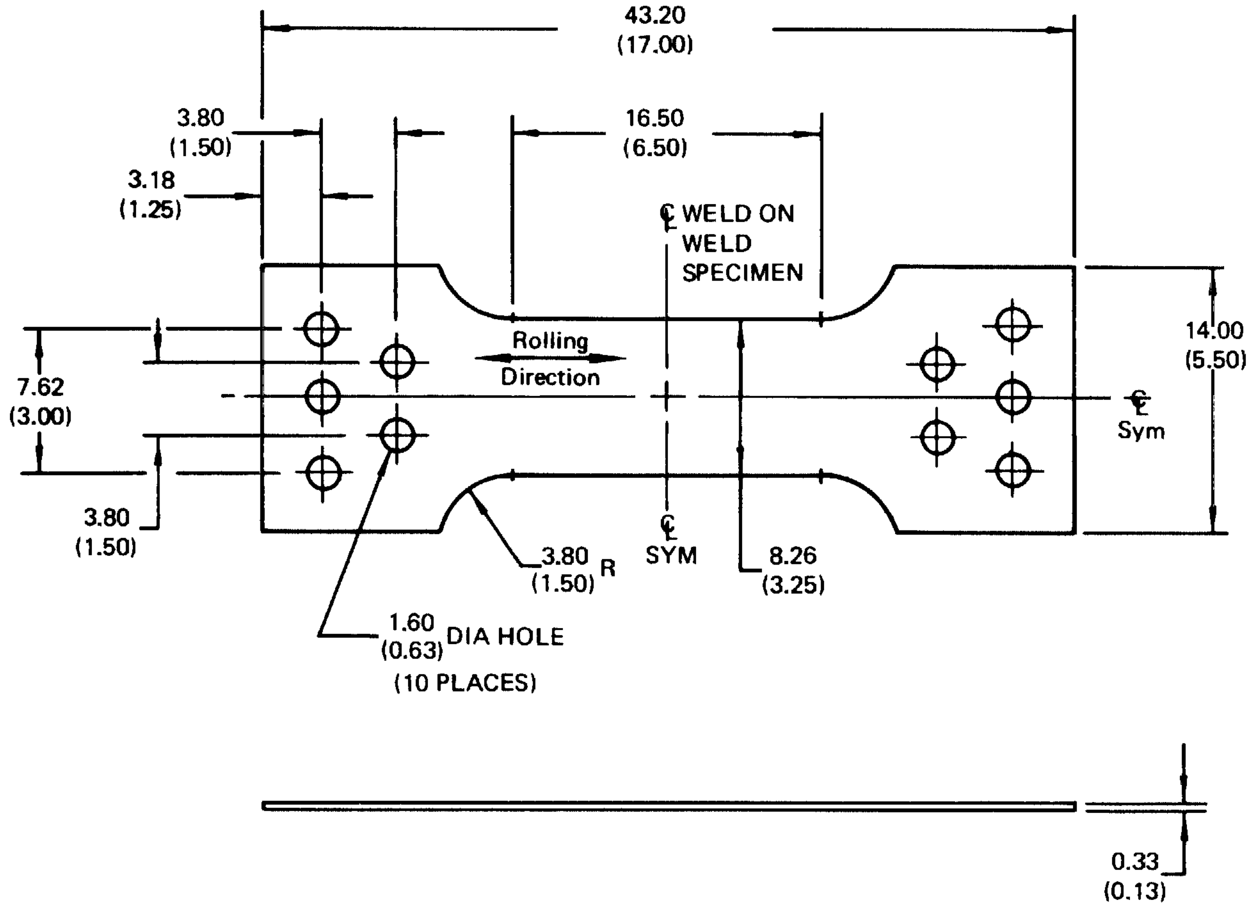

DIMENSIONS GIVEN IN CENTIMETERS (INCHES)

WELD BEAD MACHINED FLUSH ON WELDED SPECIMEN

Figure 19 : Inconel X750 STA "Thick" Fracture Specimen (Base Metal and Weld Metal)

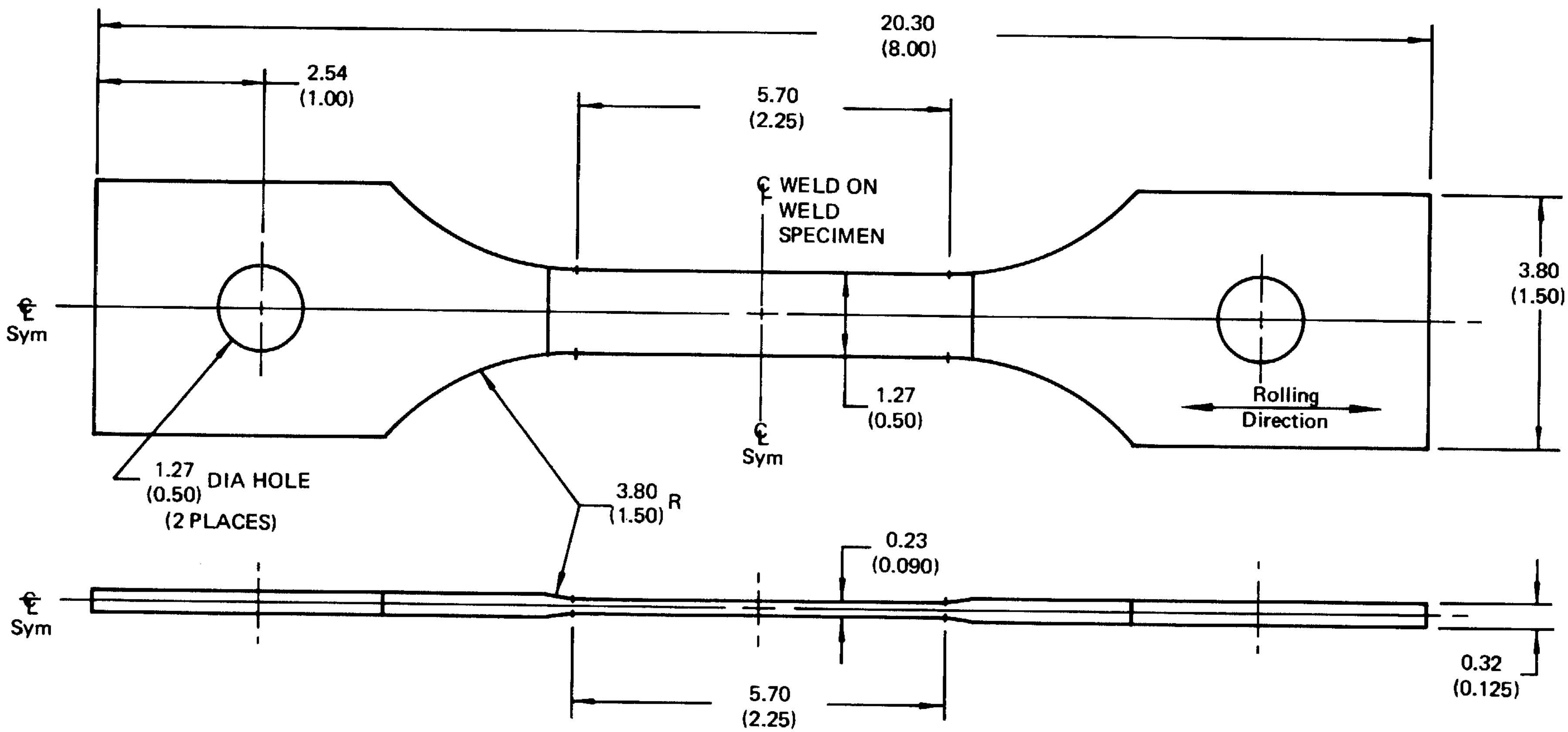

DIMENSIONS GIVEN IN CENTIMETERS (INCHES)

Figure 20 : 2219-T62 Aluminum Tensile Specimen (Base Metal and Weld Metal)

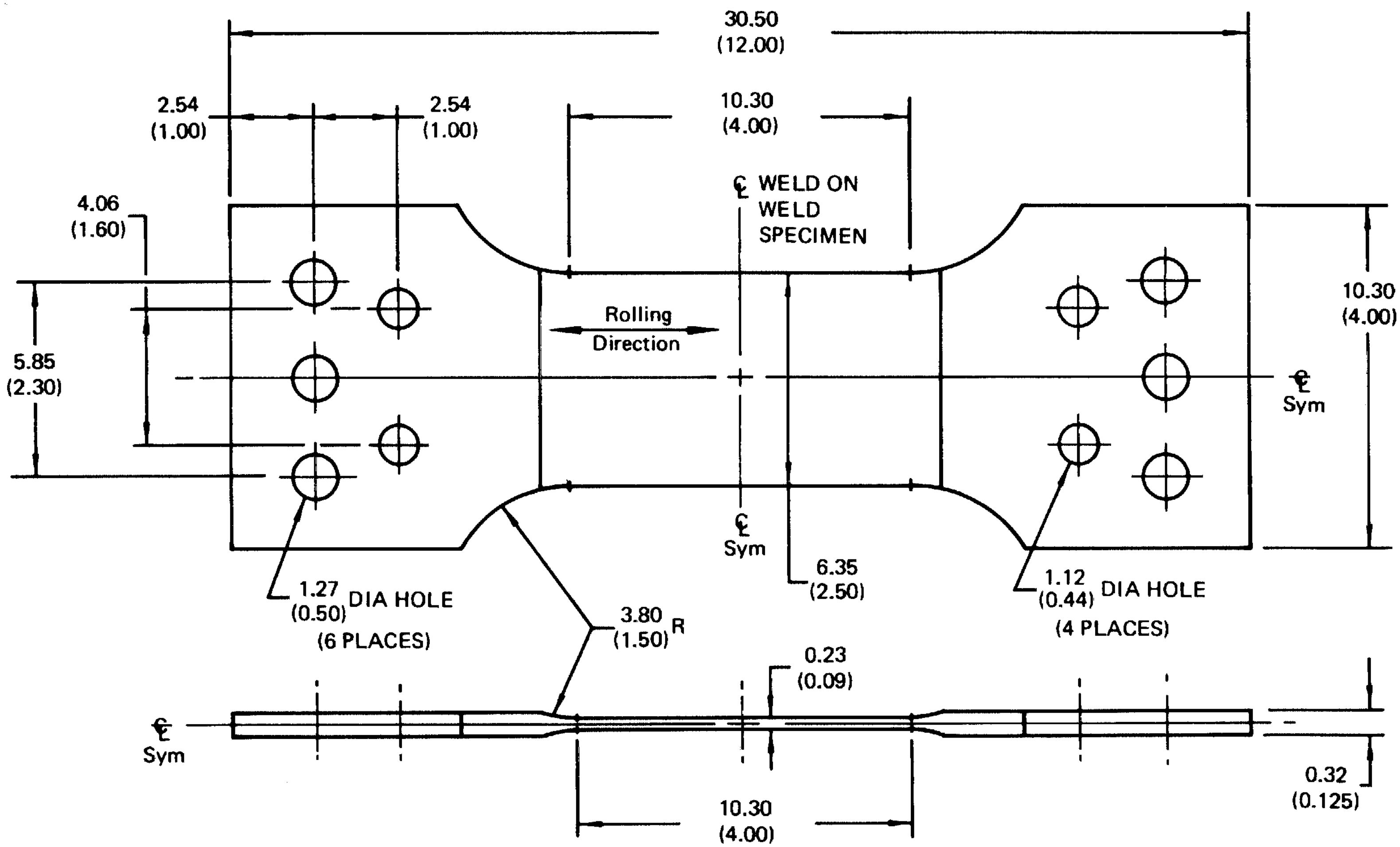

DIMENSIONS GIVEN IN CENTIMETERS (INCHES)

Figure 21 : 2219-T62 Aluminum "Thin" Fracture Specimen (Base Metal and Weld Metal)

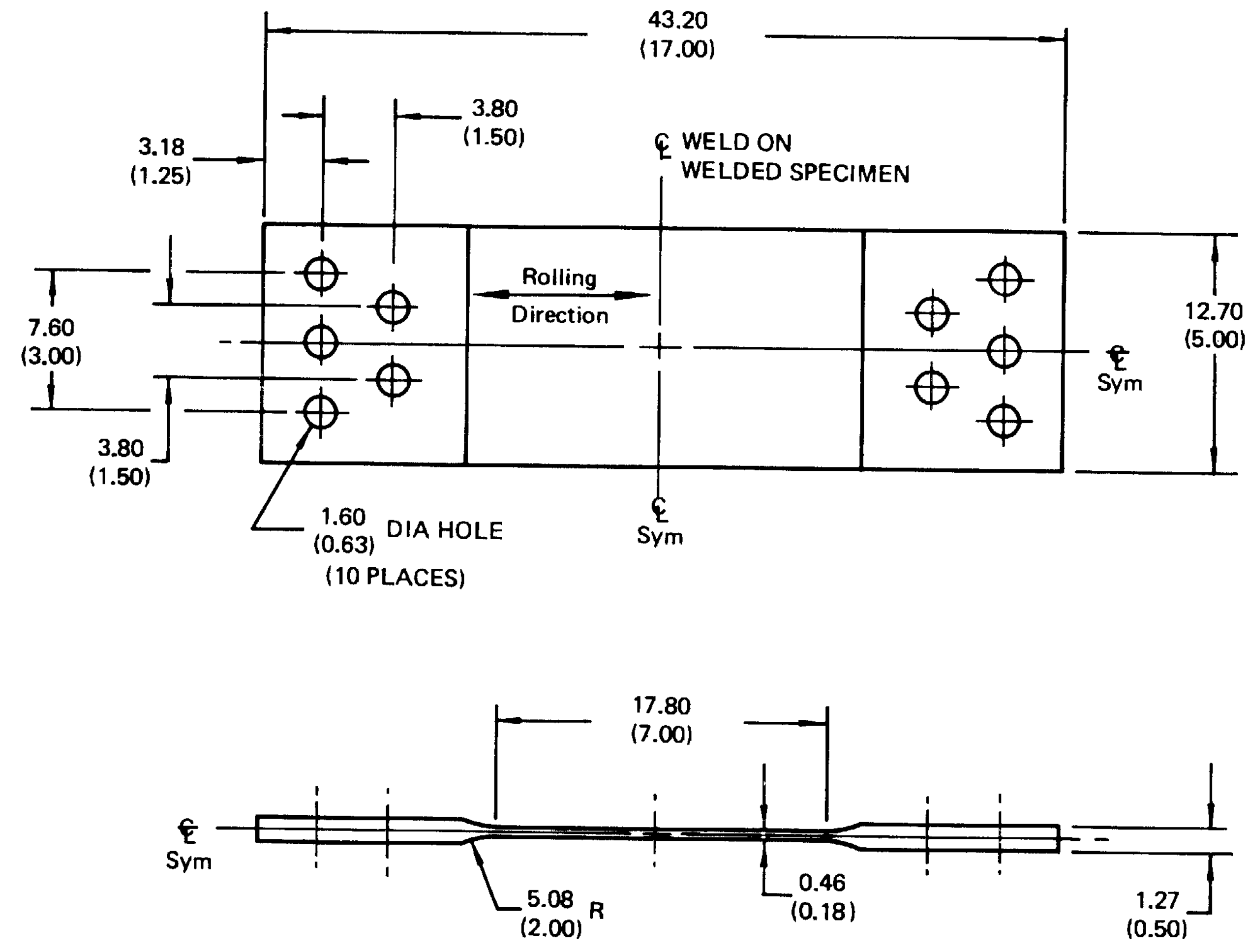

DIMENSIONS GIVEN IN CENTIMETERS (INCHES)

Figure 22 : 2219-T62 Aluminum "Thick" Fracture Specimen (Base Metal and Weld Metal)

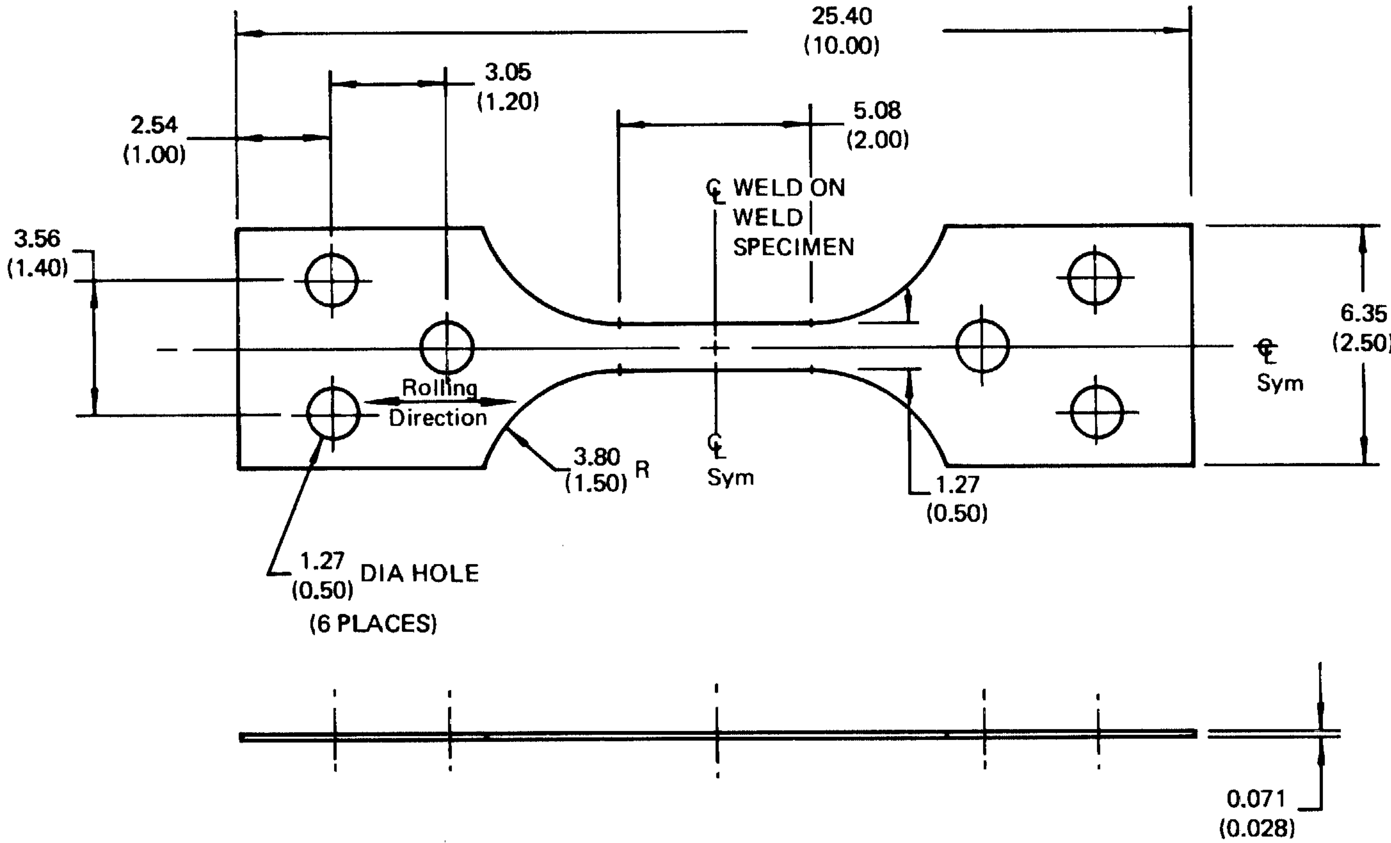

DIMENSIONS GIVEN IN CENTIMETERS (INCHES)

WELD BEAD MACHINED FLUSH ON WELDED SPECIMEN

Figure 23 : Cryostretched 301 Stainless Steel Tensile Specimen (Base Metal and Weld Metal)

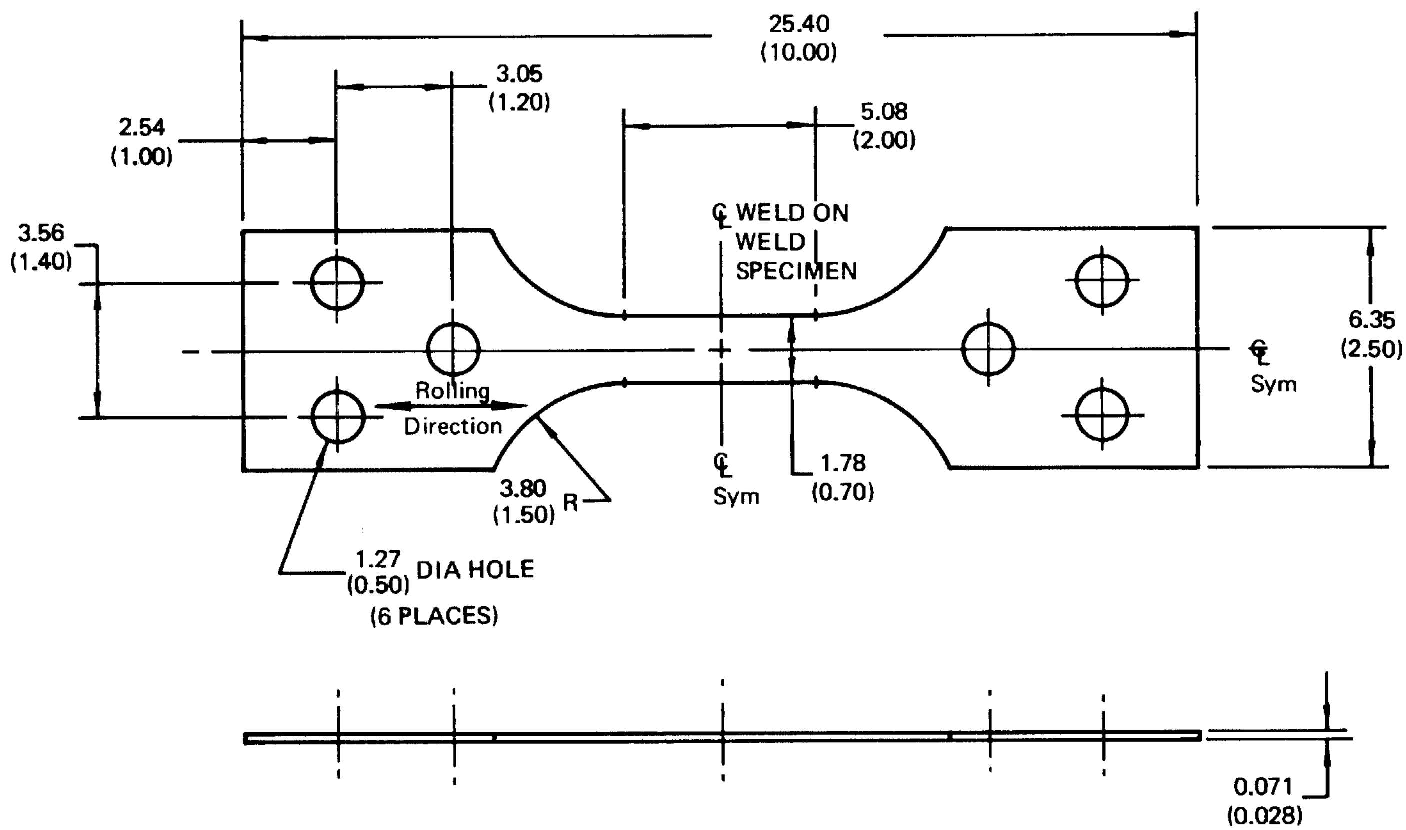

DIMENSIONS GIVEN IN CENTIMETERS (INCHES)

WELD BEAD MACHINED FLUSH ON WELDED SPECIMEN

Figure 24 : Cryostretched 301 Stainless Steel "Thin" Fracture Specimen (Base Metal and Weld Metal)

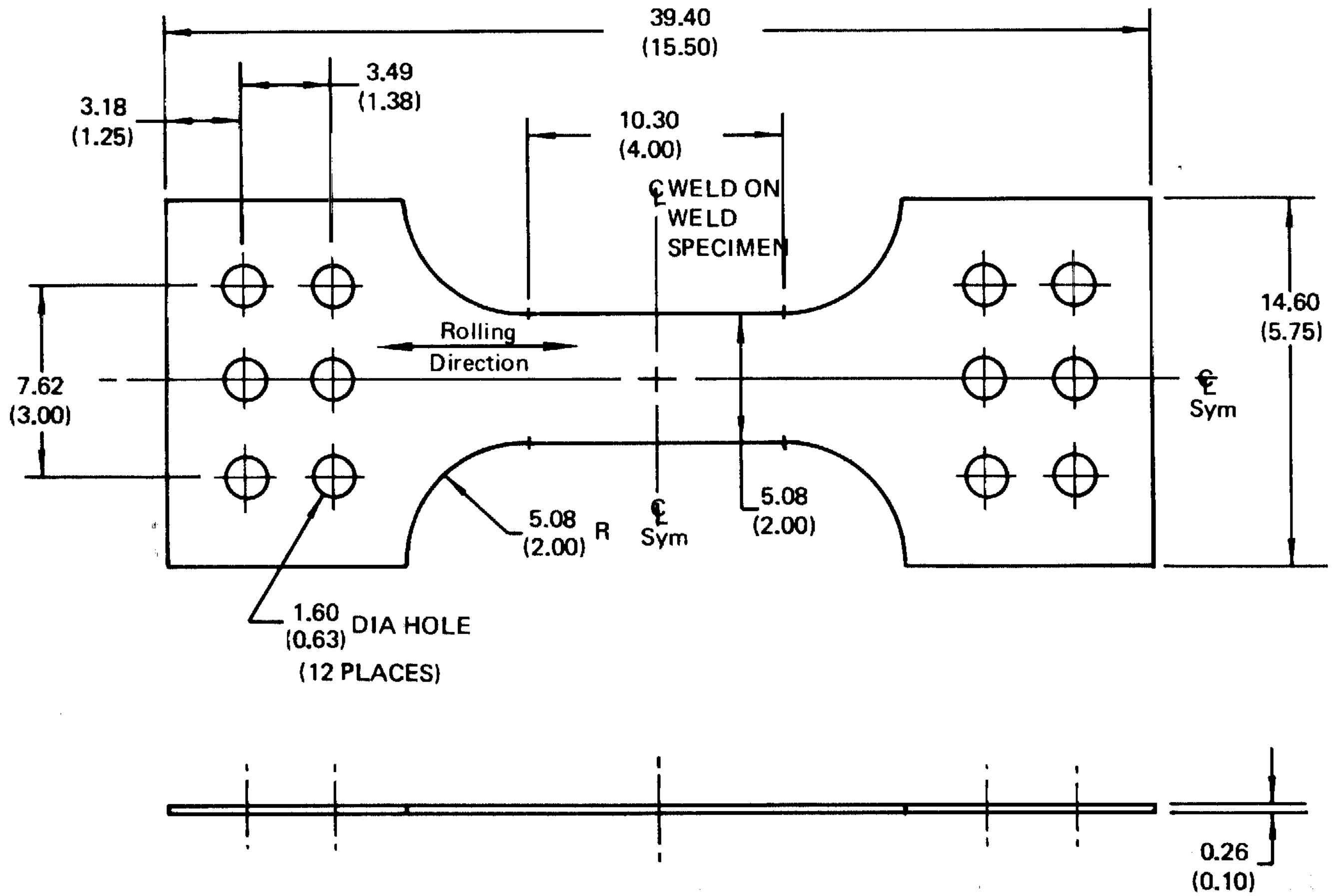

DIMENSIONS GIVEN IN CENTIMETERS (INCHES)

WELD BEAD MACHINED FLUSH ON WELDED SPECIMEN

Figure 25 : Cryostretched 301 Stainless Steel " Thick" Fracture Specimen (Base Metal and Weld Metal)

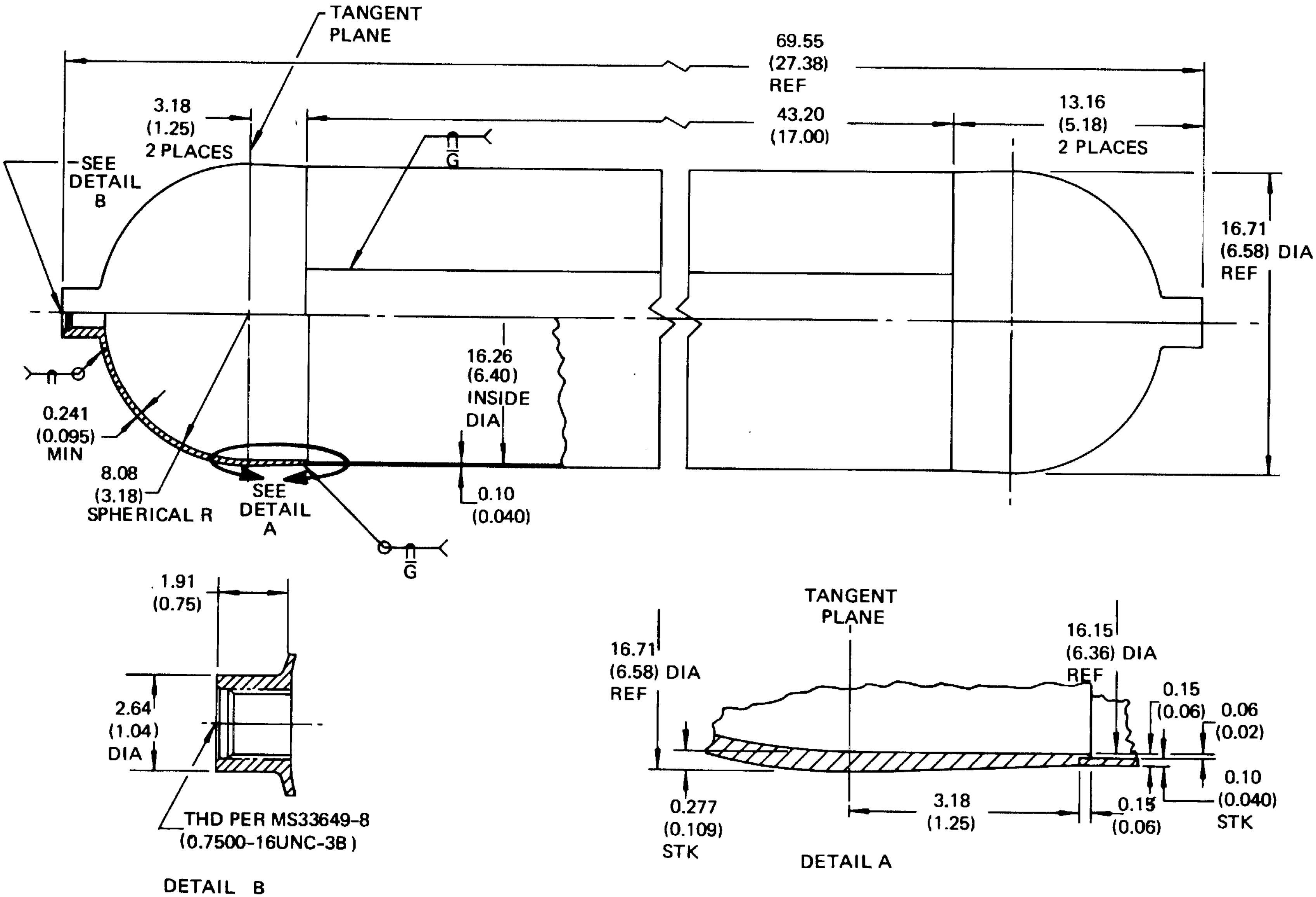

NOTE: DIMENSIONS IN CENTIMETERS (INCHES)

Figure 26 : Inconel Metal Liner

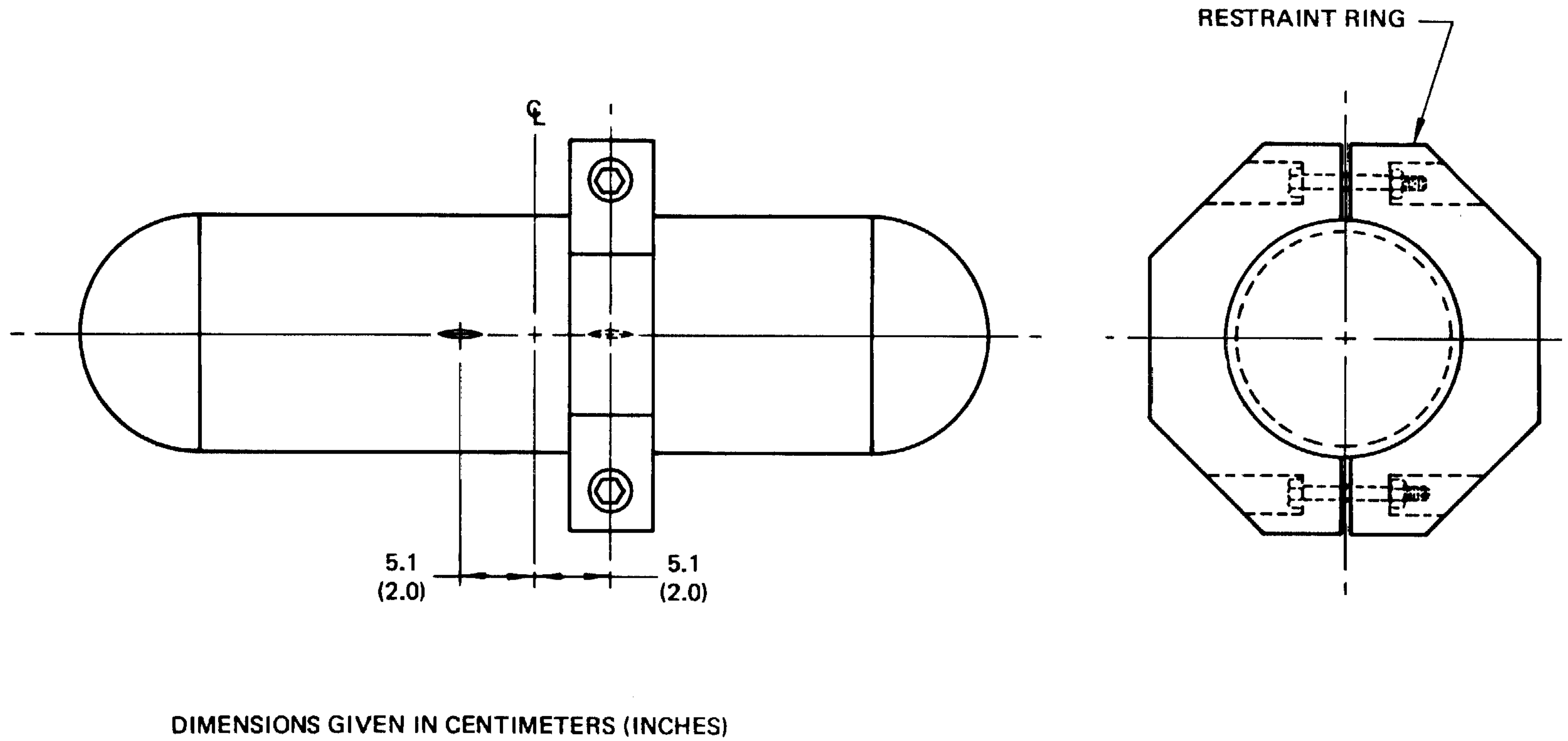

Figure 27: Restraint Ring Installation for Precracking Two Flaws in One Metal Shell

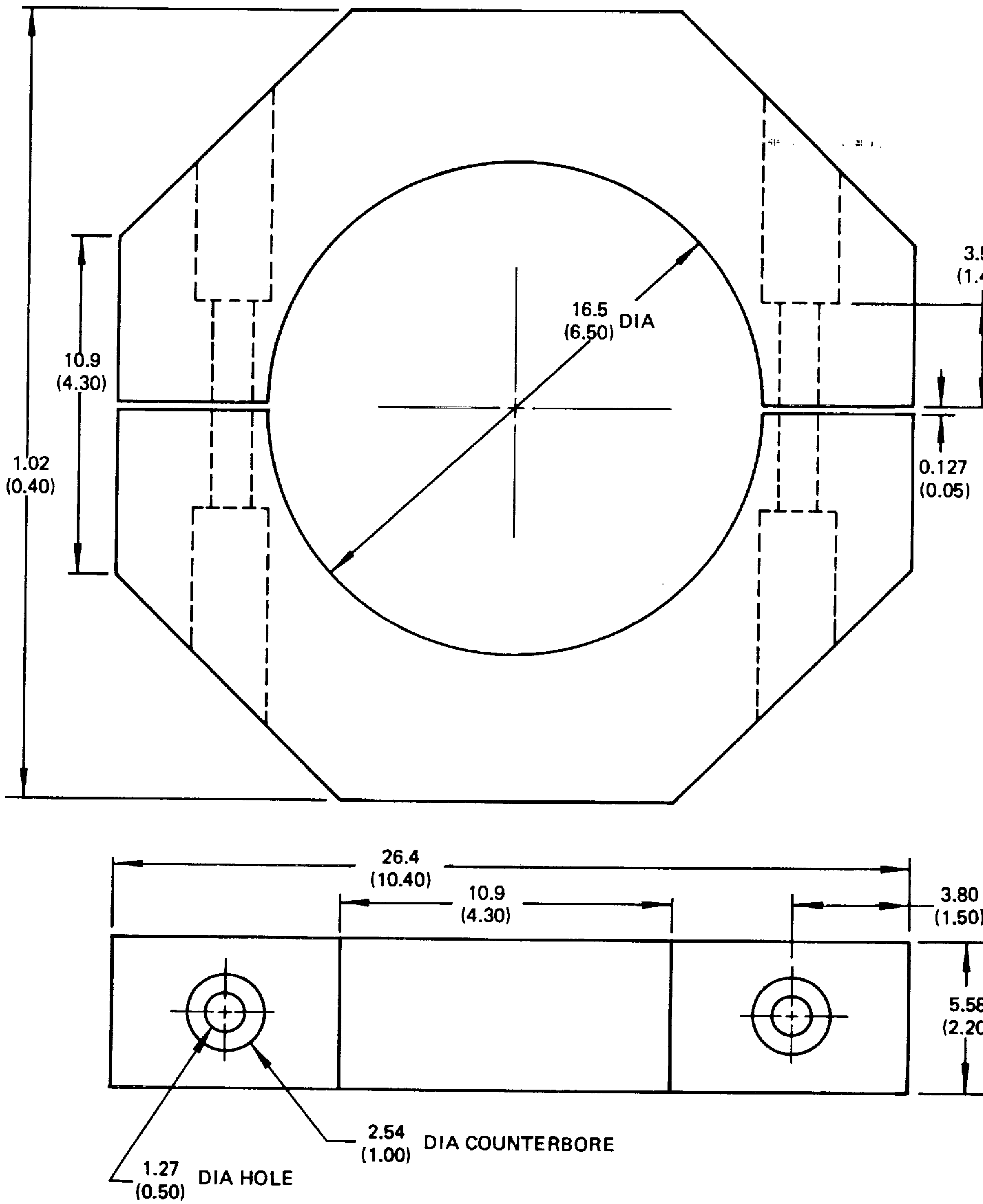

DIMENSIONS GIVEN IN CENTIMETERS (INCHES)
MATERIAL: 7075-T6 ALUMINUM

Figure 28: Hoop Restraint Ring

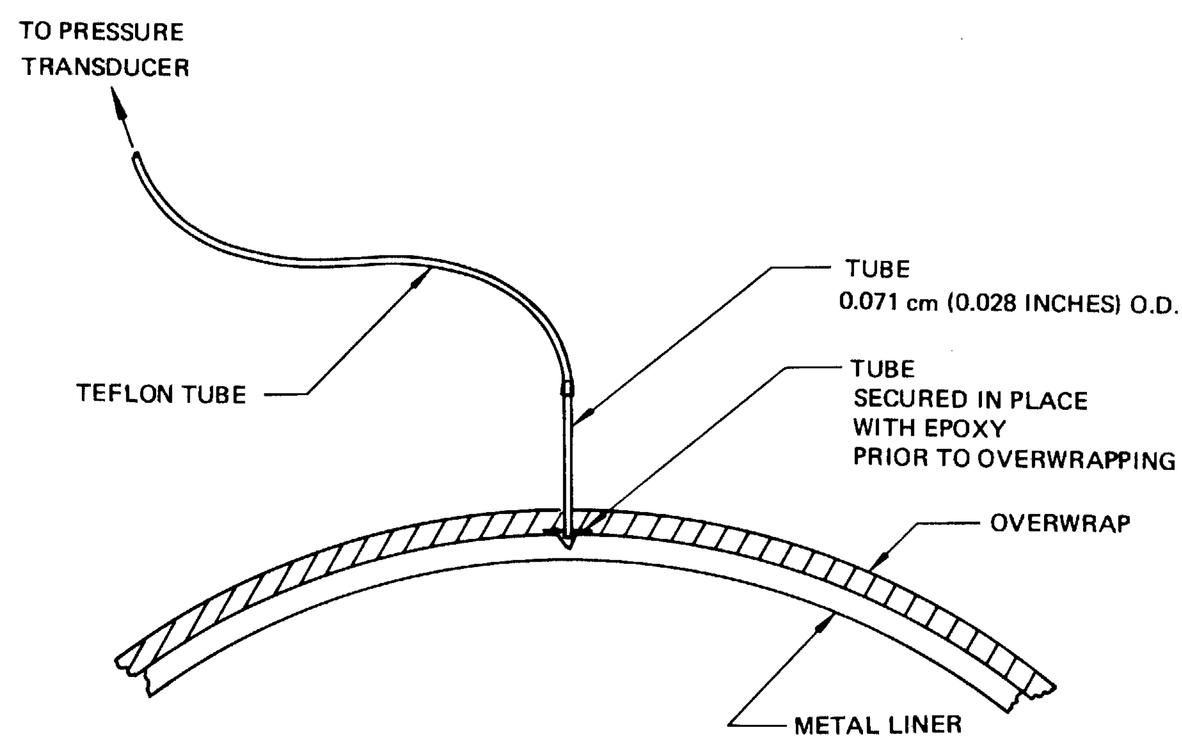

CROSS SECTION OF OVERWRAPPED TANK

Figure 29 : Flaw Breakthrough Detection Setup on Biaxial Specimens

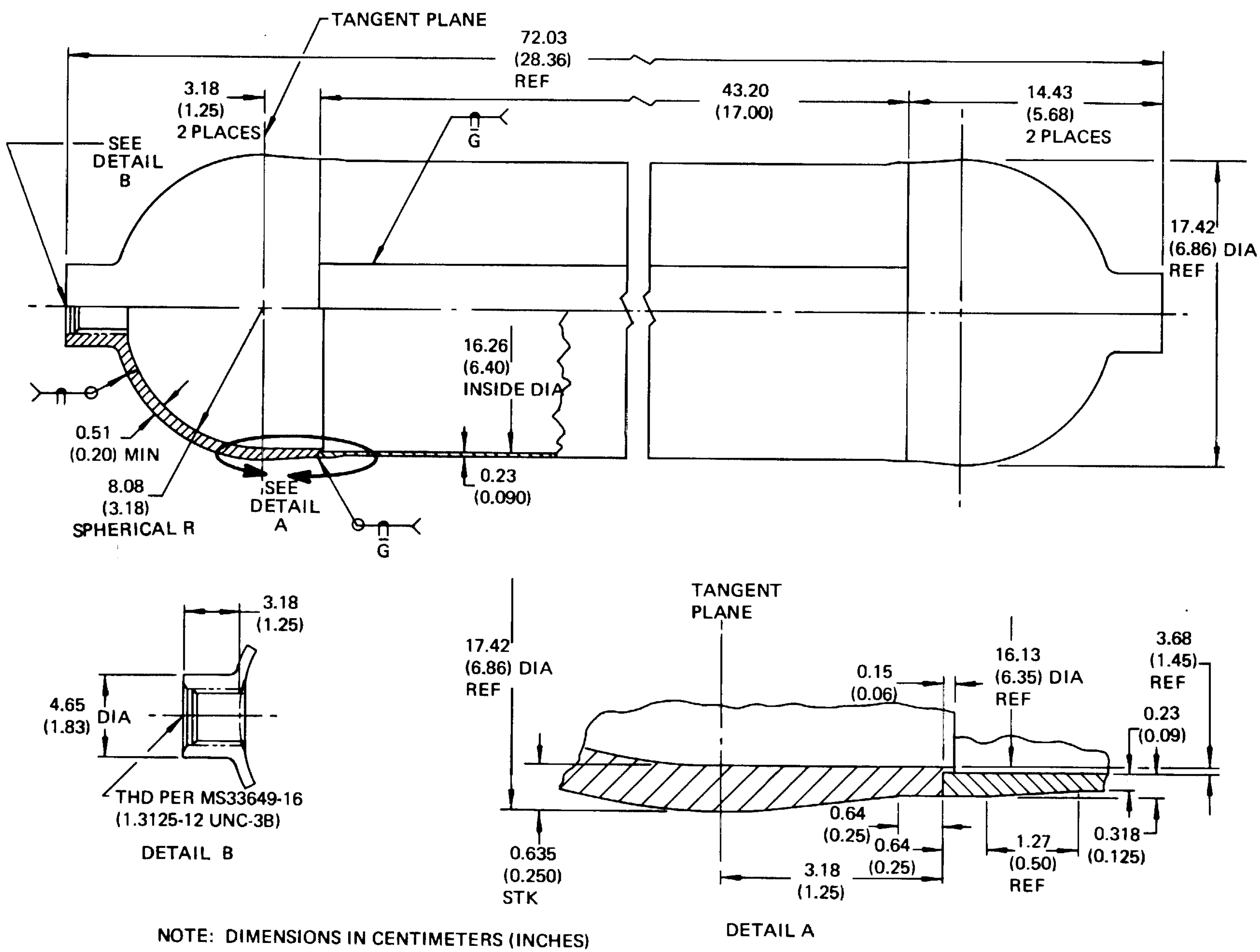

Figure 30 : Aluminum Metal Liner

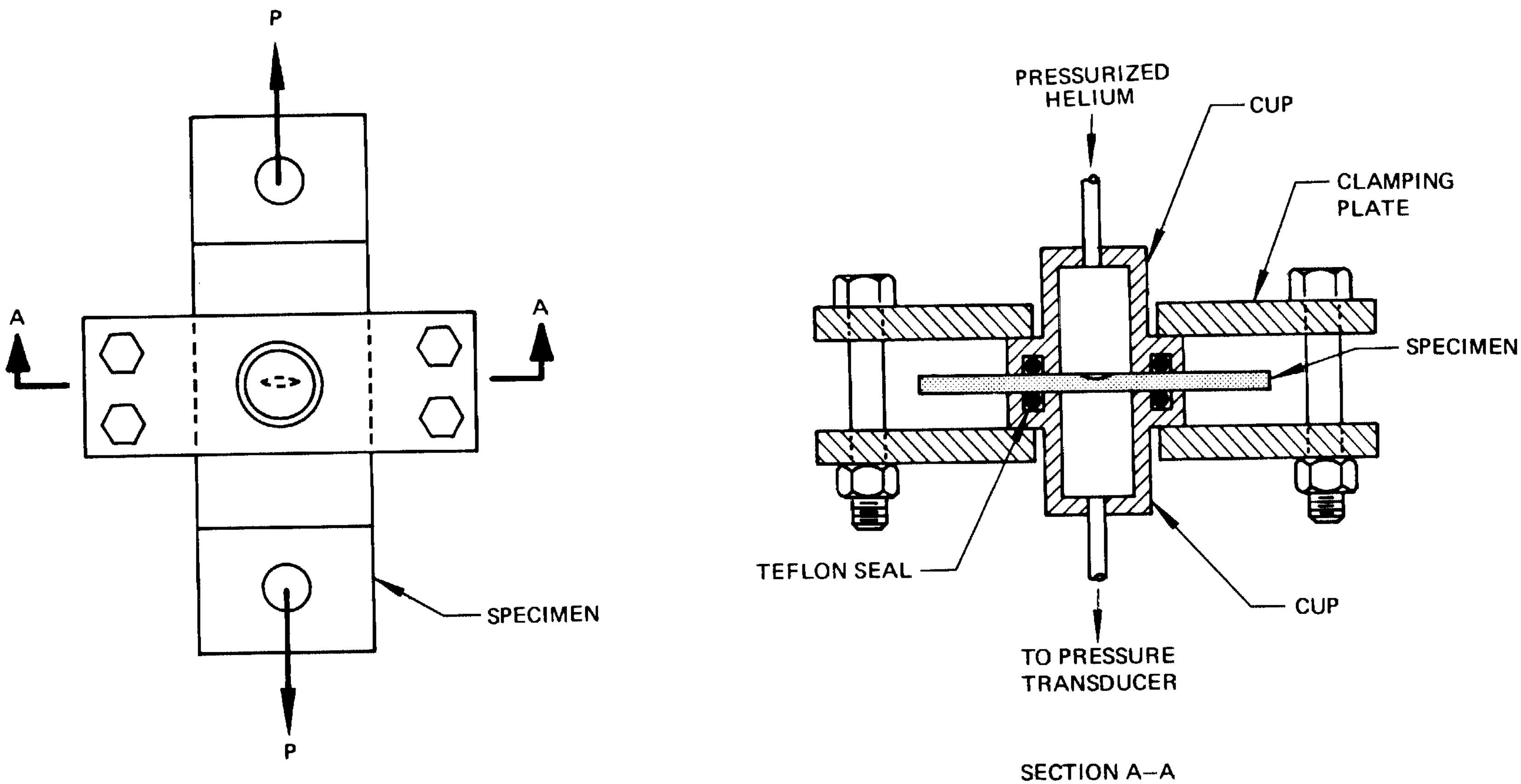

Figure 31: Pressure Cups Used for Flaw Breakthrough Detection on Uniaxial Specimens

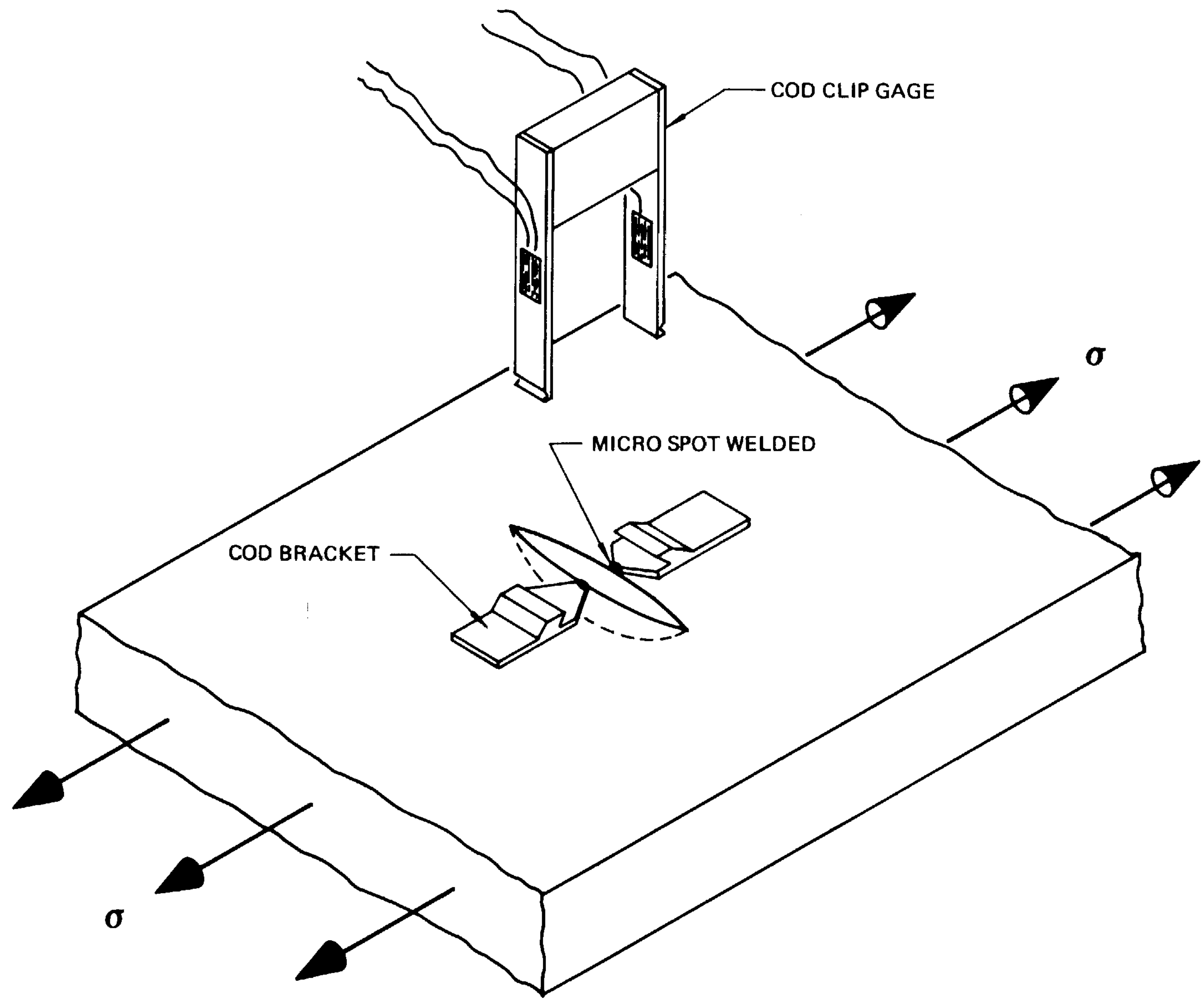

Figure 32: Clip Gage Instrumentation for Small Surface Flaws

Figure 33 : RT Tank Test Setup

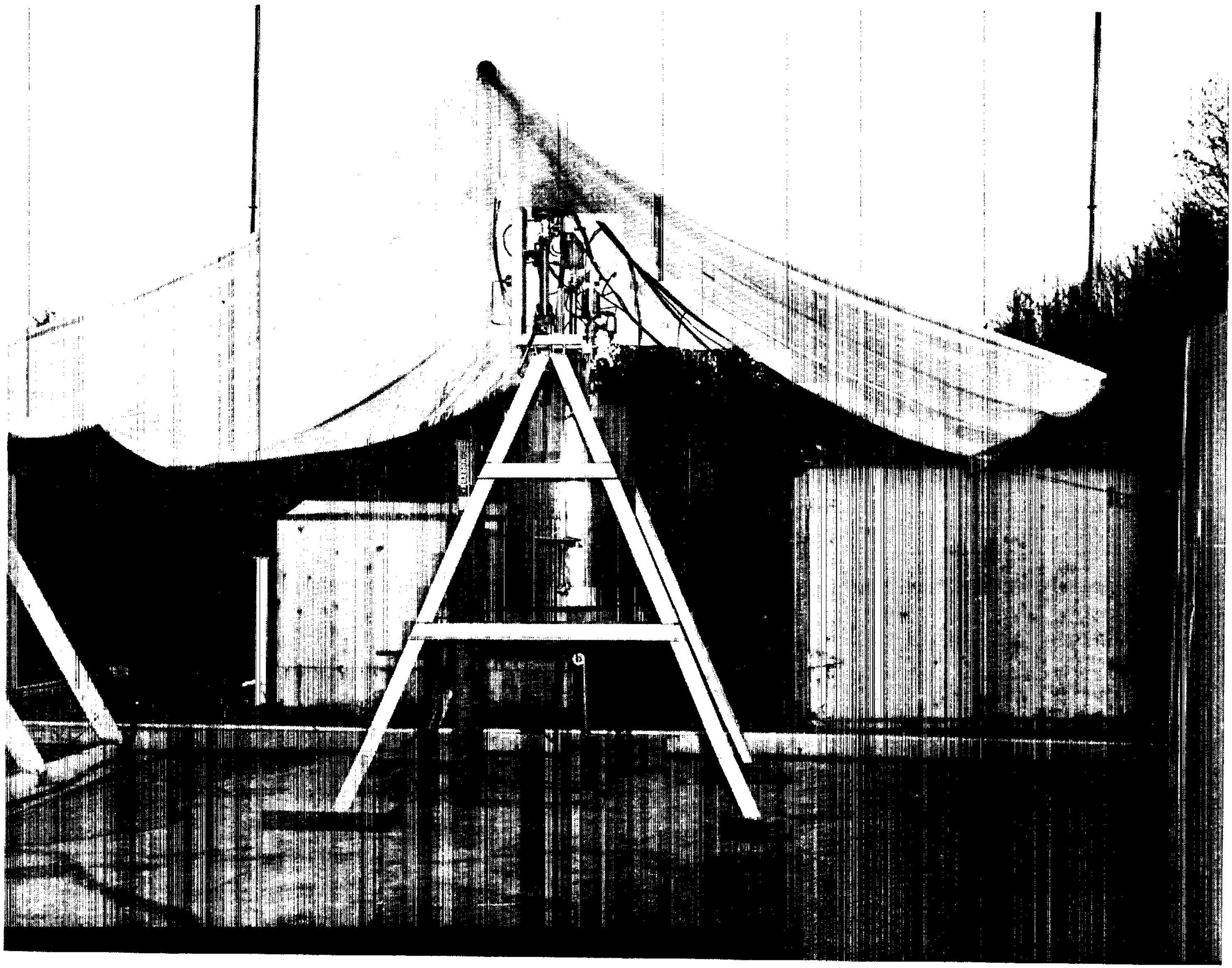

Figure 34 : Cryogenic Tank Test Setup

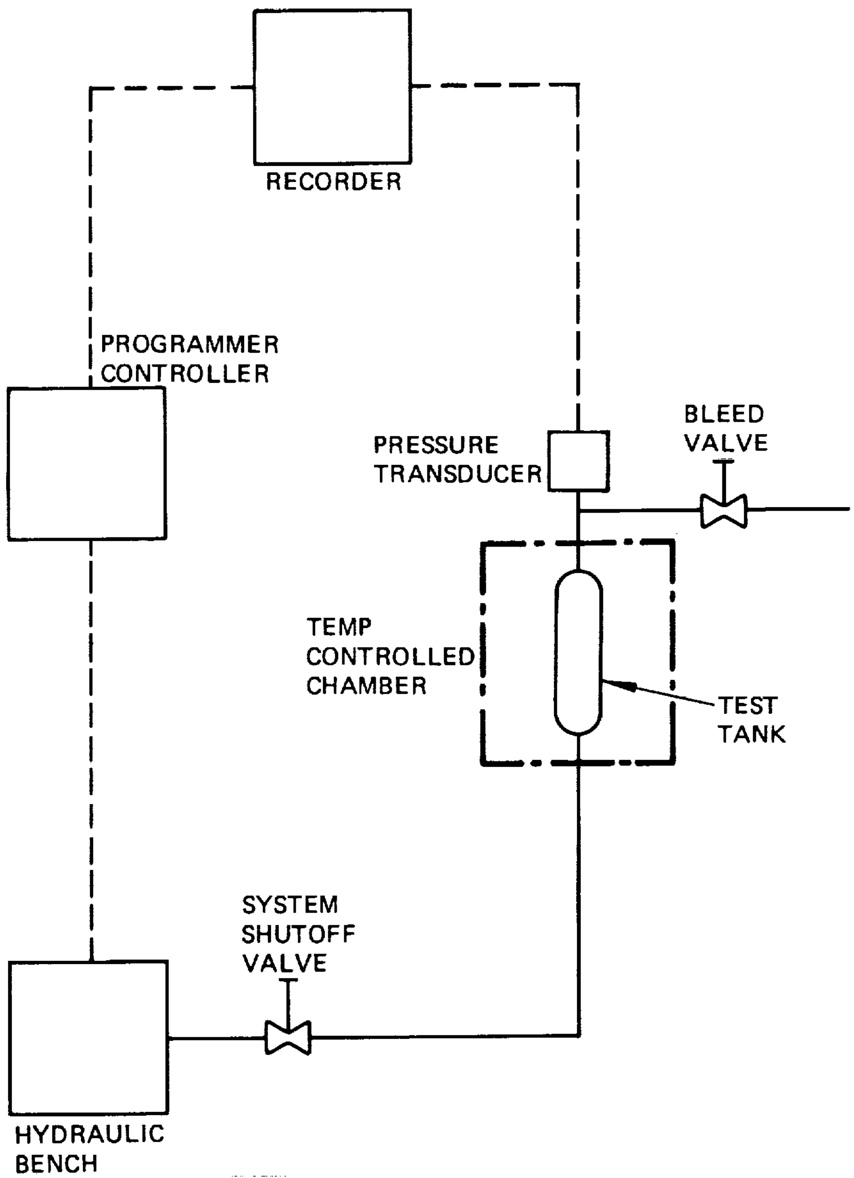

Figure 35 : Ambient Pressure Test System

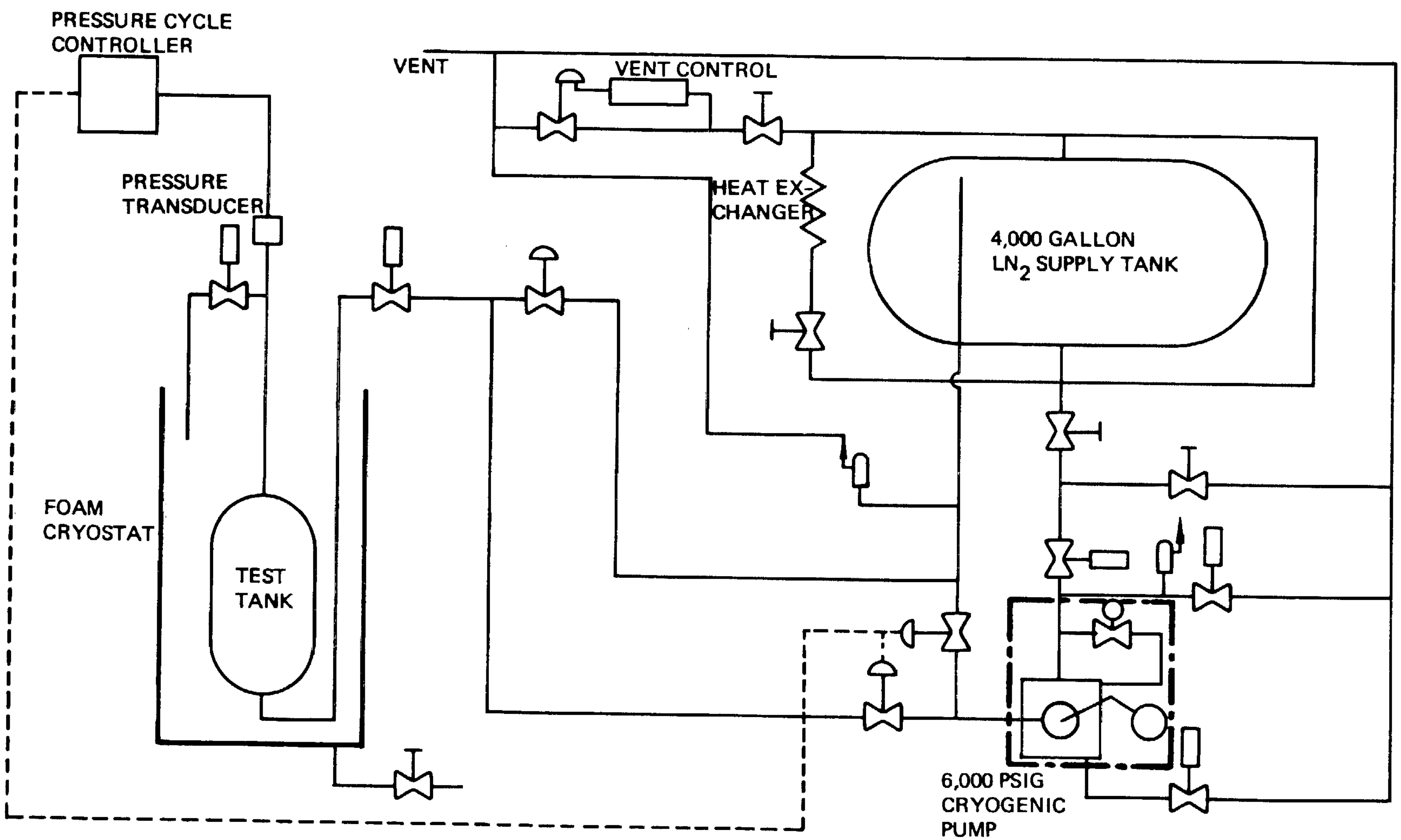

Figure 36 : LN_2 Tank Pressure Test System

Figure 37 : Hypodermic Needle Installation

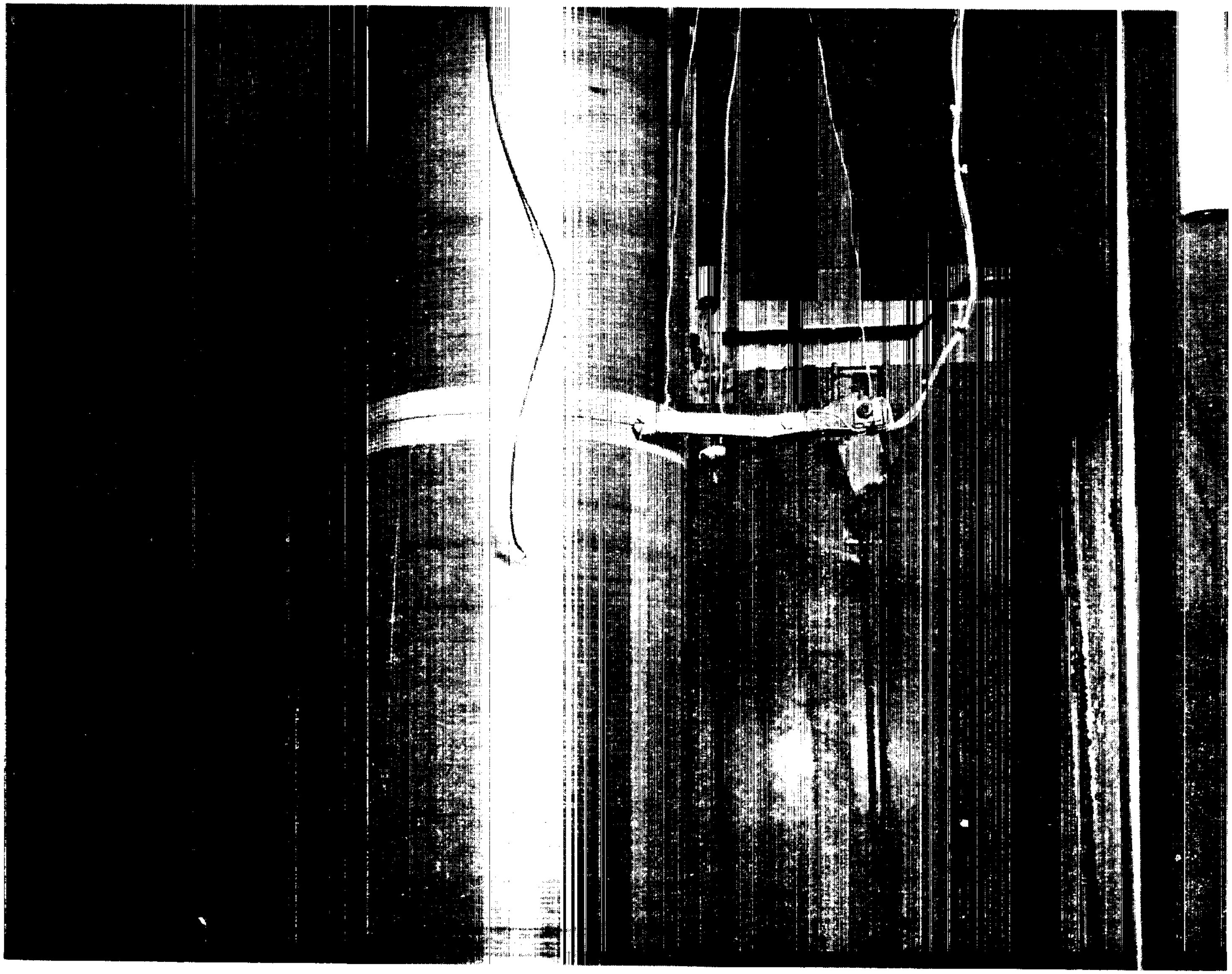

Figure 38 : Hoop Displacement Measurement Device

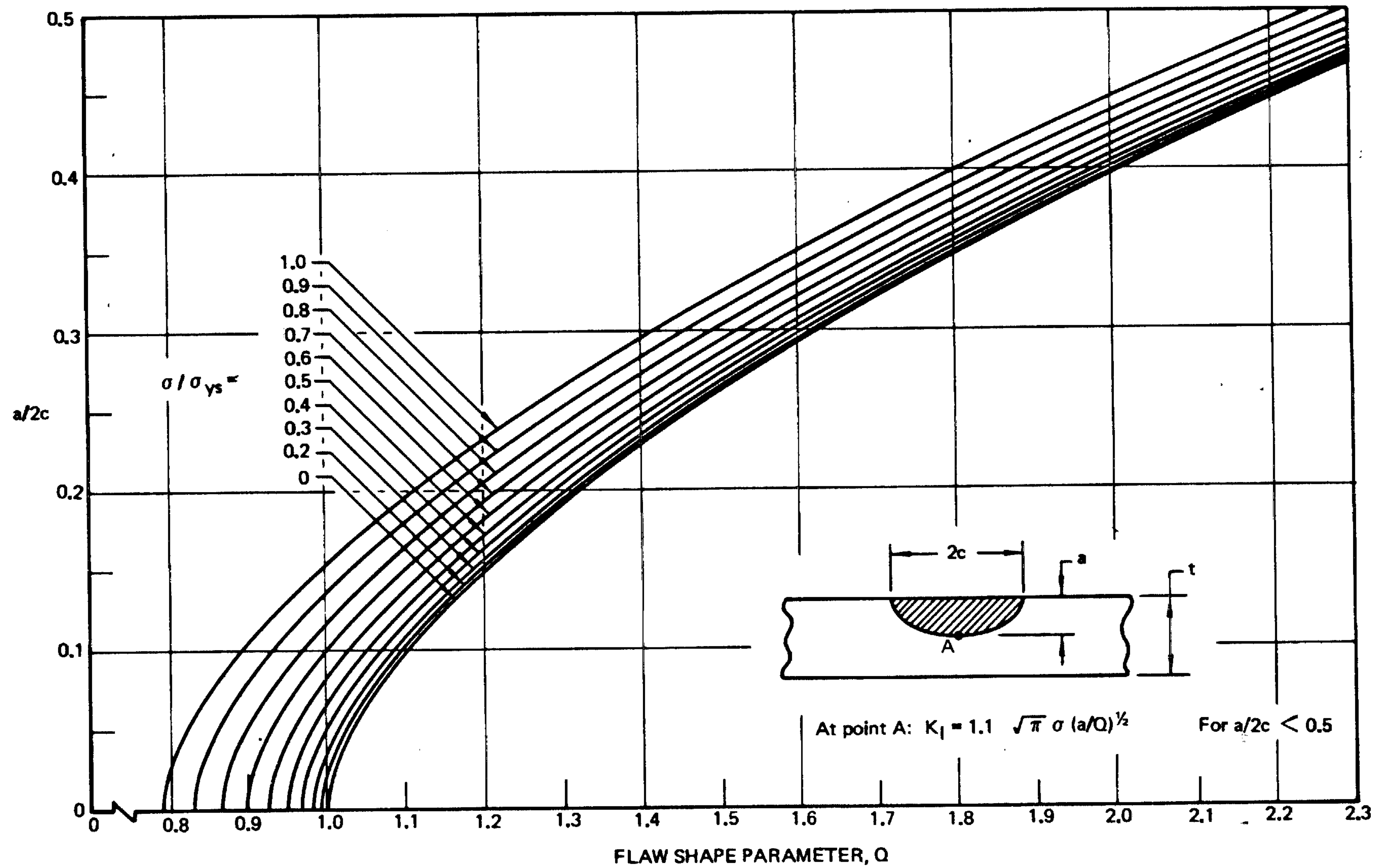

Figure 39 : Shape Parameter Curves for Surface and Internal Flaws

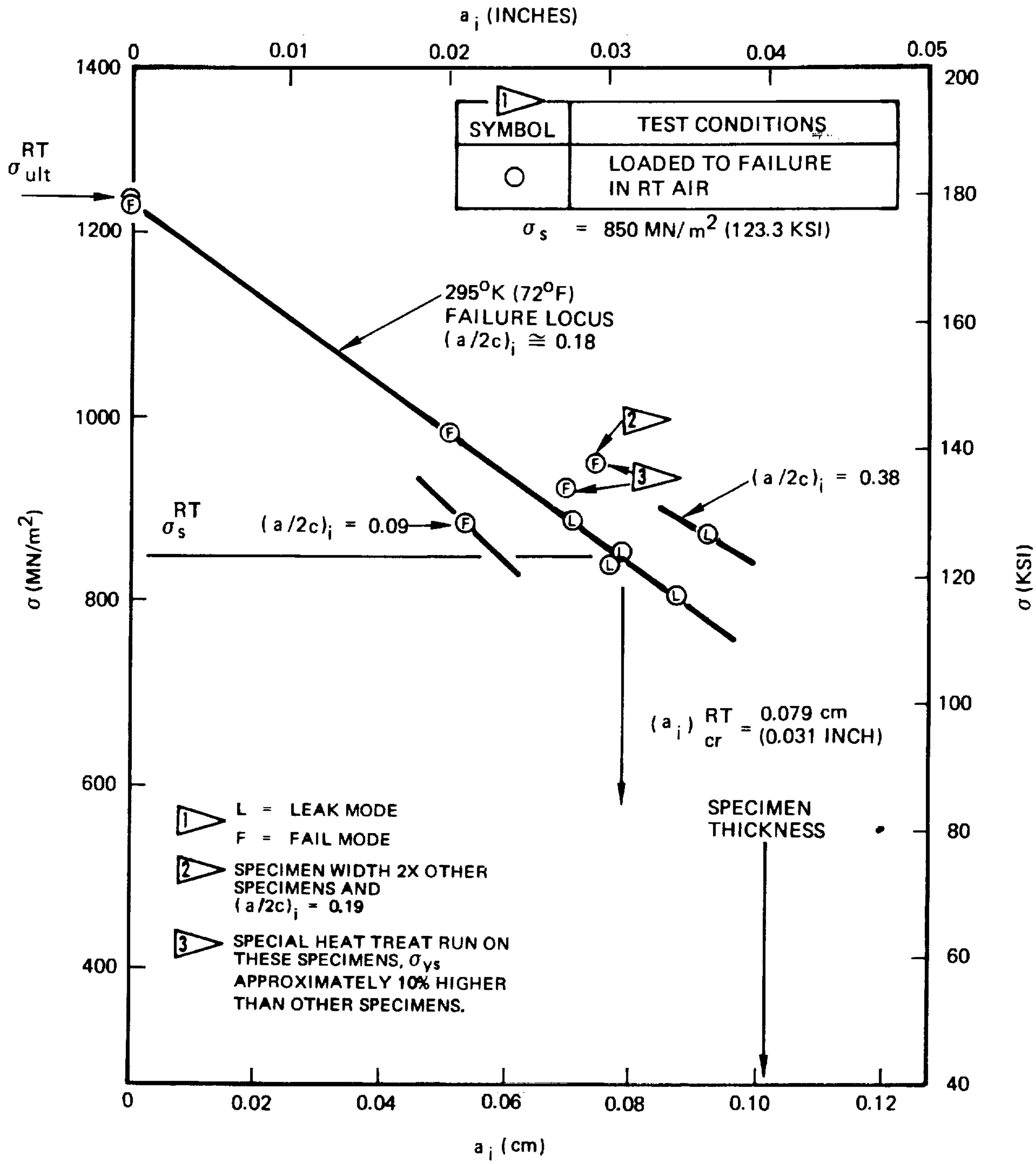

Figure 40: Uniaxial Static Fracture Results of 0.10 cm (0.040 Inch) Thick Surface Flawed Inconel X750 STA Base Metal at 295°K (72°F)

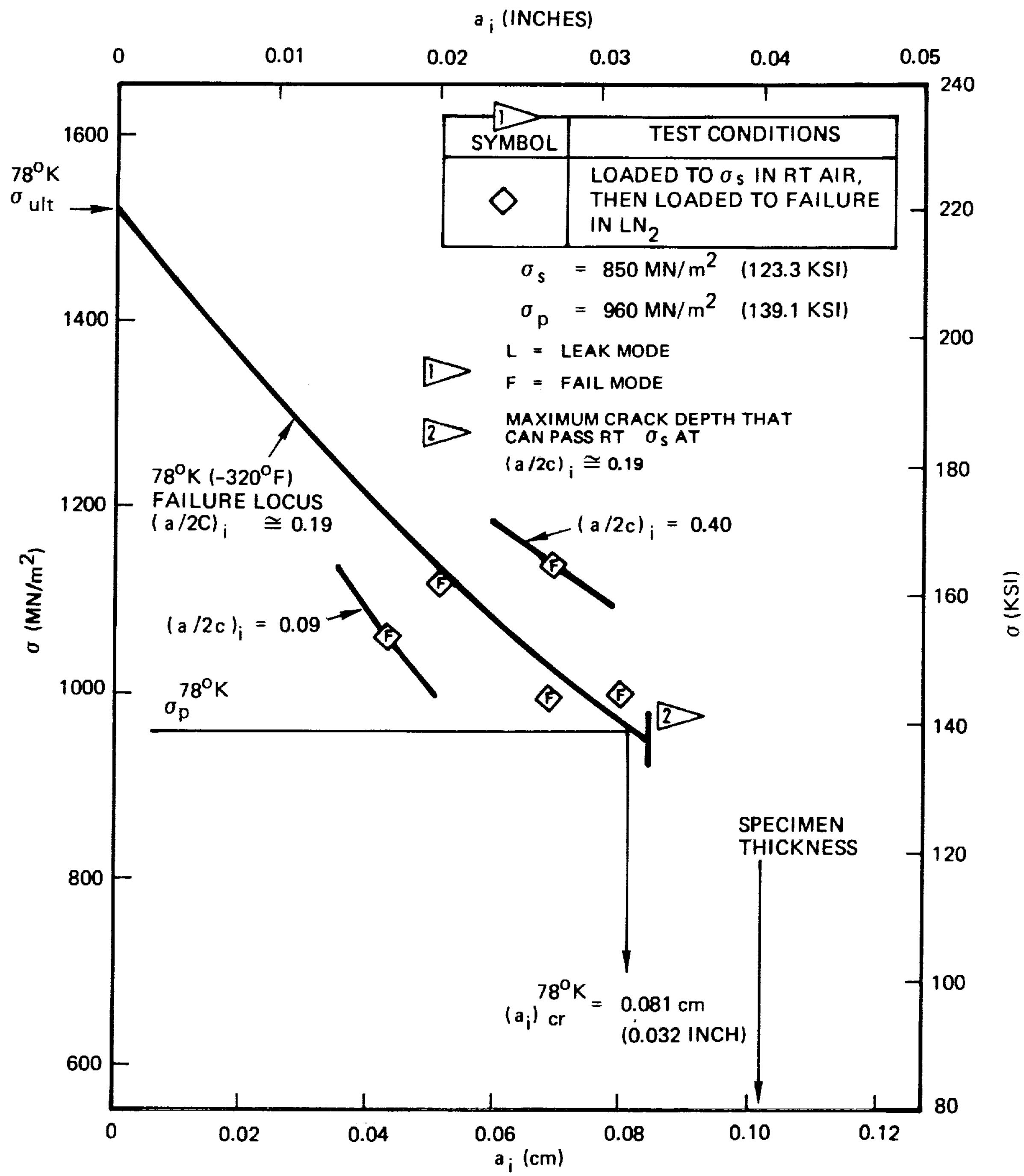

Figure 41: Uniaxial Static Fracture Results of 0.10 cm (0.040 Inch) Thick Surface Flawed Inconel X750 STA Base Metal at 78°K (-320°F)

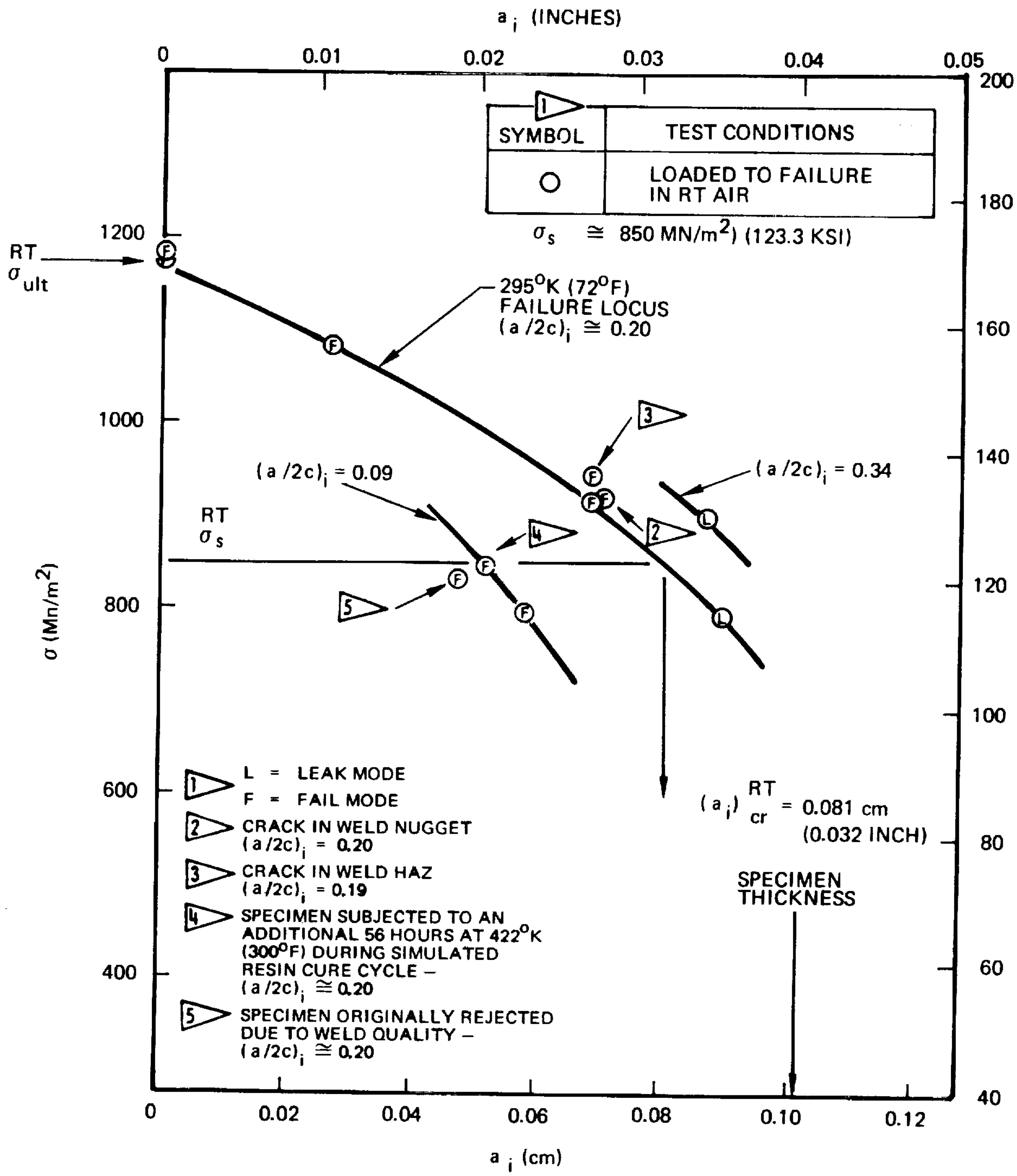

Figure 42: Uniaxial Static Fracture Results of 0.10 cm (0.040 Inch) Thick Surface Flawed Inconel X750 STA Weld Metal ℄ at 295°K (72°F)

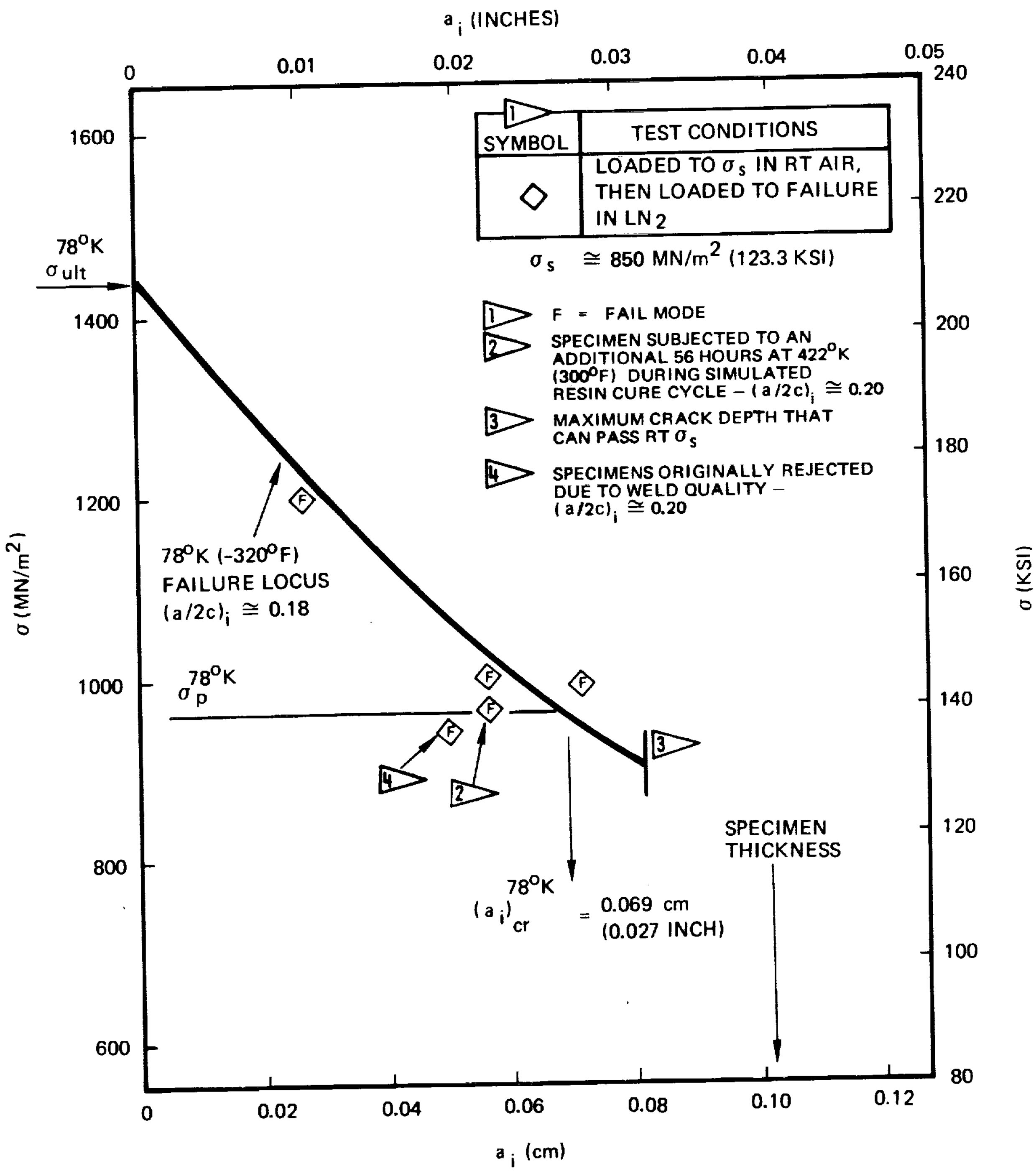

Figure 43: Uniaxial Static Fracture Results of 0.10 cm (0.040 Inch) Thick Surface Flawed Inconel X750 STA Weld Metal ℄ at 78° K (-320° F)

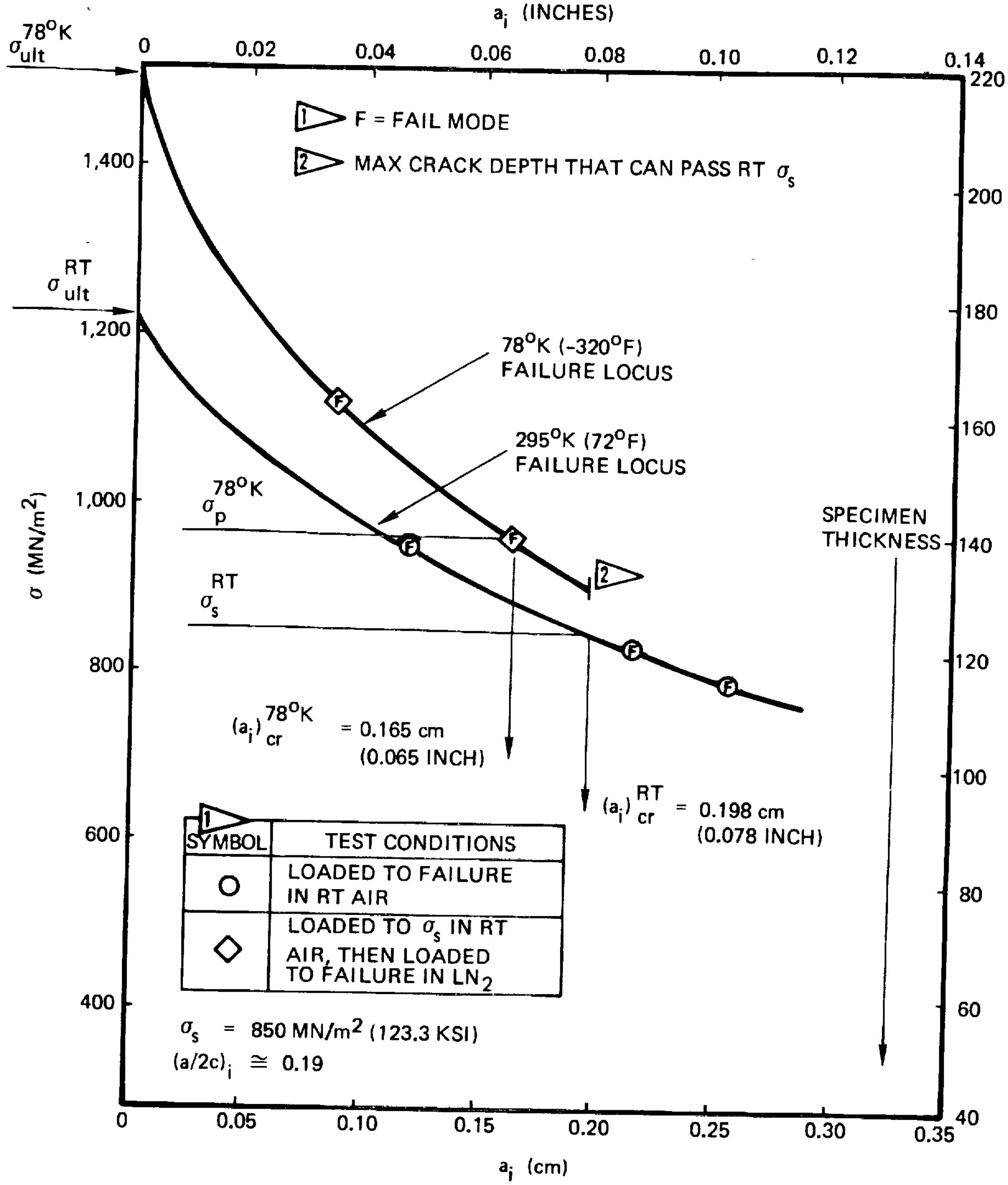

SYMBOL	TEST CONDITIONS
○	LOADED TO FAILURE IN RT AIR
◇	LOADED TO σ_s IN RT AIR, THEN LOADED TO FAILURE IN LN_2

Figure 44: Uniaxial Static Fracture Results of 0.33 cm (0.13 Inch) Thick Surface Flawed Inconel X750 STA Base Metal

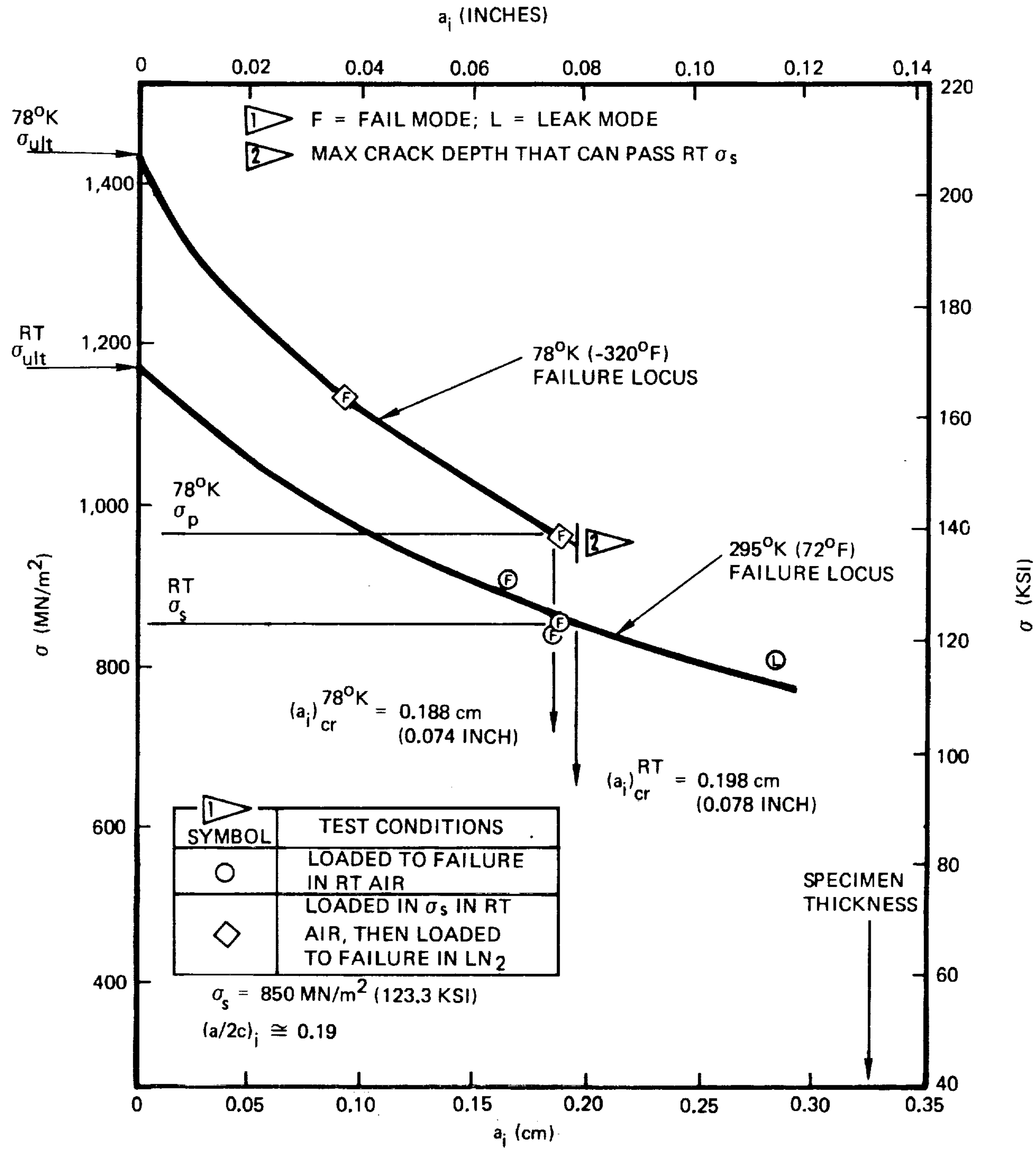

Figure 45: Uniaxial Static Fracture Results of 0.33 cm (0.13 Inch) Thick Surface Flawed Inconel X750 STA Weld Metal ℄

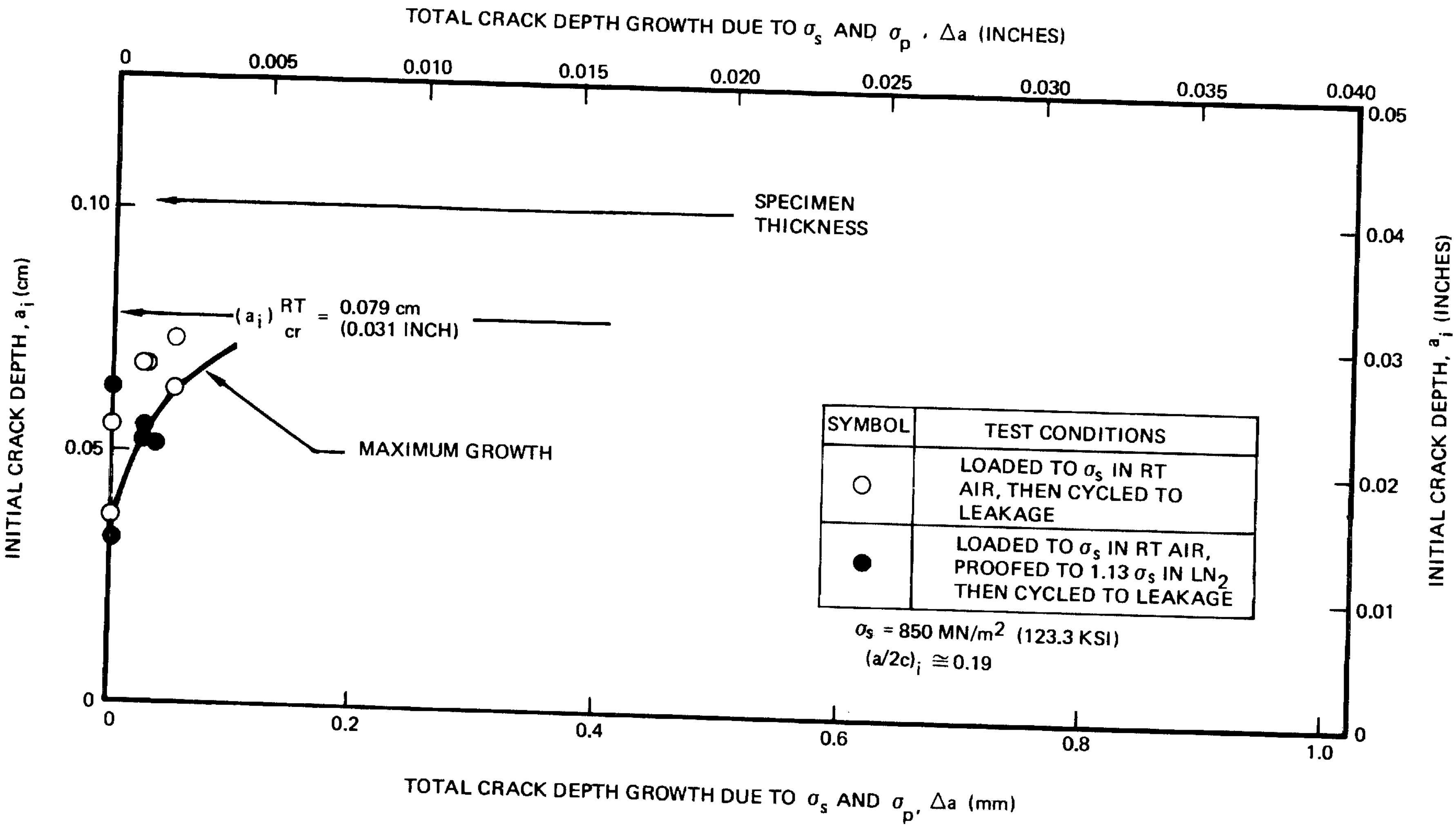

Figure 46: Growth-On-Loading Results of 0.10 cm (0.040 Inch) Thick Surface Flawed Inconel X750 STA Base Metal

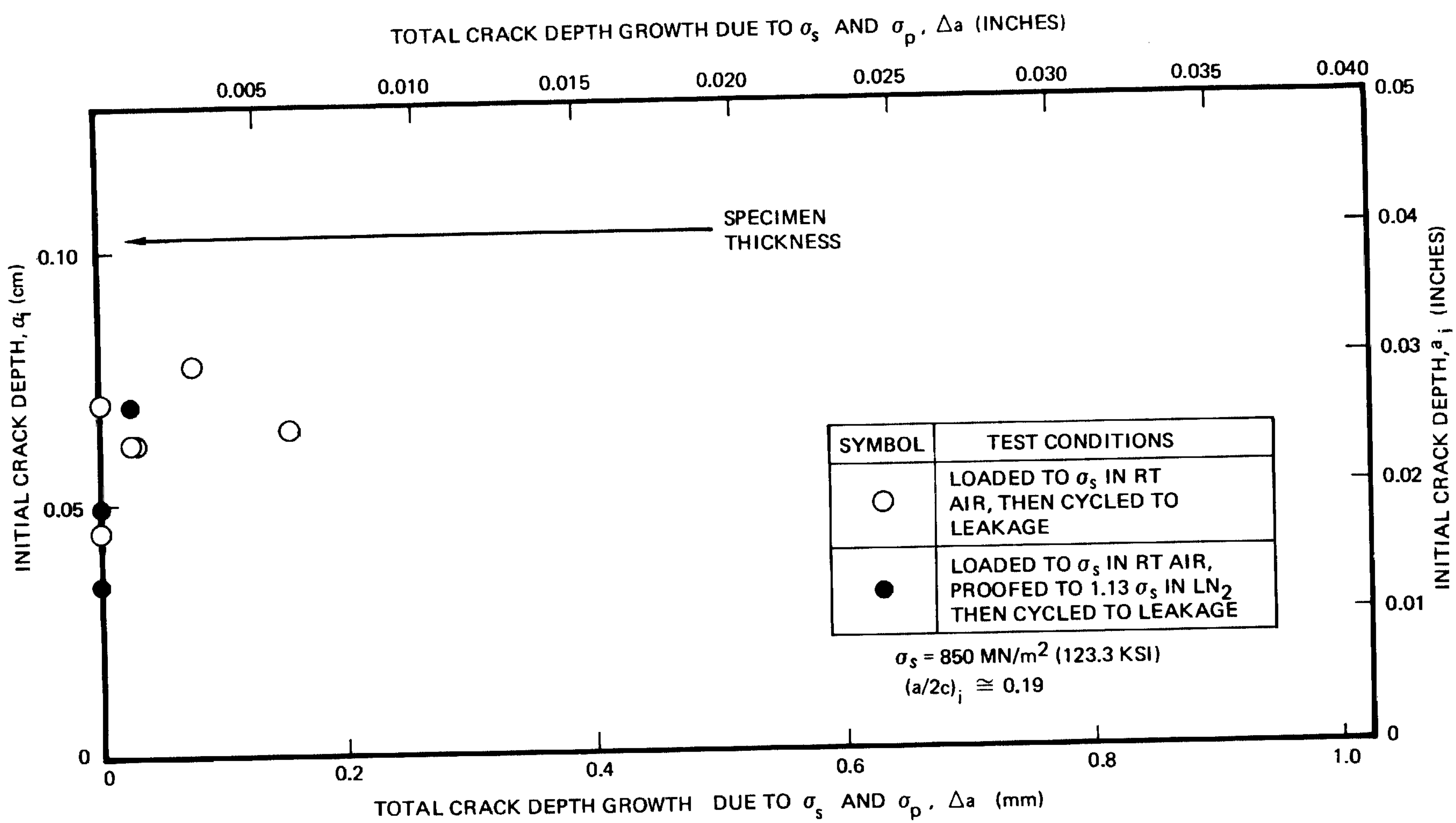

Figure 47: Growth-On-Loading Results of 0.10 cm (0.040 Inch) Thick Surface Flawed Inconel X750 STA Weld Metal ℄

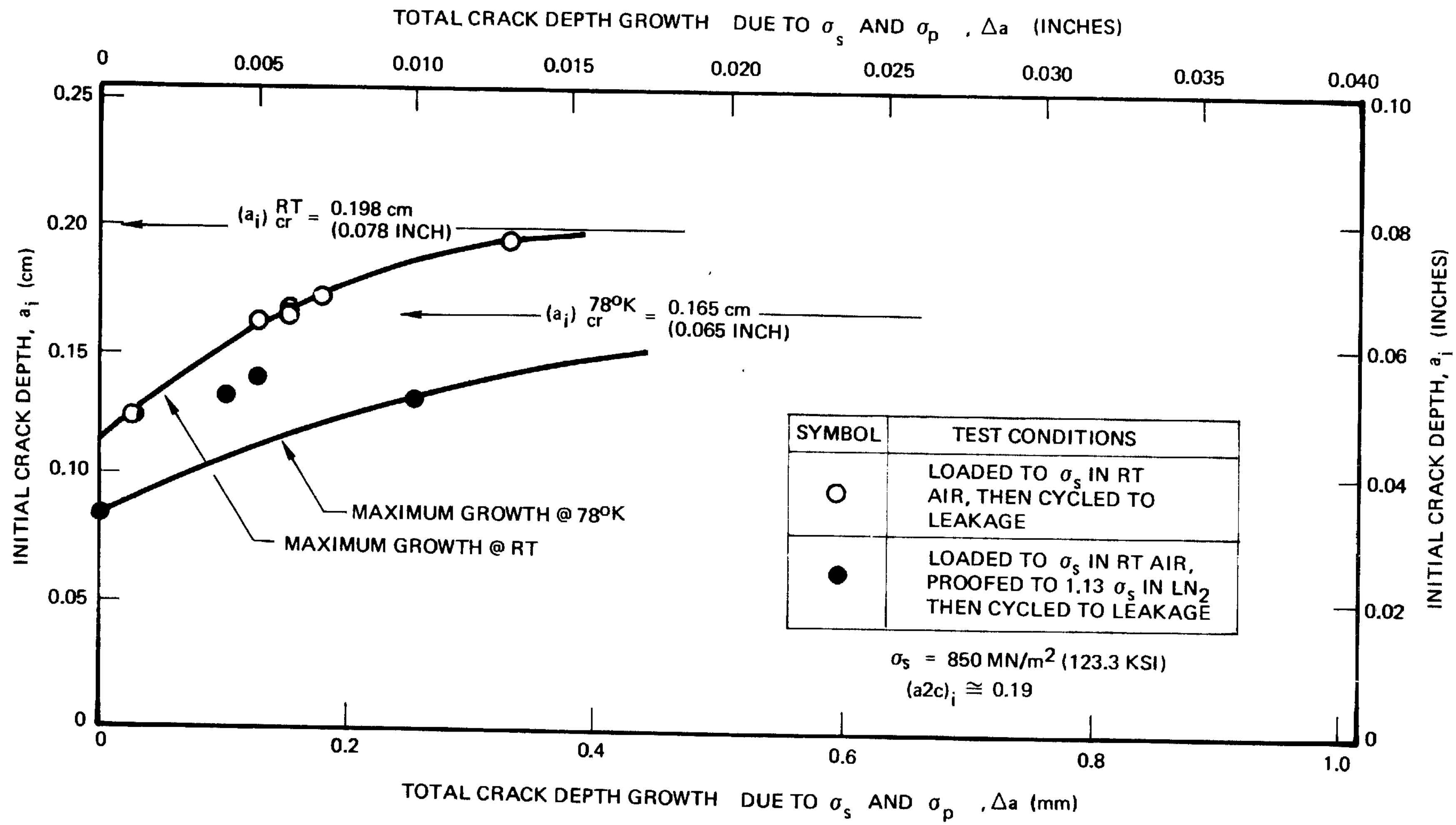

Figure 48: Growth-On-Loading Results of 0.33 cm (0.13 Inch) Thick Surface Flawed Inconel X750 STA Base Metal

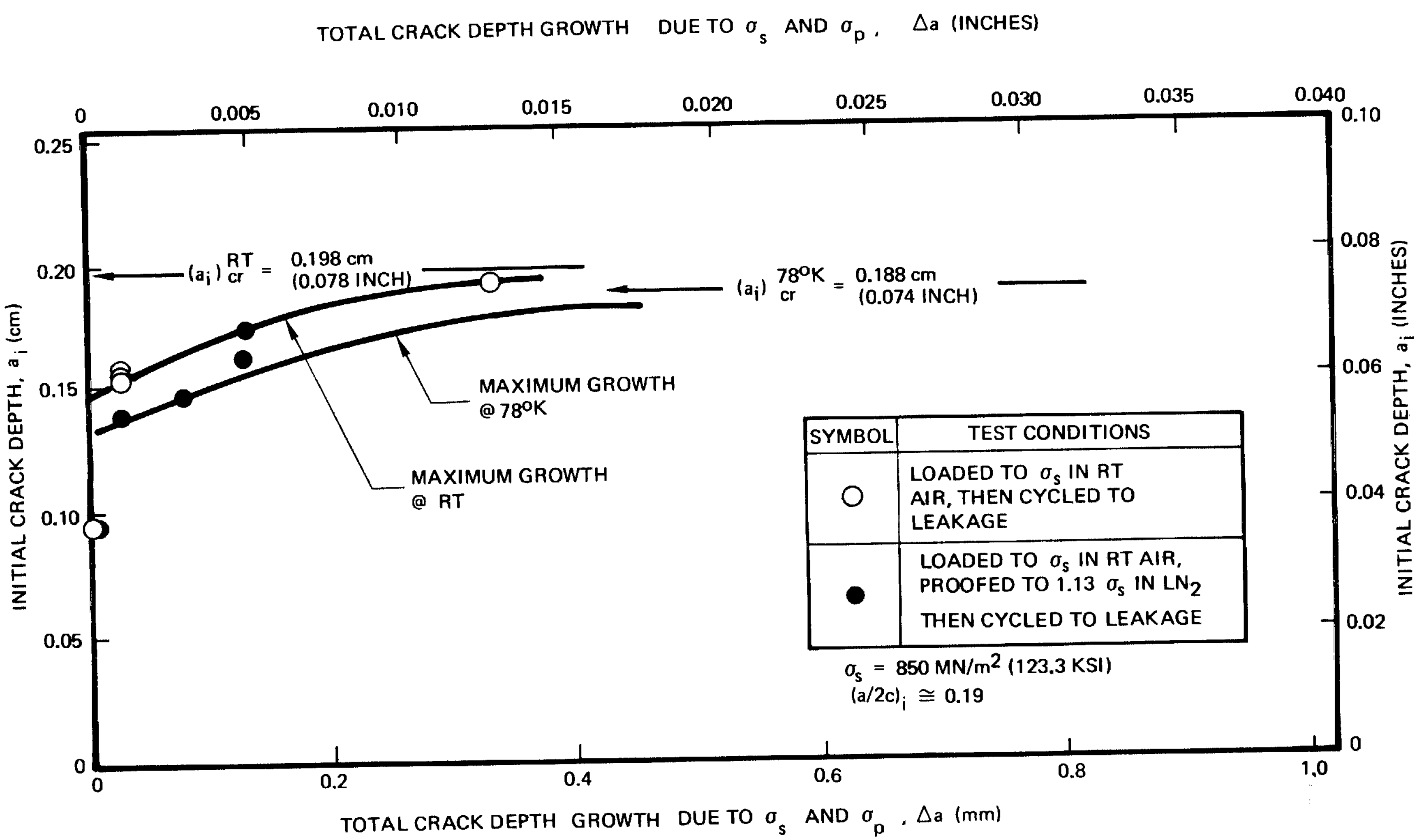

Figure 49: Growth-On-Loading Results of 0.33 cm (0.13 Inch) Thick Surface Flawed Inconel X750 STA Weld Metal ℄

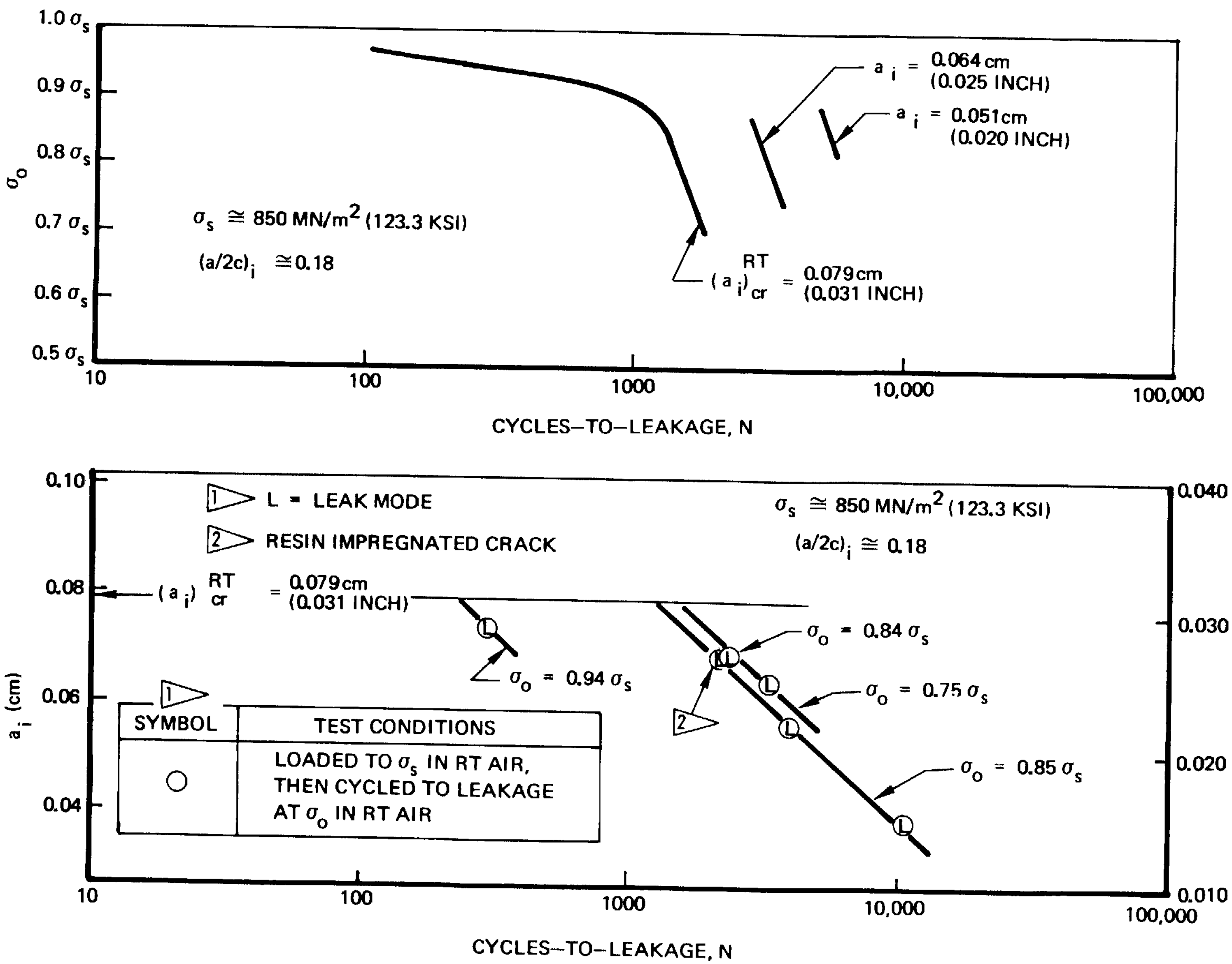

Figure 50: *Uniaxial Cyclic Life Results of 0.10cm (0.40 Inch) Thick Surface Flawed Inconel X750 STA Base Metal at 295°K (72°F)*

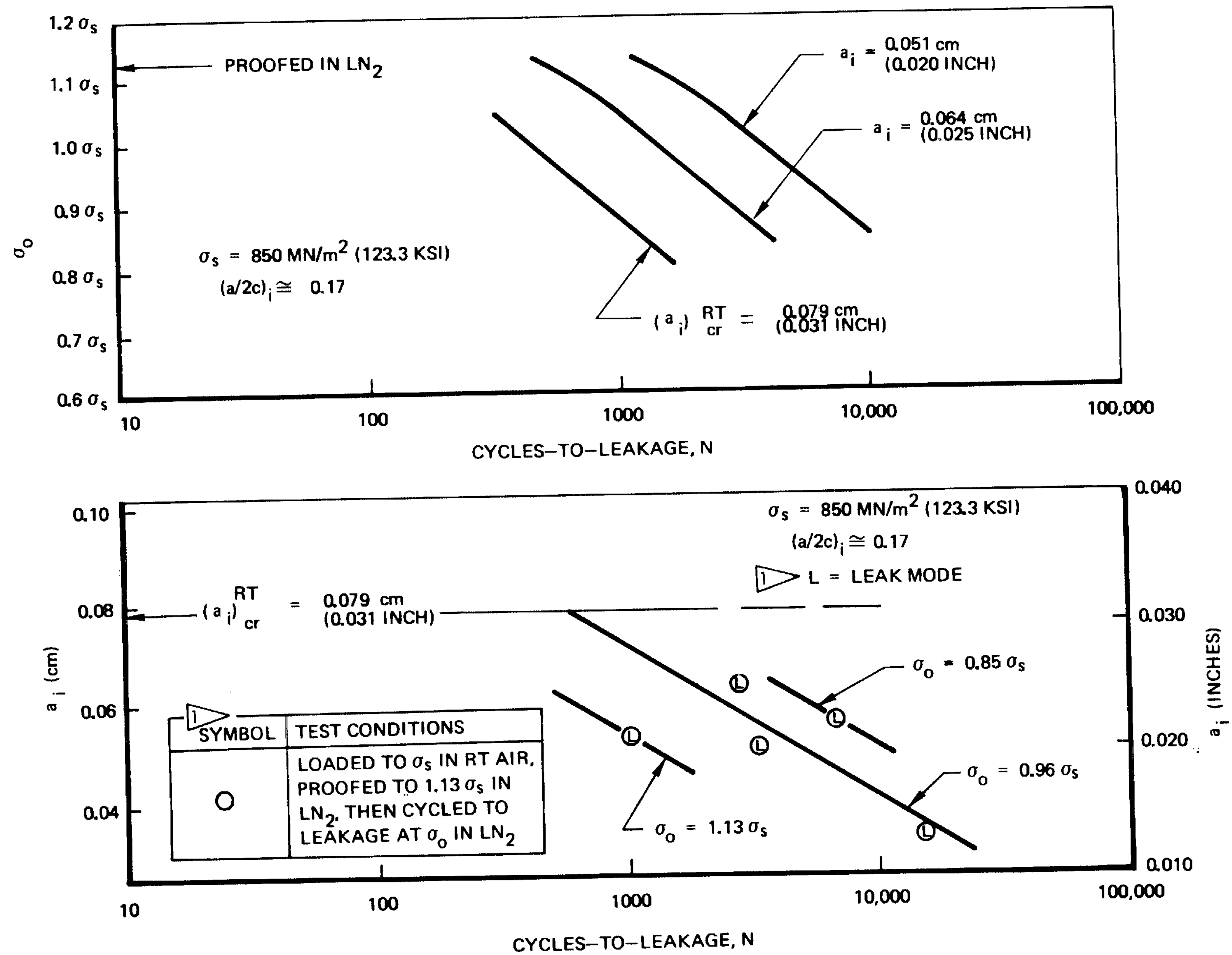

Figure 51: Uniaxial Cyclic Life Results of 0.10 cm (0.040 Inch) Thick Surface Flawed Inconel X750 STA Base Metal at 78^{0}K (-320^{0}F)

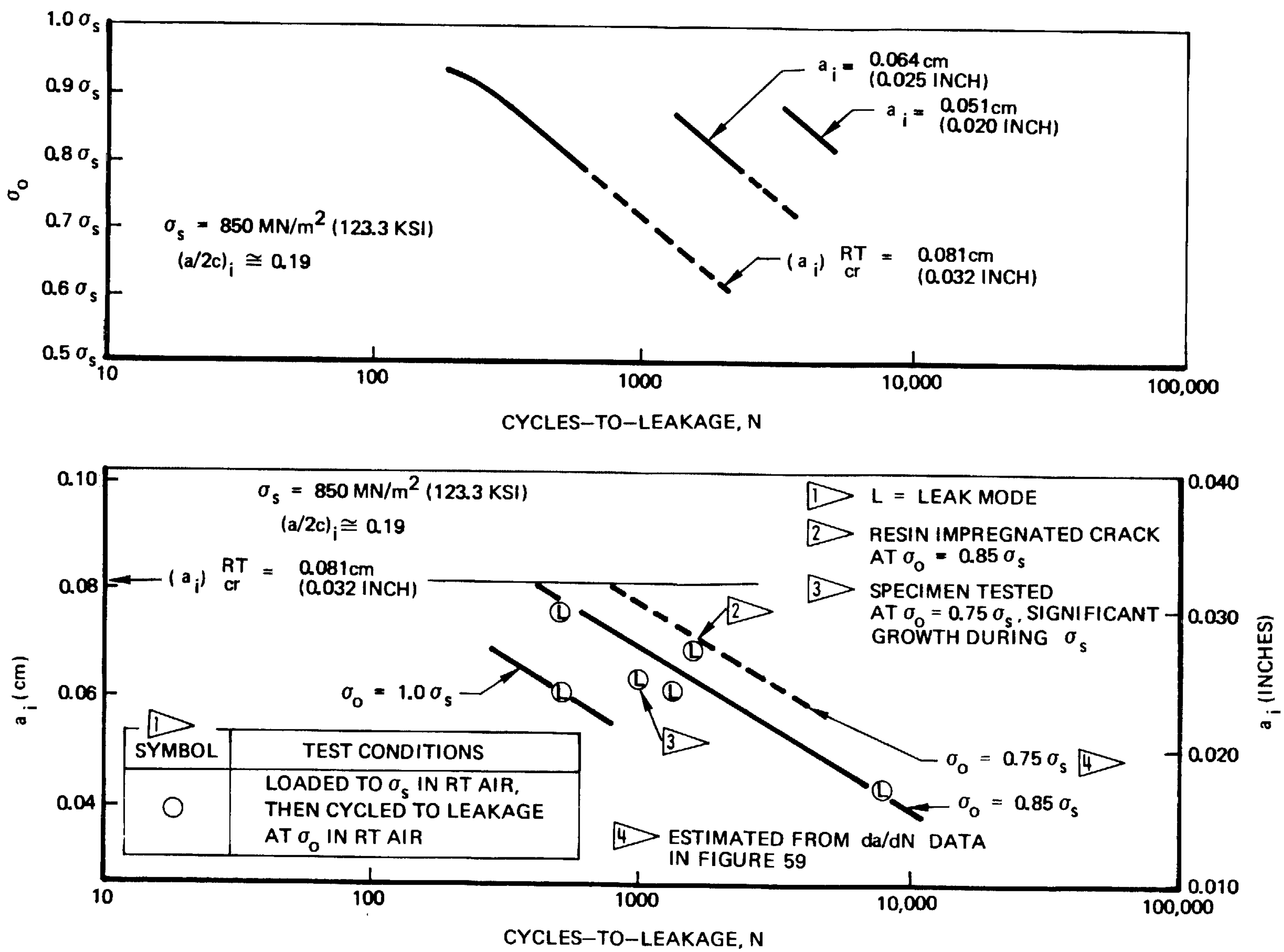

Figure 52: Uniaxial Cyclic Life Results of 0.10cm (0.040 Inch) Thick Surface Flawed Inconel X750 STA Weld Metal ℄ at 295°K (72°F)

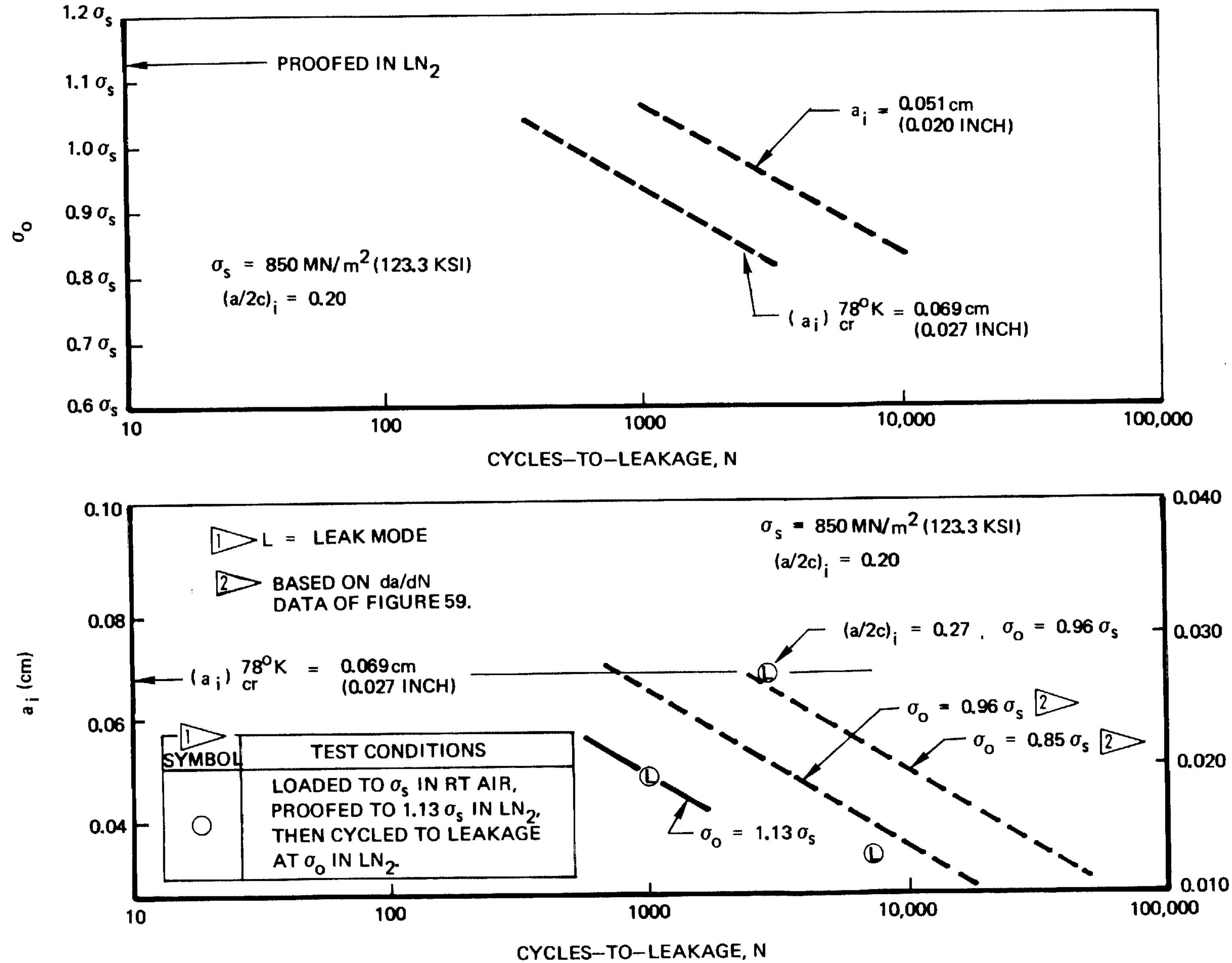

Figure 53: Uniaxial Cyclic Life Results of 0.10 cm (0.040 Inch) Thick Surface Flawed Inconel X750 STA Weld Metal ℄ at 78°K (−320°F)

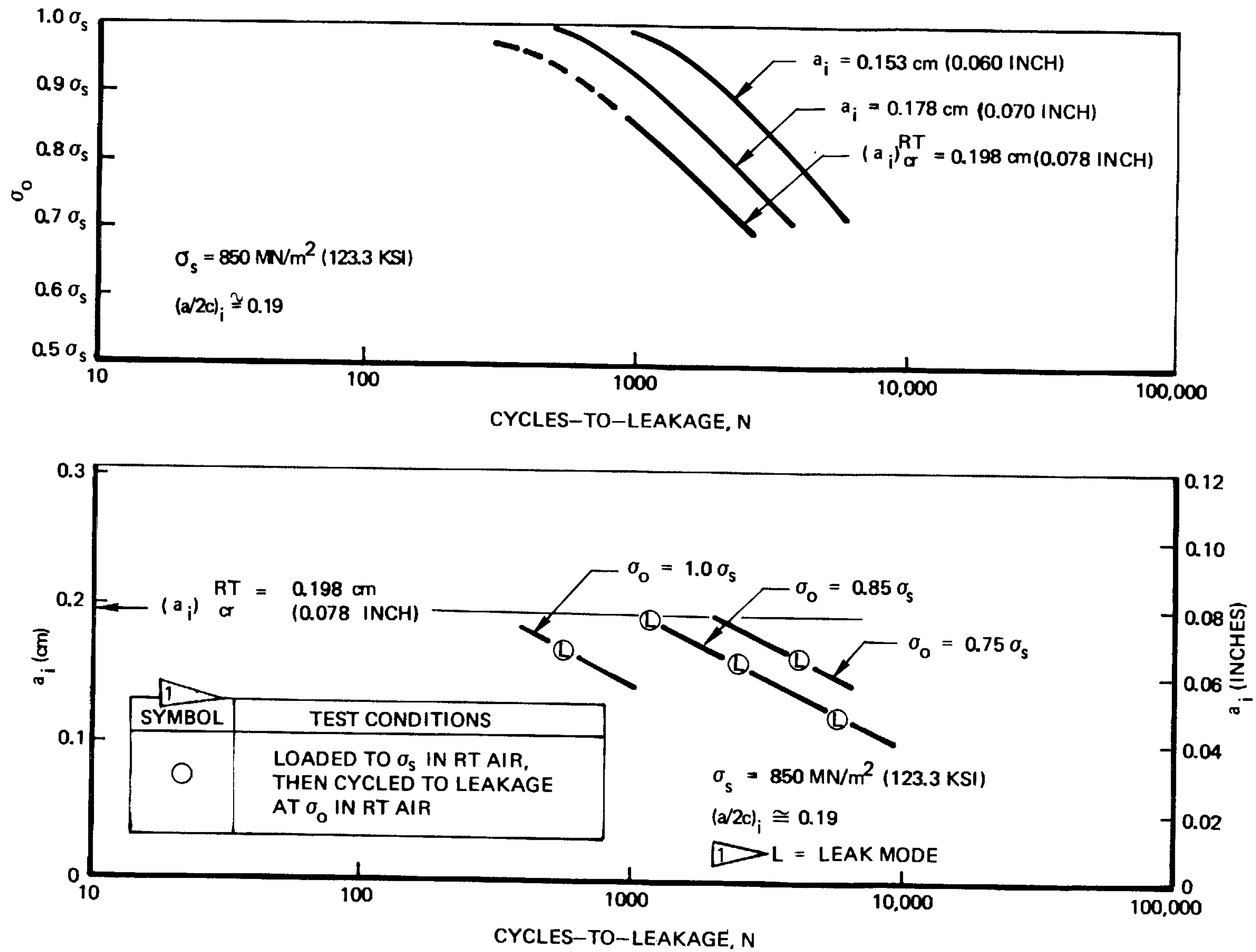

Figure 54: Uniaxial Cyclic Life Results of 0.33 cm (0.13 Inch) Thick Surface Flawed Inconel X750 STA Base Metal at 295^{0}K (72^{0}F)

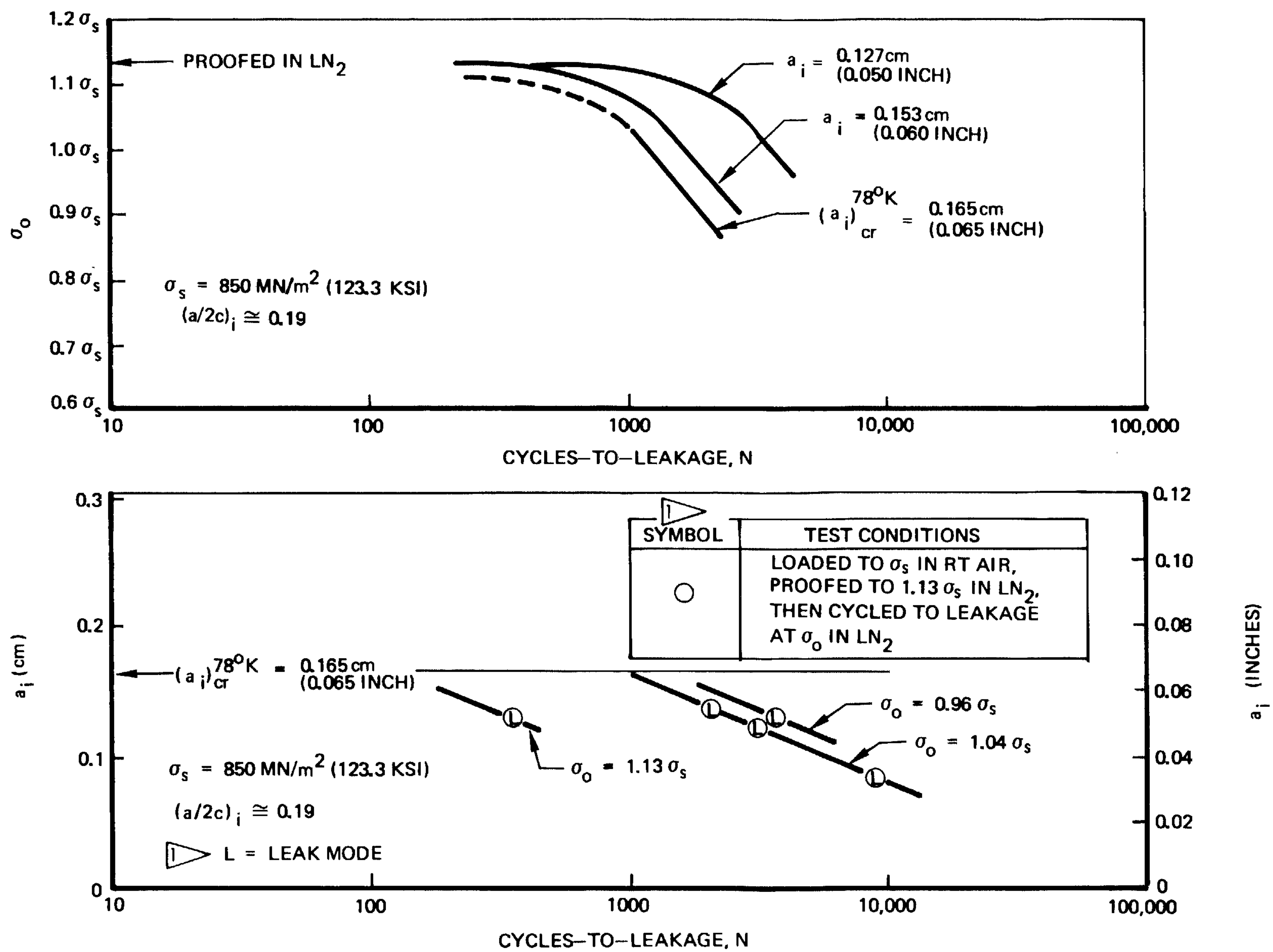

Figure 55 : Uniaxial Cyclic Life Results of 0.33 cm (0.13 Inch) Thick Surface Flawed Inconel X750 STA Base Metal at 78° K (-320° F)

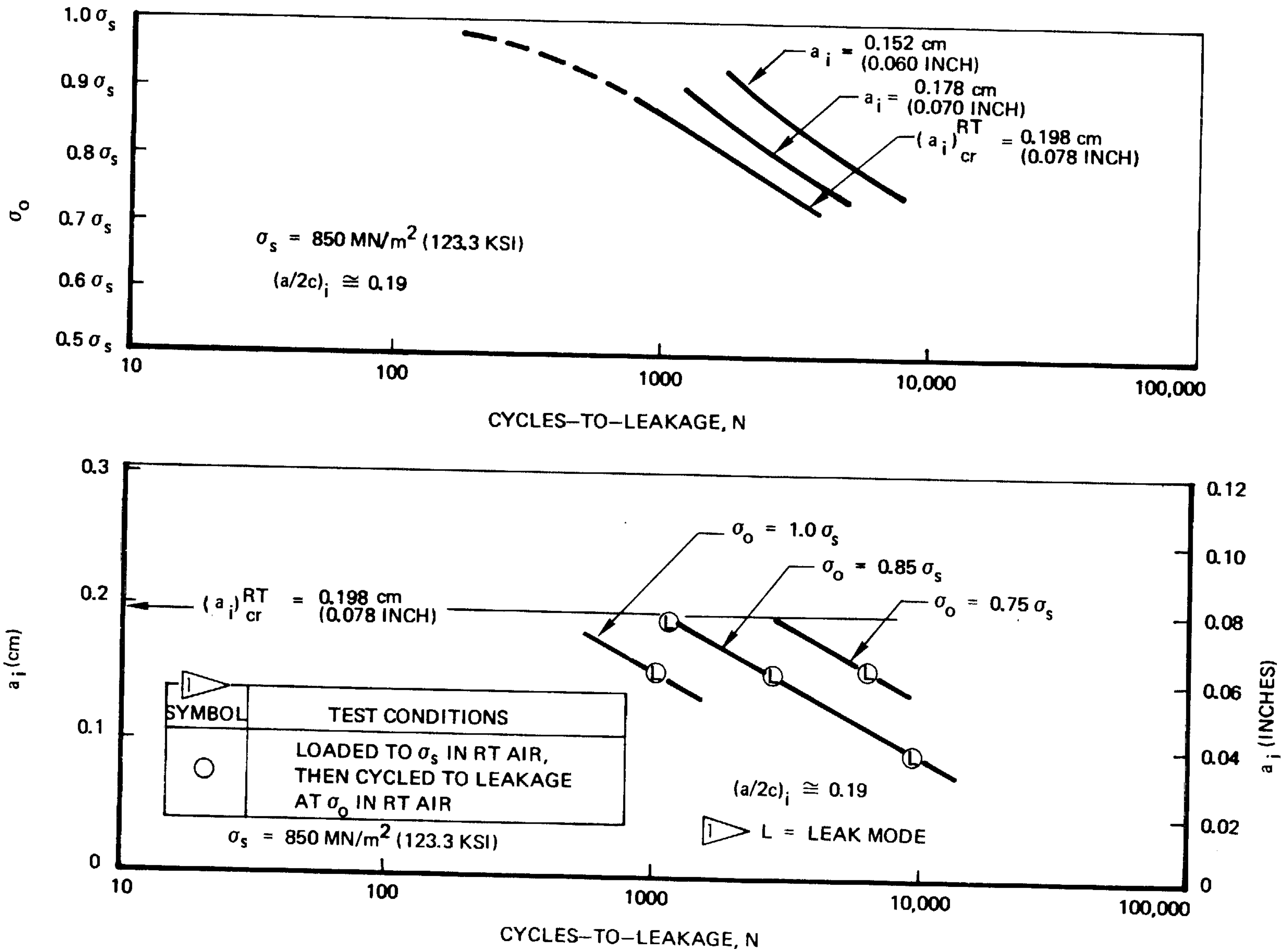

Figure 56: Uniaxial Cyclic Life Results of 0.33 cm (0.13 Inch) Thick Surface Flawed Inconel X750 STA Weld Metal ℄ at 295°K (72°F)

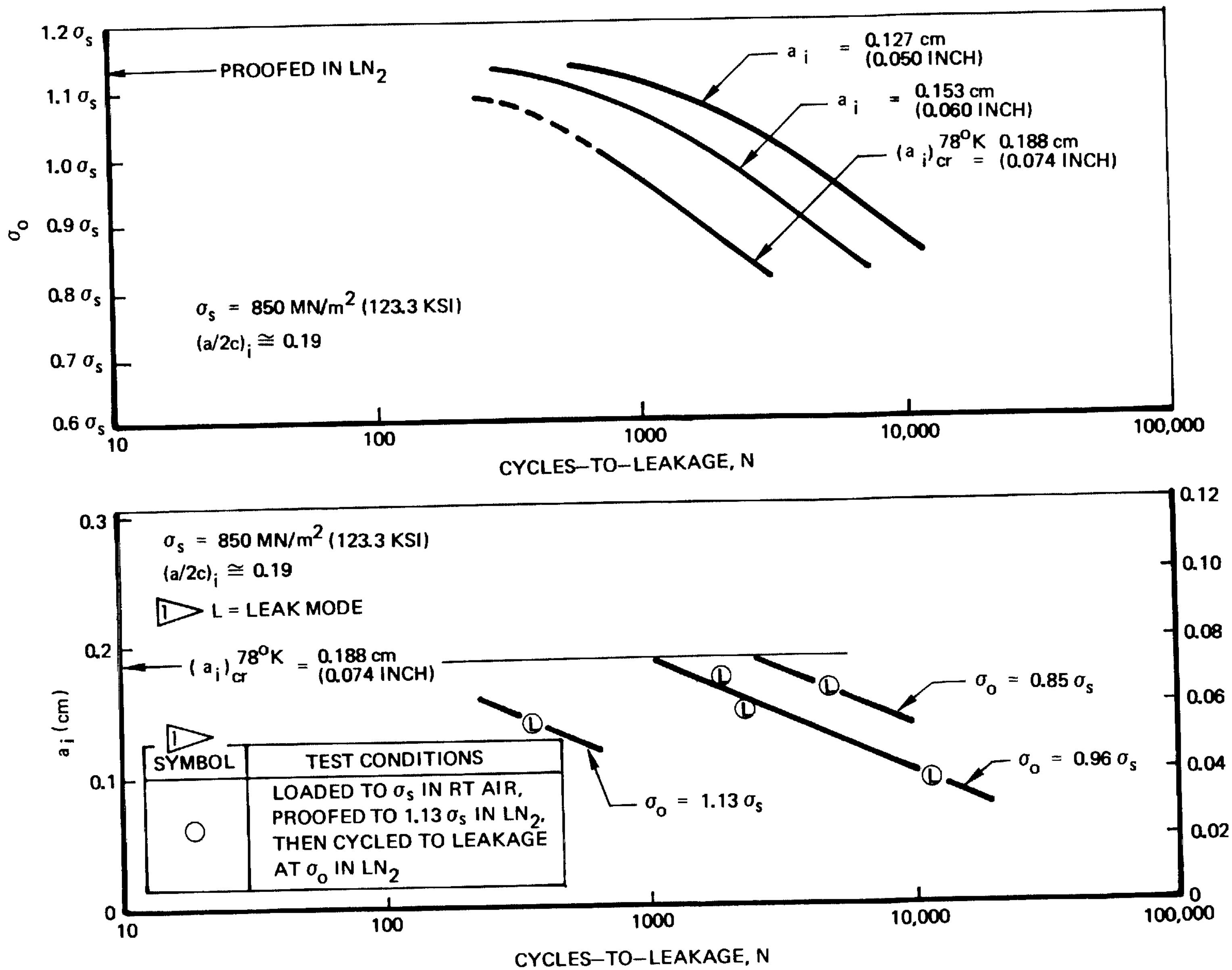

Figure 57 : Uniaxial Cyclic Life Results of 0.33 cm (0.13 Inch) Thick Surface Flawed Inconel X750 STA Weld Metal ℄ at 78^{0}K (-320^{0}F)

RT CYCLIC TESTED AT σ_o AFTER BEING LOADED TO σ_s IN RT AIR					
SYMBOL	σ_o MN/m^2	(KSI)	SYMBOL	σ_o MN/m^2	(KSI)
○ 1B-6	714	(103.5)	□ 1B-18	723	(104.9)
⬡ 1B-8	798	(115.7)	◇ 1B-22	723	(104.9)
△ 1B-16	638	92.5)	▽ 1B-26	723	(104.9)

LN_2 CYCLIC TESTED AT σ_o AFTER BEING LOADED TO σ_s IN RT AIR AND THEN PROOF LOADED TO 1.13 σ_s IN LN_2					
SYMBOL	σ_o MN/m^2	(KSI)	SYMBOL	σ_o MN/m^2	(KSI)
● 1B-21	816	(118.3)	■ 1B-25	816	(118.3)
⬢ 1B-23	959	(139.1)	◆ 1BW-3	816	(118.3)
▲ 1B-24	718	(104.2)			

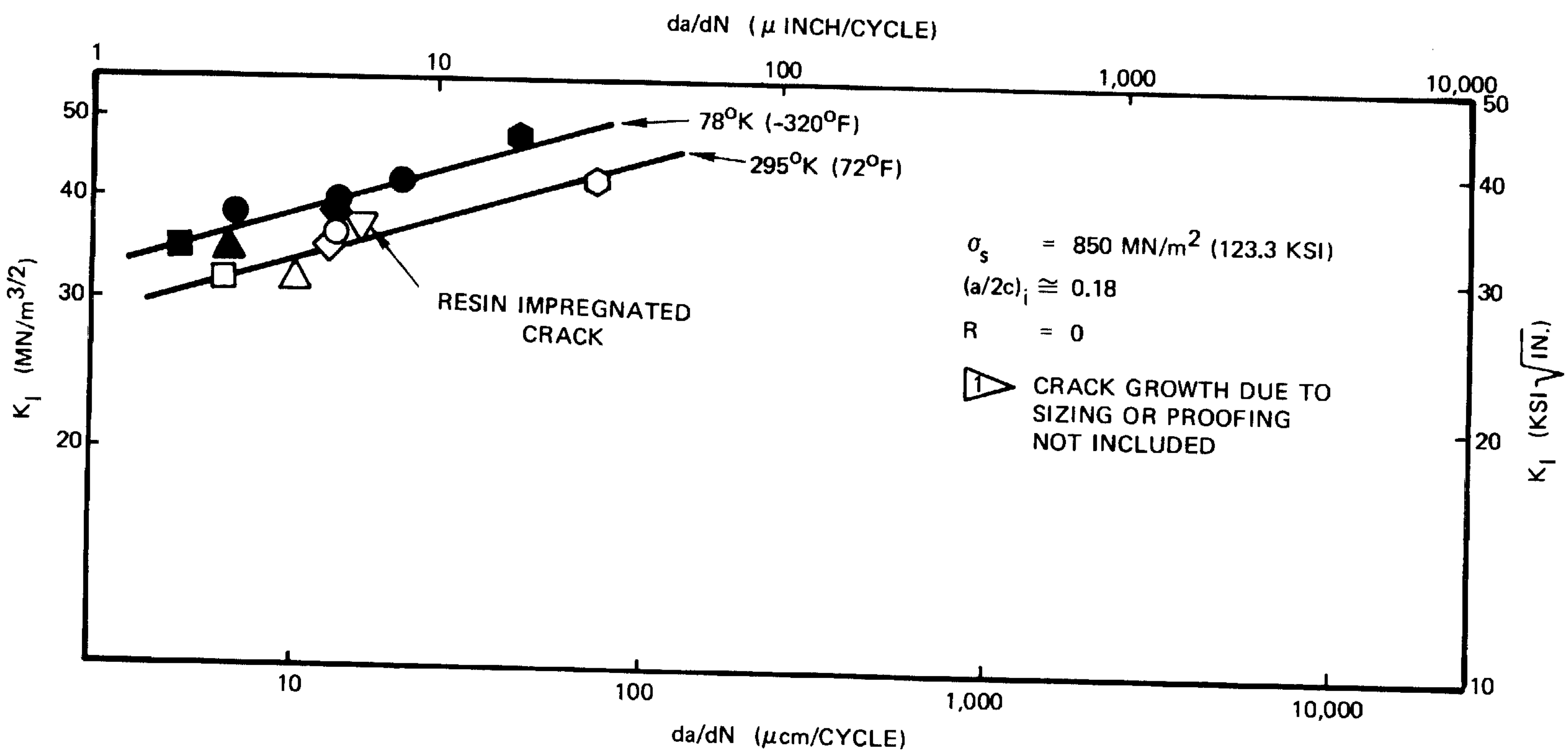

Figure 58: Uniaxial Cyclic Crack Growth Rates [1] *for 0.10 cm (0.040 Inch) Thick Surface Flawed Inconel X750 STA Base Metal*

RT CYCLIC TESTED AT σ_o AFTER BEING LOADED TO σ_s IN RT AIR			
SYMBOL	σ_o MN/m^2 (KSI)	SYMBOL	σ_o MN/m^2 (KSI)
○ 1BW-6	720 (104.4)	□ 1BW-17	638 (92.5)
⬡ 1BW-11	723 (104.9)	◇ 1BW-21	723 (104.9)
△ 1BW-13	850 (123.3)	▽ 1BW-24	723 (104.9)

LN_2 CYCLIC TESTED AT σ_o AFTER BEING LOADING TO σ_s IN RT AIR AND THEN PROOF LOADED TO 1.13 σ_s IN LN_2			
SYMBOL	σ_o MN/m^2 (KSI)	SYMBOL	σ_S MN/m^2 (KSI)
● 1BW-12	816 (118.3)		
⬢ 1BW-14	959 (139.1)		
▲ BW-6	816 (118.3)		

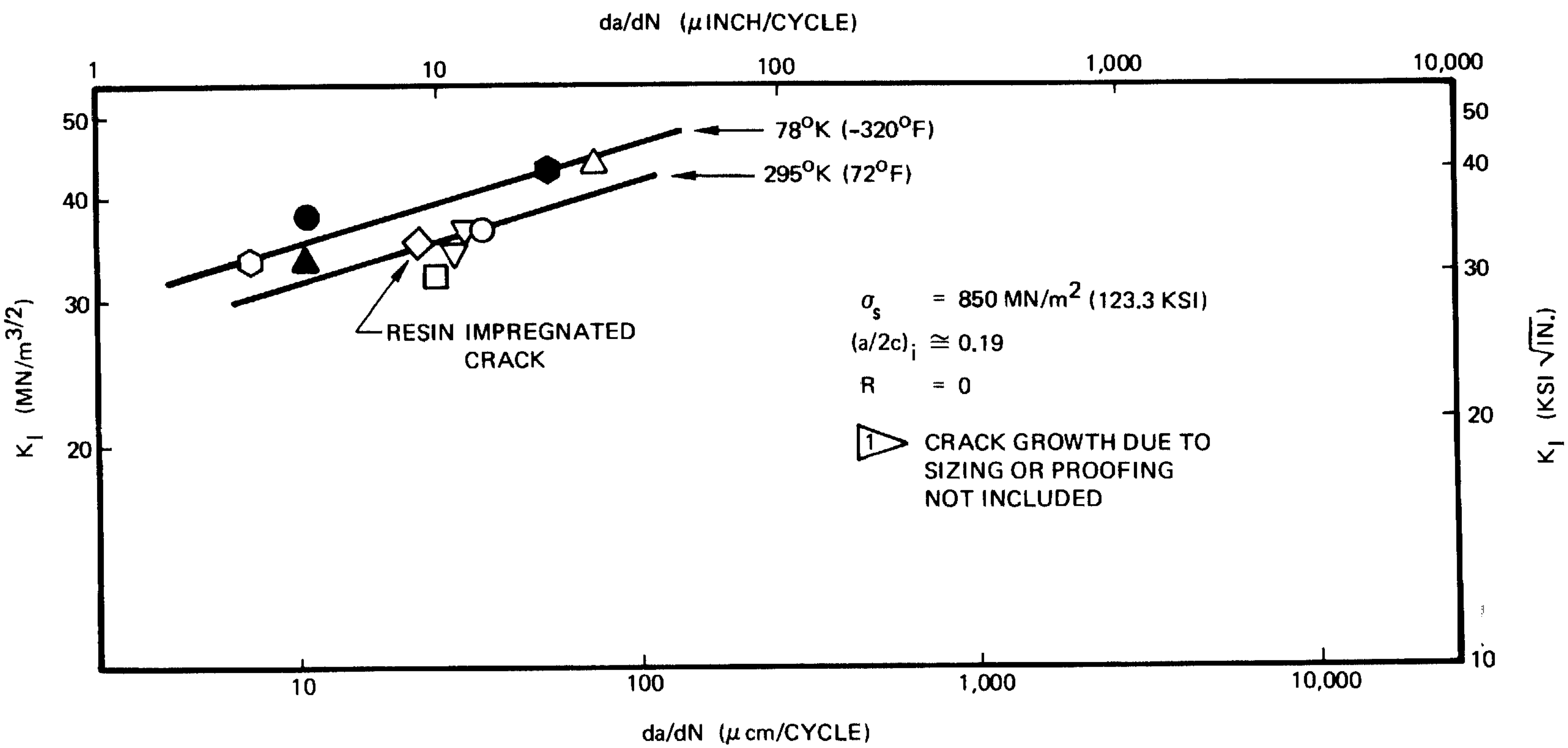

Figure 59: Uniaxial Cyclic Crack Growth Rates 1 *for 0.10 cm (0.040 Inch) Thick Surface Flawed Inconel X750 STA Weld Metal ℄*

RT CYCLIC TESTED AT σ_o AFTER BEING LOADED TO σ_s IN RT AIR			
SYMBOL	σ_o MN/m^2 (KSI)	SYMBOL	σ_o MN/m^2 (KSI)
○ 2B-5	723 (104.9)	□ 2B-13	638 (92.5)
⬡ 2B-10	850 (123.3)	◇ 2B-14	723 (104.9)
△ 2B-12	723 (104.9)	▽ 2B-16	723 (104.9)

LN_2 CYCLIC TESTED AT σ_o AFTER BEING LOADED TO σ_s IN RT AIR AND THEN PROOF LOADED TO 1.13 σ_s IN LN_2			
SYMBOL	σ_o MN/m^2 (KSI)	SYMBOL	σ_o MN/m^2 (KSI)
● 2B-6	816 (118.3)	■ 2B-9	885 (128.3)
⬢ 2B-7	959 (139.1)	◆ 2B-11	884 (128.2)
▲ 2B-8	884 (128.2)		

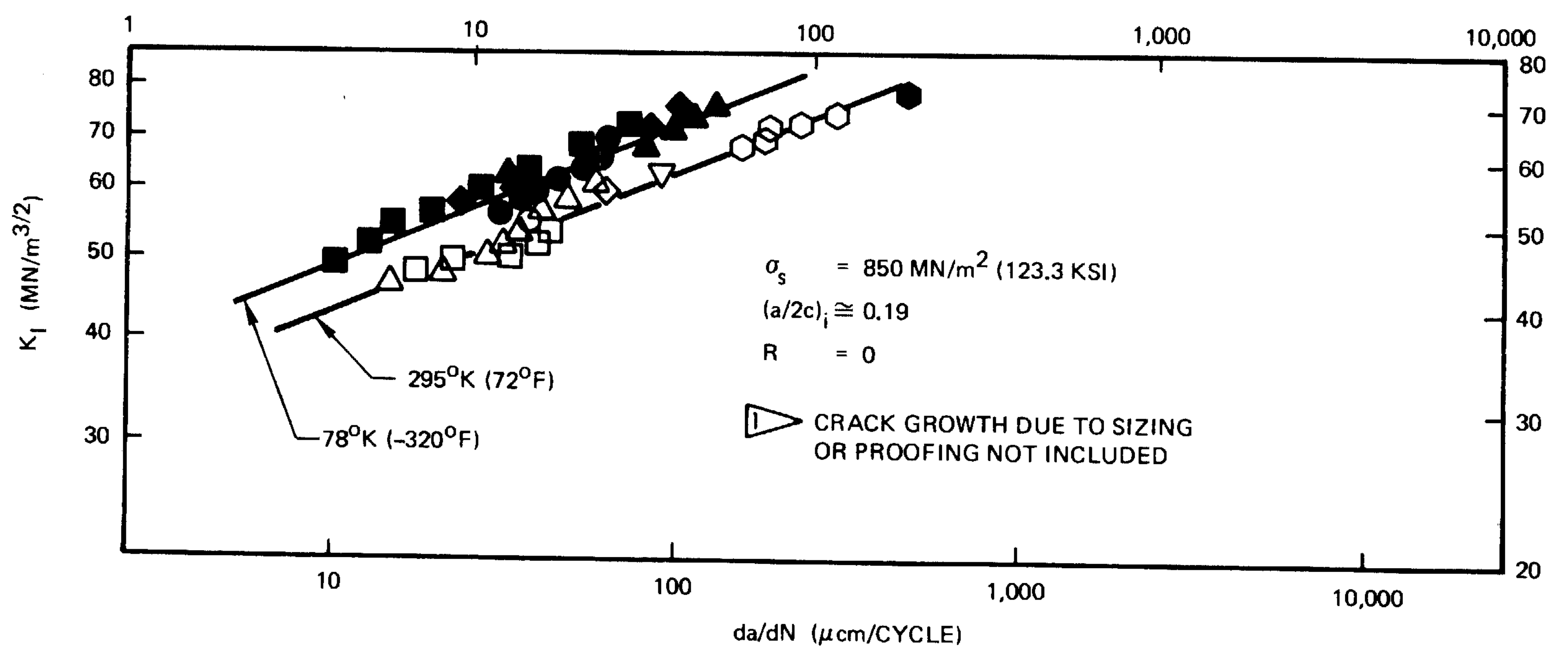

Figure 60: Uniaxial Cyclic Crack Growth Rates for 0.33 cm (0.13 Inch) Thick Surface Flawed Inconel X750 STA Base Metal

RT CYCLIC TESTED AT σ_o AFTER BEING LOADED TO σ_s IN RT AIR			
SYMBOL	σ_o MN/m^2 (KSI)	SYMBOL	σ_o MN/m^2 (KSI)
○ 2BW-6	723 (104.9)	□ 2BW-17	723 (104.9)
⬡ 2BW-13	850 (123.3)	◇ 2BW-18	638 (92.5)
△ 2BW-14	723 (104.9)		

LN_2 CYCLIC TESTED AT σ_o AFTER BEING LOADEDTO σ_s IN RT AIR AND THEN PROOF LOADED TO 1.13 σ_s IN LN_2			
SYMBOL	σ_o MN/m^2 (KSI)	SYMBOL	σ_o MN/m^2 (KSI)
● 2BW-7	816 (118.3)	■ 2BW-15	719 (104.3)
⬢ 2BW-11	959 (139.1)	◆ 2BW-16	816 (118.3)
▲ 2BW-12	816 (118.3)		

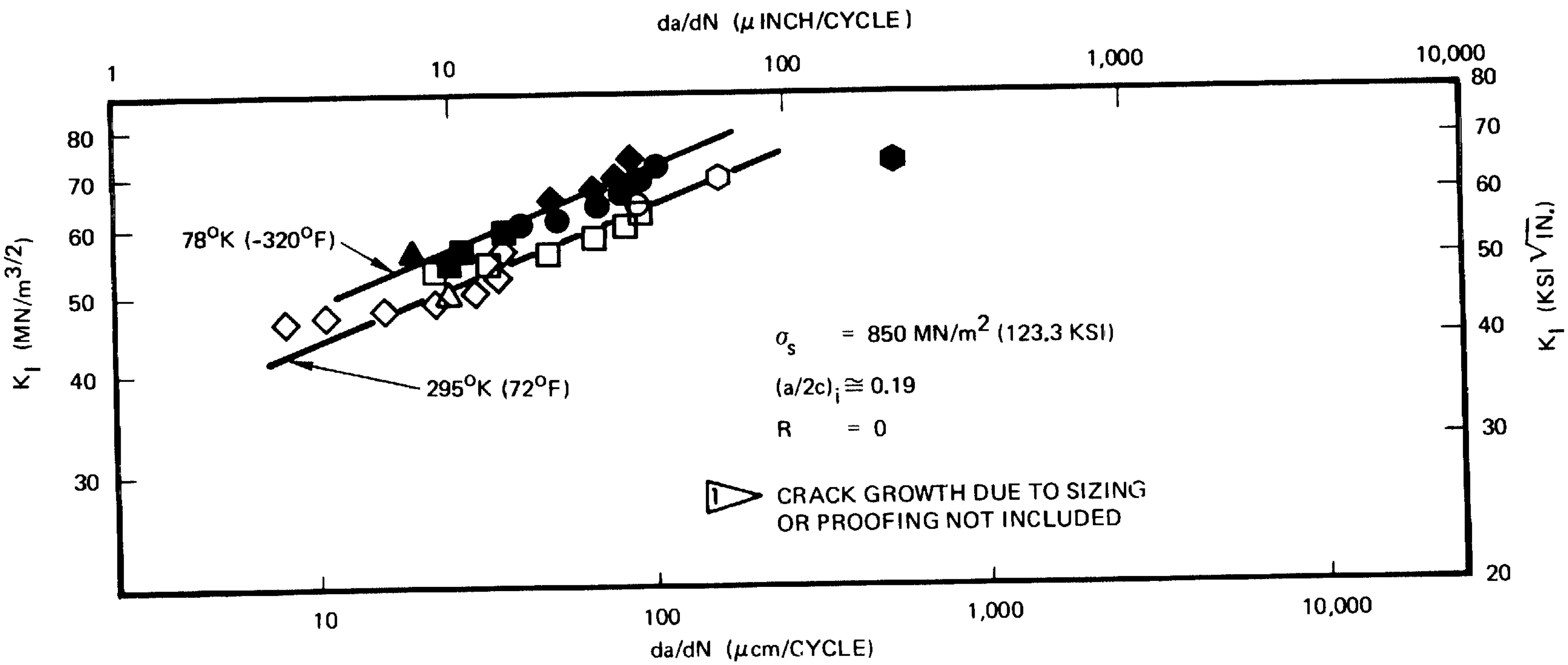

Figure 61: Uniaxial Cyclic Crack Growth Rates 1 *for 0.33 cm (0.13 Inch) Thick Surface Flawed Inconel X750 STA Weld Metal ℄*

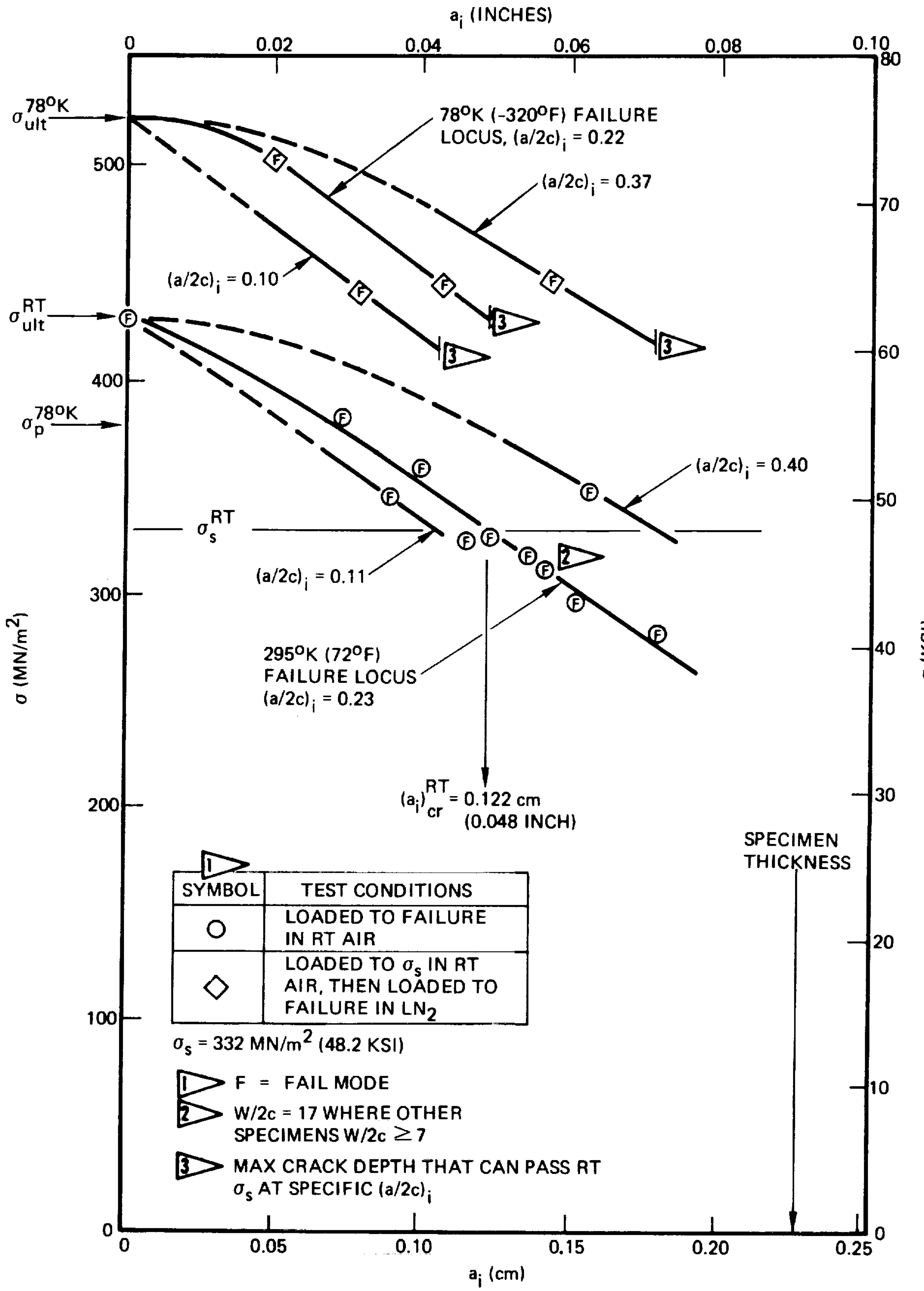

Figure 62: Uniaxial Static Fracture Results of 0.23 cm (0.090 Inch) Thick Surface Flawed 2219-T62 Aluminum Base Metal

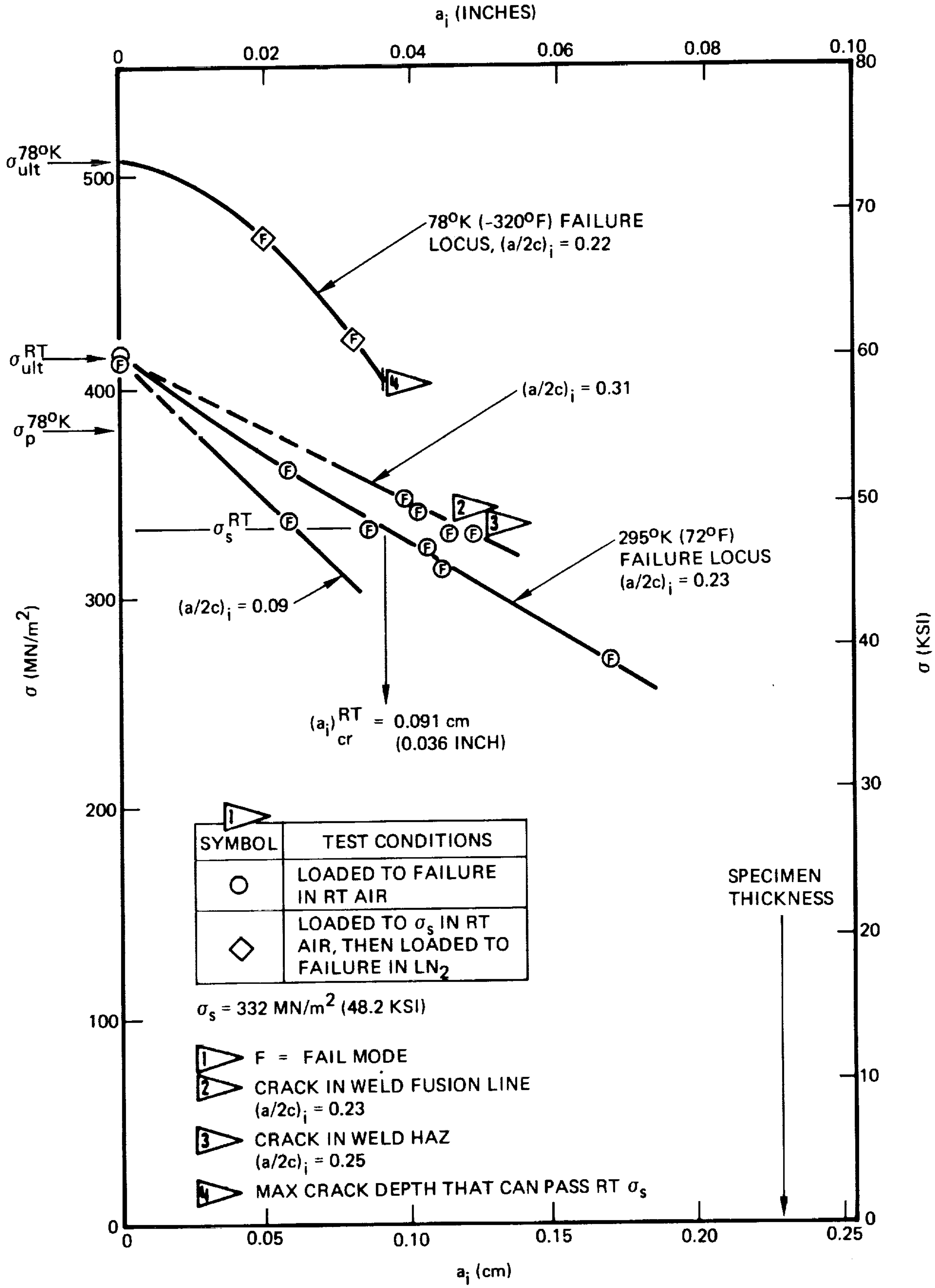

Figure 63: Uniaxial Static Fracture Results of 0.23 cm (0.090 Inch) Thick Surface Flawed 2219-T62 Aluminum Weld Metal ℄

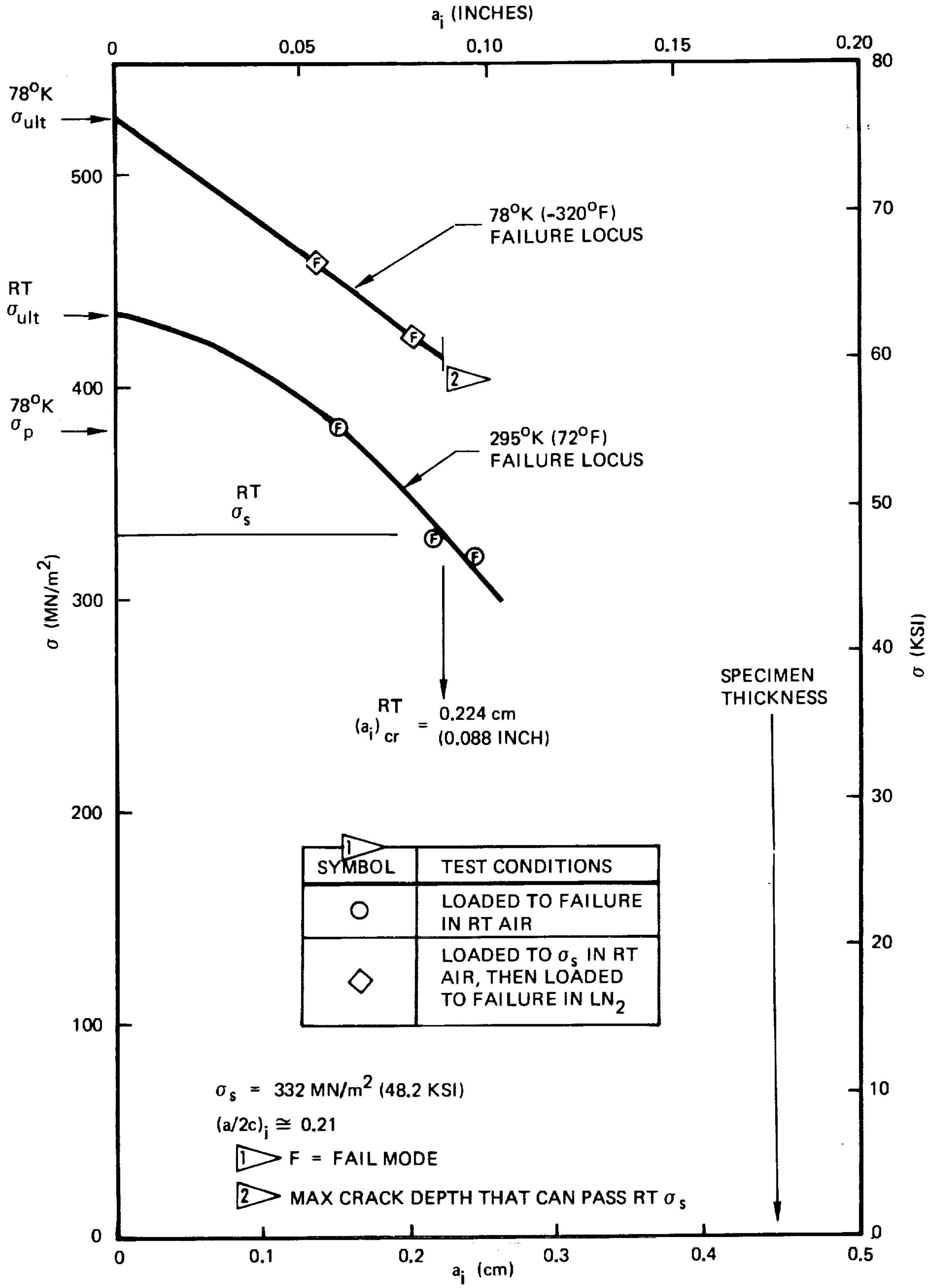

Figure 64: Uniaxial Static Fracture Results of 0.46 cm (0.18 Inch) Thick Surface Flawed 2219-T62 Aluminum Base Metal

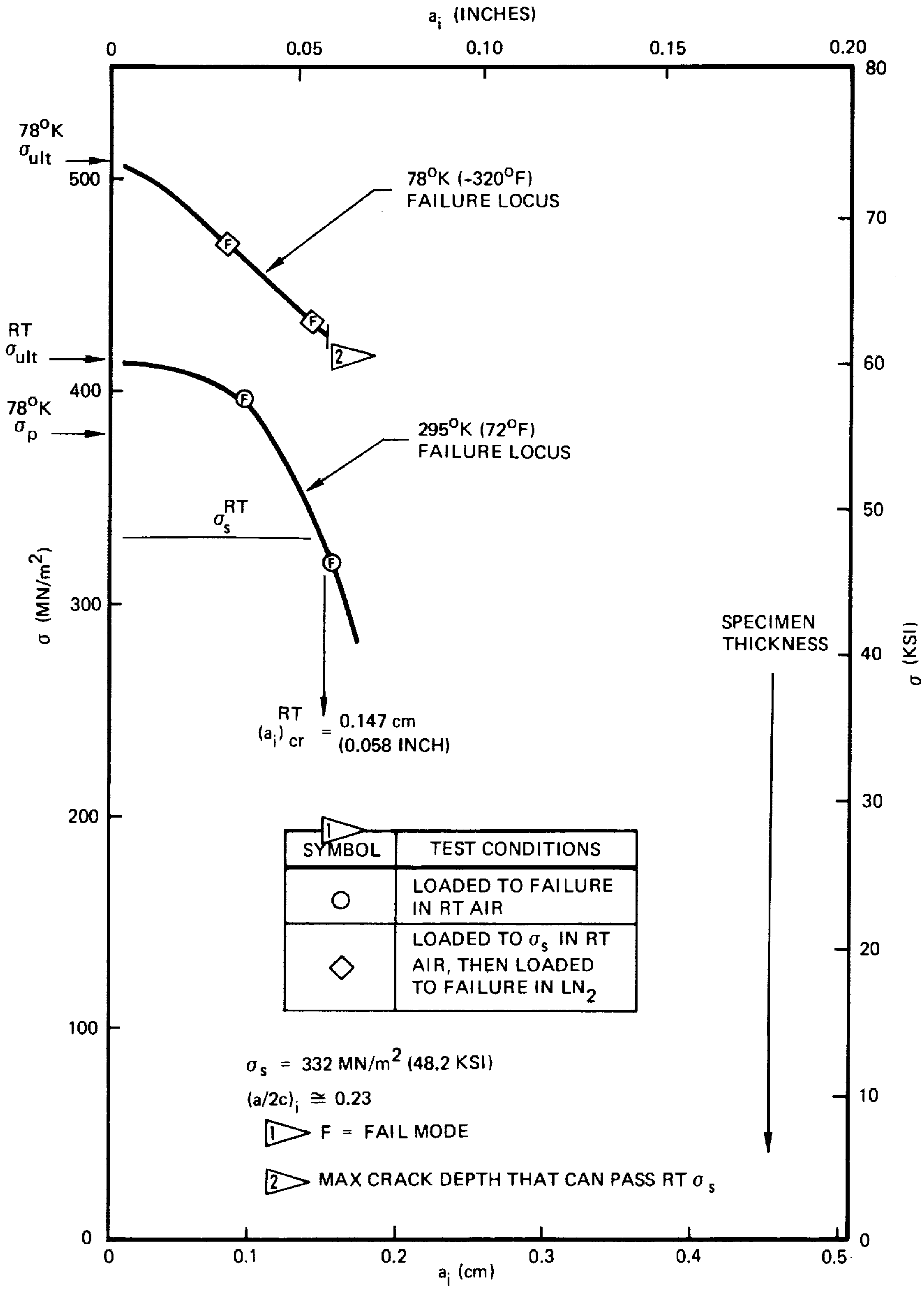

Figure 65: Uniaxial Static Fracture Results of 0.46 cm (0.18 Inch) Thick Surface Flawed 2219-T62 Aluminum Weld Metal ℄

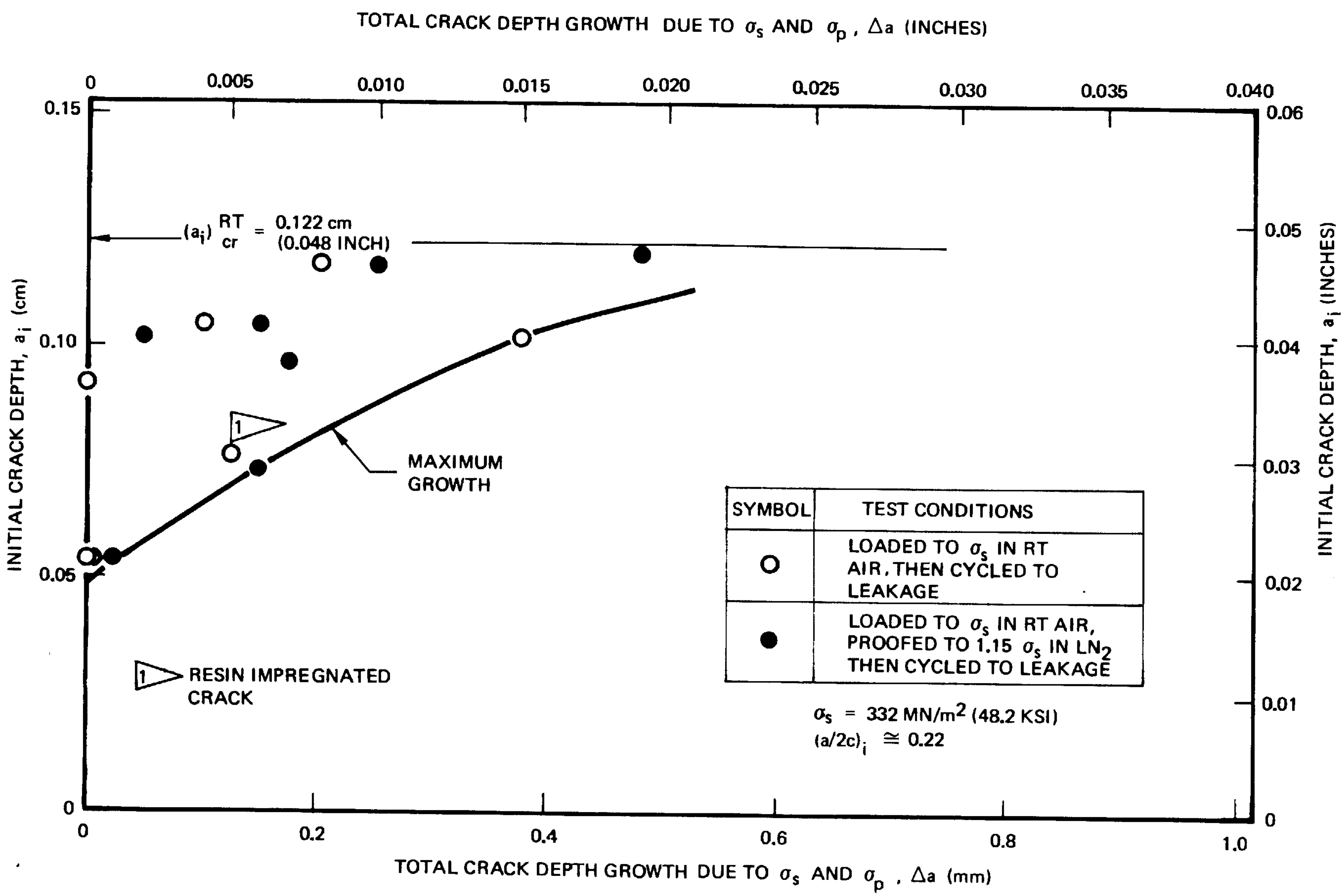

Figure 66: Growth-On-Loading of 0.23 cm (0.090 Inch) Thick Surface Flawed 2219-T62 Aluminum Base Metal

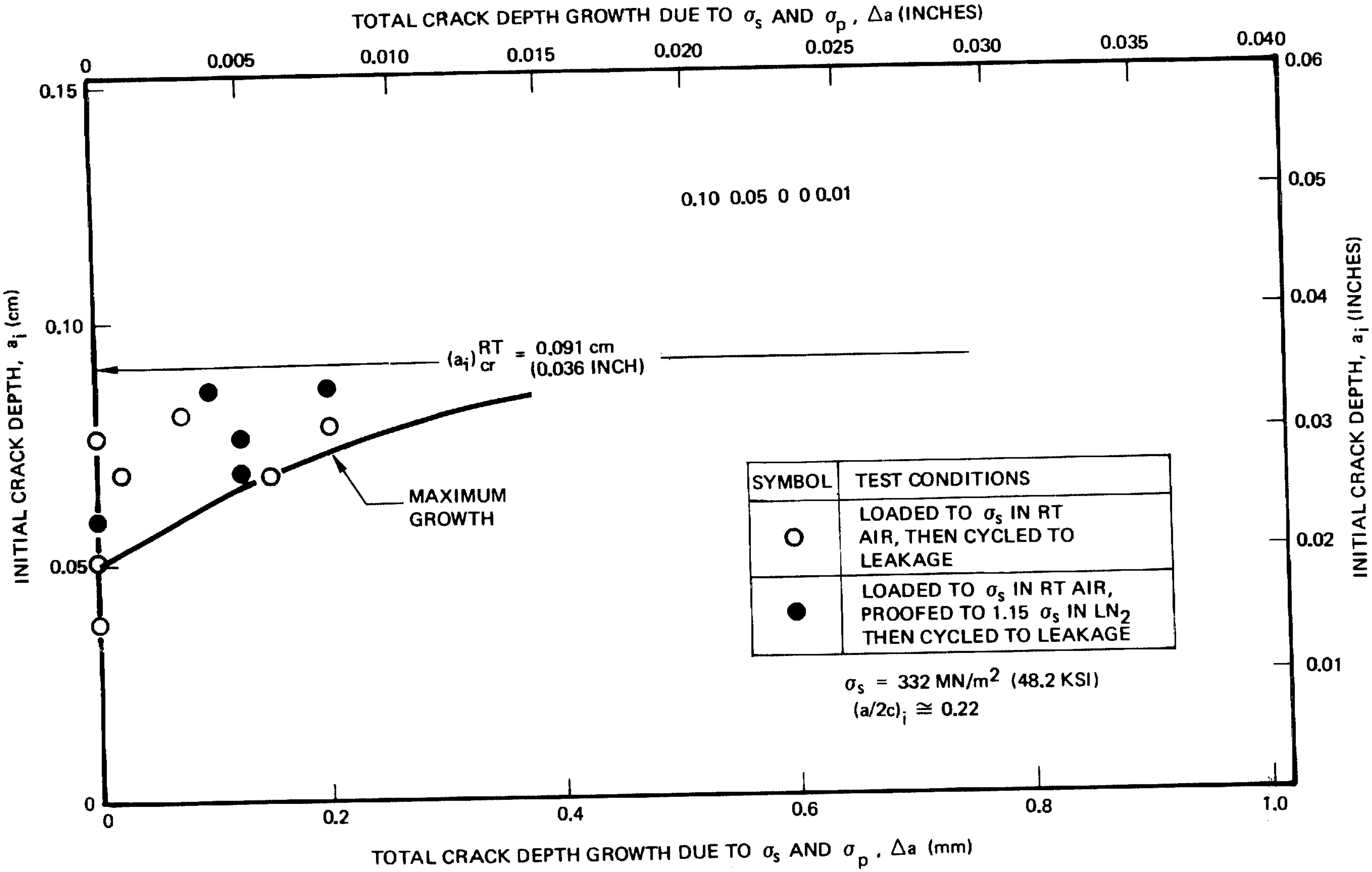

Figure 67: Growth-On-Loading of 0.23 cm (0.090 Inch) Thick Surface Flawed 2219-T62 Aluminum Weld Metal ℄

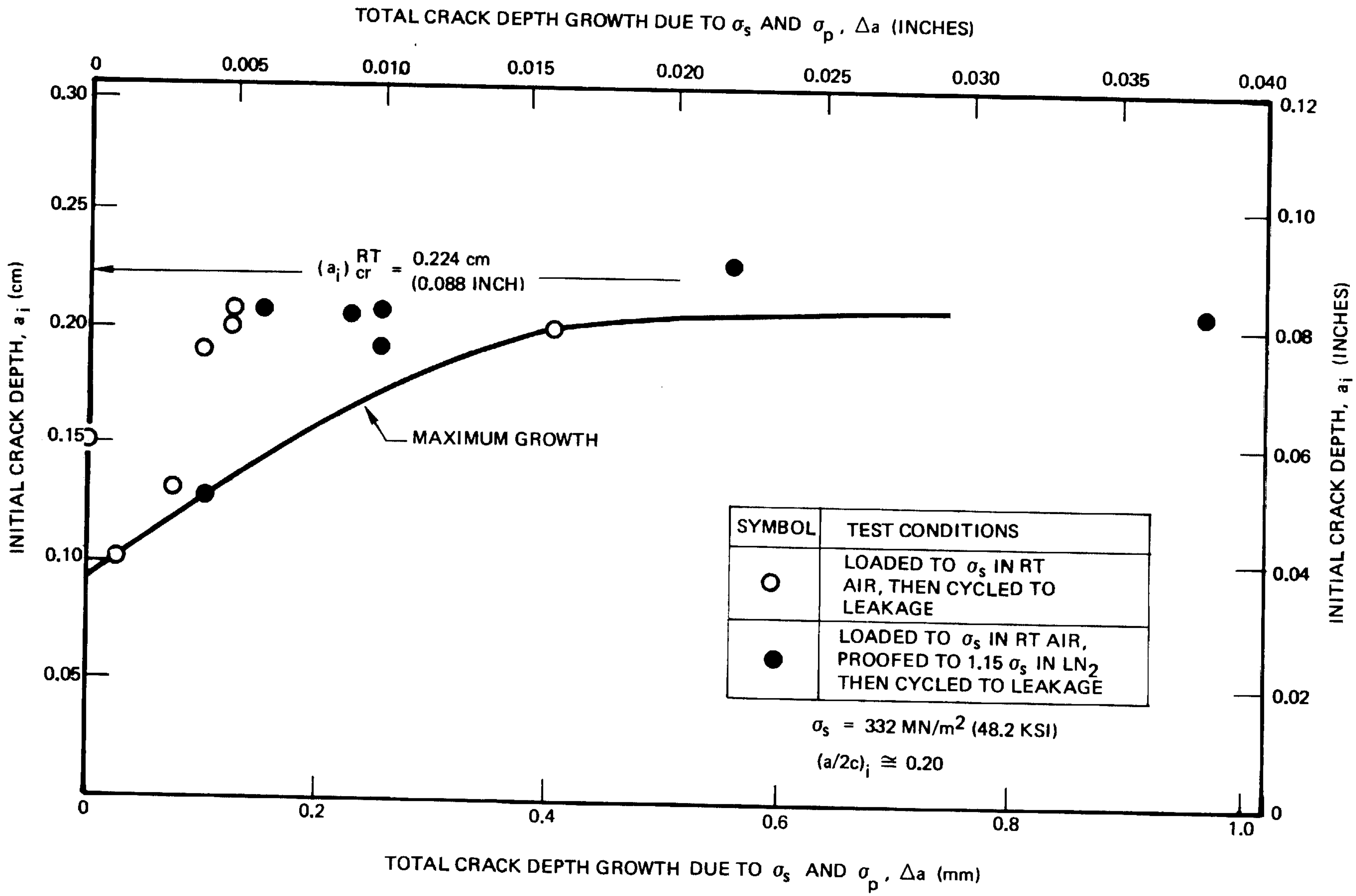

Figure 68: Growth-On-Loading Results of 0.46 cm (0.18 Inch) Thick Surface Flawed 2219-T62 Aluminum Base Metal

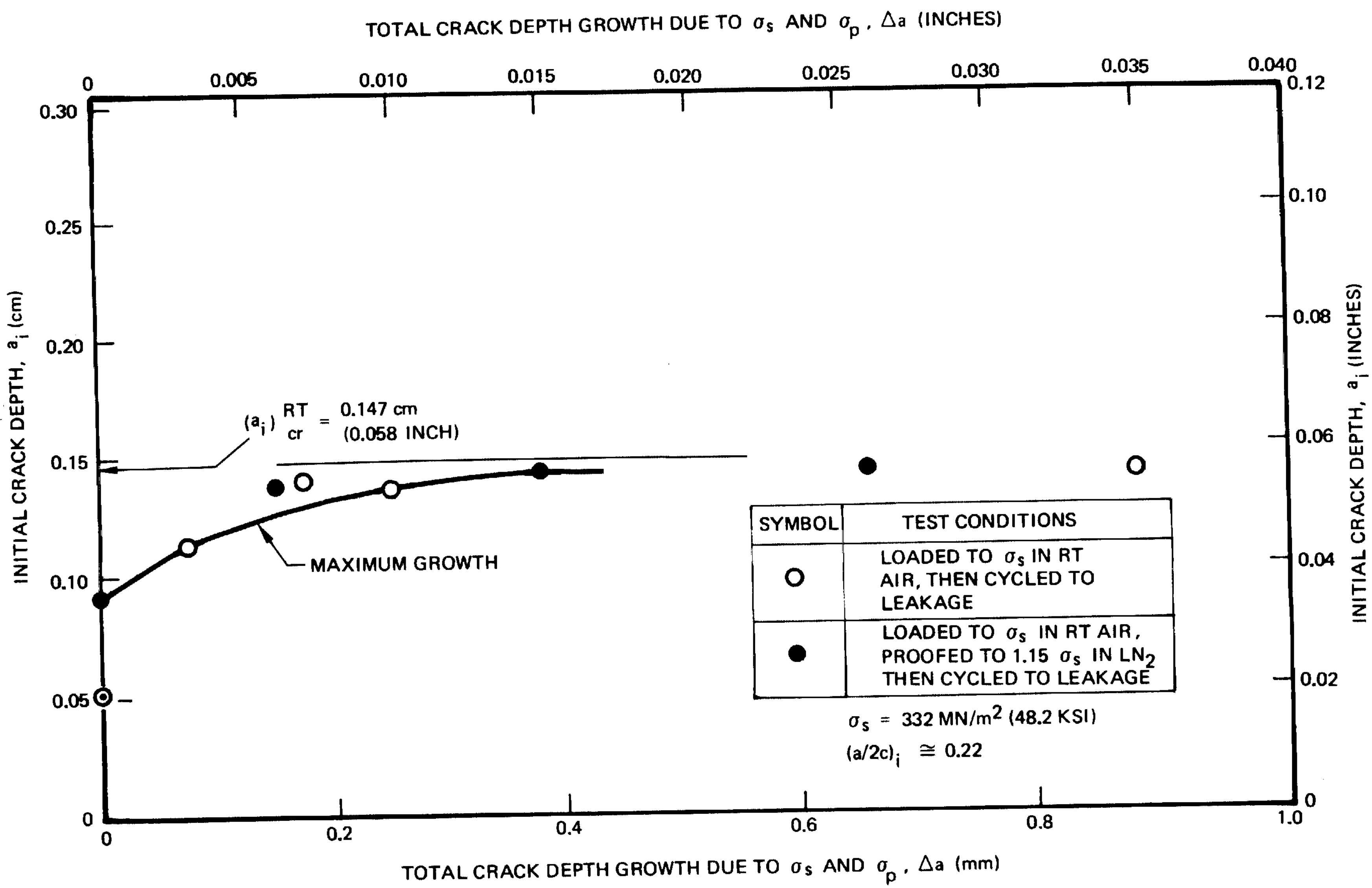

Figure 69: Growth-On-Loading Results of 0.46 cm (0.18 Inch) Thick Surface Flawed 2219-T62 Aluminum Weld Metal ℄

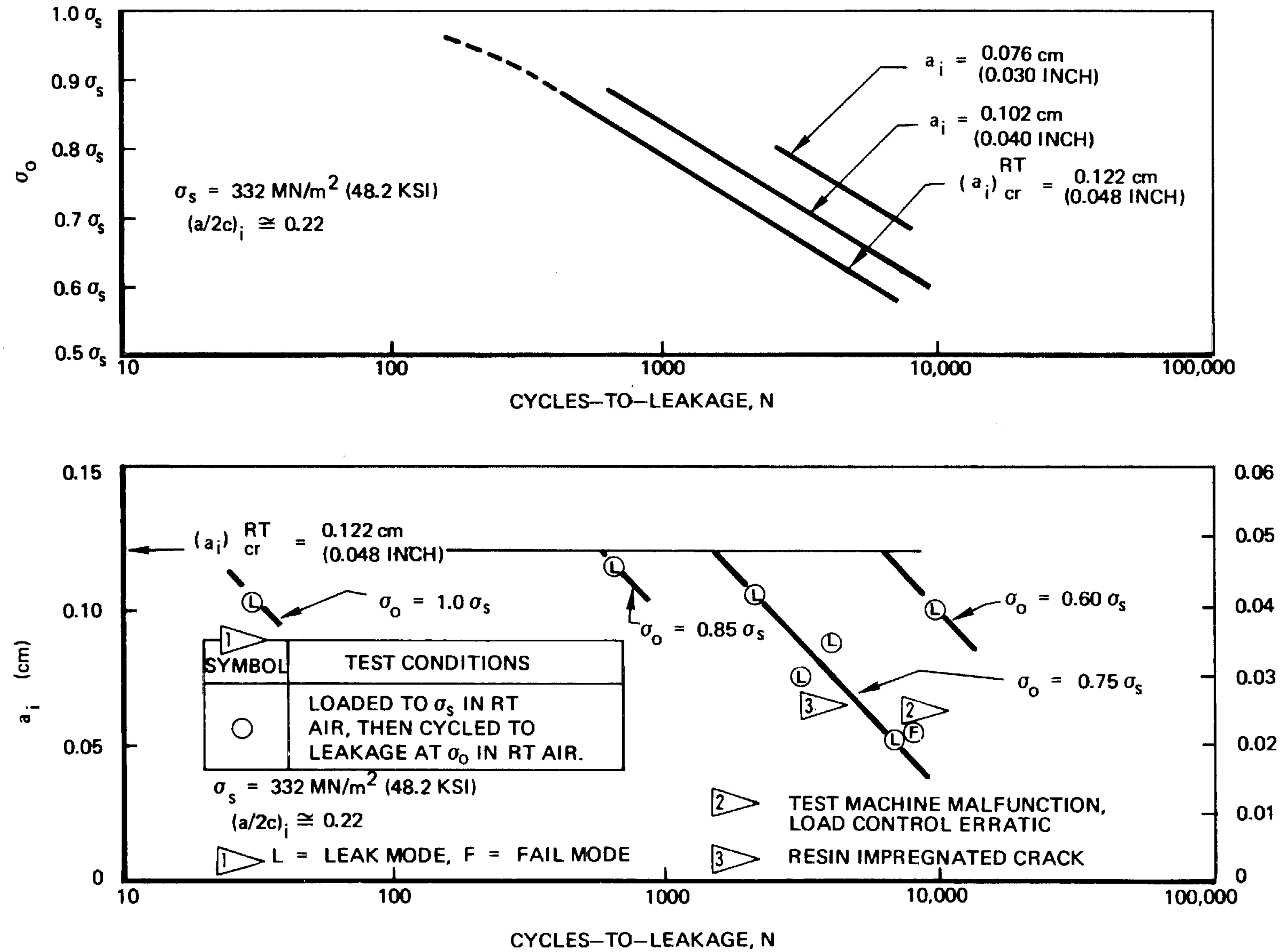

Figure 70 : Uniaxial Cyclic Life Results of 0.23 cm (0.090 Inch) Thick Surface Flawed 2219-T62 Aluminum Base Metal at 295°K (72°F)

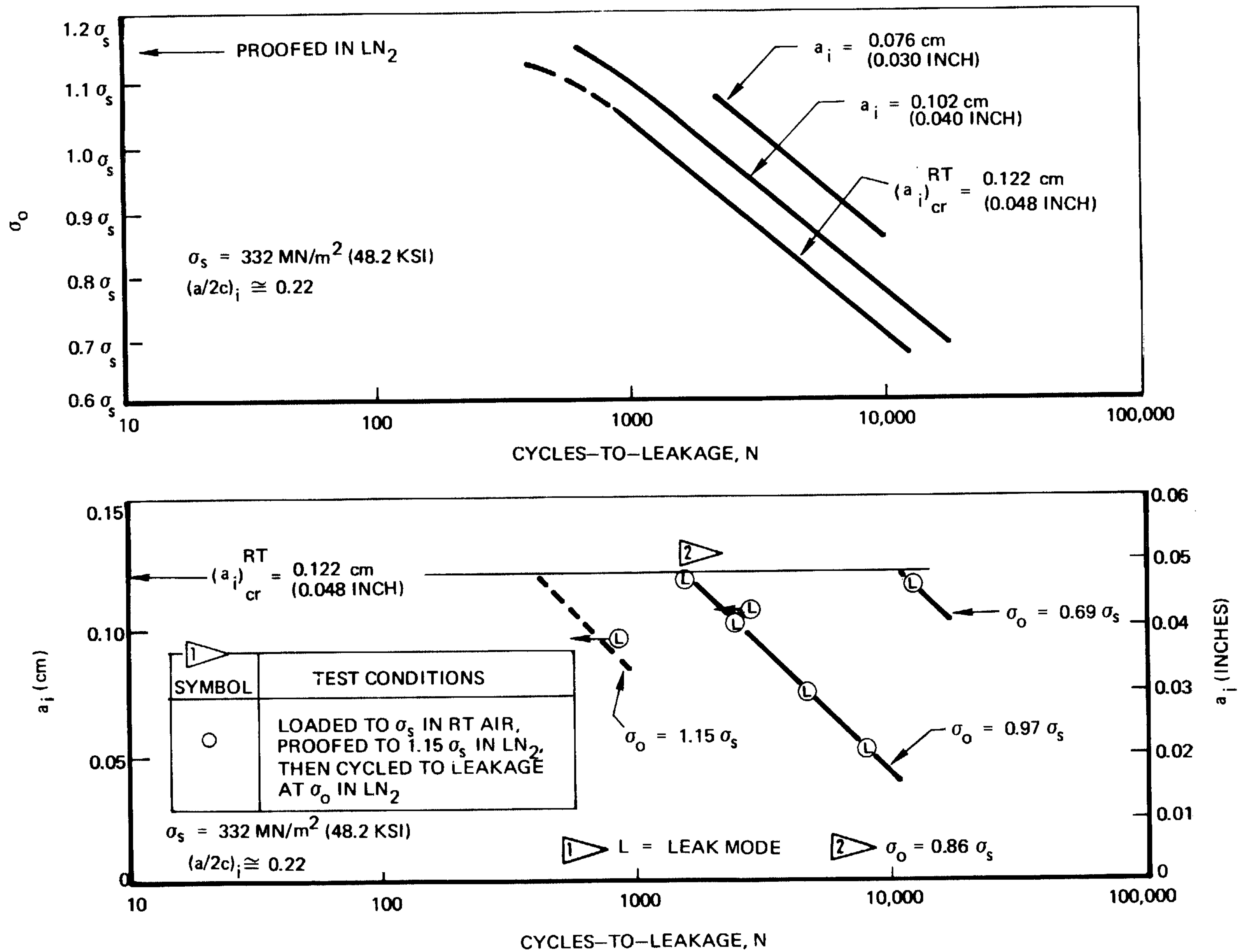

Figure 71: Uniaxial Cyclic Life Results of 0.23 cm (0.090 Inch) Thick Surface Flawed 2219-T62 Aluminum Base Metal at 78^{0}K (-320^{0}F)

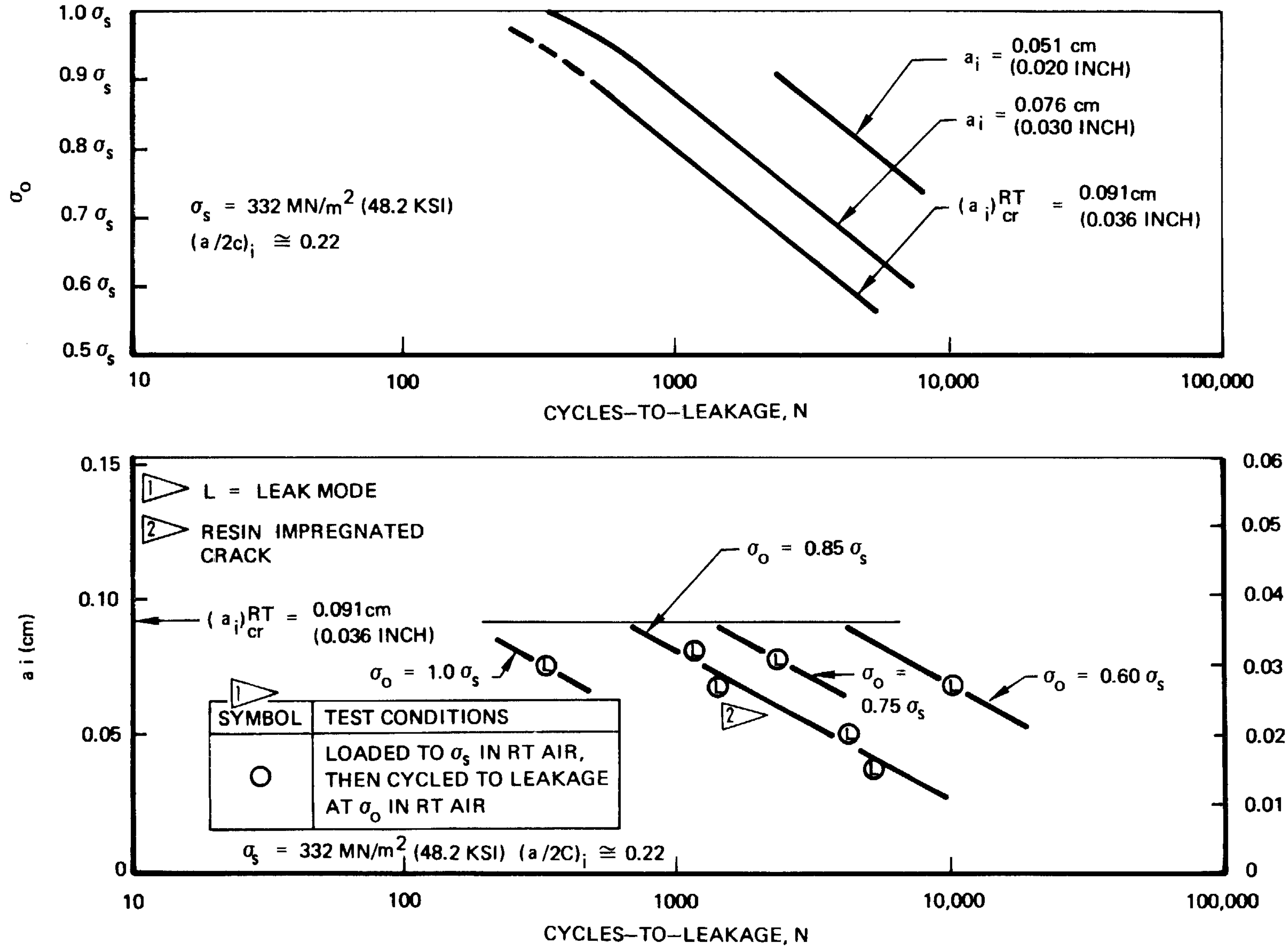

Figure 72: Uniaxial Cyclic Life Results of 0.23 cm (0.090 Inch) Thick Surface Flawed 2219-T62 Aluminum Weld Metal ℄ at 295°K (72°F)

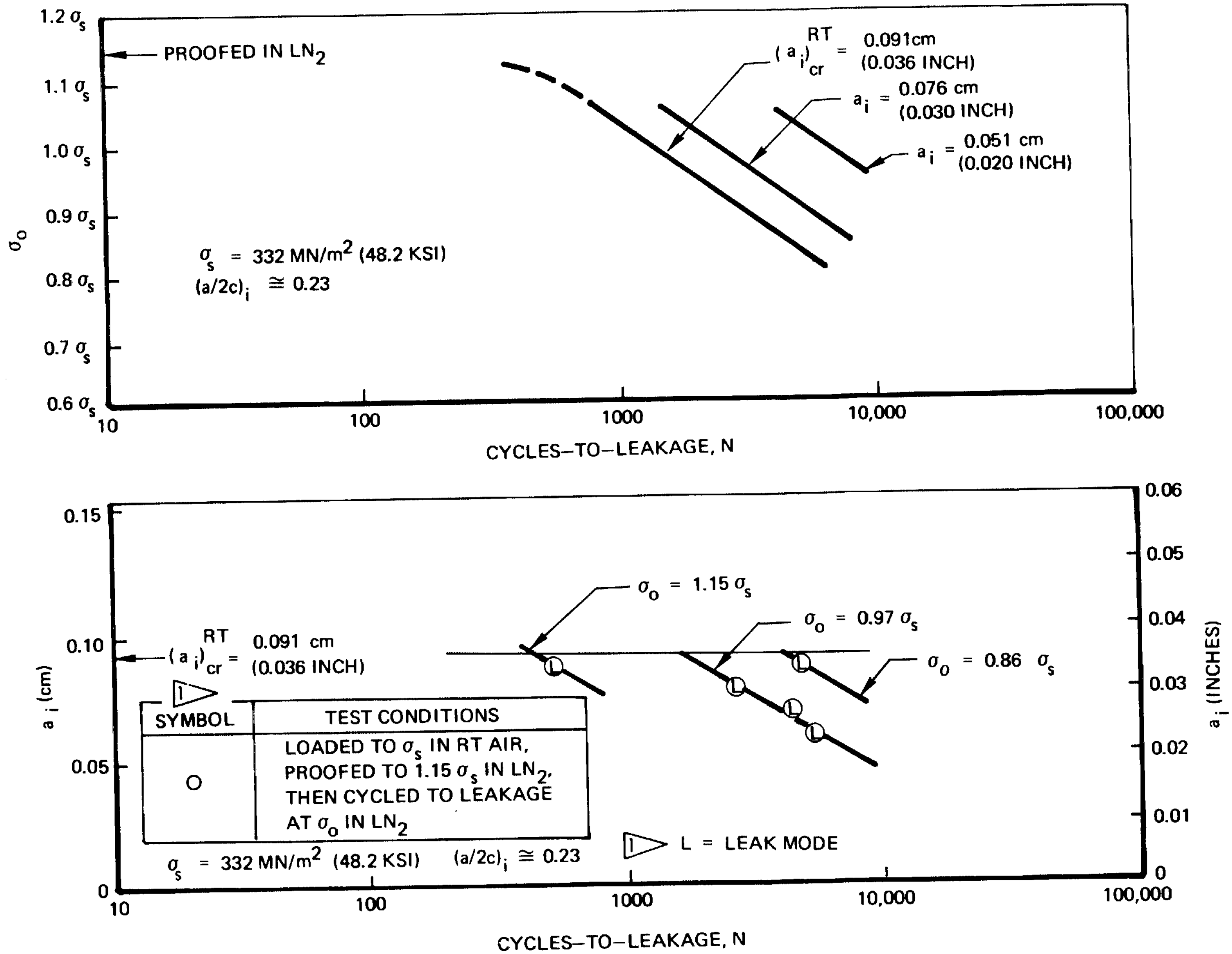

Figure 73 : *Uniaxial Cyclic Life Results of 0.23 cm (0.090 Inch) Thick Surface Flawed 2219-T62 Aluminum Weld Metal ℄ at 78^{0}K (-320^{0}F)*

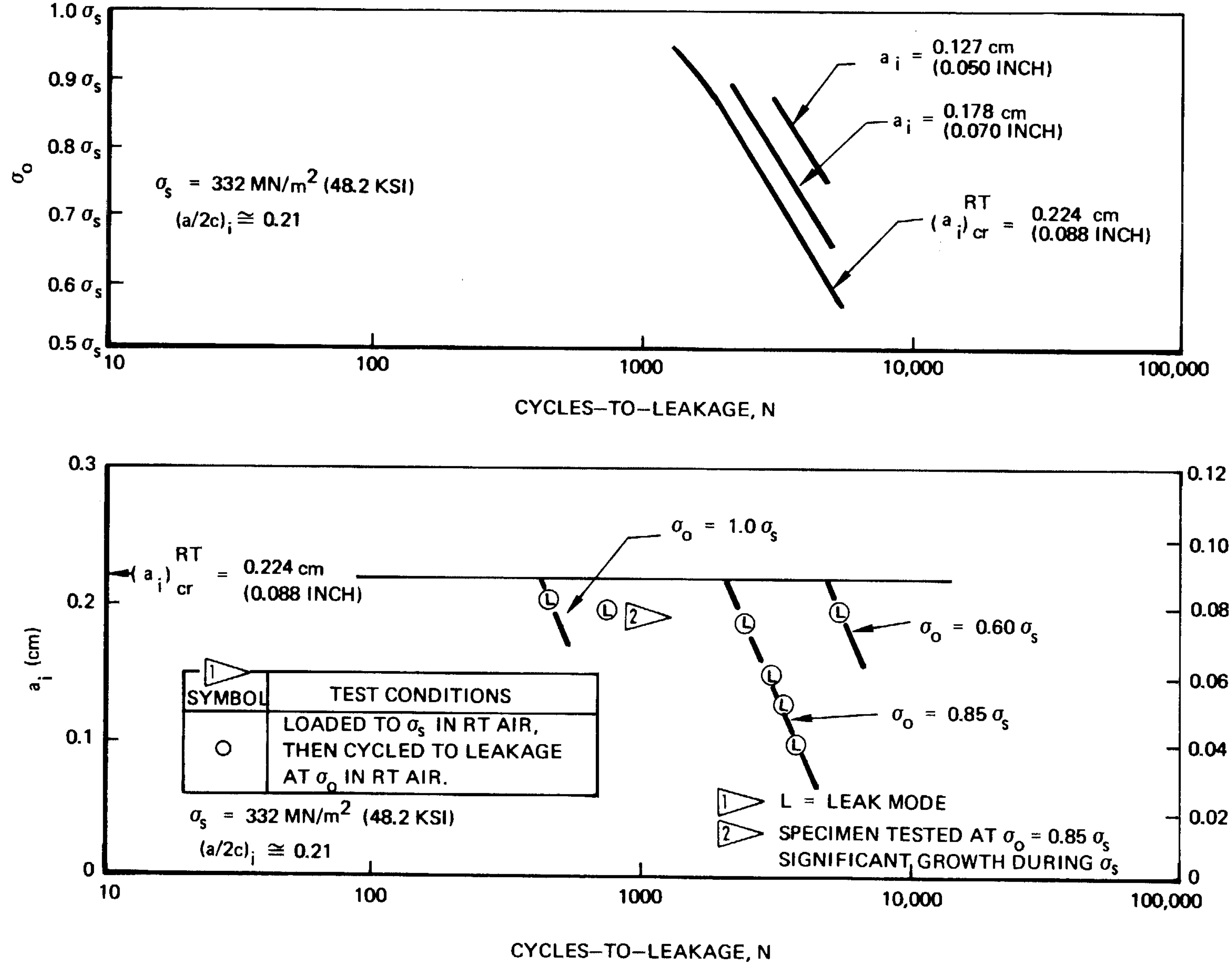

Figure 74: Uniaxial Cyclic Life Results of 0.46 cm (0.18 Inch) Thick Surface Flawed 2219-T62 Aluminum Base Metal At 295° K (72° F)

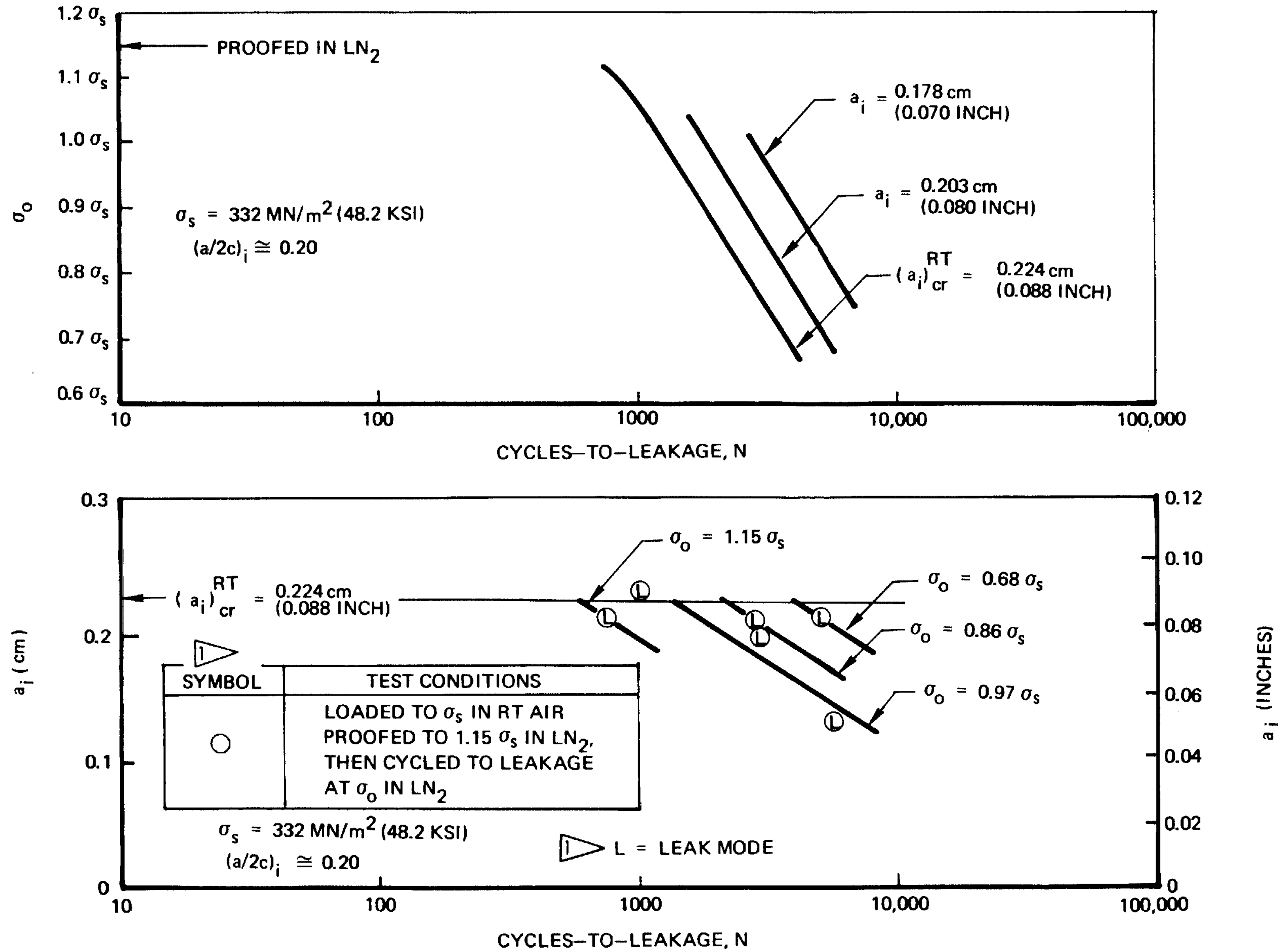

Figure 75 : Uniaxial Cyclic Life Results of 0.46 cm (0.18 Inch) Thick Surface Flawed 2219-T62 Aluminum Base Metal at 78^{0}K (-320^{0}F)

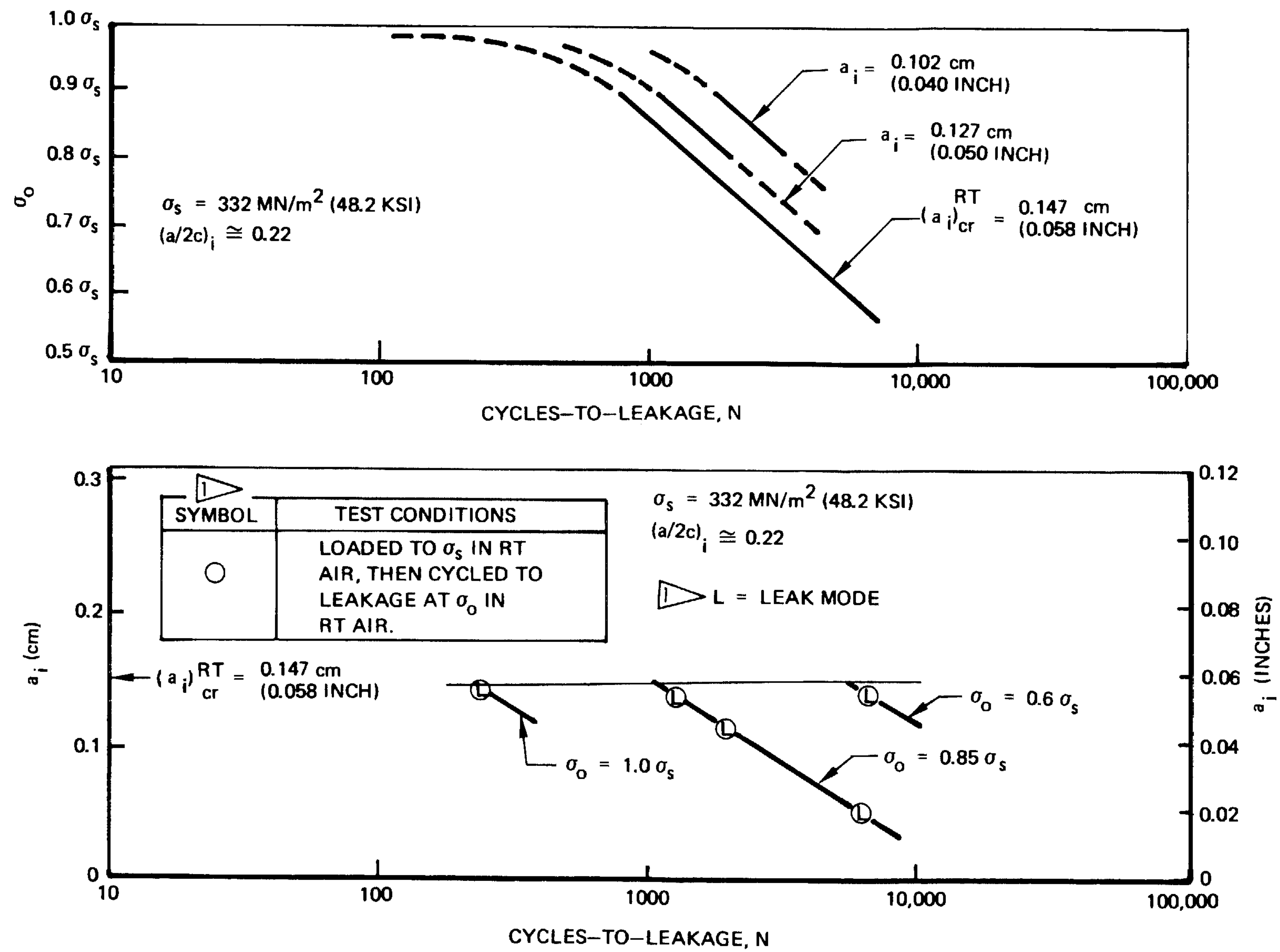

Figure 76: *Uniaxial Cyclic Life Results of 0.46 cm (0.18 INCH) Thick Surface Flawed 2219-T62 Aluminum Weld Metal ℄ at 295⁰K (72⁰F)*

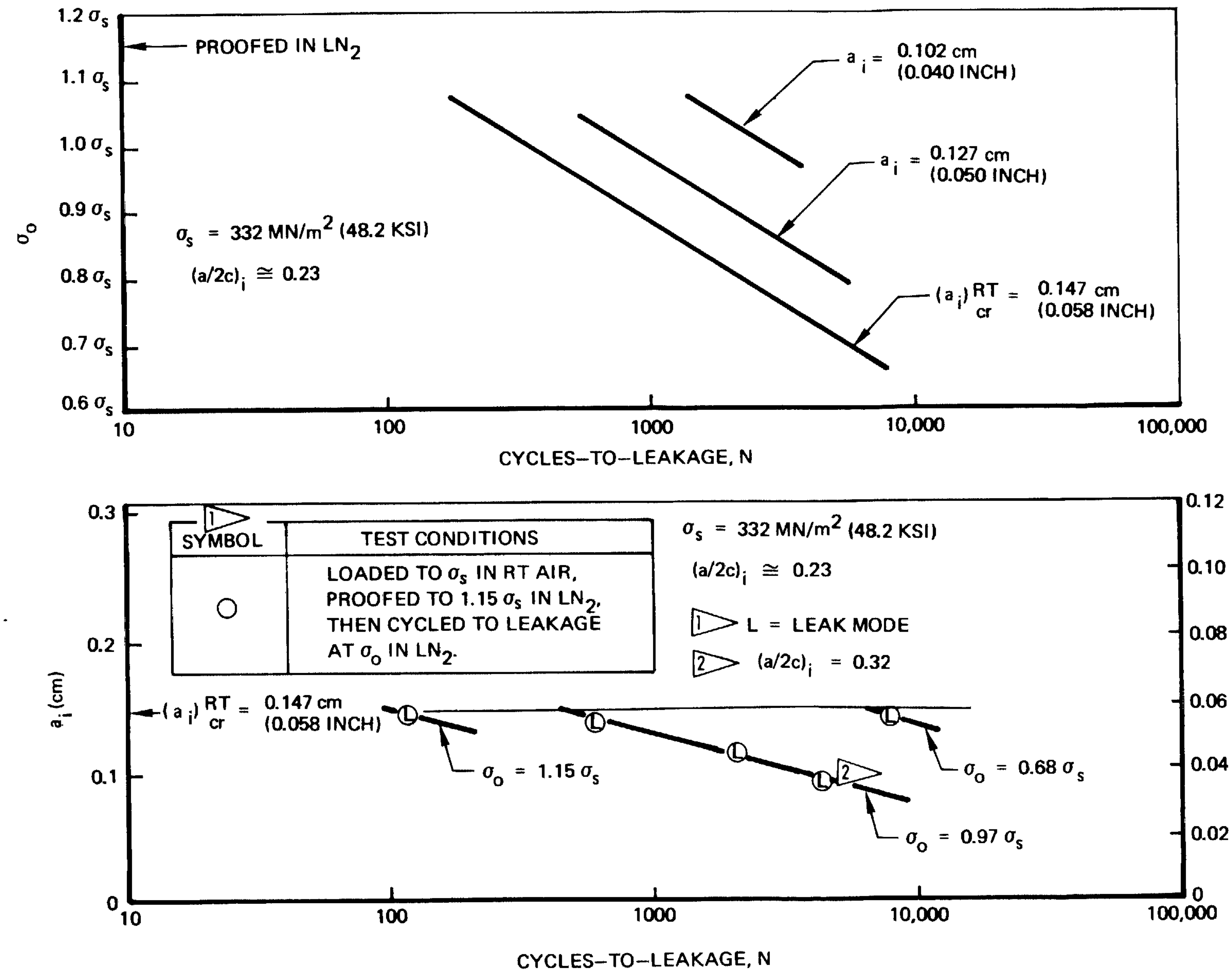

Figure 77: Uniaxial Cyclic Life Results of 0.46 cm (0.18 Inch) Thick Surface Flawed 2219-T62 Aluminum Weld Metal ℄ at 78°K (-320°F)

RT CYCLIC TESTED AT σ_o AFTER BEING LOADED TO σ_s IN RT AIR			
SYMBOL	σ_o MN/m^2 (KSI)	SYMBOL	σ_o MN/m^2 (KSI)
○ 1A-8	282 (40.9)	◇ 1A-18	249 (36.1)
⬡ 1A-11	249 (36.1)	▽ 1A-20	249 (36.1)
△ 1A-14	249 (36.1)	▷ 1A-27	249 (36.1)
□ 1A-17	199 (28.9)		

LN_2 CYLIC TESTED AT σ_o AFTER BEING LOADED TO σ_s IN RT AIR AND THEN PROOF LOADED TO 1.15 σ_s IN LN_2			
SYMBOL	σ_o MN/m^2 (KSI)	SYMBOL	σ_o MN/m^2 (KSI)
● 1A-12	229 (33.2)	▲ 1A-23	285 (41.3)
⬢ 1A-22	323 (46.8)	■ 1A-24	323 (46.8)
		◆ 1A-26	323 (46.8)

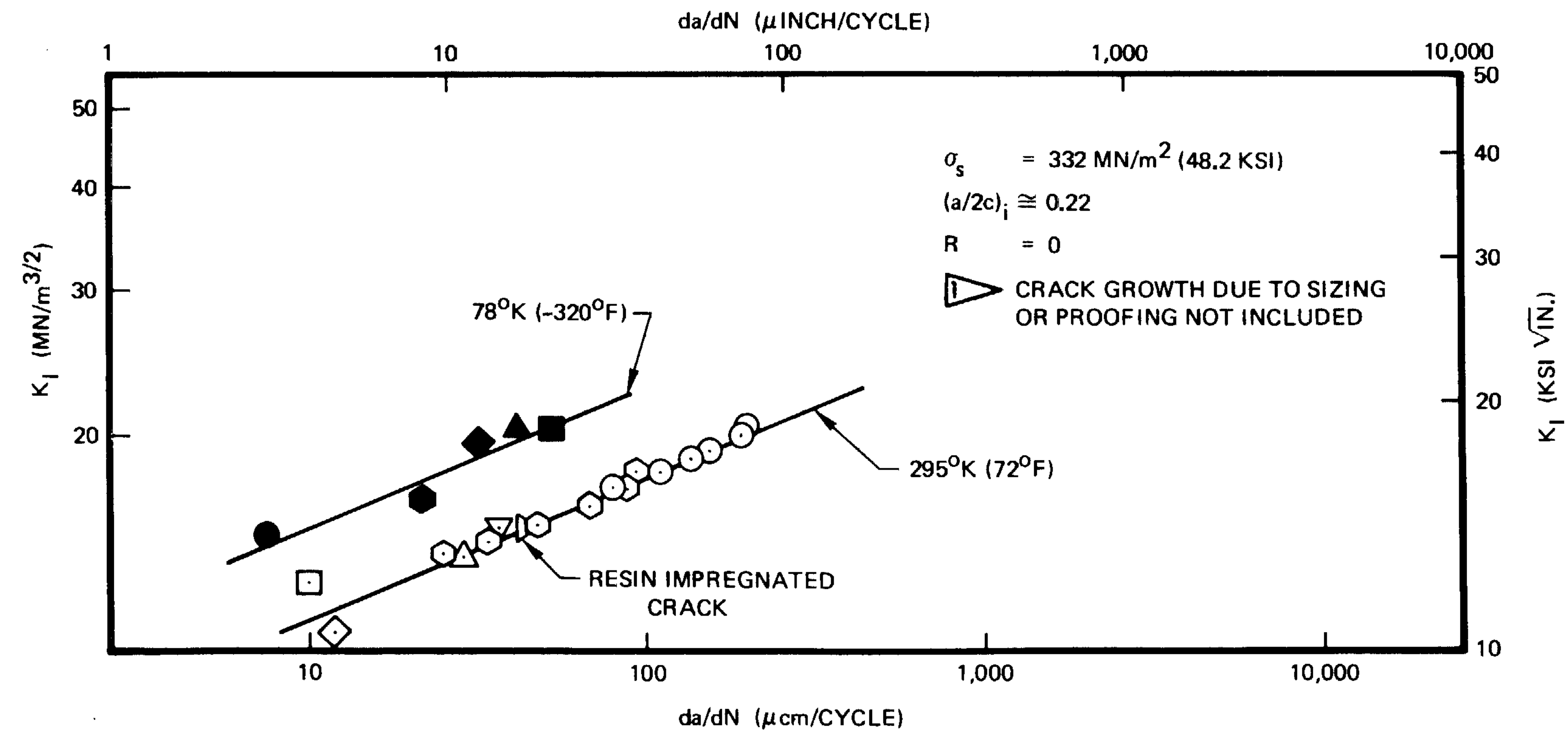

Figure 78: Uniaxial Cyclic Crack Growth Rates ⊳1 for 0.23 cm (0.090 Inch) Thick Surface Flawed 2219-T62 Aluminum Base Metal

RT CYCLIC TESTED AT σ_0 AFTER BEING LOADED IN σ_s IN RT AIR			
SYMBOL	σ_0 MN/m^2 (KSI)	SYMBOL	σ_0 MN/m^2 (KSI)
○ 1AW-12	282 (40.9)	◇ 1AW-23	282 (40.9)
⬡ 1AW-15	249 (36.1)	▽ 1AW-24	282 (40.9)
△ 1AW-17	282 (40.9)	▷ 1AW-25	199 (28.9)
□ 1AW-18	332 (48.2)		

LN_2 CYCLIC TESTED AT σ_0 AFTER BEING LOADED TO σ_s IN RT AIR AND THEN PROOF LOADED TO 1.15 σ_s IN LN_2			
SYMBOL	σ_0 MN/m^2 (KSI)	SYMBOL	σ_0 MN/m^2 (KSI)
● 1AW-16	323 (46.8)	◆ 1AW-26	323 (46.8)
⬢ 1AW-19	381 (55.2)		
▲ 1AW-20	285 (41.3)		
■ 1AW-22	323 (46.8)		

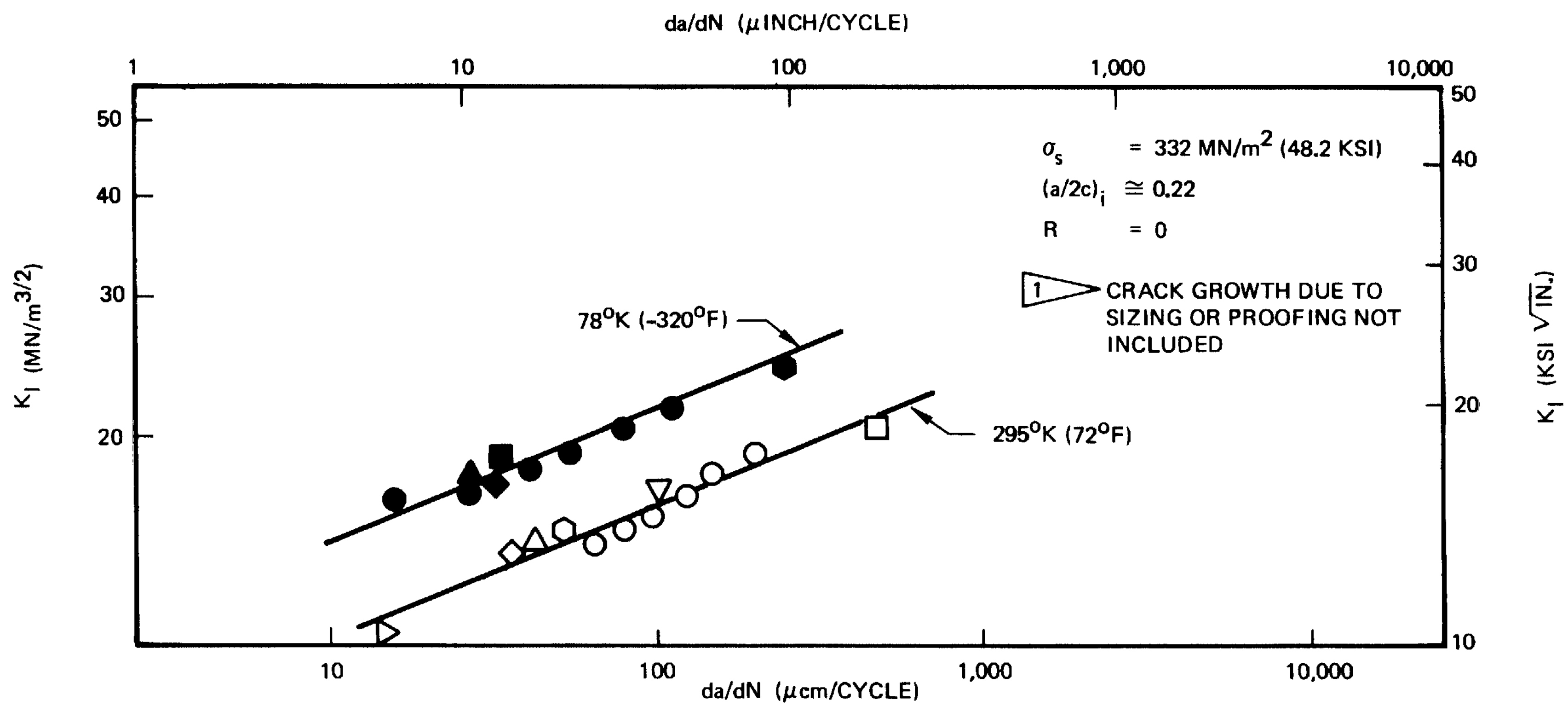

Figure 79: Uniaxial Cyclic Crack Growth Rates [1] *For 0.23 cm (0.090 Inch) Thick Surface Flawed 2219-T62 Aluminum Weld Metal ℄*

RT CYCLIC TESTED AT σ_o AFTER BEING LOADED TO σ_s IN RT AIR					
SYMBOL	σ_o MN/m^2	(KSI)	SYMBOL	σ_o MN/m^2	(KSI)
○ 2A-5	282	(40.9)	◇ 2A-15	282	(40.9)
⬡ 2A-7	332	(48.2)	▽ 2AW-16	282	(40.9)
△ 2A-8	282	(40.9)	▷ 2AW-18	282	(40.9)
□ 2A-12	199	(28.9)			

LN_2 CYCLIC TESTED AT σ_o AFTER BEING LOADED TO σ_s IN RT AIR AND THEN PROOF LOADED TO 1.15 σ_s IN LN_2					
SYMBOL	σ_o MN/m^2	(KSI)	SYMBOL	σ_o MN/m^2	(KSI)
● 2A-9	381	(55.2)	◆ 2A-16	323	(46.8)
⬢ 2A-11	323	(46.8)	▼ 2A-17	228	(33.0)
▲ 2A-13	228	(33.0)	▶ 2A-18	323	(46.8)
■ 2A-14	285	(41.3)			

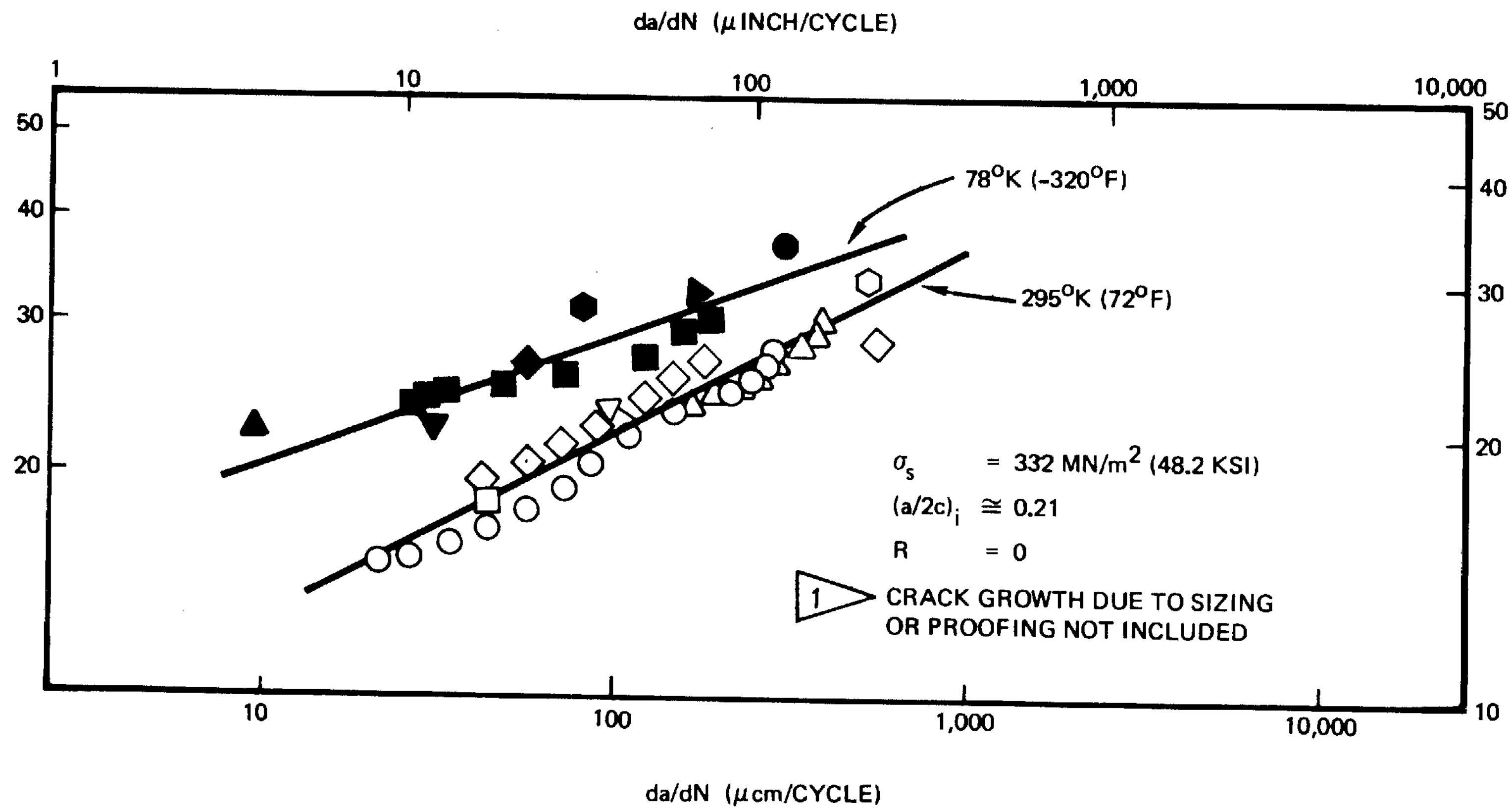

Figure 80: Uniaxial Cyclic Crack Growth Rates ▷1 *for 0.46 cm (0.18 Inch) Thick Surface Flawed 2219-T62 Aluminum Base Metal*

RT CYCLIC TESTED AT σ_o AFTER BEING LOADED TO σ_s IN RT AIR			
SYMBOL	σ_o MN/m^2 (KSI)	SYMBOL	σ_o MN/m^2 (KSI)
○ 2AW-4	332 (48.2)	□ 2AW-12	199 (28.8)
⬡ 2AW-5	282 (40.9)	◇ 2AW-13	283 (41.0)
△ 2AW-8	283 (41.0)		

LN_2 CYCLIC TESTED AT σ_o AFTER BEING LOADED TO σ_s IN RT AIR AND THEN PROOF LOADED TO 1.15 σ_s IN LN_2			
SYMBOL	σ_o MN/m^2 (KSI)	SYMBOL	σ_o MN/m^2 (KSI)
● 2AW-6	381 (55.2)	■ 2AW-10	323 (46.8)
⬢ 2AW-7	322 (46.7)	◆ 2AW-11	323 (46.8)
▲ 2AW-9	228 (33.0)		

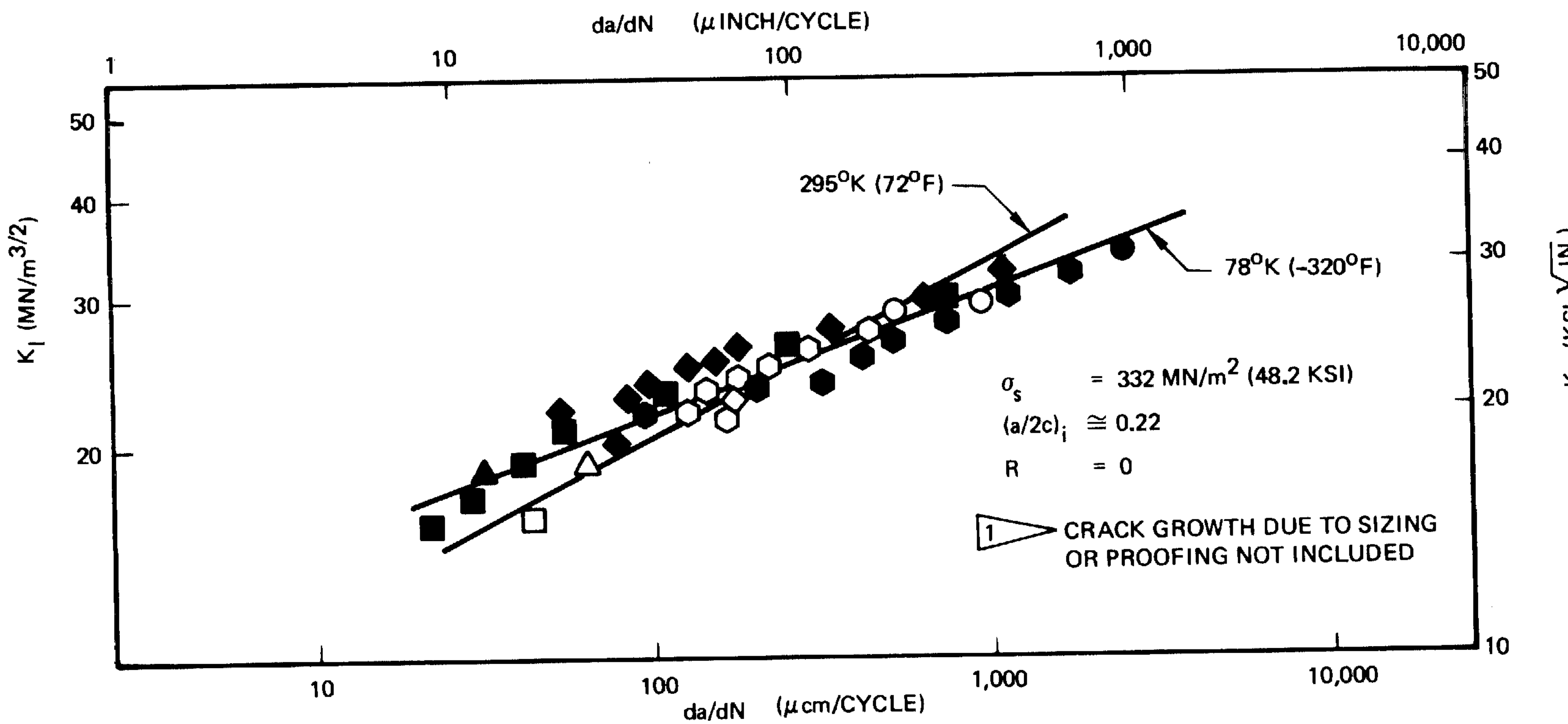

Figure 81: Uniaxial Cyclic Crack Growth Rates [1] *for 0.46 cm (0.18 Inch) Thick Surface Flawed 2219-T62 Aluminum Weld Metal ℄*

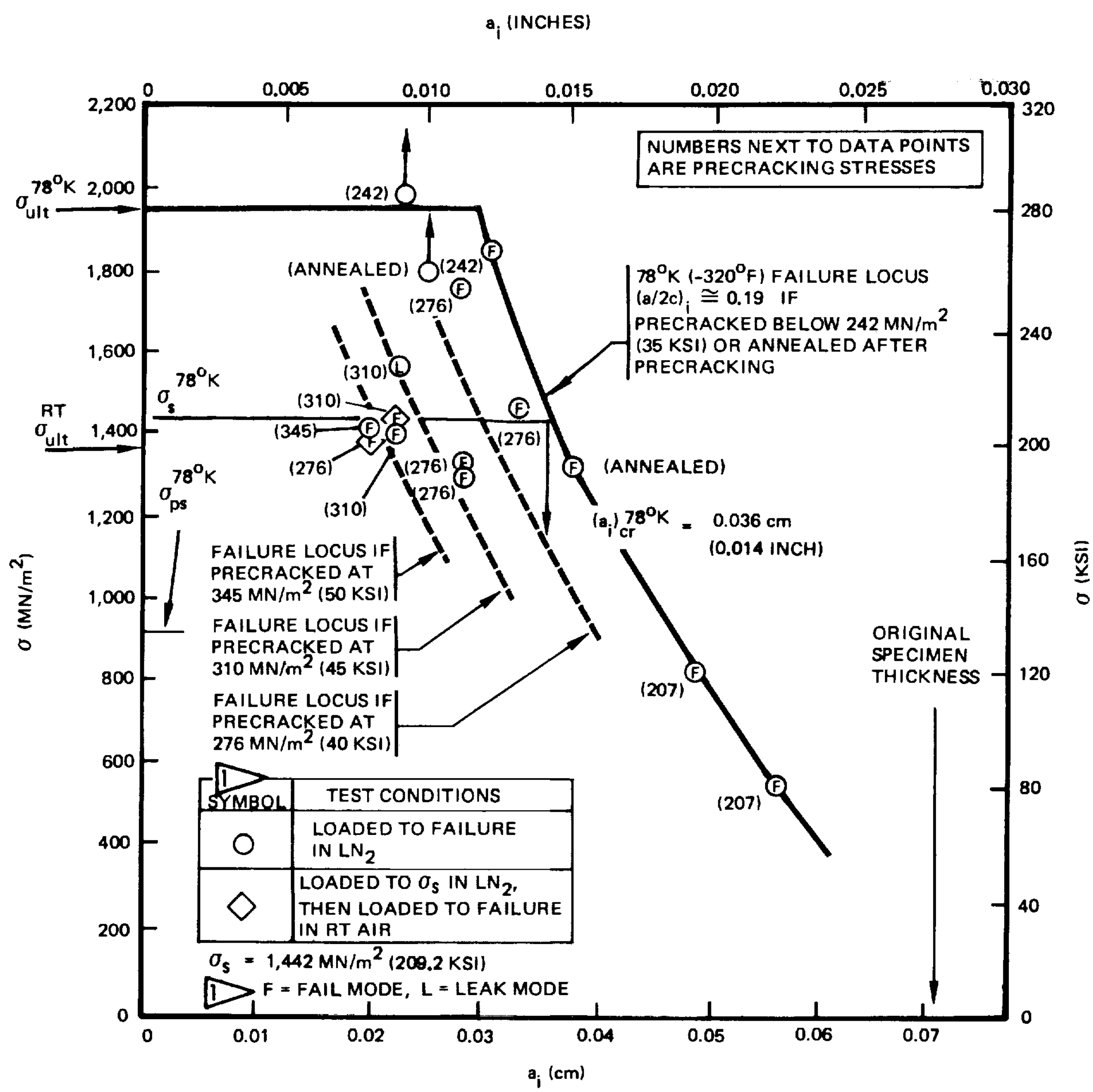

Figure 82: Uniaxial Static Fracture Results of 0.071 cm (0.028 Inch) Thick Surface Flawed Cryostretched 301 Stainless Steel Base Metal

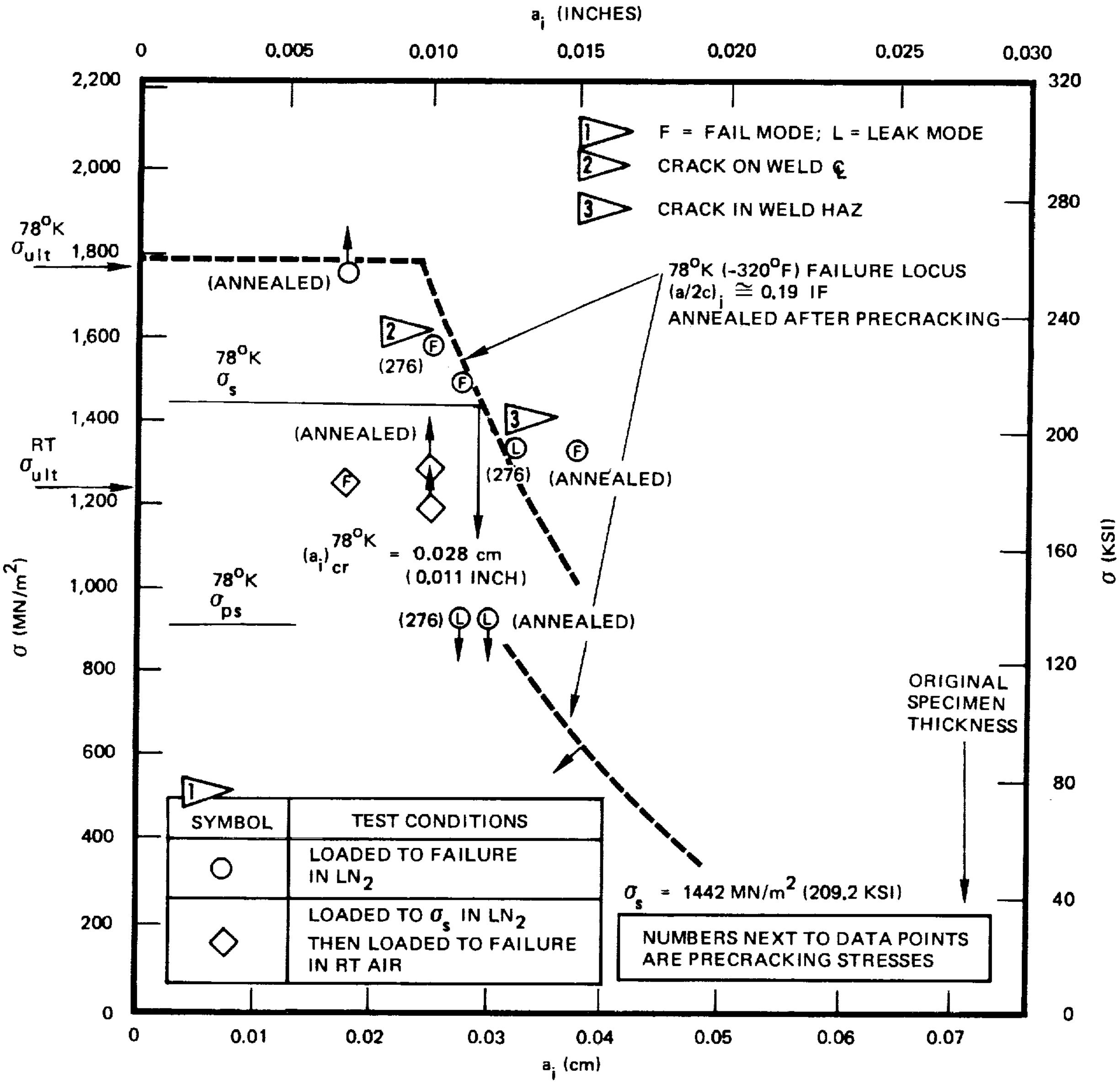

Figure 83: Uniaxial Static Fracture Results of 0.071 cm (0.028 Inch) Thick Surface Flawed Cryostretched 301 Stainless Steel Weld Metal Fusion Line

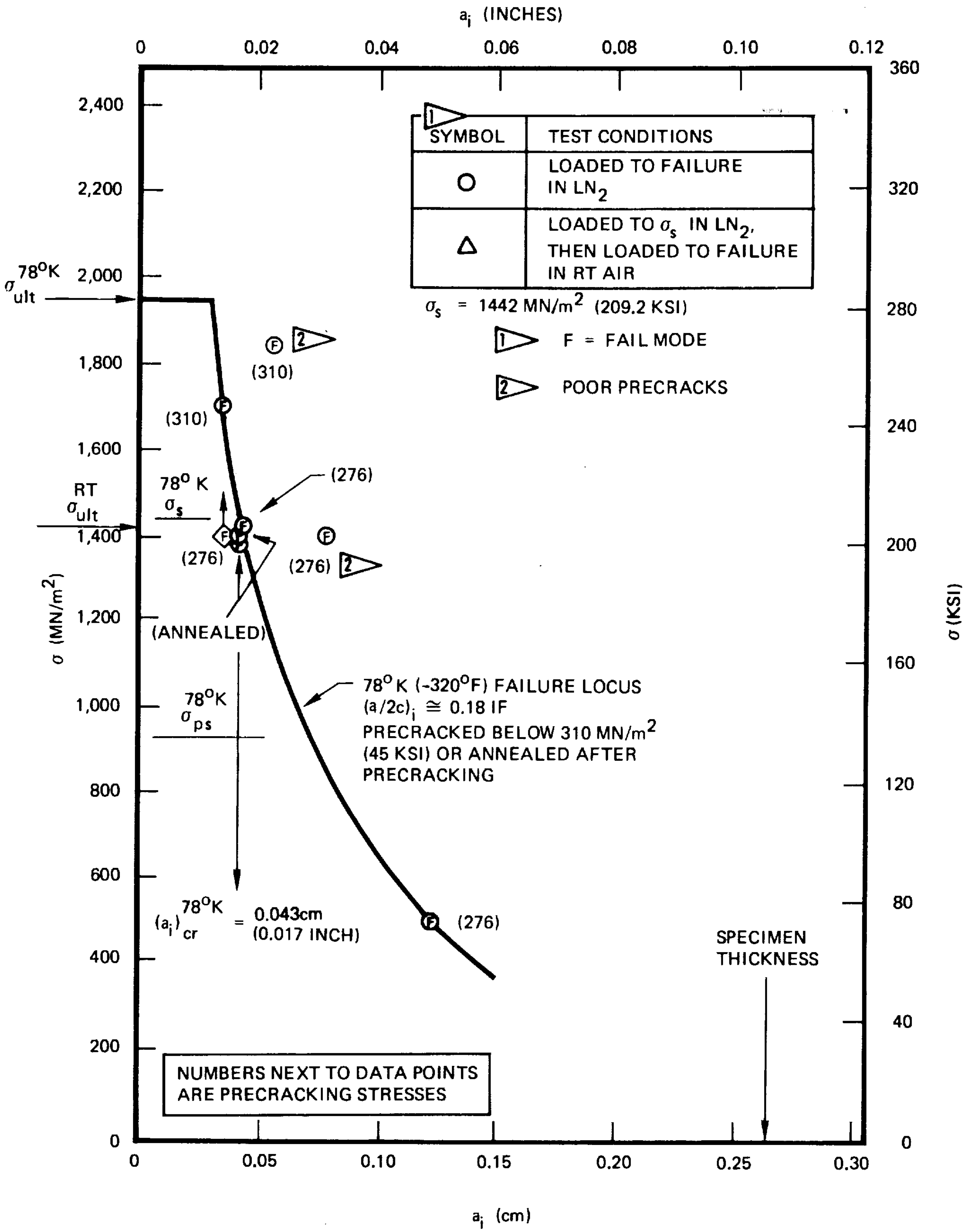

Figure 84: Uniaxial Static Fracture Results of 0.26 cm (0.10 Inch) Thick Surface Flawed Cryostretched 301 Stainless Steel Base Metal

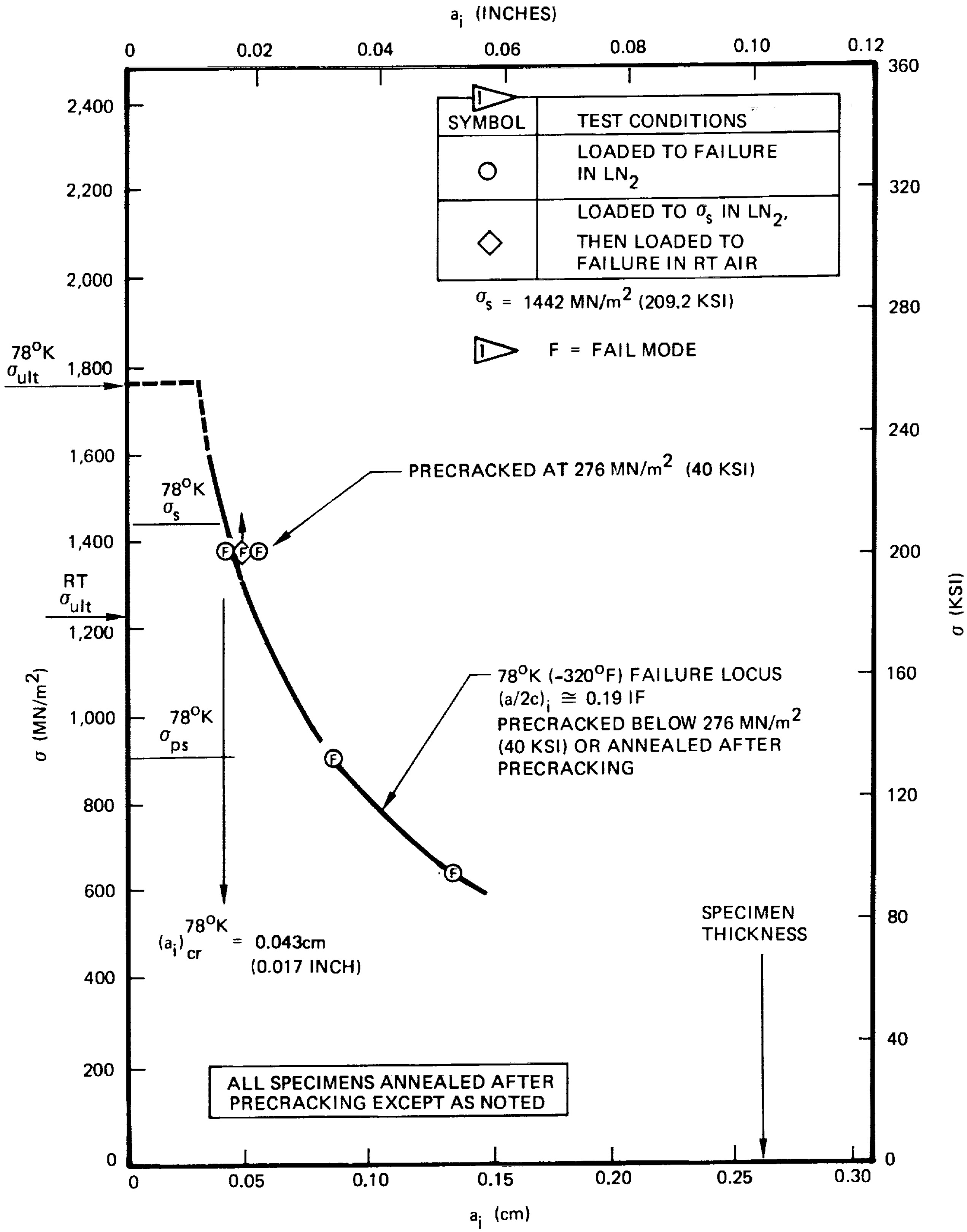

Figure 85: Uniaxial Static Fracture Results of 0.26 cm (0.10 Inch) Thick Surface Flawed Cryostretched 301 Stainless Steel Weld Metal Fusion Line

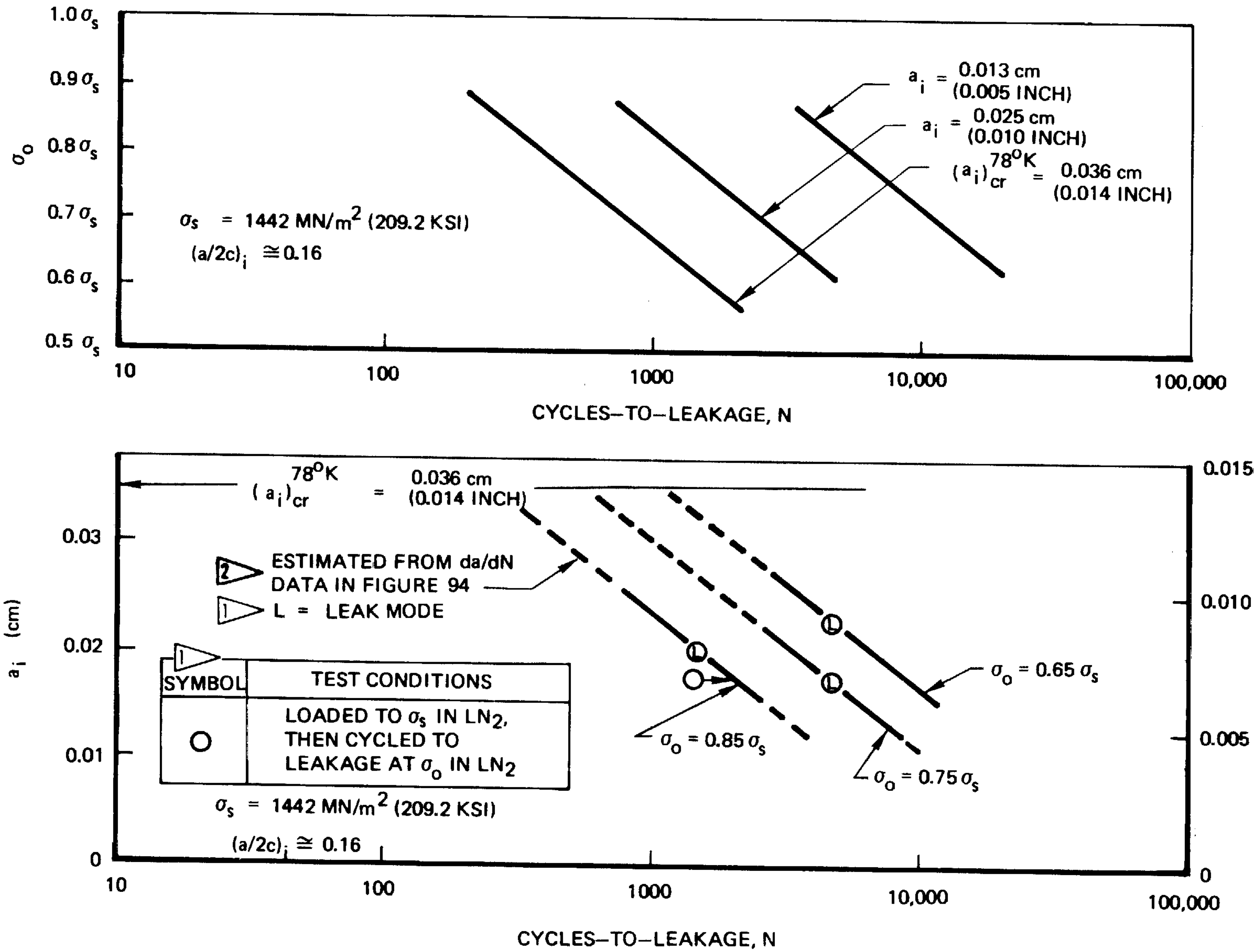

Figure 86 : *Uniaxial Cyclic Life Results of 0.071 cm (0.028 Inch) Thick Surface Flawed Cryostretched 301 Stainless Steel Base Metal at 78°K (-320°F)* [2]

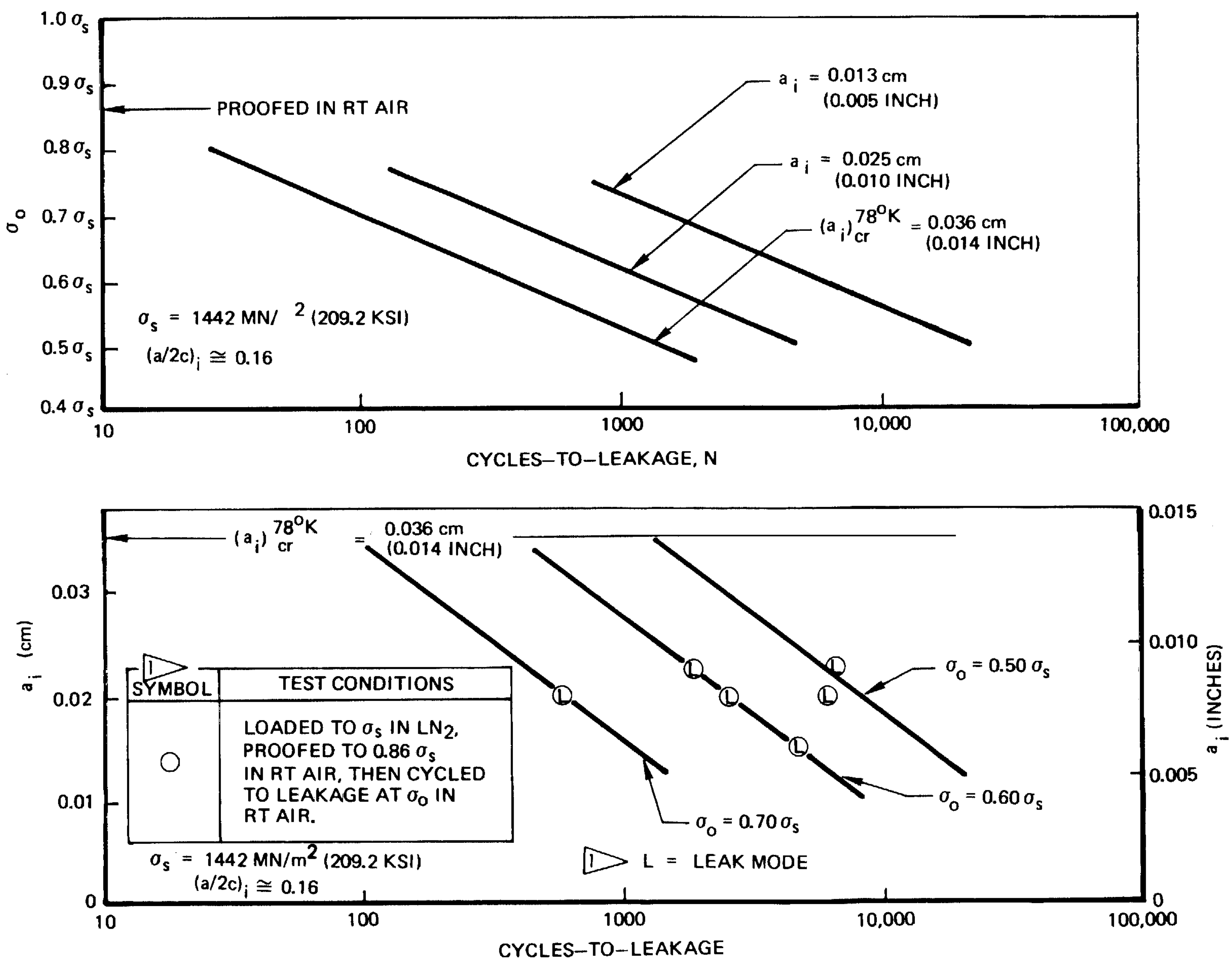

Figure 87: *Uniaxial Cyclic Life Results of 0.071 cm (0.028 Inch) Thick Surface Flawed Cryostretched 301 Stainless Steel Base Metal at 295°K (72°F)*

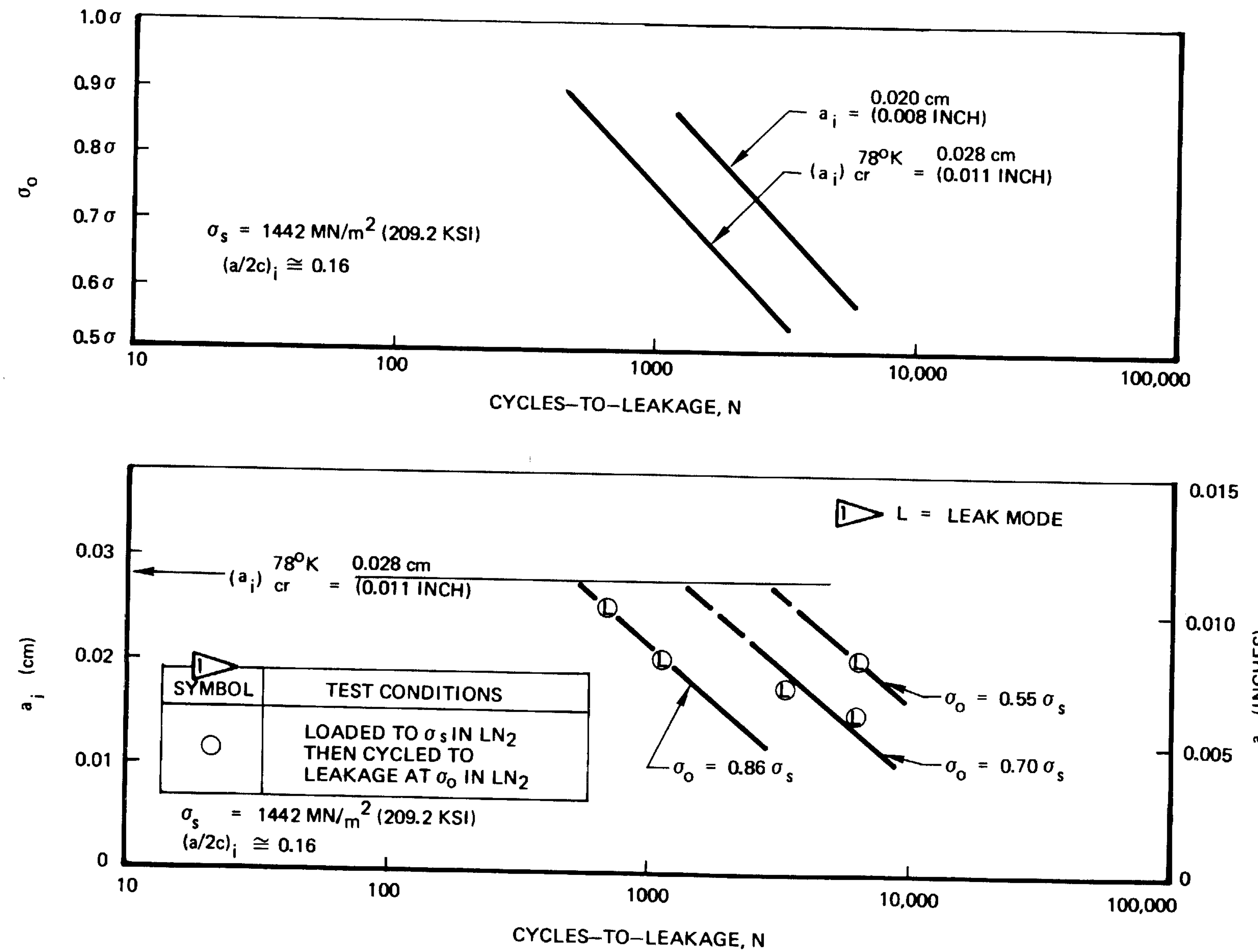

Figure 88: *Uniaxial Cyclic Life Results of 0.071 cm (0.028 Inch) Thick Surface Flawed Cryostretched 301 Stainless Steel Weld Metal Fusion Line at 78°K (-320°F)*

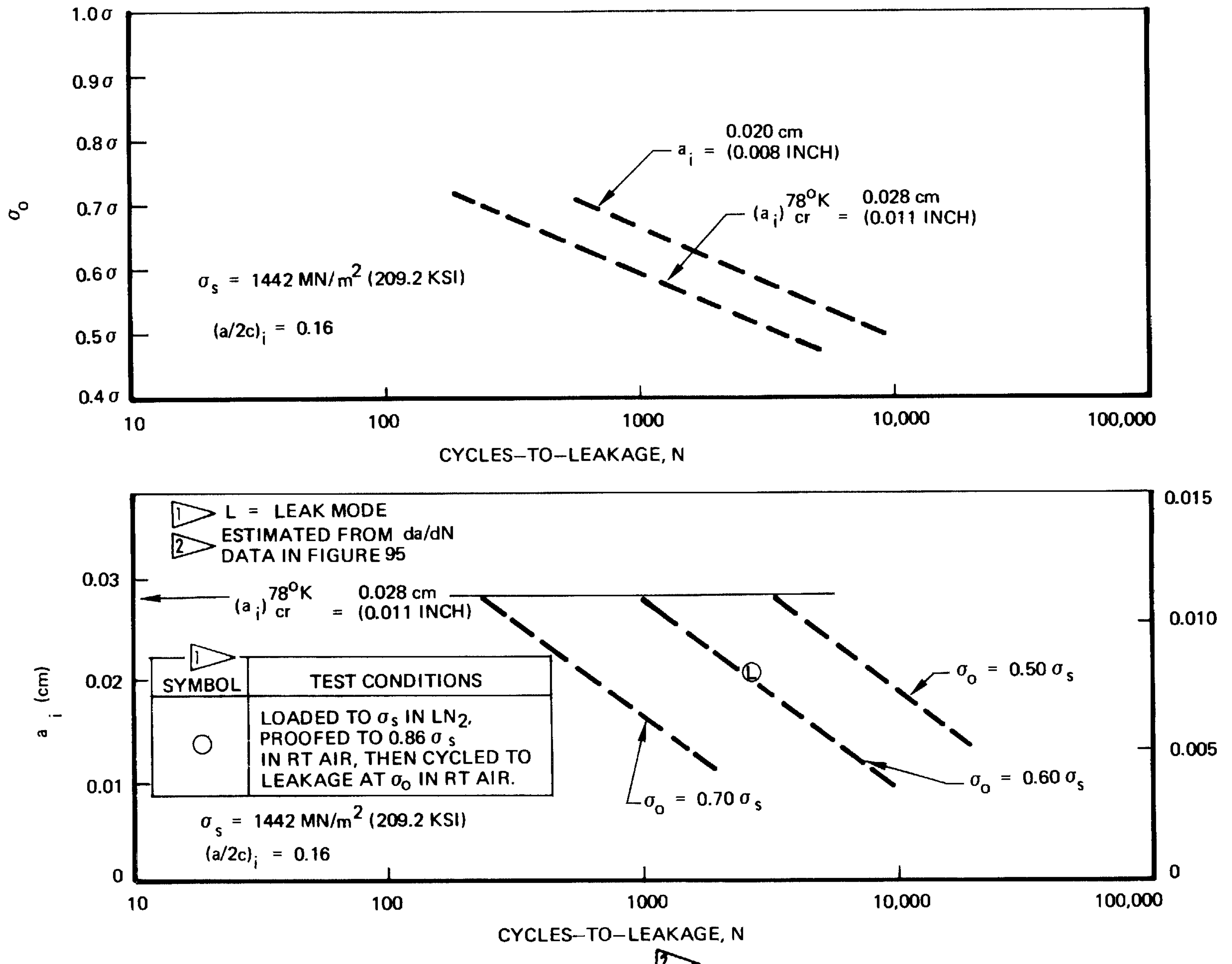

Figure 89 : *Uniaxial Cyclic Life Results of 0.071 cm (0.028 Inch) Thick Surface Flawed Cryostretched 301 Strainless Steel Weld Metal Fusion Line at 295°K (72°F)*

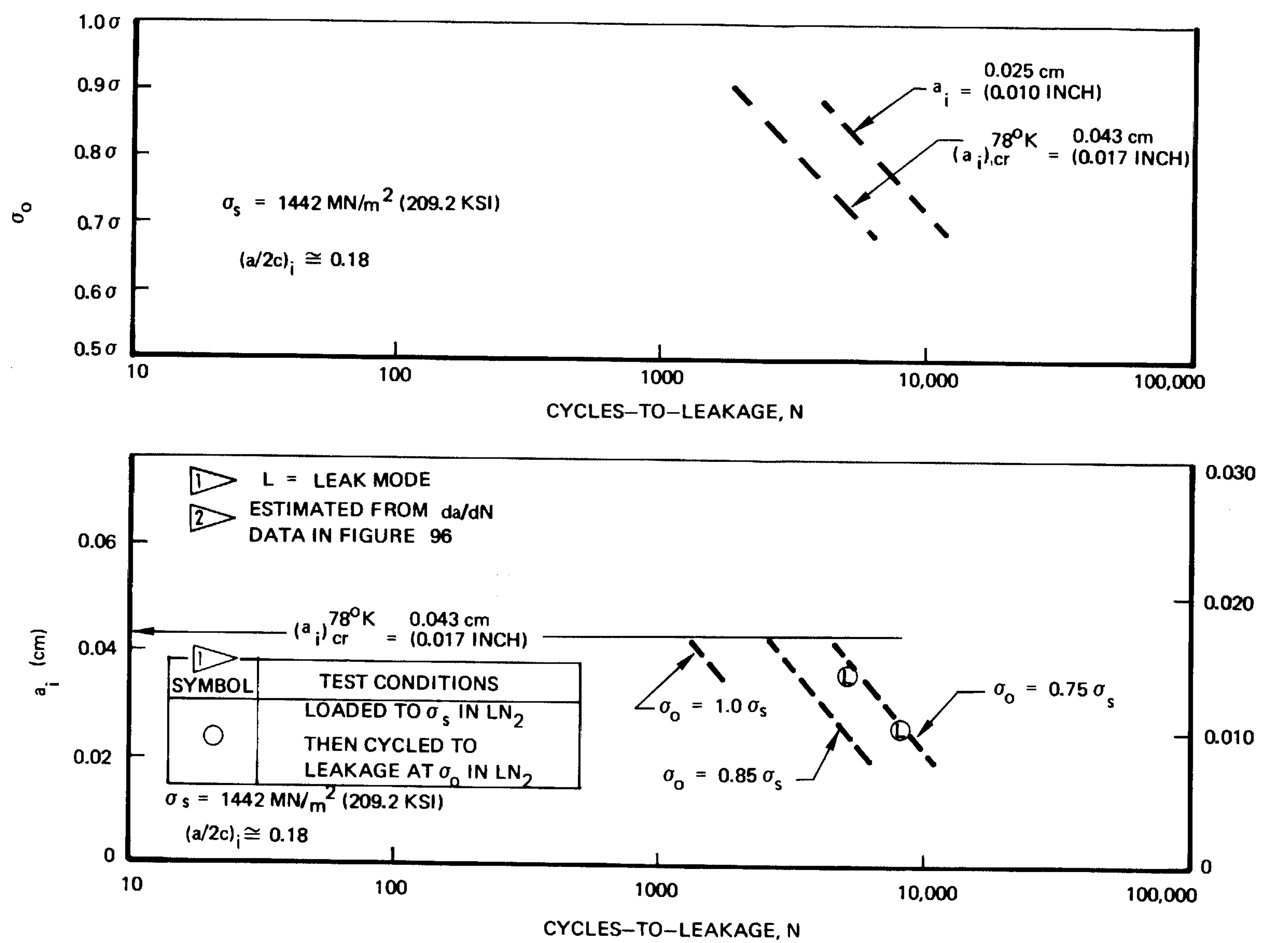

2 *Figure 90 : Uniaxial Cyclic Life Results of 0.26 cm (0.10 Inch) Thick Surface Flawed Cryostretched 301 Stainless Steel Base Metal at 78°K (-320°F)*

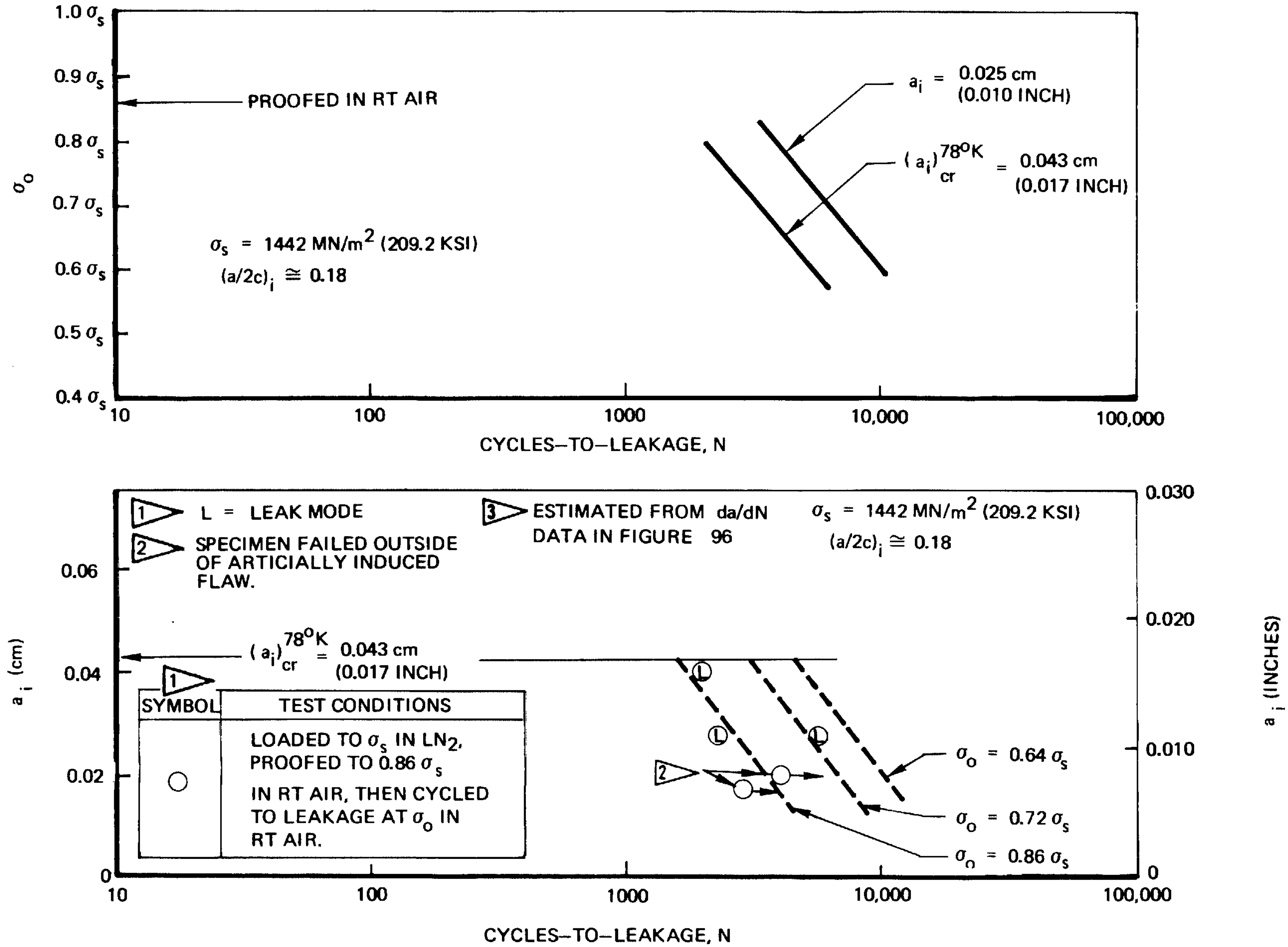

Figure 91 : Uniaxial Cyclic Life Results of 0.26 cm (0.10 Inch) Thick Surface Flawed Cryostretched 301 Stainless Steel Base Metal at 295°K (72°F) 3

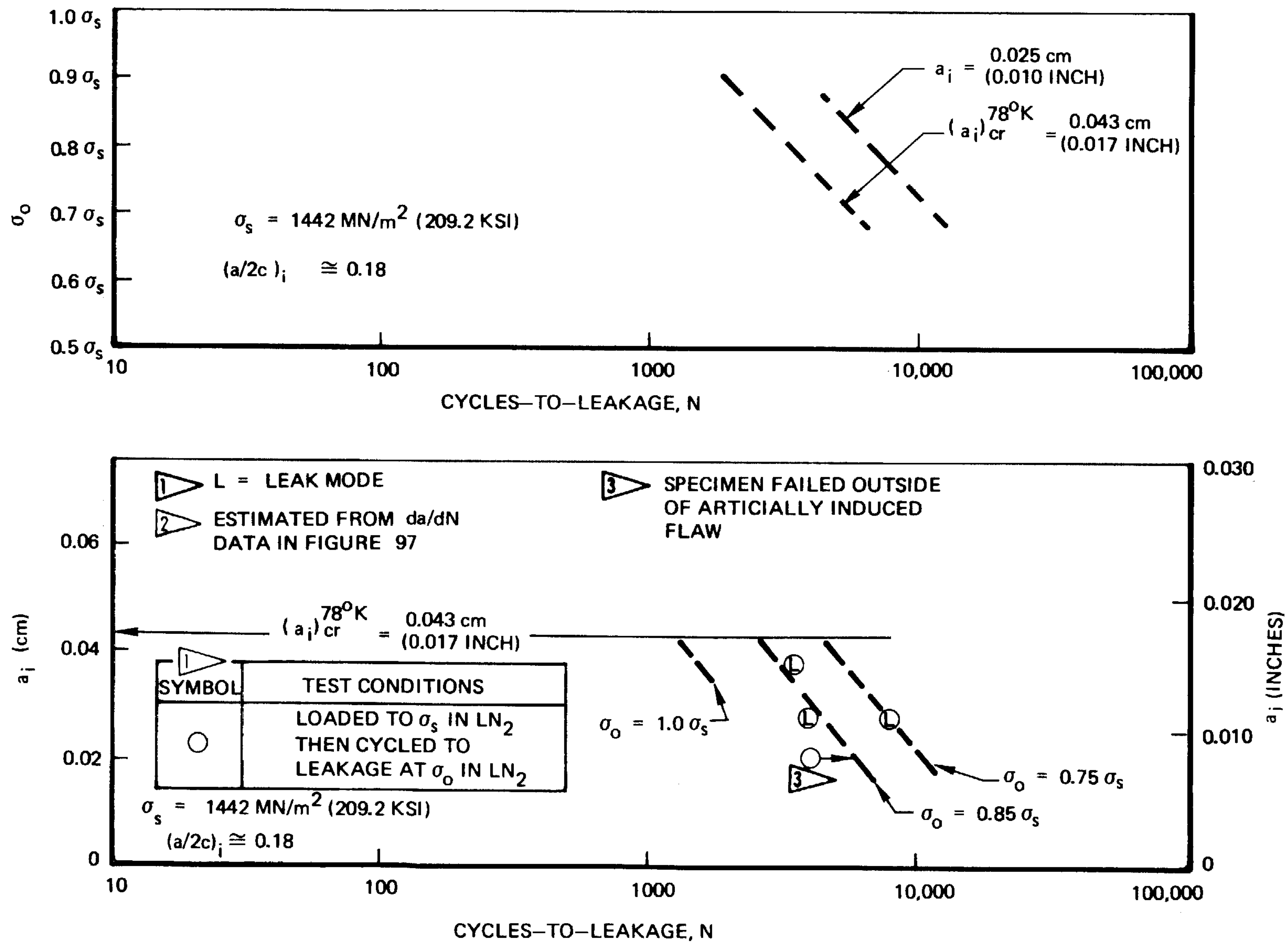

2 *Figure 92 : Uniaxial Cyclic Life Results of 0.26 cm (0.10 Inch) Thick Surface Flawed Cryostretched 301 Stainless Steel Weld Metal Fusion Line at 78°K (-320°F)*

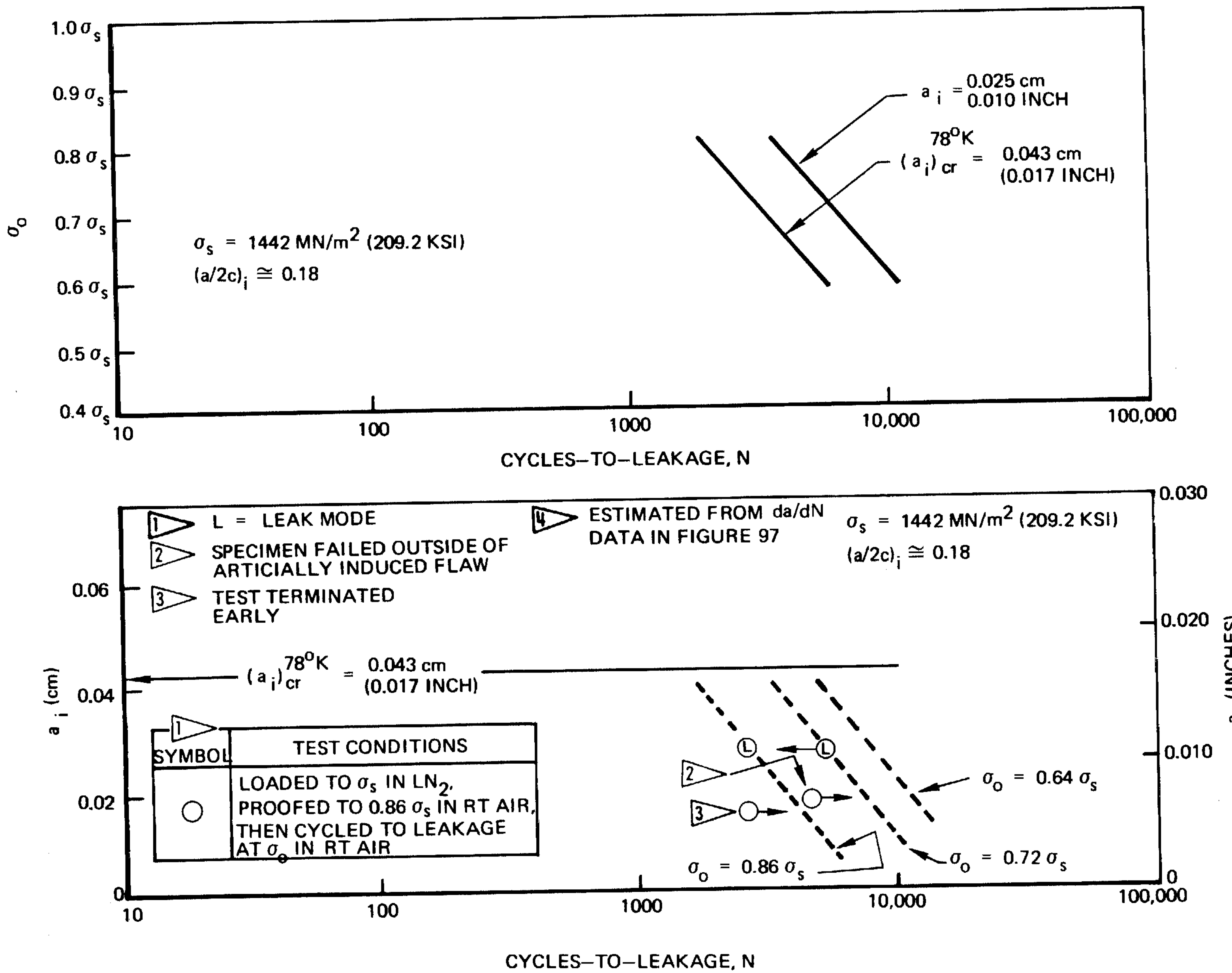

Figure 93 : *Uniaxial Cyclic Life Results of 0.26 cm (0.10 Inch) Thick Surface Flawed Cryostretched 301 Stainless Steel Weld Metal Fusion Line at 295°K (72°F)*

CYCLED AT σ_o IN LN_2 AFTER BEING LOADED TO 0.65 σ_s IN LN_2, UNLOADED, AND THEN LOADED TO σ_s IN LN_2			
SYMBOL	σ_o MN/m^2 (KSI)	SYMBOL	σ_o MN/m^2 (KSI)
○ 1C-2A	1083 (157.0)	◇ 1C-20	1227 (178.0)
⬡ 1C-14	1083 (157.0)	▽ 1C-21	1227 (178.0)
△ 1C-16	1442 (209.2)	▷ 1CW-12	(136.0)
□ 1C-17	1227 (178.0)		

CYCLED AT σ_o IN RT AIR AFTER BEING LOADED TO 0.65 σ_s IN LN_2, UNLOADED, LOADED TO σ_s IN LN_2 AND THEN PROOF LOADED TO 0.86 σ_s IN RT AIR			
SYMBOL	σ_o MN/m^2 (KSI)	SYMBOL	σ_o MN/m^2 (KSI)
● 1C-22	1007 (146.0)	◆ 1CW-17	699 (101.4)
⬢ 1C-23	817 (118.5)	▼ 1CW-18	876 (127.0)
▲ 1C-24	848 (123.0)		
■ 1CW-15	758 (110.0)		

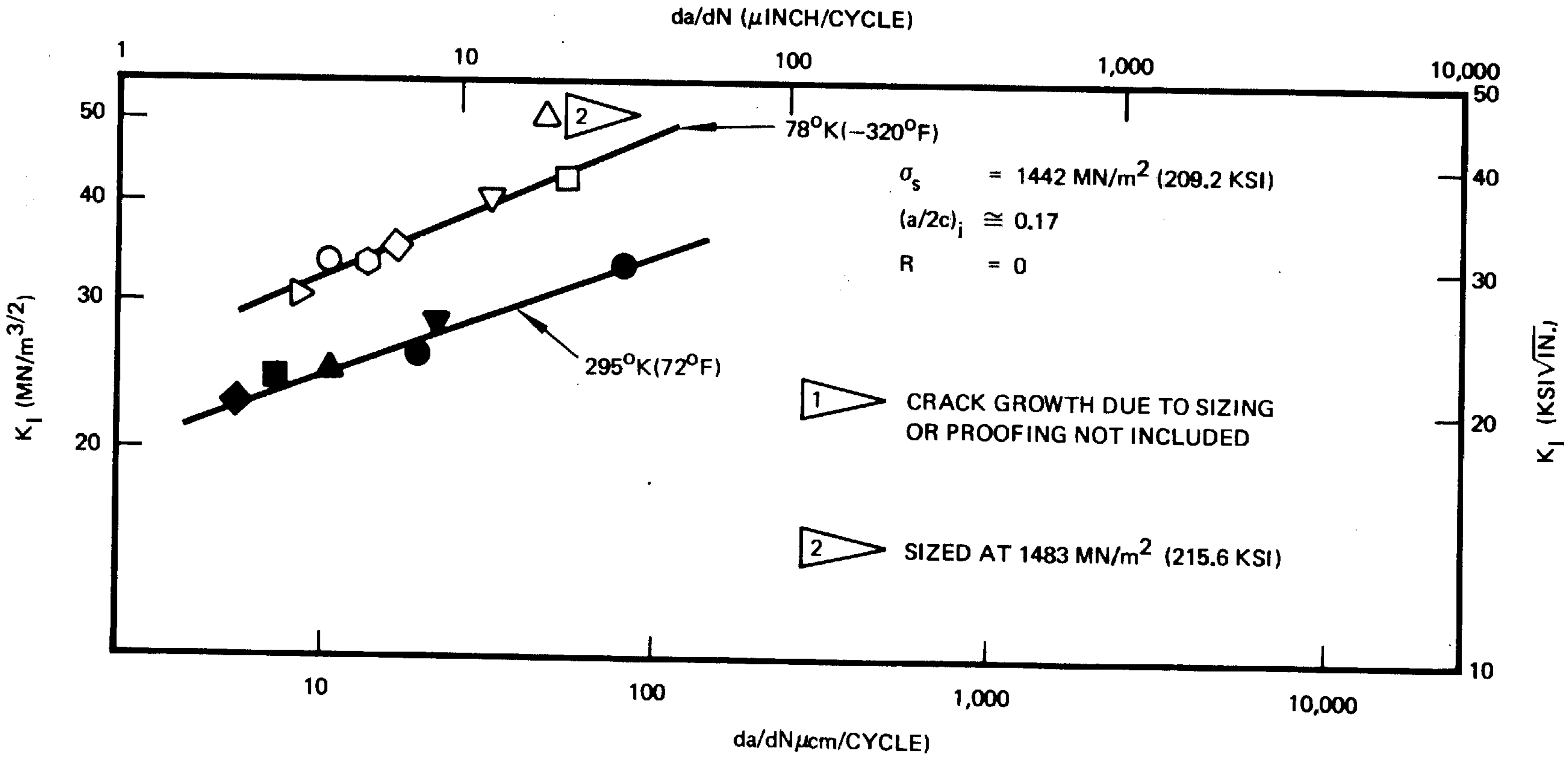

Figure 94: Uniaxial Cyclic Crack Growth Rates [1] *for 0.071 cm (0.028 Inch) Thick Surface Flawed Cryostretched 301 Stainless Steel Base Metal*

CYCLED AT σ_o IN LN_2 AFTER BEING LOADED TO 0.65 σ_s IN LN_2, UNLOADED, AND THEN LOADED TO σ_s IN LN_2			
SYMBOL	σ_o MN/m^2 (KSI)	SYMBOL	σ_o MN/m^2 (KSI)
○ 1CW-7	1010 (146.5)	□ 1CW-14	793 (115.0)
⬡ 1CW-8	1255 (182.0)	◇ 1CW-16	1234 (179.0
△ 1CW-9	1010 (146.5)		

CYCLED AT σ_o IN RT AIR AFTER BEING LOADED TO 0.65 σ_s IN LN_2, UNLOADED, LOADED TO σ_s IN LN_2 AND THEN PROOF LOADED TO 0.86 σ_s IN RT AIR			
SYMBOL	σ_o MN/m^2 (KSI)	SYMBOL	σ_o MN/m^2 (KSI)
● 1CW-19	857 (124.3)		

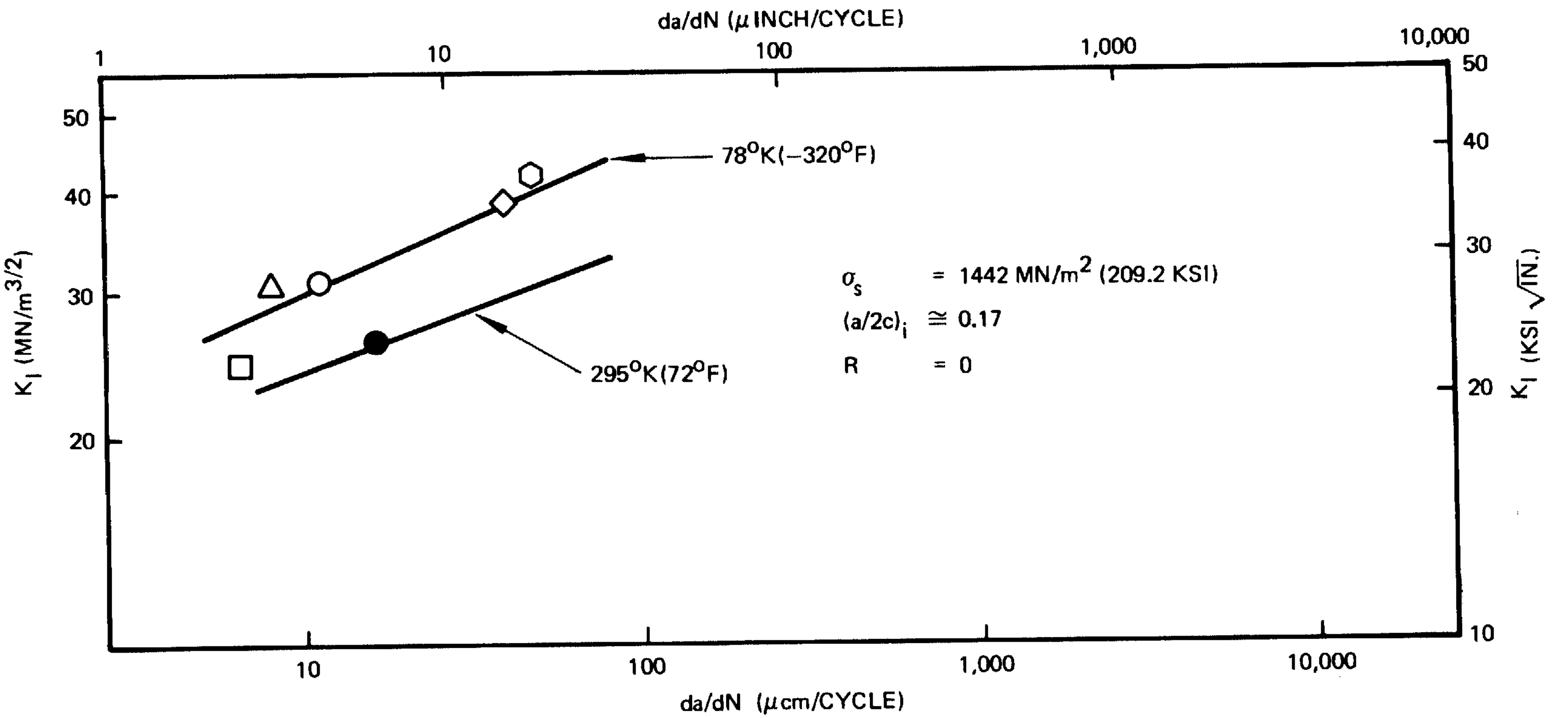

Figure 95: *Uniaxial Cyclic Crack Growth Rates for 0.071 cm (0.028 Inch) Thick Surface Flawed Cryostretched 301 Stainless Steel Weld Metal Fusion Line*

CYCLED AT σ_o IN LN_2 AFTER BEING LOADED TO 0.65 σ_s IN LN_2, UNLOADED, AND THEN LOADED TO σ_s IN LN_2			
SYMBOL	σ_o MN/m^2 (KSI)	SYMBOL	σ_o MN/m^2 (KSI)
○ 2C-6	1442 (209.2)	□ 2C-15	1083 (157.0)
⬡ 2C-7	1227 (178.0)	◇ 2CW-12	1083 (157.0)
△ 2C-13	1083 (157.0)		

CYCLED AT σ_o IN RT AIR AFTER BEING LOADED TO 0.65 σ_s IN LN_2, UNLOADED, LOADED TO σ_s IN LN_2 AND THEN PROOF LOADED TO 0.86 σ_s IN RT AIR			
SYMBOL	σ_o MN/m^2 (KSI)	SYMBOL	σ_o MN/m^2 (KSI)
● 2C-10	1214 (176.0)	■ 2CW-6	1234 (179.0)
⬢ 2C-12	1034 (150.0)	◆ 2CW-8	1234 (179.0)
▲ 2C-14	1034 (150.0)		

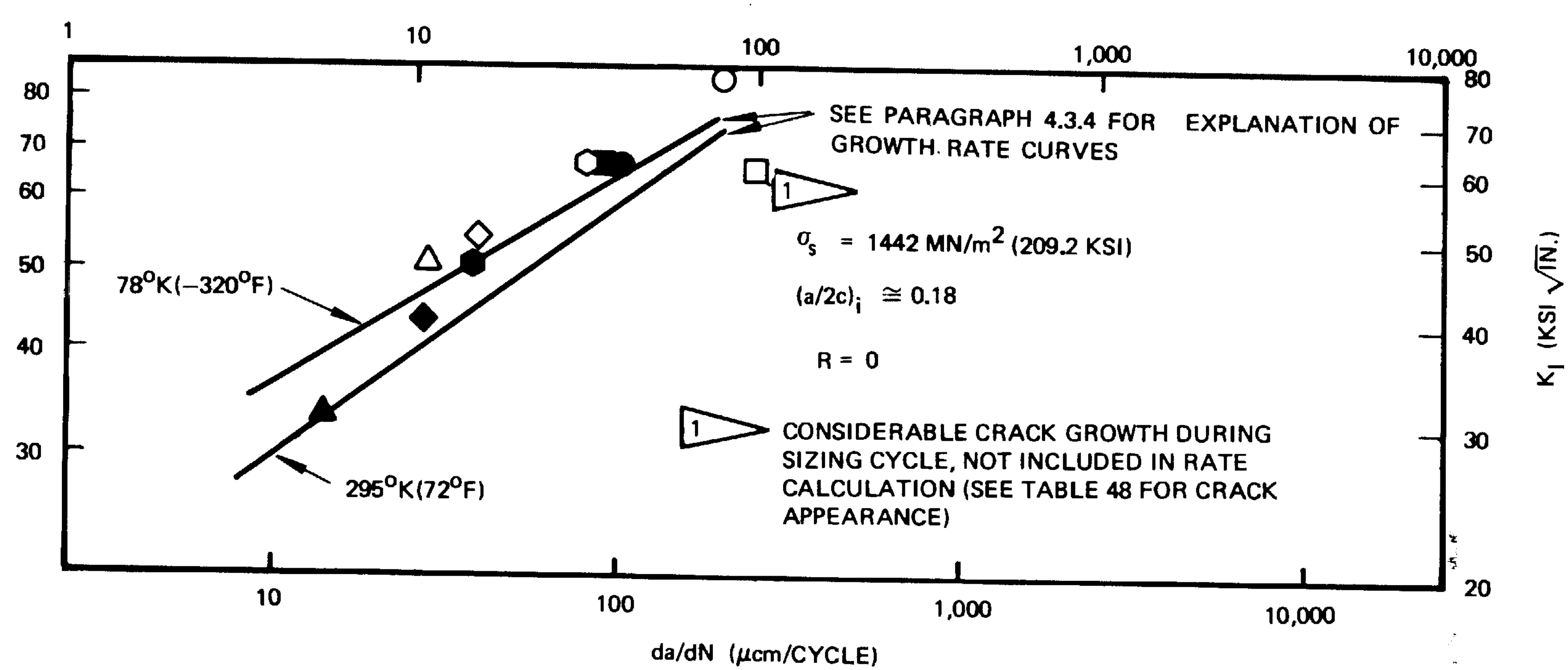

Figure 96: Uniaxial Cyclic Crack Growth Rates for 0.26 cm (0.10 Inch) Thick Surface Flawed Cryostretched 301 Stainless Steel Base Metal

CYCLED AT σ_o IN LN_2 AFTER BEING LOADED TO 0.65 σ_s IN LN_2, UNLOADED, AND THEN LOADED TO σ_s IN LN_2			
SYMBOL	σ_o MN/m^2 (KSI)	SYMBOL	σ_o MN/m^2 (KSI)
○ 2CW-5	1227 (178.0)	△ 2CW-11	1083 (157.0)
⬡ 2CW-7	1227 (178.0)	□ 2CW-14	1227 (178.0)

CYCLED AT σ_o IN RT AIR AFTER BEING LOADED TO 0.65 σ_s IN LN_2, UNLOADED, LOADED TO σ_s IN LN_2 AND THEN PROOF LOADED TO 0.86 σ_s IN RT AIR			
SYMBOL	σ_o MN/m^2 (KSI)	SYMBOL	σ_o MN/m^2 (KSI)
● 2CW-2	1027 (149.0)	▲ 2CW-4	1034 (150.0)
⬢ 2CW-3	1234 (179.0)	■ 2CW-6	1234 (179.0)

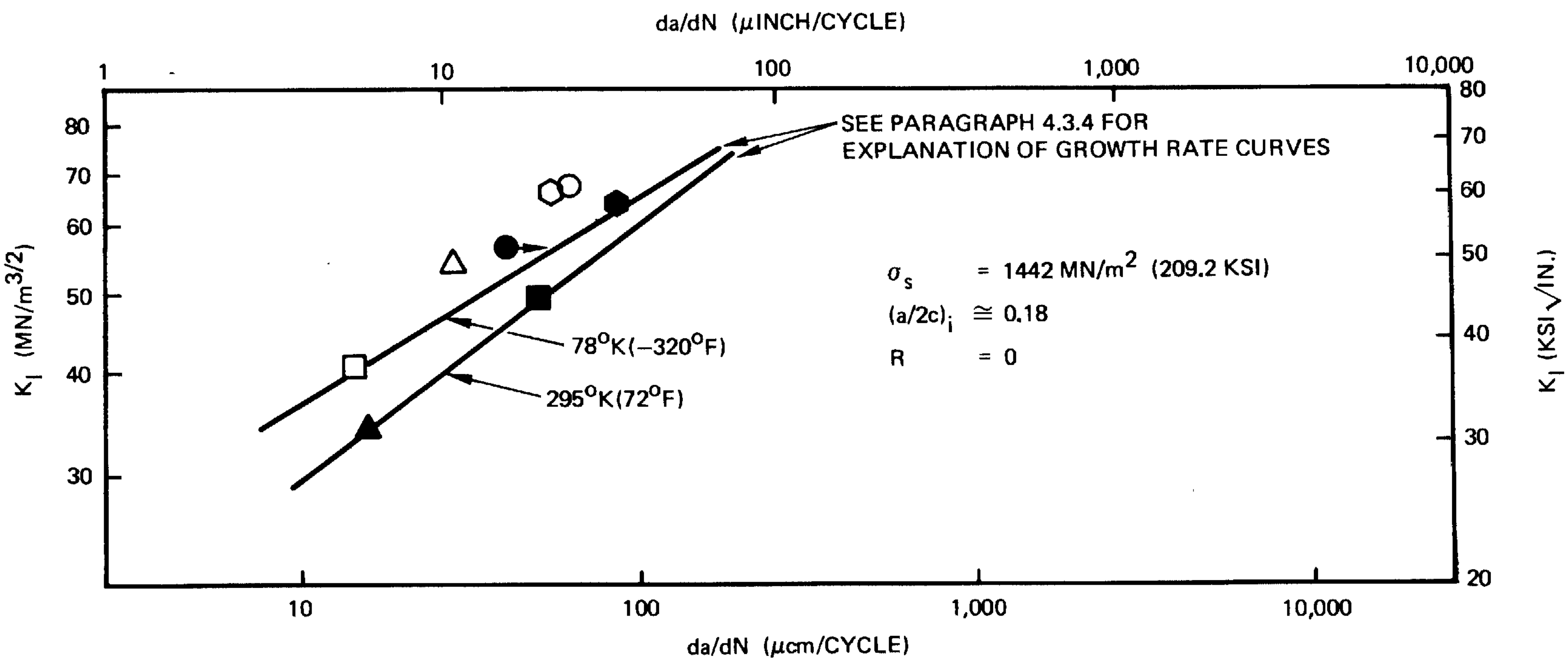

Figure 97: Uniaxial Cyclic Crack Growth Rates for 0.26 cm (0.10 Inch) Thick Surface Flawed Cryostretched 301 Stainless Steel Weld Metal Fusion Line

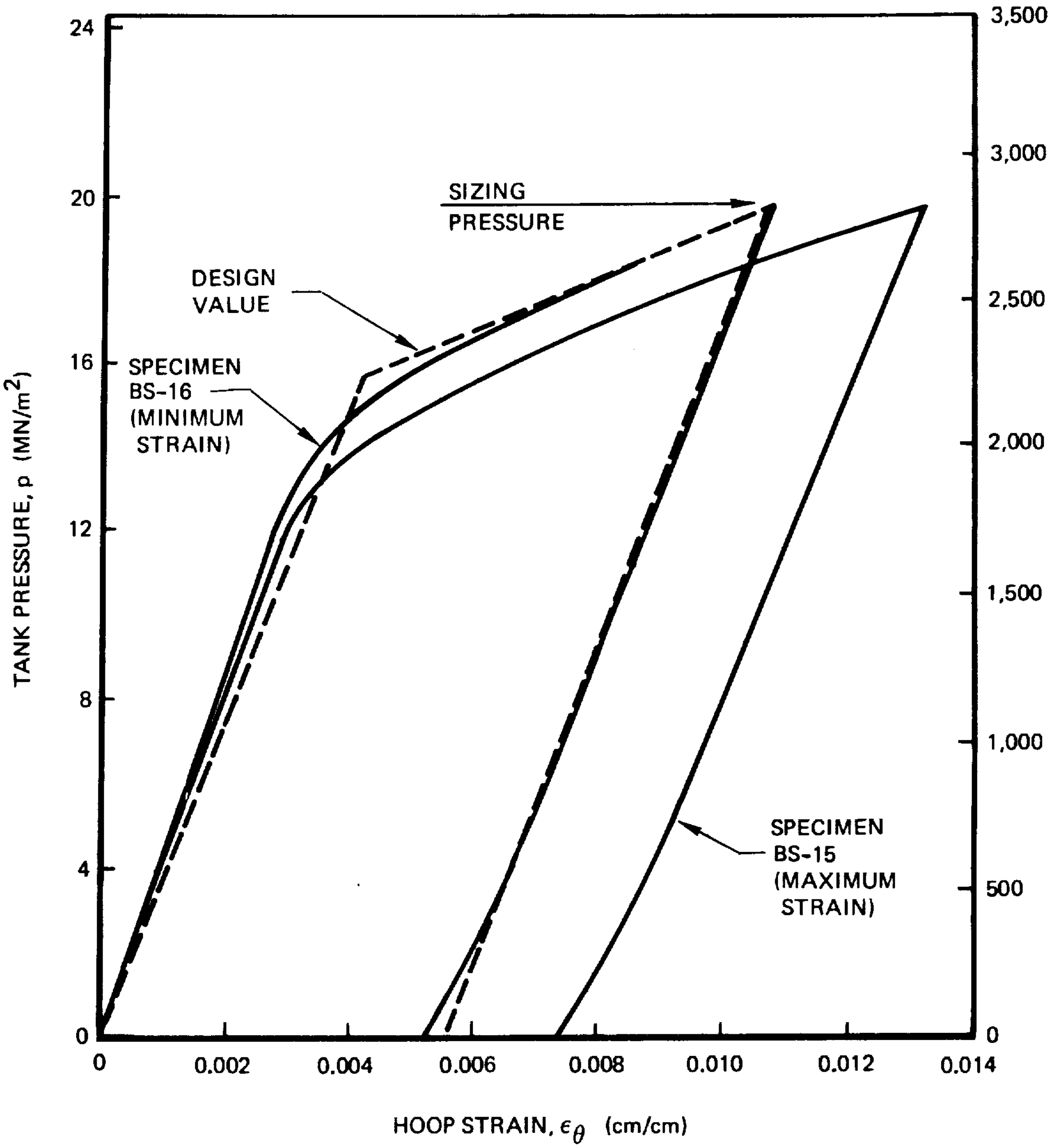

Figure 98: Comparison of Pressure/Strain Curves for Hoop GFR Inconel X750 STA Tanks at RT

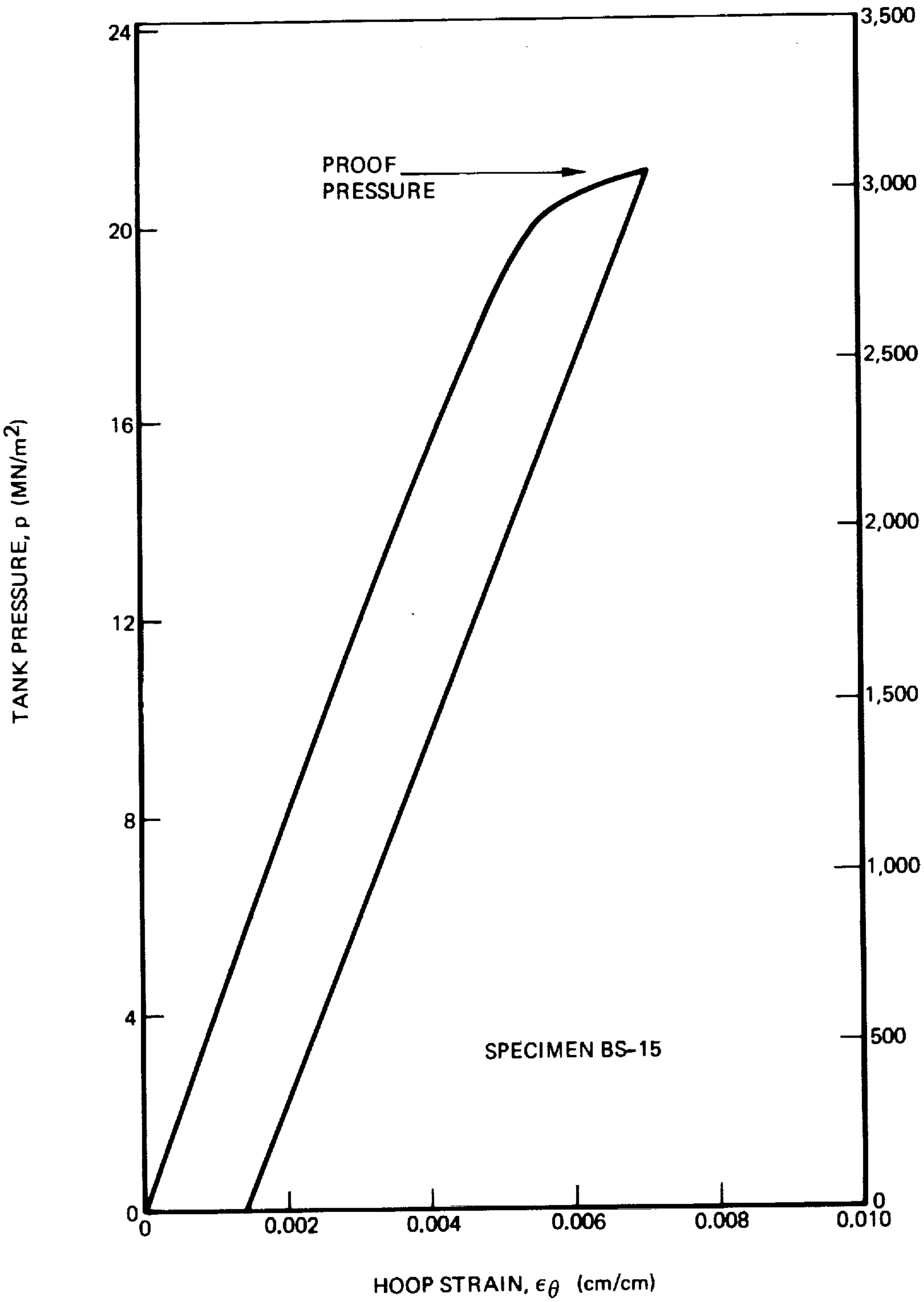

Figure 99: Cryogenic Proof Test Pressure/Strain Curve for Hoop GFR Inconel X750 STA Tank at 78°K (-320°F)

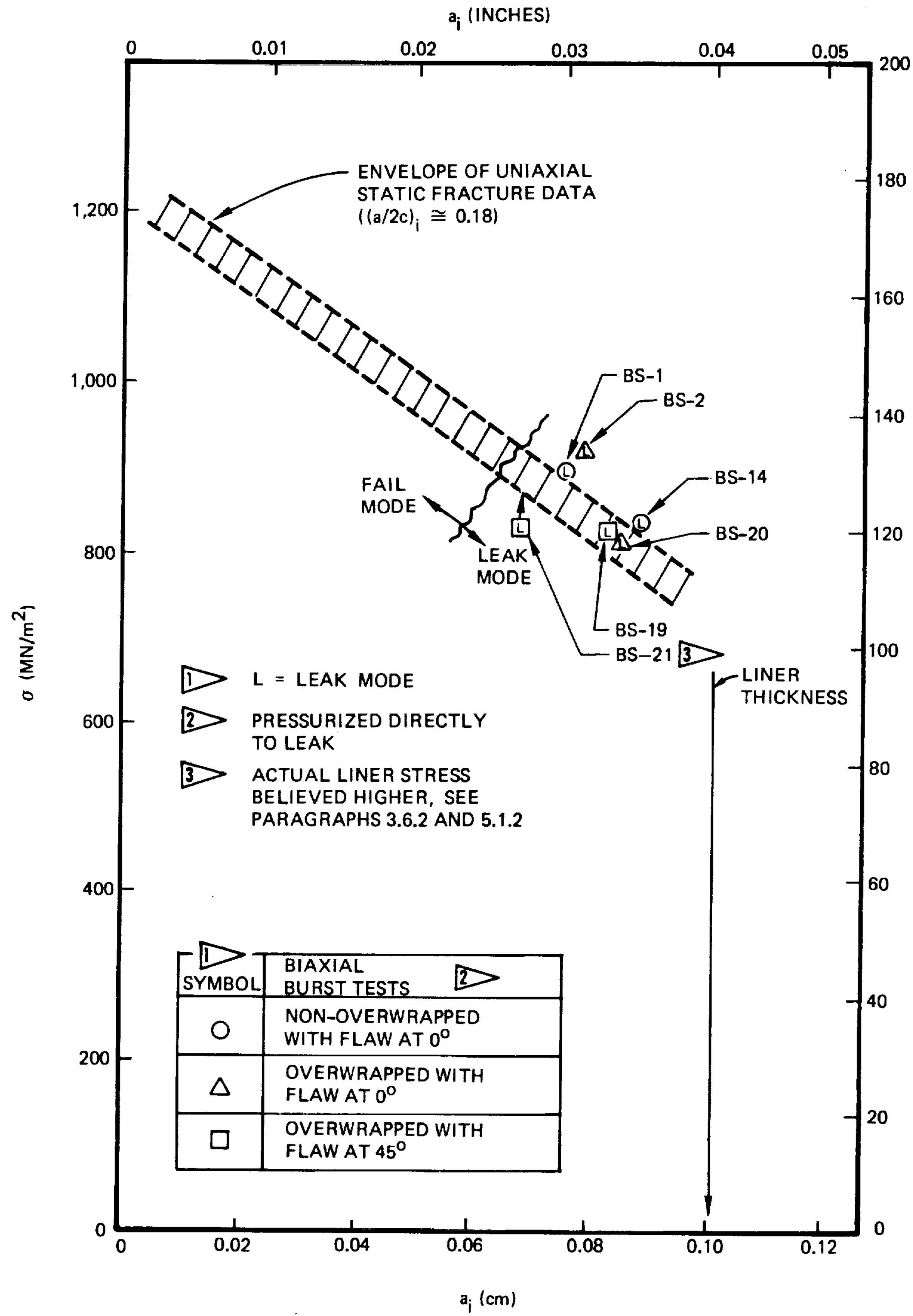

Figure 100: Comparison of Uniaxial and Biaxial Inconel X750 STA Base Metal Static Fracture Results at RT

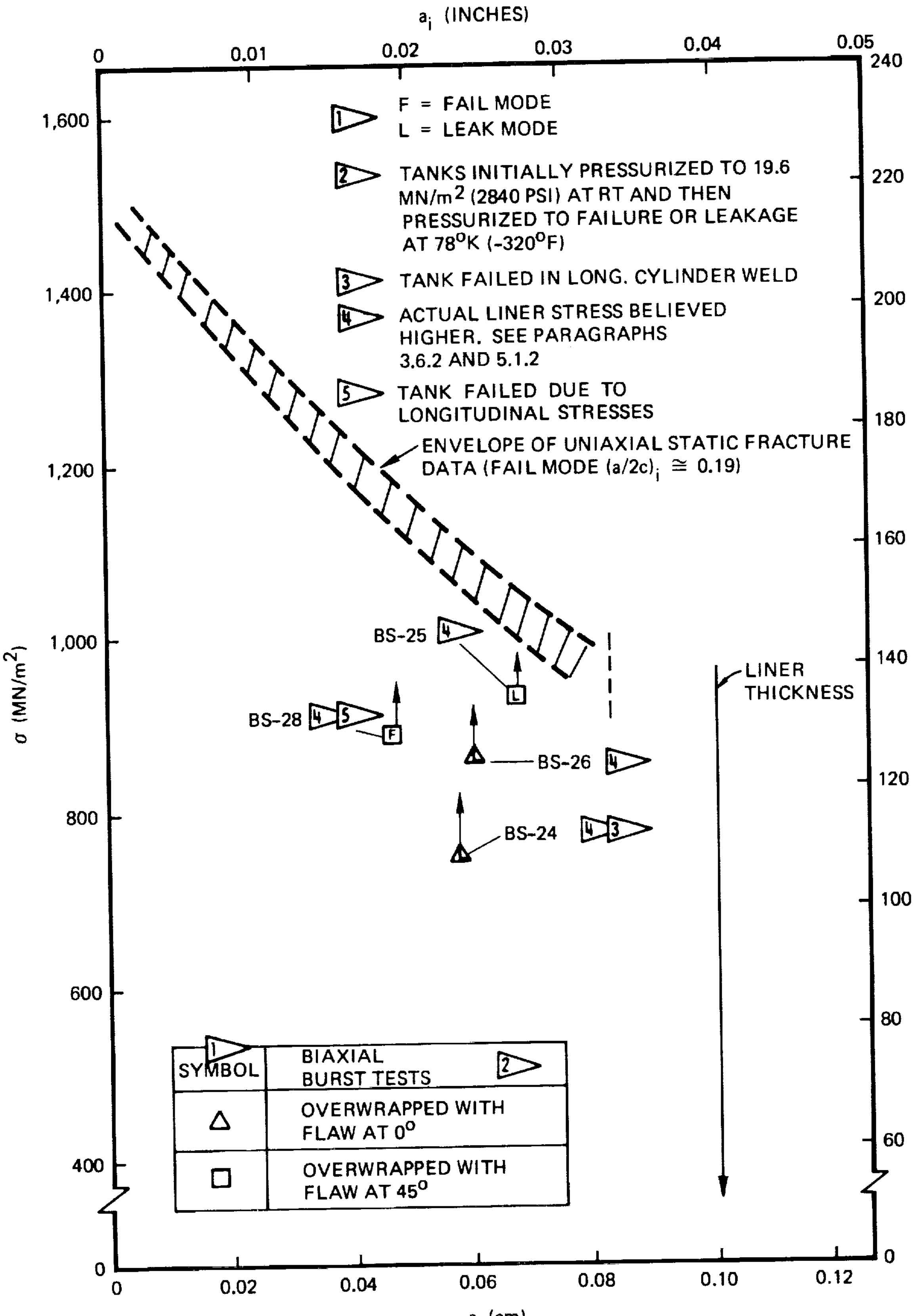

Figure 101: Comparison of Uniaxial and Biaxial Inconel X750 STA Base Metal Static Fracture Results at 78°K (-320°F)

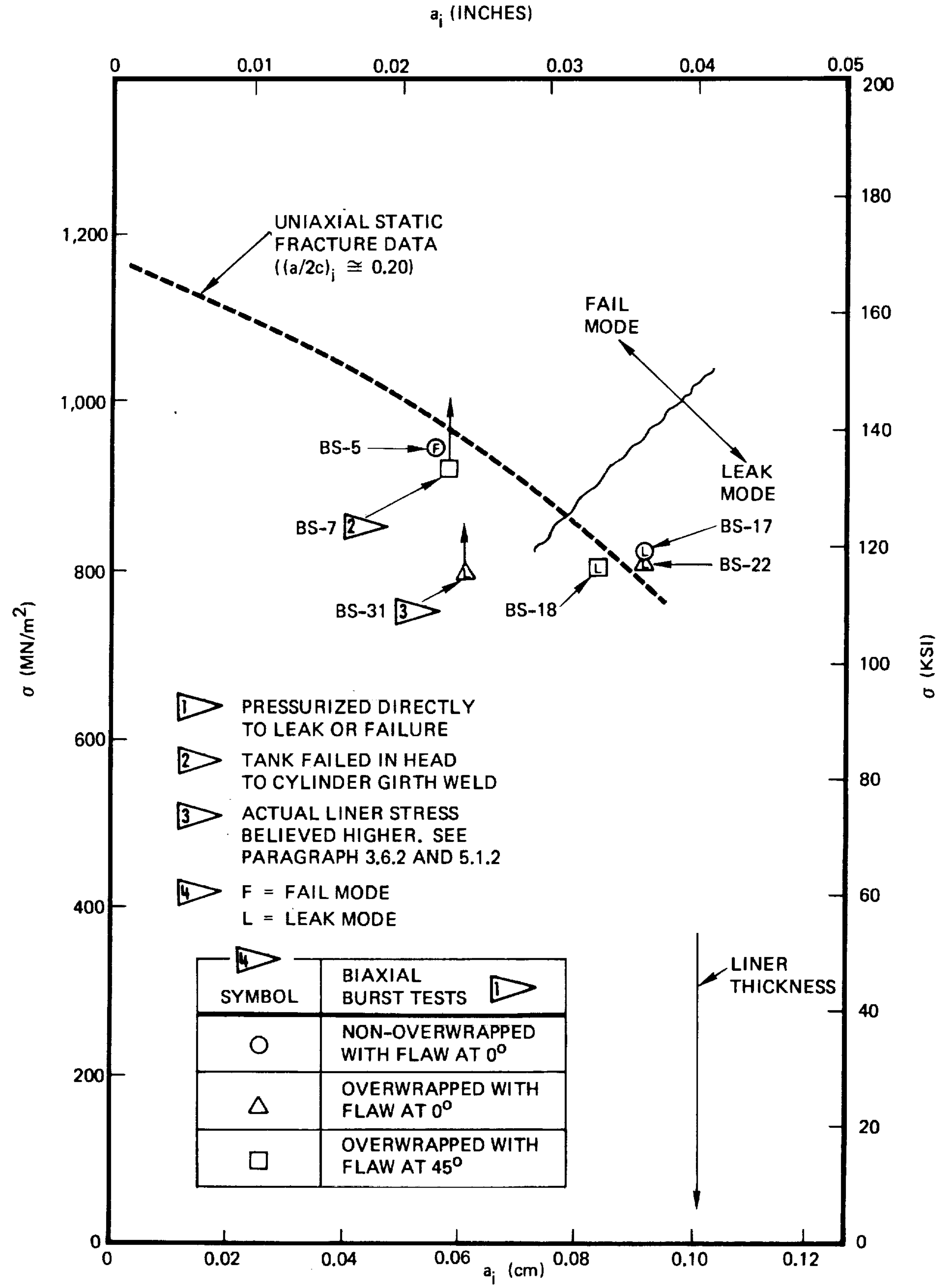

Figure 102: Comparison of Uniaxial and Biaxial Inconel X750 STA Weld Metal ℄ Static Fracture Results at RT

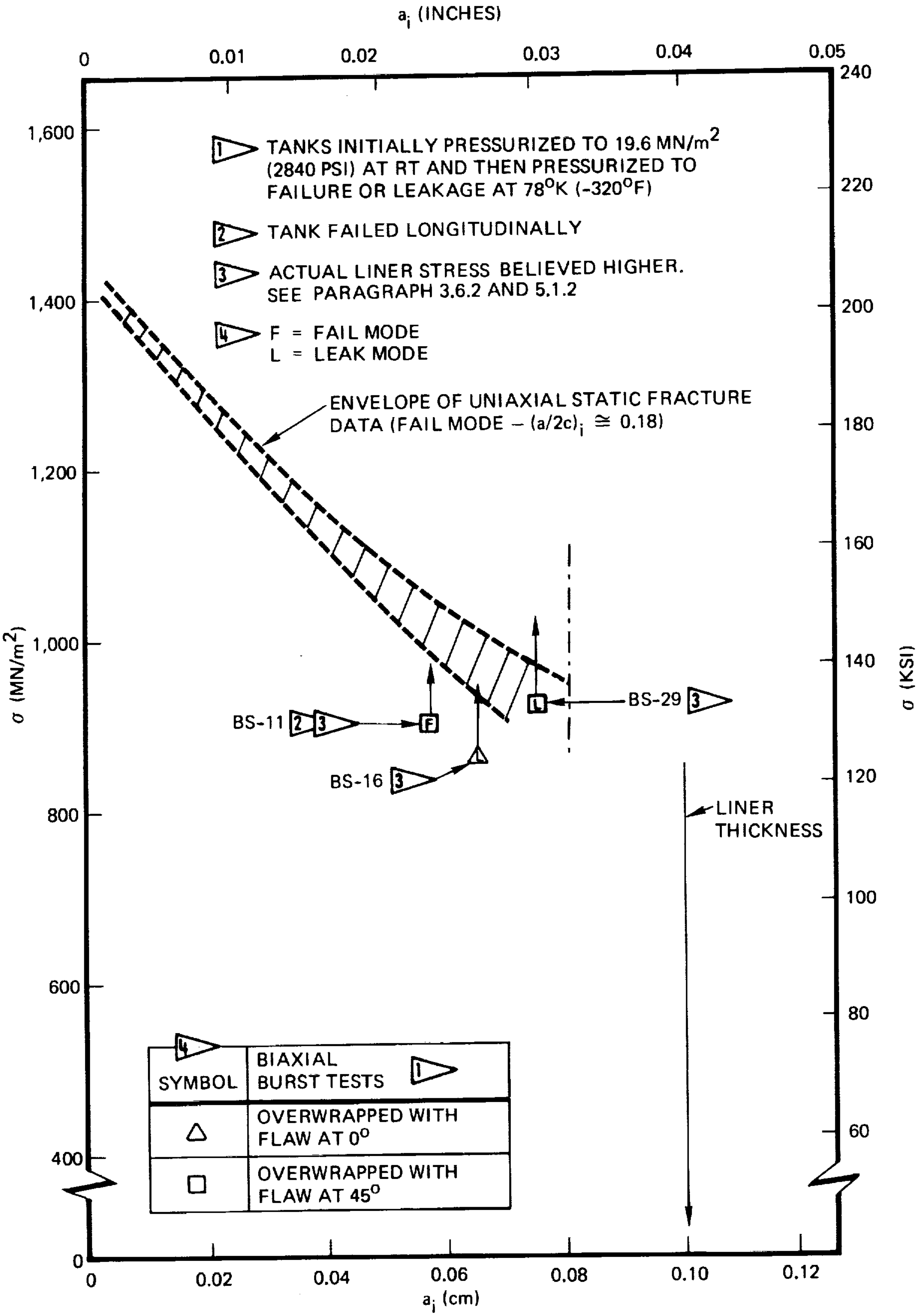

Figure 103: Comparison of Uniaxial and Biaxial X750 STA Weld Metal ℄ Static Fracture Results at 78° K (-320° F)

Figure 104: Leak Mode-of-Failure for Hoop GFR Inconel X750 STA Tank (Specimen BS–22)

Figure 105 : Hoop GFR Inconel X750 STA Tank Failure (Specimen BS-28)

1. DASHED LINES ARE UNIAXIAL RESULTS

2. TANKS CYCLED AT A $\sigma_o \approx 0.87\ \sigma_s$

3. OW TANKS WERE SIZED AT 19.6 MN/m^2 (2840 PSI) AT RT; NON–OW TANKS SIZED AT 10.6 MN/m^2 (1530 PSI)

4. L = LEAK MODE

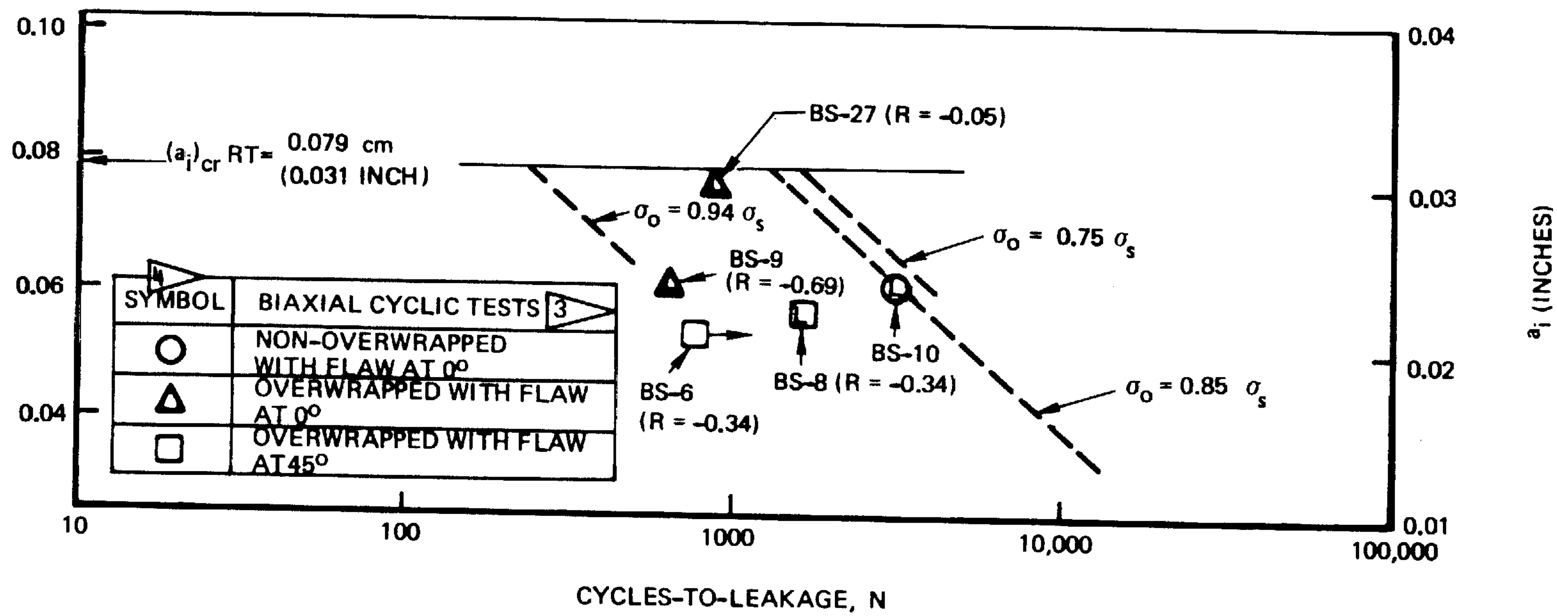

Figure 106: Comparison of Uniaxial 1 and Biaxial 2 Inconel X750 STA Base Metal Cyclic Life Results at RT

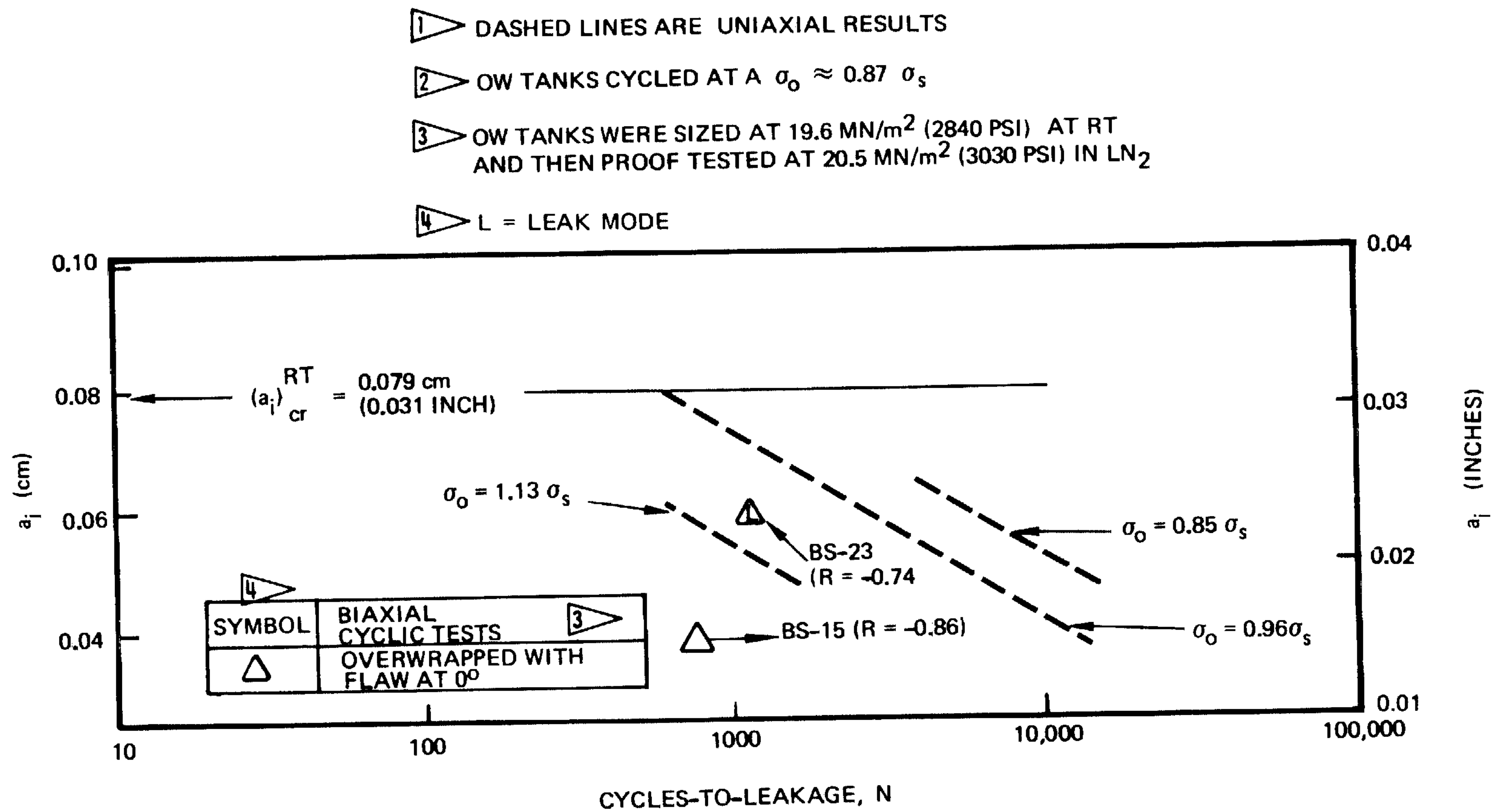

Figure 107: Comparison of Uniaxial 1 and Biaxial 2 Inconel X750 STA Base Metal Cyclic Life Results at 78°K (-320°F)

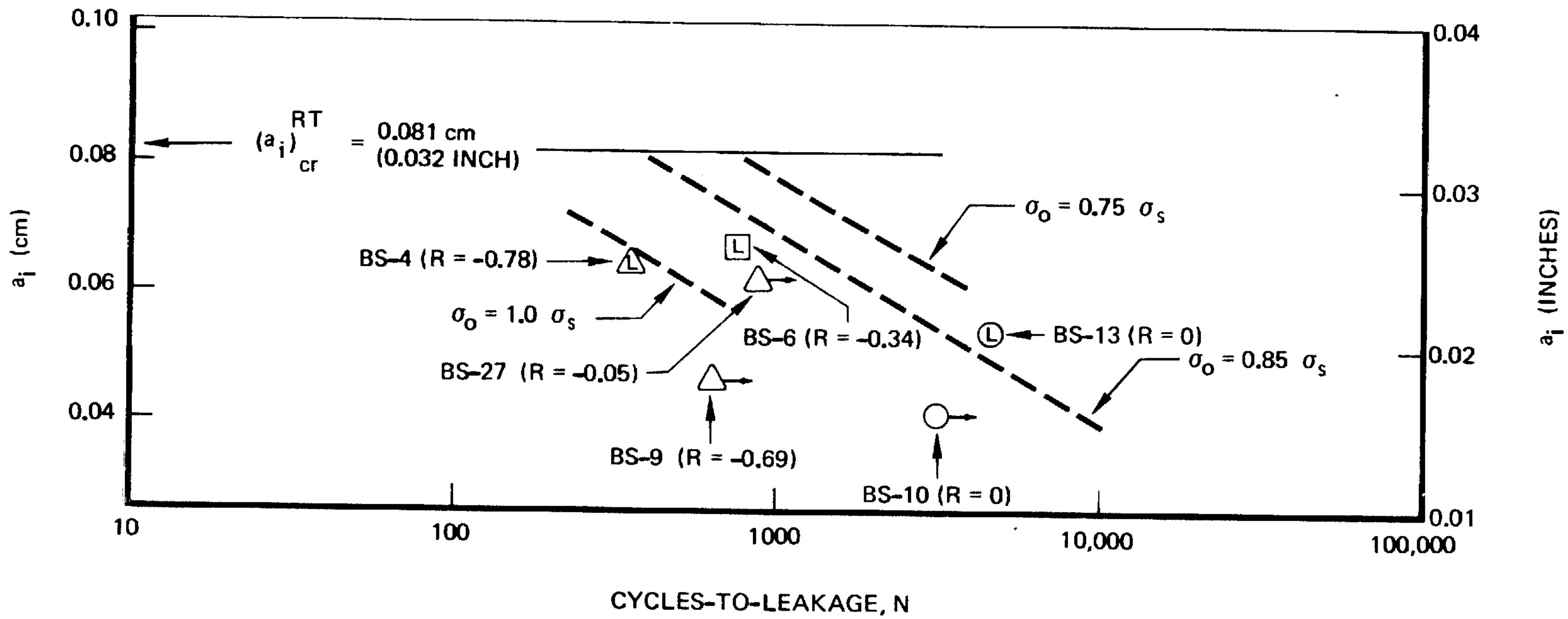

4

SYMBOL	BIAXIAL CYCLIC TESTS 3
○	NON-OVERWRAPPED WITH FLAW AT 0°
△	OVERWRAPPED WITH FLAW AT 0°
□	OVERWRAPPED WITH FLAW AT 45°

1 DASHED LINES ARE UNIAXIAL RESULTS

2 TANKS CYCLED AT A $\sigma_o \approx 0.87\ \sigma_S$

3 OW TANKS WERE SIZED AT 19.6 MN/m^2 (2840 PSI) AT RT; NON-OW TANKS SIZED AT 10.6 MN/m^2 (1530 PSI)

4 L = LEAK MODE

Figure 108: Comparison of Uniaxial 1 and Biaxial 2 Inconel X750 STA Weld Metal ℄ Cyclic Life Results at RT

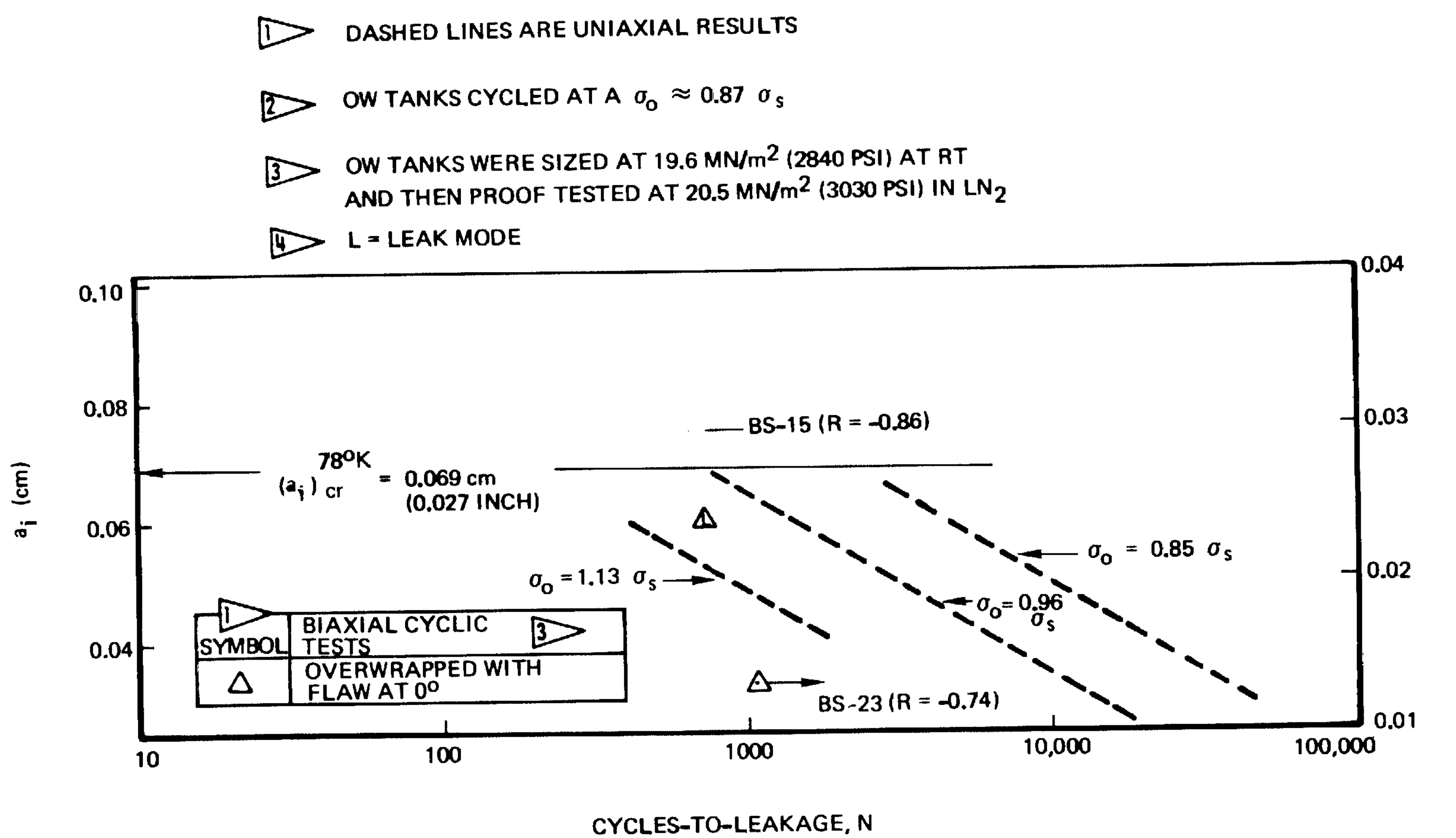

Figure 109: Comparison of Uniaxial 1 and Biaxial 2 Inconel X750 STA Weld Metal ℄ Cyclic Life Results at 78°K (-320°F)

TEST CONDITION	TANK	SYMBOL	σ_s MN/m^2 (KSI)	σ_o MN/m^2 (KSI)	R
RT CYCLIC TESTED AT σ_o AFTER BEING SIZED TO σ_s IN RT AIR	NON–OVER–WRAPPED TANK WITH 0° FLAW	○ BS-10	850 (123.3)	723 (104.9)	0
	OVERWRAPPED TANK WITH 0° FLAW	□ BS-9 ◇ BS-27	829 (120.2) 794 (115.2)	727 (105.4) 698 (101.3)	-0.69 -0.05
	OVERWRAPPED TANK WITH 45° FLAW	▷ BS-6 ◁ BS-8	810 (117.5) 821 (119.0)	718 (104.1) 714 (103.6)	-0.34 -0.34
RT CYCLIC TESTED AT σ_o AFTER BEING SIZED TO σ_s IN RT AIR AND THEN PROOFED TO 1.03 σ_s	OVERWRAPPED TANK WITH 0° FLAW	● BS-15 ⬢ BS-23	767 (111.2) 824 (119.5)	667 (96.7) 712 (103.2)	-0.86 -0.74

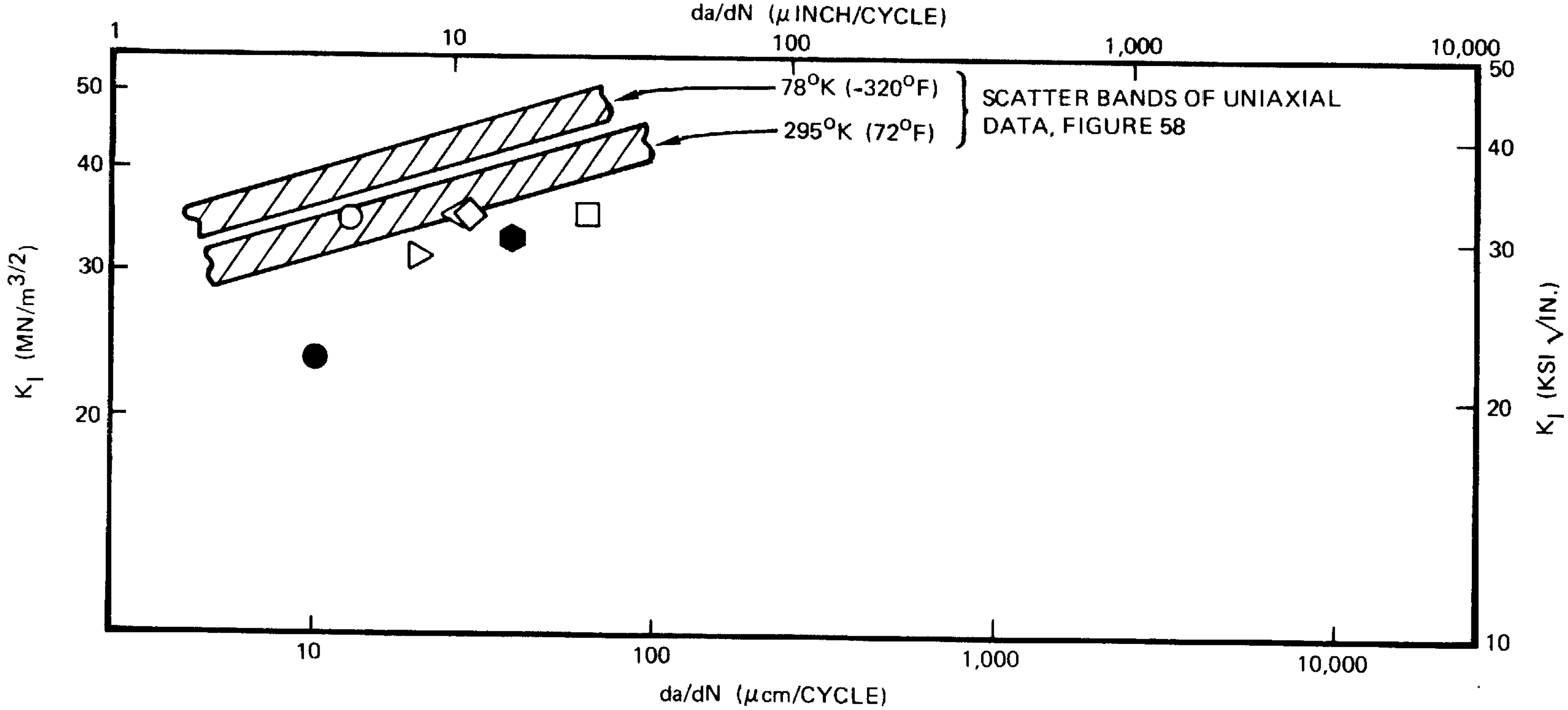

Figure 110: Comparison of Uniaxial and Biaxial Inconel X750 STA Base Metal Cyclic Flaw Growth Rates

TEST CONDITION	TANK	SYMBOL	σ_s MN/m^2 (KSI)	σ_o MN/m^2 (KSI)	R
RT CYCLIC TESTED AT σ_o AFTER BEING SIZED TO σ_s IN RT AIR	NON–OVERWRAPPED TANK WITH 0° FLAW	○ BS-10	850 (123.3)	723 (104.9)	0
		⬡ BS-13	850 (123.3)	723 (104.9)	0
	OVERWRAPPED TANK WITH 0°FLAW	△ BS-4	789 (114.4)	687 (99.7)	-0.78
		□ BS-9	829 (120.2)	727 (105.4)	-0.69
		◇ BS-27	794 (115.2)	698 (101.3)	-0.05
	OVERWRAPPED TANK WITH 45° FLAW	▷ BS-6	810 (117.5)	718 (104.1)	-0.34
RT CYCLIC TESTED AT σ_o AFTER BEING SIZED TO σ_s IN RT AIR AND THEN PROOFED TO 1.03 σ_s IN LN_2	OVERWRAPPED TANK WITH 0°FLAW	● BS-15	767 (111.2)	667 (96.7)	-0.86
		⬢ BS-23	824 (119.5)	712 (103.2)	-0.74

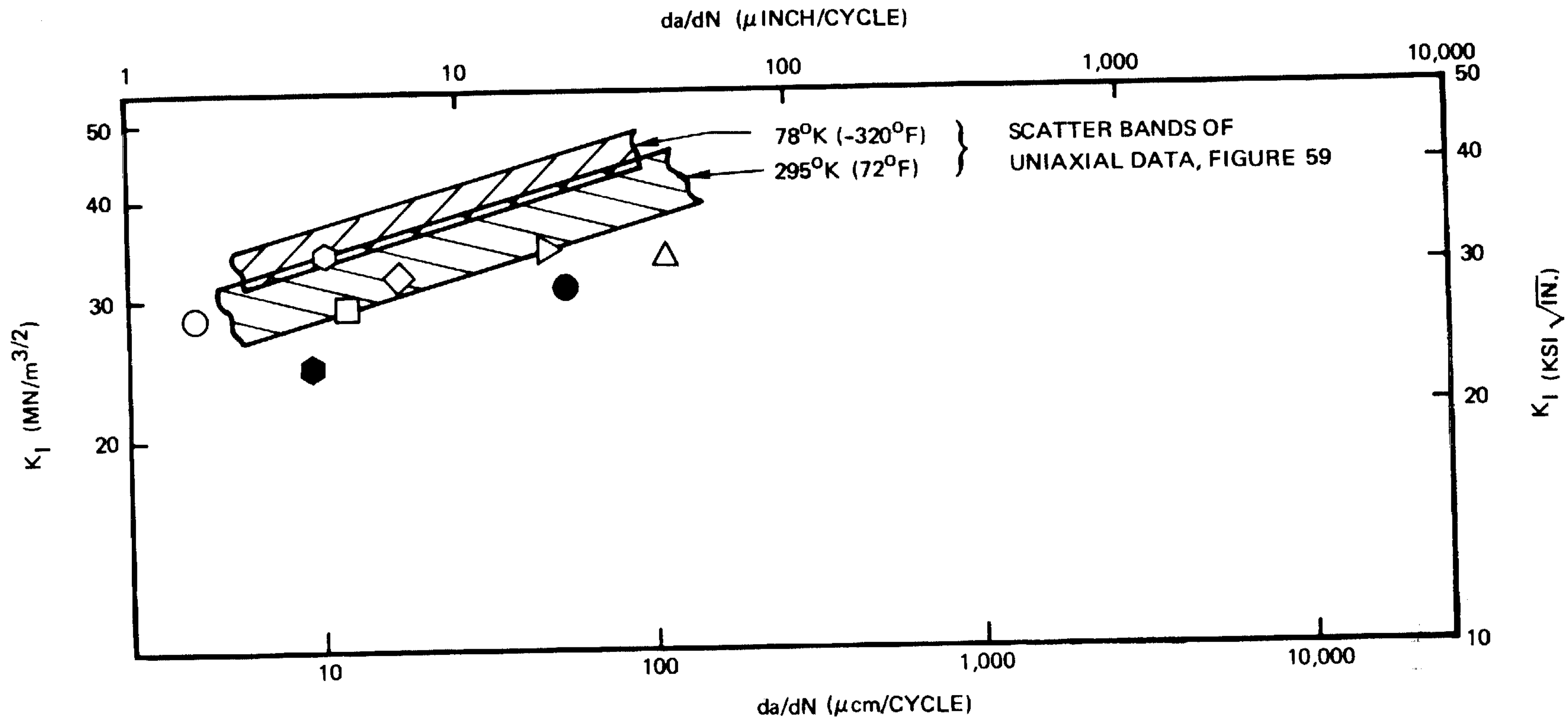

Figure 111: Comparison of Uniaxial and Biaxial Inconel X750 STA Weld Metal ℄ Cyclic Flaw Growth Rates

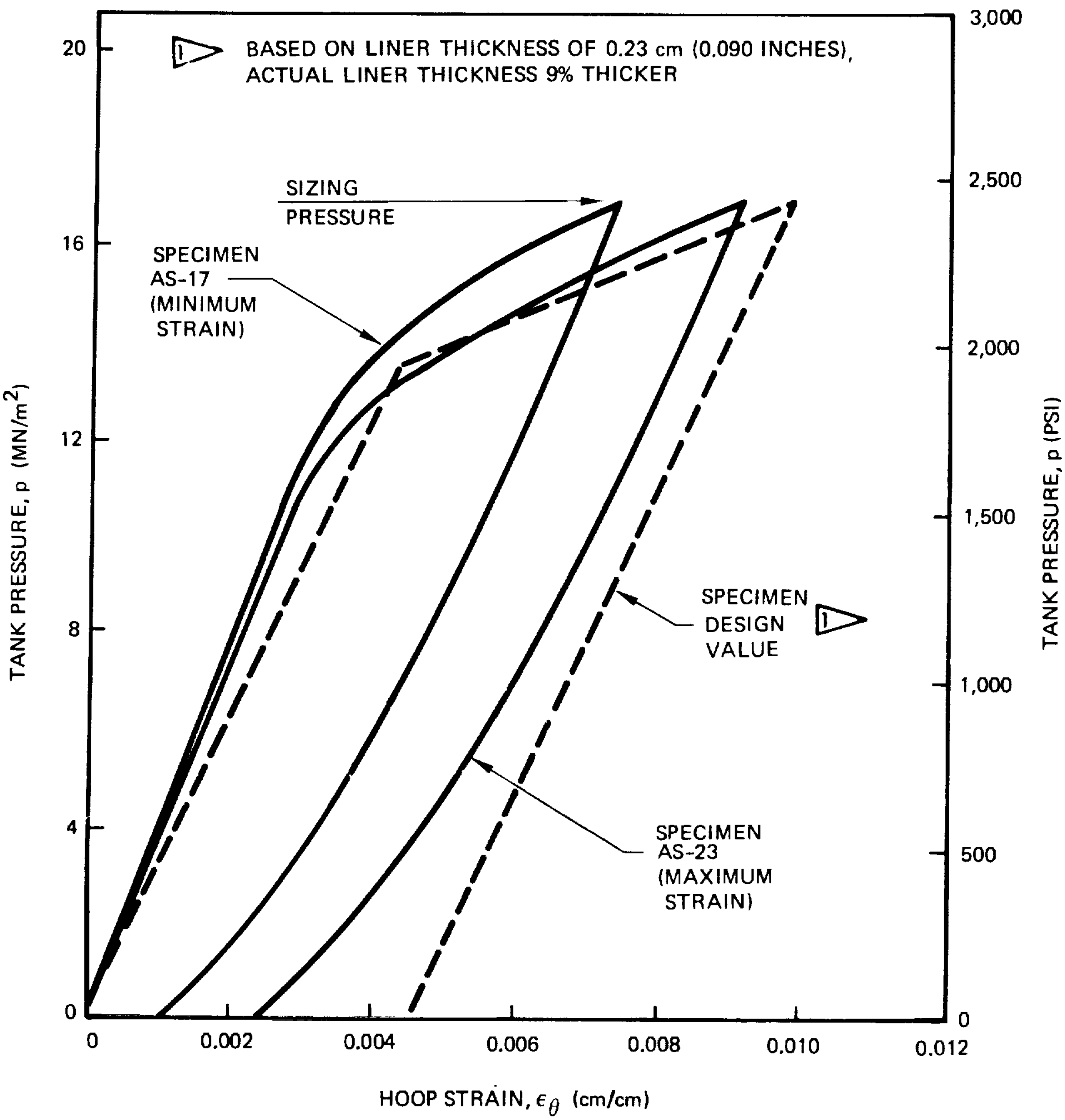

Figure 112 : Comparison of Pressure/Strain Curves for Hoop GFR 2219-T62 Aluminum Tanks at RT

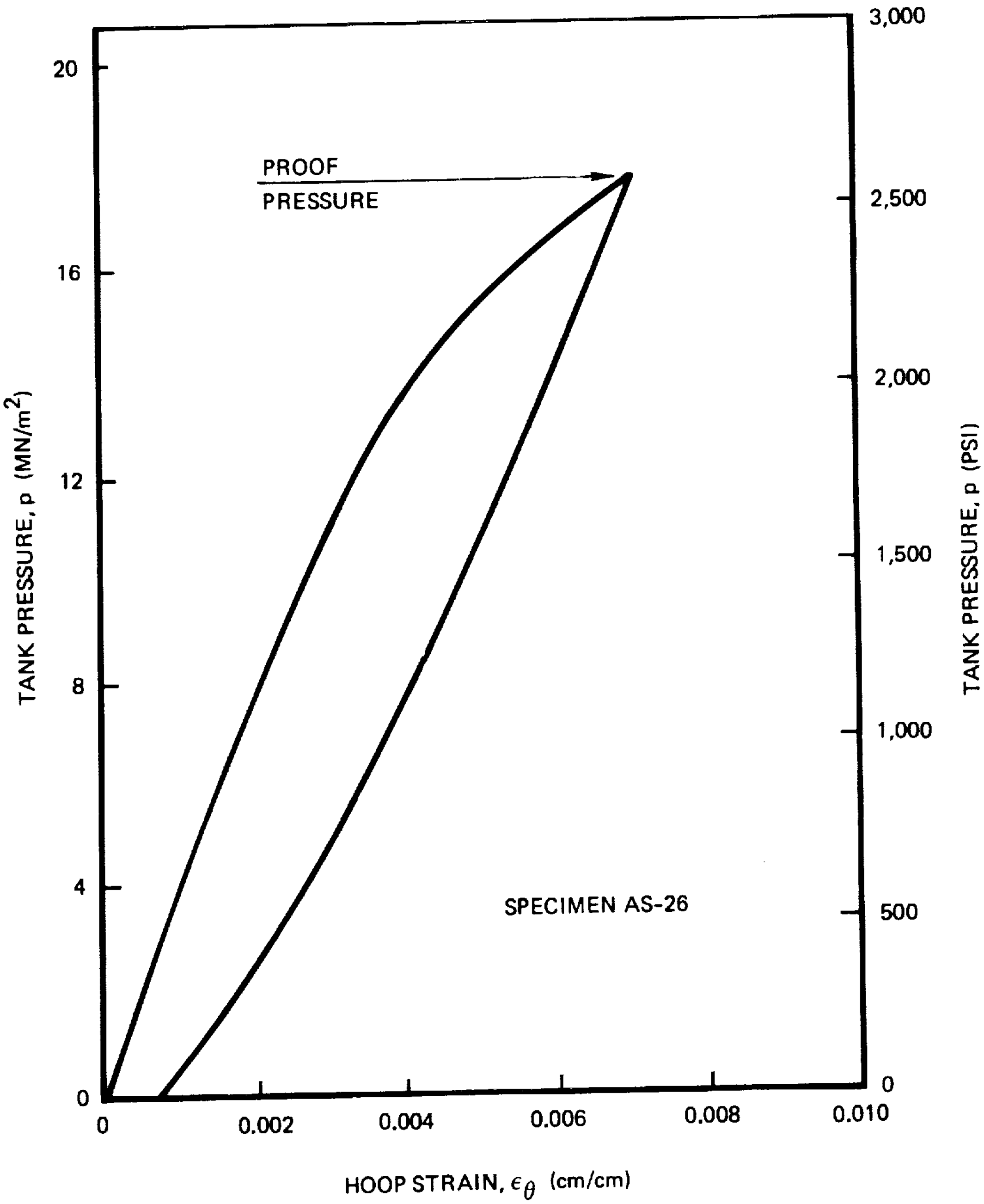

Figure 113: Cryogenic Proof Test Pressure/Strain Curve for Hoop GFR 2219-T62 Aluminum Tank at 78°K (-320°F)

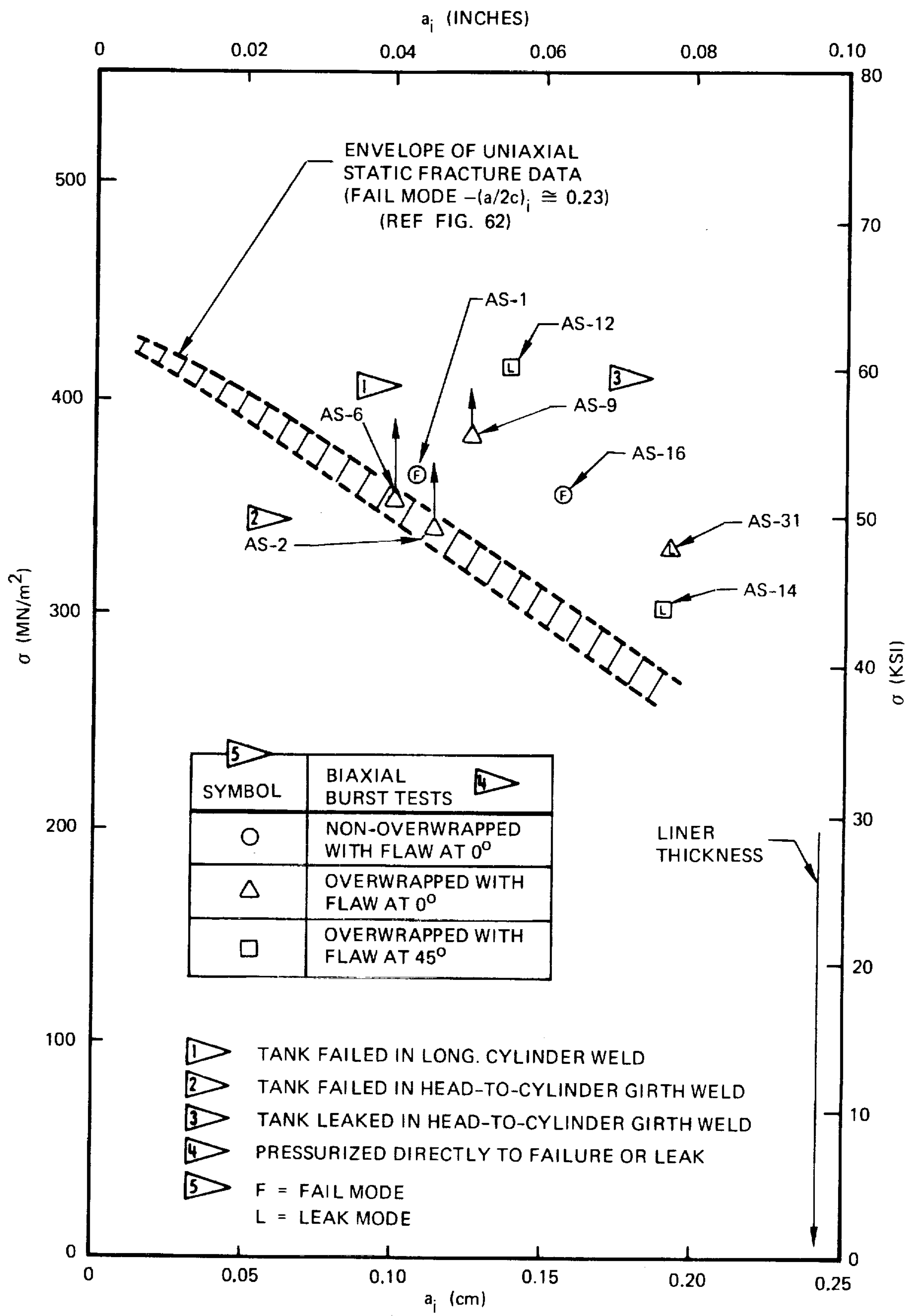

Figure 114: Comparison of Uniaxial and Biaxial 2219–T62 Aluminum Base Metal Static Fracture Results at RT

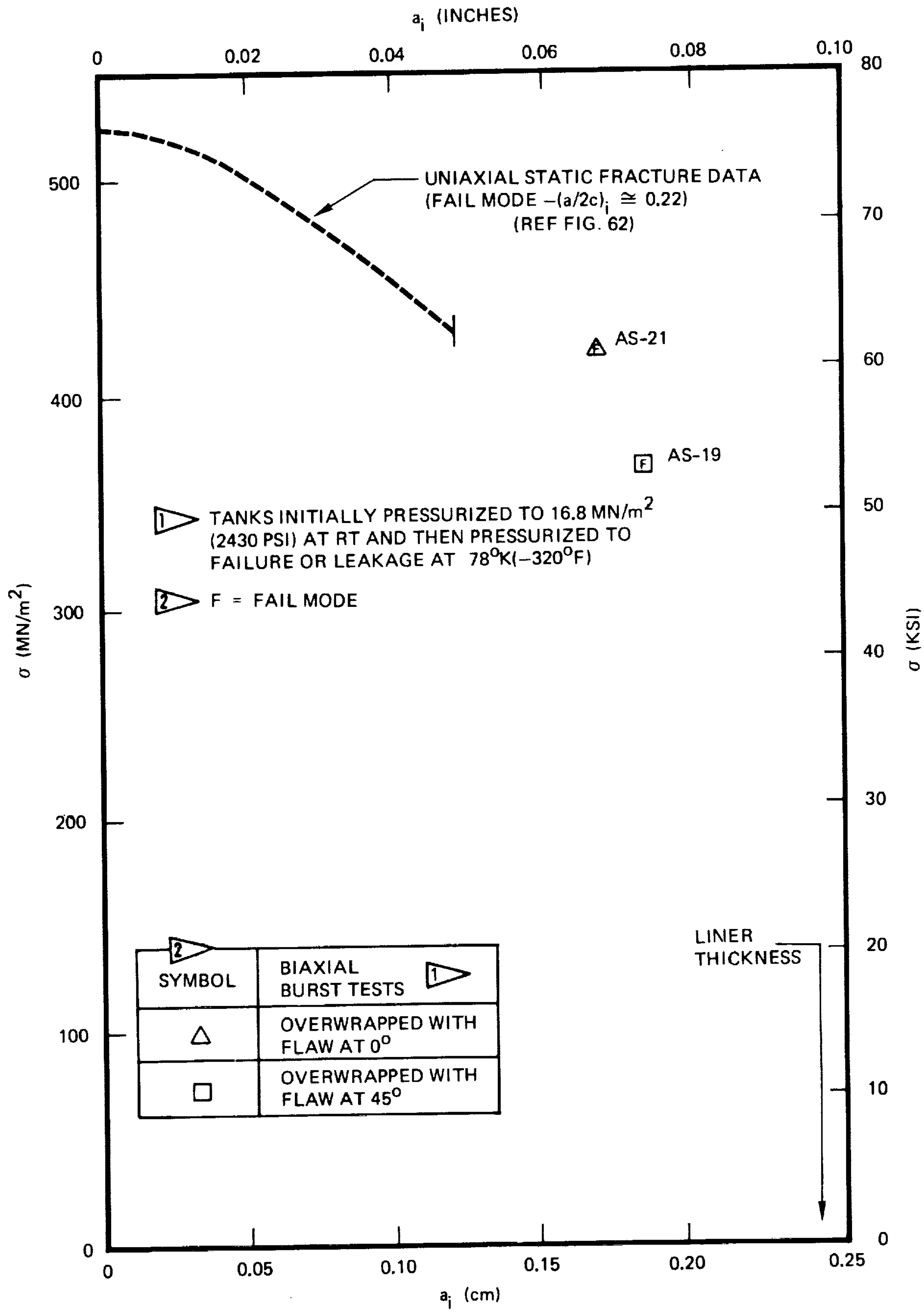

Figure 115: Comparison of Uniaxial and Biaxial 2219-T62 Aluminum Base Metal Static Fracture Results at 78°K (-320°F)

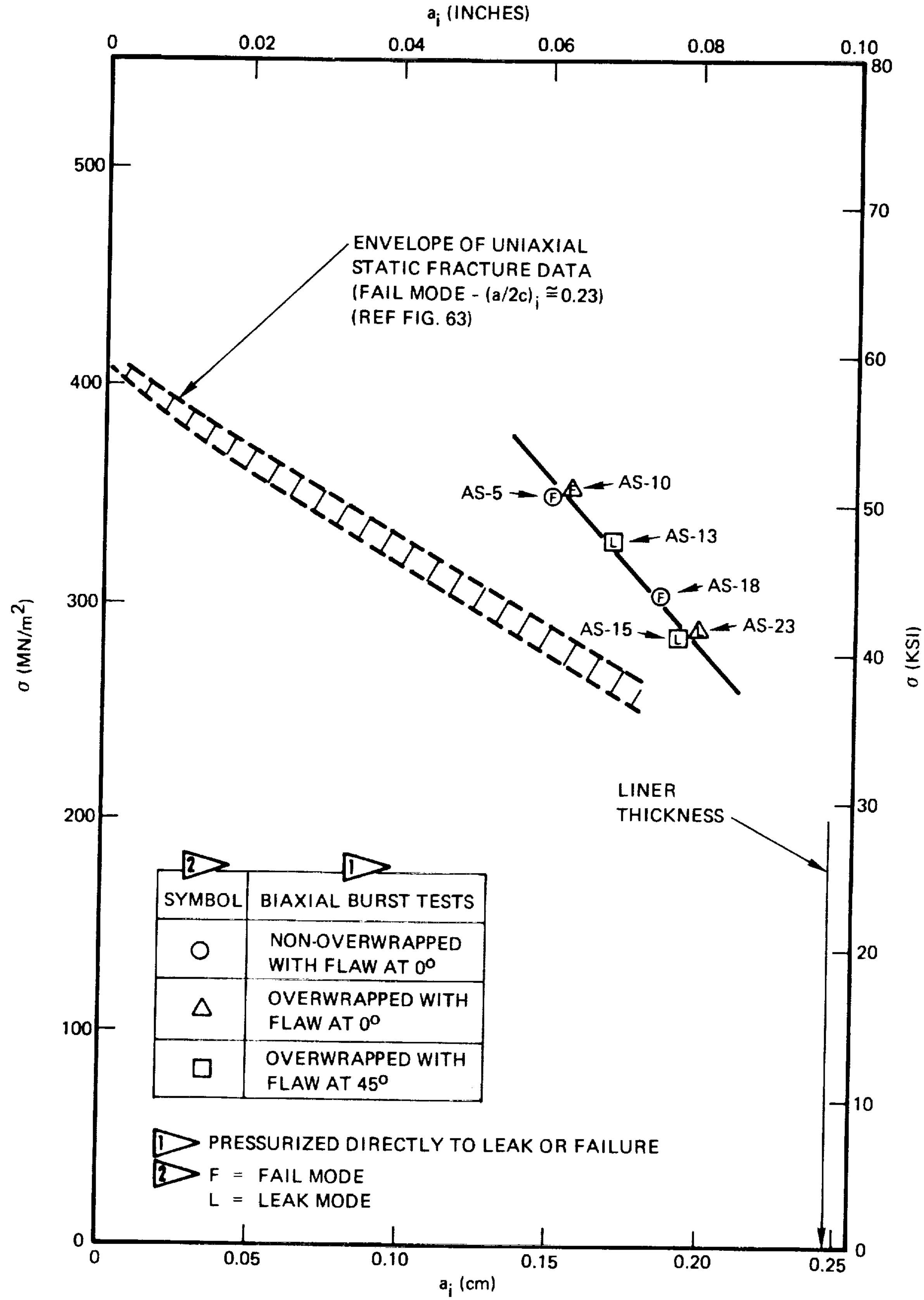

Figure 116: Comparison of Uniaxial and Biaxial 2219-T62 Aluminum Weld Metal ℄ Static Fracture Results at RT

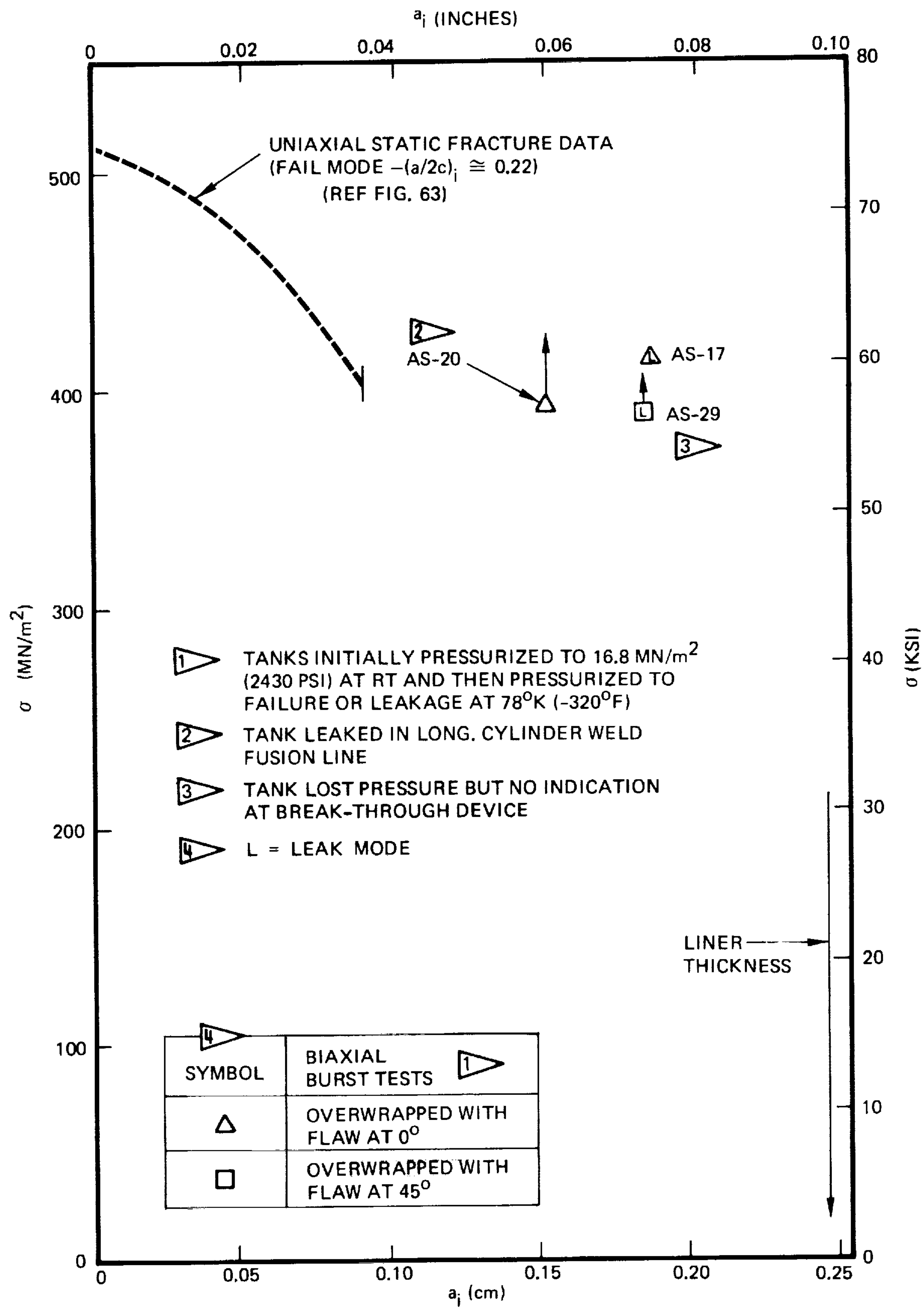

Figure 117: Comparison of Uniaxial and Biaxial 2219-T62 Aluminum Weld Metal ℄ Static Fracture Results at 78°K (-320°F)

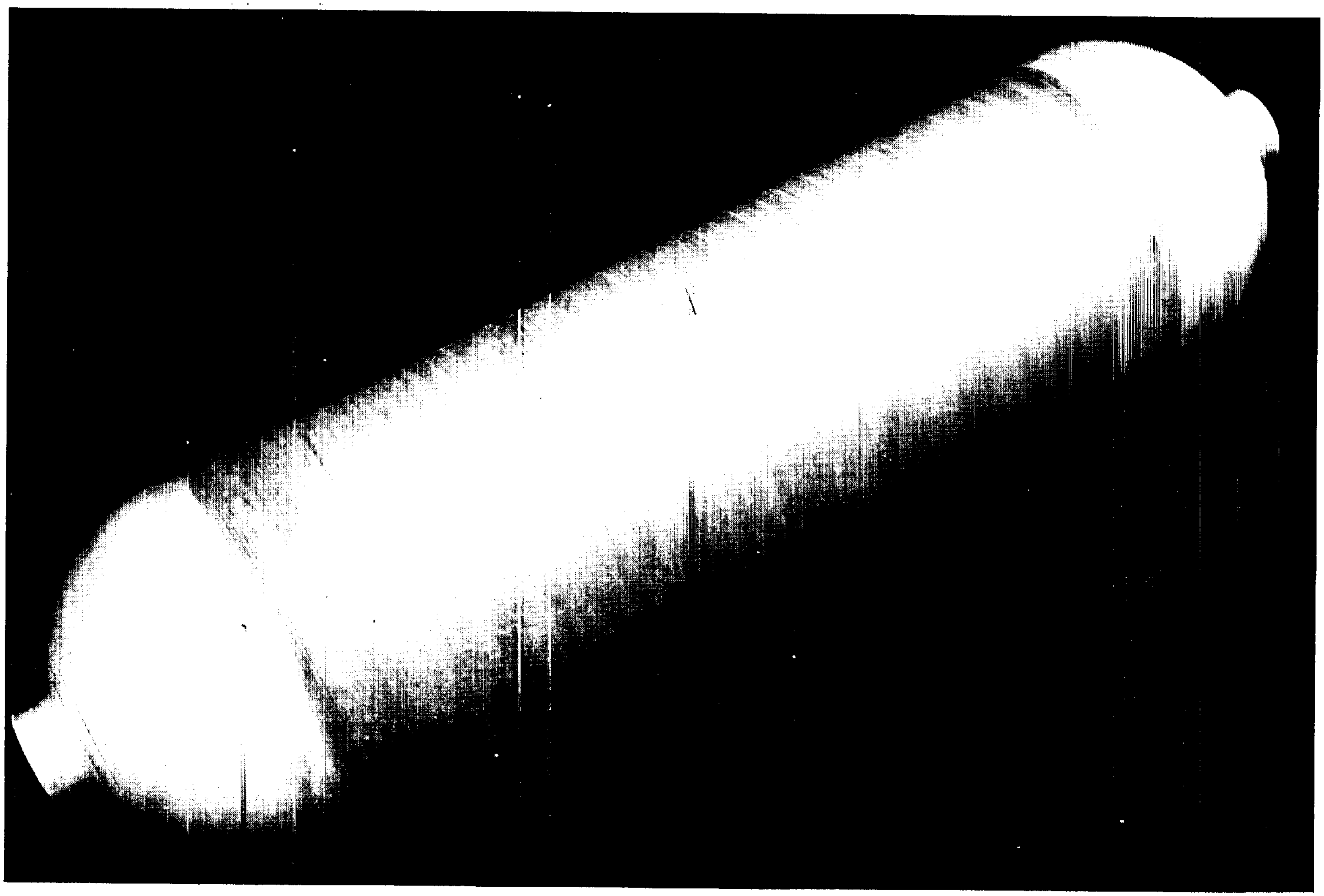

Figure 118: Leak Mode-of-Failure for Hoop GFR 2219-T62 Aluminum Tank (Specimen AS-10)

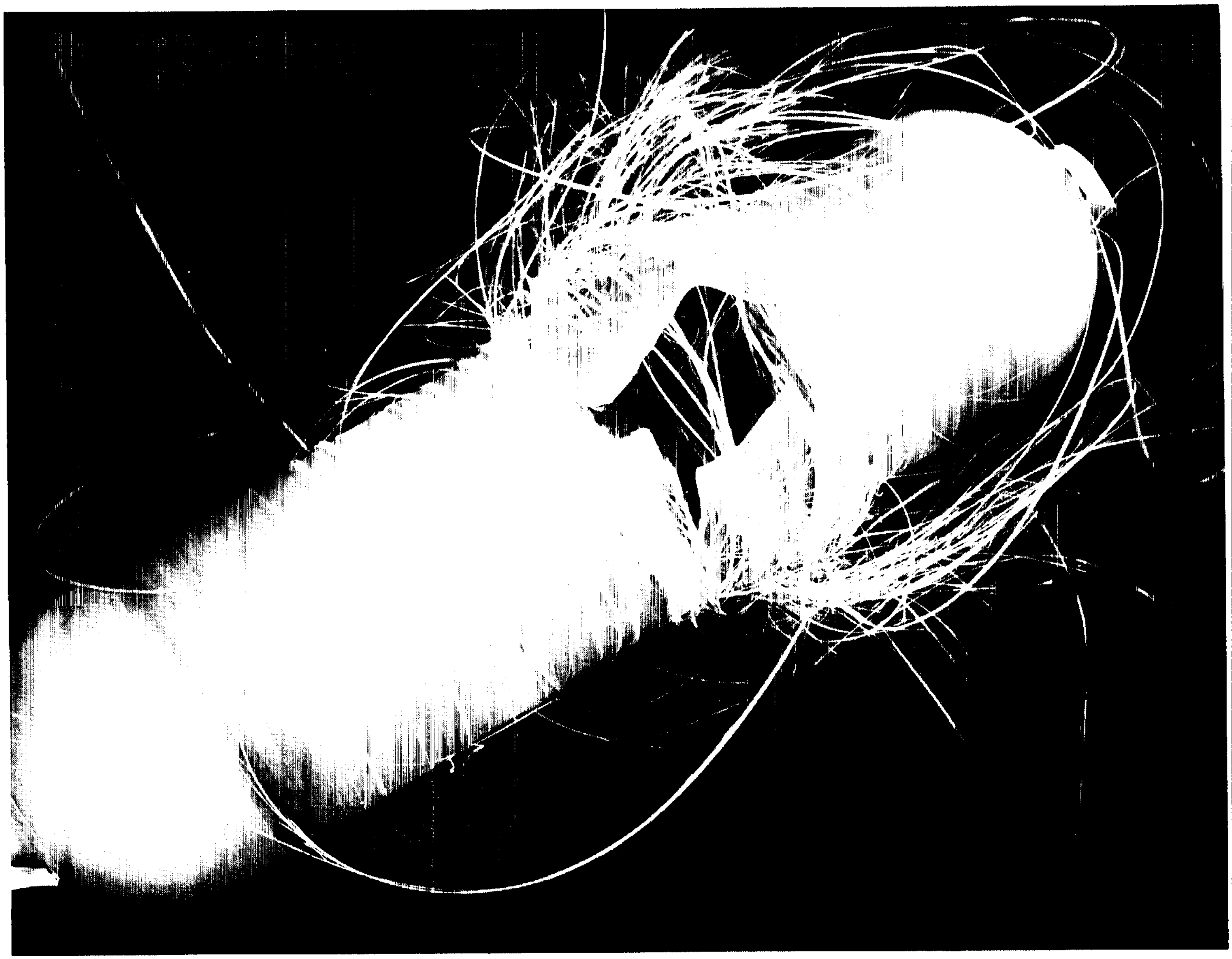

Figure 119 : Hoop GFR 2219-T62 Aluminum Tank Failure (Specimen AS-19)

1 DASHED LINES ARE UNIAXIAL RESULTS

2 OW TANKS CYCLED AT A $\sigma_o \cong 0.84\ \sigma_s$, WHEREAS NON-OW TANKS CYCLED AT A $\sigma_o = 0.75\ \sigma_s$

3 OW TANKS SIZED AT 16.8 MN/m^2 (2430 PSI); NON-OW TANKS SIZED AT ABOUT 9.7 MN/m^2 (1410 PSI)

4 L = LEAK MODE

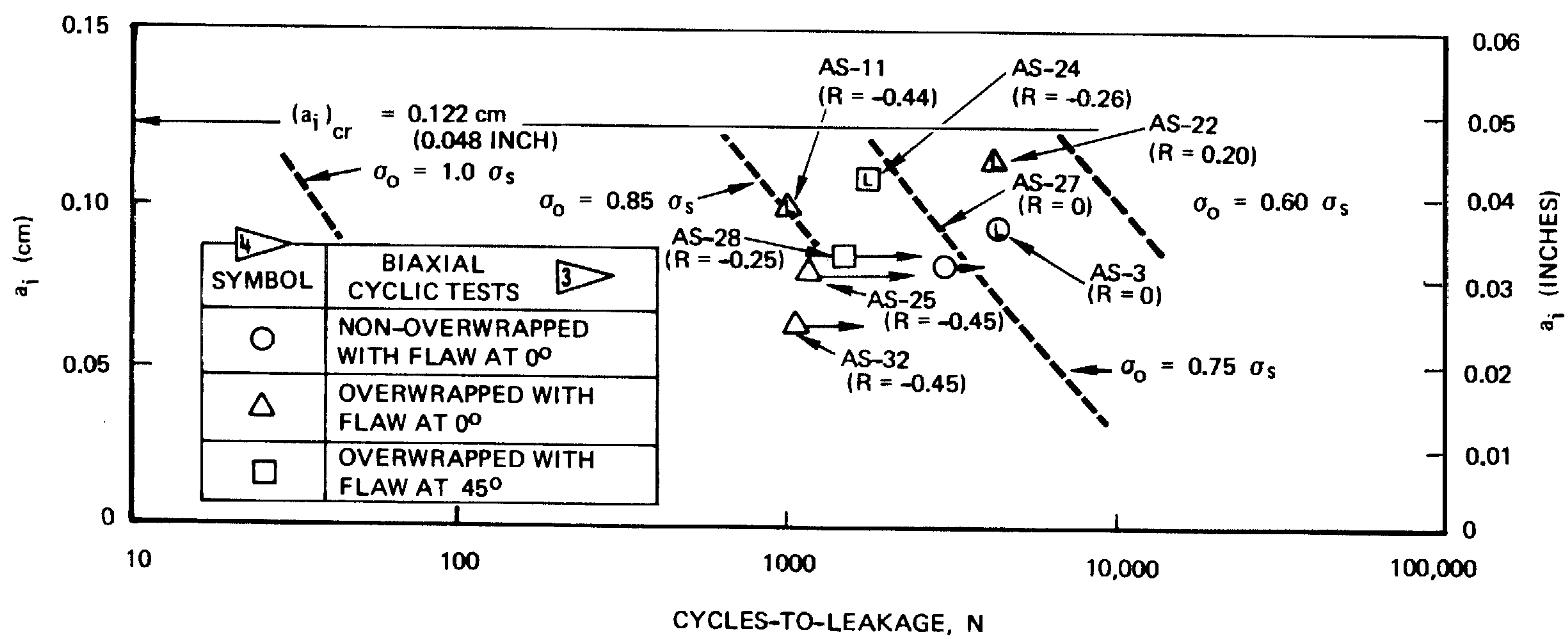

Figure 120: Comparison of Uniaxial 1 and Biaxial 2 2219-T62 Aluminum Base Metal Cyclic Life Results at RT

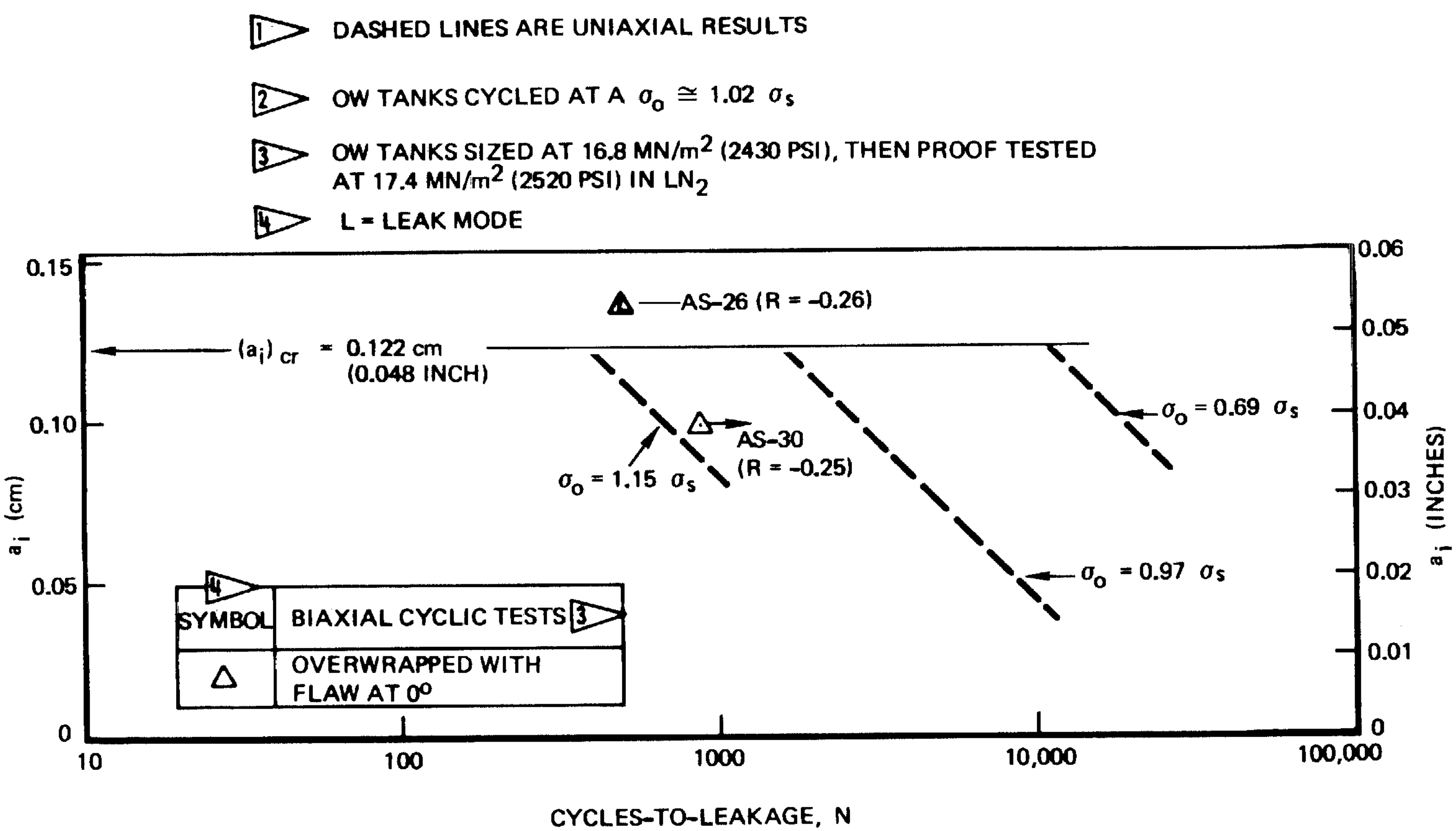

Figure 121: Comparison of Uniaxial 1 and Biaxial 2 2219-T62 Aluminum Base Metal Cyclic Life Results at 78°K (-320°F)

1 DASHED LINES ARE UNIAXIAL

2 OW TANKS CYCLED AT A $\sigma_o \cong 0.84\ \sigma_s$, WHEREAS NON-OW TANKS CYCLED AT A $\sigma_o = 0.75\ \sigma_s$

3 OW TANKS SIZED AT 16.8 MN/m² (2430 PSI); NON-OW TANKS SIZED AT ABOUT 9.7 MN/m² (1410 PSI)

4 L = LEAK MODE

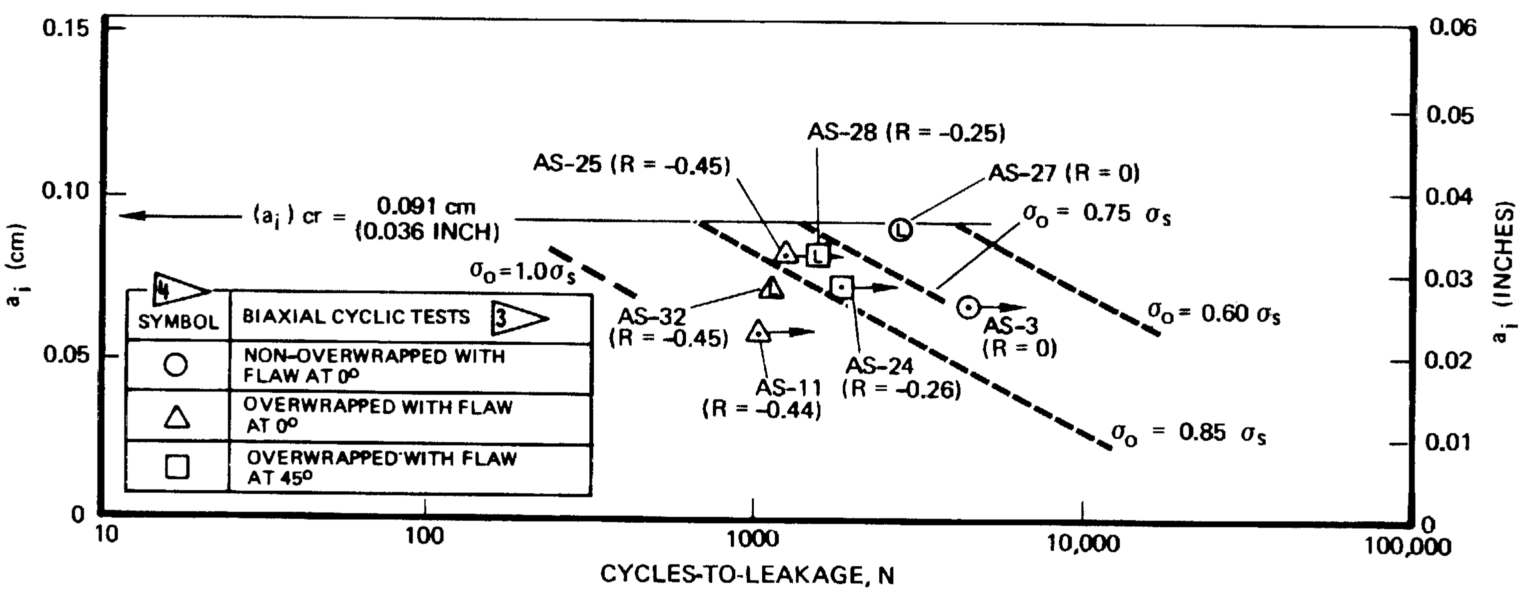

Figure 122: Comparison of Uniaxial 1 and Biaxial 2 2219-T62 Aluminum Weld Metal ℄ Cyclic Life Results at RT

1 DASHED LINES ARE UNIAXIAL RESULTS

2 OW TANKS CYCLED AT A $\sigma_o \cong 1.02\ \sigma_s$

3 OW TANKS SIZED AT 16.8 MN/m^2 (2430 PSI), THEN PROOF TESTED AT 17.4 MN/m^2 (2520 PSI) IN LN_2

4 L = LEAK MODE

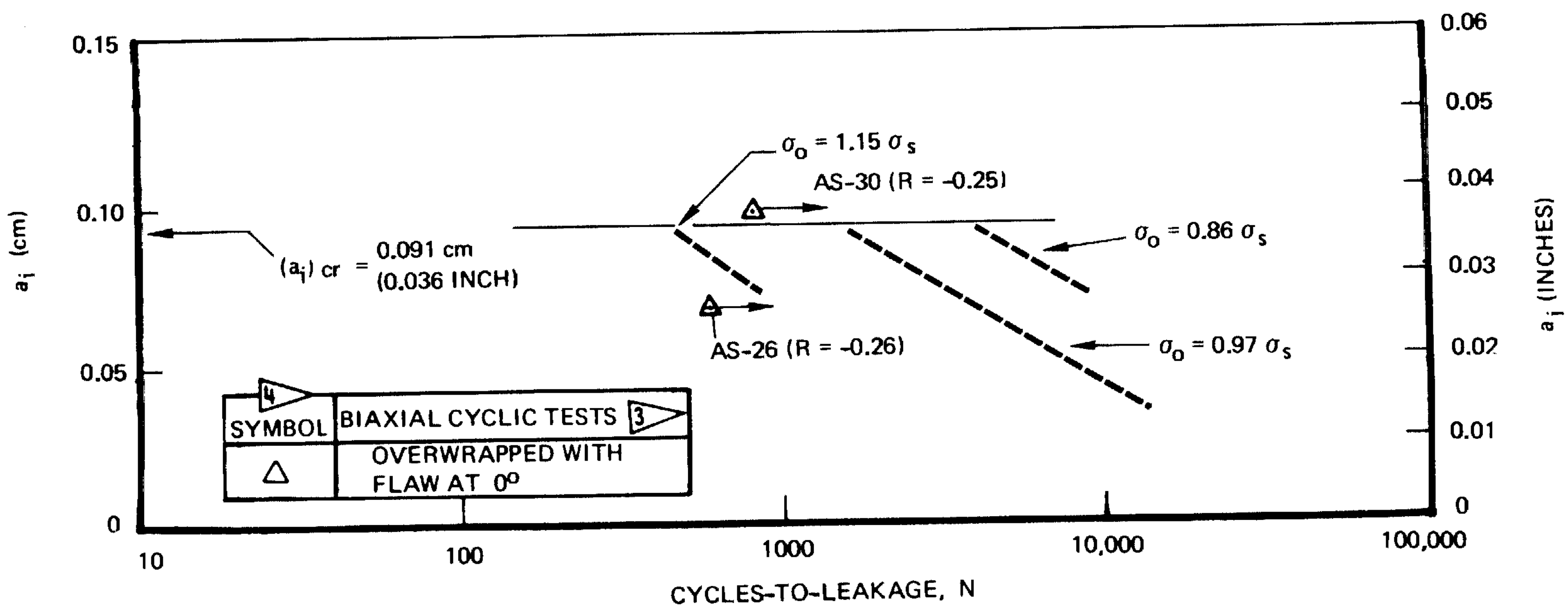

Figure 123: Comparison of Uniaxial 1 and Biaxial 2 2219-T62 Aluminum Weld Metal ℄ Cyclic Life Results at 78°K (-320°F)

TEST CONDITION	TANK	SYMBOL	σ_s MN/m^2 (KSI)		σ_o MN/m^2 (KSI)		R
RT CYCLIC TESTED AT σ_o AFTER BEING SIZED TO σ_s IN RT AIR	NON–OVER–WRAPPED TANK WITH 0° FLAW	○ AS-3	332	(48.2)	249	(36.1)	0
		⬡ AS-27	332	(48.2)	250	(36.2)	0
	OVERWRAPPED TANK WITH 0° FLAW	△ AS-11	323	(46.8)	271	(39.3)	-0.44
		□ AS-22	339	(49.2)	290	(42.1)	0.20
		◇ AS-25	319	(46.3)	264	(38.3)	-0.45
		▽ AS-32	328	(47.5)	266	(38.6)	-0.45
	OVERWRAPPED TANK WITH 45° FLAW	▷ AS-24	294	(42.7)	249	(36.1)	-0.26
		◁ AS-28	296	(43.0)	249	(36.1)	-0.25
RT CYCLIC TESTED AT σ_o AFTER BEING SIZED TO σ_s IN RT AIR AND THEN PROOFED TO 1.12 σ_s IN LN_2	OVERWRAPPED TANK WITH 0° FLAW	● AS-26	314	(45.5)	321	(46.6)	-0.26
		⬢ AS-30	323	(46.9)	328	(47.6)	-0.25

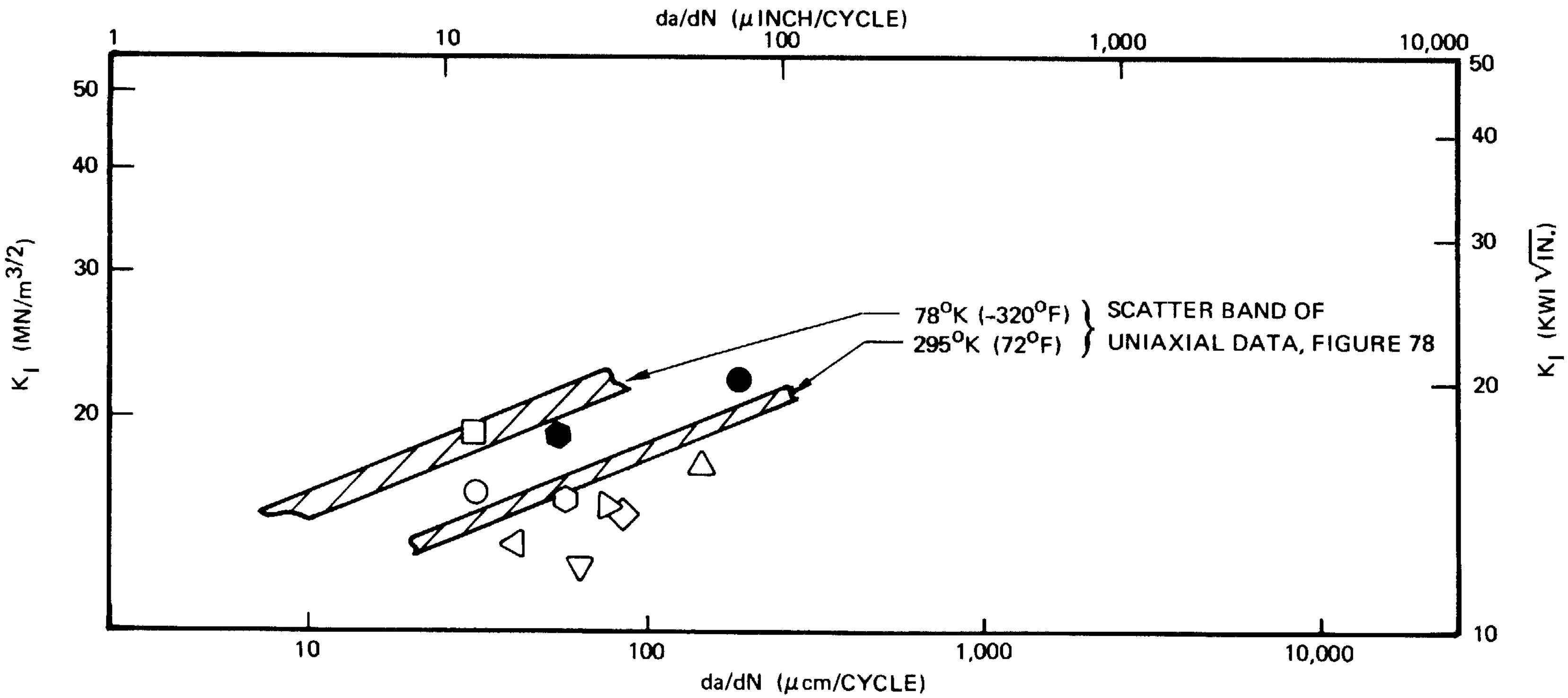

Figure 124: Comparison of Uniaxial and Biaxial 2219-T62 Aluminum Base Metal Cyclic Flaw Growth Rates

TEST CONDITION	TANK	SYMBOL	σ_s MN/m^2 (KSI)		σ_o MN/m^2 (KSI)		R
RT CYCLIC TESTED AT σ_o AFTER BEING SIZED TO σ_s IN RT AIR	NON-OVERWRAPPED TANK WITH 0° FLAW	○ AS-3	332	(48.2)	249	(36.1)	0
		⬡ AS-27	332	(48.2)	250	(36.2)	0
	OVERWRAPPED TANK WITH 0° FLAW	△ AS-11	323	(46.8)	271	(39.3)	-0.44
		□ AS-22	339	(49.2)	290	(42.1)	0.20
		◇ AS-25	319	(46.3)	264	(38.3)	-0.45
		▽ AS-32	328	(47.5)	266	(38.6)	-0.45
	OVERWRAPPED TANK WITH 45° FLAW	▷ AS-24	294	(42.7)	249	(36.1)	-0.26
		◁ AS-28	296	(43.0)	249	(36.1)	-0.25
RT CYCLIC TESTED AT σ_o AFTER BEING SIZED TO σ_s IN RT AIR AND THEN PROOFED TO 1.12 σ_s IN LN_2	OVERWRAPPED TANK WITH 0° FLAW	● AS-26	314	(45.5)	321	(46.6)	-0.26
		⬢ AS-30	323	(46.9)	328	(47.6)	-0.25

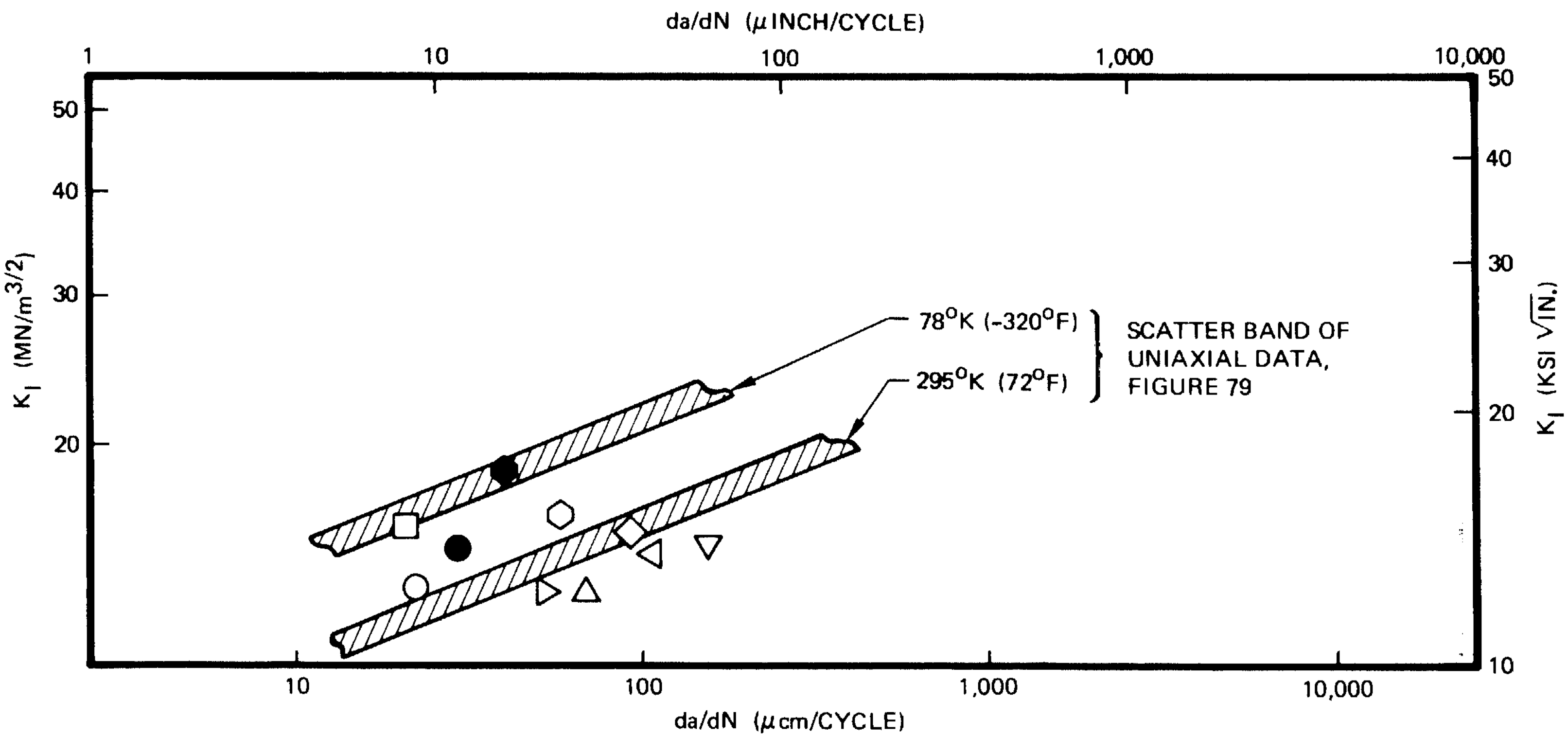

Figure 125: Comparison of Uniaxial and Biaxial 2219-T62 Aluminum Weld Metal ℄ Cyclic Flaw Growth Rates

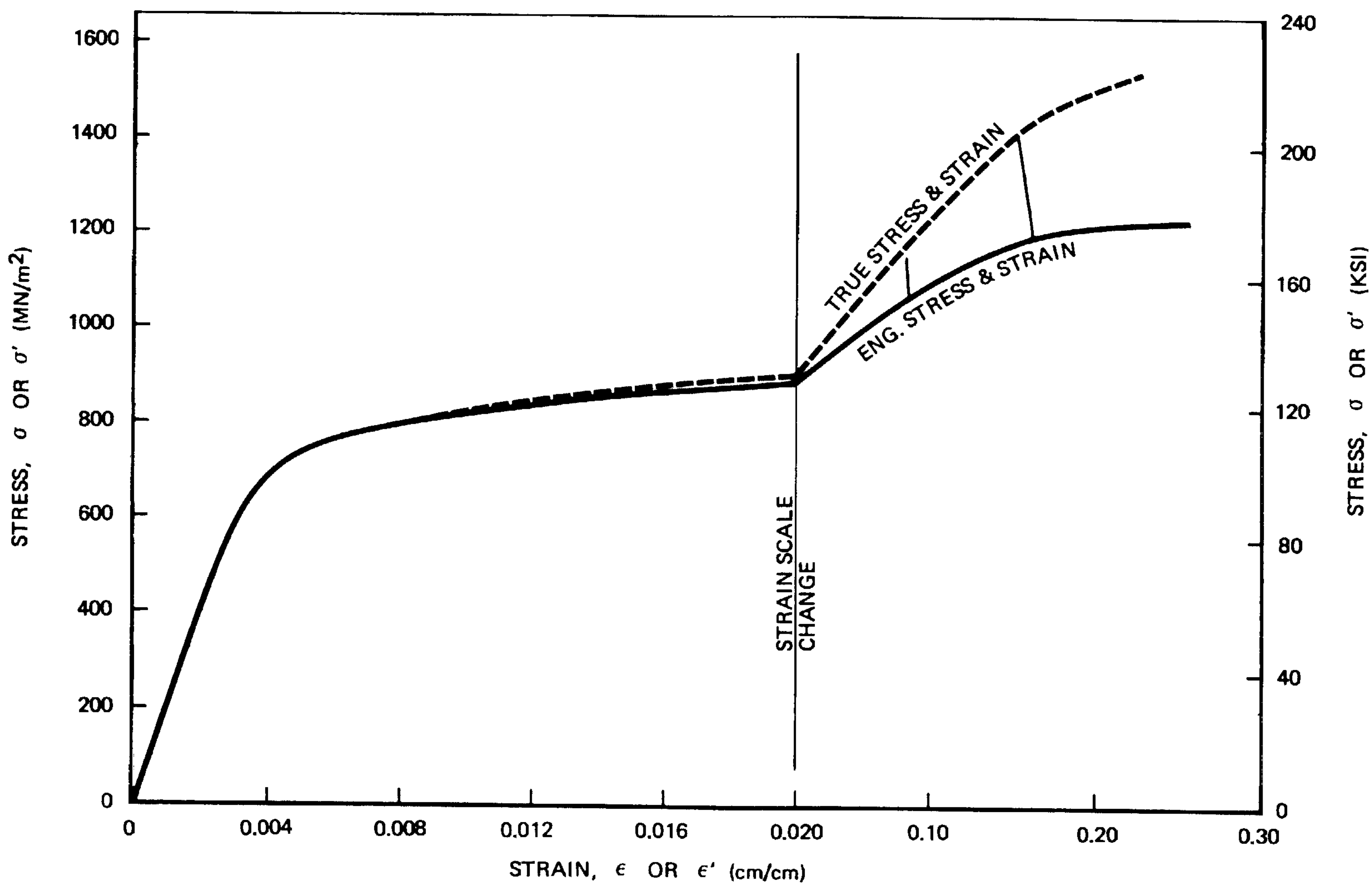

Figure A-1: Stress/Strain Relationship for 0.10 cm (0.040 Inch) Thick Inconel X750 STA Base Metal at 295°K (72°F) - Specimen B-1

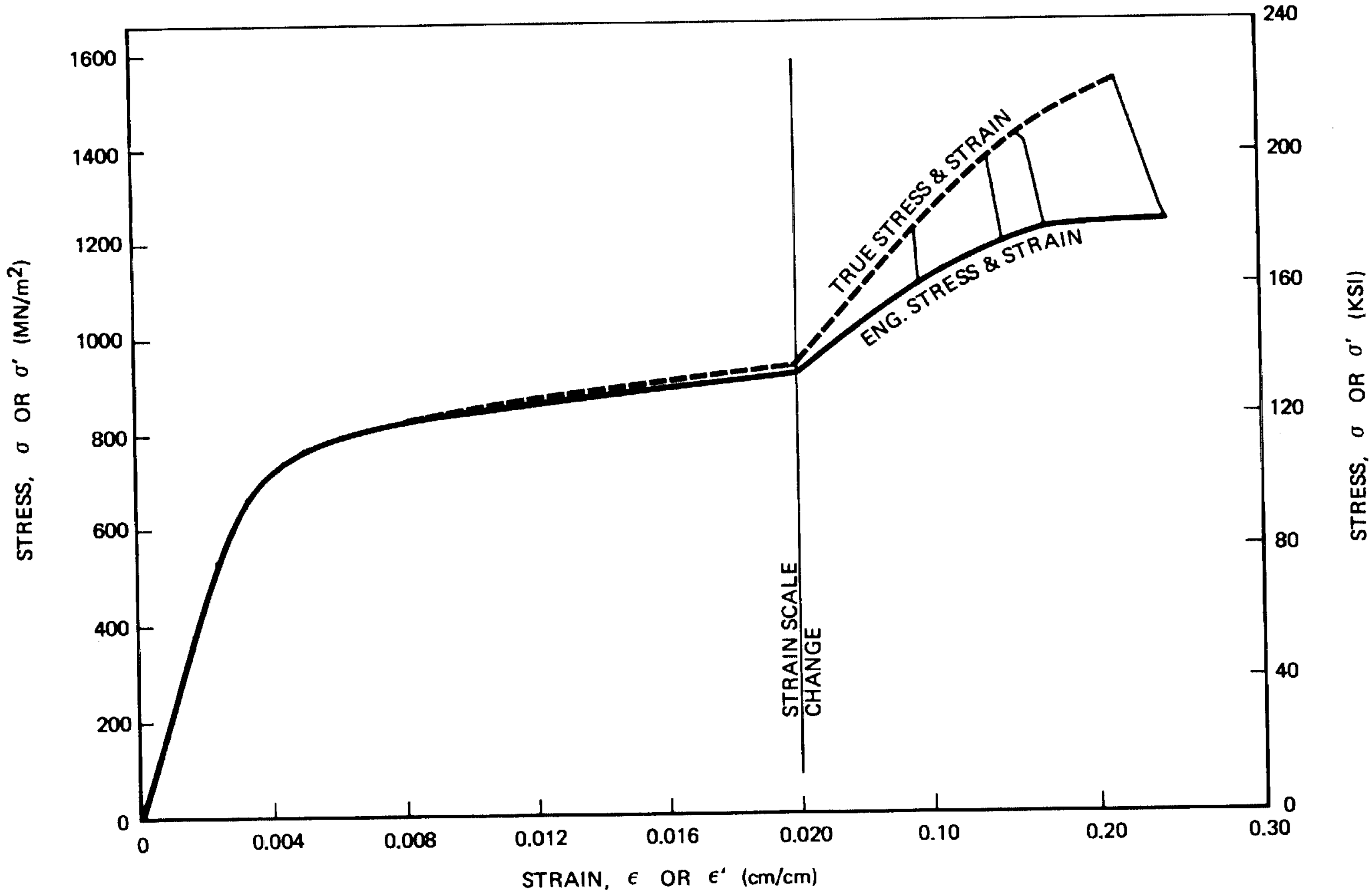

Figure A-2: Stress/Strain Relationship for 0.10 cm (0.040 Inch) Thick Inconel X750 STA Base Metal at 295⁰K (72⁰F) - Specimen B-3

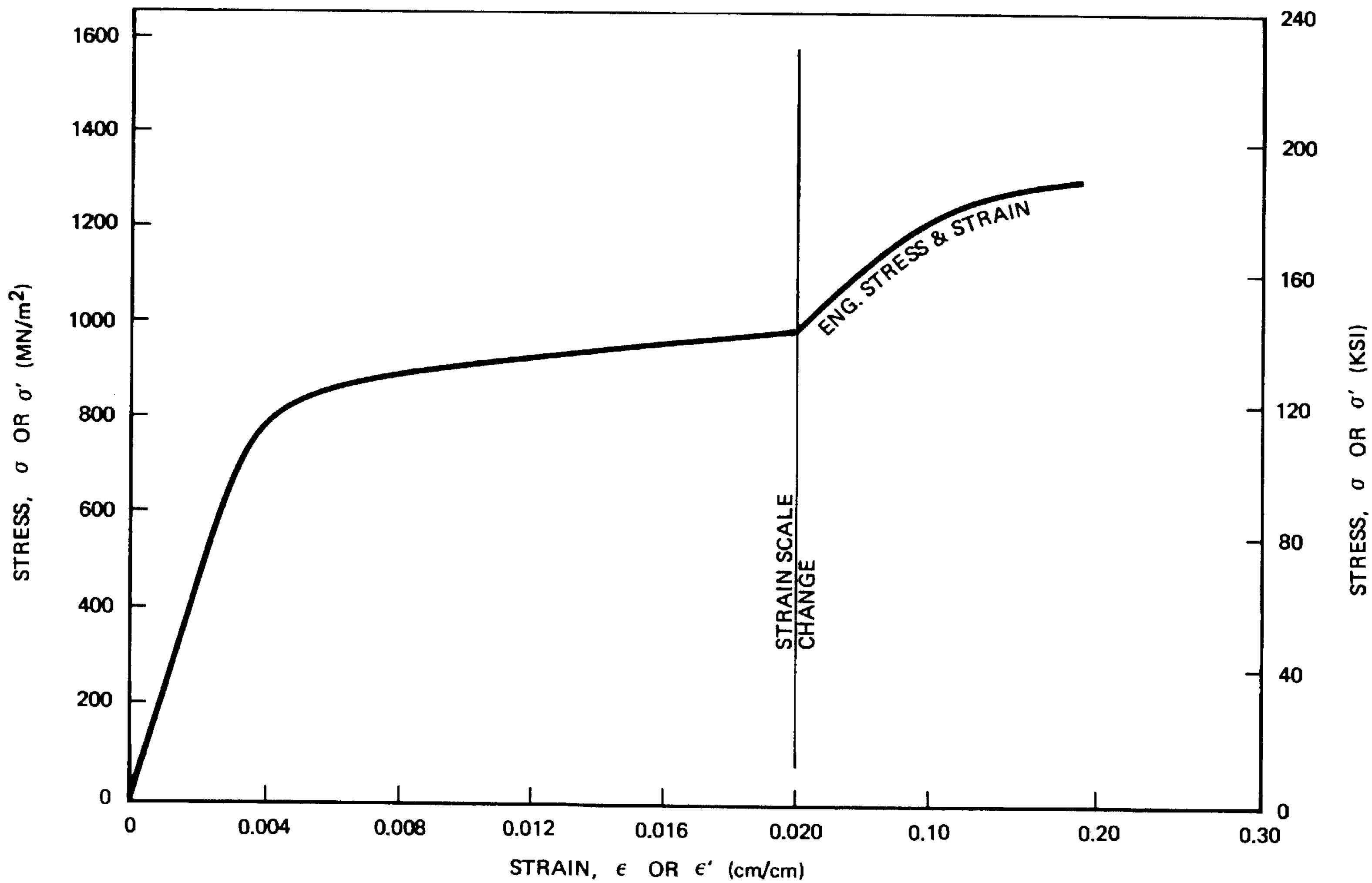

Figure A-3: Stress/Strain Relationship for 0.10 cm (0.040 Inch) Thick Inconel X750 STA Base Metal at 295°K (72°F) - Specimen B-15

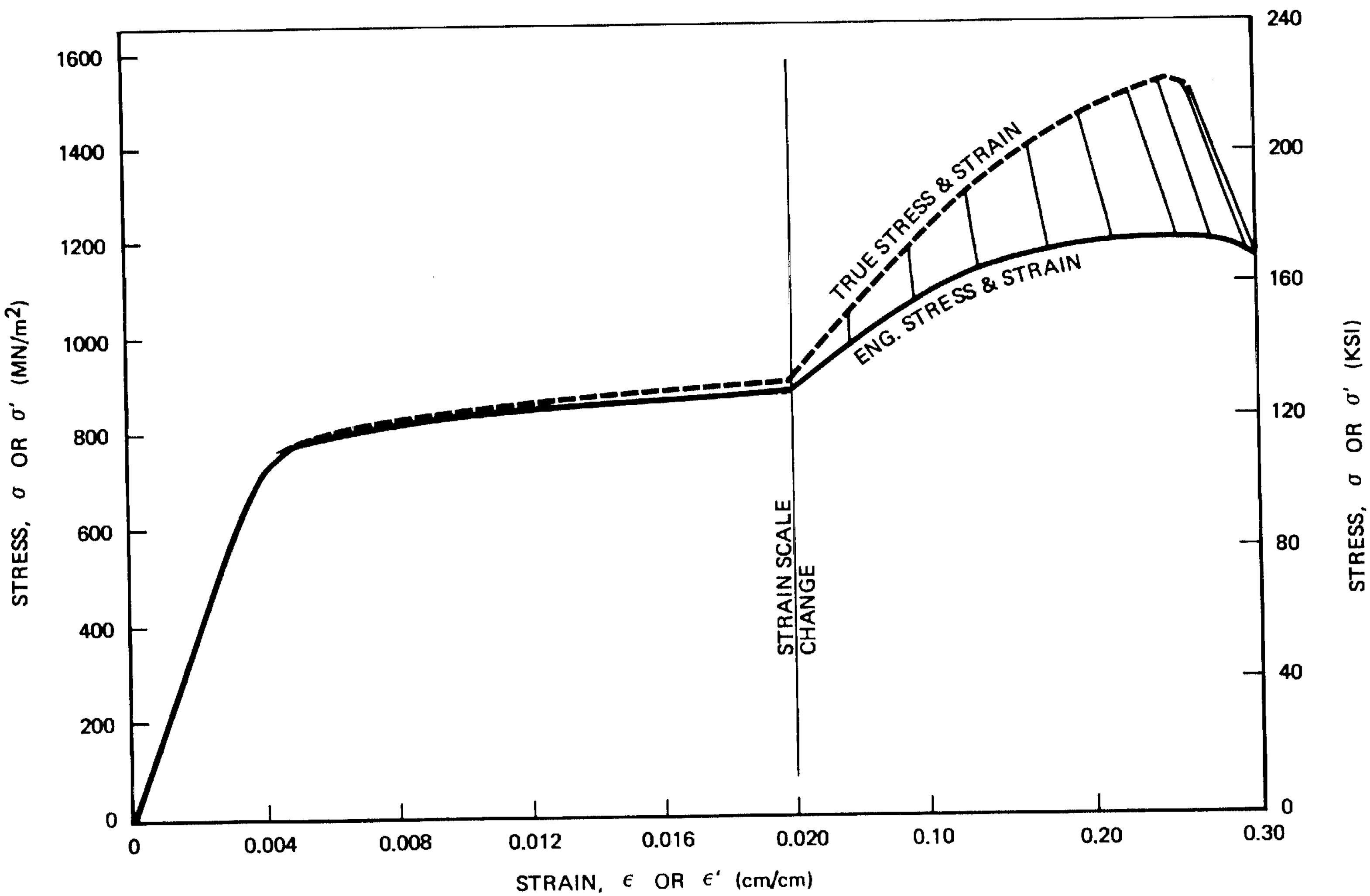

Figure A-4: Stress/Strain Relationship for 0.33 cm (0.13 Inch) Thick Inconel X750 STA Base Metal at 295°K (72°F) – Specimen 2B-15

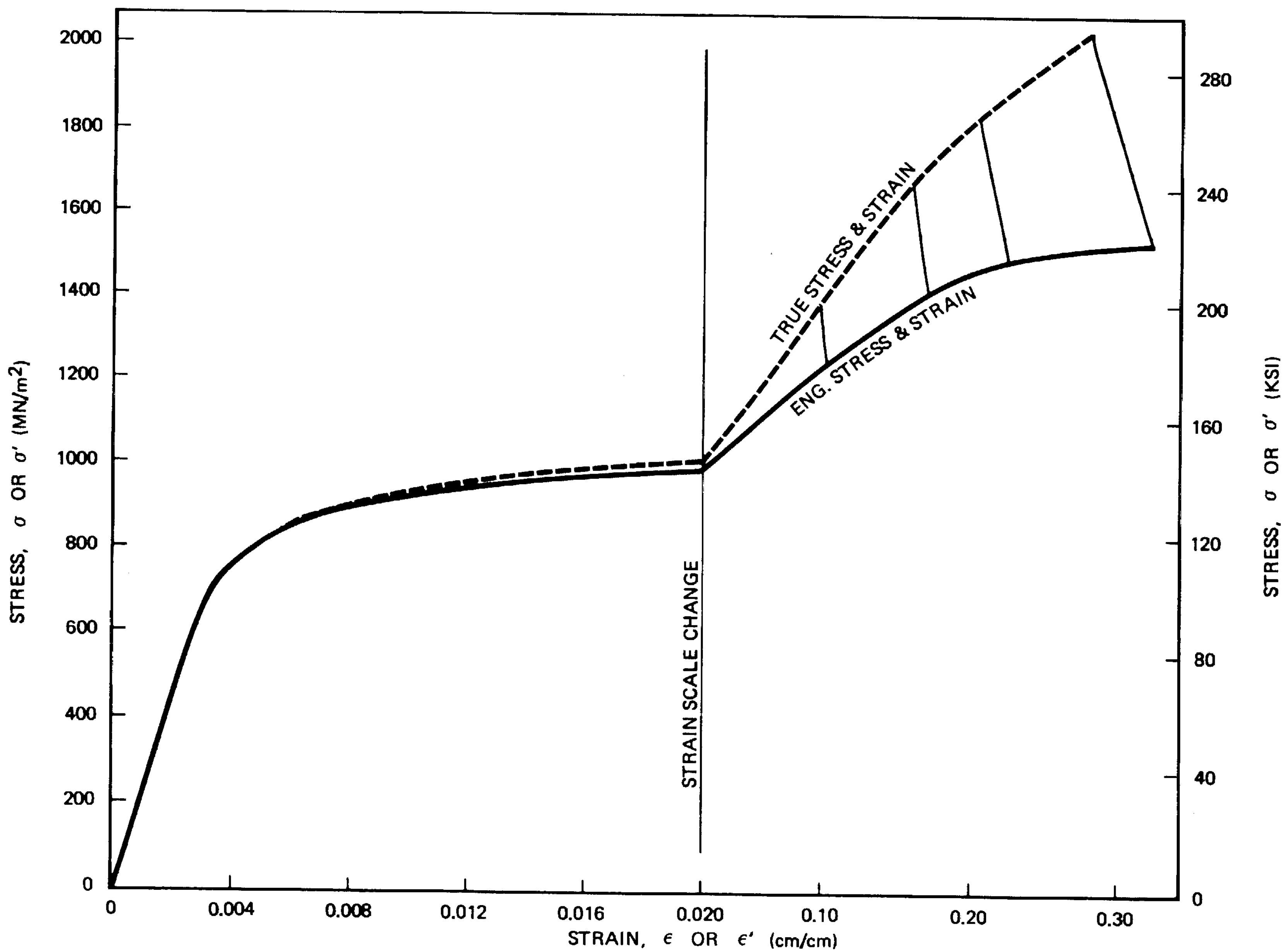

Figure A-5: Stress/Strain Relationship for 0.10 cm (0.040 Inch) Thick Inconel X750 STA Base Metal at 78°K (-320°F) - Specimen B-2

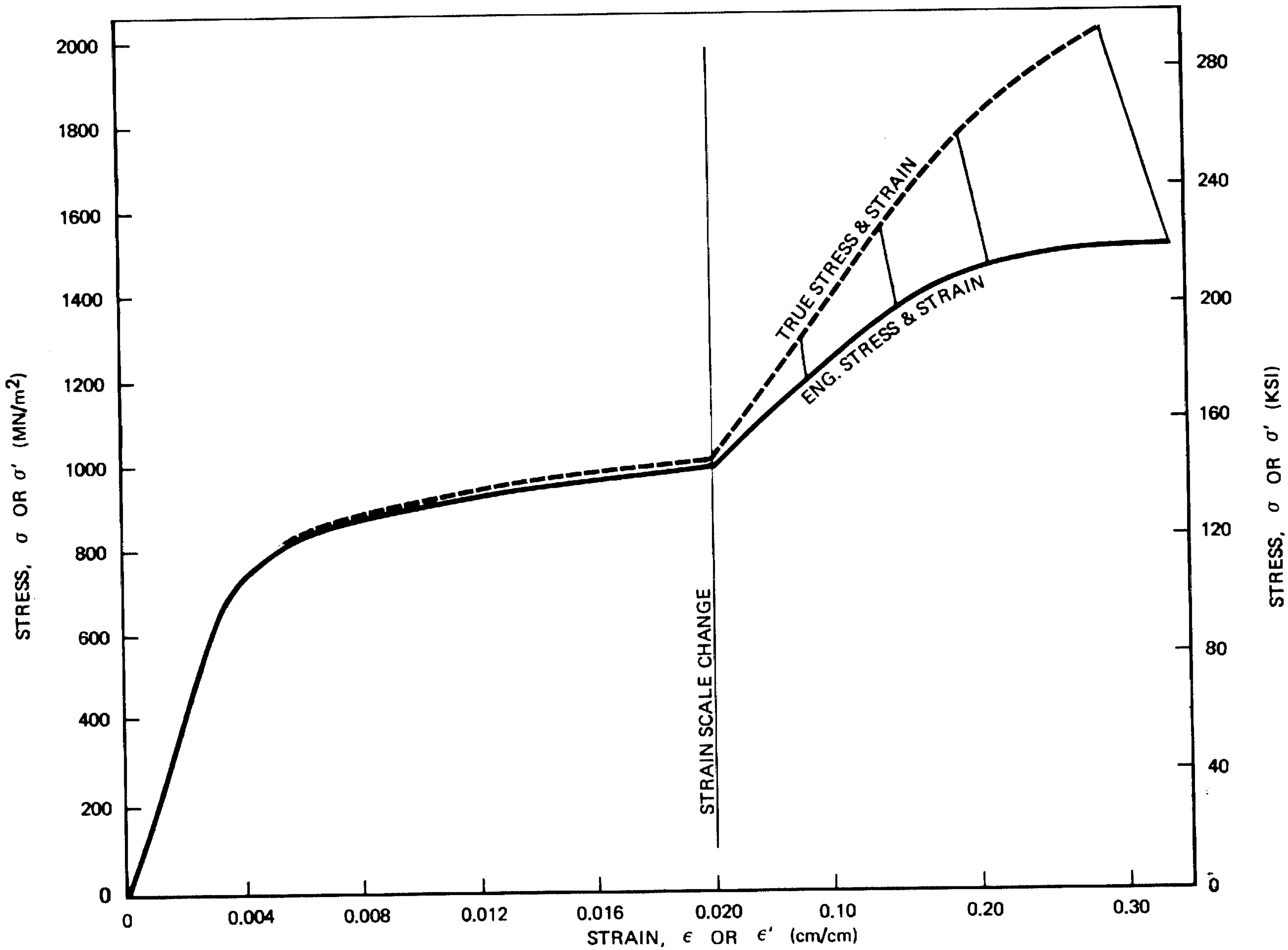

Figure A-6: Stress/Strain Relationship for 0.10 cm (0.040 Inch) Thick Inconel X750 STA Base Metal at 78°K (-320°F) - Specimen B-4

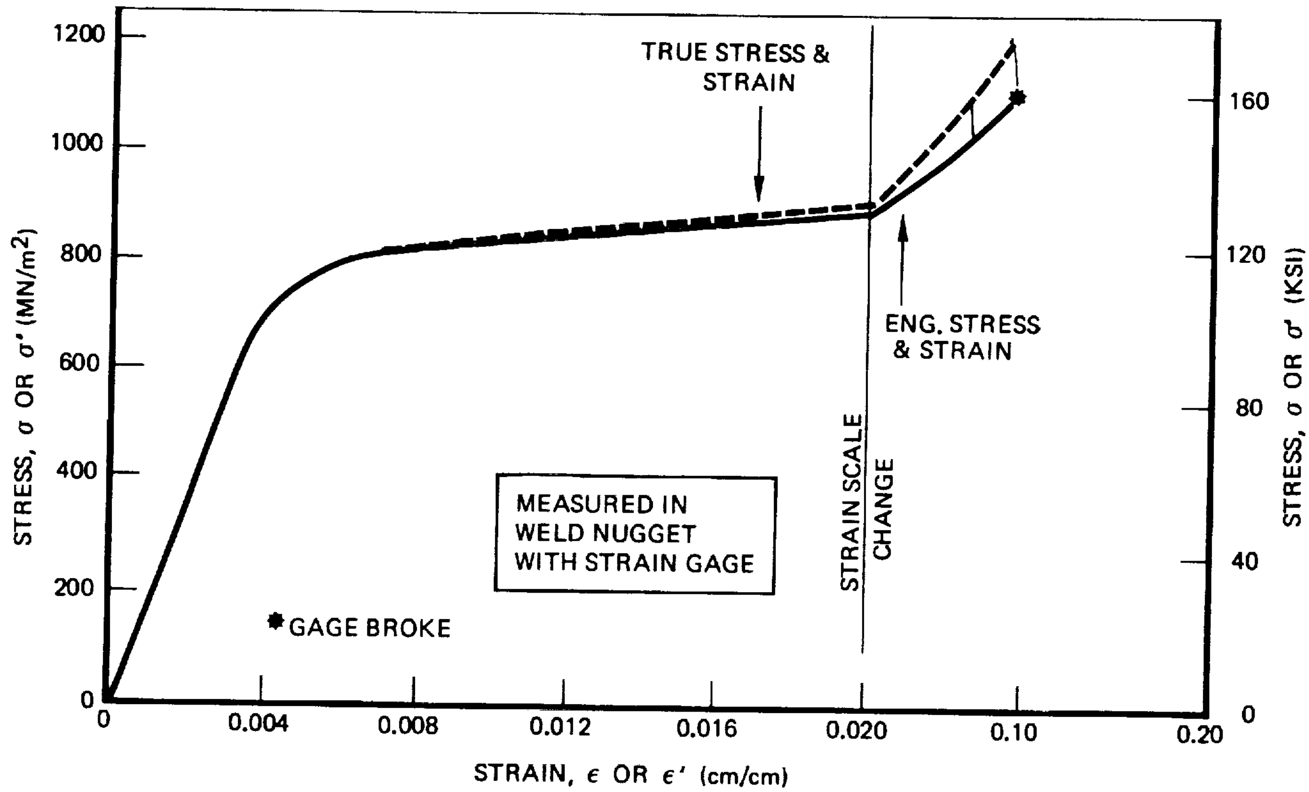

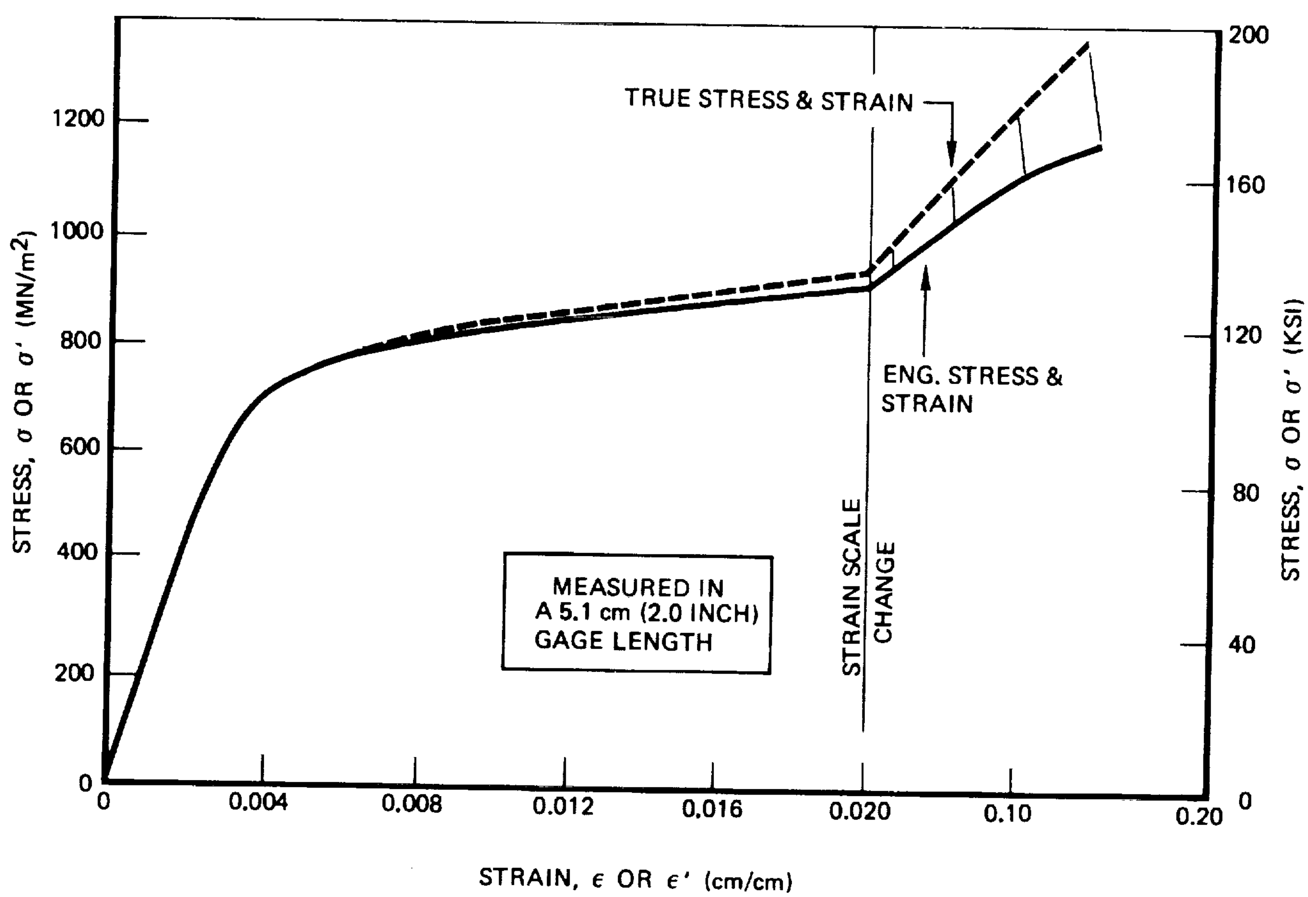

Figure A-7: Stress/Strain Relationship for 0.10 cm (0.040 Inch) Thick Inconel X750 STA Weld Metal at 295°K (72°F) - Specimen BW-2

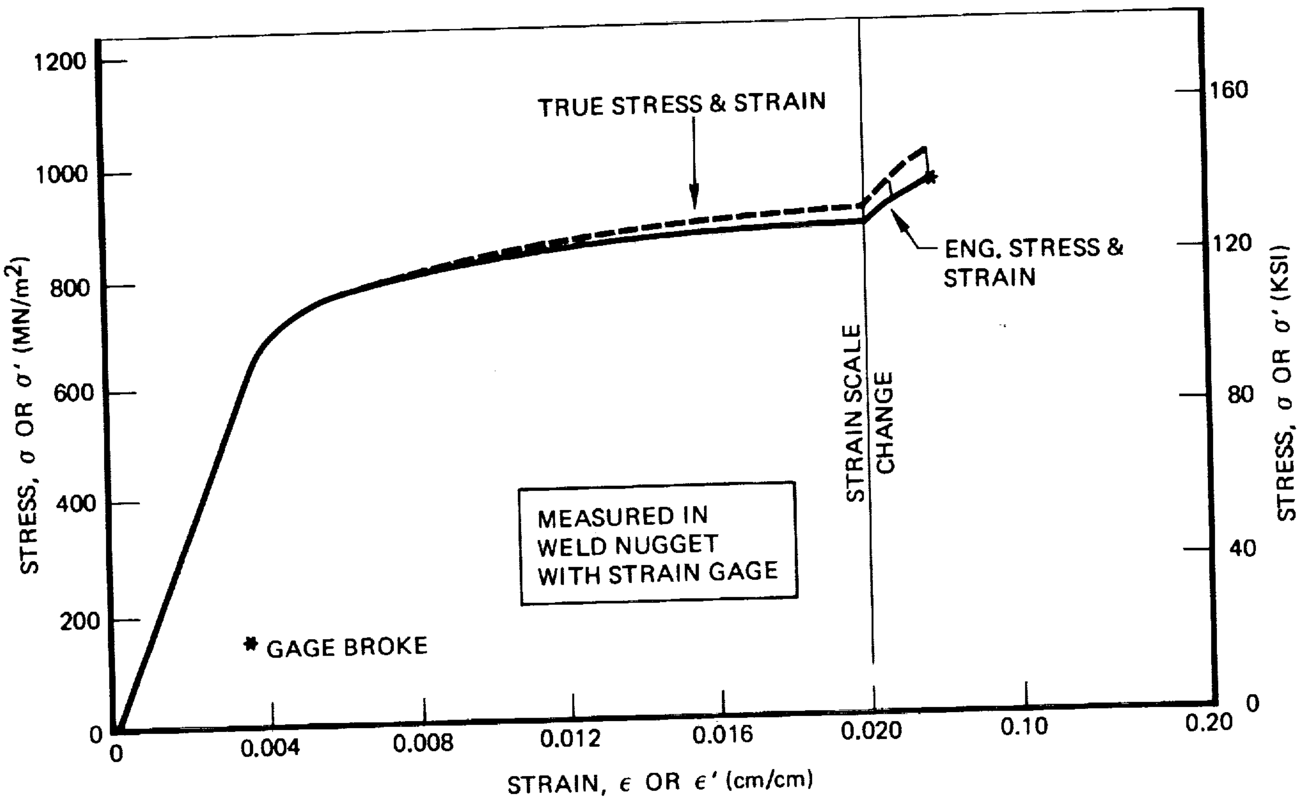

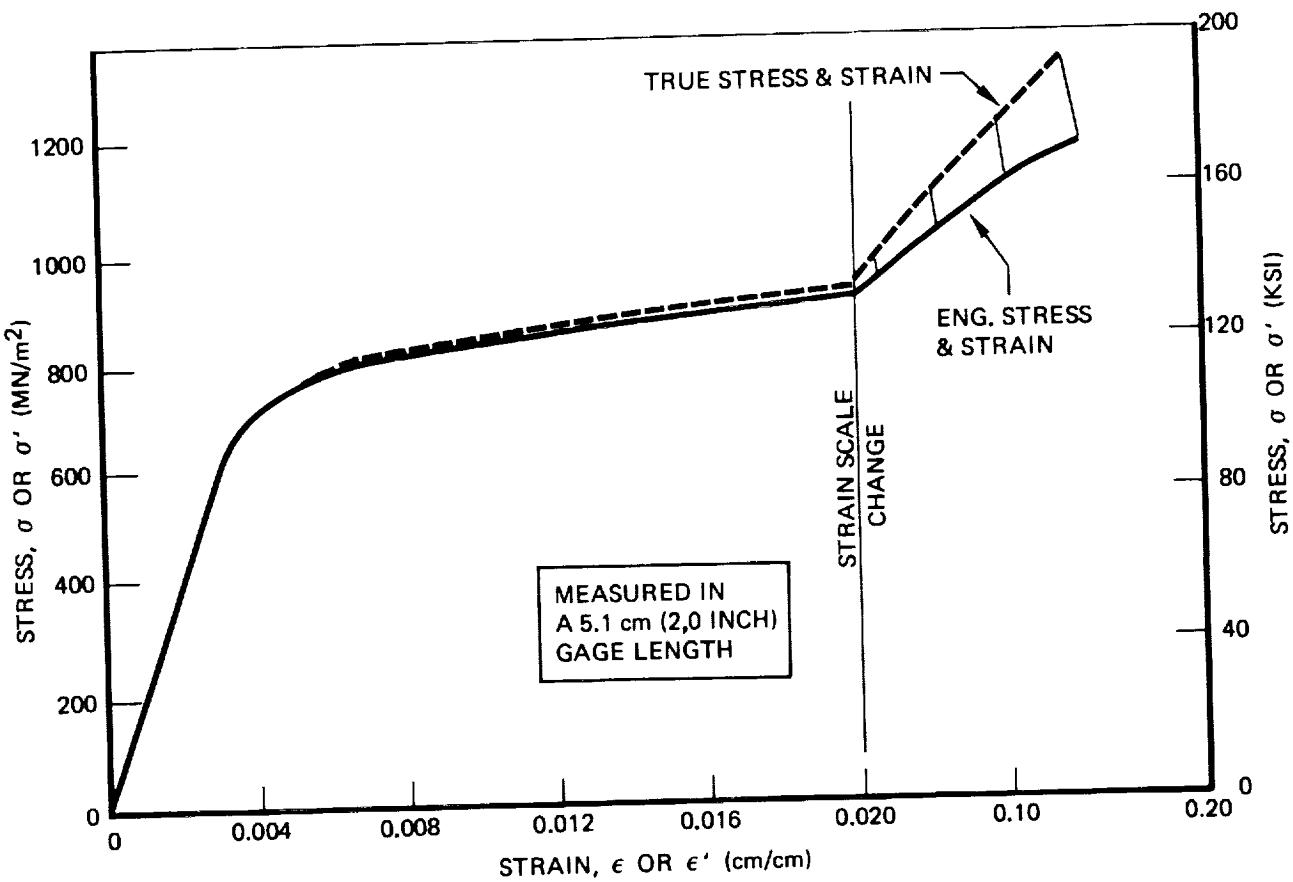

Figure A-8: Stress/Strain Relationship for 0.10 cm (0.040 Inch) Thick Inconel X750 STA Weld Metal at 295° K (72° F) - Specimen BW-4

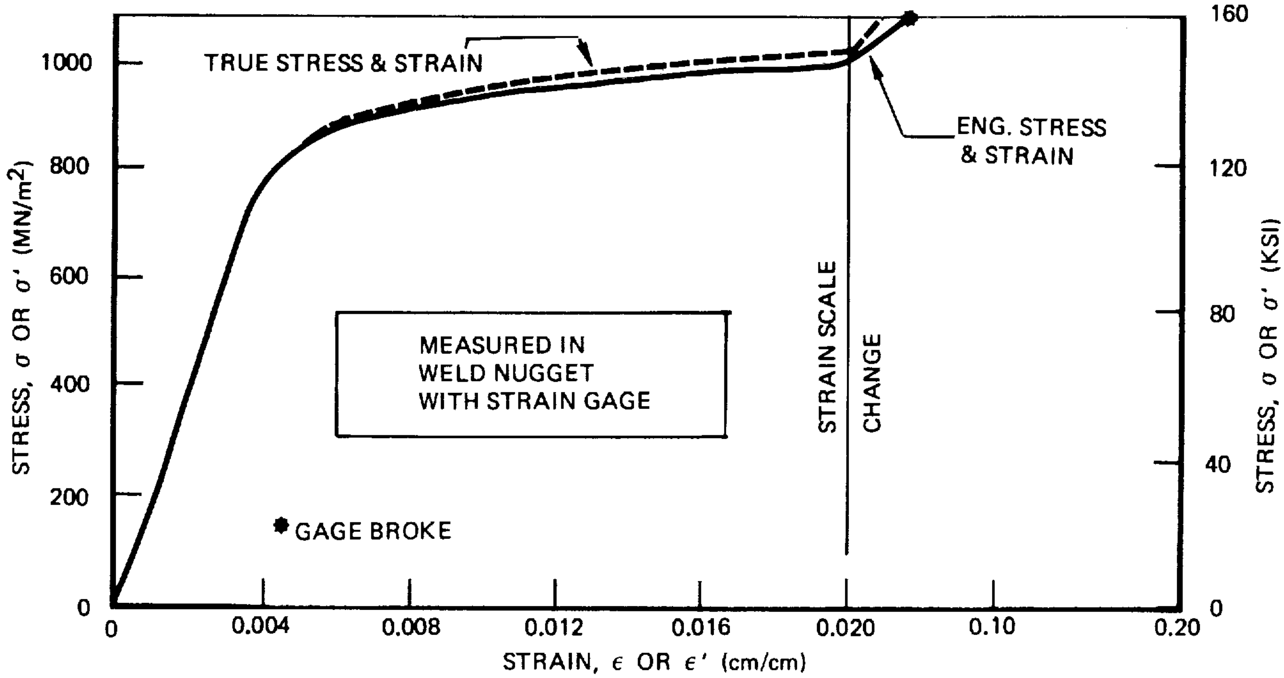

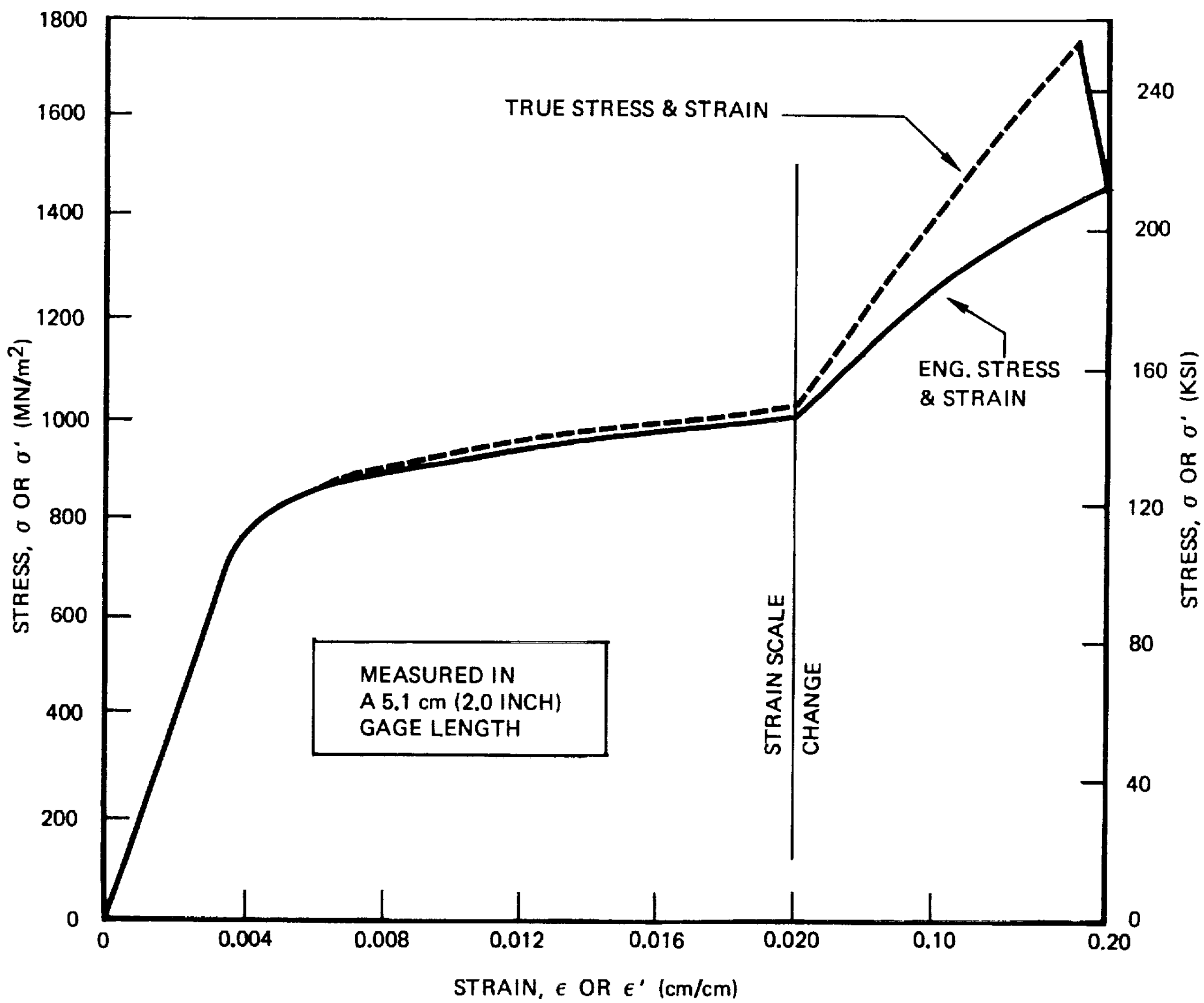

Figure A-9: Stress/Strain Relationship for 0.10 cm (0.040 Inch) Thick Inconel X750 STA Weld Metal at 78°K (-320°F) - Specimen BW-3

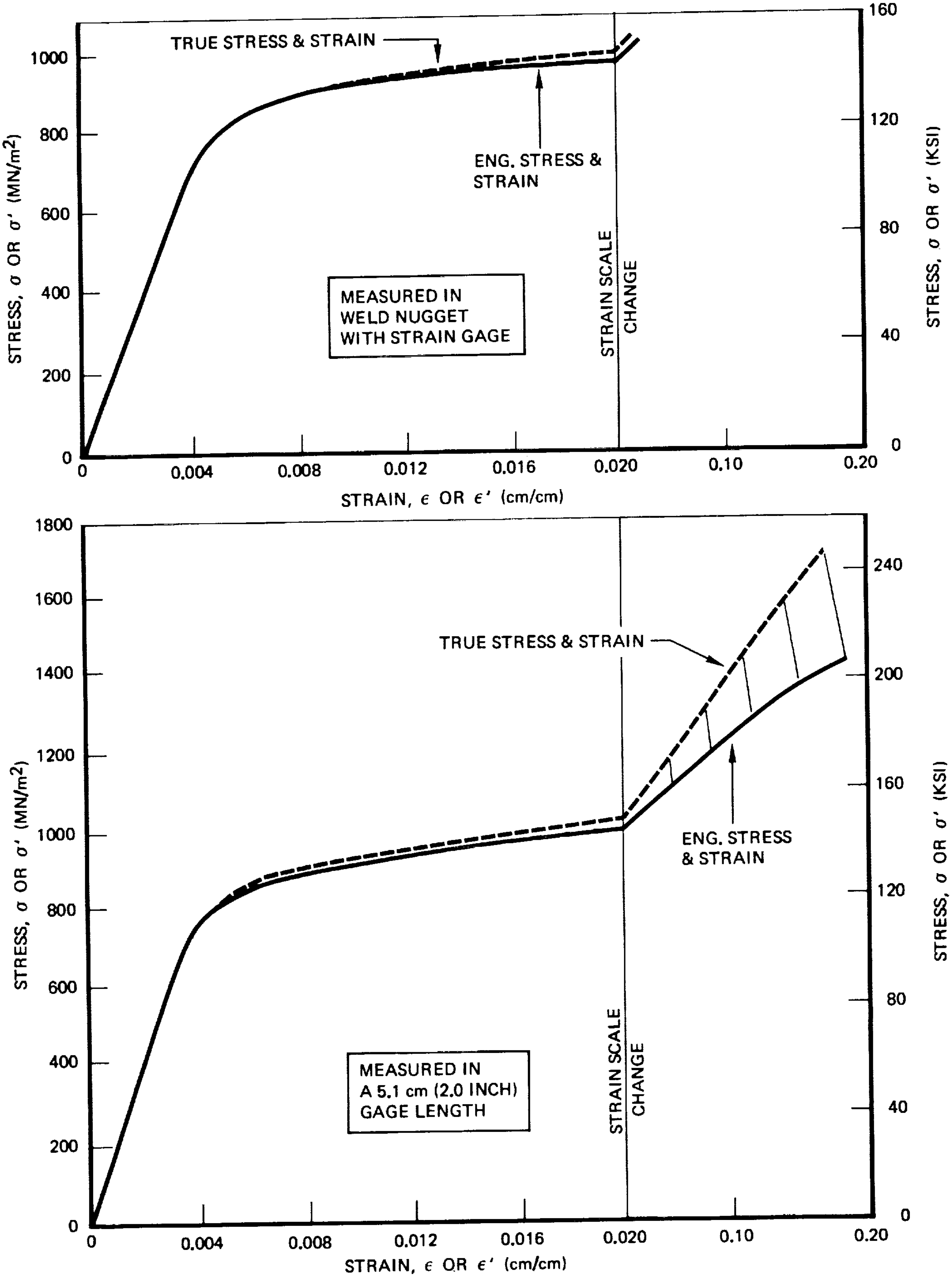

Figure A-10: Stress/Strain Relationship for 0.10 cm (0.040 Inch) Thick Inconel X750 STA Weld Metal at 78°K (-320°F) - Specimen BW-5

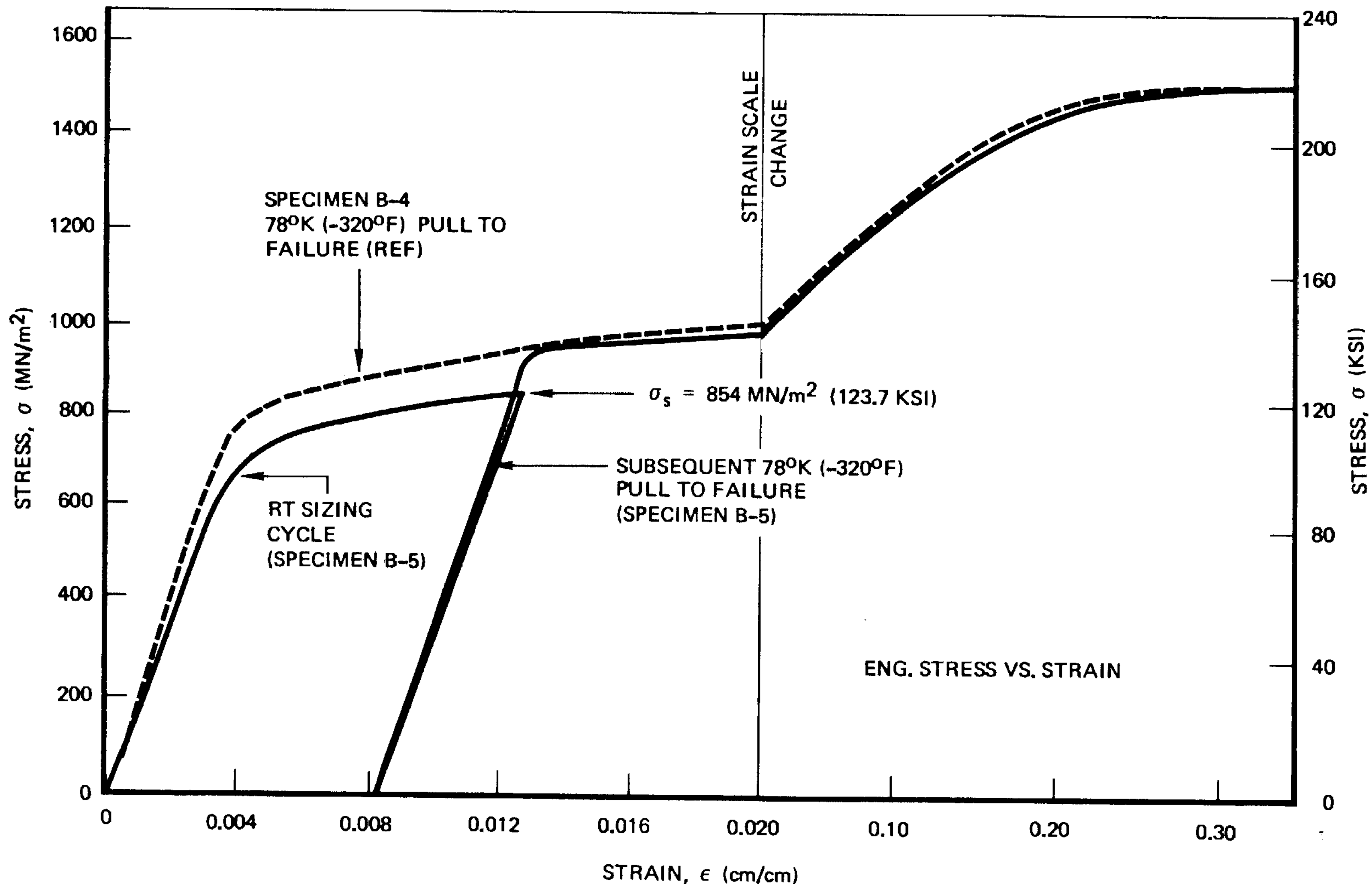

Figure A-11: Stress/Strain Relationship for 0.10 cm (0.040 Inch) Thick Inconel X750 STA Base Metal at 78°K (-320°F) - With RT Sizing Cycle - Specimen B-4

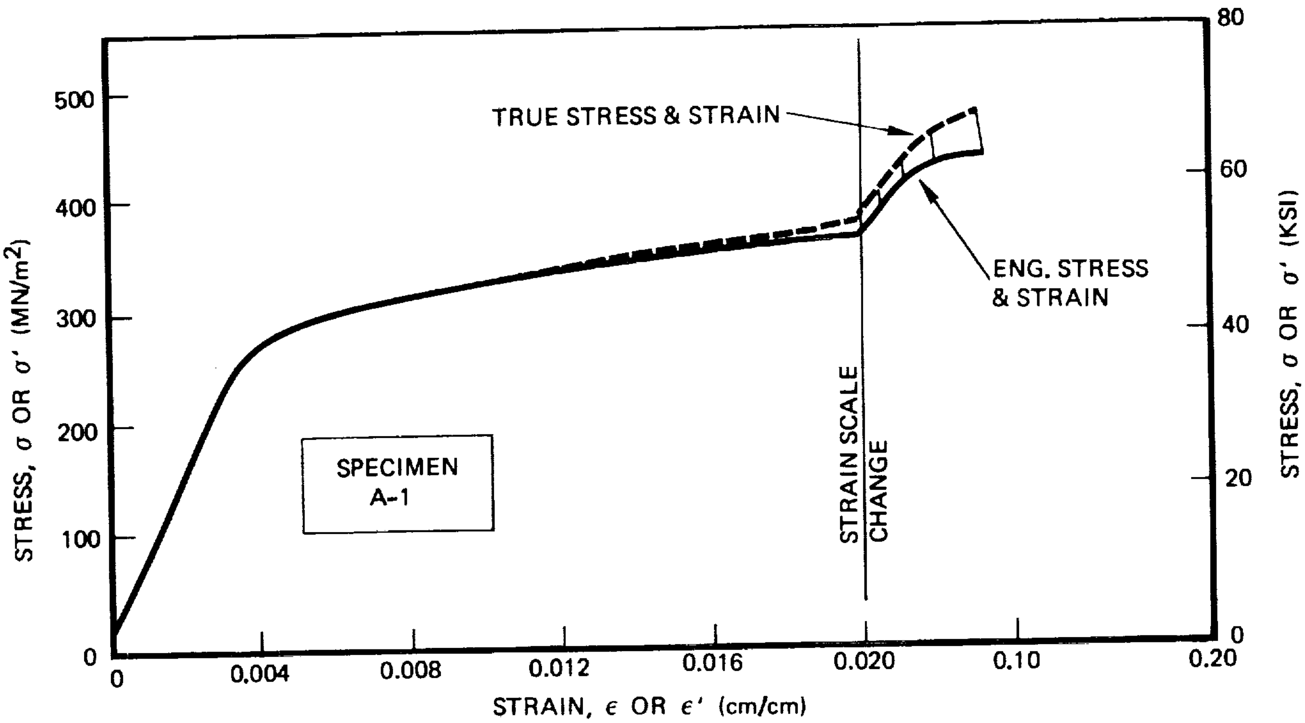

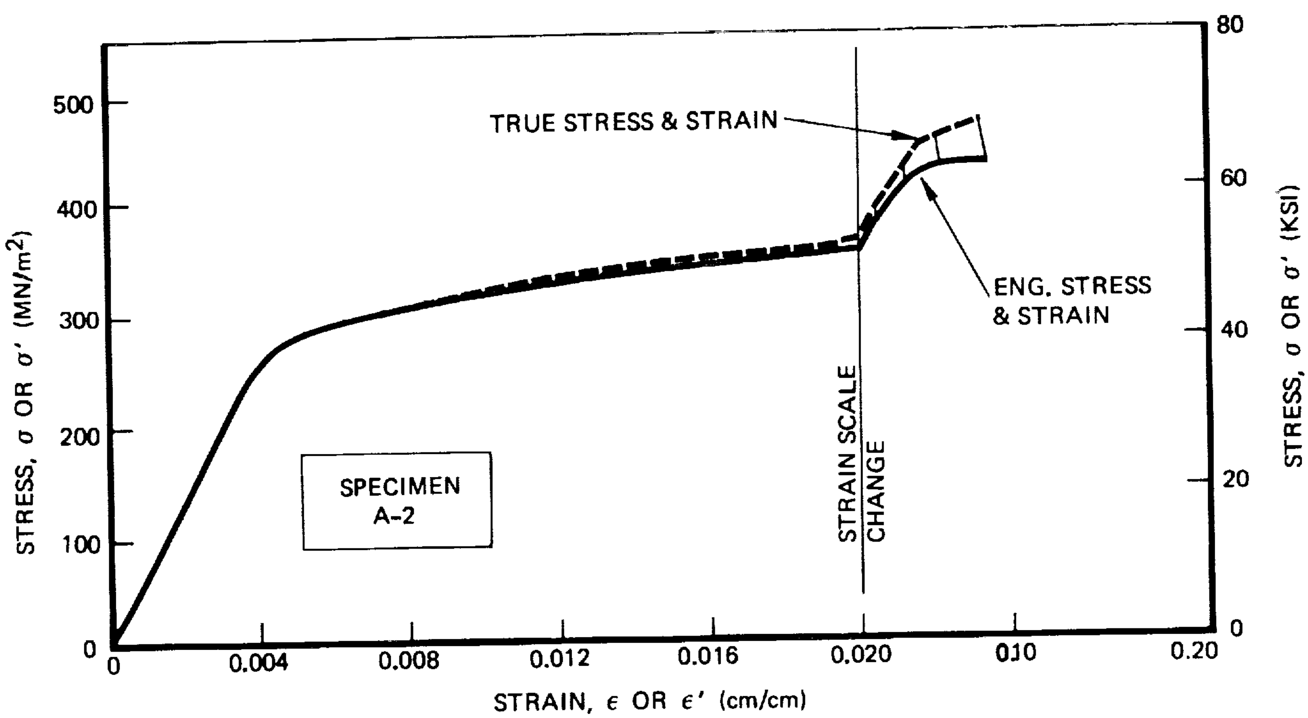

Figure A-12: Stress/Strain Relationship of 0.23 cm (0.090 Inch) Thick 2219-T62 Aluminum Base Metal at 295°K (72°F)

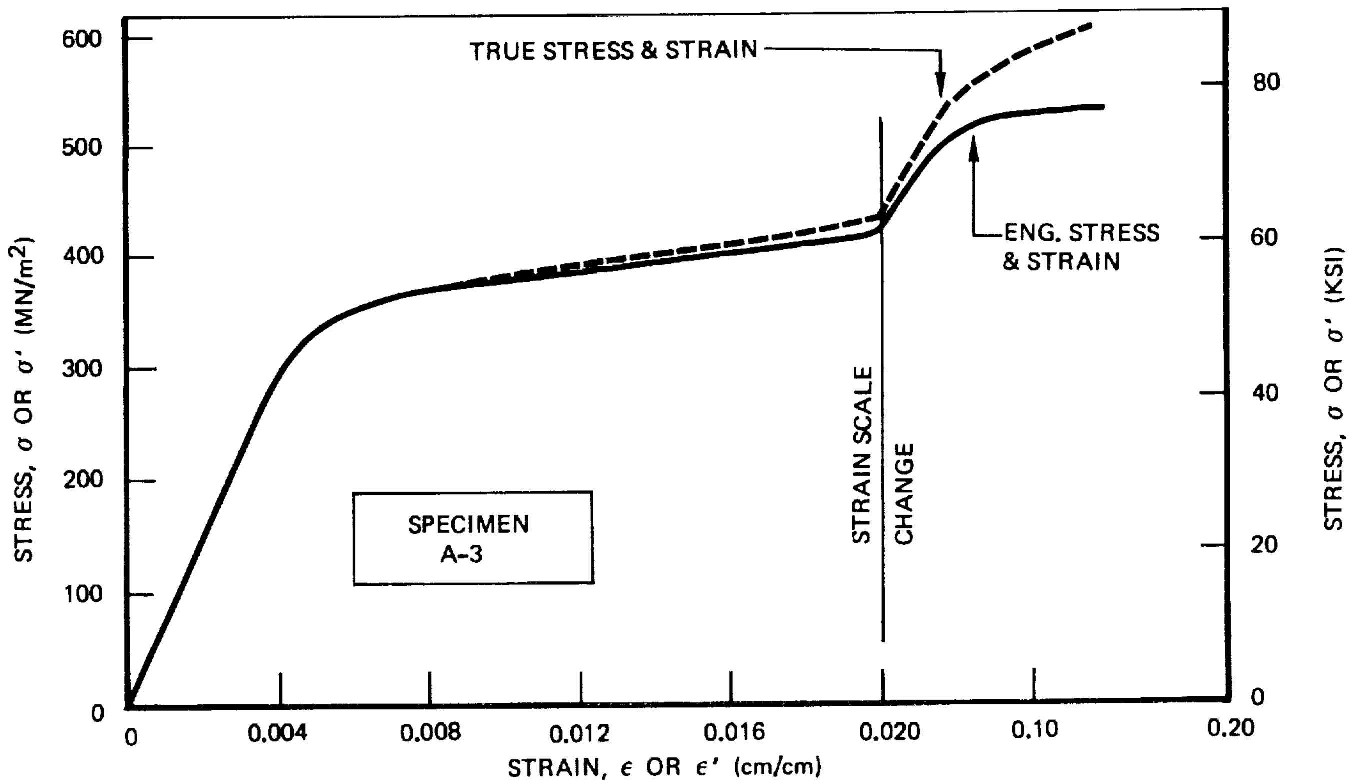

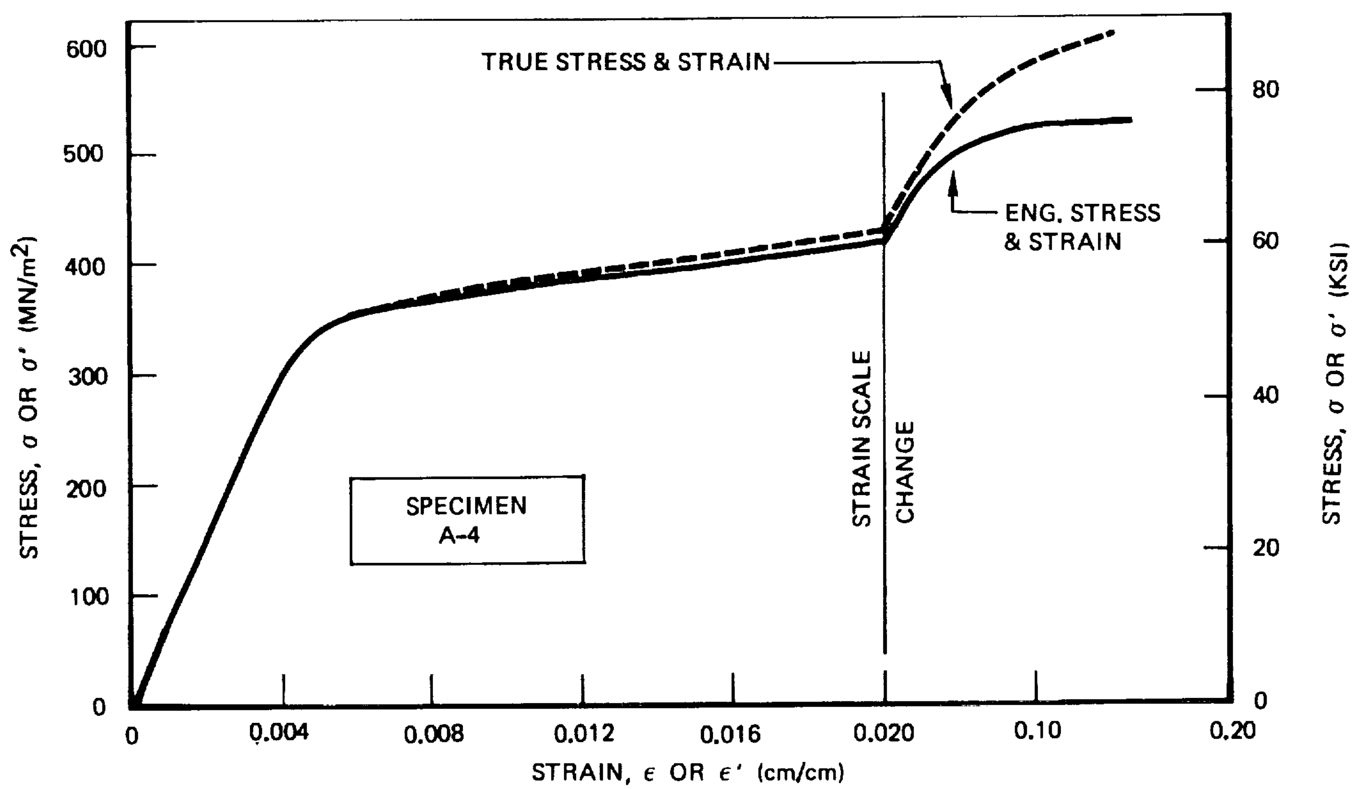

Figure A-13: Stress/Strain Relationship of 0.23 cm (0.090 Inch) Thick 2219-T62 Aluminum Base Metal at 78°K (-320°F)

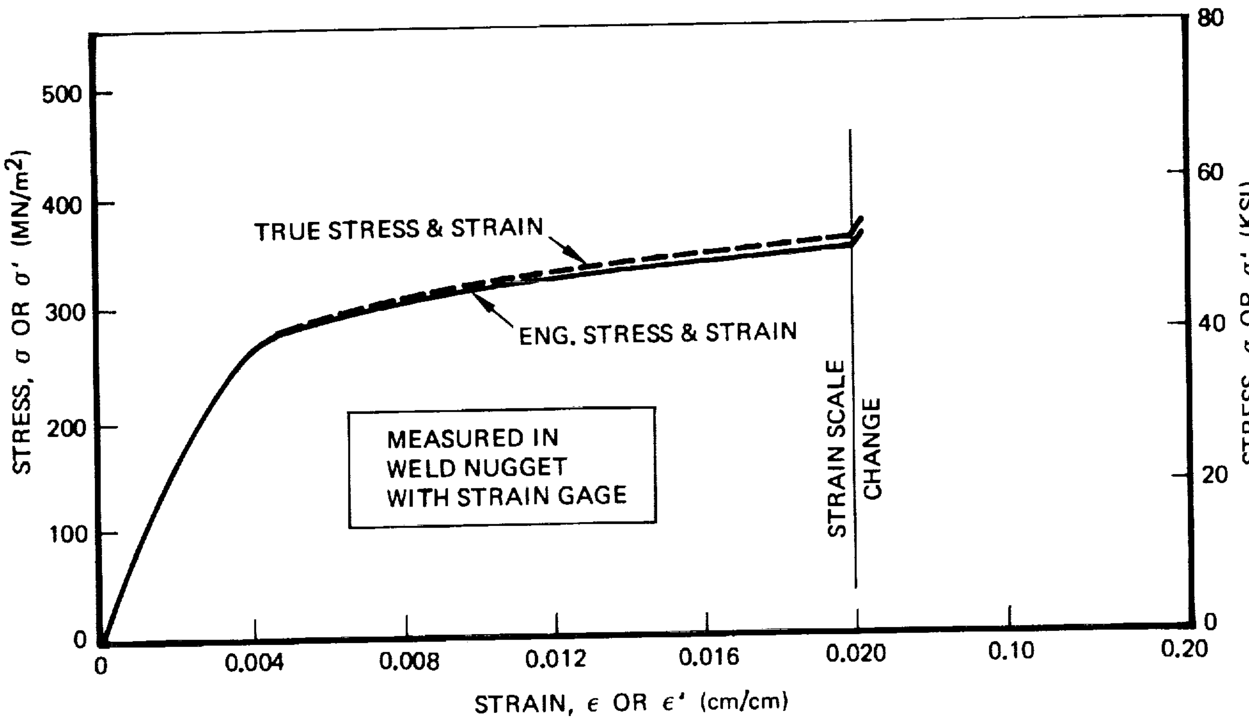

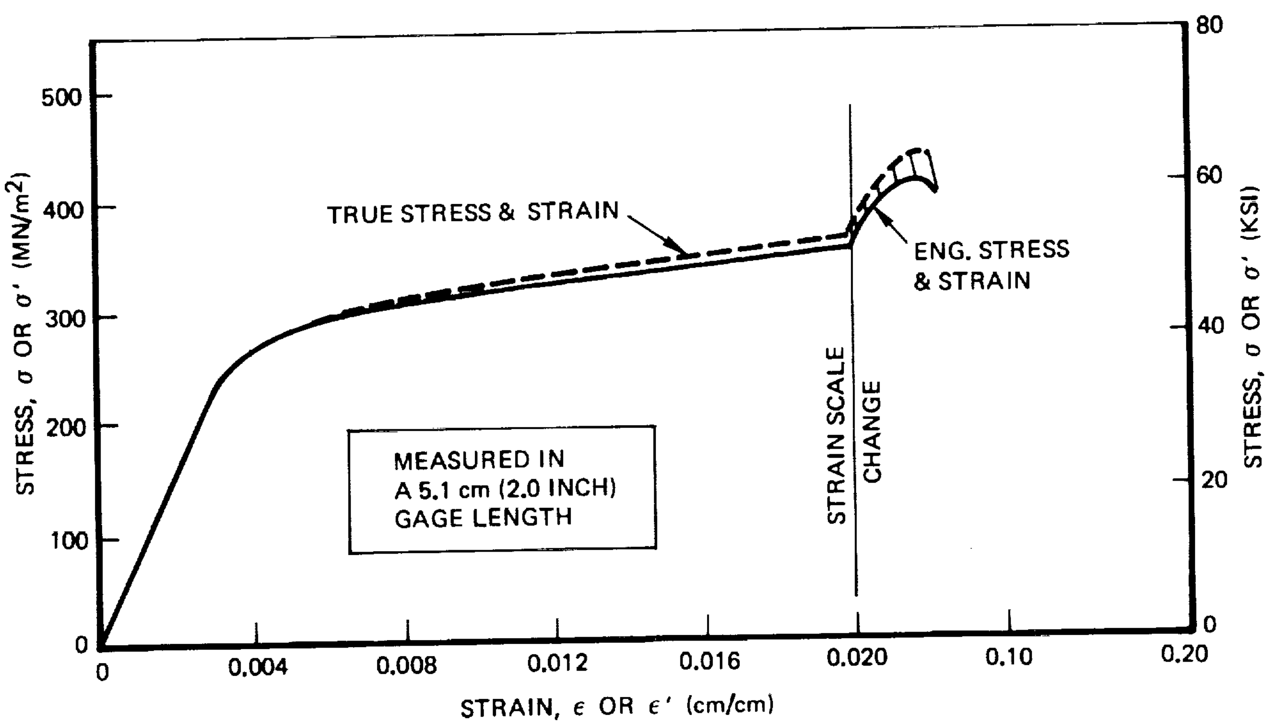

Figure A-14: Stress/Strain Relationship of 0.23 cm (0.090 Inch) Thick 2219-T62 Aluminum Weld Metal at 295°K (72°F) - Specimen AW-1

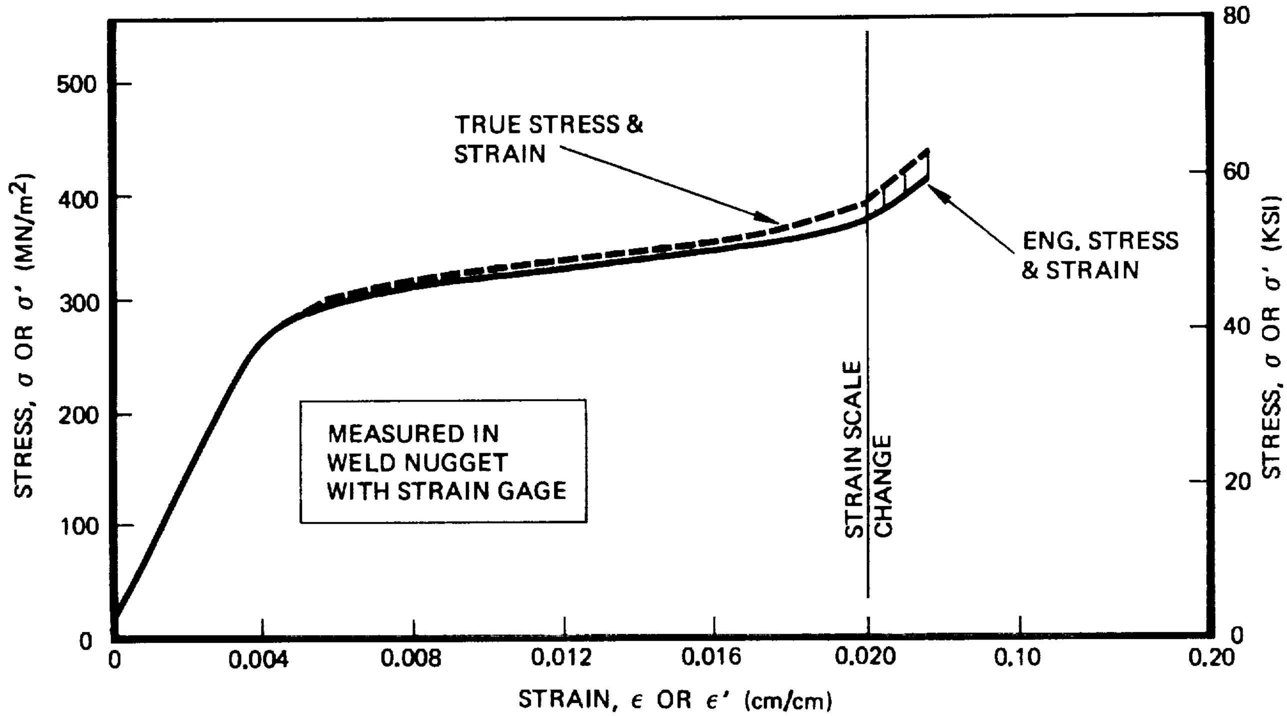

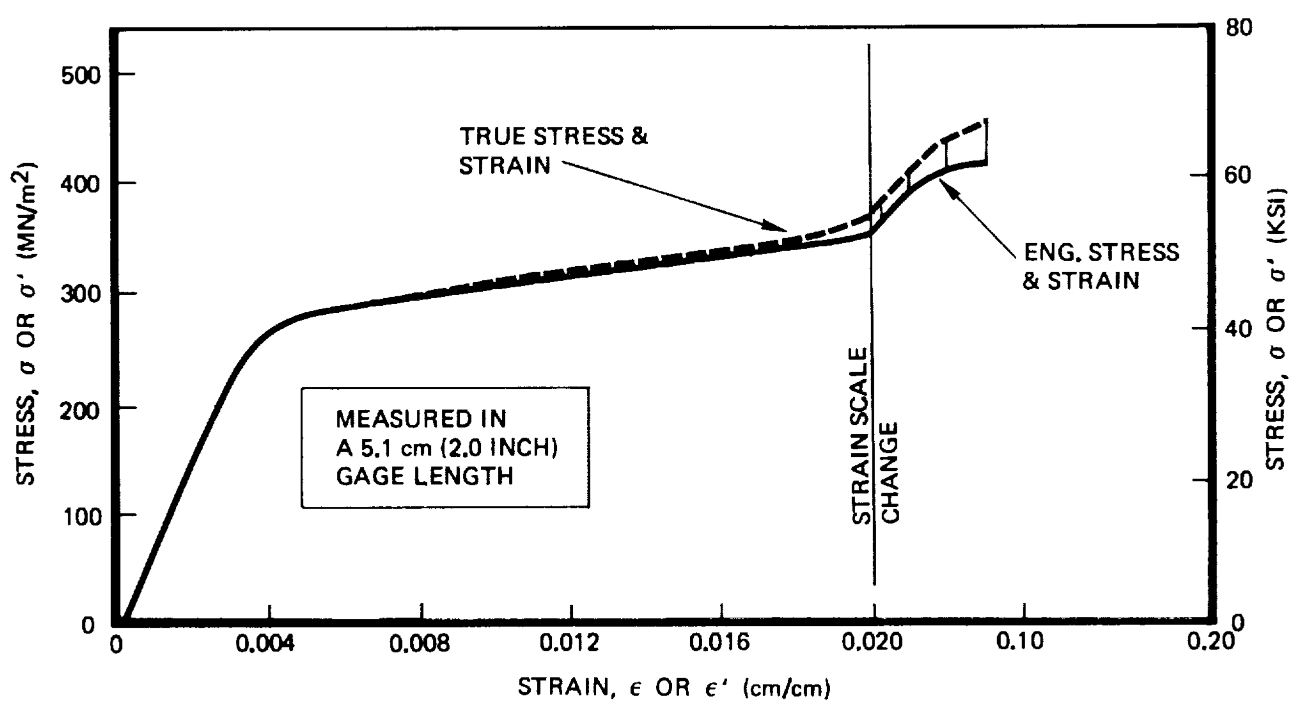

Figure A-15: Stress/Strain Relationship of 0.23 cm (0.090 Inch) Thick 2219-T62 Aluminum Weld Metal at 295°K (72°F) - Specimen AW-2

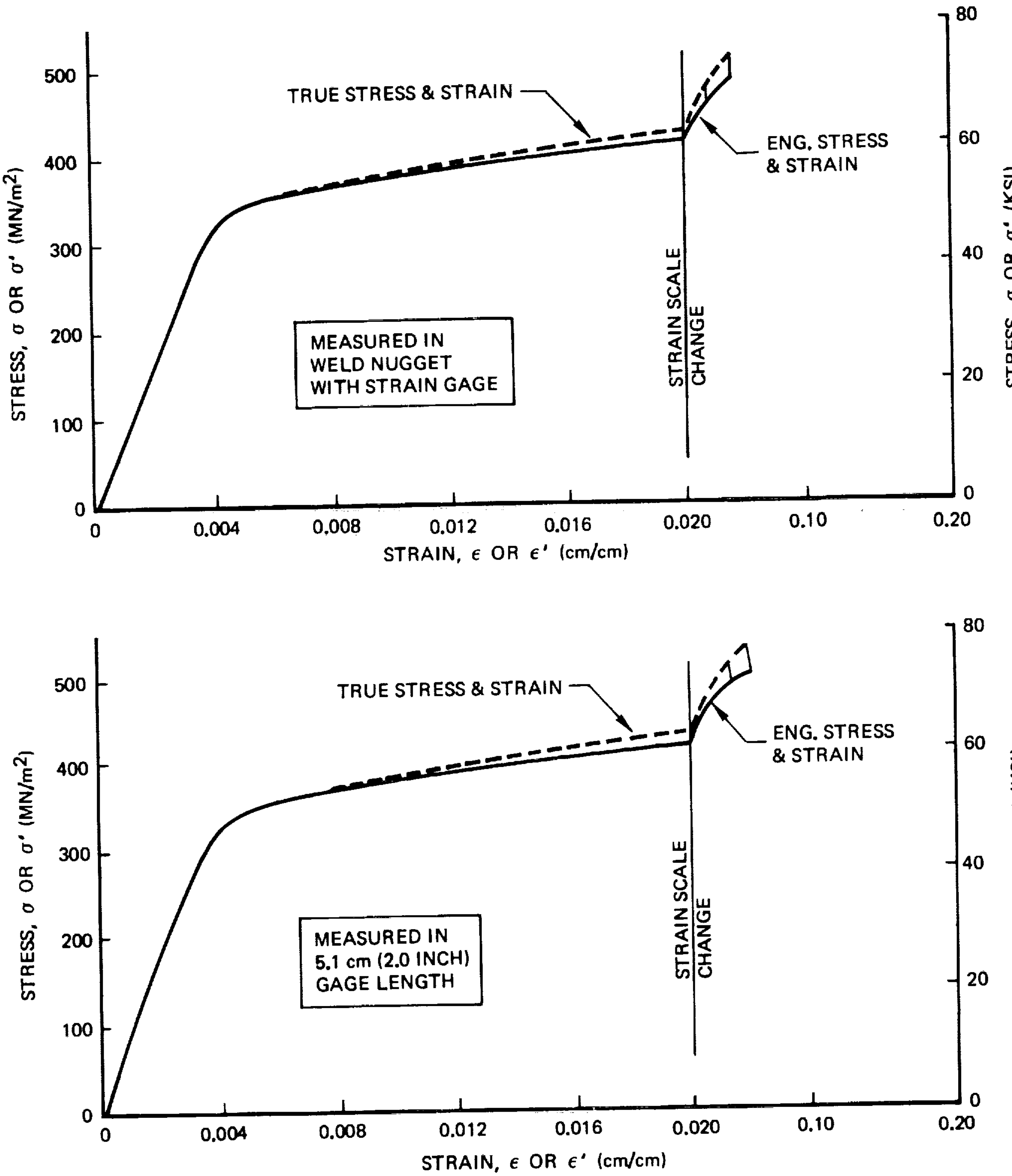

Figure A-16: Stress/Strain Relationship of 0.23 cm (0.090 Inch) Thick 2219-T62 Aluminum Weld Metal at 78° K (-320° F) - Specimen AW-4

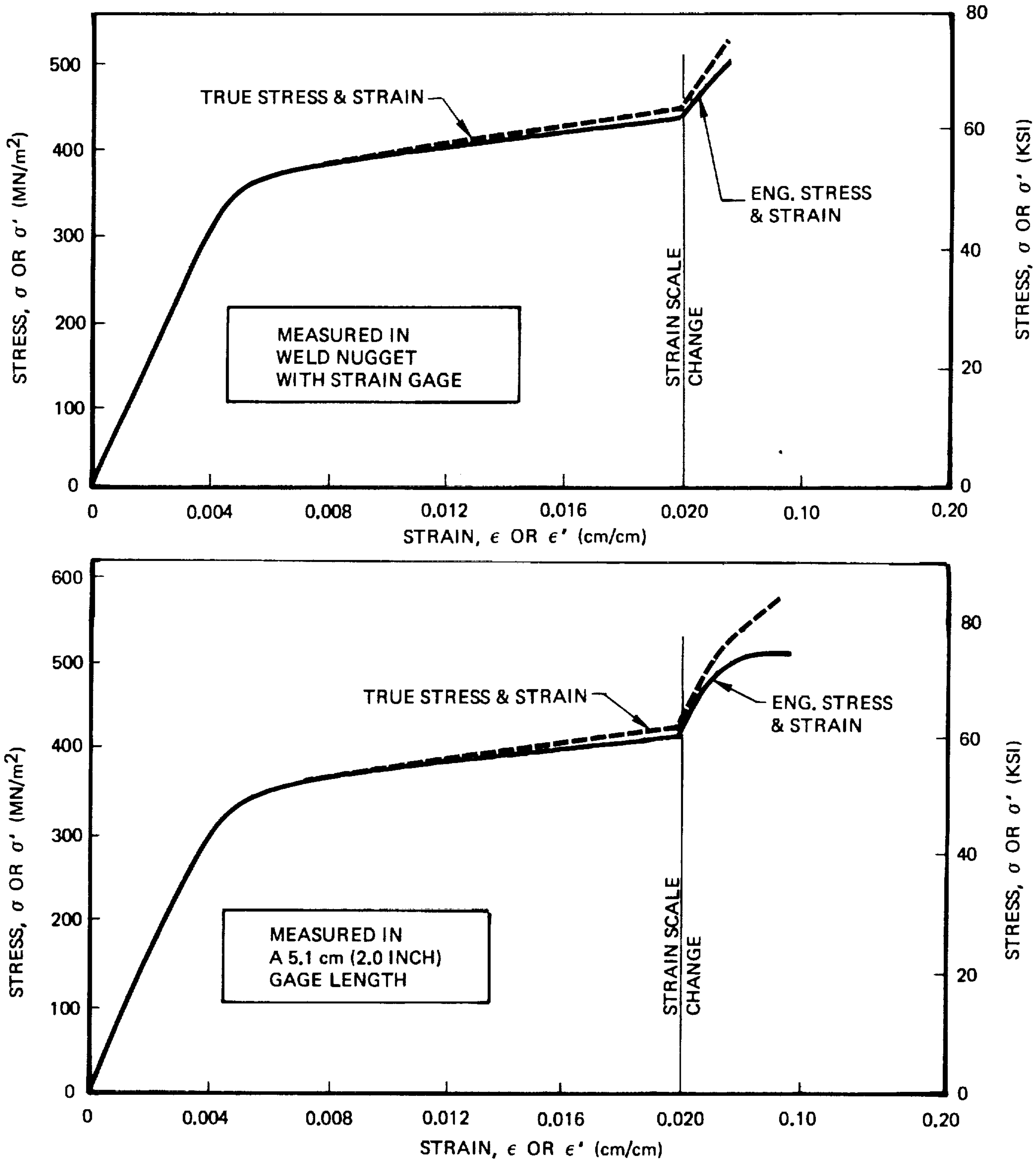

Figure A-17: Stress/Strain Relationship of 0.23 cm (0.090 Inch) Thick 2219-T62 Aluminum Weld Metal at 78°K (-320°F) - Specimen AW-6

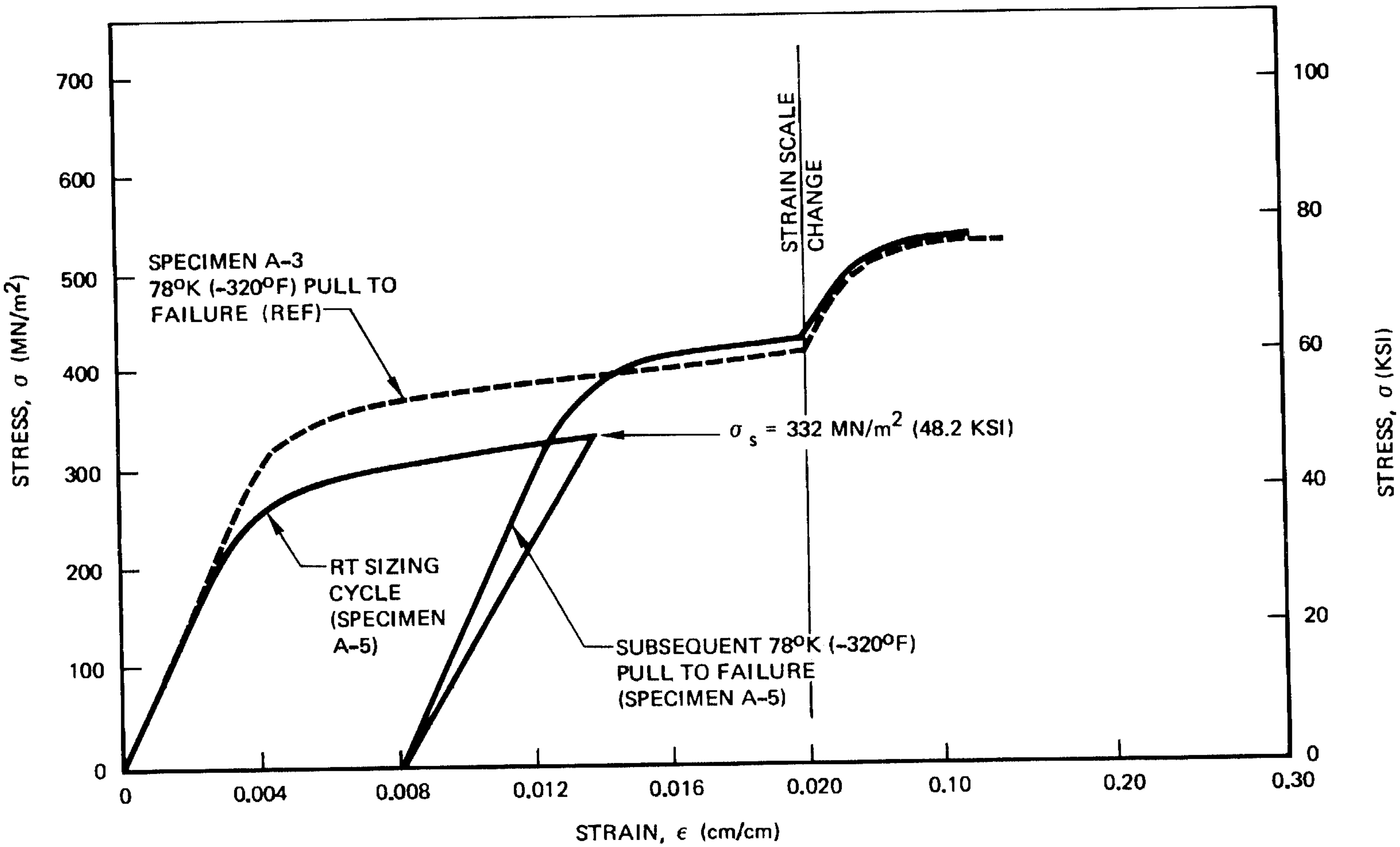

Figure A-18: Stress/Strain Relationship of 0.23 cm (0.090 Inch) Thick 2219-T62 Aluminum Base Metal at 78°K (-320°F) with RT Sizing Cycle - Specimen A-5

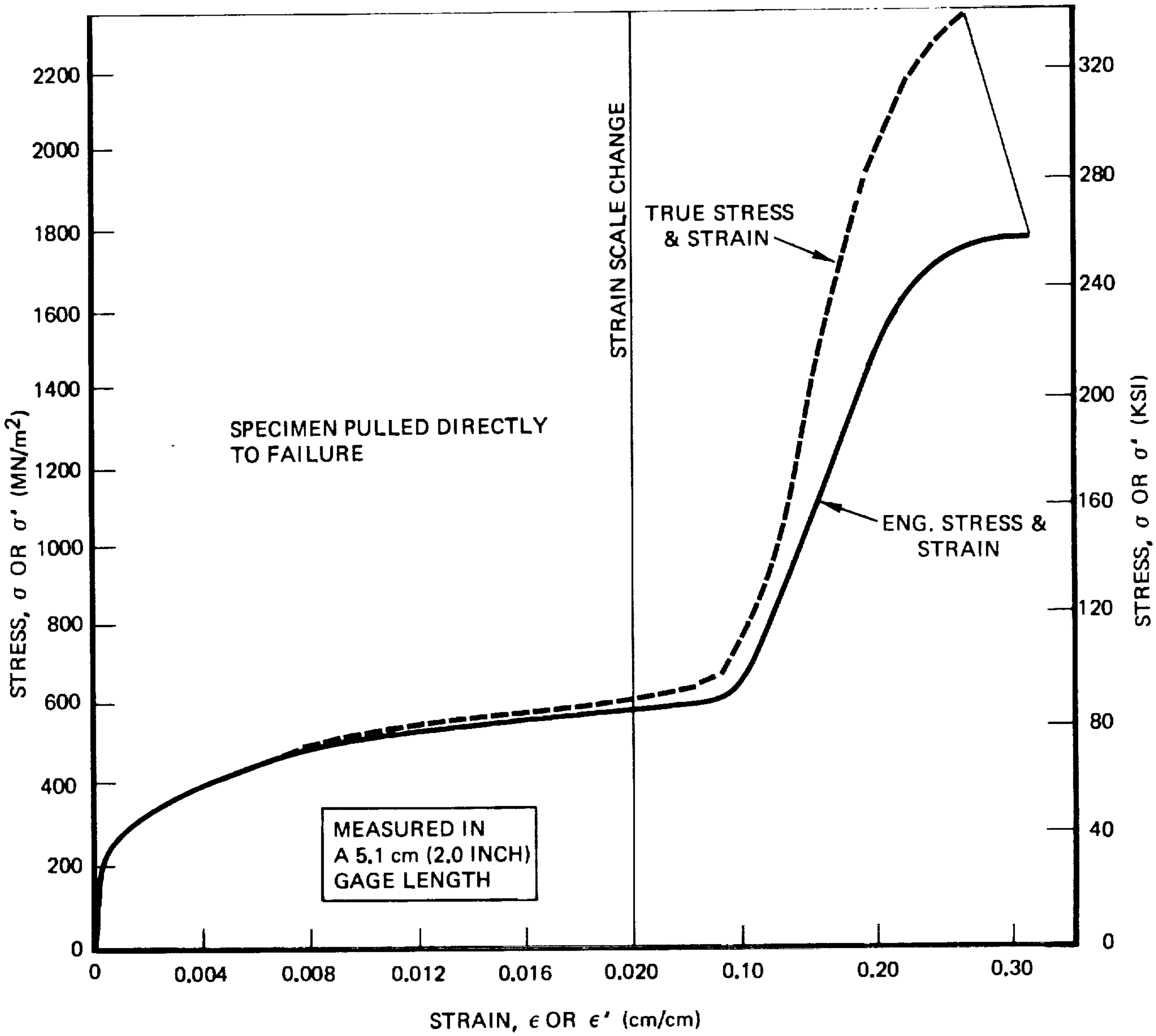

Figure A-19: Stress/Strain Relationship for 0.71 mm (0.028 Inch) Thick Cryostretched 301 Stainless Steel Base Metal at 78°K (-320°F) - Specimen C-1

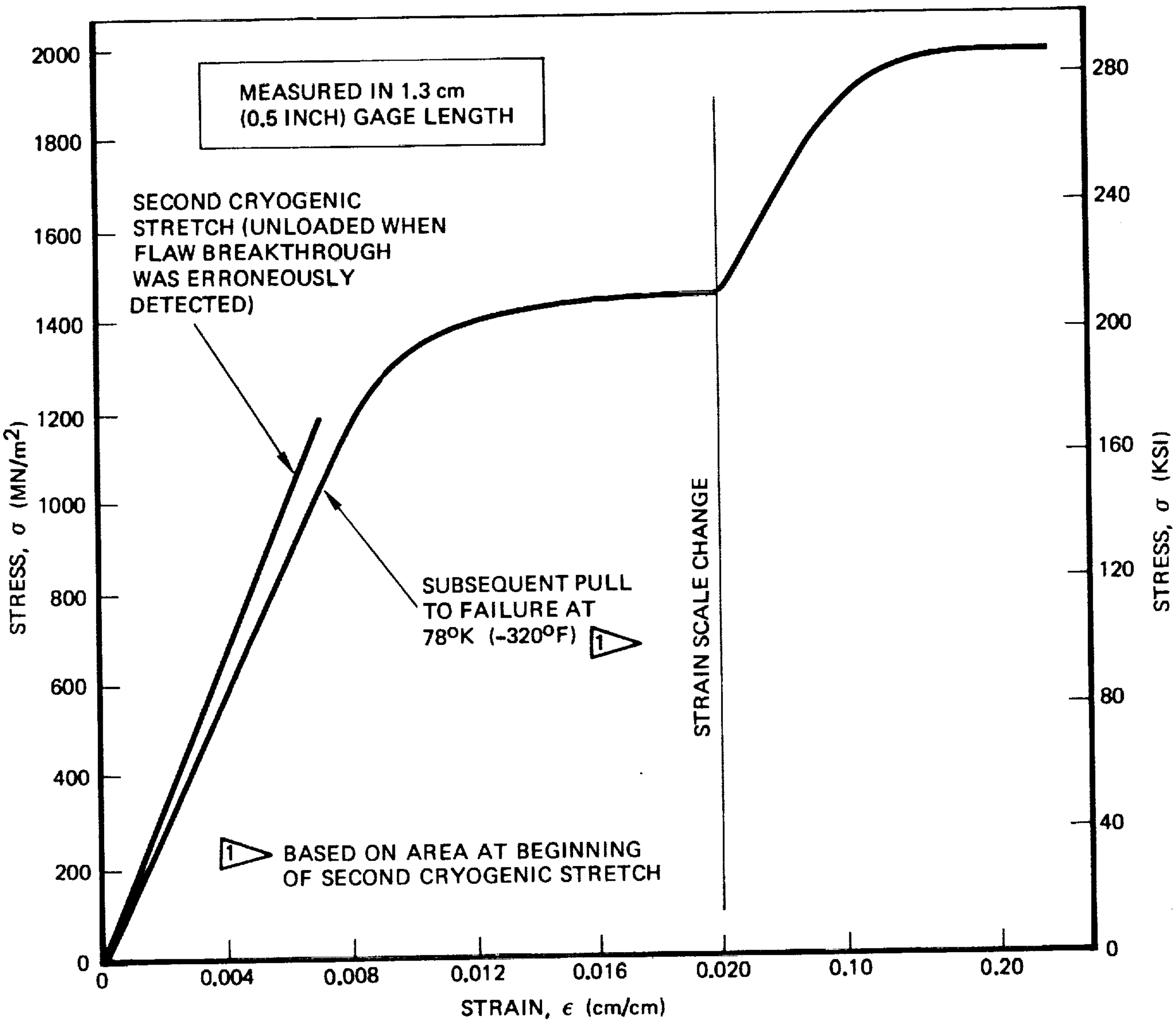

Figure A-20: Stress/Strain Relationship for 0.071 cm (0.028 Inch) Thick Cryostretched 301 Stainless Steel Base Metal at 78° K (-320° F) - Specimen 1C-5

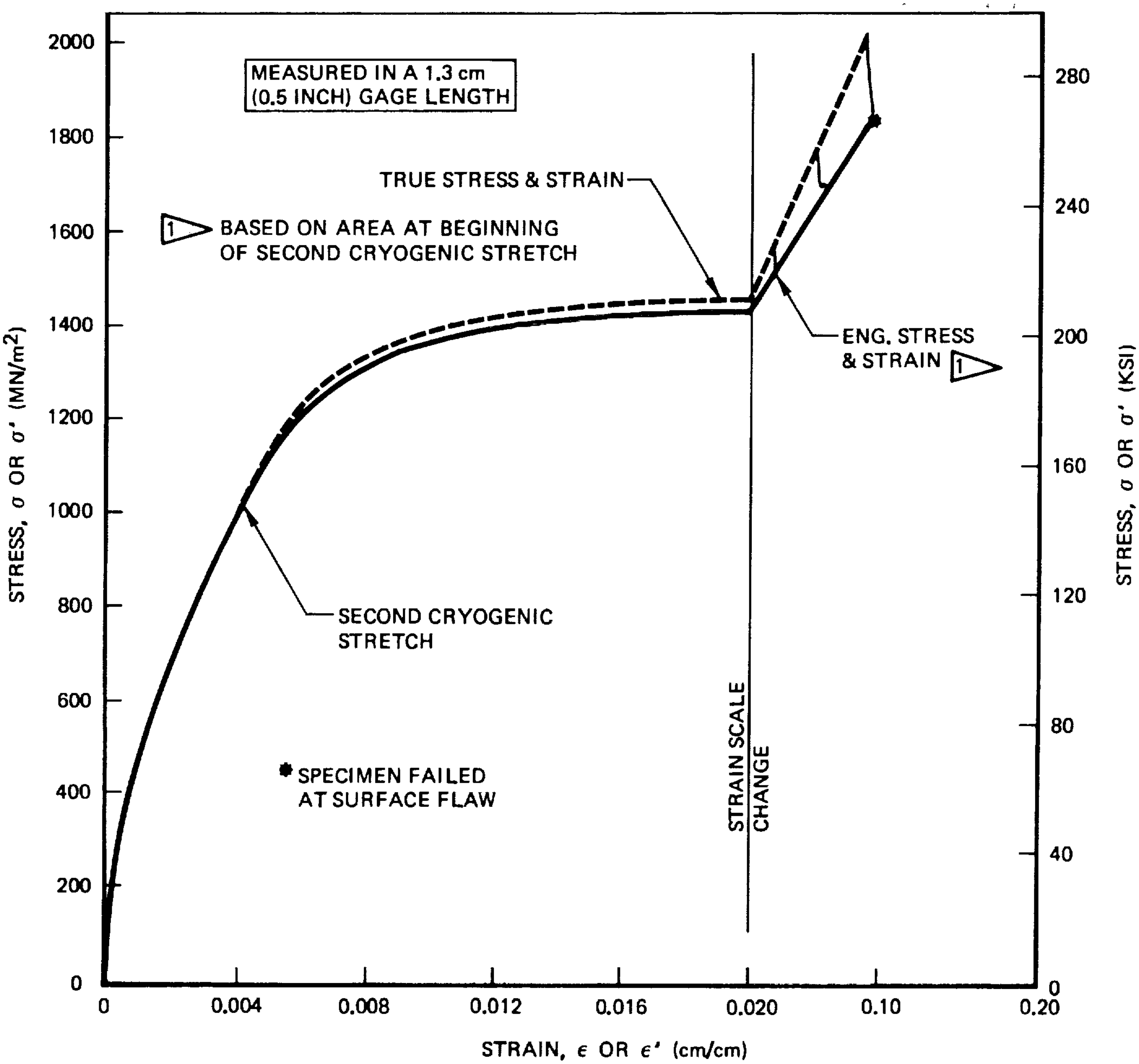

Figure A-21: Stress/Strain Relationship for 0.071 cm (0.028 Inch) Thick Cryostretched 301 Stainless Steel Base Metal at 78°K (-320°F) - Specimen 1C-6

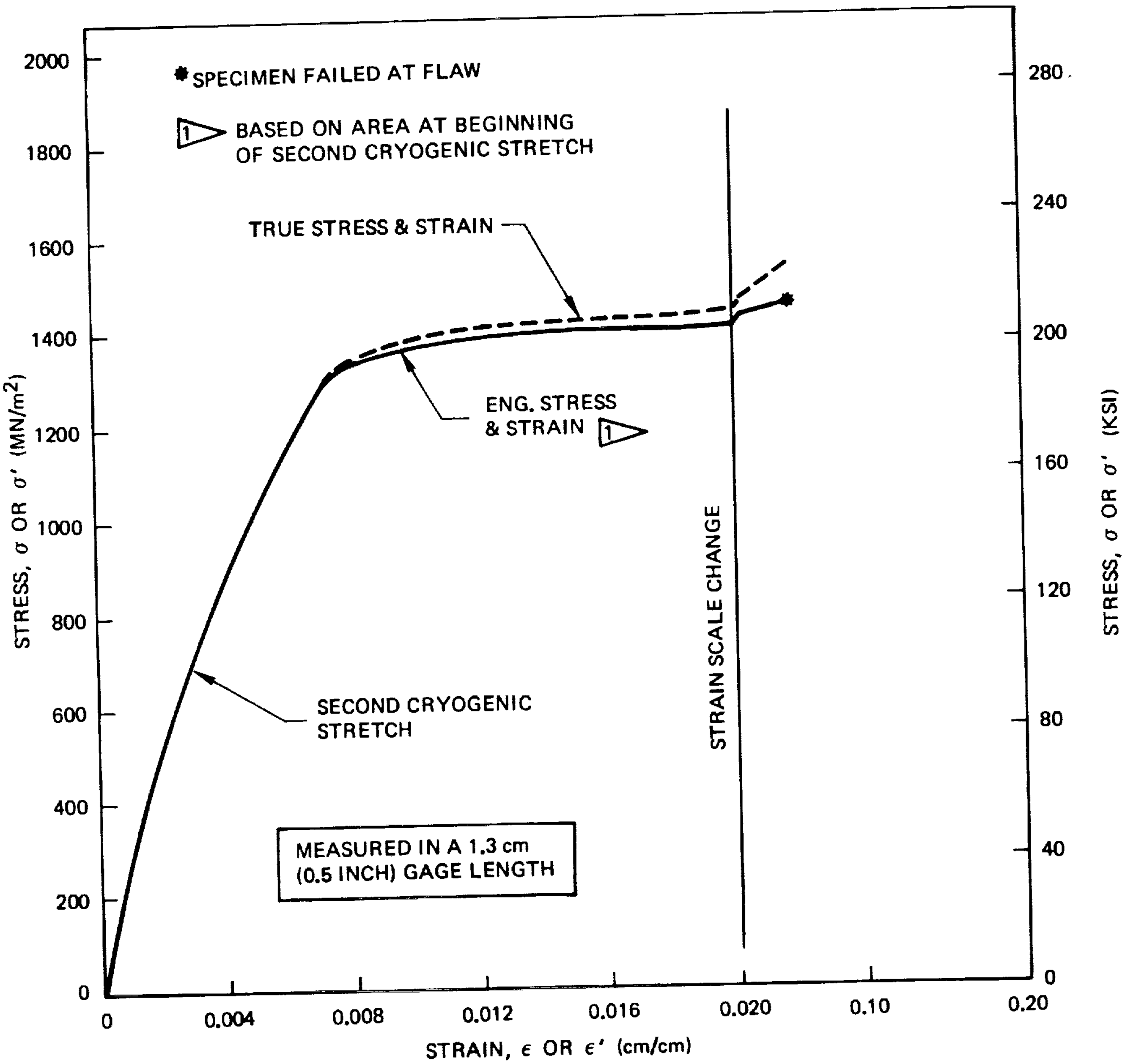

Figure A-22: Stress/Strain Relationship for 0.071 cm (0.028 Inch) Thick Cryostretched 301 Stainless Steel Base Metal at 78° K (-320° F) - Specimen 1C-8

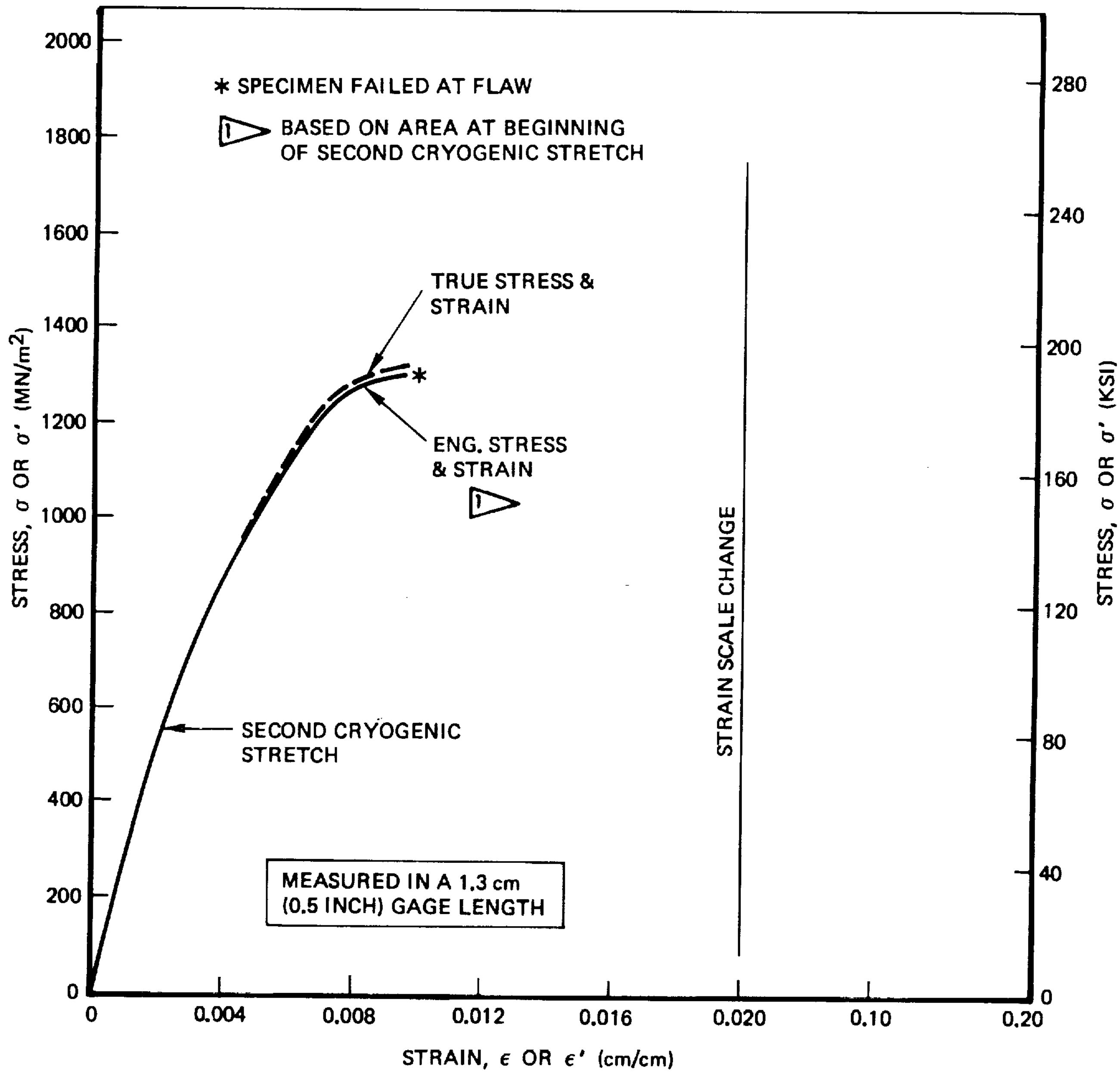

Figure A-23: Stress/Strain Relationship for 0.071 cm (0.028 Inch) Thick Cryostretched 301 Stainless Steel Base Metal at 78°K (-320°F) - Specimen 1C-9

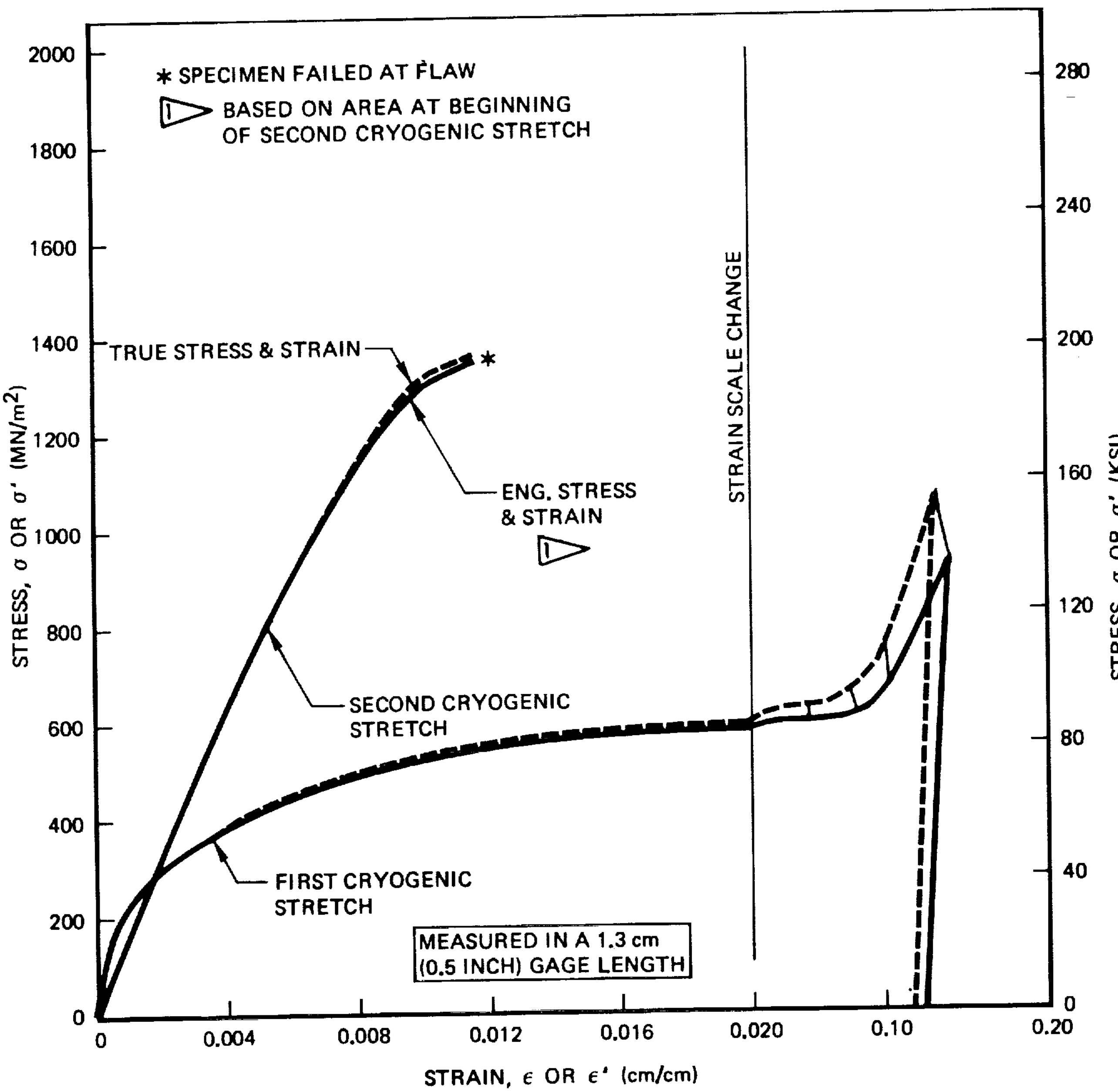

Figure A-24: Stress/Strain Relationship for 0.071 cm (0.028 Inch) Thick Cryostretched 301 Stainless Steel Base Metal at 78°K (-320°F) - Specimen 1C-10

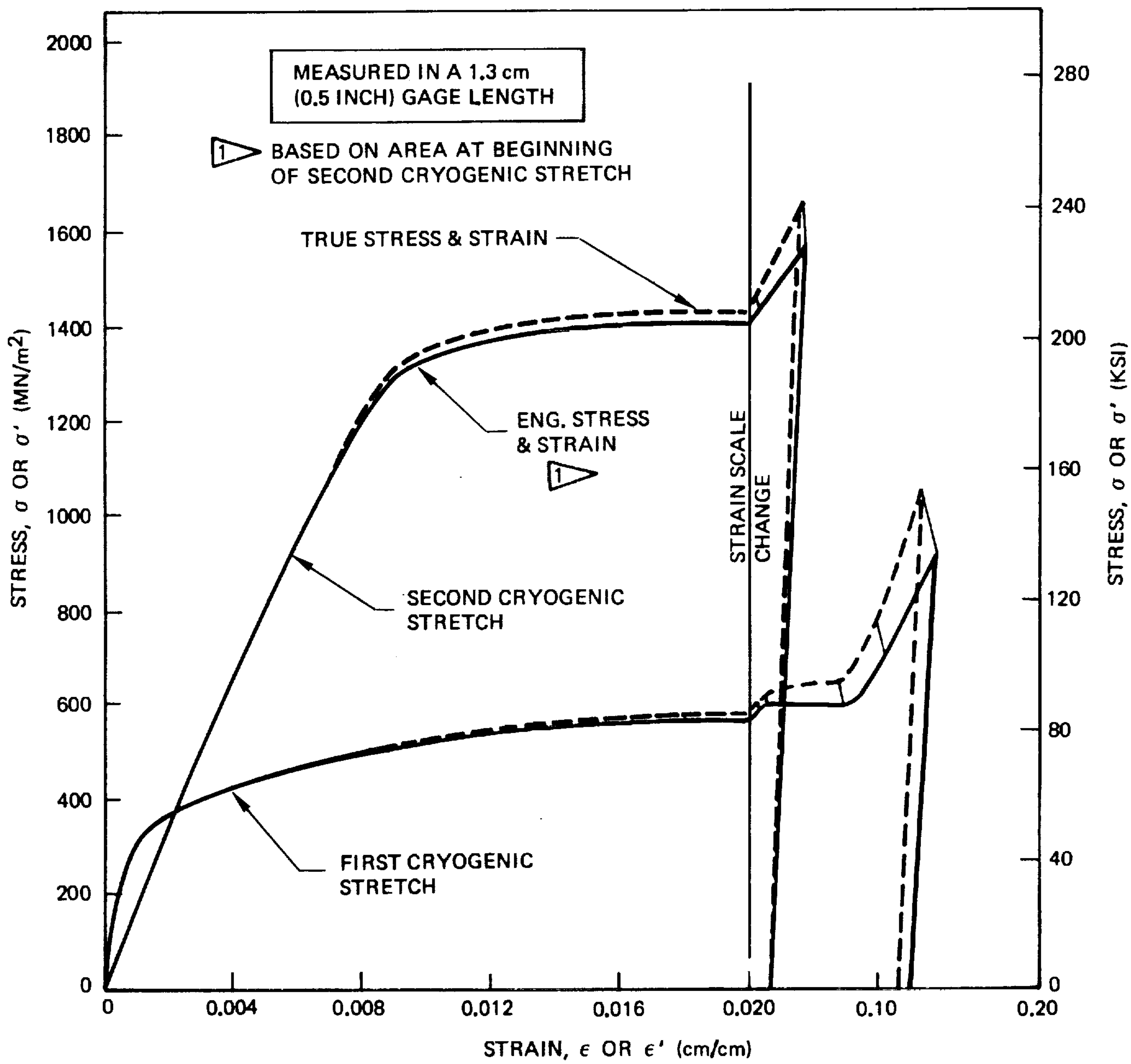

Figure A-25: Stress/Strain Relationship for 0.071 cm (0.028 Inch) Thick Cryostretched 301 Stainless Steel Base Metal at 78°K (-320°F) - Specimen 1C-15

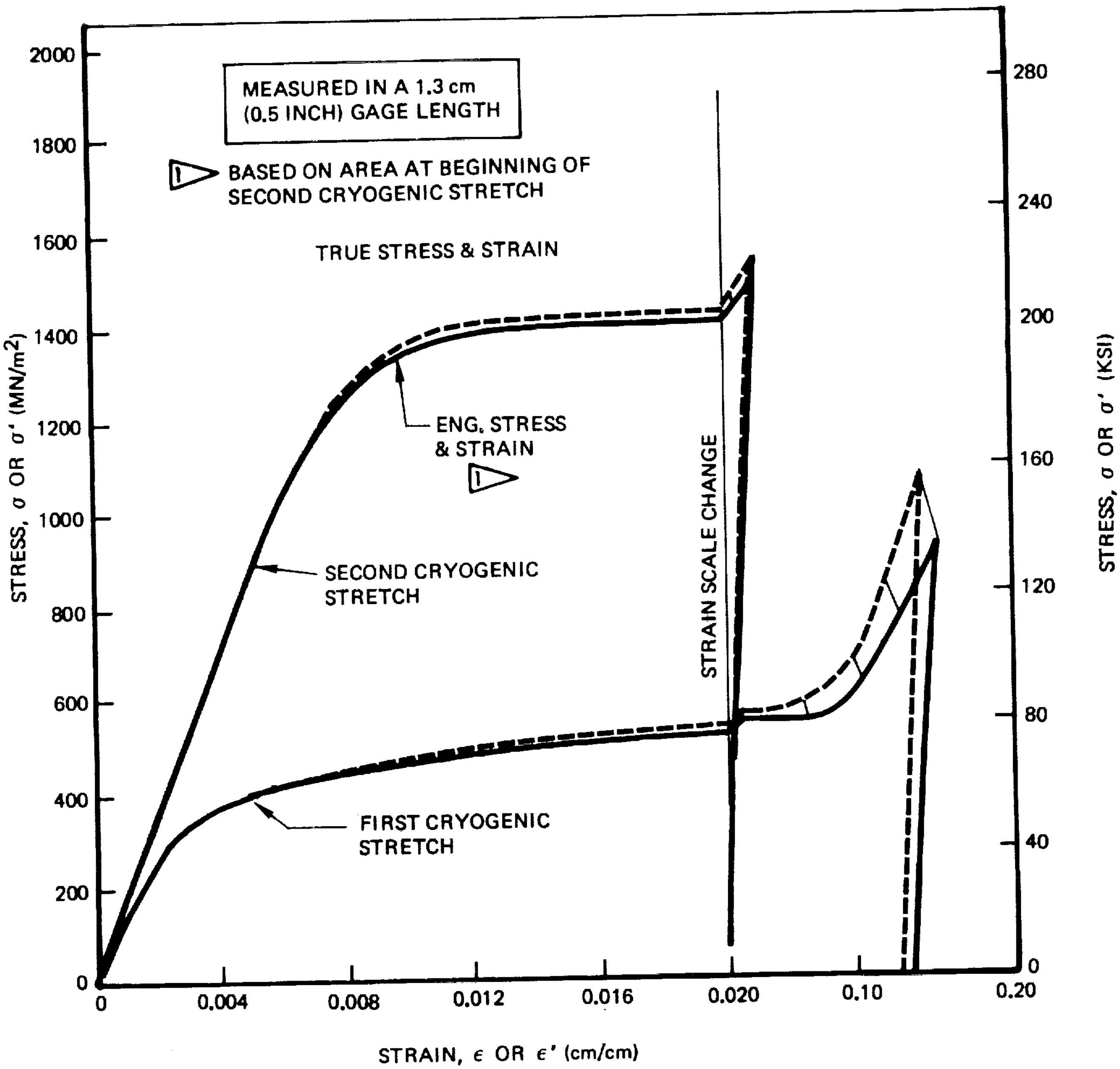

Figure A-26: Stress/Strain Relationship for 0.071 cm(0.028 Inch) Thick Cryostretched 301 Stainless Steel Base Metal at 78°K (-320°F) - Specimen 1C-16

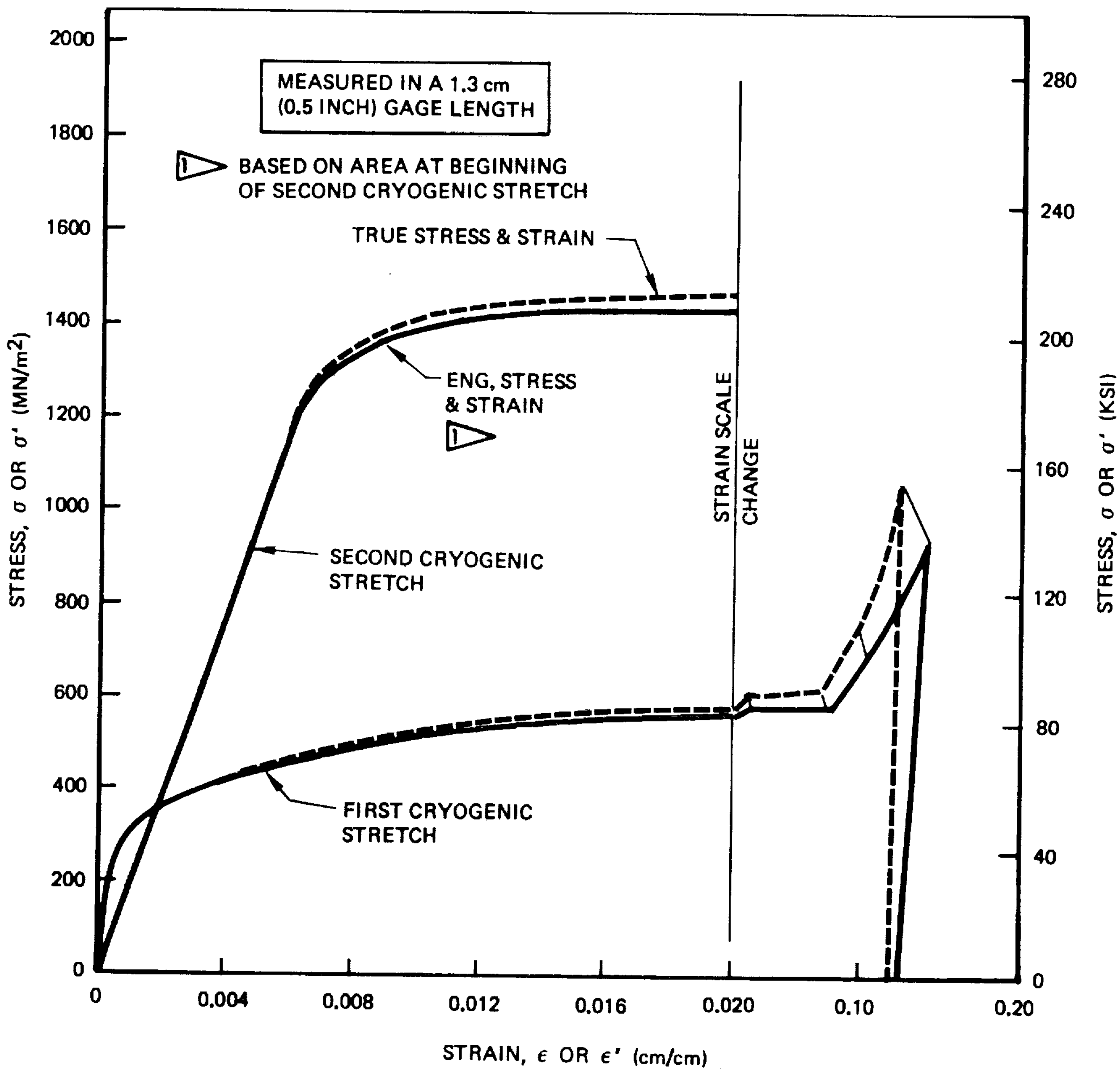

Figure A-27: Stress/Strain Relationship for 0.071 cm (0.028 Inch) Thick Cryostretched 301 Stainless Steel Base Metal at 78° K (-320° F) - Specimen 1C-17

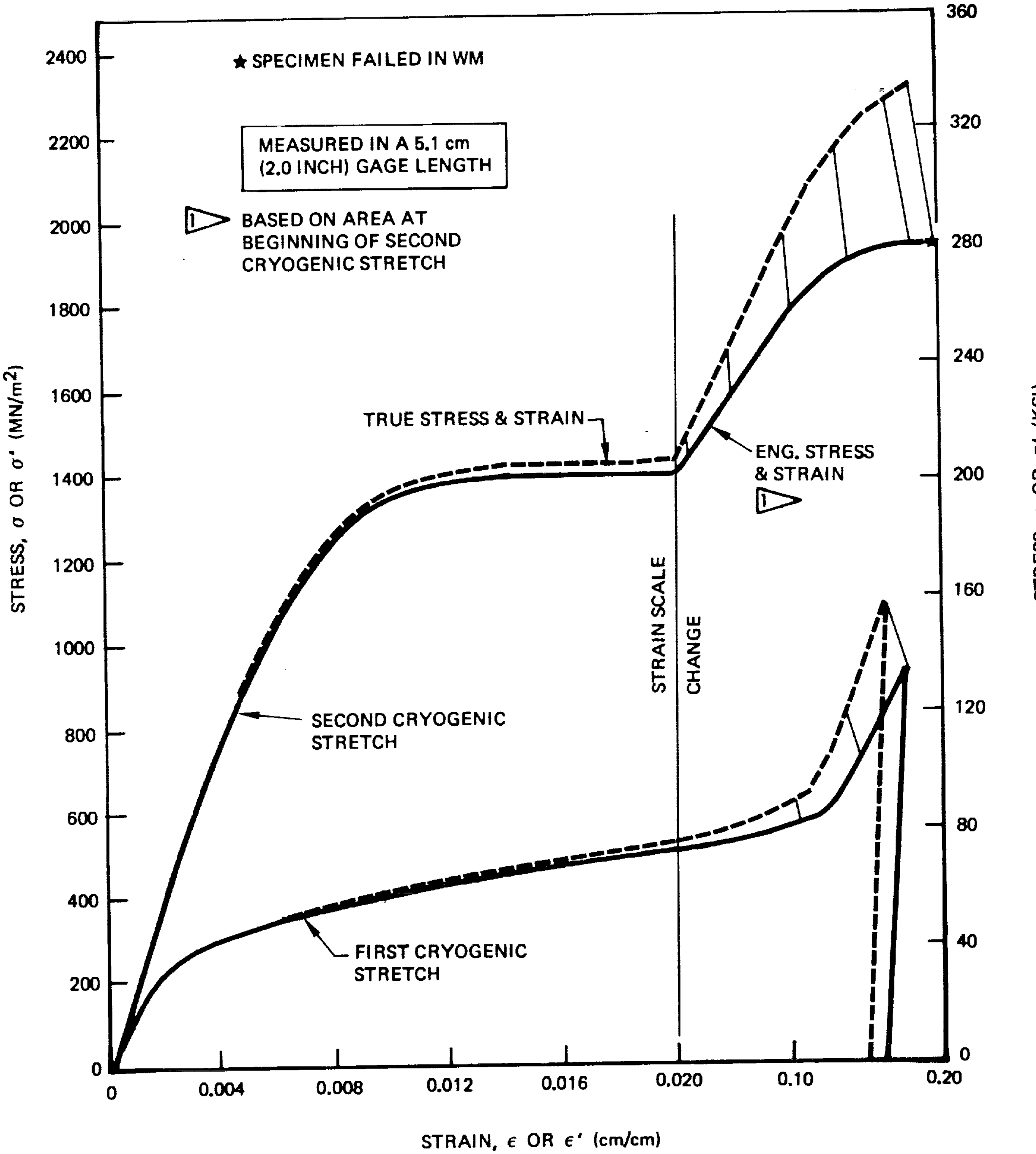

Figure A-28: Stress/Strain Relationship for 0.071 cm (0.028 Inch) Thick Cryostretched 301 Stainless Steel Base Metal at 78° K (-320° F) - Specimen CW-4

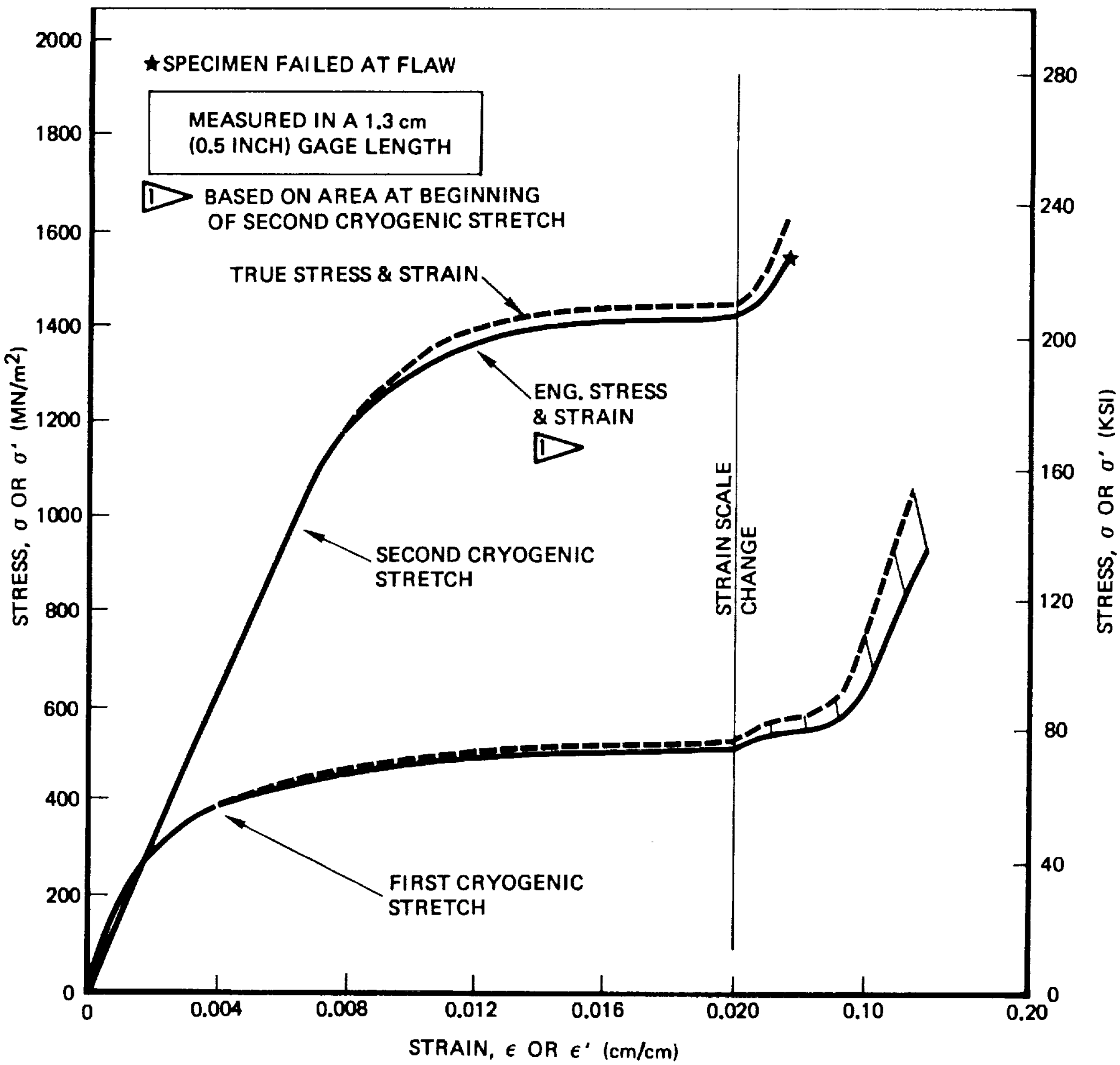

Figure A-29: Stress/Strain Relationship for 0.071 cm (0.028 Inch) Thick Cryostretched 301 Stainless Steel Base Metal at 78°K (-320°F) - Specimen 1CW-4

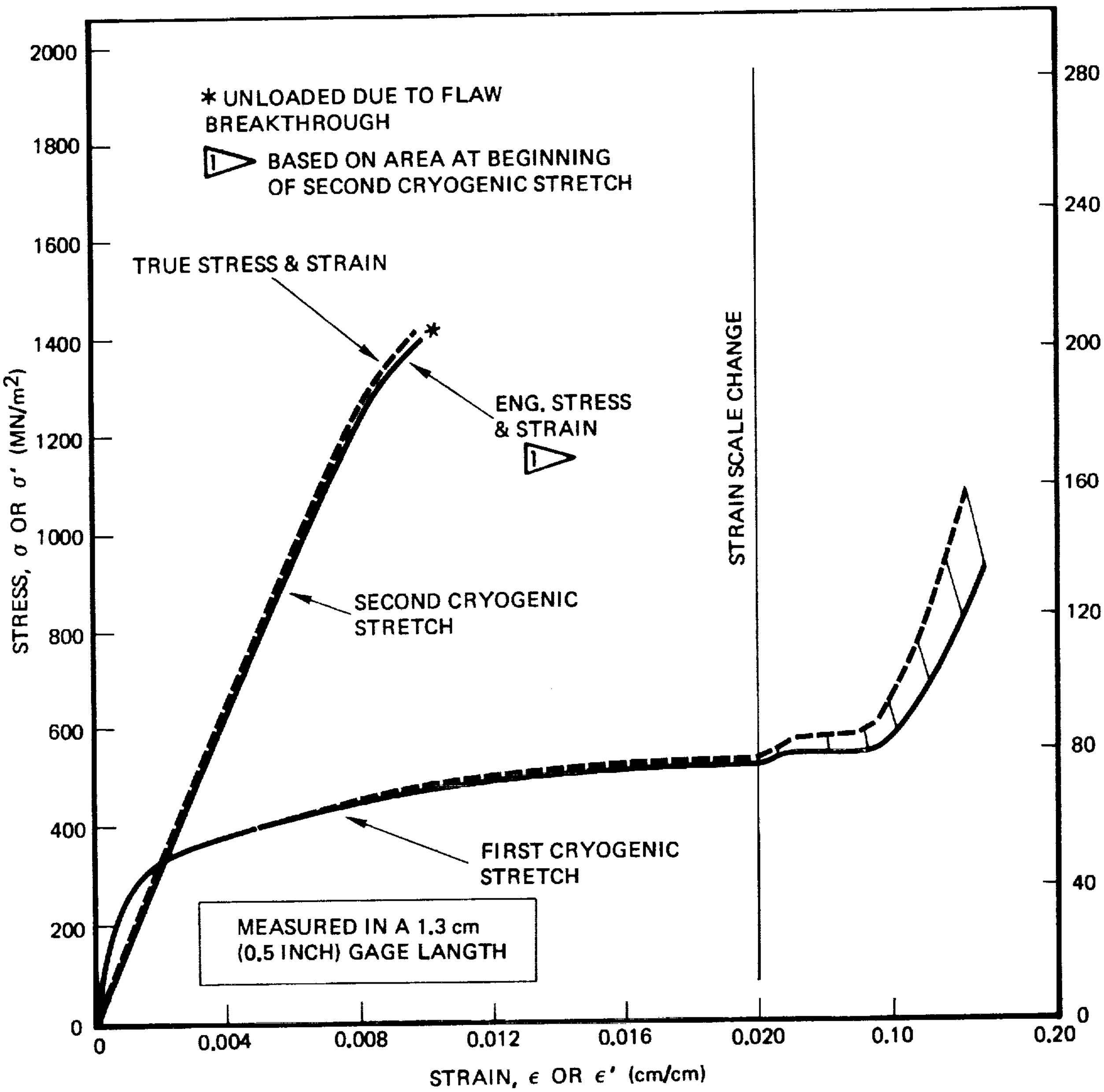

Figure A-30: Stress/Strain Relationship for 0.071 cm(0.028 Inch) Thick Cryostretched 301 Stainless Steel Base Metal at 78°K (-320°F) - Specimen 1CW-6

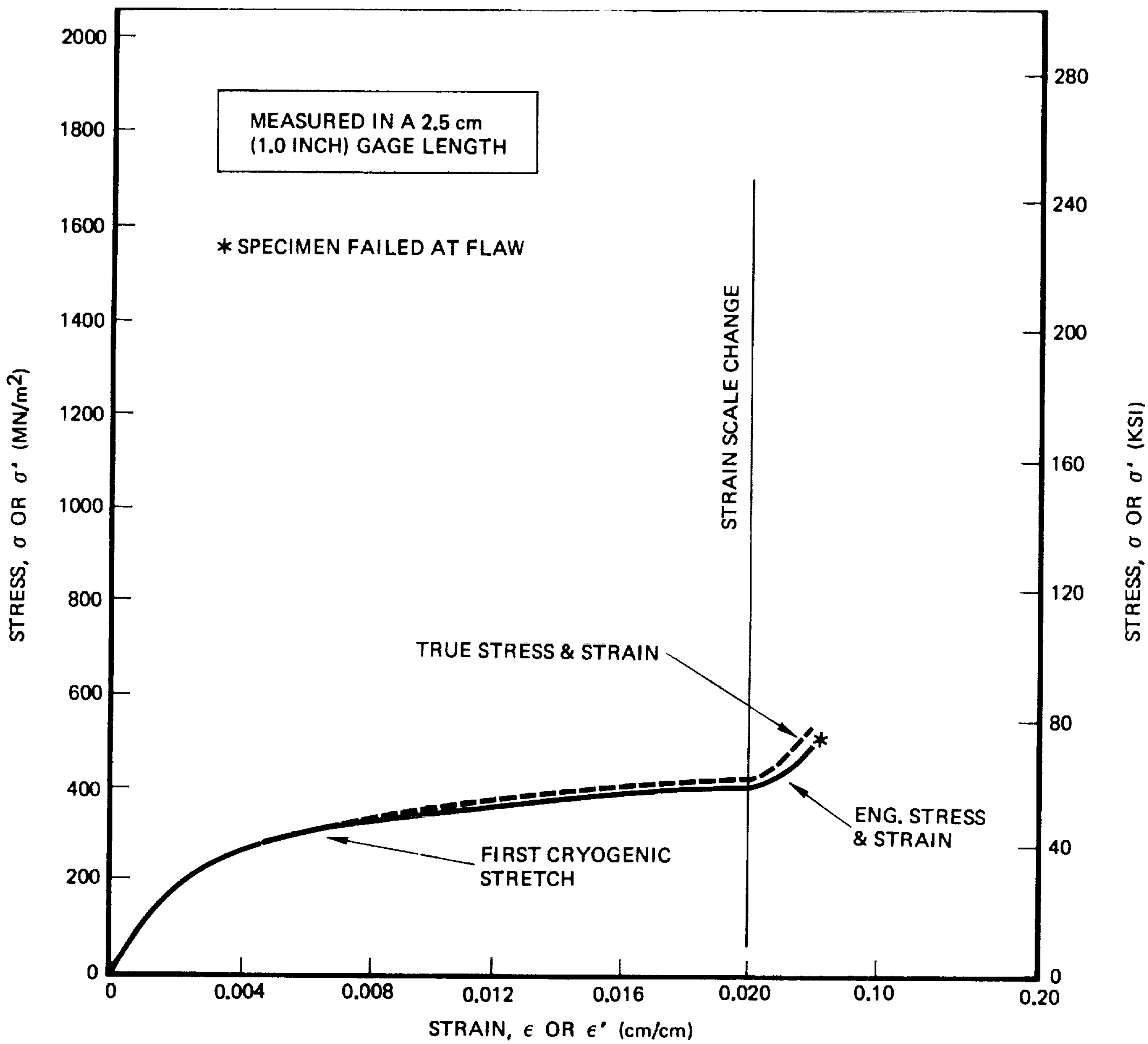

Figure A-31: Stress/Strain Relationship for 0.26 cm (0.10 Inch) Thick Cryostretched 301 Stainless Steel Base Metal at 78^{0}K (-320^{0}F) - Specimen 2C-1

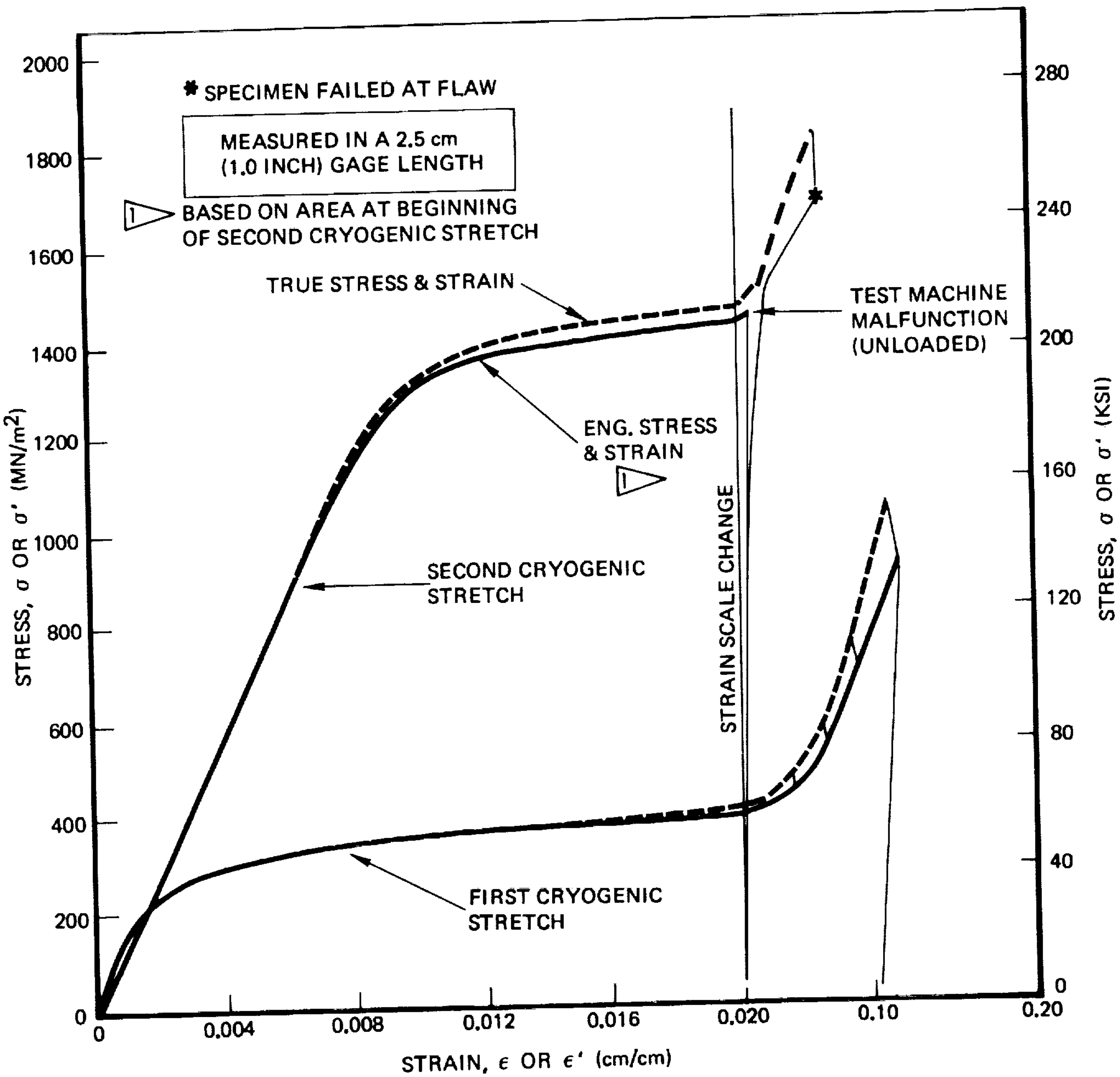

Figure A-32: Stress/Strain Relationship for 0.26 cm (0.10 Inch) Thick Cryostretched 301 Stainless Steel Base Metal at 78° K (-320° F) - Specimen 2C-2

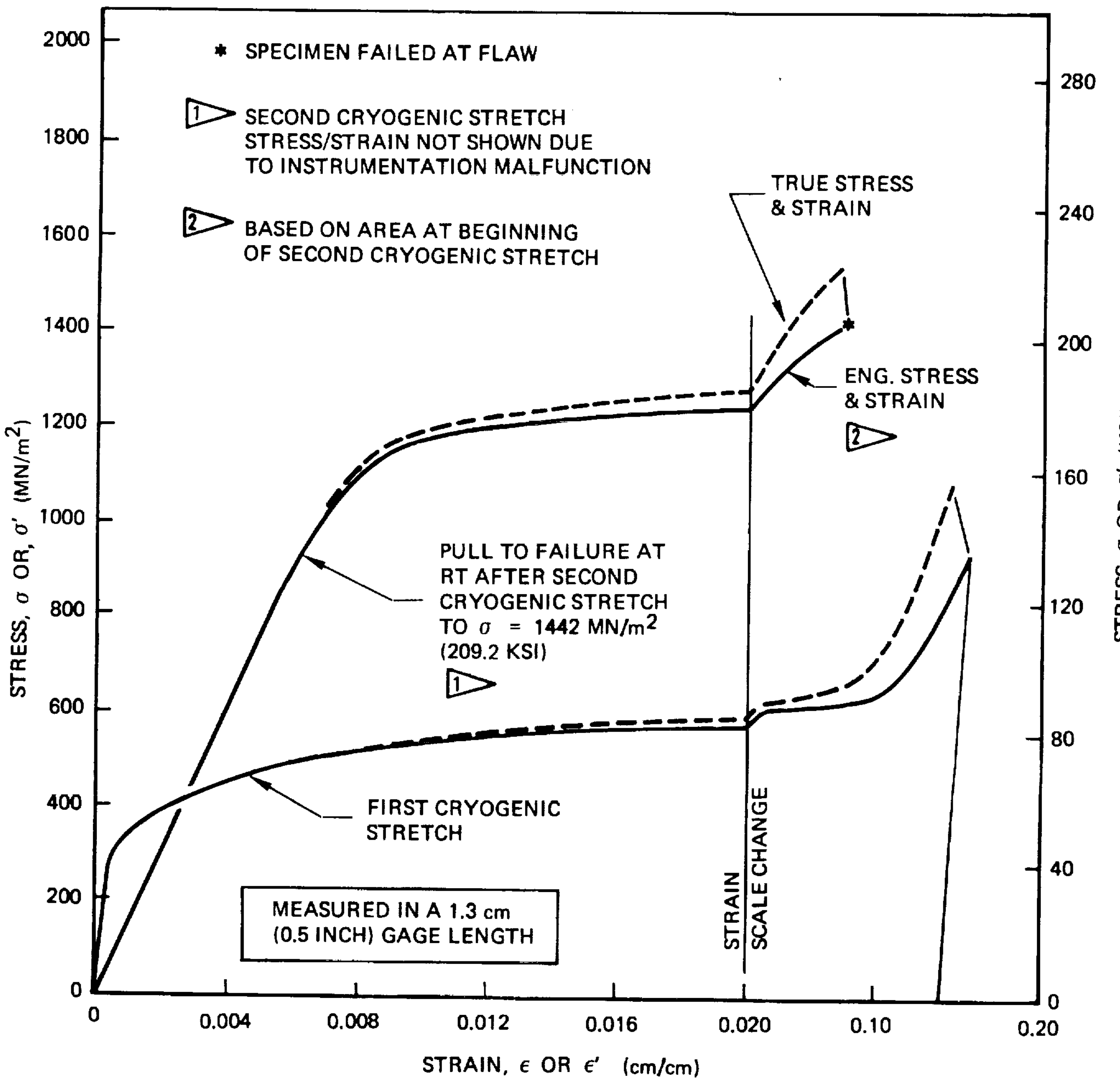

Figure A-33: Stress/Strain Relationship for 0.071 cm (0.028 Inch) Thick Cryostretched 301 Stailess Steel Base Metal at 295⁰K (72⁰F) - Specimen 1C-11

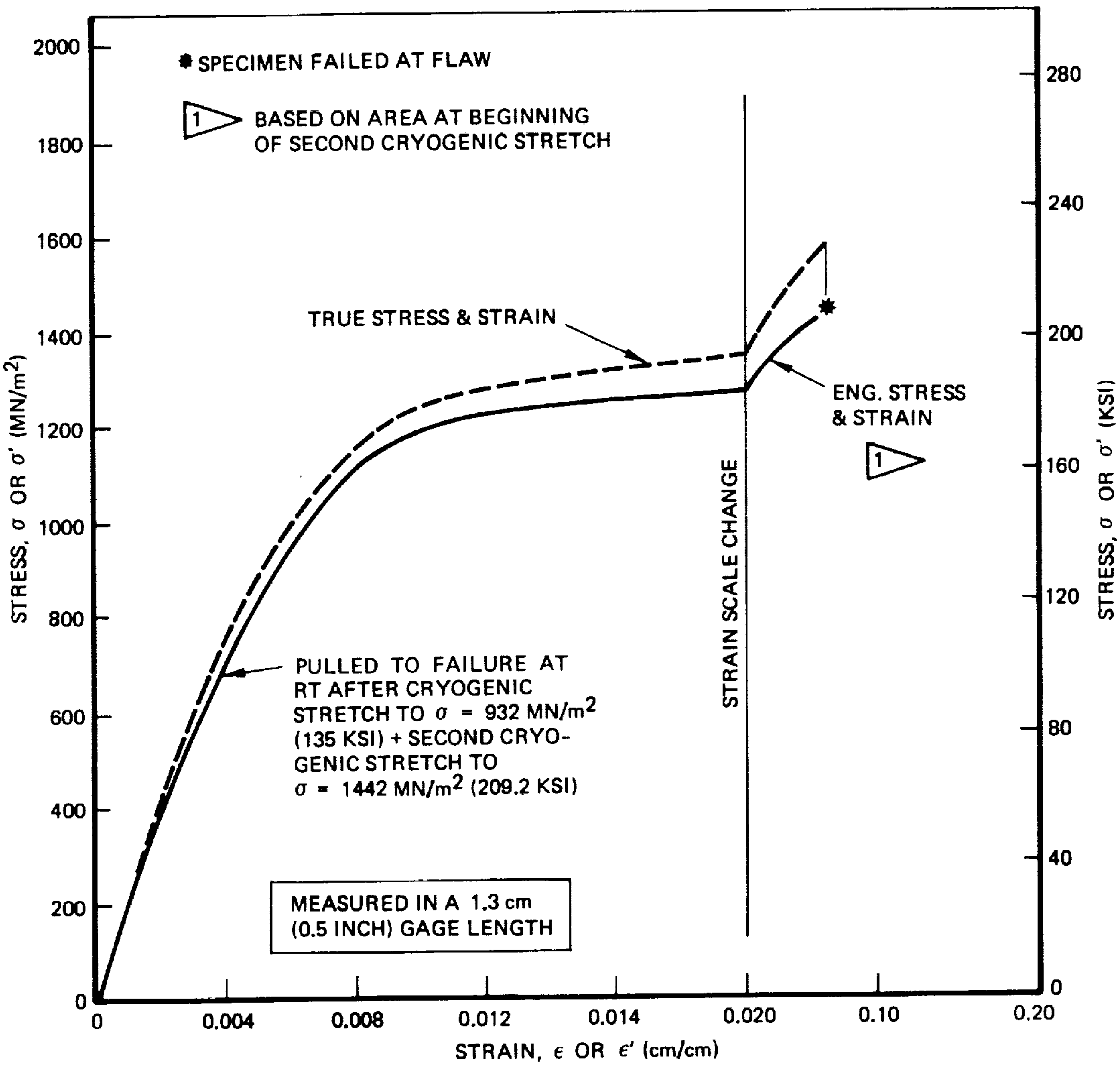

Figure A-34: Stress/Strain Relationship for 0.071 cm (0.028 Inch) Thick Cryostretched 301 Stainless Steel Base Metal at 295°K (72°F) - Specimen 1C-12

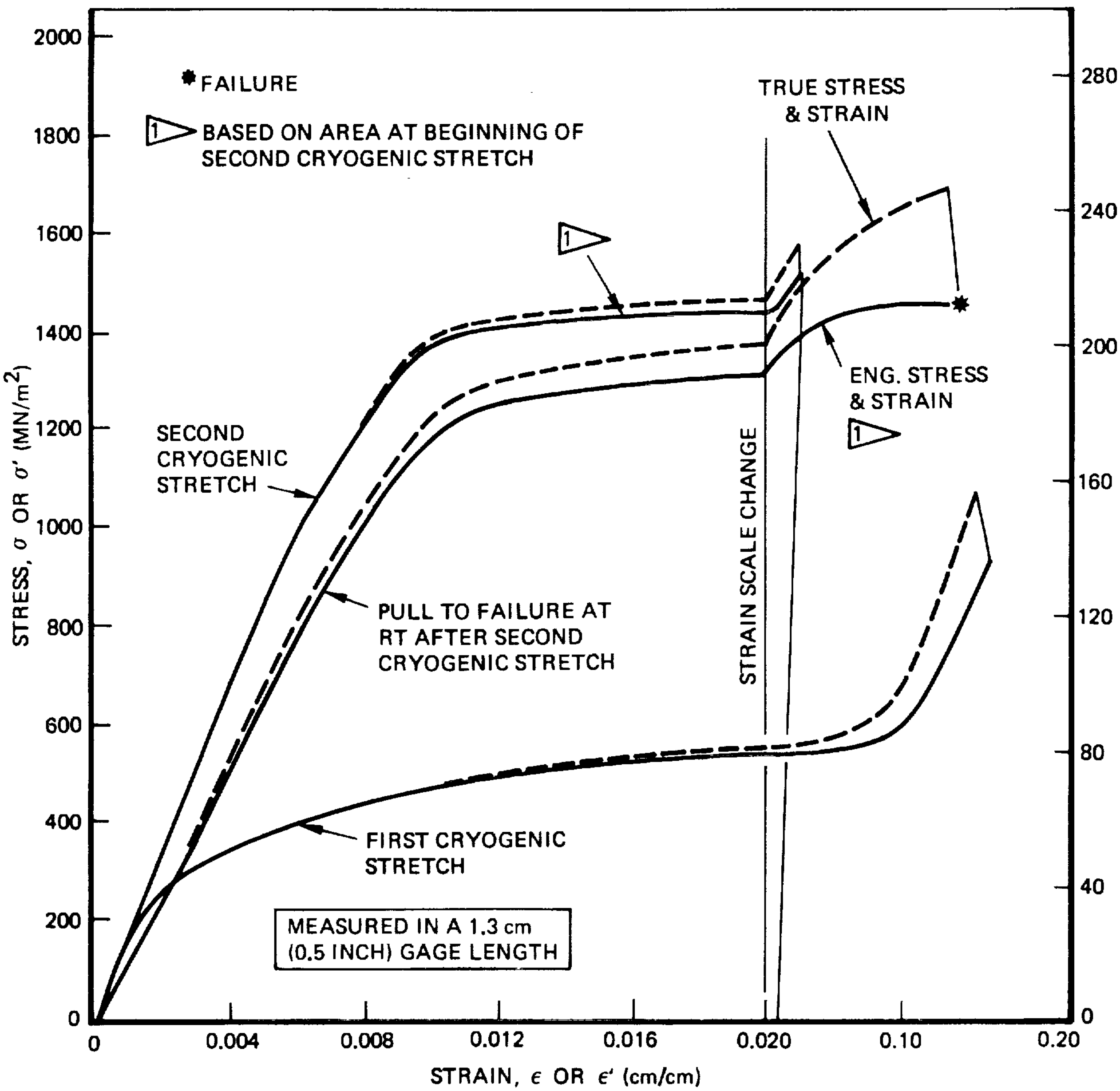

Figure A-35: Stress/Strain Relationships for 0.071 cm(0.028 Inch) Thick Cryostretched 301 Stainless Steel Base Metal at 295°K (72°F) - Specimen 1CW-3

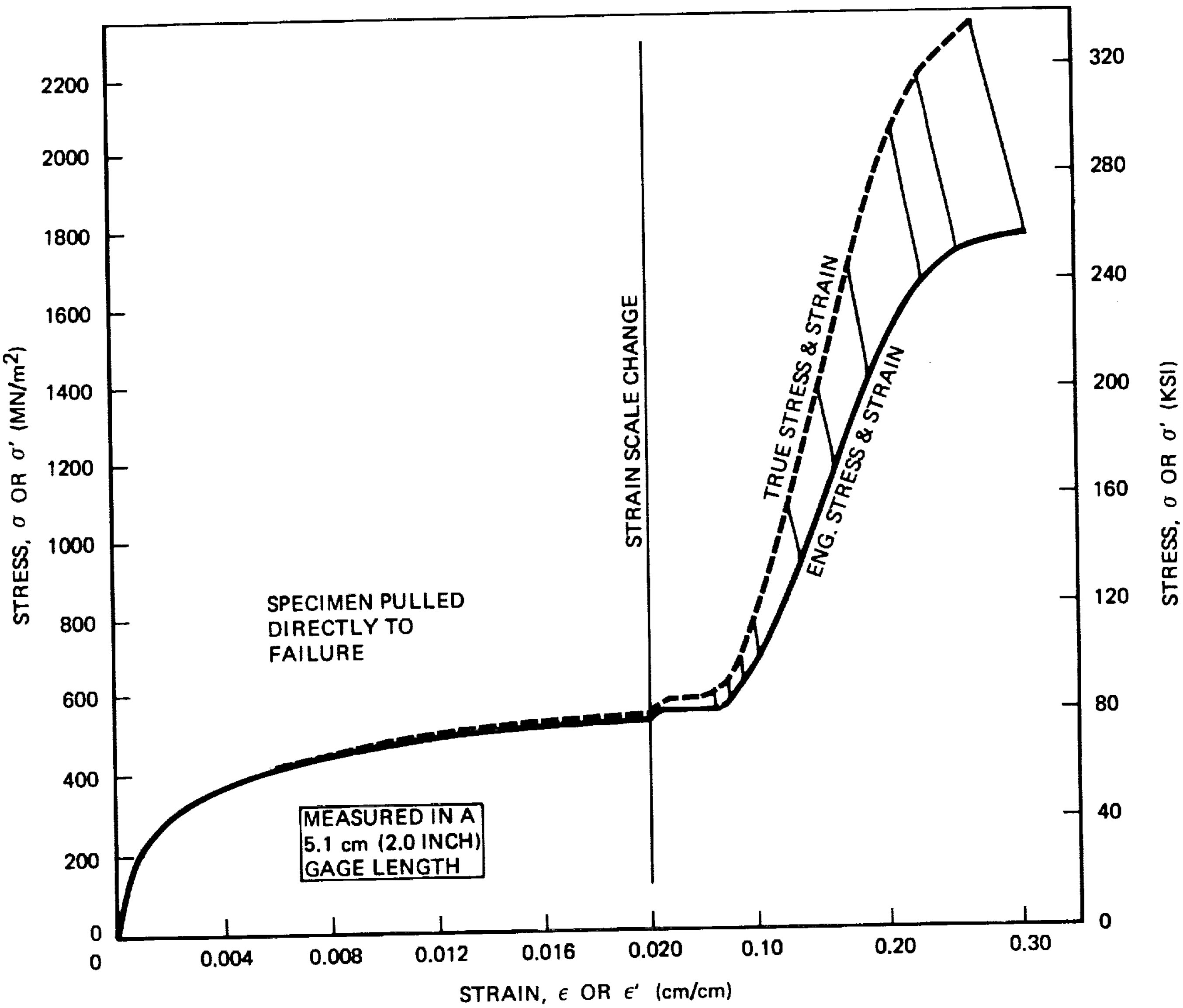

Figure A-36: Stress/Strain Relationship for 0.071 cm (0.028 Inch) Thick Cryostretched 301 Stainless Steel Weld Metal at 78°K (-320°F) - Specimen CW-1

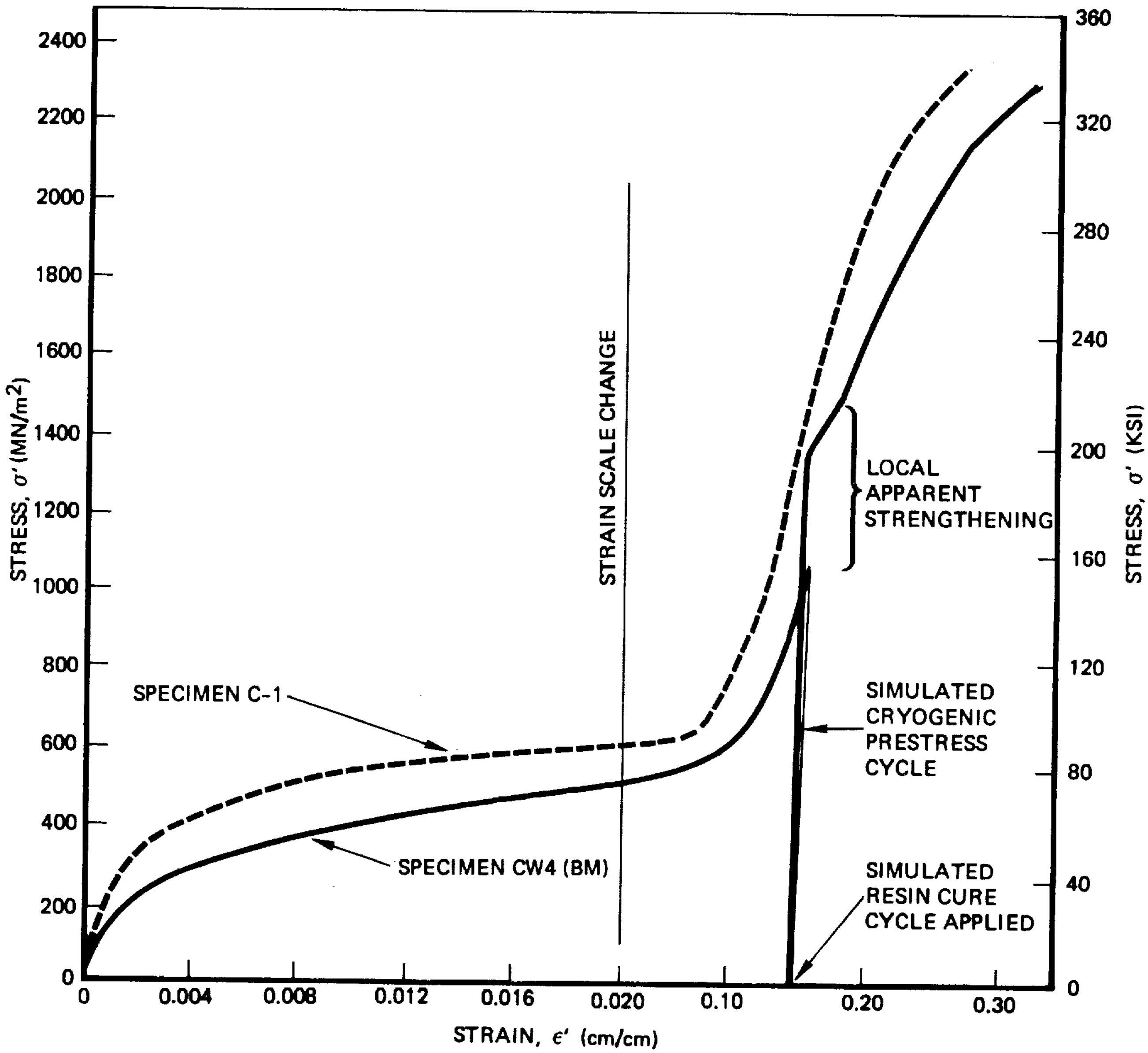

Figure A-37: Comparison of True Stress/Strain Relationships for Specimens C-1 and CW-4 (BM) at 78°K (-320°F)

Table 1: Hoop GFR Design Criteria

DESIGN PARAMETER	CRITERIA
SHAPE	CYLINDRICAL WITH HEMISPHERICAL END CLOSURES
SIZE	16.5 cm (6.5 INCH) DIAMETER BY 71.1 cm (28.0 INCH) OVERALL LENGTH
METAL SHELL	INCONEL X750 STA; 0.10 cm (0.40 INCH) CYLINDRICAL SECTION
	2219-T62 ALUMINUM; 0.23 cm (0.090 INCH) CYLINDRICAL SECTION
	CRYOSTRETCHED 301 STAINLESS STEEL; 0.71 cm (0.028 INCH) CYLINDRICAL SECTION
FIBER REINFORCE-MENT	TWENTY - END S-GLASS CONTINUOUS FILAMENTS
RESIN MATRIX	EPON 828/DSA/EMPOL 1040/BDMA (100/115.9/20/1)
WINDING PATTERN	CIRCUMFERENTIAL (CYLINDER ONLY)
OPERATING TEMPERATURE	295°K (72°F) TO 78°K (-320°F)
HOOP FILAMENT AMBIENT OPER-ATING STRESS	$\leq$1380 MN/m^2 (200 KSI)
METAL SHELL HOOP OPERATING/ SIZING STRESS RATIO	0.85
BURST PRESSURE	$\leq$34.5 MN/m^2 (5000 PSI)
SIZING CONDITION	$\leq$YIELD STRENGTH FOR UNREINFORCED PORTIONS OF LINER

Table 2: Base Metal Material Properties Used in Reference 2 Computer Program to Design Hoop GFR Tanks

PROPERTY		INCONEL X750 STA	2219-T62 ALUMINUM	CRYO-FORMED 301 STAINLESS STEEL	GLASS FILAMENT WOUND COMPOSITE
DENSITY g/m³ (LB/IN.³)		8.30 (0.300)	2.82 (0.102)	7.47 (0.270)	1.99 (0.072) [1]
COEFFICIENT OF THERMAL EXPANSION; 295°K (72°F) TO 20°K (-423°F) cm/cm – °K (IN/IN°F)		8.98 (4.99 x 10⁻⁶)	16.05 (8.915 x 10⁻⁶)	8.26 (4.59 x 10⁻⁶)	3.62 (2.01 x 10⁻⁶)
TENSILE YIELD STRENGTH MN/m² (KSI)		821 (119.0)	315 (45.7)	1186 (172.0)	—
DERIVATIVE OF YIELD STRENGTH WITH RESPECT TO TEMPERATURE kN/m²°K (PSI/°F)		-496 (-40.0)	-220 (-17.7)	-943 (-76.0)	—
ELASTIC MODULUS GN/m² (PSI)		202.0 (29.3 x 10⁶)	73.1 (10.6 x 10⁶)	131.0 (19.0 x 10⁶)	85.5 (12.4 x 10⁶)
DERIVATIVE OF ELASTIC MODULUS WITH RESPECT TO TEMPERATURE MN/m²°K (PSI/°F)		-100.4 (-8100)	-18.9 (-1520)	-207.0 (-16,700)	-29.9 (-2410)
PLASTIC MODULUS GN/m² (PSI)		4.36 (633 x 10³)	2.86 (415 x 10³)	4.14 (600 x 10³)	—
DERIVATIVE OF PLASTIC MODULUS WITH RESPECT TO TEMPERATURE kN/m²°K (PSI/°F)		-2050 (-165)	-3525 (-284)	-782 (-63)	—
POISSON'S RATIO		0.290	0.325	0.290	—
DERIVATIVE OF POISSON'S RATIO WITH RESPECT TO TEMPERATURE 1/°K (1/°F)		0	-0.36 x 10⁻⁴ (-0.2 x 10⁻⁴)	0	—
MAX ALLOWABLE OPERATING STRESS (COMPRESSIVE IN METAL; TENSILE IN FILAMENTS) MN/m² (KSI)	295°K (72°F)	690 (100.0)	245 (35.6)	772 (112.0)	1379 (200.0)
	78°K (-320°F)	800 (116.0)	283 (41.0)	903 (131.0)	1724 (250.0)
ULTIMATE STRENGTH MN/m² (KSI)	295°K (72°F)	1016 (147.4)	379 (54.9)	1407 (204.0)	2606 (378.0)
	78°K (-320°F)	1240 (179.9)	454 (65.8)	1931 (280.0)	3275 (475.0)

[1] BASED ON A VOLUME FRACTION = 0.673

Table 3: Hoop GFR Inconel X750 STA Design Membrane Stresses

CONDITION	PRESSURE MN/m^2 (PSI)	FILAMENT STRESS MN/m^2 (KSI)	METAL CYLINDER MEMBRANE STRESS MN/m^2 (KSI)	
			HOOP	LONGITUDINAL
AS FABRICATED	0	476 (69.1)	-249 (-36.1)	0
SIZING	19.6 (2840)	1413 (204.9)	850 (123.3)	794 (115.1)
AFTER SIZING	0	942 (136.6)	-491 (-71.2)	0
AMBIENT OPERATING AT 85% σ_s	17.7 (2570)	1366 (198.1)	724 (105.0)	718 (104.2)
AMBIENT BURST	25.1 (3640)	2023 (293.4)	979 (142.0)	1016 (147.4)
CRYOGENIC PROOF	20.9 (3030)	1413 (205.0)	959 (139.1)	844 (122.4)
CRYOGENIC OPERATING AT 85% σ_p	18.8 (2730)	1359 (197.1)	815 (118.2)	762 (110.5)
CRYOGENIC BURST	30.6 (4440)	2526 (366.4)	1164 (168.8)	1240 (179.9)

Table 4: Hoop GFR 2219-T62 Aluminum Design Membrane Stresses

CONDITION	PRESSURE MN/m^2 (PSI)	FILAMENT STRESS MN/m^2 (KSI)	METAL CYLINDER MEMBRANE STRESS MN/m^2 (KSI)	
			HOOP	LONGITUDINAL
AS FABRICATED	0	463 (67.2)	-97 (-14.0)	0
SIZING	16.8 (2430)	1347 (195.4)	332 (48.2)	306 (444)
AFTER SIZING	0	865 (125.4)	-180 (-26.1)	0
AMBIENT OPERATING AT 85% σ_s	15.1 (2195)	1303 (189.0)	283 (41.0)	276 (40.1)
AMBIENT BURST	20.7 (3000)	1820 (263.9)	379 (54.9)	379 (54.9)
CRYOGENIC PROOF	17.4 (2520)	1200 (174.0)	381 (55.2)	318 (46.1)
CRYOGENIC OPERATING AT 85% σ_p	15.6 (2256)	1168 (169.4)	323 (46.9)	284 (41.2)
CRYOGENIC BURST	24.1 (3500)	2064 (299.3)	454 (65.8)	441 (64.0)

Table 5: Hoop GFR Cryoformed 301 Stainless Steel Design Membrane Stresses

CONDITION		PRESSURE MN/m^2 (PSI)	FILAMENT STRESS MN/m^2 (KSI)	METAL CYLINDER MEMBRANE STRESS MN/m^2 (KSI)	
				HOOP	LONGITUDINAL
78°K (−320°F)	AS FABRICATED	0	11.7 (1.7)	−9.7 (−1.4)	0
	SIZING	23.9 (3463)	1609 (233.3)	1442 (209.2)	1371 (198.9)
	AFTER SIZING	0	748 (108.5)	−604 (−87.6)	0
	CYRO–OPERATING AT 85% σ_s	21.4 (3097)	1518 (220.2)	1227 (177.9)	1227 (177.9)
	CRYO–BURST	33.6 (4876)	2604 (377.6)	1758 (255.0)	1931 (280.0)
AMBIENT PROOF		21.8 (3161)	1627 (236.0)	1234 (179.0)	1251 (181.5)
AMBIENT OPERATING AT 85% σ_p		19.6 (2840)	1538 (223.0)	1049 (152.2)	1125 (163.1)
AMBIENT BURST		24.5 (3552)	1806 (261.9)	1353 (196.3)	1407 (204.0)

Table 6: Uniaxial Tests Conducted

MATERIAL			MECHANICAL PROPERTY		STATIC FRACTURE						CYCLIC LIFE	
					295°K (72°F)			78°K (-320°F)				
					a/2c ≈			a/2c ≈				
			295°K (72°F)	78°K (-320°F)	0.1	0.2	0.4	0.1	0.2	0.4	295°K (72°F)	78°K (-320°F)
INCONEL X750 STA	BASE METAL	t_1	3	3	2	7	1	1	3	1	6	5
		t_2	1			3			2		6	5
	WELD METAL	t_1	2	2	1	7	1		5		7	3
		t_2				4			2		5	5
2219-T62 ALUMINUM	BASE METAL	t_1	2	3	1	8	1	1	2	1	8	7
		t_2				3			2		7	7
	WELD METAL	t_1	2	2	1	8	1		2		7	5
		t_2				2			2		5	5
CRYOSTRETCHED 301 STAINLESS STEEL [1]	BASE METAL	t_1	3	12		2			15		6	7
		t_2	2	1		1			7		5	5
	WELD METAL	t_1	2	3		3			7		1	5
		t_2				1			4		4	4

[1] SOME SPECIMENS WERE USED TO OBTAIN MECHANICAL PROPERTY DATA WHEN TESTED AS STATIC FRACTURE OR CYCLIC LIFE SPECIMENS

TOTAL OF 288 TESTS

Table 7: Biaxial Tests Conducted

TANK			BURST TEST				CYCLIC LIFE TEST			
			295°K (72°F)		78°K (-320°F)		295°K (72°F)		78°K (-320°F)	
			FLAW ORIENTATION 1				FLAW ORIENTATION 1			
			0°	45°	0	45°	0	45°	0	45°
INCONEL X750 STA	NON-OW	BASE METAL	2				2			
		WELD METAL	2							
	OW	BASE METAL	2	2	2	2	3	2	2	
		WELD METAL	2	2	1	2				
2219-T62 ALUMINUM	NON-OW	BASE METAL	2				2			
		WELD METAL	2							
	OW	BASE METAL	4	2	1	1	4	2	2	
		WELD METAL	2	2	2	1				

1 PLANE OF SURFACE FLAW WITH RESPECT TO LONGITUDINAL TANK AXIS

TOTAL OF 57 TANKS TESTED

Table 8: Inconel X750 STA Mechanical Properties

TEMPERATURE, T ^oK (^oF)	MATERIAL	SPECIMEN NUMBER	THICKNESS, t cm (INCH)	WIDTH, W cm (INCH)	0.2% OFFSET σ_{ys} IN 5.1 cm (2.0 INCH) MN/m^2 (KSI)	0.2% OFFSET σ_{ys} IN WELD NUGGET MN/m^2 (KSI)	σ_{ult} MN/m^2 (KSI	% ELONGATION IN 5.1 cm (2.0 INCH)	ELASTIC MODULUS, E x 10^{-6} kN/m^2 (PSI)
295 (72)	BASE METAL	B-1	0.099 (0.039)	1.278 (0.503)	752 (109.1)		1225 (177.6)	25.8	201 (29.2)
		B-3	0.102 (0.040)	1.278 (0.503)	773 (112.1)		1232 (178.7)	24.4	202 (29.3)
		B-15 [1]	0.102 (0.040)	3.183 (1.253)	858 (124.5)		1296 (188.0)	25.0	226 (32.8)
		2B-15	0.333 (0.131)	3.172 (1.249)	805 (116.8)		1202 (174.4)	31.0	193 (28.0)
	WELD METAL	BW-2	0.102 (0.040)	1.278 (0.503)	768 (111.4)	803 (116.4)	1180 (171.1)	14.0	217 (31.5)
		BW-4	0.102 (0.040)	1.278 (0.503)	769 (111.5)	783 (113.5)	1164 (168.9)	14.0	205 (29.7)
78 (-320)	BASE METAL	B-2	0.102 (0.040)	1.280 (0.504)	849 (123.1)		1524 (221.1)	32.6	223 (32.3)
		B-4	0.099 (0.039)	1.278 (0.503)	843 (122.3)		1516 (219.9)	33.2	225 (32.6)
	WELD METAL	BW-3	0.102 (0.040)	1.275 (0.502)	847 (122.8)	902 (130.8)	1454 (210.9)	20.0	214 (31.1)
		BW-5	0.102 (0.040)	1.275 (0.502)	855 (124.0)	887 (128.7)	1421 (206.1)	18.8	213 (30.9)

[1] HEAT TREATED SEPARATELY

Table 9: Uniaxial Static Fracture Tests of 0.10 cm (0.040 inch) Thick Surface Flawed Inconel X750 STA Base Metal at 295°K (72°F)

SPECIMEN NUMBER	ORIGINAL THICKNESS, t cm (INCH)	ORIGINAL WIDTH, W cm (INCH)	TEST PARAMETERS AT	CRACK DEPTH, a cm (INCH)	CRACK LENGTH, 2c cm (INCH)	CRACK SHAPE a/2c	STRESS, σ MN/m^2 (KSI)	TEST TEMPERATURE, T °K (°F)	TEST ENVIRONMENT	REMARKS
1B-1	0.102 (0.040)	3.18 (1.25)	FAILURE	0.051 (0.020)	0.302 (0.119)	0.17	983 (142.5)	295 (72)	AIR	FAIL MODE
1B-2	0.102 (0.040)	3.18 (1.25)	LEAKAGE	0.071 (0.028)	0.386 (0.152)	0.18	892 (129.4)	295 (72)	AIR	LEAK MODE
1B-3	0.102 (0.040)	3.18 (1.25)	LEAKAGE	0.086 (0.034)	0.452 (0.178)	0.19	805 (116.8)	295 (72)	AIR	LEAK MODE
1B-10	0.102 (0.040)	3.18 (1.25)	LEAKAGE	0.076 (0.030)	0.381 (0.150)	0.20	839 (121.7)	295 (72)	AIR	LEAK MODE
1B-11	0.102 (0.040)	3.18 (1.25)	LEAKAGE	0.091 (0.036)	0.239 (0.094)	0.38	872 (126.5)	295 (72)	AIR	LEAK MODE
1B-12 [1]	0.102 (0.040)	3.18 (1.25)	FAILURE	0.071 (0.028)	1.499 (0.590)	0.05	736 (106.8)	295 (72)	AIR	FAIL MODE
1B-13	0.102 (0.040)	3.18 (1.25)	LEAKAGE	0.079 (0.031)	0.389 (0.153)	0.20	858 (124.5)	295 (72)	AIR	LEAK MODE
1B-14	0.099 (0.039)	3.18 (1.25)	FAILURE	0.069 (0.027)	0.381 (0.150)	0.18	923 (133.8)	295 (72)	AIR	FAIL MODE
1B-19	0.104 (0.041)	3.18 (1.25)	FAILURE	0.053 (0.021)	0.617 (0.243)	0.09	888 (128.8)	295 (72)	AIR	FAIL MODE
M1B-1	0.102 (0.040)	3.18 (2.50)	FAILURE	0.074 (0.029)	0.386 (0.152)	0.19	946 (137.2)	295 (72)	AIR	FAIL MODE

[1] SPECIMEN TOO NARROW, W/2c $\cong$ 2.1

Table 10: Uniaxial Static Fracture Tests of 0.10 cm (0.040 Inch) Thick Surface Flawed Inconel X750 STA Base Metal at 78° K (-320° F)

SPECIMEN NUMBER	ORIGINAL THICKNESS, t cm (INCH)	ORIGINAL WIDTH, W cm (INCH)	TEST PARAMETERS AT		CRACK DEPTH, a cm (INCH)	CRACK LENGTH, 2c cm (INCH)	CRACK SHAPE a/2c	STRESS, σ MN/m² (KSI)	TEST TEMPERATURE, T °K (°F)	TEST ENVIRONMENT	REMARKS
1B-4	0.102 (0.040)	3.18 (1.25)	SIZING	START	0.051 (0.020)	0.266 (0.103)	0.19	–	295 (72)	AIR	NO CRACK GROWTH APPARENT
				STOP	0.051 (0.020)	0.266 (0.103)	0.19	839 (121.7)	295 (72)	AIR	
			FAILURE		0.051 (0.020)	0.266 (0.103)	0.19	1116 (161.8)	78 (-320)	LN_2	FAIL MODE
1B-5	0.102 (0.040)	3.18 (1.25)	SIZING	START	0.069 (0.027)	0.363 (0.143)	0.19	–	295 (72)	AIR	NO CRACK GROWTH APPARENT
				STOP	0.069 (0.027)	0.363 (0.143)	0.19	839 (121.7)	295 (72)	AIR	
			FAILURE		0.069 (0.027)	0.363 (0.143)	0.19	996 (144.5)	78 (-320)	LN_2	FAIL MODE
1B-7	0.102 (0.040)	3.18 (1.25)	SIZING	START	0.079 (0.031)	0.389 (0.153)	0.20	–	295 (72)	AIR	NO CRACK GROWTH APPARENT
				STOP	0.079 (0.031)	0.389 (0.153)	0.20	839 (121.7)	295 (72)	AIR	
			FAILURE		0.079 (0.031)	0.389 (0.153)	0.20	998 (144.8)	78 (-320)	LN_2	FAIL MODE
1B-17	0.102 (0.040)	3.18 (1.25)	SIZING	START	0.069 (0.027)	0.170 (0.067)	0.40	–	295 (72)	AIR	NO CRACK GROWTH APPARENT
				STOP	0.069 (0.027)	0.170 (0.067)	0.40	850 (123.3)	295 (72)	AIR	
			FAILURE		0.069 (0.027)	0.170 (0.067)	0.40	1136 (164.7)	78 (-320)	LN_2	FAIL MODE
1B-20	0.104 (0.041)	3.18 (1.25)	SIZING	START	0.043 (0.017)	0.483 (0.190)	0.09	–	295 (72)	AIR	NO CRACK GROWTH APPARENT
				STOP	0.043 (0.017)	0.483 (0.190)	0.09	850 (123.3)	295 (72)	AIR	
			FAILURE		0.043 (0.017)	0.483 (0.190)	0.09	1056 (153.2)	78 (-320)	LN_2	FAIL MODE

Table 11: *Uniaxial Static Fracture Tests of 0.10 cm (0.040 Inch) Thick Surface Flawed Inconel X750 STA Weld Metal ℄ [1] at 295°K (72°F)*

SPECIMEN NUMBER	ORIGINAL THICKNESS, t cm (INCH)	ORIGINAL WIDTH, W cm (INCH)	TEST PARAMETERS AT	CRACK DEPTH, a cm (INCH)	CRACK LENGTH, 2c cm (INCH)	CRACK SHAPE a/2c	STRESS, σ MN/m² (KSI)	TEST TEMPERATURE, T °K (°F)	TEST ENVIRONMENT	REMARKS
1BW-1	0.102 (0.040)	3.18 (1.25)	FAILURE	0.069 (0.027)	0.376 (0.148)	0.18	917 (133.0)	295 (72)	AIR	FAIL MODE
1BW-2 [2]	0.099 (0.039)	3.18 (1.25)	FAILURE	0.071 (0.028)	0.361 (0.142)	0.20	925 (134.2)	295 (72)	AIR	FAIL MODE
1BW-4 [3]	0.102 (0.040)	3.18 (1.25)	FAILURE	0.069 (0.027)	0.361 (0.142)	0.19	949 (137.7)	295 (72)	AIR	FAIL MODE
1BW-8 [5]	0.114 (0.045)	3.35 (1.32)	FAILURE	0.048 (0.019)	0.229 (0.090)	0.21	834 (120.9)	295 (72)	AIR	FAIL MODE
1BW-18 [4]	0.104 (0.041)	3.18 (1.25)	FAILURE	0.053 (0.021)	0.302 (0.119)	0.18	850 (123.3)	295 (72)	AIR	FAIL MODE
1BW-22	0.104 (0.041)	3.18 (1.25)	FAILURE	0.058 (0.023)	0.686 (0.270)	0.09	800 (116.0)	295 (72)	AIR	FAIL MODE
1BW-25	0.104 (0.041)	3.18 (1.25)	LEAKAGE	0.086 (0.034)	0.251 (0.099)	0.34	899 (130.4)	295 (72)	AIR	LEAK MODE
1BW-27	0.104 (0.041)	3.18 (1.25)	FAILURE	0.028 (0.011)	0.114 (0.045)	0.24	1079 (156.5)	295 (72)	AIR	FAIL MODE
1BW-28	0.102 (0.040)	3.18 (1.25)	LEAKAGE	0.089 (0.035)	0.465 (0.183)	0.19	794 (115.1)	295 (72)	AIR	LEAK MODE

[1] UNLESS NOTED OTHERWISE
[2] CRACK LOCATED IN WELD NUGGET
[3] CRACK LOCATED IN WELD HAZ
[4] SPECIMEN SUBJECTED TO A SIMULATED RESIN CURE CYCLE AT 422°K (300°F) FOR 60 HOURS
[5] SPECIMEN ORGINALLY REJECTED DUE TO WELD QUALITY

Table 12: Uniaxial Static Fracture Tests of 0.10 cm (0.040 Inch) Thick Surface Flawed Inconel X750 STA Weld Metal ℄ at 78°K (-320°F)

SPECIMEN NUMBER	ORIGINAL THICKNESS, t cm (INCH)	ORIGINAL WIDTH, W cm (INCH)	TEST PARAMETERS AT		CRACK DEPTH, a cm (INCH)	CRACK LENGTH, 2c cm (INCH)	CRACK SHAPE a/2c	STRESS, σ MN/m² (KSI)	TEST TEMPERATURE, T °K (°F)	TEST ENVIRONMENT	REMARKS
1BW-5	0.102 (0.040)	3.18 (1.25)	SIZING	START	0.028 (0.011)	0.175 (0.069)	0.16	—	295 (72)	AIR	NO CRACK GROWTH APPARENT
				STOP	0.028 (0.011)	0.175 (0.069)	0.16	850 (123.3)	295 (72)	AIR	
			FAILURE		0.028 (0.011)	0.175 (0.069)	0.16	1205 (174.8)	78 (-320)	LN_2	FAIL MODE
[1] 1BW-7	0.114 (0.045)	3.35 (1.32)	SIZING	START	0.048 (0.019)	0.239 (0.094)	0.20	—	295 (72)	AIR	SIGNIFICANT GROWTH-ON-LOADING
				STOP	0.084 (0.033)	0.239 (0.094)	0.35	850 (123.3)	295 (72)	AIR	
			FAILURE		0.084 (0.033)	0.239 (0.094)	0.35	945 (137.0)	78 (-320)	LN_2	FAIL MODE
[2] 1BW-19	0.104 (0.041)	3.18 (1.25)	SIZING	START	0.056 (0.022)	0.310 (0.122)	0.18	—	295 (72)	AIR	NO CRACK GROWTH APPARENT
				STOP	0.056 (0.022)	0.310 (0.122)	0.18	850 (123.3)	295 (72)	AIR	
			FAILURE		0.056 (0.022)	0.310 (0.122)	0.18	959 (139.1)	78 (-320)	LN_2	FAIL MODE
1BW-23	0.104 (0.041)	3.18 (1.25)	SIZING	START	0.069 (0.027)	0.361 (0.142)	0.19	—	295 (72)	AIR	NO CRACK GROWTH APPARENT
				STOP	0.069 (0.027)	0.361 (0.142)	0.19	850 (123.3)	295 (72)	AIR	
			FAILURE		0.069 (0.027)	0.361 (0.142)	0.19	995 (144.3)	78 (-320)	LN_2	FAIL MODE
1BW-26	0.104 (0.041)	3.18 (1.25)	SIZING	START	0.056 (0.022)	0.264 (0.104)	0.21	—	295 (72)	AIR	NO CRACK GROWTH APPARENT
				STOP	0.056 (0.022)	0.264 (0.104)	0.21	839 (121.7)	295 (72)	AIR	
			FAILURE		0.056 (0.022)	0.264 (0.104)	0.21	998 (144.7)	78 (-320)	LN_2	FAIL MODE

[1] SPECIMEN ORIGINALLY REJECTED DUE TO WELD QUALITY

[2] SPECIMEN SUBJECTED TO A SIMULATED RESIN CURE CYCLE AT 422°K (300°F) FOR 60 HOURS

Table 13: Uniaxial Static Fracture Tests of 0.33 cm (0.13 Inch) Thick Surface Flawed Inconel X750 STA Base Metal

SPECIMEN NUMBER	ORIGINAL THICKNESS, t cm (INCH)	ORIGINAL WIDTH, W cm (INCH)	TEST PARAMETERS AT		CRACK DEPTH, a cm (INCH)	CRACK LENGTH, 2c cm (INCH)	CRACK SHAPE a/2c	STRESS, σ MN/m^2 (KSI)	TEST: TEMPERATURE, T ^oK (^oF)	TEST: ENVIRONMENT	REMARKS
2B-1	0.330 (0.130)	8.26 (3.25)	FAILURE		0.218 (0.086)	1.105 (0.435)	0.20	831 (120.5)	295 (72)	AIR	FAIL MODE
2B-2	0.333 (0.131)	8.26 (3.25)	FAILURE		0.119 (0.047)	0.607 (0.239)	0.20	947 (137.4)	295 (72)	AIR	FAIL MODE
2B-18	0.330 (0.130)	8.26 (3.25)	FAILURE		0.259 (0.102)	1.341 (0.528)	0.19	787 (114.2)	295 (72)	AIR	FAIL MODE
2B-3	0.333 (0.131)	8.26 (3.25)	SIZING	START	0.165 (0.065)	0.856 (0.337)	0.19	—	295 (72)	AIR	NO CRACK GROWTH
				STOP	0.165 (0.065)	0.856 (0.337)	0.19	850 (123.3)	295 (72)	AIR	
			FAILURE		0.165 (0.065)	0.856 (0.337)	0.19	958 (139.0)	78 (-320)	LN_2	FAIL MODE
2B-4	0.333 (0.131)	8.26 (3.25)	SIZING	START	0.089 (0.035)	0.483 (0.190)	0.18	—	295 (72)	AIR	NO CRACK GROWTH
				STOP	0.089 (0.035)	0.483 (0.190)	0.18	850 (123.3)	295 (72)	AIR	
			FAILURE		0.089 (0.035)	0.483 (0.190)	0.18	1122 (162.7)	78 (-320)	LN_2	FAIL MODE

Table 14: Uniaxial Static Fracture Tests of 0.33 cm (0.13 Inch) Thick Surface Flawed Inconel X750 STA Weld Metal ℄

SPECIMEN NUMBER	ORIGINAL THICKNESS, t cm (INCH)	ORIGINAL WIDTH, W cm (INCH)	TEST PARAMETERS AT		CRACK DEPTH, a cm (INCH)	CRACK LENGTH, 2c cm (INCH)	CRACK SHAPE a/2c	STRESS, σ MN/m^2 (KSI)	TEST: TEMPERATURE, T ^oK (^oF)	TEST: ENVIRONMENT	REMARKS
2BW-2	0.328 (0.129)	8.26 (3.25)	FAILURE		0.168 (0.066)	0.851 (0.335)	0.20	904 (131.1)	295 (72)	AIR	FAIL MODE
2BW-3	0.330 (0.130)	8.26 (3.25)	LEAKAGE		0.287 (0.113)	1.494 (0.588)	0.19	801 (116.1)	295 (72)	AIR	LEAK MODE
2BW-8	0.333 (0.131)	8.23 (3.24)	FAILURE		0.191 (0.075)	1.031 (0.406)	0.18	848 (123.0)	295 (72)	AIR	FAIL MODE
2BW-10	0.330 (0.130)	8.23 (3.24)	FAILURE		0.188 (0.074)	1.034 (0.407)	0.18	836 (121.3)	295 (72)	AIR	FAIL MODE
2BW-4	0.328 (0.129)	8.26 (3.25)	SIZING	START	0.191 (0.075)	0.986 (0.388)	0.19	–	295 (72)	AIR	NO CRACK GROWTH
				STOP	0.191 (0.075)	0.986 (0.358	0.19	850 (123.3)	295 (72)	AIR	
			FAILURE		0.191 (0.075)	0.986 (0.388)	0.19	954 (138.4)	78 (-320)	LN_2	FAIL MODE
2BW-5	0.333 (0.131)	8.26 (3.25)	SIZING	START	0.094 (0.037)	0.544 (0.214)	0.17	–	295 (72)	AIR	NO CRACK GROWTH
				STOP	0.094 (0.037)	0.544 (0.214)	0.17	850 (123.3)	295 (72)	AIR	
			FAILURE		0.094 (0.037)	0.544 (0.214)	0.17	1127 (163.4)	78 (-320)	LN_2	FAIL MODE

Table 15: Uniaxial Cyclic Tests of 0.10 cm (0.040 Inch) Thick Surface Flawed Inconel X750 STA Base Metal at 295°K (72°F)

SPECIMEN NUMBER	ORIGINAL THICKNESS, t cm (INCH)	ORIGINAL WIDTH, W cm (INCH)	TEST PARAMETERS AT		CRACK DEPTH, a cm (INCH)	CRACK LENGTH, 2c cm (INCH)	CRACK SHAPE a/2c	STRESS, σ MN/m² (KSI)	TEST TEMPERATURE, T °K (°F)	TEST ENVIRONMENT	REMARKS
1B-6	0.102 (0.040)	3.18 (1.25)	SIZING	START	0.069 (0.027)	0.361 (0.142)	0.19	—	295 (72)	AIR	2370 CYCLES TO BREAK-THROUGH
				STOP	0.071 (0.028)	0.361 (0.142)	0.20	839 (121.7)	295 (72)	AIR	
			CYCLING	START	0.071 (0.028)	0.361 (0.142)	0.20	714 (103.5)	295 (72)	AIR	
				STOP	0.102 (0.040)	0.378 (0.149)	0.27	714 (103.5)	295 (72)	AIR	
1B-8	0.102 (0.040)	3.18 (1.25)	SIZING	START	0.074 (0.029)	0.381 (0.150)	0.19	—	295 (72)	AIR	301 CYCLES TO BREAK-THROUGH
				STOP	0.079 (0.031)	0.381 (0.150)	0.21	839 (121.7)	295 (72)	AIR	
			CYCLING	START	0.079 (0.031)	0.381 (0.150)	0.21	798 (115.7)	295 (72)	AIR	
				STOP	0.102 (0.040)	0.381 (0.150)	0.27	798 (115.7)	295 (72)	AIR	
1B-16	0.102 (0.040)	3.18 (1.25)	SIZING	START	0.064 (0.025)	0.356 (0.140)	0.18	—	295 (72)	AIR	3315 CYCLES TO BREAK-THROUGH
				STOP	0.069 (0.027)	0.356 (0.140)	0.19	850 (123.3)	295 (72)	AIR	
			CYCLING	START	0.069 (0.027)	0.356 (0.140)	0.19	638 (92.5)	295 (72)	AIR	
				STOP	0.102 (0.040)	0.376 (0.148)	0.27	638 (92.5)	295 (72)	AIR	
1B-18	0.102 (0.040)	3.18 (1.25)	SIZING	START	0.038 (0.015)	0.254 (0.100)	0.15	—	295 (72)	AIR	10,600 CYCLES TO BREAK-THROUGH
				STOP	0.038 (0.015)	0.254 (0.100)	0.15	850 (123.3)	295 (72)	AIR	
			CYCLING	START	0.038 (0.015)	0.254 (0.100)	0.15	723 (104.9)	295 (72)	AIR	
				STOP	0.102 (0.040)	0.320 (0.126)	0.32	723 (104.9)	295 (72)	AIR	
1B-22	0.104 (0.041)	3.18 (1.25)	SIZING	START	0.056 (0.022)	0.305 (0.120)	0.18	—	295 (72)	AIR	3979 CYCLES TO BREAK-THROUGH
				STOP	0.056 (0.022)	0.305 (0.120)	0.18	850 (123.3)	295 (72)	AIR	
			CYCLING	START	0.056 (0.022)	0.305 (0.120)	0.18	723 (104.9)	295 (72)	AIR	
				STOP	0.104 (0.041)	0.348 (0.137)	0.30	723 (104.9)	295 (72)	AIR	
[1] 1B-26	0.104 (0.041)	3.18 (1.25)	SIZING	START	0.069 (0.027)	0.378 (0.149)	0.18	—	295 (72)	AIR	2200 CYCLES TO BREAK-THROUGH
				STOP	0.071 (0.028)	0.378 (0.149)	0.19	850 (123.3)	295 (72)	AIR	
			CYCLING	START	0.071 (0.028)	0.378 (0.149)	0.19	723 (104.9)	295 (72)	AIR	
				STOP	0.104 (0.041)	0.391 (0.154)	0.27	723 (104.9)	295 (72)	AIR	

[1] RESIN IMPREGNATED CRACK

Table 16: Uniaxial Cyclic Tests of 0.10 cm (0.040 Inch) Thick Surface Flawed Inconel X750 STA Base Metal at 78°K (-320°F)

SPECIMEN NUMBER	ORIGINAL THICKNESS, t cm (INCH)	ORIGINAL WIDTH, W cm (INCH)	TEST PARAMETERS AT		CRACK DEPTH, a cm (INCH)	CRACK LENGTH, 2c cm (INCH)	CRACK SHAPE a/2c	STRESS, σ MN/m^2 (KSI)	TEST TEMPERATURE, T °K (°F)	TEST ENVIRONMENT	REMARKS
1B-21	0.102 (0.040)	3.18 (1.25)	SIZING	START	0.064 (0.025)	0.335 (0.132)	0.19	—	295 (72)	AIR	
				STOP	0.064 (0.025)	0.335 (0.132)	0.19	850 (123.3)	295 (72)	AIR	
			PROOF	START	0.064 (0.025)	0.335 (0.132)	0.19	—	78 (-320)	LN_2	
				STOP	0.064 (0.025)	0.335 (0.132)	0.19	959 (139.1)	78 (-320)	LN_2	
			CYCLING	START	0.064 (0.025)	0.335 (0.132)	0.19	816 (118.3)	78 (-320)	LN_2	2835 CYCLES TO BREAK-THROUGH
				STOP	0.102 (0.040)	0.356 (0.140)	0.29	816 (118.3)	78 (-320)	LN_2	
1B-23	0.102 (0.040)	3.18 (1.25)	SIZING	START	0.053 (0.021)	0.323 (0.127)	0.17	—	295 (72)	AIR	
				STOP	[1]	0.323 (0.127)	—	850 (123.3)	295 (72)	AIR	
			PROOF	START	[1]	0.323 (0.127)	—	—	78 (-320)	LN_2	
				STOP	0.056 (0.022)	0.323 (0.127)	0.17	959 (139.1)	78 (-320)	LN_2	
			CYCLING	START	0.056 (0.022)	0.323 (0.127)	0.17	959 (139.1)	78 (-320)	LN_2	1019 CYCLES TO BREAK-THROUGH
				STOP	0.102 (0.040)	0.340 (0.134)	0.30	959 (139.1)	78 (-320)	LN_2	
1B-24	0.102 (0.040)	3.18 (1.25)	SIZING	START	0.056 (0.022)	0.320 (0.126)	0.17	—	295 (72)	AIR	
				STOP	[1]	0.320 (0.126)	—	850 (123.3)	295 (72)	AIR	
			PROOF	START	[1]	0.320 (0.126)	—	—	78 (-320)	LN_2	
				STOP	0.058 (0.023)	0.320 (0.126)	0.18	959 (139.1)	78 (-320)	LN_2	
			CYCLING	START	0.058 (0.023)	0.320 (0.126)	0.18	718 (104.2)	78 (-320)	LN_2	6744 CYCLES TO BREAK-THROUGH
				STOP	0.102 (0.040)	0.358 (0.141)	0.28	718 (104.2)	78 (-320)	LN_2	
1B-25	0.102 (0.040)	3.18 (1.25)	SIZING	START	0.033 (0.013)	0.229 (0.090)	0.14	—	295 (72)	AIR	
				STOP	0.033 (0.013)	0.229 (0.090)	0.14	850 (123.3)	295 (72)	AIR	
			PROOF	START	0.033 (0.013)	0.229 (0.090)	0.14	—	78 (-320)	LN_2	
				STOP	0.033 (0.013)	0.229 (0.090)	0.14	959 (139.1)	78 (-320)	LN_2	
			CYCLING	START	0.033 (0.013)	0.229 (0.090)	0.14	816 (118.3)	78 (-320)	LN_2	15,000 CYCLES TO BREAK-THROUGH
				STOP	0.102 (0.040)	0.307 (0.121)	0.33	816 (118.3)	78 (-320)	LN_2	
1BW-3 [2]	0.099 (0.039)	3.18 (1.25)	SIZING	START	0.053 (0.021)	0.295 (0.116)	0.18	—	295 (72)	AIR	
				STOP	[1]	0.295 (0.116)	—	850 (123.3)	295 (72)	AIR	
			PROOF	START	[1]	0.295 (0.116)	—	—	78 (-320)	LN_2	
				STOP	0.056 (0.022)	0.295 (0.116)	0.19	959 (139.1)	78 (-320)	LN_2	
			CYCLING	START	0.056 (0.022)	0.295 (0.116)	0.19	816 (118.3)	78 (-320)	LN_2	3290 CYCLES TO BREAK-THROUGH
				STOP	0.099 (0.039)	0.333 (0.131)	0.30	816 (118.3)	78 (-320)	LN_2	

[1] GROWTH DURING σ_s INDISTINGUISHABLE FROM GROWTH DURING PROOF

[2] SPECIMEN SUBJECTED TO A SIMULATED RESIN CURE CYCLE AT 422°K (300°F) FOR 60 HOURS

Table 17: Uniaxial Cyclic Tests of 0.10 cm (0.040 Inch) Thick Surface Flawed Inconel X750 STA Weld Metal ℄ at 295°K (72°F)

SPECIMEN NUMBER	ORIGINAL THICKNESS, t cm (INCH)	ORIGINAL WIDTH, W cm (INCH)	TEST PARAMETERS AT		CRACK DEPTH, a cm (INCH)	CRACK LENGTH, 2c cm (INCH)	CRACK SHAPE, a/2c	STRESS, σ MN/m² (KSI)	TEST: TEMPERATURE, T °K (°F)	TEST: ENVIRONMENT	REMARKS
1BW-6	0.102 (0.040)	3.18 (1.25)	SIZING	START	0.076 (0.030)	0.345 (0.136)	0.22	—	295 (72)	AIR	510 CYCLES TO BREAK-THROUGH
				STOP	0.084 (0.033)	0.345 (0.136)	0.24	850 (123.3)	295 (72)	AIR	
			CYCLING	START	0.084 (0.033)	0.345 (0.136)	0.24	720 (104.4)	295 (72)	AIR	
				STOP	0.102 (0.040)	0.351 (0.138)	0.29	720 (104.4)	295 (72)	AIR	
[2] 1BW-10	0.102 (0.040)	3.18 (1.25)	SIZING	START	0.064 (0.025)	0.351 (0.138)	0.18	—	295 (72)	AIR	914 CYCLES TO BREAK-THROUGH
				STOP	[1]	[1]	—	850 (123.3)	295 (72)	AIR	
			CYCLING	START	[1]	[1]	—	638 (92.5)	295 (72)	AIR	
				STOP	[1]	[1]	—	638 (92.5)	295 (72)	AIR	
1BW-11	0.102 (0.040)	3.18 (1.25)	SIZING	START	0.043 (0.017)	0.244 (0.096)	0.18	—	295 (72)	AIR	8079 CYCLES TO BREAK-THROUGH
				STOP	0.043 (0.017)	0.244 (0.096)	0.18	850 (123.3)	295 (72)	AIR	
			CYCLING	START	0.043 (0.017)	0.244 (0.096)	0.18	723 (104.9)	295 (72)	AIR	
				STOP	0.102 (0.040)	0.437 (0.172)	0.23	723 (104.9)	295 (72)	AIR	
1BW-13	0.102 (0.040)	3.18 (1.25)	SIZING	START	0.061 (0.024)	0.358 (0.141)	0.17	—	295 (72)	AIR	506 CYCLES TO BREAK-THROUGH
				STOP	0.064 (0.025)	0.358 (0.141)	0.18	850 (123.3)	295 (72)	AIR	
			CYCLING	START	0.064 (0.025)	0.358 (0.141)	0.18	850 (123.3)	295 (72)	AIR	
				STOP	0.102 (0.040)	0.414 (0.163)	0.25	850 (123.3)	295 (72)	AIR	
1BW-17	0.104 (0.041)	3.18 (1.25)	SIZING	START	0.064 (0.025)	0.353 (0.139)	0.18	—	295 (72)	AIR	1000 CYCLES TO BREAK-THROUGH
				STOP	0.079 (0.031)	0.353 (0.139)	0.22	850 (123.3)	295 (72)	AIR	
			CYCLING	START	0.079 (0.031)	0.353 (0.139)	0.22	638 (92.5)	295 (72)	AIR	
				STOP	0.104 (0.041)	0.353 (0.139)	0.30	638 (92.5)	295 (72)	AIR	
[3] 1BW-21	0.104 (0.041)	3.18 (1.25)	SIZING	START	0.069 (0.027)	0.323 (0.127)	0.21	—	295 (72)	AIR	1571 CYCLES TO BREAK-THROUGH
				STOP	0.069 (0.027)	0.323 (0.127)	0.21	850 (123.3)	295 (72)	AIR	
			CYCLING	START	0.069 (0.027)	0.323 (0.127)	0.21	723 (104.9)	295 (72)	AIR	
				STOP	0.104 (0.041)	0.340 (0.134)	0.31	723 (104.9)	295 (72)	AIR	
1BW-24	0.104 (0.041)	3.18 (1.25)	SIZING	START	0.061 (0.024)	0.351 (0.138)	0.17	—	295 (72)	AIR	1360 CYCLES TO BREAK-THROUGH
				STOP	0.064 (0.025)	0.351 (0.138)	0.18	850 (123.3)	295 (72)	AIR	
			CYCLING	START	0.064 (0.025)	0.351 (0.138)	0.18	723 (104.9)	295 (72)	AIR	
				STOP	0.104 (0.041)	0.356 (0.140)	0.29	723 (104.9)	295 (72)	AIR	

[1] NOT DISTINGUISHABLE FROM FRACTURE FACE

[2] OVERLOADED DURING LAST 150 CYCLES

[3] RESIN IMPREGNATED CRACK

Table 18: Uniaxial Cyclic Tests of 0.10 cm (0.040 Inch) Thick Surface Flawed Inconel X750 STA Weld Metal ℄ at 78°K (-320°F)

SPECIMEN NUMBER	ORIGINAL THICKNESS, t cm (INCH)	ORIGINAL WIDTH, W cm (INCH)	TEST PARAMETERS AT		CRACK DEPTH, a cm (INCH)	CRACK LENGTH, 2c cm (INCH)	CRACK SHAPE a/2c	STRESS, σ MN/m² (KSI)	TEST: TEMPERATURE, T °K (°F)	TEST: ENVIRONMENT	REMARKS
1BW-12	0.102 (0.040)	3.18 (1.25)	SIZING	START	0.069 (0.027)	0.264 (0.104)	0.26	–	295 (72)	AIR	
				STOP	[1]	0.264 (0.104)	–	850 (123.3)	295 (72)	AIR	
			PROOF	START	[1]	0.264 (0.104)	–	–	78 (-320)	LN_2	
				STOP	0.071 (0.028)	0.264 (0.104)	0.27	959 (139.1)	78 (-320)	LN_2	
			CYCLING	START	0.071 (0.028)	0.264 (0.104)	0.27	816 (118.3)	78 (-320)	LN_2	2883 CYCLES TO BREAK-THROUGH
				STOP	0.102 (0.040)	0.295 (0.116)	0.34	816 (118.3)	78 (-320)	LN_2	
1BW-14	0.102 (0.040)	3.18 (1.25)	SIZING	START	0.048 (0.019)	0.274 (0.108)	0.18	–	295 (72)	AIR	
				STOP	0.048 (0.019)	0.274 (0.108)	0.18	850 (123.3)	295 (72)	AIR	
			PROOF	START	0.048 (0.019)	0.274 (0.108)	0.18	–	78 (-320)	LN_2	
				STOP	0.048 (0.019)	0.274 (0.108)	0.18	959 (139.1)	78 (-320)	LN_2	
			CYCLING	START	0.048 (0.019)	0.274 (0.108)	0.18	959 (139.1)	78 (-320)	LN_2	990 CYCLES TO BREAK-THROUGH
				STOP	0.102 (0.040)	0.274 (0.108)	0.37	959 (139.1)	78 (-320)	LN_2	
BW-6	0.107 (0.042)	1.27 (0.50)	SIZING	START	0.033 (0.013)	0.206 (0.081)	0.16	–	295 (72)	AIR	
				STOP	0.033 (0.013)	0.206 (0.081)	0.16	850 (123.3)	295 (72)	AIR	
			PROOF	START	0.033 (0.013)	0.206 (0.081)	0.16	–	78 (-320)	LN_2	
				STOP	0.033 (0.013)	0.206 (0.081)	0.16	959 (139.1)	78 (-320)	LN_2	
			CYCLING	START	0.033 (0.013)	0.206 (0.081)	0.16	816 (118.3)	78 (-320)	LN_2	7063 CYCLES TO BREAK-THROUGH
				STOP	0.107 (0.042)	0.302 (0.119)	0.35	816 (118.3)	78 (-320)	LN_2	

[1] GROWTH DURING σ_s INDISTINGUISHABLE FROM GROWTH DURING PROOF

Table 19: Uniaxial Cyclic Tests of 0.33 cm (0.13 Inch) Thick Surface Flawed Inconel X750 STA Base Metal at 295^{0}K (72^{0}F)

SPECIMEN NUMBER	ORIGINAL THICKNESS, t cm (INCH)	ORIGINAL WIDTH, W cm (INCH)	TEST PARAMETERS AT		CRACK DEPTH, a cm (INCH)	CRACK LENGTH, 2c cm (INCH)	CRACK SHAPE a/2c	STRESS, σ MN/m^2 (KSI)	TEST TEMPERATURE, T ^{0}K (^{0}F)	TEST ENVIRONMENT	REMARKS
2B-5	0.333 (0.131)	8.26 (3.25)	SIZING	START	0.160 (0.063)	0.859 (0.338)	0.19	–	295 (72)	AIR	CYCLED FOR 128 CYCLES AND THEN TEST MACHINE OVERLOADED
			SIZING	STOP	0.173 (0.068)	0.859 (0.338)	0.20	850 (123.3)	295 (72)	AIR	
			CYCLING	START	0.173 (0.068)	0.859 (0.338)	0.20	723 (104.9)	295 (72)	AIR	
			CYCLING	STOP	0.178 (0.070)	0.859 (0.338)	0.21	723 (104.9)	295 (72)	AIR	
			FAILURE		0.178 (0.070)	0.859 (0.338)	0.21	841 (122.0)	295 (72)	AIR	FAIL MODE
2B-10	0.333 (0.131)	8.26 (3.25)	SIZING	START	0.170 (0.067)	0.881 (0.347)	0.19	–	295 (72)	AIR	558 CYCLES TO BREAKTHROUGH
			SIZING	STOP	0.188 (0.074)	0.881 (0.347)	0.21	850 (123.3)	295 (72)	AIR	
			CYCLING	START	0.188 (0.074)	0.881 (0.347)	0.21	850 (123.3)	295 (72)	AIR	
			CYCLING	STOP	0.333 (0.131)	0.945 (0.372)	0.35	850 (123.3)	295 (72)	AIR	
2B-12	0.333 (0.131)	8.26 (3.25)	SIZING	START	0.122 (0.048)	0.620 (0.244)	0.20	–	295 (72)	AIR	5815 CYCLES TO BREAK-THROUGH
			SIZING	STOP	0.124 (0.049)	0.620 (0.244)	0.20	850 (123.3)	295 (72)	AIR	
			CYCLING	START	0.124 (0.049)	0.620 (0.244)	0.20	723 (104.9)	295 (72)	AIR	
			CYCLING	STOP	0.333 (0.131)	0.894 (0.352)	0.37	723 (104.9)	295 (72)	AIR	
2B-13	0.328 (0.129)	8.26 (3.25)	SIZING	START	0.165 (0.065)	0.884 (0.348)	0.19	–	295 (72)	AIR	4143 CYCLES TO BREAK-THROUGH
			SIZING	STOP	0.180 (0.071)	0.884 (0.348)	0.20	850 (123.3)	295 (72)	AIR	
			CYCLING	START	0.180 (0.071)	0.884 (0.348)	0.20	638 (92.5)	295 (72)	AIR	
			CYCLING	STOP	0.328 (0.129)	1.024 (0.403)	0.32	638 (92.5)	295 (72)	AIR	
2B-14	0.330 (0.130)	8.28 (3.26)	SIZING	START	0.163 (0.064)	0.889 (0.350)	0.18	–	295 (72)	AIR	2477 CYCLES TO BREAK-THROUGH
			SIZING	STOP	0.178 (0.070)	0.889 (0.350)	0.20	850 (123.3)	295 (72)	AIR	
			CYCLING	START	0.178 (0.070)	0.889 (0.350)	0.20	723 (104.9)	295 (72)	AIR	
			CYCLING	STOP	0.330 (0.130)	1.036 (0.408)	0.32	723 (104.9)	295 (72)	AIR	
2B-16	0.333 (0.131)	8.26 (3.25)	SIZING	START	0.193 (0.076)	1.024 (0.403)	0.19	–	295 (72)	AIR	152 CYCLES TO BREAK-THROUGH
			SIZING	STOP	0.226 (0.089)	1.024 (0.403)	0.22	850 (123.3)	295 (72)	AIR	
			CYCLING	START	0.226 (0.089)	1.024 (0.403)	0.22	723 (104.9)	295 (72)	AIR	
			CYCLING	STOP	0.333 (0.131)	1.087 (0.428)	0.31	723 (104.9)	295 (72)	AIR	

Table 20: Uniaxial Cyclic Tests of 0.33 cm (0.13 Inch) Thick Surface Flawed Inconel X750 STA Base Metal at 78^{0}K (-320^{0}F)

SPECIMEN NUMBER	ORIGINAL THICKNESS, t cm (INCH)	ORIGINAL WIDTH, W cm (INCH)	TEST PARAMETERS AT		CRACK DEPTH, a cm (INCH)	CRACK LENGTH, 2c cm (INCH)	CRACK SHAPE, a/2c	STRESS, σ MN/m^2 (KSI)	TEST TEMPERATURE, T ^{0}K (^{0}F)	TEST ENVIRONMENT	REMARKS
2B-6	0.330 (0.130)	8.26 (3.25)	SIZING	START	0.130 (0.051)	0.691 (0.272)	0.19	—	295 (72)	AIR	3744 CYCLES TO BREAK-THROUGH
				STOP	[1]	0.691 (0.272)	—	850 (123.3)	295 (72)	AIR	
			PROOF	START	[1]	0.691 (0.272)	—	—	78 (-320)	LN_2	
				STOP	0.140 (0.055)	0.691 (0.272)	0.20	959 (139.1)	78 (-320)	LN_2	
			CYCLING	START	0.140 (0.055)	0.691 (0.272)	0.20	816 (118.3)	78 (-320)	LN_2	
				STOP	0.330 (0.130)	0.932 (0.367)	0.35	816 (118.3)	78 (-320)	LN_2	
2B-7	0.328 (0.129)	8.26 (3.25)	SIZING	START	0.130 (0.051)	0.711 (0.280)	0.18	—	295 (72)	AIR	362 CYCLES TO BREAK-THROUGH
				STOP	[1]	0.711 (0.280)	—	850 (123.3)	295 (72)	AIR	
			PROOF	START	[1]	0.711 (0.280)	—	—	78 (-320)	LN_2	
				STOP	0.155 (0.061)	0.711 (0.280)	0.22	959 (139.1)	78 (-320)	LN_2	
			CYCLING	START	0.155 (0.061)	0.711 (0.280)	0.22	959 (139.1)	78 (-320)	LN_2	
				STOP	0.328 (0.129)	0.970 (0.382)	0.34	959 (139.1)	78 (-320)	LN_2	
2B-8	0.330 (0.130)	8.26 (3.25)	SIZING	START	0.137 (0.054)	0.732 (0.288)	0.19	—	295 (72)	AIR	2112 CYCLES TO BREAK-THROUGH
				STOP	[1]	0.732 (0.288)	—	871 (126.3)	295 (72)	AIR	
			PROOF	START	[1]	0.732 (0.288)	—	—	78 (-320)	LN_2	
				STOP	0.150 (0.059)	0.732 (0.288)	0.21	966 (140.1)	78 (-320)	LN_2	
			CYCLING	START	0.150 (0.059)	0.732 (0.288)	0.21	884 (128.2)	78 (-320)	LN_2	
				STOP	0.330 (0.130)	0.917 (0.361)	0.36	884 (128.2)	78 (-320)	LN_2	
2B-9	0.333 (0.131)	8.26 (3.25)	SIZING	START	0.084 (0.033)	0.439 (0.173)	0.19	—	295 (72)	AIR	9195 CYCLES TO BREAK-THROUGH
				STOP	0.084 (0.033)	0.439 (0.173)	0.19	850 (123.3)	295 (72)	AIR	
			• PROOF	START	0.084 (0.033)	0.439 (0.173)	0.19	—	78 (-320)	LN_2	
				STOP	0.084 (0.033)	0.439 (0.173)	0.19	959 (139.1)	78 (-320)	LN_2	
			CYCLING	START	0.084 (0.033)	0.439 (0.173)	0.19	885 (123.3)	78 (-320)	LN_2	
				STOP	0.333 (0.131)	0.831 (0.327)	0.40	885 (128.3)	78 (-320)	LN_2	
2B-11	0.333 (0.131)	8.26 (3.25)	SIZING	START	0.122 (0.048)	0.630 (0.248)	0.19	—	295 (72)	AIR	3184 CYCLES TO BREAK-THROUGH
				STOP	[1]	0.630 (0.248)	—	850 (123.3)	295 (72)	AIR	
			PROOF	START	[1]	0.630 (0.248)	—	—	78 (-320)	LN_2	
				STOP	0.124 (0.049)	0.630 (0.248)	0.20	959 (139.1)	78 (-320)	LN_2	
			CYCLING	START	0.124 (0.049)	0.630 (0.248)	0.20	884 (128.2)	78 (-320)	LN_2	
				STOP	0.333 (0.131)	0.909 (0.358)	0.37	884 (128.2)	78 (-320)	LN_2	

[1] GROWTH DURING σ_s INDISTINGUISHABLE FROM GROWTH DURING PROOF

Table 21: Uniaxial Cyclic Tests of 0.33 cm (0.13 Inch) Thick Surface Flawed Inconel X750 STA Weld Metal ℄ at 295^{0}K (72^{0}F)

SPECIMEN NUMBER	ORIGINAL THICKNESS, t cm (INCH)	ORIGINAL WIDTH, W cm (INCH)	TEST PARAMETERS AT		CRACK DEPTH, a cm (INCH)	CRACK LENGTH, 2c cm (INCH)	CRACK SHAPE a/2c	STRESS, σ MN/m^2 (KSI)	TEST: TEMPERATURE, T ^{o}K (^{o}F)	TEST: ENVIRONMENT	REMARKS
2BW-6	0.330 (0.130)	8.26 (3.25)	SIZING	START	0.193 (0.076)	1.085 (0.427)	0.18	–	295 (72)	AIR	
				STOP	0.226 (0.089)	1.085 (0.427)	0.21	850 (123.3)	295 (72)	AIR	
			CYCLING	START	0.226 (0.089)	1.085 (0.427)	0.21	723 (104.9)	295 (72)	AIR	1152 CYCLES TO BREAK-THROUGH
				STOP	0.330 (0.130)	1.135 (0.447)	0.29	723 (104.9)	295 (72)	AIR	
2BW-13	0.328 (0.129)	8.26 (3.25)	SIZING	START	0.155 (0.061)	0.818 (0.322)	0.19	–	295 (72)	AIR	
				STOP	0.157 (0.062)	0.818 (0.322)	0.19	850 (123.3)	295 (72)	AIR	
			CYCLING	START	0.157 (0.062)	0.818 (0.322)	0.19	850 (123.3)	295 (72)	AIR	1058 CYCLES TO BREAK-THROUGH
				STOP	0.328 (0.129)	0.953 (0.375)	0.34	850 (123.3)	295 (72)	AIR	
2BW-14	0.333 (0.131)	8.24 (3.24)	SIZING	START	0.094 (0.037)	0.503 (0.200)	0.19	–	295 (72)	AIR	
				STOP	0.094 (0.037)	0.508 (0.200)	0.19	850 (123.3)	295 (72)	AIR	
			CYCLING	START	0.094 (0.037)	0.508 (0.200)	0.19	723 (104.9)	295 (72)	AIR	9512 CYCLES TO BREAK-THROUGH
				STOP	0.333 (0.131)	0.808 (0.318)	0.41	723 (104.9)	295 (72)	AIR	
2BW-17	0.333 (0.131)	8.24 (3.24)	SIZING	START	0.155 (0.061)	0.838 (0.330)	0.18	–	295 (72)	AIR	
				STOP	0.157 (0.062)	0.838 (0.330)	0.19	850 (123.3)	295 (72)	AIR	
			CYCLING	START	0.157 (0.062)	0.838 (0.330)	0.19	723 (104.9)	295 (72)	AIR	2891 CYCLES TO BREAK-THROUGH
				STOP	0.333 (0.131)	1.003 (0.395)	0.33	723 (104.9)	295 (72)	AIR	
2BW-18	0.323 (0.127)	8.26 (3.25)	SIZING	START	0.157 (0.062)	0.838 (0.330)	0.19	–	295 (72)	AIR	
				STOP	0.160 (0.063)	0.838 (0.330)	0.19	850 (123.3)	295 (72)	AIR	
			CYCLING	START	0.160 (0.063)	0.838 (0.330)	0.19	633 (92.5)	295 (72)	AIR	6480 CYCLES TO BREAK-THROUGH
				STOP	0.323 (0.127)	1.054 (0.415)	0.31	638 (92.5)	295 (72)	AIR	

Table 22: Uniaxial Cyclic Tests of 0.33 cm (0.13 Inch) Thick Surface Flawed Inconel X750 STA Weld Metal ℄ at 78°K (-320°F)

SPECIMEN NUMBER	ORIGINAL THICKNESS, t cm (INCH)	ORIGINAL WIDTH, W cm (INCH)	TEST PARAMETERS AT		CRACK DEPTH, a cm (INCH)	CRACK LENGTH, 2c cm (INCH)	CRACK SHAPE, a/2c	STRESS, σ MN/m² (KSI)	TEST TEMPERATURE, T °K (°F)	TEST ENVIRONMENT	REMARKS
2BW-7	0.333 (0.131)	8.26 (3.25)	SIZING	START	0.147 (0.058)	0.831 (0.327)	0.18	–	295 (72)	AIR	
				STOP	[1]	0.831 (0.327)	–	850 (123.3)	295 (72)	AIR	
			PROOF	START	[1]	0.831 (0.327)	–	–	78 (-320)	LN_2	
				STOP	0.155 (0.061)	0.831 (0.327)	0.19	959 (139.1)	78 (-320)	LN_2	
			CYCLING	START	0.155 (0.061)	0.831 (0.327)	0.19	816 (118.3)	78 (-320)	LN_2	2337 CYCLES TO BREAK-THROUGH
				STOP	0.333 (0.131)	1.011 (0.398)	0.33	816 (118.3)	78 (-320)	LN_2	
2BW-11	0.333 (0.131)	8.23 (3.24)	SIZING	START	0.140 (0.055)	0.762 (0.300)	0.18	–	295 (72)	AIR	
				STOP	[1]	0.762 (0.300)	–	850 (123.3)	295 (72)	AIR	
			PROOF	START	[1]	0.762 (0.300)	–	–	78 (-320)	LN_2	
				STOP	0.142 (0.056)	0.762 (0.300)	0.19	959 (139.1)	78 (-320)	LN_2	
			CYCLING	START	0.142 (0.056)	0.762 (0.300)	0.19	959 (139.1)	78 (-320)	LN_2	370 CYCLES TO BREAK-THROUGH
				STOP	0.333 (0.131)	0.762 (0.300)	0.44	959 (139.1)	78 (-320)	LN_2	
2BW-12	0.328 (0.129)	8.23 (3.24)	SIZING	START	0.094 (0.037)	0.495 (0.195)	0.19	–	295 (72)	AIR	
				STOP	0.094 (0.037)	0.495 (0.195)	0.19	850 (123.3)	295 (72)	AIR	
			PROOF	START	0.094 (0.037)	0.495 (0.195)	0.19	–	78 (-320)	LN_2	
				STOP	0.094 (0.037)	0.495 (0.195)	0.19	959 (139.1)	78 (-320)	LN_2	
			CYCLING	START	0.094 (0.037)	0.495 (0.195)	0.19	816 (118.3)	78 (-320)	LN_2	11,653 CYCLES TO BREAK-THROUGH
				STOP	0.328 (0.129)	0.787 (0.310)	0.42	816 (118.3)	78 (-320)	LN_2	
2BW-15	0.333 (0.131)	8.25 (3.25)	SIZING	START	0.163 (0.064)	0.810 (0.319)	0.20	–	295 (72)	AIR	
				STOP	[1]	0.810 (0.319)	–	850 (123.3)	295 (72)	AIR	
			PROOF	START	[1]	0.810 (0.319)	–	–	78 (-320)	LN_2	
				STOP	0.175 (0.069)	0.810 (0.319)	0.22	959 (139.1)	78 (-320)	LN_2	
			CYCLING	START	0.175 (0.069)	0.810 (0.319)	0.22	719 (104.3)	78 (-320)	LN_2	4886 CYCLES TO BREAK-THROUGH
				STOP	0.333 (0.131)	0.897 (0.353)	0.37	719 (104.3)	78 (-320)	LN_2	
2BW-16	0.328 (0.129)	8.23 (3.24)	SIZING	START	0.173 (0.068)	0.940 (0.370)	0.18	–	295 (72)	AIR	
				STOP	[1]	0.940 (0.370)	–	850 (123.3)	295 (72)	AIR	
			PROOF	START	[1]	0.940 (0.370)	–	–	78 (-320)	LN_2	
				STOP	0.185 (0.073	0.940 (0.370)	0.20	959 (139.1)	78 (-320)	LN_2	
			CYCLING	START	0.185 (0.073)	0.940 (0.370)	0.20	816 (118.3)	78 (-320)	LN_2	1905 CYCLES TO BREAK-THROUGH
				STOP	0.328 (0.129)	1.062 (0.418)	0.31	816 (118.3)	78 (-320)	LN_2	

[1] GROWTH DURING σ_s INDISTINGUISHABLE FROM GROWTH DURING PROOF

Table 23: Cyclic Crack Growth Rate Constants [1] *for Inconel X750 STA Tested at* $R = 0$ *and* $(a/2c)_i \approx 0.20$

MATERIAL THICKNESS cm (INCH)	MATERIAL	TEMPERATURE °K (°F)	n	C	K RANGE $MN/m^{3/2}$ (KSI$\sqrt{IN}$) FROM	TO	REMARKS
0.102 (0.040)	BASE METAL	295 (72)	8.2	0.0617×10^{-12} (2.67×10^{-12})	≈ 33.0 (30)	≈ 44.0 (40)	[2]
		78 (-320)	8.2	0.0234×10^{-12} (1.01×10^{-12})			[3]
	WELD METAL	295 (72)	8.2	0.0941×10^{-12} (4.07×10^{-12})			[2]
		78 (-320)	8.2	0.0396×10^{-12} (1.71×10^{-12})			[3]
0.330 (0.130)	BASE METAL	295 (72)	6.0	0.0250×10^{-9} (1.08×10^{-9})	≈ 44.0 (40)	≈ 77.0 (70)	[2]
		78 (-320)	6.0	0.0125×10^{-9} (0.54×10^{-9})			[3]
	WELD METAL	295 (72)	6.0	0.0215×10^{-9} (0.93×10^{-9})			[2]
		78 (-320)	6.0	0.0125×10^{-9} (0.54×10^{-9})			[3]

[1] ASSUMES $da/dN = CK^n$ (SEE FIGURES 58,59,60 AND 61) WHERE da/dN UNITS ARE μcm/CYCLE (μINCHES/CYCLE)

[2] RT CYCLIC TESTED AFTER BEING LOADED TO 850 MN/m^2 (123.3 KSI) IN RT AIR

[3] LN_2 CYCLIC TESTED AFTER BEING LOADED TO 850 MN/m^2 (123.3 KSI) IN RT AIR AND THEN LOADED TO 960 MN/m^2 (139.1 KSI) IN LN_2

Table 24: 2219-T62 Mechanical Properties

TEMPERATURE, T °K (°F)	MATERIAL	SPECIMEN NUMBER	THICKNESS, t cm (INCH)	WIDTH, W cm (INCH)	0.2% OFFSET σ_{ys} IN 5.1 cm (2.0 INCH) MN/m^2 (KSI)	0.2% OFFSET σ_{ys} IN WELD NUGGET MN/m^2 (KSI)	σ_{ult} MN/m^2 (KSI)	% ELONGATION IN 5.1 cm (2.0 INCH)	ELASTIC MODULUS, E x 10^{-6} kN/m^2 (PSI)
295 (72)	BASE METAL	A-1	0.231 (0.091)	1.270 (0.500)	294 (42.6)		432 (62.6)	8.4	79.3 (11.5)
		A-2	0.231 (0.091)	1.270 (0.500)	294 (42.6)		432 (62.6)	8.8	66.8 (9.7)
	WELD METAL	AW-1	0.229 (0.090)	1.273 (0.501)	283 (41.0)	283 (41.0)	412 (59.8)	6.6	75.8 (11.0)
		AW-2	0.229 (0.090)	1.278 (0.503)	288 (41.8)	303 (44.0)	417 (60.5)	8.4	82.7 (12.0)
78 (-320)	BASE METAL	A-3	0.231 (0.091)	1.273 (0.501)	361 (52.4)		526 (76.3)	13.8	76.5 (11.1)
		A-4	0.234 (0.092)	1.267 (0.499)	359 (52.1)		523 (75.9)	14.8	77.9 (11.3)
	WELD METAL	AW-4	0.229 (0.090)	1.273 (0.501)	355 (51.5)	356 (51.7)	501 (72.7)	6.3	91.7 (13.3)
		AW-6	0.224 (0.088)	1.270 (0.500)	365 (51.5)	370 (53.6)	514 (74.6)	9.6	77.2 (11.2)

Table 25: *Uniaxial Static Fracture Tests of 0.23 cm (0.090 Inch) Thick Surface Flawed 2219-T62 Aluminum Base Metal at 295°K (72°F)*

SPECIMEN NUMBER	ORIGINAL THICKNESS, t cm (INCH)	ORIGINAL WIDTH, W cm (INCH)	TEST PARAMETERS AT	CRACK DEPTH, a cm (INCH)	CRACK LENGTH, 2c cm (INCH)	CRACK SHAPE a/2c	STRESS, σ MN/m² (KSI)	TEST: TEMPERATURE, T °K (°F)	TEST: ENVIRONMENT	REMARKS
1A-1	0.229 (0.090)	6.35 (2.50)	FAILURE	0.152 (0.060)	0.742 (0.292)	0.21	298 (43.2)	295 (72)	AIR	FAIL MODE
1A-2	0.231 (0.091)	635 (2.50)	FAILURE	0.074 (0.029)	0.239 (0.094)	0.31	385 (55.9)	295 (72)	AIR	FAIL MODE
1A-3	0.229 (0.090)	6.35 (2.50)	FAILURE	0.122 (0.048)	0.503 (0.198)	0.24	330 (47.8)	295 (72)	AIR	FAIL MODE
1A-4	0.231 (0.091)	6.35 (2.50)	FAILURE	0.102 (0.040)	0.381 (0.150)	0.27	359 (52.1)	295 (72)	AIR	FAIL MODE
1A-5	0.229 (0.090)	6.35 (2.50)	FAILURE	0.114 (0.045)	0.516 (0.203)	0.22	328 (47.6)	295 (72)	AIR	FAIL MODE
1A-9	0.234 (0.092)	6.35 (2.50)	FAILURE	0.089 (0.035)	0.775 (0.305)	0.11	345 (50.1)	295 (72)	AIR	FAIL MODE
1A-10	0.234 (0.092)	6.35 (2.50)	FAILURE	0.157 (0.062)	0.399 (0.157)	0.40	350 (50.7)	295 (72)	AIR	FAIL MODE
1AW-13	0.234 (0.092)	6.35 (2.50)	FAILURE	0.180 (0.071)	0.940 (0.370)	0.19	285 (41.3)	295 (72)	AIR	FAIL MODE
M1A-1	0.236 (0.093)	6.35 (2.50)	FAILURE	0.135 (0.053)	0.737 (0.290)	0.18	319 (46.3)	295 (72)	AIR	FAIL MODE
M1A-2	0.231 (0.091)	12.70 (5.00)	FAILURE	0.142 (0.056)	0.737 (0.290)	0.19	312 (45.3)	295 (72)	AIR	FAIL MODE

Table 26: *Uniaxial Static Fracture Tests of 0.23 cm (0.090 Inch) Thick Surface Flawed 2219-T62 Aluminum Base Metal at 78°K (-320°F)*

SPECIMEN NUMBER	ORIGINAL THICKNESS, t cm (INCH)	ORIGINAL WIDTH, W cm (INCH)	TEST PARAMETERS AT		CRACK DEPTH, a cm (INCH)	CRACK LENGTH, 2c cm (INCH)	CRACK SHAPE, a/2c	STRESS, σ MN/m² (KSI)	TEST: TEMPERATURE, T °K (°F)	TEST: ENVIRONMENT	REMARKS
1A-6	0.229 (0.090)	6.35 (2.50)	SIZING	START	0.051 (0.020)	0.231 (0.091)	0.22	–	295 (72)	AIR	NO CRACK GROWTH
				STOP	0.051 (0.020)	0.231 (0.091)	0.22	332 (48.2)	295 (72)	AIR	
			FAILURE		0.051 (0.020)	0.231 (0.091)	0.22	505 (73.3)	78 (-320)	LN_2	FAIL MODE
1A-7	0.229 (0.090)	6.35 (2.50)	SIZING	START	0.107 (0.042)	0.488 (0.192)	0.22	–	295 (72)	AIR	Δa = 0.015 cm (0.006 INCH)
				STOP	0.122 (0.048)	0.488 (0.192)	0.25	332 (48.2)	295 (72)	AIR	
			FAILURE		0.122 (0.048)	0.488 (0.192)	0.25	447 (64.8)	78 (-320)	LN_2	FAIL MODE
1A-15	0.236 (0.093)	6.35 (2.50)	SIZING	START	0.079 (0.031)	0.762 (0.300)	0.10	–	295 (72)	AIR	NO CRACK GROWTH
				STOP	0.079 (0.031)	0.762 (0.300)	0.10	332 (48.2)	295 (72)	AIR	
			FAILURE		0.079 (0.031)	0.762 (0.300)	0.10	442 (64.1)	78 (-320)	LN_2	FAIL MODE
1A-16	0.234 (0.092)	6.35 (2.50)	SIZING	START	0.145 (0.057)	0.396 (0.156)	0.37	–	295 (72)	AIR	NO CRACK GROWTH
				STOP	0.145 (0.057)	0.396 (0.156)	0.37	332 (48.2)	295 (72)	AIR	
			FAILURE		0.145 (0.057)	0.396 (0.156)	0.37	447 (64.8)	78 (-320)	LN_2	FAIL MODE

Table 27: Uniaxial Static Fracture Tests of 0.23 cm (0.090 Inch) Thick Surface Flawed 2219-T62 Aluminum Weld Metal ℄ [1]

SPECIMEN NUMBER	ORIGINAL THICKNESS, t cm (INCH)	ORIGINAL WIDTH, W cm (INCH)	TEST PARAMETERS AT		CRACK DEPTH, a cm (INCH)	CRACK LENGTH, 2c cm (INCH)	CRACK SHAPE, a/2c	STRESS, σ MN/m² (KSI)	TEST: TEMPERATURE, T °K (°F)	TEST: ENVIRONMENT	REMARKS
1AW-1	0.236 (0.093)	6.35 (2.50)	FAILURE		0.112 (0.044)	0.488 (0.192)	0.23	312 (45.3)	295 (72)	AIR	FAIL MODE
1AW-2	0.236 (0.093)	6.35 (2.50)	FAILURE		0.104 (0.041)	0.376 (0.148)	0.28	341 (49.4)	295 (72)	AIR	FAIL MODE
[2] 1AW-3	0.234 (0.092)	6.35 (2.50)	FAILURE		0.123 (0.048)	0.490 (0.193)	0.25	330 (47.8)	295 (72)	AIR	FAIL MODE
[3] 1AW-4	0.234 (0.092)	6.35 (2.50)	FAILURE		0.117 (0.046)	0.498 (0.196)	0.23	330 (47.8)	295 (72)	AIR	FAIL MODE
1AW-5	0.221 (0.087)	6.35 (2.50)	FAILURE		0.058 (0.023)	0.323 (0.127)	0.18	361 (52.4)	295 (72)	AIR	FAIL MODE
1AW-6	0.226 (0.089)	6.35 (2.50)	FAILURE		0.170 (0.067)	0.876 (0.345)	0.19	270 (39.1)	295 (72)	AIR	FAIL MODE
1AW-7	0.236 (0.093)	6.35 (2.50)	FAILURE		0.058 (0.023)	0.660 (0.260)	0.09	336 (48.7)	295 (72)	AIR	FAIL MODE
1AW-9	0.229 (0.090)	6.35 (2.50)	FAILURE		0.099 (0.039)	0.290 (0.114)	0.34	346 (50.2)	295 (72)	AIR	FAIL MODE
1AW-11	0.234 (0.092)	6.35 (2.50)	FAILURE		0.107 (0.042)	0.490 (0.193)	0.22	323 (46.9)	295 (72)	AIR	FAIL MODE
1AW-14	0.231 (0.091)	6.35 (2.50)	FAILURE		0.086 (0.034)	0.381 (0.150)	0.23	332 (48.1)	295 (72)	AIR	FAIL MODE
1AW-8	0.231 (0.091)	6.35 (2.50)	SIZING	START	0.081 (0.032)	0.376 (0.148)	0.22	–	295 (72)	AIR	NO CRACK GROWTH
				STOP	0.081 (0.032)	0.376 (0.148)	0.22	332 (48.2)	295 (72)	AIR	
			FAILURE		0.081 (0.032)	0.376 (0.148)	0.22	415 (61.2)	78 (-320)	LN_2	FAIL MODE
1AW-10	0.226 (0.089)	6.35 (2.50)	SIZING	START	0.051 (0.020)	0.231 (0.091)	0.22	–	295 (72)	AIR	NO CRACK GROWTH
				STOP	0.051 (0.020)	0.231 (0.091)	0.22	332 (48.2)	295 (72)	AIR	
			FAILURE		0.051 (0.020)	0.231 (0.091)	0.22	470 (68.2)	78 (-320)	LN_2	FAIL MODE

[1] UNLESS NOTED OTHERWISE
[2] CRACK IN WELD HAZ
[3] CRACK IN WELD FUSION LINE

Table 28: Uniaxial Static Fracture Tests of 0.46 cm (0.18 Inch) Thick Surface Flawed 2219-T62 Aluminum Base Metal

SPECIMEN NUMBER	ORIGINAL THICKNESS, t cm (INCH)	ORIGINAL WIDTH, W cm (INCH)	TEST PARAMETERS AT		CRACK DEPTH, a cm (INCH)	CRACK LENGTH, 2c cm (INCH)	CRACK SHAPE, a/2c	STRESS, σ MN/m² (KSI)	TEST TEMPERATURE, T °K (°F)	TEST ENVIRONMENT	REMARKS
2A-1	0.462 (0.182)	12.70 (5.00)	FAILURE		0.249 (0.098)	1.262 (0.497)	0.20	322 (46.7)	295 (72)	AIR	FAIL MODE
2A-2	0.460 (0.181)	12.70 (5.00)	FAILURE		0.157 (0.062)	0.737 (0.290)	0.21	380 (55.1)	295 (72)	AIR	FAIL MODE
2AW-17	0.460 (0.181)	12.70 (5.00)	FAILURE		0.213 (0.084)	1.041 (0.410)	0.20	328 (47.5)	295 (72)	AIR	FAIL MODE
2A-3	0.460 (0.181)	12.70 (5.00)	SIZING	START	0.140 (0.055)	0.622 (0.245)	0.22	–	295 (72)	AIR	NO CRACK GROWTH
				STOP	0.140 (0.055)	0.622 (0.245)	0.22	332 (48.2)	295 (72)	AIR	
			FAILURE		0.140 (0.055)	0.622 (0.245)	0.22	457 (66.3)	78 (-320)	LN_2	FAIL MODE
2A-6	0.460 (0.181)	12.70 (5.00)	SIZING	START	0.203 (0.080)	1.011 (0.398)	0.20	–	295 (72)	AIR	Δa = 0.030 cm (0.012 INCH)
				STOP	0.234 (0.092)	1.011 (0.398)	0.23	332 (48.2)	295 (72)	AIR	
			FAILURE		0.234 (0.092)	1.011 (0.398)	0.23	425 (61.6)	78 (-320)	LN_2	FAIL MODE

Table 29: Uniaxial Static Fracture Tests of 0.46 cm (0.18 Inch) Thick Surface Flawed 2219-T62 Aluminum Weld Metal ℄

SPECIMEN NUMBER	ORIGINAL THICKNESS, t cm (INCH)	ORIGINAL WIDTH, W cm (INCH)	TEST PARAMETERS AT		CRACK DEPTH, a cm (INCH)	CRACK LENGTH, 2c cm (INCH)	CRACK SHAPE a/2c	STRESS, σ MN/m² (KSI)	TEST TEMPERATURE, T °K (°F)	TEST ENVIRONMENT	REMARKS
2AW-1	0.455 (0.179)	12.70 (5.00)	FAILURE		0.152 (0.060)	0.737 (0.290)	0.21	321 (46.5)	295 (72)	AIR	FAIL MODE
2AW-2	0.450 (0.177)	12.70 (5.00)	FAILURE		0.094 (0.037)	0.396 (0.156)	0.24	392 (56.9)	295 (72)	AIR	FAIL MODE
2AW-3	0.457 (0.180)	12.70 (5.00)	SIZING	START	0.076 (0.030)	0.300 (0.118)	0.25	–	295 (72)	AIR	NO CRACK GROWTH
				STOP	0.076 (0.030)	0.300 (0.118)	0.25	332 (48.2)	295 (72)	AIR	
			FAILURE		0.076 (0.030)	0.300 (0.118)	0.25	470 (68.1)	78 (-320)	LN_2	FAIL MODE
2AW-14	0.460 (0.181)	12.70 (5.00)	SIZING	START	0.135 (0.053)	0.617 (0.243)	0.22	–	295 (72)	AIR	Δa = 0.020 cm (0.008 INCH)
				STOP	0.155 (0.061)	0.617 (0.243)	0.25	332 (48.2)	295 (72)	AIR	
			FAILURE		0.155 (0.061)	0.617 (0.243)	0.25	434 (63.0)	78 (-320)	LN_2	FAIL MODE

Table 30: Uniaxial Cyclic Tests of 0.23 cm (0.090 Inch) Thick Surface Flawed 2219-T62 Aluminum Base Metal at 295^{o}K (72^{o}F)

SPECIMEN NUMBER	ORIGINAL THICKNESS, t cm (INCH)	ORIGINAL WIDTH, W cm (INCH)	TEST PARAMETERS AT		CRACK DEPTH, a cm (INCH)	CRACK LENGTH, 2c cm (INCH)	CRACK SHAPE, a/2c	STRESS, σ MN/m^2 (KSI)	TEST TEMPERATURE, T ^{o}K (^{o}F)	TEST ENVIRONMENT	REMARKS
1A-8	0.224 (0.088)	6.35 (2.50)	SIZING	START	0.117 (0.046)	0.495 (0.195)	0.24	–	295 (72)	AIR	655 CYCLES TO BREAKTHROUGH
				STOP	0.137 (0.054)	0.495 (0.195)	0.28	332 (48.2)	295 (72)	AIR	
			CYCLING	START	0.137 (0.054)	0.495 (0.195)	0.28	282 (40.9)	295 (72)	AIR	
				STOP	0.224 (0.088)	0.693 (0.273)	0.32	282 (40.9)	295 (72)	AIR	
1A-11	0.234 (0.092)	6.35 (2.50)	SIZING	START	0.104 (0.041)	0.483 (0.190)	0.22	–	295 (72)	AIR	2112 CYCLES TO BREAKTHROUGH
				STOP	0.114 (0.045)	0.483 (0.190)	0.24	332 (48.2)	295 (72)	AIR	
			CYCLING	START	0.114 (0.045)	0.483 (0.190)	0.24	249 (36.1)	295 (72)	AIR	
				STOP	0.234 (0.092)	0.719 (0.283)	0.33	249 (36.1)	295 (72)	AIR	
1A-14	0.234 (0.092)	6.35 (2.50)	SIZING	START	0.053 (0.021)	0.259 (0.102)	0.21	–	295 (72)	AIR	6718 CYCLES TO BREAKTHROUGH
				STOP	0.053 (0.021)	0.259 (0.102)	0.21	332 (48.2)	295 (72)	AIR	
			CYCLING	START	0.053) (0.021)	0.259 (0.102)	0.21	249 (36.1)	295 (72)	AIR	
				STOP	0.234 (0.092)	0.719 (0.283)	0.33	249 (36.1)	295 (72)	AIR	
1A-17	0.234 (0.092)	6.35 (2.50)	SIZING	START	0.102 (0.040)	0.483 (0.190)	0.21	–	295 (72)	AIR	9787 CYCLES TO BREAKTHROUGH
				STOP	0.140 (0.055)	0.483 (0.190)	0.29	332 (48.2)	295 (72)	AIR	
			CYCLING	START	0.140 (0.055)	0.483 (0.190)	0.29	199 (28.9)	295 (72)	AIR	
				STOP	0.234 (0.092)	0.752 (0.296)	0.31	199 (28.9)	295 (72)	AIR	
1A-18	0.231 (0.091)	6.35 (2.50)	SIZING	START	0.053 (0.021)	0.231 (0.091)	0.23	–	295 (72)	AIR	SPECIMEN FAILED ON 7802 CYCLE-MACHINE MALFUNCTION
				STOP	0.053 (0.021)	0.231 (0.091)	0.23	332 (48.2)	295 (72)	AIR	
			CYCLING	START	0.053 (0.021)	0.231 (0.091)	0.23	249 (36.1)	295 (72)	AIR	
				STOP	0.147 (0.058)	0.356 (0.140)	0.41	249 (36.1)	295 (72)	AIR	
1A-19	0.234 (0.092)	6.35 (2.50)	SIZING	START	0.104 (0.041)	0.493 (0.194)	0.21	–	295 (72)	AIR	31 CYCLES TO BREAKTHROUGH
				STOP	[1]	[1]	–	332 (48.2)	295 (72)	AIR	
			CYCLING	START	[1]	[1]	–	332 (48.2)	295 (72)	AIR	
				STOP	6.35 (0.092)	0.775 (0.305)	0.30	332 (48.2)	295 (72)	AIR	
1A-20	0.236 (0.093)	6.35 (2.50)	SIZING	START	0.091 (0.036)	0.381 (0.150)	0.24	–	295 (72)	AIR	4084 CYCLES TO BREAKTHROUGH
				STOP	0.091 (0.036)	0.381 (0.150)	0.24	332 (48.2)	295 (72)	AIR	
			CYCLING	START	0.091 (0.036)	0.381 (0.150)	0.24	249 (36.1)	295 (72)	AIR	
				STOP	0.236 (0.093)	0.660 (0.260)	0.36	249 (36.1)	295 (72)	AIR	
[2] 1A-27	0.226 (0.089)	6.35 (2.50)	SIZING	START	0.076 (0.030)	0.381 (0.150)	0.20	–	295 (72)	AIR	3122 CYCLES TO BREAKTHROUGH
				STOP	0.089 (0.035)	0.381 (0.150)	0.23	332 (48.2)	295 (72)	AIR	
			CYCLING	START	0.089 (0.035)	0.381 (0.150)	0.23	249 (36.1)	295 (72)	AIR	
				STOP	0.226 (0.089)	0.706 (0.278)	0.32	249 (36.1)	295 (72)	AIR	

[1] NOT DISTINGUISHABLE

[2] RESIN IMPREGNATED CRACK

Table 31: Uniaxial Cyclic Tests of 0.23 cm (0.090 Inch) Thick Surface Flawed 2219-T62 Aluminum Base Metal at 78°K (-320°F)

SPECIMEN NUMBER	ORIGINAL THICKNESS, t cm (INCH)	ORIGINAL WIDTH, W cm (INCH)	TEST PARAMETERS AT		CRACK DEPTH, a cm (INCH)	CRACK LENGTH, 2c cm (INCH)	CRACK SHAPE a/2c	STRESS, σ MN/m² (KSI)	TEST: TEMPERATURE, T °K (°F)	TEST: ENVIRONMENT	REMARKS
1A-12	0.231 (0.091)	6.35 (2.50)	SIZING	START	0.117 (0.046)	0.503 (0.198)	0.23	–	295 (72)	AIR	12,210 CYCLES TO BREAK-THROUGH
				STOP	0.142 (0.056)	0.513 (0.202)	0.28	332 (48.2)	295 (72)	AIR	
			PROOF	START	0.142 (0.056)	0.513 (0.202)	0.28	–	78 (-320)	LN_2	
				STOP	0.142 (0.056)	0.513 (0.202)	0.28	381 (55.2)	78 (-320)	LN_2	
			CYCLING	START	0.142 (0.056)	0.513 (0.202)	0.28	229 (33.2)	78 (-320)	LN_2	
				STOP	0.231 (0.091)	0.693 (0.273)	0.33	229 (33.2)	78 (-320)	LN_2	
1A-13	0.234 (0.092)	6.35 (2.50)	SIZING	START	0.107 (0.042)	0.478 (0.188)	0.22	–	295 (72)	AIR	2943 CYCLES TO BREAK-THROUGH
				STOP	0.123 (0.048)	0.478 (0.188)	0.26	332 (48.2)	295 (72)	AIR	
			PROOF	START	0.123 (0.048)	0.478 (0.188)	0.26	–	78 (-320)	LN_2	
				STOP	0.123 (0.048)	0.478 (0.188)	0.26	381 (55.2)	78 (-320)	LN_2	
			CYCLING	START	0.123 (0.048)	0.478 (0.188)	0.26	323 (46.8)	78 (-320)	LN_2	
				STOP	0.234 (0.092)	[1]	–	323 (46.8)	78 (-320)	LN_2	
1A-21	0.234 (0.092)	6.35 (2.50)	SIZING	START	0.097 (0.038)	0.483 (0.190)	0.20	–	295 (72)	AIR	865 CYCLES TO BREAKTHROUGH
				STOP	0.114 (0.045)	0.483 (0.190)	0.24	332 (48.2)	295 (72)	AIR	
			PROOF	START	0.114 (0.045)	0.483 (0.190)	0.24	–	78 (-320)	LN_2	
				STOP	0.114 (0.045)	0.483 (0.190)	0.24	381 (55.2)	78 (-320)	LN_2	
			CYCLING	START	0.114 (0.045)	0.483 (0.190)	0.24	381 (55.2)	78 (-320)	LN_2	
				STOP	0.234 (0.092)	< 0.851 (0.335) [2]	> 0.27	381 (55.2)	78 (-320)	LN_2	
1A-22	0.229 (0.090)	6.35 (2.50)	SIZING	START	0.053 (0.021)	0.259 (0.102)	0.21	–	295 (72)	AIR	8025 CYCLES TO BREAKTHROUGH
				STOP	0.056 (0.022)	0.259 (0.102)	0.22	332 (48.2)	295 (72)	AIR	
			PROOF	START	0.056 (0.022)	0.259 (0.102)	0.22	–	78 (-320)	LN_2	
				STOP	0.056 (0.022)	0.259 (0.102)	0.22	381 (55.2)	78 (-320)	LN_2	
			CYCLING	START	0.056 (0.022)	0.259 (0.102)	0.22	323 (46.8)	78 (-320)	LN_2	
				STOP	0.229 (0.090)	0.472 (0.186)	0.48	323 (46.8)	78 (-320)	LN_2	
1A-23	0.231 (0.091)	6.35 (2.50)	SIZING	START	0.119 (0.047)	0.523 (0.206)	0.23	–	295 (72)	AIR	1557 CYCLES TO BREAKTHROUGH
				STOP	0.168 (0.066)	0.635 (0.250)	0.26	332 (48.2)	295 (72)	AIR	
			PROOF	START	0.168 (0.066)	0.635 (0.250)	0.26	–	78 (-320)	LN_2	
				STOP	0.168 (0.066)	0.635 (0.250)	0.26	381 (55.2)	78 (-320)	LN_2	
			CYCLING	START	0.168 (0.066)	0.635 (0.250)	0.26	285 (41.3)	78 (-320)	LN_2	
				STOP	0.231 (0.091)	0.719 (0.283)	0.32	285 (41.3)	78 (-320)	LN_2	
1A-24	0.234 (0.092)	6.35 (2.50)	SIZING	START	0.102 (0.040)	0.427 (0.168)	0.24	–	295 (72)	AIR	2468 CYCLES TO BREAKTHROUGH
				STOP	0.107 (0.042)	0.427 (0.168)	0.25	332 (48.2)	295 (72)	AIR	
			PROOF	START	0.107 (0.042)	0.427 (0.168)	0.25	–	78 (-320)	LN_2	
				STOP	0.107 (0.042)	0.427 (0.168)	0.25	381 (55.2)	78 (-320)	LN_2	
			CYCLING	START	0.107 (0.042)	0.427 (0.168)	0.25	323 (46.8)	78 (-320)	LN_2	
				STOP	0.234 (0.092)	0.630 (0.248)	0.37	323 (46.8)	78 (-320)	LN_2	
1A-26	0.234 (0.092)	6.35 (2.50)	SIZING	START	0.074 (0.029)	0.368 (0.145)	0.20	–	295 (72)	AIR	4583 CYCLES TO BREAKTHROUGH
				STOP	0.089 (0.035)	0.368 (0.145)	0.24	332 (48.2)	295 (72)	AIR	
			PROOF	START	0.089 (0.035)	0.368 (0.145)	0.24	–	78 (-320)	LN_2	
				STOP	0.089 (0.035)	0.368 (0.145)	0.24	381 (55.2)	78 (-320)	LN_2	
			CYCLING	START	0.089 (0.035)	0.368 (0.145)	0.24	323 (46.8)	78 (-320)	LN_2	
				STOP	0.234 (0.092)	0.615 (0.242)	0.38	323 (46.8)	78 (-320)	LN_2	

[1] SPECIMEN WAS CYCLED FOR 715 CYCLES AFTER BREAKTHROUGH

[2] SPECIMEN WAS CYCLED FOR 130 CYCLES AFTER BREAKTHROUGH

Table 32: Uniaxial Cyclic Tests of 0.23 cm (0.090 Inch) Thick Surface Flawed 2219-T62 Aluminum Weld Metal ℄ at 295°K (72°F)

SPECIMEN NUMBER	ORIGINAL THICKNESS, t cm (INCH)	ORIGINAL WIDTH, W cm (INCH)	TEST PARAMETERS AT		CRACK DEPTH, a cm (INCH)	CRACK LENGTH, 2c cm (INCH)	CRACK SHAPE a/2c	STRESS, σ MN/m² (KSI)	TEST: TEMPERATURE, T °K (°F)	TEST: ENVIRONMENT	REMARKS
1AW-12	0.231 (0.091)	6.35 (2.50)	SIZING	START	0.081 (0.032)	0.361 (0.142)	0.23	–	295 (72)	AIR	1168 CYCLES TO BREAK-THROUGH
				STOP	0.089 (0.035)	0.361 (0.142)	0.25	332 (48.2)	295 (72)	AIR	
			CYCLING	START	0.089 (0.035)	0.361 (0.142)	0.25	282 (40.9)	295 (72)	AIR	
				STOP	0.231 (0.091)	0.589 (0.232)	0.39	282 (40.9)	295 (72)	AIR	
1AW-15	0.229 (0.090)	6.35 (2.50)	SIZING	START	0.079 (0.031)	0.356 (0.140)	0.22	–	295 (72)	AIR	2353 CYCLES TO BREAK-THROUGH
				STOP	0.099 (0.039)	0.356 (0.140)	0.28	332 (48.2)	295 (72)	AIR	
			CYCLING	START	0.099 (0.039)	0.356 (0.140)	0.28	249 (36.1)	295 (72)	AIR	
				STOP	0.229 (0.090)	0.640 (0.252)	0.36	249 (36.1)	295 (72)	AIR	
1AW-17	0.231 (0.091)	6.35 (2.50)	SIZING	START	0.051 (0.020)	0.198 (0.078)	0.26	–	295 (72)	AIR	4220 CYCLES TO BREAK-THROUGH
				STOP	0.051 (0.020)	0.198 (0.078)	0.26	332 (48.2)	295 (72)	AIR	
			CYCLING	START	0.051 (0.020)	0.198 (0.078)	0.26	282 (40.9)	295 (72)	AIR	
				STOP	0.231 (0.091)	0.538 (0.212)	0.43	282 (40.9)	295 (72)	AIR	
1AW-18	0.234 (0.092)	6.35 (2.50)	SIZING	START	0.076 (0.030)	0.356 (0.140)	0.21	–	295 (72)	AIR	332 CYCLES TO BREAK-THROUGH
				STOP	0.076 (0.030)	0.356 (0.140)	0.21	332 (48.2)	295 (72)	AIR	
			CYCLING	START	0.076 (0.030)	0.356 (0.140)	0.21	332 (48.2)	295 (72)	AIR	
				STOP	0.234 (0.092)	0.635 (0.250)	0.37	332 (48.2)	295 (72)	AIR	
1AW-23	0.226 (0.089)	6.35 (2.50)	SIZING	START	0.038 (0.015)	0.152 (0.060)	0.25	–	295 (72)	AIR	5316 CYCLES TO BREAK-THROUGH
				STOP	0.038 (0.015)	0.152 (0.060)	0.25	332 (48.2)	295 (72)	AIR	
			CYCLING	START	0.038 (0.015)	0.152 (0.060)	0.25	282 (40.9)	295 (72)	AIR	
				STOP	0.226 (0.089)	0.508 (0.200)	0.44	282 (40.9)	295 (72)	AIR	
[1] 1AW-24	0.229 (0.090)	6.35 (2.50)	SIZING	START	0.067 (0.027)	0.333 (0.131)	0.21	–	295 (72)	AIR	1436 CYCLES TO BREAK-THROUGH
				STOP	0.084 (0.033)	0.333 (0.131)	0.25	332 (48.2)	295 (72)	AIR	
			CYCLING	START	0.084 (0.033)	0.333 (0.131)	0.25	282 (40.9)	295 (72)	AIR	
				STOP	0.229 (0.090)	0.559 (0.220)	0.41	282 (40.9)	295 (72)	AIR	
1AW-25	0.231 (0.091)	6.35 (2.50)	SIZING	START	0.067 (0.027)	0.363 (0.143)	0.19	–	295 (72)	AIR	10,257 CYCLES TO BREAK-THROUGH
				STOP	0.071 (0.028)	0.363 (0.143)	0.20	314 (45.6)	295 (72)	AIR	
			CYCLING	START	0.071 (0.028)	0.363 (0.143)	0.20	199 (28.9)	295 (72)	AIR	
				STOP	0.231 (0.091)	0.607 (0.239)	0.38	199 (28.9)	295 (72)	AIR	

[1] RESIN IMPREGNATED CRACK

Table 33: Uniaxial Cyclic Tests of 0.23 cm (0.090 Inch) Thick Surface Flawed 2219-T62 Aluminum Weld Metal ℄ at 78°K (-320°F)

SPECIMEN NUMBER	ORIGINAL THICKNESS, t cm (INCH)	ORIGINAL WIDTH, W cm (INCH)	TEST PARAMETERS AT		CRACK DEPTH, a cm (INCH)	CRACK LENGTH, 2c cm (INCH)	CRACK SHAPE, a/2c	STRESS, σ MN/m^2 (KSI)	TEST: TEMPERATURE, T °K (°F)	TEST: ENVIRONMENT	REMARKS
1AW-16	0.231 (0.091)	6.35 (2.50)	SIZING	START	0.076 (0.030)	0.356 (0.140)	0.21	–	295 (72)	AIR	2628 CYCLES TO BREAK-THROUGH
				STOP	0.089 (0.035)	0.356 (0.140)	0.25	332 (48.2)	295 (72)	AIR	
			PROOF	START	0.089 (0.035)	0.356 (0.140)	0.25	–	78 (-320)	LN_2	
				STOP	0.089 (0.035)	0.356 (0.140)	0.25	381 (55.2)	78 (-320)	LN_2	
			CYCLING	START	0.089 (0.035)	0.356 (0.140)	0.25	323 (46.8)	78 (-320)	LN_2	
				STOP	0.231 (0.091)	0.579 (0.228)	0.40	323 (46.8)	78 (-320)	LN_2	
1AW-19	0.229 (0.090)	6.35 (2.50)	SIZING	START	0.086 (0.034)	0.371 (0.146)	0.23	–	295 (72)	AIR	527 CYCLES TO BREAK-THROUGH
				STOP	0.097 (0.038)	0.371 (0.146)	0.26	332 (48.2)	295 (72)	AIR	
			PROOF	START	0.097 (0.038)	0.371 (0.146)	0.26	–	78 (-320)	LN_2	
				STOP	0.097 (0.038)	0.371 (0.146)	0.26	381 (55.2)	78 (-320)	LN_2	
			CYCLING	START	0.097 (0.038)	0.371 (0.146)	0.26	381 (55.2)	78 (-320)	LN_2	
				STOP	0.229 (0.090)	0.660 (0.260)	0.35	381 (55.2)	78 (-320)	LN_2	
1AW-20	0.236 (0.093)	6.35 (2.50)	SIZING	START	0.086 (0.034)	0.371 (0.146)	0.23	–	295 (72)	AIR	4817 CYCLES TO BREAK-THROUGH
				STOP	0.107 (0.042)	0.371 (0.146)	0.29	332 (48.2)	295 (72)	AIR	
			PROOF	START	0.107 (0.042)	0.371 (0.146)	0.29	–	78 (-320)	LN_2	
				STOP	0.107 (0.042)	0.371 (0.146)	0.29	381 (55.2)	78 (-320)	LN_2	
			CYCLING	START	0.107 (0.042)	0.371 (0.146)	0.29	285 (41.3)	78 (-320)	LN_2	
				STOP	0.236 (0.093)	0.640 (0.252)	0.37	285 (41.3)	78 (-320)	LN_2	
1AW-22	0.234 (0.092)	6.35 (2.50)	SIZING	START	0.069 (0.027)	0.287 (0.113)	0.24	–	295 (72)	AIR	4491 CYCLES TO BREAK-THROUGH
				STOP	0.081 (0.032)	0.287 (0.113)	0.28	332 (48.2)	295 (72)	AIR	
			PROOF	START	0.081 (0.032)	0.287 (0.113)	0.28	–	78 (-320)	LN_2	
				STOP	0.081 (0.032)	0.287 (0.113)	0.28	381 (55.2)	78 (-320)	LN_2	
			CYCLING	START	0.081 (0.032)	0.287 (0.113)	0.28	323 (46.8)	78 (-320)	LN_2	
				STOP	0.234 (0.092)	0.589 (0.232)	0.40	323 (46.8)	78 (-320)	LN_2	
1AW-26	0.231 (0.091)	6.35 (2.50)	SIZING	START	0.058 (0.023)	0.231 (0.091)	0.25	–	295 (72)	AIR	5330 CYCLES TO BREAK-THROUGH
				STOP	0.058 (0.023)	0.231 (0.091)	0.25	332 (48.2)	295 (72)	AIR	
			PROOF	START	0.058 (0.023)	0.231 (0.091)	0.25	–	78 (-320)	LN_2	
				STOP	0.058 (0.023)	0.231 (0.091)	0.25	381 (55.2)	78 (-320)	LN_2	
			CYCLING	START	0.058 (0.023)	0.231 (0.091)	0.25	323 (46.8)	78 (-320)	LN_2	
				STOP	0.231 (0.091)	0.559 (0.220)	0.41	323 (46.8)	78 (-320)	LN_2	

Table 34: Uniaxial Cyclic Tests of 0.46 cm (0.18 Inch) Thick Surface Flawed 2219-T62 Aluminum Base Metal at 295°K (72°F)

SPECIMEN NUMBER	ORIGINAL THICKNESS, t cm (INCH)	ORIGINAL WIDTH, W cm (INCH)	TEST PARAMETERS AT		CRACK DEPTH, a cm (INCH)	CRACK LENGTH, 2c cm (INCH)	CRACK SHAPE a/2c	STRESS, σ MN/m^2 (KSI)	TEST TEMPERATURE, T °K (°F)	TEST ENVIRONMENT	REMARKS
2A-5	0.457 (0.180)	12.70 (5.00)	SIZING	START	0.102 (0.040)	0.404 (0.159)	0.25	–	295 (72)	AIR	3785 CYCLES TO BREAK-THROUGH
				STOP	0.104 (0.041)	0.404 (0.159)	0.26	332 (48.2)	295 (72)	AIR	
			CYCLING	START	0.104 (0.041)	0.404 (0.159)	0.26	282 (40.9)	295 (72)	AIR	
				STOP	0.457 (0.180)	1.214 (0.478)	0.38	282 (40.9)	295 (72)	AIR	
2A-7	0.462 (0.182)	12.70 (5.00)	SIZING	START	0.208 (0.082)	1.016 (0.400)	0.21	–	295 (72)	AIR	460 CYCLES TO BREAK-THROUGH
				STOP	0.221 (0.087)	1.016 (0.400)	0.22	332 (48.2)	295 (72)	AIR	
			CYCLING	START	0.221 (0.087)	1.016 (0.400)	0.22	332 (48.2)	295 (72)	AIR	
				STOP	0.462 (0.182)	1.753 (0.690)	0.26	332 (48.2)	295 (72)	AIR	
2A-8	0.455 (0.179)	12.70 (5.00)	SIZING	START	0.201 (0.079)	1.016 (0.400)	0.20	–	295 (72)	AIR	757 CYCLES TO BREAK-THROUGH
				STOP	0.241 (0.095)	1.016 (0.400)	0.23	332 (48.2)	295 (72)	AIR	
			CYCLING	START	0.241 (0.095)	1.016 (0.400)	0.23	282 (40.9)	295 (72)	AIR	
				STOP	0.455 (0.179)	1.478 (0.582)	0.31	282 (40.9)	295 (72)	AIR	
2A-12	0.457 (0.180)	12.70 (5.00)	SIZING	START	0.201 (0.079)	1.034 (0.407)	0.19	–	295 (72)	AIR	5495 CYCLES TO BREAK-THROUGH
				STOP	0.213 (0.084)	1.034 (0.407)	0.21	332 (48.2)	295 (72)	AIR	
			CYCLING	START	0.213 (0.084)	1.034 (0.407)	0.21	199 (28.9)	295 (72)	AIR	
				STOP	0.457 (0.180)	1.524 (0.600)	0.30	199 (28.9)	295 (72)	AIR	
2A-15	0.460 (0.181)	12.70 (5.00)	SIZING	START	0.152 (0.060)	0.625 (0.246)	0.24	–	295 (72)	AIR	3054 CYCLES TO BREAK-THROUGH
				STOP	0.152 (0.060)	0.625 (0.246)	0.24	332 (48.2)	295 (72)	AIR	
			CYCLING	START	0.152 (0.060)	0.625 (0.246)	0.24	282 (40.9)	295 (72)	AIR	
				STOP	0.460 (0.181)	1.359 (0.535)	0.34	282 (40.9)	295 (72)	AIR	
2AW-16	0.460 (0.181)	12.70 (5.00)	SIZING	START	0.132 (0.052)	0.653 (0.257)	0.20	–	295 (72)	AIR	3384 CYCLES TO BREAK-THROUGH
				STOP	0.140 (0.055)	0.653 (0.257)	0.21	332 (48.2)	295 (72)	AIR	
			CYCLING	START	0.140 (0.055)	0.653 (0.257)	0.21	282 (40.9)	295 (72)	AIR	
				STOP	0.460 (0.181)	1.270 (0.500)	0.36	282 (40.9)	295 (72)	AIR	
2AW-18	0.462 (0.182)	12.70 (5.00)	SIZING	START	0.191 (0.075)	1.049 (0.413)	0.18	–	295 (72)	AIR	2480 CYCLES TO BREAK-THROUGH
				STOP	0.201 (0.079)	1.049 (0.413)	0.19	327 47.4	295 (72)	AIR	
			CYCLING	START	0.201 (0.079)	1.049 (0.413)	0.19	282 40.9	295 (72)	AIR	
				STOP	0.462 (0.182)	1.488 (0.586)	0.31	282 40.9	295 (72)	AIR	

Table 35: *Uniaxial Cyclic Tests of 0.46 cm (0.18 Inch) Thick Surface Flawed 2219-T62 Aluminum Base Metal at 78° K (-320° F)*

SPECIMEN NUMBER	ORIGINAL THICKNESS, t cm (INCH)	ORIGINAL WIDTH, W cm (INCH)	TEST PARAMETERS AT		CRACK DEPTH, a cm (INCH)	CRACK LENGTH, 2c cm (INCH)	CRACK SHAPE, a/2c	STRESS, σ MN/m^2 (KSI)	TEST: TEMPERATURE, T °K (°F)	TEST: ENVIRONMENT	REMARKS
2A-8	0.457 (0.180)	12.70 (5.00)	SIZING	START	0.208 (0.082)	1.041 (0.410)	0.20	–	295 (72)	AIR	768 CYCLES TO BREAK-THROUGH
				STOP	0.224 (0.088)	1.041 (0.410)	0.21	332 (48.2)	295 (72)	AIR	
			PROOF	START	0.224 (0.088)	1.041 (0.410)	0.21	–	78 (-320)	LN_2	
				STOP	0.224 (0.088)	1.041 (0.410)	0.21	381 (55.2)	78 (-320)	LN_2	
			CYCLING	START	0.224 (0.088)	1.041 (0.410)	0.21	381 (55.2)	78 (-320)	LN_2	
				STOP	0.457 (0.180)	1.516 (0.597)	0.30	381 (55.2)	78 (-320)	LN_2	
2A-11	0.462 (0.182)	12.70 (5.00)	SIZING	START	0.193 (0.076)	1.034 (0.407)	0.19	–	295 (72)	AIR	2974 CYCLES TO BREAK-THROUGH
				STOP	0.218 (0.086)	1.034 (0.407)	0.21	332 (48.2)	295 (72)	AIR	
			PROOF	START	0.218 (0.086)	1.034 (0.407)	0.21	–	78 (-320)	LN_2	
				STOP	0.218 (0.086)	1.034 (0.407)	0.21	381 (55.2)	78 (-320)	LN_2	
			CYCLING	START	0.218 (0.086)	1.034 (0.407)	0.21	323 (46.8)	78 (-320)	LN_2	
				STOP	0.462 (0.182)	1.514 (0.596)	0.31	323 (46.8)	78 (-320)	LN_2	
2A-13	0.460 (0.181)	12.70 (5.00)	SIZING	START	0.208 (0.082)	1.054 (0.415)	0.20	–	295 (72)	AIR	SPECIMEN OVERSIZED, 23,658 CYCLES TO BREAK-THROUGH FLAW PERIPHERY IRREGULAR
				STOP	0.234 (0.092)	1.186 (0.467)	0.20	367 (53.2)	295 (72)	AIR	
			PROOF	START	0.234 (0.092)	1.186 (0.467)	0.20	–	78 (-320)	LN_2	
				STOP	0.234 (0.092)	1.186 (0.467)	0.20	381 (55.2)	78 (-320)	LN_2	
			CYCLING	START	0.234 (0.092)	1.186 (0.467)	0.20	228 (33.0)	78 (-320)	LN_2	
				STOP	0.460 (0.181)	1.727 (0.680)	0.27	228 (33.0)	78 (-320)	LN_2	
2A-14	0.460 (0.181)	12.70 (5.00)	SIZING	START	0.206 (0.081)	1.059 (0.417)	0.19	–	295 (72)	AIR	2870 CYCLES TO BREAK-THROUGH
				STOP	0.227 (0.090)	1.059 (0.417)	0.22	332 (48.2)	295 (72)	AIR	
			PROOF	START	0.227 (0.090)	1.059 (0.417)	0.22	–	78 (-320)	LN_2	
				STOP	0.227 (0.090)	1.059 (0.417)	0.22	381 (55.2)	78 (-320)	LN_2	
			CYCLING	START	0.227 (0.090)	1.059 (0.417)	0.22	285 (41.3)	78 (-320)	LN_2	
				STOP	0.460 (0.181)	1.478 (0.582)	0.31	285 (41.3)	78 (-320)	LN_2	
2A-16	0.460 (0.181)	12.70 (5.00)	SIZING	START	0.127 (0.050)	0.566 (0.223)	0.22	–	295 (72)	AIR	5695 CYCLES TO BREAK-THROUGH
				STOP	0.137 (0.054)	0.566 (0.223)	0.24	332 (48.2)	295 (72)	AIR	
			PROOF	START	0.137 (0.054)	0.566 (0.223)	0.24	–	78 (-320)	LN_2	
				STOP	0.137 (0.054)	0.592 (0.233)	0.24	381 (55.2)	78 (-320)	LN_2	
			CYCLING	START	0.137 (0.054)	0.592 (0.233)	0.24	323 (46.8)	78 (-320)	LN_2	
				STOP	0.460 (0.181)	1.290 (0.508)	0.36	323 (46.8)	78 (-320)	LN_2	
2A-17	0.460 (0.181)	12.70 (5.00)	SIZING	START	0.208 (0.082)	1.049 (0.413)	0.20	–	295 (72)	AIR	5032 CYCLES TO BREAK-THROUGH
				STOP	0.259 (0.102)	1.087 (0.428)	0.24	332 (48.2)	295 (72)	AIR	
			PROOF	START	0.259 (0.102)	1.087 (0.428)	0.24	–	78 (-320)	LN_2	
				STOP	0.305 (0.120)	1.232 (0.485)	0.25	381 (55.2)	78 (-320)	LN_2	
			CYCLING	START	0.305 (0.120)	1.232 (0.485)	0.25	228 (33.0)	78 (-320)	LN_2	
				STOP	0.460 (0.181)	1.544 (0.608)	0.30	228 (33.0)	78 (-320)	LN_2	
2A-18	0.457 (0.180)	12.70 (5.00)	SIZING	START	0.229 (0.090)	1.194 (0.470)	0.19	–	295 (72)	AIR	1025 CYCLES TO BREAK-THROUGH
				STOP	0.284 (0.112)	1.219 (0.480)	0.23	332 (48.2)	295 (72)	AIR	
			PROOF	START	0.284 (0.112)	1.219 (0.480)	0.23	–	78 (-320)	LN_2	
				STOP	0.284 (0.112)	1.219 (0.480)	0.23	381 (55.2)	78 (-320)	LN_2	
			CYCLING	START	0.284 (0.112)	1.219 (0.480)	0.23	323 (46.8)	78 (-320)	LN_2	
				STOP	0.457 (0.180)	1.656 (0.652)	0.28	323 (46.8)	78 (-320)	LN_2	

Table 36: Uniaxial Cyclic Tests of 0.46 cm (0.18 Inch) Thick Surface Flawed 2219-T62 Aluminum Weld Metal ℄ at 295°K (72°F)

SPECIMEN NUMBER	ORIGINAL THICKNESS, t cm (INCH)	ORIGINAL WIDTH, W cm (INCH)	TEST PARAMETERS AT		CRACK DEPTH, a cm (INCH)	CRACK LENGTH, 2c cm (INCH)	CRACK SHAPE, a/2c	STRESS, σ MN/m^2 (KSI)	TEST TEMPERATURE, T °K (°F)	TEST ENVIRONMENT	REMARKS
2AW-4	0.450 (0.177)	12.70 (5.00)	SIZING	START	0.142 (0.056)	0.643 (0.253)	0.22	–	295 (72)	AIR	238 CYCLES TO BREAK-THROUGH
				STOP	0.231 (0.091)	0.643 (0.253)	0.36	332 (48.2)	295 (72)	AIR	
			CYCLING	START	0.231 (0.091)	0.643 (0.253)	0.36	332 (48.2)	295 (72)	AIR	
				STOP	0.450 (0.177)	1.270 (0.500)	0.35	332 (48.2)	295 (72)	AIR	
2AW-5	0.460 (0.181)	12.70 (5.00)	SIZING	START	0.137 (0.054)	0.638 (0.251)	0.22	–	295 (72)	AIR	1265 CYCLES TO BREAK-THROUGH
				STOP	0.163 (0.064)	0.638 (0.251)	0.26	332 (48.2)	295 (72)	AIR	
			CYCLING	START	0.163 (0.064)	0.638 (0.251)	0.26	282 (40.9)	295 (72)	AIR	
				STOP	0.460 (0.181)	1.354 (0.533)	0.34	282 (40.9)	295 (72)	AIR	
2AW-8	0.457 (0.180)	12.70 (5.00)	SIZING	START	0.051 (0.020)	0.244 (0.096)	0.21	–	295 (72)	AIR	6325 CYCLES TO BREAK-THROUGH
				STOP	0.051 (0.020)	0.244 (0.096)	0.21	332 (48.2)	295 (72)	AIR	
			CYCLING	START	0.051 (0.020)	0.244 (0.096)	0.21	283 (41.0)	295 (72)	AIR	
				STOP	0.457 (0.180)	1.041 (0.410)	0.44	283 (41.0)	295 (72)	AIR	
2AW-12	0.455 (0.179)	12.70 (5.00)	SIZING	START	0.140 (0.055)	0.605 (0.238)	0.23	–	295 (72)	AIR	6600 CYCLES TO BREAK-THROUGH
				STOP	0.157 (0.062)	0.605 (0.238)	0.26	332 (48.2)	295 (72)	AIR	
			CYCLING	START	0.157 (0.062)	0.605 (0.238)	0.26	199 (28.8)	295 (72)	AIR	
				STOP	0.455 (0.179)	1.252 (0.493)	0.36	199 (28.8)	295 (72)	AIR	
2AW-13	0.462 (0.182)	12.70 (5.00)	SIZING	START	0.114 (0.045)	0.488 (0.192)	0.23	–	295 (72)	AIR	1938 CYCLES TO BREAK-THROUGH
				STOP	0.122 (0.048)	0.488 (0.192)	0.25	332 (48.2)	295 (72)	AIR	
			CYCLING	START	0.122 (0.048)	0.488 (0.192)	0.25	283 (41.0)	295 (72)	AIR	
				STOP	0.462 (0.182)	1.181 (0.465)	0.39	283 (41.0)	295 (72)	AIR	

Table 37: Uniaxial Cyclic Tests of 0.46 cm (0.18 Inch) Thick Surface Flawed 2219-T62 Aluminum Weld Metal ℄ at 78°K (-320°F)

SPECIMEN NUMBER	ORIGINAL THICKNESS, t cm (INCH)	ORIGINAL WIDTH, W cm (INCH)	TEST PARAMETERS AT		CRACK DEPTH, a cm (INCH)	CRACK LENGTH, 2c cm (INCH)	CRACK SHAPE a/2c	STRESS, σ MN/m² (KSI)	TEST		REMARKS
									TEMPERATURE, T °K (°F)	ENVIRONMENT	
2AW-6	0.460 (0.181)	12.70 (5.00)	SIZING	START	0.145 (0.057)	0.635 (0.250)	0.23	–	295 (72)	AIR	115 CYCLES TO BREAK-THROUGH
				STOP	0.183 (0.072)	0.635 (0.250)	0.29	332 (48.2)	295 (72)	AIR	
			PROOF	START	0.183 (0.072)	0.635 (0.250)	0.29	–	78 (-320)	LN_2	
				STOP	0.183 (0.072)	0.635 (0.250)	0.29	381 (55.2)	78 (-320)	LN_2	
			CYCLING	START	0.183 (0.072)	0.635 (0.250)	0.29	381 (55.2)	78 (-320)	LN_2	
				STOP	0.460 (0.181)	1.346 (0.530)	0.34	381 (55.2)	78 (-320)	LN_2	
2AW-7	0.460 (0.181)	12.70 (5.00)	SIZING	START	0.137 (0.054)	0.635 (0.250)	0.22	–	295 (72)	AIR	586 CYCLES TO BREAK-THROUGH
				STOP	0.152 (0.060)	0.635 (0.250)	0.24	332 (48.2)	295 (72)	AIR	
			PROOF	START	0.152 (0.060)	0.635 (0.250)	0.24	–	78 (-320)	LN_2	
				STOP	0.152 (0.060)	0.635 (0.250)	0.24	381 (55.2)	78 (-320)	LN_2	
			CYCLING	START	0.152 (0.060)	0.635 (0.250)	0.24	322 (46.7)	78 (-320)	LN_2	
				STOP	0.460 (0.181)	1.270 (0.500)	0.36	322 (46.7)	78 (-320)	LN_2	
2AW-9	0.457 (0.180)	12.70 (5.00)	SIZING	START	0.142 (0.056)	0.610 (0.240)	0.23	–	295 (72)	AIR	7910 CYCLES TO BREAK-THROUGH
				STOP	0.208 (0.082)	0.635 (0.250)	0.33	332 (48.2)	295 (72)	AIR	
			PROOF	START	0.208 (0.082)	0.635 (0.250)	0.33	–	78 (-320)	LN_2	
				STOP	0.208 (0.082)	0.635 (0.250)	0.33	381 (55.2)	78 (-320)	LN_2	
			CYCLING	START	0.208 (0.082)	0.635 (0.250)	0.33	228 (33.0)	78 (-320)	LN_2	
				STOP	0.457 (0.180)	1.130 (0.445)	0.40	228 (33.0)	78 (-320)	LN_2	
2AW-10	0.462 (0.182)	12.70 (5.00)	SIZING	START	0.091 (0.036)	0.287 (0.113)	0.32	–	295 (72)	AIR	4333 CYCLES TO BREAK-THROUGH
				STOP	0.091 (0.036)	0.287 (0.113)	0.32	332 (48.2)	295 (72)	AIR	
			PROOF	START	0.091 (0.036)	0.287 (0.113)	0.32	–	78 (-320)	LN_2	
				STOP	0.091 (0.036)	0.287 (0.113)	0.32	381 (55.2)	78 (-320)	LN_2	
			CYCLING	START	0.091 (0.036)	0.287 (0.113)	0.32	323 (46.8)	78 (-320)	LN_2	
				STOP	0.462 (0.182)	1.117 (0.440)	0.41	323 (46.8)	78 (-320)	LN_2	
2AW-11	0.460 (0.181)	12.70 (5.00)	SIZING	START	0.117 (0.046)	0.483 (0.190)	0.24	–	295 (72)	AIR	2050 CYCLES TO BREAK-THROUGH
				STOP	0.117 (0.046)	0.483 (0.190)	0.24	332 (48.2)	295 (72)	AIR	
			PROOF	START	0.117 (0.046)	0.483 (0.190)	0.24	–	78 (-320)	LN_2	
				STOP	0.117 (0.046)	0.483 (0.190)	0.24	381 (55.2)	78 (-320)	LN_2	
			CYCLING	START	0.117 (0.046)	0.483 (0.190)	0.24	323 (46.8)	78 (-320)	LN_2	
				STOP	0.460 (0.181)	1.270 (0.500)	0.36	323 (46.8)	78 (-320)	LN_2	

Table 38: Cyclic Crack Growth Rate Constants [1] for 2219-T62 Aluminum Tested at $R = 0$ $(a/2c)_i \approx 0.20$

MATERIAL THICKNESS cm (INCH)	MATERIAL	TEMPERATURE ^oK (^oF)	n	C	K RANGE $MN/m^{3/2}$, (KSI $\sqrt{IN}$) FROM	TO	REMARKS
0.229 (0.090)	BASE METAL	295 (72)	5.8	0.0885×10^{-6} (3.82×10^{-6})	≈ 11.0 (10)	≈ 22.0 (20)	[2]
		78 (-320)	5.8	0.0204×10^{-6} (0.88×10^{-6})			[3]
	WELD METAL	295 (72)	5.8	0.1428×10^{-6} (6.16×10^{-6})			[2]
		78 (-320)	5.8	0.0288×10^{-6} (1.24×10^{-6})			[3]
0.457 (0.180)	BASE METAL	295 (72)	4.6	0.0909×10^{-5} (3.92×10^{-5})	≈ 16.5 (15)	≈ 33.0 (30)	[2]
		78 (-320)	7.1	0.0893×10^{-9} (3.85×10^{-9})			[3]
	WELD METAL	295 (72)	4.6	0.1389×10^{-5} (5.98×10^{-5})			[2]
		78 (-320)	7.1	0.0658×10^{-8} (2.84×10^{-8})			[3]

[1] ASSUMES $da/dN = CK^n$ (SEE FIGURES 78, 79, 80 AND 81) WHERE da/dN UNITS ARE IN μcm/CYCLE (μ INCHES/CYCLE)

[2] RT CYCLIC TESTED AFTER BEING LOADED TO 332 MN/m^2 (48.2 KSI) IN RT AIR

[3] LN_2 CYCLIC TESTED AFTER BEING LOADED TO 332 MN/m^2 (48.2 KSI) IN RT AIR AND THEN LOADED TO 381 MN/m^2 (55.2 KSI) IN LN_2

Table 39: Cryostretched 301 Stainless Steel Mechanical Properties (Based On Area at End of Cryo-Prestress [1])

MATERIAL	TEMPERATURE, T ^oK (^oF)	SPECIMEN NUMBER	ORIGINAL THICKNESS, t cm (INCH)	ORIGINAL WIDTH, W cm (INCH)	0.2% OFFSET σ_{ys} IN 1.27 cm (0.5 INCH) MN/m^2 (KSI)	σ_{ult} MN/m^2 (KSI)	% ELONGATION IN 1.27 cm (0.5 INCH)	ELASTIC MODULUS, E $\times 10^{-6}$ kN/m^2 (PSI)
BASE METAL	78 (-320)	IC-5	0.076 (0.030)	1.75 (0.69)	1338 (194.0)	1979 (287.0)	23.4	169.5 (24.6)
		IC-6	0.073 (0.029)	1.80 (0.71)	1365 (198.0)	[3]	[3]	175.0 (25.4)
		IC-8	0.071 (0.028)	1.78 (0.70)	1365 (198.0)	[3]	[3]	190.3 (27.6)
		IC-9	0.071 (0.028)	1.78 (0.70)	1310 (190.0)	[3]	[3]	178.0 (25.8)
		IC-10	0.073 (0.029)	1.80 (0.71)	1345 (195.0)	[3]	[3]	138.0 (20.0)
		IC-15	0.073 (0.029)	1.80 (0.71)	1365 (198.0)	[3]	[3]	151.0 (21.9)
		IC-16	0.071 (0.028)	1.78 (0.70)	1338 (194.0)	[3]	[3]	178.0 (25.8)
		IC-17	0.073 (0.029)	1.80 (0.71)	1365 (198.0)	[3]	[3]	197.0 (28.6)
		CW-4	0.073 (0.029)	1.27 (0.50)	1338 (1940) [5]	1931 (280.0)	19.0 [5]	175.2 (25.4)
		ICW-3	0.073 (0.029)	1.80 (0.71)	1393 (202.0)	[3]	[3]	165.0 (23.9)
		ICW-4	0.071 (0.028)	1.78 (0.70)	1324 (192.0)	[3]	[3]	158.0 (22.9)
		2C-2	0.262 (0.103)	5.08 (2.00)	1351 (196.0) [6]	[3]	[3]	145.4 (21.1)
	295 (72) [2]	IC-11	0.073 (0.029)	1.75 (0.69)	1165 (169.0)	[3]	[3]	151.8 (22.0)
		IC-12	0.073 (0.029)	1.78 (0.70)	1186 (172.6)	[3]	[3]	149.0 (21.6)
		ICW-3	0.073 (0.029)	1.80 (0.71)	1241 (180.0)	1448 (210.0)	13.6	131.7 (19.1)
		2C-5	0.262 (0.103)	5.08 (2.00)	[4]	1407 (204.0)	[4]	[4]
		2CW-16	0.262 (0.103)	5.08 (2.00)	[4]	1372 (199.0)	[4]	[4]
WELD METAL	78 (-320)	ICW-11	0.071 (0.028)	1.78 (0.70)	[4]	1744 (253.0)	[4]	[4]
		ICW-24	0.069 (0.027)	1.78 (0.70)	[4]	1800 (261.0)	[4]	[4]
	295 (72) [2]	ICW-10	0.061 (0.024)	1.78 (0.70)	[4]	1201 (174.2)	[4]	[4]
		ICW-13	0.064 (0.025)	1.78 (0.70)	[4]	1288 (186.8)	[4]	[4]

[1] ALL SPECIMENS SUBJECTED TO A CRYO-PRESTRESS OF 932 MN/m^2 (135 KSI – BASED ON ORIGINAL AREA) PRIOR TO TESTS SHOWN

[2] SPECIMENS SUBJECTED TO A SIMULATED SIZING LOADING IN LN_2 TO 1442 MN/m^2 (209.2 KSI) PRIOR TO RT TESTS

[3] SPECIMENS FAILED AT ARTIFICIALLY INDUCED FLAWS

[4] SPECIMENS NOT INSTRUMENTED

[5] MEASURED IN A 5.1 cm (2.0 INCH) GAGE LENGTH

[6] MEASURED IN A 2.5 cm (1.0 INCH) GAGE LENGTH

Table 40: Uniaxial Static Fracture Tests of 0.071 cm (0.028 Inch) Thick Surface Flawed Cryostretched 301 Stainless Steel Base Metal

SPECIMEN NUMBER	ORIGINAL THICKNESS, t cm (INCH)	ORIGINAL WIDTH, W cm (INCH)	TEST PARAMETERS AT		CRACK DEPTH, a cm (INCH)	CRACK LENGTH, 2c cm (INCH)	CRACK SHAPE, a/2c	[2] STRESS, σ MN/m² (KSI)	TEST: TEMPERATURE, T °K (°F)	TEST: ENVIRONMENT	REMARKS
1C-1	0.071 (0.028)	1.78 (0.70)	FAILURE		0.023 (0.009)	0.142 (0.056)	0.16	2055 (298.0)	78 (-320)	LN_2	DID NOT [1] [3] FAIL AT F LAW
1C-2	0.071 (0.028)	1.78 (0.70)	FAILURE		0.048 (0.019)	0.290 (0.114)	0.17	829 (120.2)	78 (-320)	LN_2	FAIL MODE [3]
1C-3	0.074 (0.029)	1.78 (0.70)	FAILURE		0.033 (0.013)	0.198 (0.078)	0.17	1214 (176.0)	78 (-320)	LN_2	FAIL MODE [3]
1C-4	0.076 (0.030)	1.80 (0.71)	FAILURE		0.056 (0.022)	0.292 (0.115)	0.19	564 (81.8)	78 (-320)	LN_2	FAIL MODE [3]
1C-5	0.076 (0.030)	1.75 (0.69)	FAILURE		0.023 (0.009)	0.097 (0.038)	0.24	1979 (287.0)	78 (-320)	LN_2	DID NOT F AT FLAW [3] [4]
1C-6	0.074 (0.029)	1.80 (0.71)	FAILURE		0.030 (0.012)	0.170 (0.067)	0.18	1848 (268.0)	78 (-320)	LN_2	FAIL MODE [3] [4]
1C-7	0.071 (0.028)	1.78 (0.70)	FAILURE		0.028 (0.011)	0.147 (0.058)	0.19	1758 (255.0)	78 (-320)	LN_2	FAIL MODE [3] [4]
1C-8	0.071 (0.028)	1.78 (0.70)	FAILURE		0.033 (0.013)	0.183 (0.072)	0.18	1465 (212.5)	78 (-320)	LN_2	FAIL MODE [3] [4]
1C-9	0.071 (0.028)	1.78 (0.70)	FAILURE		0.028 (0.011)	0.140 (0.055)	0.20	1311 (190.2)	78 (-320)	LN_2	FAIL MODE [3] [4]
1C-10	0.074 (0.029)	1.80 (0.71)	FAILURE		0.028 (0.011)	0.140 (0.055)	0.20	1345 (195.0)	78 (-320)	LN_2	FAIL MODE [3] [4]
1C-15	0.074 (0.029)	1.80 (0.71)	LEAKAGE		0.023 (0.009)	0.119 (0.047)	0.19	1579 (229.0)	78 (-320)	LN_2	LEAK MODE [3] [4]
1C-18	0.074 (0.029)	1.78 (0.70)	FAILURE		0.023 (0.009)	0.119 (0.047)	0.19	1410 (204.5)	78 (-320)	LN_2	FAIL MODE [3] [4]
1C-19	0.071 (0.028)	1.80 (0.71)	FAILURE		0.020 (0.008)	0.094 (0.037)	0.22	1422 (206.3)	78 (-320)	LN_2	FAIL MODE [3] [4]
1CW-23	0.069 (0.027)	1.75 (0.69)	FAILURE		0.038 (0.015)	0.213 (0.084)	0.18	1338 (194.0)	78 (-320)	LN_2	FAIL MODE [4]
1CW-24	0.069 (0.027)	1.78 (0.70)	FAILURE		0.025 (0.010)	0.155 (0.061)	0.16	1800 (261.0)	78 (-320)	LN_2	DID NOT FAIL AT FLAW [4]
1C-11	0.069 (0.029)	1.75 (0.69)	SIZING	START	0.020 (0.008)	0.112 (0.044)	0.18	–	78 (-320)	LN_2	FAIL MODE [3] [4]
				STOP	0.020 (0.008)	0.112 (0.044)	0.18	1442 (209.2)	78 (-320)	LN_2	
			FAILURE		0.020 (0.008)	0.112 (0.044)	0.18	1417 (205.5)	295 (72)	AIR	
1C-12	0.074 (0.029)	1.78 (0.70)	SIZING	START	0.023 (0.009)	0.114 (0.045)	0.20	–	78 (-320)	LN_2	FAIL MODE [3] [4]
				STOP	0.023 (0.009)	0.114 (0.045)	0.20	1442 (209.2)	78 (-320)	LN_2	
			FAILURE		0.023 (0.009)	0.114 (0.045)	0.20	1436 (208.3)	295 (72)	AIR	

[1] SPECIMEN SUBJECTED TO A CRYO-PRESTRESS OF 1450 MN/m² (210 KSI-BASED ON ORIGINAL AREA) PRIOR TO LOADING SHOWN

[2] BASED ON AREA AT BEGINNING OF LOADING SHOWN

[3] SPECIMEN NOT REANNEALED AFTER PRECRACKING

[4] SPECIMEN SUBJECTED TO A CRYO-PRESTRESS OF 932 MN/m² (135 KSI – BASED ON ORIGINAL AREA) PRIOR TO LOADING SHOWN

Table 41: *Uniaxial Static Fracture Tests of 0.071 cm (0.028 Inch) Thick Surface Flawed Cryostretched 301 Stainless Steel Weld Metal Fusion Line* [4]

SPECIMEN NUMBER	ORIGINAL THICKNESS, t cm (INCH)	ORIGINAL WIDTH, W cm (INCH)	TEST PARAMETERS AT		CRACK DEPTH, a cm (INCH)	CRACK LENGTH, 2c cm (INCH)	CRACK SHAPE, a/2c	[2] STRESS, σ MN/m^2 (KSI)	TEST TEMPERATURE, T °K (°F)	TEST ENVIRONMENT	REMARKS
1CW-2	0.069 (0.027)	1.80 (0.71)	FAILURE		0.028 (0.011)	0.150 (0.059)	0.19	1493 (216.5)	78 (-320)	LN_2	FAIL MODE [1]
1CW-4 [5]	0.071 (0.028)	1.78 (0.70)	FAILURE		0.025 (0.010)	0.160 (0.063)	0.16	1582 (229.5)	78 (-320)	LN_2	FAIL MODE [1][3]
1CW-5	0.071 (0.028)	1.78 (0.70)	LEAKAGE		0.028 (0.011)	0.155 (0.061)	0.18	931 (135.0)	78 (-320)	LN_2	[3][7]
1CW-6 [6]	0.076 (0.030)	1.78 (0.70)	LEAKAGE		0.033 (0.013)	0.170 (0.067)	0.19	1338 (194.0)	78 (-320)	LN_2	LEAK MODE [1][3]
1CW-11	0.071 (0.028)	1.78 (0.70)	FAILURE		0.018 (0.007)	0.109 (0.043)	0.16	1744 (253.0)	78 (-320)	LN_2	DID NOT FAIL AT FLAW [1]
1CW-20	0.064 (0.025)	1.78 (0.70)	LEAKAGE		0.030 (0.012)	0.127 (0.060)	0.24	931 (135.0)	78 (-320)	LN_2	[7]
1CW-22	0.069 (0.027)	1.78 (0.70)	FAILURE		0.038 (0.015)	0.208 (0.082)	0.18	1331 (193.0)	78 (-320)	LN_2	FAIL MODE [1]
1CW-10	0.061 (0.024)	1.78 (0.70)	SIZING	START	0.025 (0.010)	0.132 (0.052)	0.19	–	78 (-320)	LN_2	DID NOT FAIL AT FLAW [1]
				STOP	0.025 (0.010)	0.132 (0.052)	0.19	1442 (209.2)	78 (-320)	LN_2	
			FAILURE		0.025 (0.010)	0.132 (0.052	0.19	1201 (174.2)	295 (72)	AIR	
1CW-13	0.064 (0.025)	1.78 (0.70)	SIZING	START	0.025 (0.010)	0.132 (0.052)	0.19	–	78 (-320)	LN_2	DID NOT FAIL AT FLAW [1]
				STOP	0.025 (0.010)	0.132 (0.052)	0.19	1442 (209.2)	78 (-320)	LN_2	
			FAILURE		0.025 (0.010)	0.132 (0.052)	0.19	1288 (186.8)	295 (72)	AIR	
1CW-21	0.069 (0.027)	1.78 (0.70)	SIZING	START	0.018 (0.007)	0.114 (0.045)	0.16	–	78 (-320)	LN_2	FAIL MODE [1]
				STOP	0.018 (0.007)	0.114 (0.045)	0.16	1442 (209.2)	78 (-320)	LN_2	
			FAILURE		0.018 (0.007)	0.114 (0.045)	0.16	1251 (181.5)	295 (72)	AIR	

[1] SPECIMEN SUBJECTED TO A CRYO-PRESTRESS OF 932 MN/m^2 (135 KSI – BASED ON ORIGINAL AREA) PRIOR TO LOADING SHOWN

[2] BASED ON AREA AT BEGINNING OF LOADING SHOWN

[3] SPECIMEN NOT REANNEALED AFTER PRECRACKING

[4] UNLESS NOTED OTHERWISE

[5] CRACK LOCATED ON WELD ℄

[6] CRACK LOCATED IN WELD HAZ

[7] LEAK MODE PRIOR TO σ_{PS} = 932 MN/m^2

Table 42: Uniaxial Static Fracture Tests of 0.26 cm (0.10 Inch) Thick Surface Flawed Cryostretched 301 Stainless Steel Base Metal

SPECIMEN NUMBER	ORIGINAL THICKNESS, t cm (INCH)	ORIGINAL WIDTH, W cm (INCH)	TEST PARAMETERS AT		CRACK DEPTH, a cm (INCH)	CRACK LENGTH, 2c cm (INCH)	CRACK SHAPE, a/2c	STRESS, σ MN/m² (KSI) [2]	TEST TEMPERATURE, T °K (°F)	TEST ENVIRONMENT	REMARKS
2C-1	0.262 (0.103)	5.08 (2.00)	FAILURE		0.127 (0.050)	0.691 (0.272)	0.18	505 (73.2)	78 (-320)	LN_2	FAIL MODE [3]
2C-2	0.262 (0.103)	5.08 (2.00)	FAILURE		0.036 (0.014)	0.229 (0.090)	0.16	1710 (248.0)	78 (-320)	LN_2	FAIL MODE [1][3][4]
2C-3	0.262 (0.103)	5.05 (1.99)	FAILURE		0.056 (0.022)	0.287 (0.113)	0.19	1848 (268.0)	78 (-320)	LN_2	FAIL MODE [1][3]
2C-4	0.264 (0.104)	5.08 (2.00)	FAILURE		0.079 (0.031)	0.414 (0.163)	0.19	1403 (203.5)	78 (-320)	LN_2	FAIL MODE [1][3]
2C-8	0.264 (0.104)	5.05 (1.99)	FAILURE		0.046 (0.018)	0.257 (0.101)	0.18	1434 (208.0)	78 (-320)	LN_2	FAIL MODE [1][3]
2C-9	0.262 (0.103)	5.08 (2.00)	FAILURE		0.043 (0.017)	0.211 (0.083)	0.20	1386 (201.0)	78 (-320)	LN_2	FAIL MODE [1]
2C-16	0.262 (0.103)	5.08 (2.00)	FAILURE		0.043 (0.017)	0.224 (0.088)	0.19	1415 (205.2)	78 (-320)	LN_2	FAIL MODE [1]
2C-5	0.262 (0.103)	5.08 (2.00)	SIZING	START	0.038 (0.015)	0.193 (0.076)	0.20	–	78 (-320)	LN_2	NO CRACK GROWTH
				STOP	0.038 (0.015)	0.193 (0.076)	0.20	1442 (209.2)	78 (-320)	LN_2	
			FAILURE		0.038 (0.015)	0.193 (0.076)	0.20	1407 (204.0)	295 (72)	AIR	FAILED OUTSIDE OF FLAW AREA [1][3]

[1] SPECIMEN SUBJECTED TO A CYRO-PRESTRESS OF 932 MN/m² (135 KSI – BASED ON ORIGINAL AREA) PRIOR TO LOADING SHOWN

[2] BASED ON AREA AT BEGINNING OF LOAD CYCLE

[3] SPECIMEN NOT REANNEALED AFTER PRECRACKING

[4] SPECIMEN LOADED TO 1464 MN/m² (212 KSI) CYROGENICALLY AND UNLOADED DUE TO TEST MACHINE MALFUNCTION THEN LOADED TO FAILURE

Table 43: Uniaxial Static Fracture Tests of 0.26 cm (0.10 Inch) Thick Surface Flawed Cryostretched 301 Stainless Steel Weld Metal Fusion Line

SPECIMEN NUMBER	ORIGINAL THICKNESS, t cm (INCH)	ORIGINAL WIDTH, W cm (INCH)	TEST PARAMETERS AT		CRACK DEPTH, a cm (INCH)	CRACK LENGTH, 2c cm (INCH)	CRACK SHAPE, a/2c	[2] STRESS, σ MN/m² (KSI)	TEST TEMPERATURE, T °K (°F)	TEST ENVIRONMENT	REMARKS
2CW-1	0.262 (0.103)	5.08 (2.00)	FAILURE		0.051 (0.020)	0.295 (0.116)	0.17	1379 (200.0)	78 (-320)	LN_2	FAIL MODE [1] [3]
2CW-9	0.267 (0.105)	5.08 (2.00)	FAILURE		0.041 (0.016)	0.218 (0.086)	0.19	1390 (201.6)	78 (-320)	LN_2	FAIL MODE [1]
2CW-13	0.264 (0.104)	5.08 (2.00)	FAILURE		0.135 (0.053)	0.747 (0.294)	0.18	656 (95.2)	78 (-320)	LN_2	FAIL MODE
2CW-15	0.267 (0.105)	5.08 (2.00)	FAILURE		0.081 (0.032)	0.414 (0.163)	0.20	929 (134.7)	78 (-320)	LN_2	FAIL MODE
2CW-16	0.262 (0.103)	5.08 (2.00)	SIZING	START	0.048 (0.019)	0.152 (0.060)	0.32	–	78 (-320)	LN_2	NO CRACK GROWTH
				STOP	0.048 (0.019)	0.152 (0.060)	0.32	1442 (209.2)	78 (-320)	LN_2	
			FAILURE		0.048 (0.019)	0.152 (0.060)	0.32	1372 (199.0)	295 (72)	AIR	FAILED OUTSIDE OF FLAW AREA [1]

[1] SPECIMEN SUBJECTED TO A CRYO-PRESTRESS OF 932 MN/m² (135 KSI – BASED ON ORIGINAL AREA) PRIOR TO LOADING SHOWN

[2] BASED ON AREA AT BEGINNING OF LOAD CYCLE

[3] SPECIMEN NOT REANNEALED AFTER PRECRACKING

Table 44: Uniaxial Cyclic Tests of 0.071 cm (0.028 Inch) Thick Surface Flawed Cryostretched [1] 301 Stainless Steel Base Metal at 78°K (-320°F)

SPECIMEN NUMBER	ORIGINAL THICKNESS, t cm (INCH)	ORIGINAL WIDTH, W cm (INCH)	TEST PARAMETERS AT		CRACK DEPTH, a cm (INCH)	CRACK LENGTH, 2c cm (INCH)	CRACK SHAPE, a/2c	[2] STRESS, σ MN/m^2 (KSI)	TEST: TEMPERATURE, T °K (°F)	TEST: ENVIRONMENT	REMARKS
1C-2A	0.076 (0.030)	1.80 (0.71)	SIZING	START	0.018 (0.007)	0.099 (0.039)	0.18	–	78 (-320)	LN_2	4791 CYCLES TO BREAK-THROUGH
				STOP	0.018 (0.007)	0.099 (0.039)	0.18	1442 (209.2)	78 (-320)	LN_2	
			CYCLING	START	0.018 (0.007)	0.099 (0.039)	0.18	1083 (157.0)	78 (-320)	LN_2	
				STOP	0.069 (0.027)	0.173 (0.068)	0.40	1083 (157.0)	78 (-320)	LN_2	
1C-14	0.074 (0.029)	1.80 (0.71)	SIZING	START	0.018 (0.007)	0.099 (0.039)	0.18	–	78 (-320)	LN_2	[3] 3618 CYCLES TO BREAK-THROUGH
				STOP	0.018 (0.007)	0.099 (0.039)	0.18	1442 (209.2)	78 (-320)	LN_2	
			CYCLING	START	0.018 (0.007)	0.099 (0.039)	0.18	1083 (157.0)	78 (-320)	LN_2	
				STOP	0.069 (0.027)	0.168 (0.066)	0.41	1083 (157.0)	78 (-320)	LN_2	
1C-16	0.071 (0.028)	1.78 (0.70)	SIZING	START	0.025 (0.010)	0.142 (0.056)	0.18	–	78 (-320)	LN_2	[3] 810 CYCLES TO BREAK-THROUGH
				STOP	0.030 (0.012)	0.142 (0.056)	0.21	1487 (215.6)	78 (-320)	LN_2	
			CYCLING	START	0.030 (0.012)	0.142 (0.056)	0.21	1442 (209.2)	78 (-320)	LN_2	
				STOP	0.069 (0.027)	0.170 (0.067)	0.40	1442 (209.2)	78 (-320)	LN_2	
1C-17	0.074 (0.029)	1.80 (0.71)	SIZING	START	0.023 (0.009)	0.132 (0.052)	0.17	–	78 (-320)	LN_2	[3] 420 CYCLES TO BREAK-THROUGH
				STOP	0.048 (0.019)	0.132 (0.052)	0.37	1442 (209.2)	78 (-320)	LN_2	
			CYCLING	START	0.048 (0.019)	0.132 (0.052)	0.37	1227 (178.0)	78 (-320)	LN_2	
				STOP	0.071 (0.028)	0.155 (0.061)	0.46	1227 (178.0)	78 (-320)	LN_2	
1C-20	0.074 (0.029)	1.78 (0.70)	SIZING	START	0.018 (0.007)	0.112 (0.044)	0.16	–	78 (-320)	LN_2	CYCLED FOR 1485 CYCLES
				STOP	0.018 (0.007)	0.112 (0.044)	0.16	1442 (209.2)	78 (-320)	LN_2	
			CYCLING	START	0.018 (0.007)	0.112 (0.044)	0.16	1227 (178.0)	78 (-320)	LN_2	
				STOP	0.043 (0.017)	0.122 (0.048)	0.35	1227 (178.0)	78 (-320)	LN_2	
1C-21	0.071 (0.028)	1.80 (0.71)	SIZING	START	0.020 (0.008)	0.130 (0.051)	0.16	–	78 (-320)	LN_2	1490 CYCLES TO BREAK-THROUGH
				STOP	0.020 (0.008)	0.130 (0.051)	0.16	1442 (209.2)	78 (-320)	LN_2	
			CYCLING	START	0.020 (0.008)	0.130 (0.051)	0.16	1227 (178.0)	78 (-320)	LN_2	
				STOP	0.069 (0.027)	0.178 (0.070)	0.39	1227 (178.0)	78 (-320)	LN_2	
1CW-12 (BM)	0.069 (0.027)	1.78 (0.70)	SIZING	START	0.023 (0.009)	0.142 (0.056)	0.16	–	78 (-320)	LN_2	4730 CYCLES TO BREAK-THROUGH
				STOP	0.023 (0.009)	0.142 (0.056)	0.16	1442 (209.2)	78 (-320)	LN_2	
			CYCLING	START	0.023 (0.009)	0.142 (0.056)	0.16	938 (136.0)	78 (-320)	LN_2	
				STOP	0.064 (0.025)	0.173 (0.068)	0.37	938 (136.0)	78 (-320)	LN_2	

[1] SPECIMENS SUBJECTED TO A CRYO-PRESTRESS OF 932 MN/m^2 (135 KSI – BASED ON ORIGINAL AREA) PRIOR TO LOADINGS SHOWN

[2] BASED ON AREA AT BEGINNING OF SIZING CYCLE

[3] SPECIMEN NOT REANNEALED AFTER PRECRACKING

Table 45: *Uniaxial Cyclic Tests of 0.071 cm (0.028 Inch) Thick Surface Flawed Cryostretched [1] 301 Stainless Steel Base Metal at 295^{o}K (72^{o}F)*

SPECIMEN NUMBER	ORIGINAL THICKNESS, t cm (INCH)	ORIGINAL WIDTH, W cm (INCH)	TEST PARAMETERS AT		CRACK DEPTH, a cm (INCH)	CRACK LENGTH, 2c cm (INCH)	CRACK SHAPE, a/2c	[2] STRESS, σ MN/m^2 (KSI)	TEST: TEMPERATURE, T ^{o}K (^{o}F)	TEST: ENVIRONMENT	REMARKS
1C-22	0.071 (0.028)	1.78 (0.70)	SIZING	START	0.020 (0.008)	0.130 (0.051)	0.16	–	78 (-320)	LN_2	
				STOP	0.020 (0.008)	0.130 (0.051)	0.16	1442 (209.2)	78 (-320)	LN_2	
			PROOF	START	0.020 (0.008)	0.130 (0.051)	0.16	–	295 (72)	AIR	
				STOP	0.020 (0.008)	0.130 (0.051)	0.16	1234 (179.0)	295 (72)	AIR	
			CYCLING	START	0.020 (0.008)	0.130 (0.051)	0.16	1007 (146.0)	295 (72)	AIR	691 CYCLES TO TO BREAK-THROUGH
				STOP	0.069 (0.027)	0.185 (0.073)	0.37	1007 (146.0)	295 (72)	AIR	
1C-23	0.074 (0.029)	1.80 (0.71)	SIZING	START	0.020 (0.008)	0.122 (0.048)	0.17	–	78 (-320)	LN_2	
				STOP	0.020 (0.008)	0.122 (0.048)	0.17	1442 (209.2)	78 (-320)	LN_2	
			PROOF	START	0.020 (0.008)	0.122 (0.048)	0.17	–	295 (72)	AIR	
				STOP	0.020 (0.008)	0.122 (0.048)	0.17	1234 (179.0)	295 (72)	AIR	
			CYCLING	START	0.020 (0.008)	0.122 (0.048)	0.17	817 (118.5)	295 (72)	AIR	2558 CYCLES TO BREAK-THROUGH
				STOP	0.071 (0.028)	0.168 (0.066)	0.42	817 (118.5)	295 (72)	AIR	
1C-24	0.074 (0.029)	1.78 (0.70)	SIZING	START	0.015 (0.006)	0.089 (0.035)	0.17	–	78 (-320)	LN_2	
				STOP	0.015 (0.006)	0.089 (0.035)	0.17	1442 (209.2)	78 (-320)	LN_2	
			PROOF	START	0.015 (0.006)	0.089 (0.035)	0.17	–	295 (72)	AIR	
				STOP	0.015 (0.006)	0.089 (0.035)	0.17	1234 (179.0)	295 (72)	AIR	
			CYCLING	START	0.015 (0.006)	0.089 (0.035)	0.17	848 (123.0)	295 (72)	AIR	4758 CYCLES TO BREAK-THROUGH
				STOP	0.066 (0.026)	0.152 (0.060)	0.43	848 (123.0)	295 (72)	AIR	
1CW-16 (BM)	0.071 (0.028)	1.75 (0.69)	SIZING	START	0.020 (0.008)	0.130 (0.051)	0.16	–	78 (-320)	LN_2	
				STOP	0.020 (0.008)	0.130 (0.051)	0.16	1442 (209.2)	78 (-320)	LN_2	
			PROOF	START	0.020 (0.008)	0.130 (0.051)	0.16	–	295 (72)	AIR	
				STOP	0.020 (0.008)	0.130 (0.051)	0.16	1096 (159.0)	295 (72)	AIR	
			CYCLING	START	0.020 (0.008)	0.130 (0.051)	0.16	758 (110.0)	295 (72)	AIR	6244 CYCLES TO BREAK-THROUGH
				STOP	0.066 (0.026)	0.175 (0.069)	0.38	758 (110.0)	295 (72)	AIR	
1CW-17 (BM)	0.066 (0.026)	1.75 (0.69)	SIZING	START	0.023 (0.009)	0.140 (0.055)	0.16	–	78 (-320)	LN_2	
				STOP	0.023 (0.009)	0.140 (0.055)	0.16	1442 (209.2)	78 (-320)	LN_2	
			PROOF	START	0.023 (0.009)	0.140 (0.055)	0.16	–	295 (72)	AIR	
				STOP	0.023 (0.009)	0.140 (0.055)	0.16	1234 (179.0)	295 (72)	AIR	
			CYCLING	START	0.023 (0.009)	0.140 (0.055)	0.16	699 (101.4)	295 (72)	AIR	6534 CYCLES TO BREAK-THROUGH
				STOP	0.061 (0.024)	0.183 (0.072)	0.33	699 (101.4)	295 (72)	AIR	
1CW-18	0.069 (0.027)	1.75 (0.68)	SIZING	START	0.023 (0.009)	0.140 (0.055)	0.16	–	78 (-320)	LN_2	SPECIMEN FAILED AT WELD FUSION LINE DURING RT PROOF; SPECIMEN THEN GRIPPED IN FRICTION GRIPS AND CYCLED FOR 1941 CYCLES TO BREAK-THROUGH
				STOP	0.023 (0.009)	0.140 (0.055)	0.16	1442 (209.2)	78 (-320)	LN_2	
			PROOF	START	0.023 (0.009)	0.140 (0.055)	0.16	–	295 (72)	AIR	
				STOP	0.023 (0.009)	0.140 (0.055)	0.16	1234 (179.0)	295 (72)	AIR	
			CYCLING	START	0.023 (0.009)	0.140 (0.055)	0.16	876 (127.0)	295 (72)	AIR	
				STOP	0.066 (0.026)	0.170 (0.067)	0.39	876 (127.0)	295 (72)	AIR	

[1] SPECIMENS SUBJECTED TO A CRYO-PRESTRESS OF 932 MN/m^2 (135 KSI – BASED ON ORIGINAL AREA) PRIOR TO LOADINGS SHOWN

[2] BASED ON AREA AT BEGINNING OF SIZING CYCLE

Table 46: Uniaxial Cyclic Tests of 0.071 cm (0.028 Inch) Thick Surface Flawed Cryostretched [1] 301 Stainless Steel Weld Metal Fusion Line at 78°K (-320°F)

SPECIMEN NUMBER	ORIGINAL THICKNESS, t cm (INCH)	ORIGINAL WIDTH, W cm (INCH)	TEST PARAMETERS AT		CRACK DEPTH, a cm (INCH)	CRACK LENGTH, 2c cm (INCH)	CRACK SHAPE, a/2c	[2] STRESS, σ MN/m^2 (KSI)	TEST TEMPERATURE, T °K (°F)	TEST ENVIRONMENT	REMARKS
1CW-7	0.061 (0.024)	1.78 (0.70)	SIZING	START	0.018 (0.007)	0.132 (0.052)	0.13	–	78 (-320)	LN_2	3273 CYCLES TO BREAK-THROUGH
				STOP	0.018 (0.007)	0.132 (0.052)	0.13	1442 (209.2)	78 (-320)	LN_2	
			CYCLING	START	0.018 (0.007)	0.132 (0.052)	0.13	1010 (146.5)	78 (-320)	LN_2	
				STOP	0.053 (0.021)	0.160 (0.063)	0.33	1010 (146.5)	78 (-320)	LN_2	
1CW-8	0.064 (0.025)	1.75 (0.69)	SIZING	START	0.025 (0.010)	0.152 (0.060)	0.17	–	78 (-320)	LN_2	701 CYCLES TO BREAK-THROUGH
				STOP	0.025 (0.010)	0.152 (0.060)	0.17	1442 (209.2)	78 (-320)	LN_2	
			CYCLING	START	0.025 (0.010)	0.152 (0.060)	0.17	1255 (182.0)	78 (-320)	LN_2	
				STOP	0.058 (0.023)	0.152 (0.060)	0.38	1255 (182.0)	78 (-320)	LN_2	
1CW-9	0.069 (0.027)	1.78 (0.70)	SIZING	START	0.015 (0.006)	0.104 (0.041)	0.15	–	78 (-320)	LN_2	6113 CYCLES TO BREAK-THROUGH
				STOP	0.015 (0.006)	0.104 (0.041)	0.15	1442 (209.2)	78 (-320)	LN_2	
			CYCLING	START	0.015 (0.006)	0.104 (0.041)	0.15	1010 (146.5)	78 (-320)	LN_2	
				STOP	0.064 (0.025)	0.165 (0.065)	0.38	1010 (146.5)	78 (-320)	LN_2	
1CW-14	0.064 (0.025)	1.78 (0.70)	SIZING	START	0.020 (0.008)	0.127 (0.050)	0.16	–	78 (-320)	LN_2	6350 CYCLES TO BREAK-THROUGH
				STOP	0.020 (0.008)	0.127 (0.050)	0.16	1442 (209.2)	78 (-320)	LN_2	
			CYCLING	START	0.020 (0.008)	0.127 (0.050)	0.16	793 (115.0)	78 (-320)	LN_2	
				STOP	0.061 (0.024)	0.155 (0.061)	0.39	793 (115.0)	78 (-320)	LN_2	
1CW-16	0.066 (0.026)	1.75 (0.69)	SIZING	START	0.020 (0.008)	0.122 (0.048)	0.17	–	78 (-320)	LN_2	1123 CYCLES TO BREAK-THROUGH
				STOP	0.020 (0.008)	0.122 (0.048)	0.17	1442 (209.2)	78 (-320)	LN_2	
			CYCLING	START	0.020 (0.008)	0.122 (0.048)	0.17	1234 (179.0)	78 (-320)	LN_2	
				STOP	0.064 (0.025)	0.150 (0.059)	0.42	1234 (179.0)	78 (-320)	LN_2	

[1] SPECIMENS SUBJECTED TO A CRYO-PRESTRESS OF 932 MN/m^2 (135 KSI – BASED ON ORIGINAL AREA) PRIOR TO LOADINGS SHOWN

[2] BASED ON AREA AT BEGINNING OF SIZING CYCLE

Table 47: Uniaxial Cyclic Tests of 0.071 cm (0.028 Inch) Thick Surface Flawed Cryostretched [1] 301 Stainless Steel Weld Metal Fusion Line at 295°K (72°F)

SPECIMEN NUMBER	ORIGINAL THICKNESS, t cm (INCH)	ORIGINAL WIDTH, W cm (INCH)	TEST PARAMETERS AT		CRACK DEPTH, a cm (INCH)	CRACK LENGTH, 2c cm (INCH)	CRACK SHAPE, a/2c	[2] STRESS, σ MN/m^2 (KSI)	TEST TEMPERATURE, T °K (°F)	TEST ENVIRONMENT	REMARKS
1CW-19	0.066 (0.026)	1.78 (0.70)	SIZING	START	0.020 (0.008)	0.091 (0.036)	0.22	–	78 (-320)	LN_2	2718 CYCLES TO BREAK-THROUGH
				STOP	0.020 (0.008)	0.091 (0.036)	0.22	1442 (209.2)	78 (-320)	LN_2	
			PROOF	START	0.020 (0.008)	0.091 (0.036)	0.22	–	295 (72)	AIR	
				STOP	0.020 (0.008)	0.091 (0.036)	0.22	1234 (179.0)	295 (72)	AIR	
			CYCLING	START	0.020 (0.008)	0.091 (0.036)	0.22	857 (124.3)	295 (72)	AIR	
				STOP	0.064 (0.025)	0.152 (0.060)	0.42	857 (124.3)	295 (72)	AIR	

[1] SPECIMEN SUBJECTED TO A CRYO-PRESTRESS OF 932 MN/m^2 (135 KSI – ON ORIGINAL AREA) PRIOR TO LOADINGS SHOWN

[2] BASED ON AREA AT BEGINNING OF SIZING CYCLE

Table 48: Uniaxial Cyclic Tests of 0.26 cm (0.10 Inch) Thick Surface Flawed Cryostretched [1] 301 Stainless Steel Base Metal at 78°K (-320°F)

SPECIMEN NUMBER	ORIGINAL THICKNESS, t cm (INCH)	ORIGINAL WIDTH, W cm (INCH)	TEST PARAMETERS AT		CRACK DEPTH, a cm (INCH)	CRACK LENGTH, 2c cm (INCH)	CRACK SHAPE, a/2c	[2] STRESS, σ MN/m^2 (KSI)	TEST TEMPERATURE, T °K (°F)	TEST ENVIRONMENT	REMARKS
2C-6	0.262 (0.103)	5.08 (2.00)	SIZING	START	0.046 (0.018)	0.262 (0.103)	0.17	–	78 (-320)	LN_2	[3] 1000 CYCLES TO FAILURE
				STOP	0.046 (0.018)	0.262 (0.103)	0.17	1442 (209.2)	78 (-320)	LN_2	
			CYCLING	START	0.046 (0.018)	0.262 (0.103)	0.17	1442 (209.2)	78 (-320)	LN_2	
				STOP	0.251 (0.099)	0.686 (0.270)	0.37	1442 (209.2)	78 (-320)	LN_2	
2C-7	0.262 (0.103)	5.08 (2.00)	SIZING	START	0.048 (0.019)	0.267 (0.105)	0.18	–	78 (-320)	LN_2	[3] 2433 CYCLES TO BREAK-THROUGH
				STOP	0.048 (0.019)	0.267 (0.105)	0.18	1442 (209.2)	78 (-320)	LN_2	
			CYCLING	START	0.048 (0.019)	0.267 (0.105)	0.18	1227 (178.0)	78 (-320)	LN_2	
				STOP	0.251 (0.099)	0.584 (0.230)	0.43	1227 (178.0)	78 (-320)	LN_2	
2C-13	0.262 (0.103)	5.11 (2.01)	SIZING	START	0.025 (0.010)	0.152 (0.060)	0.17	–	78 (-320)	LN_2	8012 CYCLES TO BREAK-THROUGH
				STOP	0.025 (0.010)	0.152 (0.060)	0.17	1442 (209.2)	78 (-320)	LN_2	
			CYCLING	START	0.025 (0.010)	0.152 (0.060)	0.17	1083 (157.0)	78 (-320)	LN_2	
				STOP	0.254 (0.100)	0.533 (0.210)	0.48	1083 (157.0)	78 (-320)	LN_2	
2C-15	0.264 (0.104)	5.08 (2.00)	SIZING	START	0.041 (0.016)	0.244 (0.096)	0.17	–	78 (-320)	LN_2	CRACK APPEARANCE  GROWTH-ON-LOADING CYCLIC GROWTH 47 CYCLES TO BREAKTHROUGH
				STOP	0.206 (0.081)	0.526 (0.207)	0.39	1442 (209.2)	78 (-320)	LN_2	
			CYCLING	START	0.206 (0.081)	0.526 (0.207)	0.39	1083 (157.0)	78 (-320)	LN_2	
				STOP	0.249 (0.098)	0.533 (0.210)	0.47	1083 (157.0)	78 (-320)	LN_2	
2CW-12 (BM)	0.259 (0.102)	5.08 (2.00)	SIZING	START	0.036 (0.014)	0.175 (0.069)	0.20	–	78 (-320)	LN_2	5116 CYCLES TO BREAK-THROUGH
				STOP	0.036 (0.014)	0.175 (0.069)	0.20	1442 (209.2)	78 (-320)	LN_2	
			CYCLING	START	0.036 (0.014)	0.175 (0.069)	0.20	1082 (157.0)	78 (-320)	LN_2	
				STOP	0.241 (0.095)	0.572 [4] (0.225)	0.42	1082 (157.0)	78 (-320)	LN_2	

[1] SPECIMENS SUBJECTED TO A CRYO-PRESTRESS OF 932 MN/m^2 (135 KSI BASED ON ORIGINAL AREA) PRIOR TO LOADINGS SHOWN

[2] BASED ON AREA AT BEGINNING OF SIZING CYCLE

[3] SPECIMEN NOT REANNEALED AFTER PRECRACKING

[4] APPROXIMATE DIMENSION

Table 49: Uniaxial Cyclic Tests of 0.26 cm (0.10 Inch) Thick Surface Flawed Cryostretched [1] 301 Stainless Steel Base Metal at 295°K (72°F)

SPECIMEN NUMBER	ORIGINAL THICKNESS, t cm (INCH)	ORIGINAL WIDTH, W cm (INCH)	TEST PARAMETERS AT		CRACK DEPTH, a cm (INCH)	CRACK LENGTH, 2c cm (INCH)	CRACK SHAPE, a/2c	[2] STRESS, σ MN/m^2 (KSI)	TEST TEMPERATURE, T °K (°F)	TEST ENVIRONMENT	REMARKS
2C-10	0.262 (0.103)	5.08 (2.00)	SIZING	START	0.041 (0.016)	0.229 (0.090)	0.18	–	78 (-320)	LN_2	1992 CYCLES TO BREAK-THROUGH
				STOP	0.041 (0.016)	0.229 (0.090)	0.18	1442 (209.2)	78 (-320)	LN_2	
			PROOF	START	0.041 (0.016)	0.229 (0.090)	0.18	–	295 (72)	AIR	
				STOP	0.041 (0.016)	0.229 (0.090)	0.18	1234 (179.0)	295 (72)	AIR	
			CYCLING	START	0.041 (0.016)	0.229 (0.090)	0.18	1214 (176.0)	295 (72)	AIR	
				STOP	0.249 (0.098)	0.625 (0.246)	0.40	1214 (176.0)	295 (72)	AIR	
2C-12	0.264 (0.104)	5.08 (2.00)	SIZING	START	0.028 (0.011)	0.157 (0.062)	0.18	–	78 (-320)	LN_2	5665 CYCLES TO BREAK-THROUGH
				STOP	0.028 (0.011)	0.157 (0.062)	0.18	1442 (209.2)	78 (-320)	LN_2	
			PROOF	START	0.028 (0.011)	0.157 (0.062)	0.18	–	295 (72)	AIR	
				STOP	0.028 (0.011)	0.157 (0.062)	0.18	1234 (179.0)	295 (72)	AIR	
			CYCLING	START	0.028 (0.011)	0.157 (0.062)	0.18	1034 (150.0)	295 (72)	AIR	
				STOP	0.249 (0.098)	0.559 (0.220)	0.45	1034 (150.0)	295 (72)	AIR	
2C-14	0.264 (0.104)	5.05 (1.99)	SIZING	START	0.020 (0.008)	0.114 (0.045)	0.18	–	78 (-320)	LN_2	FAILED OUTSIDE OF ARTIFICIALLY INDUCED FLAW AFTER 4044 CYCLES
				STOP	0.020 (0.008)	0.114 (0.045)	0.18	1442 (209.2)	78 (-320)	LN_2	
			PROOF	START	0.020 (0.008)	0.114 (0.045)	0.18	–	295 (72)	AIR	
				STOP	0.020 (0.008)	0.114 (0.045)	0.18	1234 (179.0)	295 (72)	AIR	
			CYCLING	START	0.020 (0.008)	0.114 (0.045)	0.18	1034 (150.0)	295 (72)	AIR	
				STOP	0.079 (0.031)	0.178 (0.070)	0.44	1034 (150.0)	295 (72)	AIR	
2CW-6 (BM)	0.269 (0.106)	5.08 (2.00)	SIZING	START	0.028 (0.011)	0.130 (0.051)	0.22	–	78 (-320)	LN_2	2281 CYCLES TO BREAK-THROUGH
				STOP	0.028 (0.011)	0.130 (0.051)	0.22	1442 (209.2)	78 (-320)	LN_2	
			PROOF	START	0.028 (0.011)	0.130 (0.051)	0.22	–	295 (72)	AIR	
				STOP	0.028 (0.011)	0.130 (0.051)	0.22	1234 (179.0)	295 (72)	AIR	
			CYCLING	START	0.028 (0.011)	0.130 (0.051)	0.22	1234 (179.0)	295 (72)	AIR	
				STOP	0.244 (0.096)	0.749 (0.295)	0.33	1234 (179.0)	295 (72)	AIR	
2CW-8 (BM)	0.262 (0.103)	5.08 (2.00)	SIZING	START	0.018 (0.007)	0.119 (0.047)	0.15	–	78 (-320)	LN_2	FAILED OUTSIDE OF ARITIFICIALLY INDUCED FLAW AFTER 2814 CYCLES
				STOP	0.018 (0.007)	0.119 (0.047)	0.15	1442 (209.2)	78 (-320)	LN_2	
			PROOF	START	0.018 (0.007)	0.119 (0.047)	0.15	–	295 (72)	AIR	
				STOP	0.018 (0.007)	0.119 (0.047)	0.15	1234 (179.0)	295 (72)	AIR	
			CYCLING	START	0.018 (0.007)	0.119 (0.047)	0.15	1234 (179.0)	295 (72)	AIR	
				STOP	0.097 (0.038)	0.226 (0.089)	0.43	1234 (179.0)	295 (72)	AIR	

[1] SPECIMENS SUBJECTED TO A CRYO-PRESTRESS OF 932 MN/m^2 (135 KSI BASED ON ORIGINAL AREA) PRIOR TO LOADINGS SHOWN

[2] BASED ON AREA AT BEGINNING OF SIZING CYCLE

Table 50: Uniaxial Cyclic Tests of 0.26 cm (0.10 Inch) Thick Surface Flawed Cryostretched [1] 301 Stainless Steel Weld Metal Fusion Line at 78°K (-320°F)

SPECIMEN NUMBER	ORIGINAL THICKNESS, t cm (INCH)	ORIGINAL WIDTH, W cm (INCH)	TEST PARAMETERS AT		CRACK DEPTH, a cm (INCH)	CRACK LENGTH, 2c cm (INCH)	CRACK SHAPE, a/2c	[2] STRESS, σ MN/m² (KSI)	TEST: TEMPERATURE, T °K (°F)	TEST: ENVIRONMENT	REMARKS
2CW-5	0.264 (0.104)	5.08 (2.00)	SIZING	START	0.038 (0.015)	0.191 (0.075)	0.20	–	78 (-320)	LN_2	
				STOP	0.038 (0.015)	0.191 (0.075)	0.20	1442 (209.2)	78 (-320)	LN_2	
			CYCLING	START	0.038 (0.015)	0191 (0.075)	0.20	1227 (178.0)	78 (-320)	LN_2	3490 CYCLES TO BREAKTHROUGH
				STOP	0.249 (0.098)	0.630 (0.248)	0.40	1227 (178.0)	78 (-320)	LN_2	
2CW-7	0.259 (0.102)	5.08 (2.00)	SIZING	START	0.028 (0.011)	0.155 (0.061)	0.18	–	78 (-320)	LN_2	3985 CYCLES TO BREAKTHROUGH
				STOP	0.028 (0.011)	0.155 (0.061)	0.18	1442 (209.2)	78 (-320)	LN_2	
			CYCLING	START	0.028 (0.011)	0.155 (0.061)	0.18	1227 (178.0)	78 (-820	LN_2	
				STOP	0.244 (0.096)	0.627 (0.247)	0.39	1227 (178.0)	78 (-320)	LN_2	
2CW-11	0.264 (0.104)	5.08 (2.00)	SIZING	START	0.028 (0.011)	0.155 (0.061)	0.18	–	78 (-320)	LN_2	7900 CYCLES TO BREAK-THROUGH
				STOP	0.028 (0.011)	0.155 (0.061)	0.18	1442 (209.2)	78 (-320)	LN_2	
			CYCLING	START	0.028 (0.011)	0.155 (0.061)	0.18	1083 (157.0)	78 (-320)	LN_2	
				STOP	0.249 (0.098)	0.569 (0.224)	0.44	1083 (157.0)	78 (-320)	LN_2	
2CW-14	0.264 (0.104)	5.08 (2.00)	SIZING	START	0.020 (0.008)	0.117 (0.046)	0.17	–	78 (-320)	LN_2	FAILED OUTSIDE OF ARTIFICIALLY INDUCED FLAW AFTER 4033 CYCLES
				STOP	0.020 (0.008)	0.117 (0.046)	0.17	1442 (209.2)	78 (-320)	LN_2	
			CYCLING	START	0.020 (0.008)	0.117 (0.046)	0.17	1227 (178.0)	78 (-320)	LN_2	
				STOP	0.076 (0.030)	0.178 (0.070)	0.43	1227 (178.0)	78 (-320)	LN_2	

[1] SPECIMENS SUBJECTED TO A CRYO-PRESTRESS OF 932 MN/m² (135 KSI – BASED ON ORIGINAL AREA) PRIOR TO LOADINGS SHOWN

[2] BASED ON AREA AT BEGINNING OF SIZING CYCLE

Table 51: *Uniaxial Cyclic Tests of 0.26 cm (0.10 Inch) Thick Surface Flawed Cryostretched [1] 301 Stainless Steel Weld Metal Fusion Line at 295°K (72°F)*

SPECIMEN NUMBER	ORIGINAL THICKNESS, t cm (INCH)	ORIGINAL WIDTH, W cm (INCH)	TEST PARAMETERS AT		CRACK DEPTH, a cm (INCH)	CRACK LENGTH, 2c cm (INCH)	CRACK SHAPE, a/2c	STRESS, σ [2] MN/m^2 (KSI)	TEST TEMPERATURE, T °K (°F)	TEST ENVIRONMENT	REMARKS
2CW-2	0.254 (0.100)	5.03 (1.98)	SIZING	START	0.028 (0.011)	0.163 (0.064)	0.17	–	78 (-320)	LN_2	LESS THAN 5475 CYCLES TO BREAK-THROUGH
				STOP	0.028 (0.011)	0.163 (0.064)	0.17	1442 (209.2)	78 (-320)	LN_2	
			PROOF	START	0.028 (0.011)	0.163 (0.064)	0.17	–	295 (72)	AIR	
				STOP	0.028 (0.011)	0.163 (0.064)	0.17	1234 (179.0)	295 (72)	AIR	
			CYCLING	START	0.028 (0.011)	0.163 (0.064)	0.17	1027 (149.0)	295 (72)	AIR	
				STOP	0.246 (0.097)	< 0.742 (0.292)	>0.33	1027 (149.0)	295 (72)	AIR	
2CW-3	0.262 (0.103)	5.08 (2.00)	SIZING	START	0.028 (0.011)	0.155 (0.061)	0.18	–	78 (-320)	LN_2	2605 CYCLES TO BREAK-THROUGH
				STOP	0.028 (0.011)	0.155 (0.061)	0.18	1442 (209.2)	78 (-320)	LN_2	
			PROOF	START	0.028 (0.011)	0.155 (0.061)	0.18	–	295 (72)	AIR	
				STOP	0.028 (0.011)	0.155 (0.061)	0.18	1234 (179.0)	295 (72)	AIR	
			CYCLING	START	0.028 (0.011)	0.155 (0.061)	0.18	1234 (179.0)	295 (72)	AIR	
				STOP	0.246 (0.097)	0.574 (0.226)	0.43	1234 (179.0)	295 (72)	AIR	
2CW-4	0.259 (0.102)	5.08 (2.00)	SIZING	START	0.018 (0.007)	0.114 (0.045)	0.16	–	78 (-320)	LN_2	FAILED OUTSIDE OF ARTIFICIALLY INDUCED FLAW AFTER 4600 CYCLES
				STOP	0.018 (0.007)	0.114 (0.045)	0.16	1442 (209.2)	78 (-320)	LN_2	
			PROOF	START	0.018 (0.007)	0.114 (0.045)	0.16	–	295 (72)	AIR	
				STOP	0.018 (0.007)	0.114 (0.045)	0.16	1234 (179.0)	295 (72)	AIR	
			CYCLING	START	0.018 (0.007)	0.114 (0.045)	0.16	1034 (150.0)	295 (72)	AIR	
				STOP	0.086 (0.034)	0.198 (0.078)	0.44	1034 (150.0)	295 (72)	AIR	
2CW-6 (WM)	0.269 (0.106)	5.08 (2.00)	SIZING	START	0.015 (0.006)	0.094 (0.037)	0.16	–	78 (-320)	LN_2	CYCLED FOR 2669 CYCLES
				STOP	0.015 (0.006)	0.094 (0.037)	0.16	1442 (209.2)	78 (-320)	LN_2	
			PROOF	START	0.015 (0.006)	0.094 (0.037)	0.16	–	295 (72)	AIR	
				STOP	0.015 (0.006)	0.094 (0.037)	0.16	1234 (179.0)	295 (72)	AIR	
			CYCLING	START	0.015 (0.006)	0.094 (0.037)	0.16	1234 (179.0)	295 (72)	AIR	
				STOP	0.145 (0.057)	0.361 (0.142)	0.40	1234 (179.0)	295 (72)	AIR	

[1] SPECIMENS SUBJECTED TO A CRYO-PRESTRESS OF 932 MN/m^2 (135 KSI BASED ON ORIGINAL AREA) PRIOR TO LOADINGS SHOWN

[2] BASED ON AREA AT BEGINNING OF SIZING CYCLE

Table 52: Cyclic Crack Growth Rate Constants [1] for Cryostretched 301 Stainless Steel Tested at $R = 0$ and $(a/2c)_i \approx 0.16$

MATERIAL THICKNESS cm (INCH)	MATERIAL	TEMPERATURE °K (°F)	n	C	K RANGE $MN/m^{3/2}$ (KSI$\sqrt{IN}$) FROM	TO	REMARKS
0.071 (0.028)	BASE METAL	78 (-320)	5.6	0.0585×10^{-8} (2.52×10^{-8})	≈ 22.0 (20)	≈ 44.0 (40)	[2]
		295 (72)	6.9	0.0533×10^{-9} (2.30×10^{-9})			[3]
	WELD METAL	78 (-320)	5.6	0.0773×10^{-8} (3.33×10^{-8})			[2]
		296 (72)	6.9	0.0533×10^{-9} (2.30×10^{-9})			[3]
0.25 (0.10)	BASE METAL	78 (-320)	4.0	0.0766×10^{-6} (3.30×10^{-6})	≈ 27.5 (25)	≈ 109.9 (100)	[2]
		295 (72)	3.3	0.0174×10^{-4} (0.75×10^{-4})			[3]
	WELD METAL	78 (-320)	4.0	0.0766×10^{-6} (3.30×10^{-6})			[2]
		295 (72)	3.3	0.0174×10^{-4} (0.75×10^{-4})			[3]

[1] ASSUMES $da/dN = CK^n$ (SEE FIGURES 94,95,96 AND 97) WHERE da/dN UNITS ARE IN μcm/CYCLE (μINCHES/CYCLE)

[2] LN_2 CYCLIC TESTED AFTER BEING LOADED TO 1442 MN/m^2 (209.2 KSI) in LN_2

[3] RT CYCLIC TESTED AFTER BEING LOADED TO 1442 MN/m^2 (109.1 KSI) IN LN_2 AND THEN LOADED TO 1235 MN/m^2 (179.0 KSI) IN RT AIR

Table 53: Burst Tests of Tanks With Inconel X750 STA Shells at 295°K (72°F)

TANK	SPECIMEN NUMBER	LINER THICKNESS, t_L cm (INCH)	OVERWRAP THICKNESS, t_c cm (INCH)	LINER OUTSIDE DIAMETER, D_L cm (INCH)	TEST PARAMETERS AT	CRACK PLANE ORIENTATION RELATIVE TO TANK LONG. AXIS, ψ rad (DEG)	SURFACE CRACK DIMENSIONS: BASE METAL: DEPTH, a cm (INCH)	BASE METAL: LENGTH, 2c cm (INCH)	BASE METAL: SHAPE, a/2c	WELD METAL ℄: DEPTH, a cm (INCH)	WELD METAL ℄: LENGTH, 2c cm (INCH)	WELD METAL ℄: SHAPE, a/2c	TANK PRESSURE, p MN/m² (PSIG)	TANK STRESSES: OVERWRAP: HOOP, $\sigma_{t\theta}$ MN/m² (KSI)	LINER: HOOP, $\sigma_{L\theta}$ MN/m² (KSI)	LINER: LONG., $\sigma_{L\phi}$ MN/m² (KSI)	LINER: PERPEND. TO CRACK, $\sigma_{L\psi}$ MN/m² (KSI)	TEST: TEMPERATURE, T °K (°F)	TEST: ENVIRONMENT	REMARKS
NON-OVERWRAPPED	BS-1	0.102 (0.040)	–	16.469 (6.484)	MAX PRESSURE	0	0.076 (0.030)	0.394 (0.155)	0.19	–	–	–	11.1 (1610)	–	895 (129.8)	147 (64.9)	895 (129.8)	295 (72)	AIR	TANK LEAKED AT FLAW
	BS-6	0.102 (0.040)	–	16.469 (6.484)	MAX PRESSURE	0	–	–	–	0.056 (0.022)	0.297 (0.117)	0.19	11.7 (1690)	–	939 (136.2)	470 (68.1)	939 (136.2)	295 (72)	AIR	TANK RUPTURED AT FLAW
	BS-14	0.102 (0.040)	–	16.469 (6.484)	MAX PRESSURE	0	0.089 (0.035)	0.424 (0.167)	0.21	–	–	–	10.3 (1500)	–	834 (120.9)	417 (60.5)	834 (120.9)	295 (72)	AIR	TANK LEAKED AT FLAW
	BS-17	0.102 (0.040)	–	16.469 (6.484)	MAX PRESSURE	0	–	–	–	0.091 (0.036)	0.401 (0.158)	0.23	10.2 (1480)	–	822 (119.2)	411 (59.6)	822 (119.2)	295 (72)	AIR	TANK LEAKED AT FLAW
OVERWRAPPED	BS-2	0.102 (0.040)	0.076 (0.030)	16.447 (6.475)	AS FABRICATED	0	0.069 (0.027)	0.396 (0.156)	0.17	–	–	–	0	460 (66.7)	-232 (-33.6)	0	-232 (-33.6)	295 (72)	AIR	TANK LEAKED AT FLAW
					MAX PRESSURE								22.8 (3300)	1731 (251.0)	958 (138.9)	915 (132.7)	958 (138.9)			
	BS-7	0.102 (0.040)	0.076 (0.030)	16.454 (6.478)	AS FABRICATED	π/4 (45)	–	–	–	0.058 (0.023)	0.297 (0.117)	0.20	0	460 (66.7)	-232 (-33.6)	0	-116 (-16.8)	295 (72)	AIR	TANK FAILED IN HEAD-TO-CYLINDER GIRTH WELD
					MAX PRESSURE								22.7 (3290)	1979 (287.0)	829 (120.2)	913 (132.4)	871 (126.3)			
	BS-18	0.102 (0.040)	0.076 (0.030)	16.429 (6.468)	AS FABRICATED	π/4 (45)	–	–	–	0.084 (0.033)	0.419 (0.165)	0.20	0	460 (66.7)	-232 (-33.6)	0	-116 (-16.8)	295 (72)	AIR	TANK LEAKED AT FLAW
					MAX PRESSURE								20.3 (2950)	1689 (245.0)	783 (113.5)	817 (118.5)	800 (116.0)			
	BS-19	0.102 (0.040)	0.076 (0.030)	16.444 (6.474)	AS FABRICATED	π/4 (45)	0.084 (0.033)	0.442 (0.174)	0.19	–	–	–	0	460 (66.7)	-232 (-33.6)	0	-116 (-16.8)	295 (72)	AIR	TANK LEAKED AT FLAW
					MAX PRESSURE								20.4 (2960)	1634 (237.0)	818 (118.6)	821 (119.0)	819 (118.8)			
	BS-20	0.102 (0.040)	0.076 (0.030)	16.434 (6.470)	AS FABRICATED	0	0.086 (0.034)	0.452 (0.178)	0.19	–	–	–	0	460 (66.7)	-232 (-33.6)	0	-232 (-33.6)	295 (72)	AIR	TANK LEAKED AT FLAW
					MAX PRESSURE								16.5 (2400)	1048 (152.0)	803 (116.4)	665 (96.5)	803 (116.4)			
	BS-21	0.102 (0.040)	0.076 (0.030)	16.452 (6.477)	AS FABRICATED	π/4 (45)	0.069 (0.027)	0.323 (0.127)	0.21	–	–	–	0	460 (66.7)	-232 (-33.6)	0	-116 (-16.8)	295 (72)	AIR	TANK LEAKED AT FLAW
					MAX PRESSURE								24.5 (3550)	2572 (373.0)	673 (97.6)	986 (142.8)	829 (120.2)			
	BS-22	0.102 (0.040)	0.076 (0.030)	16.447 (6.475)	AS FABRICATED	0	–	–	–	0.091 (0.036)	0.452 (0.178)	0.20	0	460 (66.7)	-232 (-33.6)	0	-232 (-33.6)	295 (72)	AIR	TANK LEAKED AT FLAW
					MAX PRESSURE								16.4 (2380)	1007 (146.0)	812 (117.8)	660 (95.7)	812 (117.8)			
	BS-31	0.102 (0.040)	0.076 (0.030)	16.454 (6.478)	AS FABRICATED	0	–	–	–	0.061 (0.024)	0.351 (0.138)	0.17	0	460 (66.7)	-232 (-33.6)	0	-232 (-33.6)	295 (72)	AIR	TANK LEAKED AT FLAW
					MAX PRESSURE								25.2 (3660)	2455 (356.0)	794 (115.2)	1016 (147.3)	794 (115.2)			

Table 54: Burst Tests of Tanks With Inconel X750 STA Liners at 78°K (−320°F)

TANK	SPECIMEN NUMBER	LINER THICKNESS, t_L cm (INCH)	OVERWRAP THICKNESS, t_c cm (INCH)	LINER OUTSIDE DIAMETER, D_L cm (INCH)	TEST PARAMETERS AT	CRACK PLANE ORIENTATION RELATIVE TO TANK LONG. AXIS, ψ Rad. (DEG.)	SURFACE CRACK DIMENSIONS: BASE METAL DEPTH, a cm (INCH)	BASE METAL LENGTH, 2c cm (INCH)	BASE METAL SHAPE, a/2c	WELD METAL ℄ DEPTH, a cm (INCH)	WELD METAL ℄ LENGTH, 2c cm (INCH)	WELD METAL ℄ SHAPE, a/2c	TANK PRESSURE, p MN/m² (PSIG)	TANK STRESSES: OVER-WRAP HOOP, $\sigma_{f\theta}$ MN/m² (KSI)	LINER HOOP, $\sigma_{L\theta}$ MN/m² (KSI)	LINER LONG., $\sigma_{L\phi}$ MN/m² (KSI)	LINER PERPEND. TO CRACK, $\sigma_{L\psi}$ MN/m² (KSI)	TEST TEMPERATURE, T °K (°F)	TEST ENVIRONMENT	REMARKS
OVERWRAPPED	BS-11	0.102 (0.040)	0.076 (0.030)	16.434 (6.470)	AS FABRICATED	π/4 (45)	—	—	—	0.058 (0.023)	0.312 (0.123)	0.19	0	460 (66.7)	-232 (-33.6)	0	-116 (-16.8)	295 (72)	AIR	TANK RUPTURED AT FLAW – LONGITUDINALLY
					SIZING PRESSURE								19.6 (2840)	1420 (206.0)	858 (124.4)	787 (114.1)	826 (119.8)			
					RT ZERO PRESS								0	958 (139.0)	-484 (-70.2)	0	-242 (-35.1)			
					78°K ZERO PRESS								0	938 (136.0)	-472 (-68.5)	0	-236 (-34.3)	78 (-320)	LN_2	
					MAX PRESSURE								27.1 (3925)	2951 (428.0)	687 (99.6)	1087 (157.7)	887 (128.7)			
	BS-16	0.102 (0.040)	0.076 (0.030)	16.434 (6.470)	AS FABRICATED	0	—	—	—	0.066 (0.026)	0.378 (0.149)	0.17	0	460 (66.7)	-232 (-33.6)	0	-232 (-33.6)	295 (72)	AIR	TANK LEAKED AT FLAW
					SIZING PRESSURE								19.6 (2840)	1400 (203.0)	868 (125.9)	787 (114.1)	868 (125.9)			
					RT ZERO PRESS								0	924 (134.0)	-467 (-67.7)	0	-467 (-67.7)			
					78°K ZERO PRESS								0	903 (131.0)	-454 (-65.8)	0	-454 (-65.8)	78 (-320)	LN_2	
					MAX PRESSURE								22.8 (3300)	1896 (275.0)	874 (126.7)	914 (132.6)	874 (126.7)			
	BS-24	0.102 (0.040)	0.076 (0.030)	16.447 (6.475)	AS FABRICATED	0	0.058 (0.023)	0.345 (0.136)	0.17	—	—	—	0	460 (66.7)	-232 (-33.6)	0	-232 (-33.6)	295 (72)	AIR	TANK FAILED IN LONGITUDINAL CYLINDER WELD
					SIZING PRESSURE								19.6 (2840)	1427 (207.0)	856 (124.1)	787 (114.2)	856 (124.1)			
					RT ZERO PRESS								0	958 (139.0)	-482 (-69.9)	0	-482 (-69.9)			
					78°K ZERO PRESS								0	931 (135.0)	-470 (-68.2)	0	-470 (-68.2)	78 (-320)	LN_2	
					MAX PRESSURE								31.0 (4500)	3482 (505.0)	741 (107.4)	1248 (181.0)	741 (107.4)			
	BS-25	0.102 (0.040)	0.076 (0.030)	16.447 (6.475)	AS FABRICATED	π/4 (45)	0.069 (0.027)	0.361 (0.142)	0.19	—	—	—	0	460 (66.7)	-232 (-33.6)	0	-116 (-16.8)	295 (72)	AIR	TANK LEAKED AT FLAW
					SIZING PRESSURE								19.6 (2840)	1434 (208.0)	852 (123.6)	787 (114.2)	820 (118.9)			
					RT ZERO PRESS								0	965 (140.0)	-485 (-70.4)	0	-243 (-35.2)			
					78°K ZERO PRESS								0	938 (136.0)	-474 (-68.7)	0	-237 (-34.4)	78 (-320)	LN_2	
					MAX PRESSURE								25.7 (3730)	2468 (358.0)	825 (119.6)	1034 (150.0)	929 (134.8)			

Table 54: Burst Tests of Tanks With Inconel X750 STA Liners at 78°K (−320°F) (Continued)

TANK	SPECIMEN NUMBER	LINEAR THICKNESS, t_L cm (INCH)	OVERWRAP THICKNESS, t_c cm (INCH)	LINER OUTSIDE DIAMERER, D_L cm (INCH)	TEST PARAMETERS AT	CRACK PLANE ORIENTATION RELATIVE TO TANK LONG. AXIS, ψ Rad. (DEG.)	SURFACE CRACK DIMENSIONS – BASE METAL – DEPTH, a cm (INCH)	BASE METAL – LENGTH, 2c cm (INCH)	BASE METAL – SHAPE, a/2c	WELD METAL ℄ – DEPTH, a cm (INCH)	WELD METAL ℄ – LENGTH, 2c cm (INCH)	WELD METAL ℄ – SHAPE, a/2c	TANK PRESSURE, p MN/m² (PSIG)	TANK STRESSES – OVER-WRAP – HOOP, $\sigma_{f\theta}$ MN/m² (KSI)	LINER – HOOP, $\sigma_{L\theta}$ MN/m² (KSI)	LINER – LONG., $\sigma_{L\phi}$ MN/m² (KSI)	LINER – PERPEND. TO CRACK, $\sigma_{L\psi}$ MN/m² (KSI)	TEST – TEMPERATURE, T °K (°F)	TEST – ENVIRONMENT	REMARKS
OVERWRAPPED	BS-26	0.094 (0.037)	0.076 (0.030)	16.467 (6.483)	AS FABRICATED	0	0.061 (0.024)	0.376 (0148)	0.16	—	—	—	0	460 (66.7)	-250 (-36.3)	0	-250 (-36.3)	295 (72)	AIR	TANK LEAKED AT FLAW
					SIZING PRESSURE								19.6 (2840)	1586 (230.0)	841 (121.9)	862 (123.6)	841 (121.9)			
					RT ZERO PRESS								0	1089 (158.0)	-594 (-86.1)	0	-594 (-86.1)			
					78°K ZERO PRESS								0	1083 (157.0)	-588 (-85.3)	0	-588 (-85.3)	78 (-320)	LN_2	
					MAX PRESSURE								23.5 (3410)	2179 (316.0)	860 (124.7)	1023 (148.4)	860 (124.7)			
	BS-28	0.102 (0.040)	0.076 (0.030)	16.444 (6.474)	AS FABRICATED	π/4 (45)	0.048 (0.019)	0.312 (0.123)	0.15	—	—	—	0	460 (66.7)	-232 (-33.6)	0	-116 (-16.8)	295 (72)	AIR	TANK RUPTURE AT FLAW – CIRCUMFERENTIALLY
					SIZING PRESSURE								19.6 (2840)	1565 (227.0)	786 (114.0)	787 (114.2)	787 (114.1)			
					RT ZERO PRESS								0	1076 (156.0)	-642 (-78.6)	0	-271 (-39.3)			
					78°K ZERO PRESS								0	1062 (154.0)	-535 (-77.6)	0	-268 (-38.8)	78 (-320)	LN_2	
					MAX PRESSURE								29.5 (4280)	3537 (513.0)	590 (85.6)	1187 (172.1)	888 (128.8)			
	BS-29	0.102 (0.040)	0.076 (0.030)	16.434 (6.470	AS FABRICATED	π/4 (45)	—	—	—	0.071 (0.028)	0.361 (0.142)	0.20	0	460 (66.7)	-232 (-33.6)	0	-116 (-16.8)	295 (72)	AIR	TANK LEAKED AT FLAW
					SIZING PRESSURE								19.6 (2840)	1489 (216.0)	823 (119.3)	787 (114.1)	805 (116.7)			
					RT ZERO PRESS								0	993 (144.0)	-499 (-72.3)	0	-250 (-36.2)			
					78°K ZERO PRESS								0	972 (141.0)	-488 (-70.8)	0	-244 (-35.4)	78 (-320)	LN_2	
					MAX PRESSURE								24.5 (3560)	2241 (325.0)	845 (122.5)	987 (143.1)	916 (132.8)			

Table 55: Cyclic Life Tests of Tanks With Inconel X750 STA Shells at 295°K (72°F)

TANK	SPECIMEN NUMBER	LINER THICKNESS, t_L cm (INCH)	OVERWRAP THICKNESS, t_c cm (INCH)	LINER OUTSIDE DIAMETER, D_L cm (INCH)	TEST PARAMETERS AT	CRACK PLANE ORIENTATION RELATIVE TO TANK LONG. AXIS, ψ rad. (DEG.)	SURFACE CRACK DIMENSIONS: BASE METAL DEPTH, a cm (INCH)	BASE METAL LENGTH, 2c cm (INCH)	BASE METAL SHAPE, a/2c	WELD METAL ℄ DEPTH, a cm (INCH)	WELD METAL ℄ LENGTH, 2c cm (INCH)	WELD METAL ℄ SHAPE, a/2c	TANK PRESSURE, p MN/m² (KSI)	TANK STRESSES: OVERWRAP HOOP, $\sigma_{f\theta}$ MN/m² (KSI)	LINER HOOP, $\sigma_{L\theta}$ MN/m² (KSI)	LINER LONG., $\sigma_{L\phi}$ MN/m² (KSI)	LINER PERPEND. TO CRACK, $\sigma_{L\psi}$ MN/m² (KSI)	TEST TEMPERATURE, T °K (°F)	TEST ENVIRONMENT	REMARKS
NON-OVERWRAPPED	BS-10	0.102 (0.040)	–	16.469 (6.484)	SIZING PRESSURE	0	0.061 (0.024)	0.310 (0.122)	0.20	0.041 (0.016)	0.254 (0.100)	0.16	10.5 (1530)	–	850 (123.3)	425 (61.7)	850 (123.3)	295 (72)	AIR	TANK LEAKED AT BASE METAL FLAW IN 3185 CYCLES R = 0
					MAX OPER PRESS ▷1		0.102 (0.040)	0.363 (0.143)	0.28	0.053 (0.021)	0.254 (0.100)	0.21	9.0 (1300)	–	723 (104.9)	362 (52.5)	723 (104.9)			
	BS-13	0.102 (0.040)	–	16.469 (6.484)	SIZING PRESSURE	0	–	–	–	0.053 (0.021)	0.312 (0.123)	0.17	10.5 (1530)	–	850 (123.3)	425 (61.7)	850 (123.3)	295 (72)	AIR	TANK LEAKED AT WELD METAL FLAW IN 4807 CYCLES R = 0
					MAX OPER PRESS ▷1		–	–	–	0.102 (0.040)	0.361 (0.142)	0.28	9.0 (1300)	–	723 (104.9)	362 (52.5)	723 (104.9)			
OVERWRAPPED	BS-4	0.102 (0.040)	0.076 (0.030)	16.449 (6.476)	AS FABRICATED	0							0	460 (66.7)	-232 (-33.6)	0	-232 (-33.6)	295 (72)	AIR	TANK LEAKED AT WELD METAL FLAW IN ABOUT 350 CYCLES R = -0.78
					SIZING PRESSURE		–	–	–	0.064 (0.025)	0.330 (0.130)	0.19	19.6 (2840)	1565 (227.0)	789 (114.4)	788 (114.3)	789 (114.4)			
					RT ZERO PRESSURE								0	1062 (154.0)	-536 (-77.7)	0	-536 (-77.7)			
					MAX OPER PRESS ▷1		–	–	–	0.102 (0.040)	0.373 (0.147)	0.27	17.8 (2580)	1476 (214.0)	687 (99.7)	716 (103.8)	687 (99.7)			
	BS-6	0.102 (0.040)	0.076 (0.030)	16.434 (6.470)	AS FABRICATED	π/4 (45)							0	460 (66.7)	-232 (-33.6)	0	-116 (-16.8)	295 (72)	AIR	TANK LEAKED AT WELD METAL FLAW IN 763 CYCLES R = -0.34
					SIZING PRESSURE		0.053 (0.021)	0.277 (0.109)	0.19	0.066 (0.026)	0.312 (0.123)	0.21	19.6 (2840)	1469 (213.0)	833 (120.8)	787 (114.1)	810 (117.5)			
					RT ZERO PRESSURE								0	979 (142.0)	-492 (-71.4)	0	-246 (-35.7)			
					MAX OPER PRESS ▷1		0.069 (0.027)	0.284 (0.112)	0.24	0.102 (0.040)	0.335 (0.132)	0.30	17.7 (2570)	1393 (202.0)	723 (104.8)	712 (103.3)	718 (104.1)			
	BS-8	0.102 (0.040)	0.076 (0.030)	16.449 (6.476)	AS FABRICATED	π/4 (45)							0	460 (66.7)	-232 (-33.6)	0	-116 (-16.8)	295 (72)	AIR	TANK LEAKED IN BASE METAL FLAW IN 1629 CYCLES R = -0.34
					SIZING PRESSURE		0.056 (0.022)	0.310 (0.122)	0.18	–	–	–	19.6 (2840)	1434 (208.0)	853 (123.7)	788 (114.3)	821 (119.0)			
					RT ZERO PRESSURE								0	965 (140.0)	-487 (-70.7)	0	-244 (-35.4)			
					MAX OPER PRESS ▷1		0.102 (0.040)	0.335 (0.132)	0.30	–	–	–	17.8 (2580)	1427 (207.0)	712 (103.3)	716 (103.8)	750 (108.8)			
	BS-9	0.102 (0.040)	0.076 (0.030)	16.424 (6.466)	AS FABRICATED	0							0	460 (66.7)	-232 (-33.6)	0	-232 (-33.6)	295 (72)	AIR	TANK LEAKED IN BASE METAL FLAW IN 644 CYCLCES R = -0.69
					SIZING PRESSURE		0.061 (0.024)	0.323 (0.127)	0.19	0.046 (0.018)	0.259 (0.102)	0.18	19.6 (2840)	1476 (214.0)	829 (120.2)	787 (114.1)	829 (120.2)			
					RT ZERO PRESSURE								0	1000 (145.0)	-503 (-72.9)	0	-503 (-72.9)			
					MAX OPER PRESS ▷1		0.102 (0.040)	0.353 (0.139)	0.29	0.053 (0.021)	0.259 (0.102)	0.21	17.8 (2580)	1393 (202.0)	727 (105.4)	714 (103.6)	727 (105.4)			
	BS-27	0.102 (0.040)	0.076 (0.030)	16.457 (6.479)	AS FABRICATED	0							0	460 (66.7)	-232 (-33.6)	0	-232 (-33.6)	295 (72)	AIR	TANK LEAKED AT BASE METAL FLAW IN CYCLES 890 CYCLES R = -0.05
					SIZING PRESSURE		0.076 (0.030)	0.340 (0.134)	0.22	0.061 (0.024)	0.300 (0.118)	0.20	19.6 (2840)	1551 (225.0)	794 (115.2)	788 (114.3)	794 (115.2)			
					RT ZERO PRESSURE								0	1062 (154.0)	-534 (-77.4)	0	-534 (-77.4)			
					MAX OPER PRESS ▷1		0.102 (0.040)	0.366 (0.144)	0.28	0.076 (0.030)	0.305 (0.120)	0.25	17.8 (2580)	1455 (211.0)	698 (101.3)	716 (103.8)	698 (101.3)			
					MIN OPER PRESS ▷1								7.2 (1050)	1227 (178.0)	-35 (-5.1)	292 (42.3)	-35 (-5.1)			

▷1 FLAW DIMENSIONS AT TEST TERMINATION

Table 56: Cyclic Life Tests of Tanks With Inconel X750 STA Liners at 78°K (−320°F)

TANK	SPECIMEN NUMBER	LINER THICKNESS, t_L cm (INCH)	OVERWRAP THICKNESS, t_c cm (INCH)	LINER OUTSIDE DIAMETER, D_L cm (INCH)	TEST PARAMETERS AT	CRACK PLANE ORIENTATION RELATIVE TO TANK LONG. AXIS, ψ rad (DEG)	SURFACE CRACK DIMENSIONS: BASE METAL: DEPTH, a cm (INCH)			SURFACE CRACK DIMENSIONS: WELD METAL ℄: DEPTH, a cm (INCH)			TANK PRESSURE, p MN/m² (PSIG)	TANK STRESSES: OVERWRAP: HOOP, $\sigma_{f\theta}$ MN/m² (KSI)	TANK STRESSES: LINER: HOOP, $\sigma_{L\theta}$ MN/m² (KSI)			TEST: TEMPERATURE, T °K (°F)		REMARKS
							DEPTH, a cm (INCH)	LENGTH, 2c cm (INCH)	SHAPE, a/2c	DEPTH, a cm (INCH)	LENGTH, 2c cm (INCH)	SHAPE, a/2c			HOOP, $\sigma_{L\theta}$ MN/m² (KSI)	LONG., $\sigma_{L\phi}$ MN/m² (KSI)	PERPEND. TO CRACK, $\sigma_{L\psi}$ MN/m² (KSI)	TEMPERATURE, T °K (°F)	ENVIRONMENT	
OVERWRAPPED	BS-15	0.102 (0.040)	0.076 (0.030)	16.452 (6.477)	AS FABRICATED	0	0.038 (0.015)	0.196 (0.077)	0.20	0.061 (0.024)	0.284 (0.112)	0.21	0	460 (66.7)	-232 (-33.6)	0	-232 (-33.6)	295 (72)	AIR	TANK LEAKED AT WELD METAL FLAW IN 749 CYCLES R = - 0.86
					SIZING PRESSURE								19.6 (2840)	1607 (233.0)	767 (111.2)	788 (114.3)	767 (111.2)			
					RT ZERO PRESSURE								0	1110 (161.0)	-559 (-81.1)	0	-559 (-81.1)			
					78°K ZERO PRESSURE								0	1096 (159.0)	-554 (-80.3)	0	-554 (-80.3)	78 (-320)	LN$_2$	
					PROOF PRESSURE								20.9 (3030)	1765 (256.0)	791 (114.7)	841 (121.9)	791 (114.7)			
					78°K MIN PRESSURE								0.7 (100)	1248 (181.0)	-573 (-83.1)	28 (4.0)	-573 (-83.1)			
					MAX OPER PRESS [1]		0.046 (0.018)	0.196 (0.077)	0.23	0.102 (0.040)	0.312 (0.123)	0.33	18.8 (2730)	1682 (244.0)	667 (96.7)	757 (109.8)	667 (96.7)			
	BS-23	0.102 (0.040)	0.076 (0.030)	16.190 (6.374)	AS FABRICATED	0	0.058 (0.023)	0.274 (0.108)	0.21	0.033 (0.013)	0.191 (0.075)	0.17	0	460 (66.7)	-232 (-33.6)	0	-232 (-33.6)	295 (72)	AIR	TANK LEAKED AT BASE METAL FLAW IN 1122 CYCLES R = - 0.74
					SIZING PRESSURE								19.6 (2840)	1489 (216.0)	824 (119.5)	787 (114.2)	824 (119.5)			
					RT ZERO PRESSURE								0	986 (143.0)	-497 (-72.1)	0	-497 (-72.1)			
					78°K ZERO PRESSURE								0	965 (140.0)	-486 (-70.5)	0	-486 (-70.5)	78 (-320)	LN$_2$	
					PROOF PRESSURE								20.9 (3030)	1648 (239.0)	848 (123.0)	840 (121.8)	848 (123.0)			
					78°K MIN PRESSURE								0.7 (100)	1151 (167.0)	-526 (-76.3)	28 (4.0)	-526 (-76.3)			
					MAX OPER PRESS [1]		0.102 (0.040)	0.315 (0.124)	0.32	0.043 (0.017)	0.191 (0.075)	0.23	18.8 (2730)	1593 (231.0)	712 (103.2)	757 (109.8)	712 (103.2)			

[1] FLAW DIMENSIONS AT TEST TERMINATION

Table 57: Burst Tests of Tanks With 2219-T62 Aluminum Shells at 295°K (72°F)

TANK	SPECIMEN NUMBER	LINER THICKNESS, t_L cm (INCH)	OVERWRAP THICKNESS, t_c cm (INCH)	LINER OUTSIDE DIAMETER, D_L cm (INCH)	TEST PARAMETERS AT	CRACK PLANE ORIENTATION RELATIVE TO TANK LONG. AXIS, ψ rad (DEG)	SURFACE CRACK DIMENSIONS: BASE METAL: DEPTH, a cm (INCH)	BASE METAL: LENGTH, 2c cm (INCH)	BASE METAL: SHAPE, a/2c	WELD METAL ℄: DEPTH, a cm (INCH)	WELD METAL ℄: LENGTH, 2c cm (INCH)	WELD METAL ℄: SHAPE, a/2c	TANK PRESSURE, p MN/m^2 (PSIG)	TANK STRESSES: OVERWRAP: HOOP, $\sigma_{t\theta}$ MN/m^2 (KSI)	LINER: HOOP, $\sigma_{L\theta}$ MN/m^2 (KSI)	LINER: LONG., $\sigma_{L\phi}$ MN/m^2 (KSI)	LINER: PERPEND. TO CRACK, $\sigma_{L\psi}$ MN/m^2 (KSI)	TEST: TEMPERATURE, T °K (°F)	TEST: ENVIRONMENT	REMARKS
NON-OVERWRAPPED	AS-1	0.244 (0.096)	–	16.767 (6.601)	MAX PRESSURE	0	0.107 (0.042)	0.584 (0.230)	0.18	–	–	–	10.7 (1550)	–	362 (52.5)	181 (26.2)	362 (52.5)	295 (72)	AIR	TANK RUPTURED AT FLAW
	AS-5	0.251 (0.099)	–	16.787 (6.609)	MAX PRESSURE	0	–	–	–	0.152 (0.060)	0.681 (0.268)	0.22	10.5 (1530)	–	347 (50.3)	174 (25.2)	347 (50.3)	295 (72)	AIR	TANK RUPTURED AT FLAW
	AS-16	0.246 (0.097)	–	16.789 (6.610)	MAX PRESSURE	0	0.157 (0.062)	0.747 (0.294)	0.21	–	–	–	10.5 (1520)	–	352 (51.0)	176 (25.5)	352 (51.0)	295 (72)	AIR	TANK RUPTURED AT FLAW
	AS-18	0.249 (0.098)	–	16.806 (6.616)	MAX PRESSURE	0	–	–	–	0.191 (0.075)	1.003 (0.395)	0.19	9.2 (1330)	–	305 (44.2)	152 (22.1)	305 (44.2)	295 (72)	AIR	TANK RUPTURED AT FLAW
OVERWRAPPED	AS-2	0.236 (0.093)	0.074 (0.029)	16.726 (6.585)	AS FABRICATED	0	0.114 (0.045)	0.579 (0.228)	0.20	–	–	–	0	460 (66.7)	-96 (-13.9)	0	-96 (-13.9)	295 (72)	AIR	TANK FAILED IN HEAD-TO-CYLINDER GIRTH WELD
					MAX PRESSURE								17.2 (2500)	1269 (184.0)	338 (49.0)	301 (43.6)	338 (49.0)			
	AS-6	0.246 (0.097)	0.074 (0.029)	16.764 (6.600)	AS FABRICATED	0	0.102 (0.040)	0.478 (0.188)	0.21	–	–	–	0	460 (66.7)	-92 (-13.3)	0	-92 (-13.3)	296 (72)	AIR	TANK FAILED IN LONG. CYLINDER WELD
					MAX PRESSURE								19.0 (2760)	1441 (209.0)	351 (50.9)	319 (46.3)	351 (50.9)			
	AS-8	0.249 (0.098)	0.074 (0.029)	16.744 (6.592)	AS FABRICATED	0	0.127 (0.050) [1]	0.643 (0.253)	0.20	–	–	–	0	460 (66.7)	-91 (-13.2)	0	-91 (-13.2)	295 (72)	AIR	TANK LEAKED IN HEAD-TO-CYLINDER GIRTH WELD
					MAX PRESSURE								20.9 (3025)	1579 (229.0)	379 (55.0)	345 (50.1)	379 (55.0)			
	AS-10	0.254 (0.100)	0.074 (0.029)	16.749 (6.594)	AS FABRICATED	0	–	–	–	0.157 (0.062)	0.749 (0.295)	0.21	0	460 (66.7)	-89 (-12.9)	0	-89 (-12.9)	295 (72)	AIR	TANK LEAKED AT FLAW
					MAX PRESSURE								19.6 (2840)	1482 (215.0)	352 (51.0)	319 (46.3)	352 (51.0)			
	AS-12	0.246 (0.097)	0.074 (0.029)	16.751 (6.595)	AS FABRICATED	π/4 (45)	0.137 (0.054)	0.749 (0.295)	0.18	–	–	–	0	460 (66.7)	-92 (-13.3)	0	-46 (-6.7)	295 (72)	AIR	TANK LEAKED AT FLAW
					MAX PRESSURE								23.9 (3470)	1931 (280.0)	416 (60.4)	401 (58.1)	409 (59.3)			
	AS-13	0.251 (0.099)	0.074 (0.029)	16.754 (6.596)	AS FABRICATED	π/4 (45)	–	–	–	0.173 (0.068)	0.881 (0.347)	0.20	0	460 (66.7)	-90 (-13.0)	0	90 (-13.0)	295 (72)	AIR	TANK LEAKED AT FLAW
					MAX PRESSURE								18.6 (2700)	1338 (194.0)	350 (50.7)	305 (44.3)	328 (47.5)			
	AS-14	0.251 (0.099)	0.074 (0.029)	16.764 (6.600)	AS FABRICATED	π/4 (45)	0.191 (0.075)	0.965 (0.380)	0.20	–	–	–	0	460 (66.7)	-90 (13.0)	0	-90 (-13.0)	295 (72)	AIR	TANK LEAKED AT FLAW
					MAX PRESSURE								16.8 (2430)	1165 (169.0)	323 (46.8)	275 (39.9)	299 (43.4)			
	AS-15	0.254 (0.100)	0.074 (0.029)	16.777 (6.606)	AS FABRICATED	π/4 (45)	–	–	–	0.196 (0.077)	1.041 (0.410)	0.19	0	460 (66.7)	-89 (-12.9)	0	-89 (-12.9)	295 (72)	AIR	TANK LEAKED AT FLAW
					MAX PRESSURE								15.7 (2280)	1069 (155.0)	305 (44.2)	256 (37.1)	281 (40.7)			
	AS-23	0.254 (0.100)	0.074 (0.029)	16.759 (6.598)	AS FABRICATED	0	–	–	–	0.203 (0.080)	1.080 (0.425)	0.19	0	460 (66.7)	-89 (-12.9)	0	-89 (-12.9)	295 (72)	AIR	TANK LEAKED AT FLAW
					MAX PRESSURE								14.1 (2050)	938 (136.0)	284 (41.2)	232 (33.7)	284 (41.2)			
	AS-31	0.249 (0.098)	0.074 (0.029)	16.769 (6.602)	AS FABRICATED	0	0.198 (0.078)	0.996 (0.392)	0.20	–	–	–	0	460 (66.7)	-91 (-13.2)	0	-91 (-13.2)	295 (72)	AIR	TANK LEAKED AT FLAW
					MAX PRESSURE								17.1 (2480)	1220 (177.0)	326 (47.3)	283 (41.1)	326 (47.3)			

[1] FLAW GREW IN DEPTH 0.010 cm (0.004 INCH) AT MAX PRESSURE – FLAW AREA MARKED AND FAILED

Table 58: Burst Tests of Tanks With 2219-T62 Aluminum Liners at 78°K (–320°F)

TANK	SPECIMEN NUMBER	LINER THICKNESS, t_L cm (INCH)	OVERWRAP THICKNESS, t_c cm (INCH)	LINER OUTSIDE DIAMETER, D_L cm (INCH)	TEST PARAMETERS AT	CRACK PLANE ORIENTATION RELATIVE TO TANK LONG. AXIS, ψ rad. (DEG.)	SURFACE CRACK DIMENSIONS: BASE METAL DEPTH, a cm (INCH)	BASE METAL LENGTH, 2c cm (INCH)	BASE METAL SHAPE, a/2c	WELD METAL ℄ DEPTH, a cm (INCH)	WELD METAL ℄ LENGTH, 2c cm (INCH)	WELD METAL ℄ SHAPE, a/2c	TANK PRESSURE, p MN/m² (PSIG)	TANK STRESSES: OVERWRAP HOOP, σ_θ MN/m² (KSI)	LINER HOOP, $\sigma_L\theta$ MN/m² (KSI)	LINER LONG., $\sigma_L\phi$ MN/m² (KSI)	LINER PERPEND. TO CRACK, $\sigma_L\psi$ MN/m² (KSI)	TEST TEMPERATURE, T °K (°F)	TEST ENVIRONMENT	REMARKS
OVERWRAPPED	AS-17	0.257 (0.101)	0.074 (0.029)	16.772 (6.603)	AS FABRICATED	0	–	–	–	0.188 (0.074)	0.899 (0.354)	0.21	0	460 (66.7)	-88 (-12.8)	0	-88 (-12.8)	295 (72)	AIR	TANK LEAKED AT FLAW
					SIZING PRESSURE								16.8 (2430)	1069 (155.0)	335 (48.6)	270 (39.1)	335 (48.6)			
					RT ZERO PRESS								0	554 (80.3)	-106 (-15.4)	0	-106 (-15.4)			
					78°K ZERO PRESS								0	379 (54.9)	-72 (-10.5)	0	-72 (-10.5)	78 (-320)	LN_2	
					MAX PRESSURE								21.0 (3050)	1393 (202.0)	411 (59.6)	339 (49.1)	411 (59.6)			
	AS-19	0.259 (0.102)	0.074 (0.029)	16.756 (6.597)	AS FABRICATED	π/4 (45)	0.185 (0.073)	0.902 (0.355)	0.21	–	–	–	0	460 (66.7)	-87 (-12.6)	0	-43 (-6.3)	295 (72)	AIR	TANK RUPTURED AT FLAW
					SIZING PRESSURE								16.8 (2430)	1083 (157.0)	329 (47.7)	267 (38.7)	299 (43.2)			
					RT ZERO PRESS								0	566 (82.1)	-107 (-15.5)	0	-54 (-7.8)			
					78°K ZERO PRESS								0	390 (56.5)	-74 (-10.7)	0	-37 (-5.4)	78 (-320)	LN_2	
					MAX PRESSURE								21.0 (3050)	1469 (213.0)	392 (56.9)	335 (48.6)	364 (52.8)			
	AS-20	0.264 (0.104)	0.074 (0.029)	16.751 (6.595)	AS FABRICATED	0	–	–	–	0.152 (0.060)	0.749 (0.295)	0.20	0	460 (66.7)	-85 (-12.4)	0	-85 (-12.4)	295 (72)	AIR	TANK LEAKED IN LONG CYLINDER WELD FUSION LINE
					SIZING PRESSURE								16.8 (2430)	1117 (162.0)	315 (45.7)	261 (37.9)	315 (45.7)			
					RT ZERO PRESS								0	601 (87.2)	-112 (-16.2)	0	-112 (-16.2)			
					78°K ZERO PRESS								0	427 (61.9)	-79 (-11.5)	0	-79 (-11.5)	78 (-320)	LN_2	
					MAX PRESSURE								21.0 (3050)	1441 (209.0)	389 (56.4)	328 (47.6)	389 (56.4)			
	AS-21	0.246 (0.097)	0.074 (0.029)	16.749 (6.594)	AS FABRICATED	0	0.168 (0.066)	0.737 (0.290)	0.23	–	–	–	0	460 (66.7)	-92 (-13.3)	0	-92 (-13.3)	295 (72)	AIR	TANK FAILED AT FLAW
					SIZING PRESSURE								16.8 (2430)	1158 (168.0)	330 (47.9)	281 (40.7)	330 (47.9)			
					RT ZERO PRESS								0	599 (86.9)	-119 (-17.3)	0	-119 (-17.3)			
					78°K ZERO PRESS								0	429 (62.2)	-85 (-12.4)	0	-85 (-12.4)	78 (-320)	LN_2	
					MAX PRESSURE								22.4 (3250)	1655 (240.0)	421 (61.0)	375 (54.4)	421 (61.0)			
	AS-29	0.249 (0.098)	0.074 (0.029)	16.761 (6.599)	AS FABRICATED	π/4 (45)	–	–	–	0.185 (0.073)	0.879 (0.346)	0.21	0	460 (66.7)	-91 (-13.2)	0	-46 (-6.6)	295 (72)	AIR	TANK LOST PRESSURE BUT NO INDICATION AT BREAKTHROUGH DEVICE
					SIZING PRESSURE								16.8 (2430)	1103 (160.0)	339 (49.1)	278 (40.3)	308 (44.7)			
					RT ZERO PRESS								0	545 (79.1)	-108 (-15.6)	0	-54 (-7.8)			
					78°K ZERO PRESS								0	371 (53.8)	-73 (-10.6)	0	-37 (-5.3)	78 (-320)	LN_2	
					MAX PRESSURE								22.3 (3240)	1703 (247.0)	404 (58.6)	370 (53.7)	387 (56.2)			

Table 59: Cyclic Life Tests of Tanks With 2219-T62 Aluminum Shells at 295°K (72°F)

TANK	SPECIMEN NUMBER	LINER THICKNESS, t_L cm (INCH)	OVERWRAP THICKNESS, t_c cm (INCH)	LINER OUTSIDE DIAMETER, D_L cm (INCH)	TEST PARAMETERS AT	CRACK PLANE ORIENTATION RELATIVE TO TANK LONG. AXIS, ψ rad (DEG)	SURFACE CRACK DIMENSIONS: BASE METAL: DEPTH, a cm (INCH)	BASE METAL: LENGTH, 2c cm (INCH)	BASE METAL: SHAPE, a/2c	WELD METAL ℄: DEPTH, a cm (INCH)	WELD METAL ℄: LENGTH, 2c cm (INCH)	WELD METAL ℄: SHAPE, a/2c	TANK PRESSURE, p MN/m² (PSIG)	TANK STRESSES: OVERWRAP: HOOP, $\sigma_{f\theta}$ MN/m² (KSI)	LINER: HOOP, $\sigma_{L\theta}$ MN/m² (KSI)	LINER: LONG., $\sigma_{L\phi}$ MN/m² (KSI)	LINER: PERPEND. TO CRACK, $\sigma_{L\psi}$ MN/m² (KSI)	TEST: TEMPERATURE, T °K (°F)	TEST: ENVIRONMENT	REMARKS
NON-OVERWRAPPED	AS-3	0.236 (0.093)	–	16.772 (6.603)	SIZING PRESSURE	0	0.094 (0.037)	0.516 (0.203)	0.18	0.066 (0.026)	0.345 (0.136)	0.19	9.4 (1375)	–	332 (48.2)	166 (24.1)	332 (48.2)	295 (72)	AIR	TANK LEAKED AT BASE METAL FLAW IN 4492 CYCLES R = 0
					MAX OPER PRESS. [1]		0.236 (0.093)	0.744 (0.293)	0.32	0.165 (0.065)	0.503 (0.198)	0.33	7.1 (1030)	–	249 (36.1)	125 (18.1)	249 (36.1)			
	AS-27	0.249 (0.098)	–	16.784 (6.608)	SIZING PRESSURE	0	0.086 (0.034)	0.406 (0.160)	0.21	0.089 (0.035)	0.424 (0.167)	0.21	10.0 (1450)	–	332 (48.2)	166 (24.1)	332 (48.2)	295 (72)	AIR	TANK LEAKED AT WELD METAL FLAW IN 2769 CYCLES R = 0
					MAX OPER PRESS. [1]		0.249 (0.098)	0.744 (0.293)	0.33	0.249 (0.098)	0.876 (0.345)	0.28	7.5 (1090)	–	250 (36.2)	125 (18.1)	250 (36.2)			
OVERWRAPPED	AS-11	0.249 (0.098)	0.074 (0.029)	16.744 (6.592)	AS FABRICATED	0	0.097 (0.038)	0.457 (0.180)	0.21	0.058 (0.023)	0.318 (0.125)	0.18	0	460 (66.7)	-91 (-13.2)	0	-91 (-13.2)	295 (72)	AIR	TANK LEAKED AT BASE METAL FLAW IN 1015 CYCLES R = - 0.44
					SIZING PRESSURE								16.8 (2430)	1179 (171.0)	323 (46.8)	278 (40.3)	323 (46.8)			
					RT ZERO PRESSURE								0	607 (88.0)	-120 (-17.4)	0	-120 (-17.4)			
					MAX OPER PRESS. [1]		0.249 (0.098)	0.686 (0.270)	0.36	0.130 [2] (0.061)	0.371 (0.146)	0.35	14.1 (2040)	993 (144.0)	271 (39.3)	233 (33.8)	271 (39.3)			
	AS-22	0.249 (0.098)	0.074 (0.029)	16.751 (6.595)	AS FABRICATED	0	0.114 (0.045)	0.495 (0.195)	0.23	0.079 (0.031)	0.361 (0.142)	0.22	0	460 (66.7)	-91 (-13.2)	0	-91 (-13.2)	295 (72)	AIR	TANK LEAKED AT BASE METAL FLAW IN 4287 CYCLES R = 0.20
					SIZING PRESSURE								16.8 (2430)	1096 (159.0)	339 (49.2)	278 (40.3)	339 (49.2)			
					RT ZERO PRESSURE								0	563 (81.6)	-111 (-16.1)	0	-111 (-16.1)			
					MAX OPER PRESS [1]		0.249 (0.098)	0.660 (0.260)	0.38	0.168 (0.066)	0.470 (0.185)	0.36	14.1 (2040)	889 (129.0)	290 (42.1)	233 (33.8)	290 (42.1)			
					MIN OPER PRESS. [1]								5.9 (860)	696 (101.0)	59 (8.6)	99 (14.3)	59 (8.6)			
	AS-24	0.249 (0.098)	0.074 (0.029)	16.777 (6.605)	AS FABRICATED	π/4 (45)	0.104 (0.041)	0.452 (0.178)	0.23	0.071 (0.028)	0.318 (0.125)	0.22	0	460 (66.7)	-91 (-13.2)	0	-46 (-6.6)	295 (72)	AIR	TANK LEAKED AT BASE METAL FLAW IN 1854 CYCLES R = - 0.26
					SIZING PRESSURE								16.8 (2430)	1241 (180.0)	311 (45.1)	278 (40.3)	311 (42.7)			
					RT ZERO PRESSURE								0	660 (95.7)	-130 (-18.9)	0	-130 (-9.5)			
					MAX OPER PRESS [1]		0.249 (0.098)	0.579 (0.228)	0.43	0.168 (0.066)	0.439 (0.173)	0.38	14.1 (2040)	1034 (150.0)	264 (38.3)	234 (33.9)	249 (36.1)			
	AS-25	0.254 (0.100)	0.074 (0.029)	16.774 (6.604)	AS FABRICATED	0	0.079 (0.031)	0.389 (0.153)	0.20	0.081 (0.032)	0.381 (0.150)	0.21	0	460 (66.7)	-89 (-12.9)	0	-89 (-12.9)	295 (72)	AIR	TANK LEAKED AT LONG. WELD FUSION LINE IN 1206 CYCLES R = - 0.45
					SIZING PRESSURE								16.8 (2430)	1166 (169.0)	319 (46.3)	272 (39.5)	319 (46.3)			
					RT ZERO PRESSURE								0	619 (89.8)	-119 (-17.3)	0	-119 (-17.3)			
					MAX OPER PRESS. [1]		0.185 (0.073)	0.533 (0.210)	0.35	0.193 (0.076)	0.622 (0.245)	0.31	14.1 (2040)	1000 (145.0)	264 (38.3)	229 (33.2)	264 (38.3)			
	AS-28	0.251 (0.099)	0.074 (0.029)	16.769 (6.602)	AS FABRICATED	π/4 (45)	0.081 (0.032)	0.406 (0.160)	0.20	0.081 (0.032)	0.394 (0.155)	0.21	0	460 (66.7)	-90 (-13.0)	0	-45 (-6.5)	295 (72)	AIR	TANK LEAKED AT WELD METAL FLAW IN 1584 CYCLES R = - 0.25
					SIZING PRESSURE								19.6 (2840)	1193 (173.0)	317 (46.0)	275 (39.9)	296 (43.0)			
					RT ZERO PRESSURE								0	632 (91.6)	-123 (-17.9)	0	-62 (-9.0)			
					MAX OPER PRESS. [1]		0.147 (0.058)	0.472 (0.186)	0.31	0.251 (0.099)	0.584 (0.230)	0.43	14.1 (2040)	1014 (147.0)	265 (38.4)	231 (33.5)	248 (36.0)			
	AS-32	0.249 (0.098)	0.074 (0.029)	16.373 (6.446)	AS FABRICATED	0	0.064 (0.025)	0.269 (0.106)	0.24	0.071 (0.028)	0.323 (0.127)	0.22	0	460 (66.7)	-91 (-13.2)	0	-91 (-13.2)	295 (72)	AIR	TANK LEAKED AT WELD METAL FLAW IN 1132 CYCLES R = - 0.45
					SIZING PRESSURE								16.8 (2430)	1158 (168.0)	328 (47.5)	278 (40.3)	328 (47.5)			
					RT ZERO PRESSURE								0	603 (87.4)	-119 (-17.2)	0	-119 (-17.2)			
					MAX OPER PRESS. [1]		0.137 (0.054)	0.386 (0.152)	0.36	0.249 (0.098)	0.592 (0.233)	0.42	14.1 (2040)	1014 (147.0)	266 (38.6)	233 (33.8)	266 (38.6)

[1] FLAW DIMENSIONS AT TEST TERMINATION

[2] ESTIMATE

Table 60: Cyclic Life Tests of Tanks With 2219-T62 Aluminum Liners at 78°K (−320°F)

TANK	SPECIMEN NUMBER	LINER THICKNESS, t_L cm (INCH)	OVERWRAP THICKNESS, t_c cm (INCH)	LINER OUTSIDE DIAMETER, D_L cm (INCH)	TEST PARAMETERS AT	CRACK PLANE ORIENTATION RELATIVE TO TANK LONG. AXIS, ψ rad. (DEG.)	SURFACE CRACK DIMENSIONS: BASE METAL: DEPTH, a cm (INCH)	BASE METAL: LENGTH, 2c cm (INCH)	BASE METAL: SHAPE, a/2c	WELD METAL ℄: DEPTH, a cm (INCH)	WELD METAL ℄: LENGTH, 2c cm (INCH)	WELD METAL ℄: SHAPE, a/2c	TANK PRESSURE, p MN/m² (PSIG)	TANK STRESSES: OVERWRAP: HOOP, $\sigma_{f\theta}$ MN/m² (KSI)	LINER: HOOP, $\sigma_{L\theta}$ MN/m² (KSI)	LINER: LONG., $\sigma_{L\phi}$ MN/m² (KSI)	LINER: PERPEND. TO CRACK, $\sigma_{L\psi}$ MN/m² (KSI)	TEST: TEMPERATURE, T °K (°F)	TEST: ENVIRONMENT	REMARKS
OVERWRAPPED	AS-26	0.254 (0.100)	0.074 (0.029)	16.764 (6.600)	AS FABRICATED	0	0.140 (0.055)	0.526 (0.207)	0.27	0.066 (0.026)	0.312 (0.123)	0.21	0	460 (66.7)	-89 (-12.9)	0	-89 (-12.9)	295 (72)	AIR	TANK LEAKED AT BASE METAL FLAW IN 597 CYCLES R = -0.26
					SIZING PRESSURE								16.8 (2430)	1193 (173.0)	314 (45.5)	272 (39.5)	314 (45.5)			
					RT ZERO PRESSURE								0	628 (91.1)	-121 (-17.6)	0	-121 (-17.6)			
					78°K ZERO PRESSURE								0	457 (66.3)	-88 (-12.8)	0	-88 (-12.8)	78 (-320)	LN_2	
					PROOF PRESSURE								17.4 (2520)	406 (160.0)	352 (51.1)	283 (41.0)	352 (51.1)			
					78°K MIN PRESSURE								0.7 (100)	202 (79.7)	-84 (-12.2)	11 (1.6)	-84 (-12.2)			
					MAX OPER PRESS [1]		0.254 (0.100)	0.673 (0.265)	0.38	0.084 (0.033)	0.312 (0.123)	0.27	15.4 (2240)	938 (136.0)	321 (46.6)	251 (36.4)	321 (46.6)			
	AS-30	0.249 (0.098)	0.074 (0.029)	16.373 (6.446)	AS FABRICATED	0	0.099 (0.039)	0.429 (0.169)	0.23	0.097 (0.038)	0.411 (0.162)	0.23	0	460 (66.7)	-91 (-13.2)	0	-91 (-13.2)	295 (72)	AIR	TANK ACCIDENTLY PROOF LOADED IN LIQUID NITROGEN TO ABOUT 20.7 MN/m² (3000 PSI); THEN LINER SPLIT OPEN AT WELD FUSION LINE AFTER 818 CYCLES R = -0.25
					SIZING PRESSURE								16.8 (2430)	1179 (171.0)	323 (46.9)	278 (40.3)	323 (46.9)			
					RT ZERO PRESSURE								0	632 (91.6)	-125 (-18.1)	0	-125 (-18.1)			
					78°K ZERO PRESSURE								0	462 (67.0)	-91 (-13.2)	0	-91 (-13.2)	78 (-320)	LN_2	
					PROOF PRESSURE								17.4 (2530)	1041 (151.0)	374 (54.3)	290 (42.0)	374 (54.3)			
					78°K MIN PRESSURE								0.7 (100)	536 (77.8)	-82 (-11.9)	12 (1.7)	-82 (-11.9)			
					MAX OPER PRESS [1]		0.145 (0.057)	0.490 (0.193)	0.30	0.130 (0.051)	0.478 (0.188)	0.27	15.4 (2240)	938 (136.0)	328 (47.6)	256 (37.2)	328 (47.6)			

[1] FLAW DIMENSIONS AT TEST TERMINATION

DISTRIBUTION LIST FOR NASA CR-120918
CONTRACT NAS3-14380

DEVELOPMENT OF A FRACTURE CONTROL METHOD FOR COMPOSITE TANKS WITH LOAD SHARING LINERS (Interim Report)

BOEING AEROSPACE COMPANY
SEATTLE, WASHINGTON

NASA-Lewis Research Center
21000 Brookpark Rd.
Cleveland, OH 44135

Attn:	E. J. Kolman, MS 500-313	1
	J. R. Faddoul, MS 49-3	6
	R. H. Kemp, MS 49-3	1
	G. T. Smith, MS 49-3	1
	T. Gulko, MS 49-3	1
	H. W. Douglas, MS 500-205	1
	Library, MS 60-3	1
	AFSC Liaison Office, MS 501-3	3
	Technical Utilization, MS 3-19	1
	R. H. Johns, MS 49-3	1
	R. F. Lark, MS 49-3	1
	W. F. Brown, MS 105-1	1
	G. M. Ault, MS 3-13	1

National Aeronautics and Space Administration
Washington, D.C. 20546

Attn:	MTG/J. G. Malament	1
	MHE/N. G. Peil	1
	KT/Technology Utilization Office	1
	RWM/J. J. Gangler	1
	RWS/D. A. Gilstead	1
	RW/G. C. Deutsch	1
	Library	1

NASA-Ames Research Center
Moffett Field, CA 94035

Attn:	Library	1

Arnold Engineering Development Center
Air Force Systems Command
Tullahoma, TN 37389

Attn: Library 1

Bureau of Naval Weapons
Department of the Navy
Washington, D.C.

Attn: Library 1

Commander
U.S. Naval Missile Center
Point Mugu, CA 93041

Attn: Technical Library 1

Commander
U.S. Naval Weapons Center
China Lake, CA 93557

Attn: Library 1

Commanding Officer
Naval Research Branch Office
1030 E. Green Street
Pasadena, CA 91101

Attn: Library 1

U.S. Army Missile Command
Redstone Scientific Information Center
Redstone Arsenal, AL 35808

Attn: Document Section 1

Commanding Officer
U.S. Army Research Office (Durham)
Box CM, Duke Station
Durham, NC 27706

Attn: Library 1

Director (Code 6T80)
U.S. Naval Research Laboratory
Washington, D.C. 20390

Attn: Library 1

Office of Research Analyses (OAR) Holloman Air Force Base, NM 88330	
Attn: Library RRRD	1
Picatinny Arsenal Dover, N J 07801	
Attn: Library	1
Plastics Technical Evaluation Center Picatinny Arsenal Dover, NJ 07801	1
Space & Missile Systems Organization Air Force Unit Post Office Los Angeles, CA 90045	
Attn: Technical Data Center	1
U.S. Air Force Washington, D.C.	
Attn: Library	1
U.S. Air Force Wright-Patterson AFB, OH 45433	
Attn: AFFDL/W. H. Goesch	1
AFML/T. J. Reinhart, Jr.	1
AFML/J. Whitney	1
U.S. Naval Ordnance Laboratory White Oak Silver Spring, MD 20910	
Attn: R. Simon, Nonmetallic Mat'ls. Div.	1
Library	1
Aerojet Nuclear Systems Company P.O. Box 13070 Sacramento, CA 95813	
Attn: Library	1
Ordnance Division Aerojet-General Corporation 11711 South Woodruff Avenue Downey, CA 90241	
Attn: Library	1

Propulsion Division
Aerojet-General Corporation
P.O. Box 15847
Sacramento, CA 95803

Attn: Technical Library 2484-2015A 1

Space Division
Aerojet-General Corporation
9200 East Flair Drive
El Monte, CA 91734

Attn: Library 1

Aeronautronic Division of Philco Ford Corp.
Ford Road
Newport Beach, CA 92663

Attn: Technical Information Department 1

Aerospace Corporation
P.O. Box 95085
Los Angeles, CA 90045

Attn: Library-Documents 1

Air Products and Chemicals Company
Allentown, PA 18105

Attn: P. J. DeRea 1

Allegheny Ballistics Laboratory
Hercules, Inc.
P.O. Box 210
Cumberland, MD 21052

Attn: W. T. Freeman 1
Library 1

Atlantic Research Corporation
Shirley Highway & Edsall Road
Alexandria, VA 22314

Attn: Security Office for Library 1

Arde, Inc.
19 Industrial Ave.
Mahwah, NJ 07430 1

ARO, Incorporated Arnold Engineering Development Center Arnold Air Force Station, TN 37389	1
Battelle Memorial Institute 505 King Avenue Columbus, OH 43201	
Attn: Defense Metals Information Center	1
Report Library, Room 6A	1
L. E. Hulbert	1
Beech Aircraft Corp. Wichita, KS 67201	
Attn: Library	1
Bell Aerosystems Box 1, Buffalo, NY 14205	
Attn: T. Reinhardt	1
Library	1
B. F. Goodrich Company Aerospace & Defense Products 500 South Main Street Akron, OH 44311	
Attn: Library	1
Brunswick Corporation Defense Products Division P.O. Box 4594 43000 Industrial Avenue Lincoln, NE 68504	
Attn: J. Carter	1
W. Morse	1
General Dynamics/Convair P.O. Box 1128 San Diego, CA 92112	
Attn: H. F. Rodgers, MS 549-00	1
Library	1

Goodyear Aerospace Corporation
1210 Massilon Road
Akron, OH 44306

Attn: Library 1

Grumman Aircraft Engineering Corp.
Bethpage, Long Island, NY 11714

Attn: W. Ludwig, Bldg. 25, Dept. 589 1
L. Mead, Bldg. 25 1
Library 1

Hamilton Standard Corporation
Windsor Locks, CT 06096

Attn: H. P. Borie 1
Library 1

IIT Research Institute
Technology Center
Chicago, IL 60616

Attn: R. H. Cornish, Mech. & Materials Div. 1

Lawrence Livermore Laboratory
Box 808
Livermore, CA 94550

Attn: T. T. Chiako 1

Lockheed-California Co.
Burbank, CA 91503

Attn: R. H. Stone/Dept 74-52, Bldg. 243, Plant 2 1

Lockheed-Georgia Company
Advanced Composites Information Center
Dept. 72-14, Zone 402
Marietta, GA 30060 1

Lockheed Missiles and Space Co.
P.O. Box 504
Sunnyvale ,CA 95087

Attn: J. F. Milton, Dept. 66-01, Bldg. 562 1
R. E. Lewis 1
Library 1

LTV Corporation
P.O. Box 5003
Dallas, TX 75222

Attn: Library 1

Marine Engineering Laboratory
NSRDC ANNADIV
Annapolis, MD 21402

Attn: Karl H. Keller, Code 560 1

Martin Marietta Corp.
P.O. Box 179
Denver, CO 80201

Attn: W. F. Barrett, Mail No. 1631 1
F. Swartzberg, Mail No. 1633 1
C. A. Hall 1
Dr. A. Feldman 1
Library 1

McDonnell-Douglas Corp.
5301 Bolsa Ave.
Huntington Beach CA 92647

Attn: R. F. Zemer, Dept. A3-250 1
H. Babel 1
R. Rawe 1
Library 1

McDonnell-Douglas Corp.
P.O. Box 516
St. Louis, MO 63166

Attn: R. Hepper, Dept. E400 1
Library 1

North American-Rockwell
12214 Lakewood Blvd.
Downey, CA 90241

Attn: R. Field, Mail Code AD75 1
L. J. Koob, Mail Code AD-88 1
J. Colipriest 1
Library 1

Rocketdyne Division
North American Rockwell
6633 Canoga Ave.
Canoga Park, CA 91304

Attn: E. L. Hawkinson D/956 AC10 1
R. P. Frohmberg BA-19 1
Library 1

Oak Ridge National Laboratory
Oak Ridge, TN 37830

Attn: T. W. Pickel 1

Owens-Corning Fiberglas
Technical Center
Granville, OH 43023

Attn: A. B. Isham 1

Rohr Corporation
Department 145
Chula Vista, CA 91312 1

Sandia Laboratories
Albuquerque, NM 87115

Attn: H. M. Stoller, Dept. 5310 1

Thiokol Chemical Corporation
Wasatch Division
P.O. Box 524
Brigham City, UT 84302

Attn: Library Section 1

TRW Systems
1 Space Park
Redondo Beach, CA. 90200

Attn: Tech. Lib. Doc. Acquisitions 1

United Aircraft Corporation
400 Main Street
East Hartford, CT 06108 1

United Aircraft Corporation United Technology Center P.O. Box 358 Sunnyvale, CA 94088 Attn: Librarian	1
U.S. Rubber Company Mishawaka, IN 46544	1
Whittaker Corporation 3640 Aero Court San Diego, CA 92123 Attn: V. Chase	1
University of Nebraska Dept. of Engineering Mechanics Lincoln, NE 68503 Attn: R. Foral	1
University of Oklahoma School of Aerospace, Mechanical and Nuclear Engineering 865 Asp Avenue, Room 200 Norman, OK 73069 Attn: C. W. Bert	1
National Technical Information Service Springfield, VA 22151	20